SYNTHESIS, CHARACTERIZATION AND EXPLORATION OF ANTICANCER ACTIVITY OF 5-METHOXY, 5-HYDROXY AND 5, 7-DIBROMO ISATIN THIOSEMICARBAZONES

A THESIS SUBMITTED TO THE

CENTRAL DEPARTMENT OF CHEMISTRY

INSTITUTE OF SCIENCE AND TECHNOLOGY

TRIBHUVAN UNIVERSITY

NEPAL

FOR THE AWARD OF

DOCTOR OF PHILOSOPHY

IN CHEMISTRY

BY

UPENDRA CHAUDHARY

FEBRUARY 2023

SYNTHESIS, CHARACTERIZATION AND EXPLORATION OF ANTICANCER ACTIVITY OF 5-METHOXY, 5-HYDROXY AND 5, 7-DIBROMO ISATIN THIOSEMICARBAZONES

A THESIS SUBMITTED TO THE

CENTRAL DEPARTMENT OF CHEMISTRY

INSTITUTE OF SCIENCE AND TECHNOLOGY

TRIBHUVAN UNIVERSITY

NEPAL

FOR THE AWARD OF

DOCTOR OF PHILOSOPHY

IN CHEMISTRY

BY

UPENDRA CHAUDHARY

FEBRUARY 2023

TRIBHUVAN UNIVERSITY

Institute of Science and Technology

DEAN'S OFFICE

Kirtipur, Kathmandu, Nepal

Reference No.:

Institute of Science & Technology
Dean's Office
Kirtipur 2045

EXTERNAL EXAMINERS

The Title of Ph.D. Thesis: **"Synthesis, Characterization and Exploration of Anticancer Activity of 5-methoxy, 5-hydroxy and 5,7-dibromoisatin Thiosemicarbazones,"**

Name of Candidate: **Upendra Chaudhary**

External Examiners:

(1) Dr. Bhushan Shakya
Amrit Campus
Tribhuvan University, NEPAL

(2) Prof. Dr. Ram Charitra Maurya
Department of Chemistry
Rani Durgavati Vishwavidyalaya
Jabalpur, INDIA

(3) Prof. Dr. Robert A. Gossage
Toronto Metropolitan University
Toronto, CANADA

June 13, 2023

Dr. Surendra Kumar Gautam
Asst. Dean

DECLARATION

Thesis entitled "**Synthesis, Characterization and Exploration of Anticancer Activity of 5-methoxy, 5-hydroxy and 5,7-dibromoisatin Thiosemicarbazones**," which is being submitted to the Central Department of Chemistry, Institute of Science and Technology (IOST), Tribhuvan University, Nepal for the award of the degree of Doctor of Philosophy (Ph.D.), is a research work carried out by me under the supervision of Prof. Dr. Paras Nath Yadav of Central Department of Chemistry, Tribhuvan University.

This research is original and has not been submitted earlier in part or full in this of any other form to any university or institute, here or elsewhere, for the award of any degree.

.....

Upendra Chaudhary

Date:...6../..1.8./...2023...

RECOMMENDATION

This is to recommend that **Upendra Chaudhary** has carried out research entitled **"Synthesis, Characterization and Exploration of Anticancer Activity of 5-methoxy, 5-hydroxy and 5,7-dibromoisatin Thiosemicarbazones,"** for the award of Doctor of Philosophy (Ph.D.) in **Chemistry** under my supervision. To my knowledge, this work has not been submitted for any other degree.

He has fulfilled all the requirements laid down by the Institute of Science and Technology (IOST), Tribhuvan University, Kirtipur for the submission of the thesis for the award of Ph.D. degree.

.....

Central Department of Chemistry
Kirtipur

Prof. Dr. Paras Nath Yadav

(Supervisor)

Central Department of Chemistry

Tribhuvan University

Kirtipur, Kathmandu

Nepal

Date: ...6/18/2023.....

त्रिभुवन विश्वविद्यालय
TRIBHUVAN UNIVERSITY
विज्ञान तथा प्रविधि अध्ययन संस्थान
Institute of Science and Technology
रसायन शास्त्र केन्द्रीय विभाग
CENTRAL DEPARTMENT OF CHEMISTRY
कीर्तिपुर, काठमाडौं, नेपाल
Kirtipur, Kathmandu, NEPAL

पत्र संख्या:
Ref. No.:

LETTER OF APPROVAL

Date: 23/02/2023

On the recommendation of **Prof. Dr. Paras Nath Yadav**, this Ph. D. thesis submitted by **Upendra Chaudhary**, entitled "**Synthesis, Characterization and Exploration of Anticancer Activity of 5-methoxy, 5-hydroxy and 5,7-dibromoisatin Thiosemicarbazones**," is forwarded by Central Department Research Committee (CDRC) to the Dean, IOST, T.U.

.....

Prof. Dr. Jagadeesh Bhattarai

Head of Department

Central Department of Chemistry

Tribhuvan University

Kirtipur, Kathmandu

Nepal

Tel.: 977-1-4332034, Fax No.: +977-1-4330537, http://www.cdctu.edu.np e-mail: info@cdctu.edu.np

ACKNOWLEDGEMENTS

It has been truly life-changing experience for me to pursue this Ph. D., and I could not have done it without the support and direction I received from so many individuals.

My sincere gratitude goes out to my supervisor, **Prof. Dr. Paras Nath Yadav**, for his inspirational leadership, kindness, encouragement, and unwavering support during the duration of the study and the writing of this thesis. His astute criticism inspired me to think more clearly and elevated the quality of my work and his continuous good mood and humor helped me and encouraged me in every moment

I am really appreciative of the financial support I obtained from Nepal Academy of Science and Technology (NAST) in 2018/2019 AD for my Ph. D. I am very grateful for the assistance I have received from Dr. Yuba Raj Pokharel for the anticancer screening of synthetic compounds, Dr. Kuldeep Mahiya from Haridwar, India, for the single crystal X-ray analysis simulation of compounds, Dr. Abdur Rauf from the University of Swabi, Pakistan, for Molecular Docking, IIT Madras for CHN analysis, Mass and NMR, and IISc Bangalore for NMR, Dr. Jhashanath Adhikari Subin from D.A.V. College, Lalitpur, Nepal for Molecular Docking.

I am grateful to the Head of Department Prof. Dr. Jagadeesh Bhattarai and former Head of Department Prof. Dr. Ram Chandra Basnyat, Central department of Chemistry (TU) for providing me with all the facilities there. Similarly, my sincere gratitude goes to all teaching and non-teaching staffs of the department for their prompt assistance and kind cooperation during the course of my research.

I appreciate the Dean's office at Tribhuvan University's Institute of Science and Technology (IOST) and the Chemistry Department at Premier College for helping me with my research studies and granting me time off for research. I am appreciative of Premier College's Mr. Chhabi Lal Pandey, Mr. Meen Bahadur Karki, and Mr. Mukesh Pandey for their assistance with my research.

I am so grateful to my Dream Team, my lab family, for all the support and all the help in every laboratory. Thanks Dr. Bhushan Shakya, Dr. Narendra Kumar Singh, Dr. Hari Sharan Adhikari, Dr. Dipak Kumar Gupta, Late Narayan Bhattrai, Anand Yadav, Ramina Shrestha, Lekh Nath Khanal, Prakash Gautam, Manoj Kumar, Janaki Baral,

and Sanjay Singh, along with everyone else who assisted me in any way during my research.

For everything they have done for me, my father Bhim Chandra Chaudhary, mother Bhuna Devi Chaudhary, my elder brother Prem Kant Chaudhary and my sister-in-law Tika Laxmi Chaudhary deserve special recognition. I wouldn't be who I am now without them.

Above everything, I want to thank my wife Kalpana Chaudhary for her love and unwavering support throughout the past few months, as well as for all the late nights and early mornings she put up with. I appreciate you being my best friend and muse. You are all I owe.

Last but not least my precious son Anay Chaudhary and my angelic daughter Ananya Chaudhary provided the comfort and support needed to maintain the human psyche throughout the entire period of intense labor required to complete this task. I have no words to adequately express my gratitude to them for their unending love, patience, understanding, and angelic guidance.

Upendra Chaudhary

February, 2023

ABSTRACT

Thiosemicarbazones are synthetic compounds which are formed by the condensation of carbonyl compounds with thiosemicarbazides. In thiosemicarbazone, sulphur (S) and nitrogen (N) as donor atoms which are the combination of hard soft donor character and having versatile co-ordination character. They have many chemical, biological and medical properties *e.g.*, antiviral. Thiosemicarbazones are believed to inhibit ribonucleotide reductase, a necessary enzyme for DNA synthesis, as part of their anticancer properties. As a viral enzyme involved in DNA synthesis and a major target for the production of anticancer drugs, ribonucleotide reductase transforms ribonucleotides into deoxy ribonucleotides.

All of the compounds (**1-26**) had greater inhibitory effects on the cancer cell lines MCF-7, A431, A549, MDA-MB-231, and PNT-2 than the positive control (DMSO), with IC_{50}; values for MCF-7 (IC_{50}; 2.93 µM, **2**), A431 (IC_{50}; 4.80 µM, **3**), A549 (IC_{50}; 2.52 µM, **3**), MDA-MB-231 (IC_{50}; 2.47 µM, **20**) and PNT-2 (IC_{50}; 2.54 µM, **20**).

In this study, a series of 5-substituted (-OMe, -OH) and 5,7-disubstituted (-Br) N(4)-thiosemicarbazones were synthesized and analyzed by elemental analysis, FTIR, ^{1}H-NMR, ^{13}C-NMR, ESI-HRMS, UV-Vis, and single crystal X-ray crystallography. The CHN, UV-Vis, and ESI-HRMS data all agreed with the hypothesized structures.

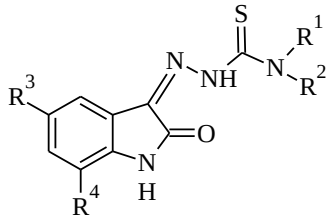

R^3 and R^4 = OCH_3, OH, Br, H

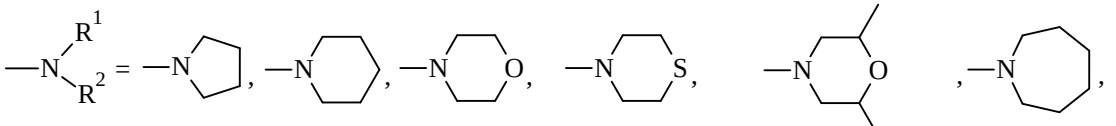

2º amine Pyrrolidine Piperidine Morpholine Thiomorpholine 2,6-dimethylmorpholine Azepane

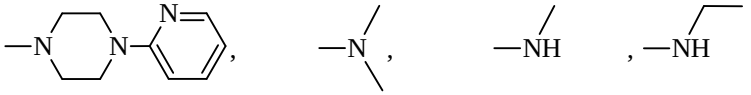

(Pyridin-2-yl)piperazine Dimethyl amine Methyl amine Ethyl amine

Keywords: Anticancer properties, DNA synthesis, inhibitory effects, major target, necessary enzyme, ribonucleotide reductase, thiosemicarbazones

LIST OF ACRONYMS AND ABBREVIATIONS

A431	: Epidermoid Carcinoma
A549	: Human Lung Adenocarcinoma
AcOH	: Acetic Acid
ADMET	: Absorption, Distribution, Metabolism, Excretion, and Toxicity
AKT	: Ak Strain Transforming
AML	: Acute Myeloid Leukemia
ARG	: Arginine
ASP	: Aspartic
ATP	: Adenosine Triphosphate
B16	: Murine Melanoma Cell
BFGS	: Broyden–Fletcher–Goldfarb–Shanno
BHT	: 2,6-di(tert-butyl)-4-hydroxytoluene
BLYP	: Becke-Lee-Yang-Parr
CCDC	: Cambridge Crystallographic Data Centre
CCRF-CEM	: Methotrexate-resistant Human T-lymphoblast Leukemia Cells
^{13}C	: NMR Carbon Nuclear Magnetic Resonance
Cdk	: Cyclin-Dependent Kinase
CNS	: Central Nervous System
CoMFA	: Comparative Molecular Field Analysis
DPBS	: Dulbecco's Phosphate-Buffered Saline
DMEM	: Dulbecco's Modified Eagle Medium
DMF	: Dimethyl Formamide
DMS	: Darmouth Medical School

DMSO : Dimethyl Sulphoxide

DMSO-d_6 : Deuterated Dimethyl Sulphoxide

DNA : Deoxyribonucleic Acid

Dp44mT : Di-2-pyridylketone-4,4-dimethyl-3-thiosemicarbazone

EA : Elemental Analysis

EAC : Ehrlich Ascetic Carcinoma Cell

e. g. : Example

EPR : Electron Paramagnetic Resonance

ESI-HRMS : High Resolution Electron Spray Ionization Mass Spectrometry

Et_2O : Diethyl Ether

EtOH : Ethyl Alcohol/ Absolute Alcohol

ERK : Extracellular Signal-Regulated Kinase

FACS : Fluorescence-Activated Cell Sorting

FDA : Food and Drug Administration

FGF : Fibroblast Growth Factor

Fig. : Figure

FLT3 : Fetal Liver Tyrosine Kinase Receptor 3

5-FU : 5-Fluorouracil

GLU : Glutamic Acid

HBD : Hydrogen Bond Donors

HBA : Hydrogen Bond Acceptor

HCT : Heterocyclic Thiosemicarbazone

HCT116 : Human Colorectal Cancer Cell

3-HP : 3-Hydroxy-2-Formylpyridine Thiosemicarbazone

5-HP : 5-Hydroxypyridine-2-Carboxaldehyde Thiosemicarbazone

HEK293 : Human Embryonic Kidney Cell

HeLa : Immortal Cervical Carcinoma

Hela S3 : Uterine Carcinoma/Human Cervix Carcinoma

HepG2 : Human Liver Cancer Cell

HDAC : Histone Deacetylase

HGPRTase : Hypoxanthine-Guanine Phosphoribosyl Transferase

HGF/SF : Hepatocyte Growth Factor/Scatter Factor

HL60 : Promyelocytic Cell

HT29 : Human Colon Cancer Cell

^{1}H NMR : Proton Nuclear Magnetic Resonance

HRMS : High-Resolution Mass Spectrometry

HUVEC : Human Umbilical Vein Endothelial Cells

ILE : Isoleucine

IR : Infrared

IUPAC : International Union of Pure and Applied Chemistry

JNK : c-Jun N-terminal Kinase

K-562 : Multipotential Leukemia Cell Line

LECO : Laboratory Equipment Corporation

LEU : Leucine

LYS : Lysine

L1210 : Mouse Lymphocytic Leukemia Cell

MABA : Microplate Alamar Blue Assay

MAO : Monoamine Oxidase

MAPK : Mitogen-Activated Protein Kinase

MCF-7 : Human Breast Carcinoma

MCT : Medium Chain Triglycerides

MDA-MB-231: Human Breast Carcinoma

MDR1 : Multidrug Resistance Protein

MET : Methionine

MeCN : Acetonitrile

Me_2CO : Acetone

MeOH : Methyl Alcohol

6-MP : 6-Mercaptopurine

MS : Mass Spectrometry

4-mpt : 4-Methyl- 4-phenyl-3-thiosemicarbazide

NCIH-460 : Hypotriploid Human Cell Line

NIH 3T3 : Mouse Embryonic Fibroblast Cells

N1E-115 : Neuroblastoma Cell

PBD : Protein Data Bank

PBMC : Peripheral Blood Mononuclear Cell

PC-12 : Pheochromocytoma Cell

PC-3 : Prostate Cancer Cell Line

PDGF : Platelet-Derived Growth Factor

PHE : Phenylalanine

PNT-2 : Normal Prostate Epithelial Cell

PTK : Protein Tyrosine Kinases

PVDF : Polyvinylidene Fluoride

QToF : Quadrupole Time-of-Flight

QSAR : Quantitative Structure-Activity Relationship

RKT : Receptor Tyrosine Kinase

RMSD : Root Mean Square Deviation

RNA : Ribonucleic Acid

RNase : Ribonuclease

ROS : Reactive Oxygen Species

RR : Ribonucleotide Reductase

RSC : Rous Sarcoma Virus

SAR : Structure Activity Relationship

SH-SY5Y : Neuroblastoma Cell

SK-BR-3 : Human Breast Cancer Cell

STAT : Signal Transducer and Activator of Transcription

TACE : Transarterial Chemoembolization

THF : Tetrahydrofuran

THR : Threonine

TKI : Tyrosine Kinase Inhibitor

U937 : Human Histiocytic Lymphoma/Human Myeloid Leukemia Cell

UV : Ultraviolet

VAL : Valine

VEGF : Vascular Endothelial Growth Factor

viz. : Such as

WHO : World Health Organization

LIST OF SYMBOLS

%	: Percentage
^{o} C	: Degree Celsius
µ	: Micro
M	: Molar or Moles Per Liter
δ	: Chemical Shift
ν	: Stretching Vibration
s	: Singlet (NMR); Strong Intensity (IR)
w	: Weak Intensity (IR)
br	: Broad Intensity (IR)
d	: Doublet (NMR)
dd	: Doublet of Doublets (NMR)
t	: Triplet (NMR)
m	: Multiplet (NMR); Medium Intensity (IR)
IC_{50}	: Maximal Concentration to Cause 50% Inhibition of Activity
GI_{50}	: Concentration for 50% of Maximal Inhibition of Cell Proliferation
LC_{50}	: Lethal Concentration Causing 50% Cell Death
CC_{50}	: 50% Cytotoxic Concentration
cm^{-1}	: Per Centimeter
ppm	: Part Per Million
MHz	: Megahertz
GHz	: Gigahertz
K	: Kelvin
Å	: Angstrom

mmol	: Milimol
mL	: Mililiter
g	: Gram
min	: Minute
amu	: Atomic Mass Unit
nm	: Nanometer
h	: Hour
>	: Greater Than
<	: Less Than
Gs	: Gauss
mT	: Milli Tesla
B_o	: Magnetic Field
h	: Planck’s Constant
et al.	: et alia (and others)
C	: Concentration

LIST OF TABLES

Page No.

Table 1: N-substituted carbothiohydrazide 30

Table 2: The physical properties of N(4)-substituted 5-methoxyisatin thiosemicarbazones (1-6) 36

Table 3: Elemental analysis data of N(4)-substituted 5-methoxyisatin thiosemicarbazones (1-6) 37

Table 4: Diagnostic bands in the IR spectra (cm^{-1}) of compounds (1-6) 39

Table 5: ^{1}H NMR spectral assignments (δ ppm) of compounds (1-6) 41

Table 6: ^{13}C NMR spectral assignments (δ ppm) of compounds (1-6) 42

Table 7: The mass spectral data of the synthesized compounds (1-6) 44

Table 8: UV-Visible spectroscopic data of compounds (1-6) 47

Table 9: Cell viability (μM) against cancer cell lines for 72 h. 53

Table 10: Short details of receptors used in molecular docking 62

Table 11: Short details of compounds and FDA approved drugs2 64

Table 12: Adsorption, distribution, metabolism, excretion and toxicity of the drug candidates 65

Table 13: Binding affinities (kCal/mol) of various chemical compounds and drugs against different receptor proteins (PDB ID) related to malignant tumors 67

Table 14: Residues involved in major interactions with MeOIstEth and distances (Å) 72

Table 15: Physical properties of 5-hydroxyisatin N(4)-substituted thiosemicarbazones (7-16) 76

Table 16: Elemental analysis data of 5-hydroxyisatin N(4)-substituted thiosemicarbazones (7-16) 79

Table 17: Diagnostic bands in the IR spectra (cm^{-1}) of compounds (7-16) 80

Table 18: ^{1}H NMR spectral assignments (δ ppm) of compounds (7-16) 82

Table 19: ^{13}C NMR spectral assignments (δ ppm) of compounds (7-16) 85

Table 20: Mass spectrometric data of compounds (7-16) 87

Table 21: UV-Visible spectroscopic data of compounds (7-16) 89

Table 22: Physical properties of 5,7-dibromoisatin N(4)-substituted thiosemicarbazones (17-26) 96

Table 23: Elemental analysis data of 5,7-dibromoisatin N(4)-substituted thiosemicarbazones (17-26) 98

Table 24: Diagnostic bands in the IR spectra (cm^{-1}) of compounds (17-26) 100

Table 25: ^{1}H NMR spectral assignments (δ ppm) of compounds (17-26) 102

Table 26: ^{13}C NMR spectral assignments (δ ppm) of compounds (17-26) 104

Table 27: Mass spectrometric data of compounds (17-26) 106

Table 28: UV-Visible spectroscopic data of compounds (17-26) 108

Table 29: Cell viability (μM) against cancer cell lines for 72 h. 111

Table 30: Brief details of receptors taken for molecular docking calculations .. 116

Table 31: Short details of the test compounds and two FDA approved drugs; Isomeric/canonical SMILES 117

Table 32: Physicochemical properties of two test molecules 118

Table 33: ADMET predicted by pkCSM server 119

Table 34: Toxicity profile of two test compounds by Pro Tox II server 120

Table 35: Binding affinities (kCal/mol) of two test compounds and two drugs against different receptor proteins (PDB ID) related to malignant tumors 123

Table 36: Key amino residues involved in major interactions in different complexes 127

LIST OF FIGURES

Page No.

Figure 1: Systematic procedure of N-substituted thiosemicarbazones.....2

Figure 2: The possible tautomer of isatin-3-thiosemicarbazone (I-VI).....3

Figure 3: General procedures of N(4)-substituted thiosemicarbazones. 3

Figure 4: Structure of ifosfamide, thiotepa, altretamine.....4

Figure 5: Structure of 5-FU and 6-MP 5

Figure 6: Structure of daunorubicin and epirubicin 5

Figure 7: Structure of etoposide and teniposide 6

Figure 8: Structure of vinblastin and vincristine.....6

Figure 9: Synthetic scheme of 5-OMe, 5-OH and 5,7-disubstituted (-Br) isatin derived N(4)-thiosemicarbazones 8

Figure 10: Structure of triapine and thiacetazone.....9

Figure 11: Structure of methisazone, and 5-AP.....10

Figure 12: Structure of Di-2-pyridylketone-4,4-dimethyl-3-thiosemicarbazone and 6-methoxycarbonyl substituted indolinone 10

Figure 13: Structure of 5-chloroisatin capped hydroxamic acid and isatin-β-thiosemicarbazone and key part shows cytotoxicity.....11

Figure 14: Structure of isatin (1H-indole-2,3-dione) 11

Figure 15: *Couroupita guianensis* Aubl (A) *Isatis tinctoria* (B) Bufo frog (D) The marine mollusc (E).....12

Figure 16: Various substitution patterns for the development of different isatin analogues.....13

Figure 17: Structure of O-acyl oximes, aminomethylene-lysine indolinone, 5, 6, 7-tribromoisatin, azaaurone 14

Figure 18: Highly cytotoxic brominated derivatives and structure of N-phenethyl derivative 15

Figure 19: Structure of isatin-benzothiazole, 5-bromoisatin derivative and 5-chloroisatin derivative 16

Figure 20: Structure of 5-fluoro-isatin-3-thiosemicarbazone and (Z)-2-(5-fluoro-2-oxoindolin-3-ylidene)-N-phenylhydrazinecarbothioamide 16

Figure 21: Structure of 5-methoxyisatin-3-thiosemicarbazone and 5-nitroisatin-3-thiosemicarbazones derivatives (a-c) 17

Figure 22: Structure of 5-chloro-1H-indole-2,3-dione 3-thiosemicarbazones derivatives and isatin-β-thiosemicarbazones 18

Figure 23: Structure of 1-(4-dimethylamino) benzylidene)-5-(2-oxoindolin-3-ylidene) thiocarbohydrazone and 5-nitroisatin-4-thiomorpholinyl-3-thiosemicarbazone 19

Figure 24: Structure of 5-chloroisatin derivatives and 4-piperazinylquinoline-isatin-thiosemicarbazone 20

Figure 25: Structure of isatin-β-thiocarbohydrazone 20

Figure 26: Structure of 5-methoxyisatin and its derivative (SU9516) 21

Figure 27: Structure of 5-hydroxyisatin and isatinic acid 21

Figure 28: Structure of 5,7-dibromoisatin and its hybrid 22

Figure 29: Systematic scheme for N-substituted carbothiohydrazide 29

Figure 30: General structure of synthesized thiosemicarbazones 33

Figure 31: Systematic scheme of 5-hydroxyisatin N(4)-substituted thiosemicarbazones 34

Figure 32: Systematic scheme of 5,7-dibromoisatin N(4)-substituted thiosemicarbazones 35

Figure 33: IR spectrum of compound (2) 39

Figure 34: ^{1}H NMR spectrum (400 MHz, DMSO-d6) of compound (2) 41

Figure 35: ^{13}C NMR spectrum (400MHz, DMSO-d6) of compound (2) 43

Figure 36: ESI-HRMS of compound (2) 46

Figure 37: UV-Visible spectra of compound (2) 47

Figure 38: ORTEP diagram of compound MeOIstDm drawn in 30% thermal probability ellipsoids showing atomic numbering scheme. 49

Figure 39: ORTEP diagram of MeOIstDmMor drawn in 20% thermal probability ellipsoids showing atomic numbering scheme. 50

Figure 40: Hydrogen bonding interactions in the crystal lattice of MeOIstDmMor viewed along the crystallographic c-axis. 50

Figure 41: Two-dimensional hydrogen bonding networks in the crystal lattice of MeOIstDmMor viewed along crystallographic a-axis. 51

Figure 42: Cell viability assay synthetic compounds with different concentration. 54

Figure 43: Colony formation assay and flow cytometric analysis of apoptosis by propidium iodide (PI) staining. 55

Figure 44: MeOIstDmMor causes G0/G1 cell cycle arrest in A431 cell line (A) control (DMSO). 56

Figure 45: A Western blotting analysis of compound MeOIstDmMor in A431 cell line. 57

Figure 46: Graphical abstract of MeOIstDmMor mediated anticancer activity in A431 cells lines 58

Figure 47: (a-b) 3D and 2D interaction plots of native ligand sorafenib into the binding site of VEGFR2 enzyme (PDB ID = 4ASD) 59

Figure 48: (a-b) 3D and 2D interaction plots of MeOIstDmMor into the binding site of VEGFR2 enzyme (PDB ID = 4ASD) 59

Figure 49: (a-b) 3D and 2D interaction plots of MeOIstDmMor into the binding site of VEGFR2 enzyme (PDB ID = 4ASD) 60

Figure 50: Cartoon representation of a docked pose of MeOIstEth in the active site of protein with PDB ID: 4ASD 61

Figure 51: Geometry optimized molecular structure of (a) MeOIstEth and of (b) MeOIstMet 63

Figure 52: Radar plots of (a) MeOIstEth and of (b) MeOIstMet showing physicochemical data 65

Figure 53: Best docked pose of MeOIstEth with 4ASD as (a) 3D with H-bond surface and (b) 2D plots 68

Figure 54: Best docked pose of MeOIstEth with 3MJG as (a) 3D with H-bond surface and (b) 2D plots 69

Figure 55: Best docked pose of MeOIstEth with 3MJK as (a) 3D with H-bond surface and (b) 2D plots 69

Figure 56: Best docked pose of MeOIstEth with 7BJ6 as (a) 3D with H-bond surface and (b) 2D plots 70

Figure 57: Best docked pose of MeOIstEth with 2VTA as (a) 3D with H-bond surface and (b) 2D plots 70

Figure 58: Best docked pose of MeOIstEth with 3VHE as (a) 3D with H-bond surface and (b) 2D plots 71

Figure 59: Best docked pose of MeOIstEth with 6LVK as (a) 3D with H-bond surface and (b) 2D plots 71

Figure 60: IR spectrum of 5-hydroxyisatin 75

Figure 61: Mass spectrum of 5-hydroxyisatin 76

Figure 62: IR spectrum of compound (11) 81

Figure 63: ^{1}H NMR spectrum (400 MHz, DMSO-d6) of compound (13) 83

Figure 64: ^{13}C NMR spectrum (400 MHz, DMSO-d6) of compound (13) 86

Figure 65: ESI-HRMS of compound (13) 88

Figure 66: UV-Visible spectra of compound (15) 89

Figure 67: ORTEP diagram of compound (9) drawn in 20% thermal probability ellipsoids showing atomic numbering scheme. 90

Figure 68: ORTEP diagram of compound (12) drawn in 30% thermal probability ellipsoids showing atomic numbering scheme. 91

Figure 69*:* ORTEP diagram of compound (16) drawn in 20% thermal probability ellipsoids showing atomic numbering scheme. 93

Figure 70: Cell viability assay of synthetic compounds with different concentration in different cell lines (7-16) 94

Figure 71: IR spectrum of compound (22) 101

Figure 72: ^{1}H NMR spectrum (400 MHz, DMSO-d6) of compound (22) 103

Figure 73: ^{13}C NMR spectrum (400 MHz, DMSO-d6) of compound (26) 105

Figure 74: ESI-HRMS of compound (20) 107

Figure 75: UV-Visible spectra of compound (26) 108

Figure 76: ORTEP diagram of compound (22) drawn in 20% thermal probability ellipsoids showing atomic numbering scheme. 109

Figure 77: The ORTEP diagram of compound (26) showing the thermal ellipsoid at 30% probability level. 110

Figure 78: Cell viability assay of synthetic compounds with different concentration in different cell lines (17-26).....112

Figure 79: Illustration of a ligand (DiBrIstEth) docked in the active site of protein with PDB ID: 3MJG 114

Figure 80: Geometry optimized molecular structure of (a) DiBrIstEth and of (b) HydIstAzep 117

Figure 81: Best docked pose of DiBrIstEth with receptor 4ASD as (a) 3D and (b) 2D plot with different types of interactions 124

Figure 82: Best docked pose of HydIstAzep with 4ASD as (a) 3D and (b) 2D plot with different types of interactions.....124

Figure 83: Best docked pose of DiBrIstEth with 2VTA as (a) 3D and (b) 2D plot with different types of interactions.....125

Figure 84: Best docked pose of HydIstAzep with 2VTA as (a) 3D and (b) 2D plot with different types of interactions.....125

Figure 85: Best docked pose of HydIstAzep with 3VHE as (a) 3D and (b) 2D plot with different types of interactions.....126

LIST OF SCHEMES

Page No.

Scheme 1: Synthesis of S-carboxymethyl N-substituted dithiocarbamate (I) 29

Scheme 2: Synthesis of N-substituted carbothiohydrazide (II) 29

Scheme 3: Synthesis of carboxy methyl-N-methyl-N-phenyldithiocarbamate (I)31

Scheme 4: Synthesis of N-methyl-N-phenyl-3-thiosemicarbazide (II) 31

Scheme 5: Synthesis of 4-(pyridin-2-yl)piperazine-1-carbothiohydrazide (III)...32

Scheme 6: Synthesis of 5-hydroxyisatin.....33

TABLE OF CONTENTS

Page No.

Declaration ii

Recommendation iii

Letter of Approval iv

Acknowledgements v

Abstract vii

List of Acronyms and Abbreviations viii

List of Symbols xiii

List of Tables xv

List of Figures xviii

List of Schemes xxiv

Table of Contents xxv

CHAPTER 1

1. INTRODUCTION 1

1.1 Introduction 1

1.2 General structure of thiosemicarbazones 2

1.2.1 Tautomerization of thiosemicarbazone 2

1.2.3 Synthetic procedures of N(4)-substituted thiosemicarbazides / thiosemicarbazones 3

1.3 Modes of action of anticancer drug 4

1.3.1 Alkylating agent 4

1.3.2 Antimetabolites 4

1.3.3 Anthracyclines 5

1.3.4 Topoisomerase inhibitors 5

1.3.5 Mitotic inhibitors 6

1.4 Rationale 7

1.5 Objectives 7

1.5.1 General objectives 7

1.5.2 Specific objectives 7

CHAPTER 2

2. LITERATURE REVIEW 9

2.1 Biological importance of thiosemicarbazones 9

2.2 Isatin 11

2.3 Reactivity of isatin 13

2.4 Cytotoxic effects of isatin 14

2.5 Cytotoxic effect of isatin derivatives 15

2.6 Biological activities of isatin thiosemicarbazones derivatives 16

2.7 Biological importance of 5-methoxyisatin 20

2.8 Biological importance of 5-hydroxyisatin 21

2.9 Biological importance of 5,7-dibromoisatin analogue 22

CHAPTER 3

3. MATERIALS AND METHODS 23

3.1 Materials 23

3.1.1 Cell lines of compounds (1 – 6) 23

3.1.2 Cell viability assay 23

3.1.3 Colony formation assay 24
3.1.4 Propidium iodide staining 24
3.1.5 Cell cycle analysis 24
3.1.6 Cell lysate preparation 24
3.1.7 Protein estimation by BCA kit 25
3.1.8 SDS gel running 25
3.1.9 Transferring proteins from gel to PVDF membrane 25
3.1.10 Blocking the membrane 26
3.2 Biological screening of compounds (7-26) 26
3.2.1 Materials 26
3.2.2 Cell culture and treatment 26
3.2.3 Cell viability assay 26
3.3 Instrumentation 27
3.3.1 Melting point determination 27
3.3.2 Elemental analysis 27
3.3.3 Infrared spectroscopy 27
3.3.4 Nuclear magnetic resonance spectroscopy (NMR) 27
3.3.5 High resolution mass spectroscopy (HRMS) 27
3.3.6 UV-Visible spectroscopy 27
3.3.7 Single crystal X-ray crystallography Study 28
3.4 Synthesis of thiosemicarbazones precursors 28
3.4.1 Synthesis of N-substituted carbothiohydrazide 28
3.4.2 4-(pyridin-2-yl)piperazine-1-carbothiohydrazide (Scovill, 1991) 31
3.5 General procedure for the synthesis of 5-methoxyisatin N(4)-substituted thiosemicarbazones (1-6) 32
3.6 Synthesis of 5-hydroxyisatin (Yasuda *et al*., 2013) 33

3.7 General procedure for the synthesis of 5-hydroxyisatin N(4)-substituted thiosemicarbazones (7-16) 33

3.8 General procedure for the synthesis of 5, 7-dibromoisatin N(4)-substituted thiosemicarbazones (17-26) 34

CHAPTER 4

4. RESULTS AND DISCUSSION 36

4.1 Synthesis, Characterization and Anticancer Activity of N(4)-Substituted 5-Methoxyisatin Thiosemicarbazones 36

4.1.1 General discussion 36

4.1.2 Spectral studies 38

4.1.2.1 IR spectra 38

4.1.2.2 NMR spectra 40

4.1.2.3 Mass spectroscopy 44

4.1.2.4 UV-Visible spectroscopy 46

4.1.2.5 Single crystal X-ray crystallographic study 48

4.1.2.6 Crystal structure description 48

4.1.3 Anticancer activity 52

4.1.3.1 Anticancer activity of 5-methoxyisatin N(4)-substituted thiosemicarbazones 53

4.1.3.2 Molecular docking of compound MeOIstDmMor 58

4.1.4 Molecular docking of compounds MeOIstEth and MeOIstMet 60

4.1.4.1 Density functional theory 60

4.1.4.2 Molecular docking 60

4.1.4.3 Target proteins 61

4.1.4.4 Test compounds and control drugs 63

4.1.4.5 Computational resources 64

4.1.5 Results and discussion 64

4.1.5.1 Druglikeness and pharmacology studies 64

4.1.5.2 Anticancer properties by graph-based signatures.....66
4.1.5.3 Flexible receptor molecular docking.....67
4.1.5.4 Interactions at the atomic-level 67
4.1.5.5 Future work 73
4.1.5.6 Conclusion.....74
4.2 Synthesis, Characterization and Anticancer Activity of 5-Hydroxyisatin N(4)-Substituted Thiosemicarbazones 75
4.2.1 IR spectra of 5-hydroxyisatin.....75
4.2.2 ESI-HRMS spectra of 5-hydroxyisatin 76
4.2.3 General discussion.....76
4.2.4 Spectral studies.....79
4.2.4.1. IR spectra.....79
4.2.4.2 NMR spectra 81
4.2.4.3 Mass spectrometry.....86
4.2.4.4 UV-Visible spectra.....88
4.2.4.5 Single crystal X-ray crystallographic study 90
4.2.4.6 Anticancer activity of 5-hydroxyisatin N(4)-substituted.....93
thiosemicar bazones (7 – 16).....93
4.2.4.7 Conclusion.....94
4.3 Synthesis, Chracterization and Anticancer Activity of 5,7-Dibromoisatin N(4)-Substituted Thiosemicarbazones 96
4.3.1 General discussion.....96
4.3.2 Spectral studies.....99
4.3.2.1 IR spectra.....99
4.3.2.2 NMR spectra 101
4.3.2.3 Mass spectrometry.....105
4.3.2.4 UV-Visible spectra.....107
4.3.2.5 Single crystal X-ray crystallographic study 109

4.3.3 Anticancer activity of 5,7-dibromoisatin N(4)-substituted thiosemicarbazones (17 – 26) 111

4.3.3.1 Conclusion 112

4.3.4 Molecular docking of compound HydIstAzep and DiBrIstEth 113

4.3.4.1 Density functional theory approximations 113

4.3.4.2 Molecular docking calculations 114

4.3.4.3 Receptor proteins 115

4.3.4.4 Test compounds, control drugs and ADMET prediction 116

4.3.4.5 Computational resources 118

4.3.5 Results and discussion 118

4.3.5.1 Physicochemical properties of test molecules 118

4.3.5.2 Druglikeness and pharmacology studies 119

4.3.5.3 Anticancer properties by graph-based signatures 121

4.3.5.4 Flexible receptor molecular docking 122

4.3.5.5 Non-covalent interactions present in adduct 123

4.3.5.6 Conclusion and prospective 128

CHAPTER 5

5. CONCLUSION AND RECOMMENDATIONS 130

5.1. Conclusion 130

5.2. Recommendation for further work 131

CHAPTER 6

6. SUMMARY 132

REFERENCES 137

APPENDICES 167

Appendix A

Appendix B

Appendix C

Appendix D

Appendix E

CHAPTER 1

1. INTRODUCTION

1.1 Introduction

Cancer is a class of diseases that are characterized by uncontrolled cell proliferation combined with malignant activity, and it is the major cause of death globally (Paulmurugan, 2012). According to the International Agency for Research on Cancer's GLOBOCAN series, there were 14.1 million new cases recorded and 8.2 million deaths worldwide in 2012. As with the reported rate, the main causes of death were stomach cancer (745 000 fatalities), liver cancer (1.6 million fatalities), and (723,000 deaths), followed by breast cancer (1.67 million), colorectal cancer (1.82 million), and lung cancer (1.36 million) (Ferlay *et al*., 2015). The estimated number of new cases of cancer in 2018 was 18.1 million, with 9.5 million fatalities. Lung cancer is the leading cause of cancer death in men, followed by prostate and stomach cancer, whereas breast cancer is the leading cause of cancer mortality in women, followed by lung and colorectal cancer (Bray *et al*., 2018). With 24.1 million new cases and 13.0 million deaths anticipated from cancer by 2030, the mortality and morbidity of the disease would likely continue to rise (Sánchez *et al*., 2019). GLOBOCAN 2018, in Nepal, estimated new cancer were 103.7 and death rate were 77.8 per 100,000 population (Shrestha *et al*., 2020). According to GLOBOCAN, there can be estimated 4,820,000 and 2,370,000 cancer cases in China and the United States, respectively, and 3,210,000 and 640,000 cancer fatalities in 2022 (Xia *et al*., 2022).

There are many cancer treatment methods like chemotherapy, surgery radiation, immunotherapy, gene therapy and nanomedicine (Arruebo *et al*., 2011). A significant obstacle for chemotherapy is the impact of multidrug resistance as cancer progresses. MDR to biochemically unrelated medicines is caused by genetic changes in the drug-induced apoptotic mechanism, which result in resistance to chemotherapy-induced cancer cell death (Aung *et al*., 2017). Most genotoxic chemotherapy drugs have devastating side effects, as well as causing cellular senescence in healthy tissues. Senescent cells persist in the body for a long time, where they can induce or intensify various chemotherapy adverse effects by promoting systemic and local inflammation (Demaria *et al*., 2017).

Drugs used in chemotherapy destroy healthy tissues in addition to malignant cells. It also has a number of side effects, including bone marrow suppression, nausea and vomiting, neurotoxicity, and temporary baldness, due to less accurate drug carriers and less effective targeting medicines (Haiguang *et al*., 2015). Reactive oxygen species are responsible for or contribute to a number of anticancer medicine adverse effects, including gastrointestinal toxicity and mutagenesis. It has specific side effects such doxorubicin-induced cardiotoxicity, cisplatin-induced nephrotoxicity, and bleomycin-induced pulmonary fibrosis (Conklin, 2000).

1.2 General structure of thiosemicarbazones

Thiosemicarbazones are an important class of Schiff bases that synthesize by reacting thiosemicarbazides with carbonyl compounds (aldehydes or ketones). In thiosemicarbazone sulphur (S) and nitrogen (N) act as donor atoms which are the combination of hard soft donor character and having versatile co-ordination character (Harness *et al*., 2008). The nitrogen (N) and sulphur (S) act as chelating agents which cause decrease in solubility of the complexes and allow the complex to be isolated from the solution. These chelating agents give complexes with many metal ions by linking with thionate sulphur and hydrazine nitrogen atoms (Suvarapu & Baek, 2015).

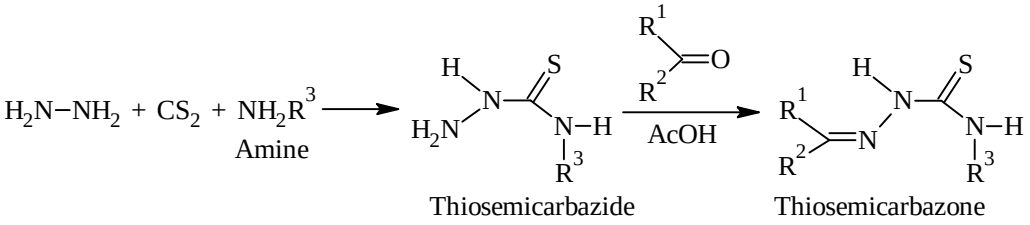

Figure 1: Systematic procedure of N-substituted thiosemicarbazones

1.2.1 Tautomerization of thiosemicarbazone

The isatin ring and the thiosemicarbazone chain combine to form isatin-3-thiosemicarbazone. The isatin moiety has planar six and five membered rings. An -NH_2 group, a keto group, an imine linkage (C=N), a hydrazine hydrogen (NH), and a thione (C=S) group are all possible hydrogen bond donors and acceptors. The presence of the -NH group next to the keto group, as well as the -NH and -NH_2 groups next to the thione group (C=S), results in a significant number of possible tautomer (Kohli *et al.*, 2014).

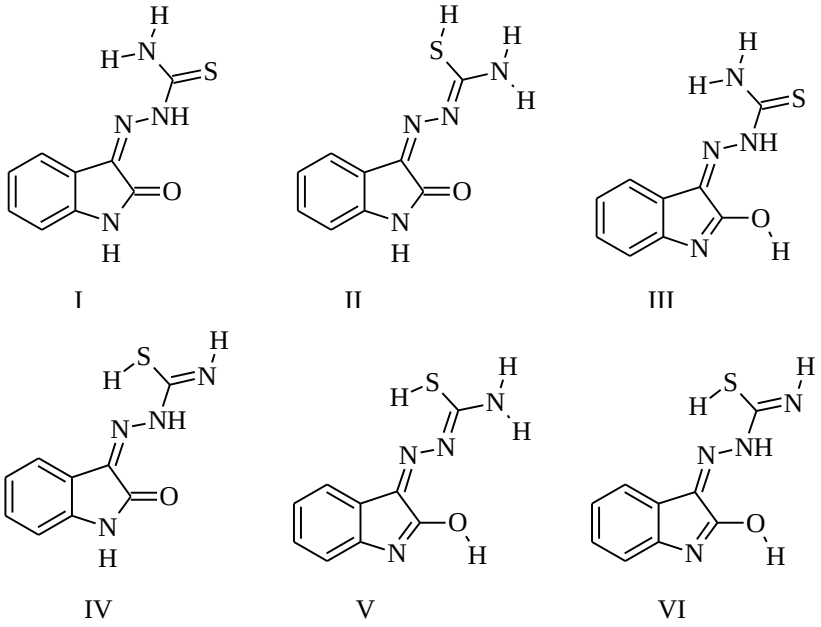

Figure 2: The possible tautomer of isatin-3-thiosemicarbazone (I-VI)

1.2.3 Synthetic procedures of N(4)-substituted thiosemicarbazides / thiosemicarbazones

Thiosemicarbazides can be synthesized by reacting hydrazine hydrate with 4-methyl-4-phenyl-3-thiosemicarbazide (4-mpt), carbon disulphide, sodium chloroacetate, and 2^{o} amine (Scovill, 1991, El-Sawaf *et al*., 2018).

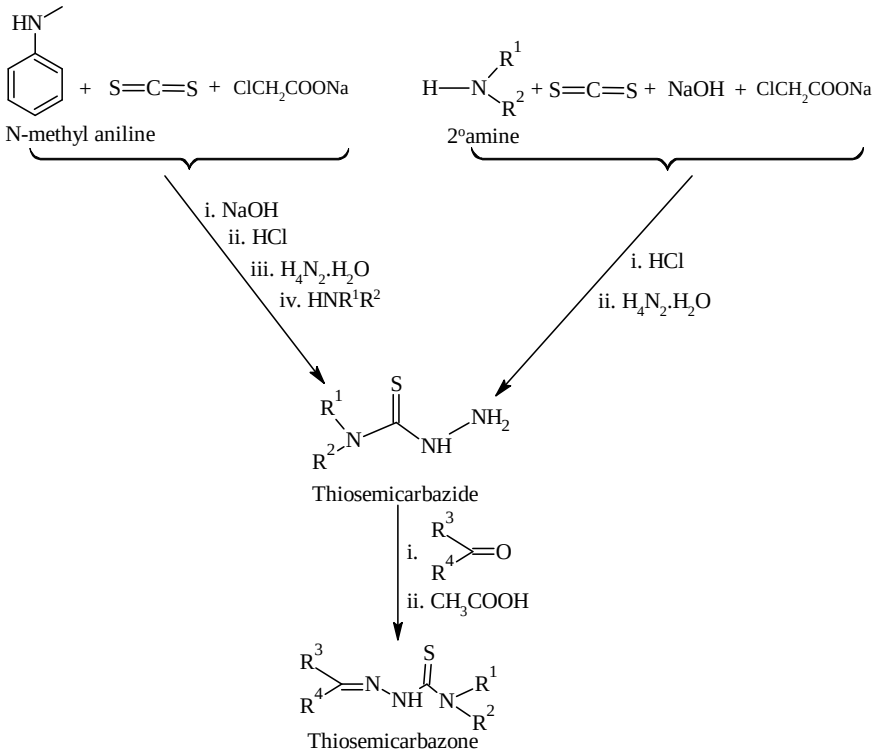

Figure 3: General procedures of N(4)-substituted thiosemicarbazones.

Thiosemicarbazones can be synthesized using a variety of methods like condensation of an equimolar amount of aldehyde or ketone with thiosemicarbazide in the presence of a catalytic amount of acetic acid (Ali *et al*., 2014, Muralisankar *et al*., 2016).

1.3 Modes of action of anticancer drug

Chemotherapy treatments are classified based on their mode of action, chemical structure, composition, and homology to other drugs. Due to its various modes of action, several drugs may fit into more than one category (Ratain, 2003).

1.3.1 Alkylating agent

Alkylating agents cause direct DNA damage to cancer cells, which stops them from dividing and is effective at all phases of the cell cycle. Alkylating drugs are used to treat a variety of malignancies, including lymphoma, leukemia, multiple myeloma, Hodgkin's disease, and sarcomas (Abbas & Rehman, 2018). Examples; ifosfamide, and melphalan, busulfan, thiotepa and altretamine (Ralhan & Kaur, 2007). Despite being categorized as an alkylating anti-neoplastic drug, it is unknown exactly how altretamine causes its cytotoxic effects. N-demethylation is the mechanism by which the drug is converted into alkylating agents. As a result, these alkylating species damage tumor cells (Keldsen *et al*., 2003).

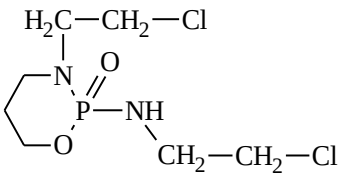

Ifosfamide

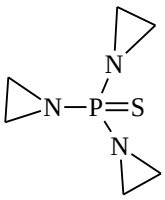

Thiotepa

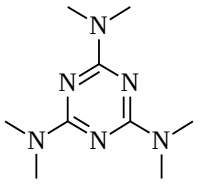

Altretamine

Figure 4: Structure of ifosfamide, thiotepa, altretamine

1.3.2 Antimetabolites

These drugs prevent DNA and RNA from growing. They have a strong influence on the S phase and have been used to treat leukemia, ovarian, breast, intestinal cancers and many others (Abbas & Rehman, 2018). Examples of antimetabolites are 5-Fluorouracil (5-FU), 6-Mercaptopurine (6-MP), Cytarabine (Damaraju *et al*., 2008). Mercaptopurine is converted to thioinosinic acid (TIMP) by the enzyme hypoxanthine-guanine phosphoribosyltransferase (HGPRTase) in competition with hypoxanthine and guanine. TIMP blocks a number of inosinic acid (IMP)-dependent processes, including the conversion of IMP to xanthylic acid (XMP) and the conversion of IMP to adenylic

acid (AMP) *via* adenylosuccinate (SAMP). TIMP is methylated to create 6-methylthioinosinate (MTIMP), which in addition to inhibiting TIMP, also inhibits glutamine-5-phosphoribosylpyrophosphate amidotransferase. The first enzyme specific to the *de novo* pathway for purine ribonucleotide synthesis is glutamine-5-phosphoribosylpyrophosphate amidotransferase (Sahasranaman *et al*., 2008).

5-FU 6-MP

Figure 5: Structure of 5-FU and 6-MP

1.3.3 Anthracyclines

These drugs are a class of antibiotics effect all phase of cell cycle by targeting DNA replication of enzymes. Excess dose can damage heart permanently (Abbas & Rehman, 2018). Examples of anthracyclines are Daunorubicin, Doxorubicin, Epirubicin, Idarubicin (Le Bot *et al*., 1988). Epirubicin exhibits cytotoxic and antimitotic effects. Through a number of proposed mechanisms of action, it prevents the synthesis of proteins and nucleic acids (DNA and RNA): Epirubicin binds to DNA to form complexes by intercalating between base pairs, and by stabilizing the DNA-topoisomerase II complex, it inhibits the activity of topoisomerase II by preventing the religation step of the ligation-religation reaction that topoisomerase II catalyzes. By preventing DNA helicase function, it also hinders DNA replication and transcription (Cersosimo & Hong, 1986).

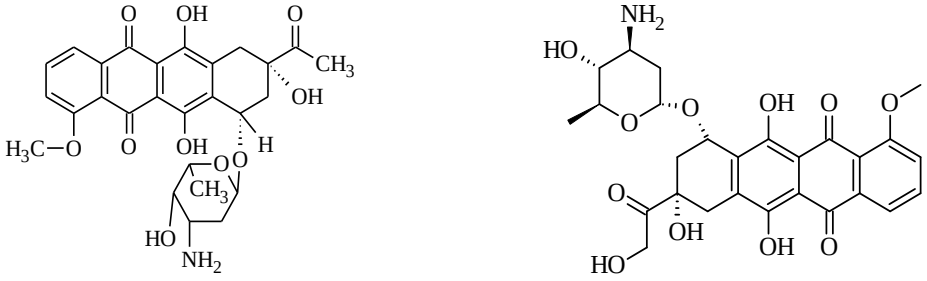

Daunorubicin Epirubicin

Figure 6: Structure of daunorubicin and epirubicin

1.3.4 Topoisomerase inhibitors

Topoisomerase inhibitors drugs stop DNA replication and are used to treated ovarian, gastrointestinal and lung cancers (Abbas & Rehman, 2018). Examples of topoisomerase

I inhibitors are topotecan and irinotecan (CPT-11), and topoisomerase II inhibitors are etoposide (VP-16) and teniposide (VM-26) (Sorensen *et al*., 1995). Teniposide does not facilitate the interaction into DNA or have a strong DNA-binding affinity, hence the mechanism of action seems to be associated to the inhibition of type II topoisomerase activity. DNA topoisomerase II interacts to and is inhibited by teniposide. Teniposide has cytotoxic effects on cells based on the proportion of double-stranded DNA breaks that are generated in cells as a result of the stabilization of a topoisomerase II-DNA intermediate (Hande, 2008).

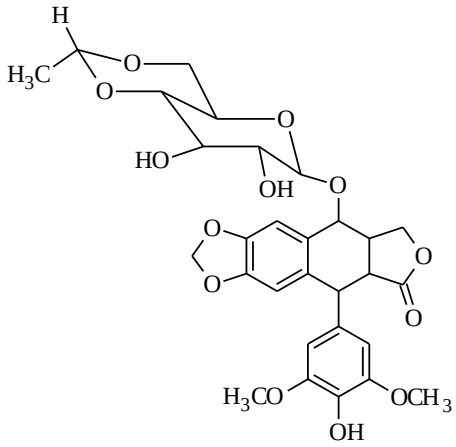

Etoposide

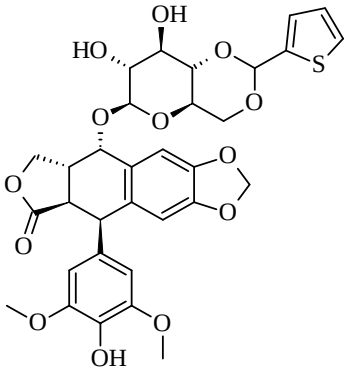

Teniposide

Figure 7: Structure of etoposide and teniposide

1.3.5 Mitotic inhibitors

These drugs are plant alkaloids and inhibit mitotic phase of the cell cycle by damaging another phase also. They are used to treat lung, breast, myelomas, leukemia and lymphoma cancer (Abbas & Rehman, 2018). Example of mitotic inhibitors are paclitaxel, docetaxel, vinblastine, vincristine and vinorelbine (Luqmani, 2005). Vincristine is believed to have an anticancer effect principally through inhibiting mitosis at metaphase through its interaction with tubulin (Graf *et al*., 1996).

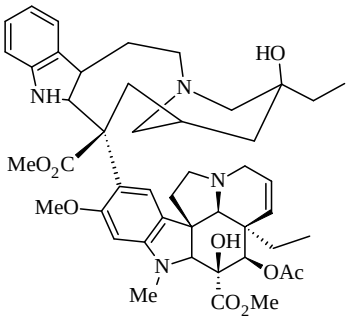

Vinblastin

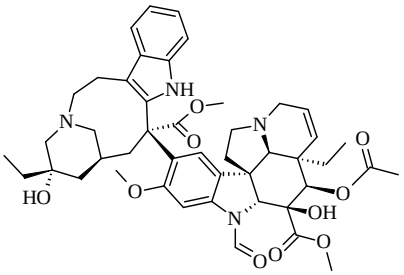

Vincristine

Figure 8: Structure of vinblastin and vincristine

1.4 Rationale

Cancer is a major global health issue that affects both developing and advanced countries. Cytotoxic activity refers to the ability of synthetic or natural chemotherapy agents to inhibit, slow, or stop the progression of cancer.

The isatin molecule is a multifunctional moiety with a wide range of biological capabilities, including cytotoxic activity. Anticancer pharmacophores were incorporated into the isatin moiety to produce isatin derivatives, which showed promise in overcoming medication resistance while reducing adverse effects (Ding *et al*., 2020). The sulphur present in the thiosemicarbazone increase the anticancer potency that can be compared with the corresponding semicarbazones (Osman *et al*., 2020). The modification of N(4) position in cyclic ring of thiosemicarbazones enhance the antitumor activities, increase solubility in organic solvent as well as inorganic solvent and decrease toxicity. The synthetic adaptability of isatin has made it possible to produce a wide range of derivatives with different structural characteristics, such as those in which the aryl ring has been substituted and/or the nitrogen of isatin and C2/C3 carbonyl moieties have been modified. The mode of action of isatin derivatives consists of the inhibition and/or modulation of proteases, translation initiation, neo-vascularisation and tubulin polymerization (Vine *et al*., 2012). With regard to cancer cell lines like breast, lung, and leukemia, a number of isatin-hydrazine hybrid structures shown effective anticancer properties (Ferraz de Paiva *et al*., 2021). Isatin-triazole hydrazones were identified as anticancer drugs but also powerful inhibitors of breast cancer cell migration and Microtubule affinity-regulating kinase 4 (MARK4) (Hou *et al*., 2020).

1.5 Objectives

The objectives of the present study are classified into two parts:

1.5.1 General objectives

i. Synthesis, characterization and exploration of anticancer activity of 5-methoxy, 5-hydroxy and 5,7-dibromoisatin thiosemicarbazones

1.5.2 Specific objectives

i. The synthesis of a series of 5-methoxy, 5-hydroxy and 5,7-dibromoisatin derived N(4)-substituted thiosemicarbazones having general structure shown in Fig. 9.

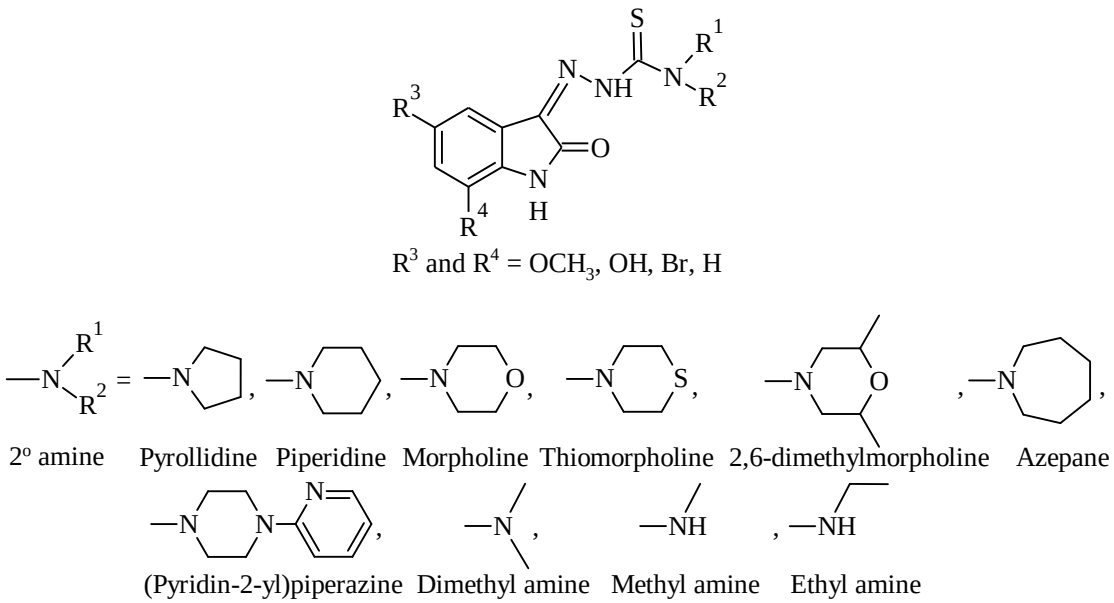

Figure 9: Synthetic scheme of 5-OMe, 5-OH and 5,7-disubstituted (-Br) isatin derived N(4)-thiosemicarbazones

ii. Characterization of thiosemicarbazones by CHN analysis and various spectroscopic techniques *viz.* IR, NMR, Mass spectrometry and UV-Visible spectroscopy.

iii. To study the structure of the thiosemicarbazones by single crystal X-ray diffraction crystallographic methods.

iv. Study the influence of different derivatives of isatin thiosemicarbazones on anticancer activity against Breast cancer cells (MCF-7, MDA-MB-231), Epidemoid carcinoma (A431), Human lung adenocarcinoma (A549) and Normal prostate epithelial cell (PNT2)

v. To predict the structure of the ligand-receptor complex using computational methods, look at the molecular docking of a molecule with a single X-ray crystal.

CHAPTER 2

2. LITERATURE REVIEW

2.1 Biological importance of thiosemicarbazones

The biological activity of thiosemicarbazones depends upon the nature of parent aldehyde or ketone (Padhye, 1985). Medicinal importance of thiosemicarbazones is well known due to a range of biological activities like antineoplastic (Yu *et al*., 2009), antimicrobial (Souza *et al*., 2013), antibacterial (Aly *et al*., 2010), antifungal (Agarwal *et al*., 2006), antiviral (Arora *et al*., 2014), and antimalarial (Khan *et al*., 2018). Triapine (3-aminopyridine-2-carboxaldehyde thiosemicarbazone, 3-AP) is the most interesting compound conducting clinical phase II research among the thiosemicarbazones (De Oliveira *et al*., 2015). The enzyme ribonucleotide reductase (RR), which facilitates the conversion of ribonucleotides to deoxyribonucleotides, is highly inhibited by 3-AP, which slows or stops DNA synthesis and cellular proliferation (Nutting *et al*., 2009). Thiacetazone, also known as p-acetamidobenzaldehyde thiosemicarbazone, is one of the most effective and affordable medications used to treat tuberculosis (Kaplancikli *et al*., 2016). Mycolic acid cyclopropanation is inhibited by thiacetazone (TAC) and its chemical equivalents. After receiving the medications, significant changes in the amount and ratio of mycolic acids were seen in both the vaccination strain *Mycobacterium bovis* BCG and the associated pathogenic species *Mycobacterium marinum* (Alahari *et al*., 2007).

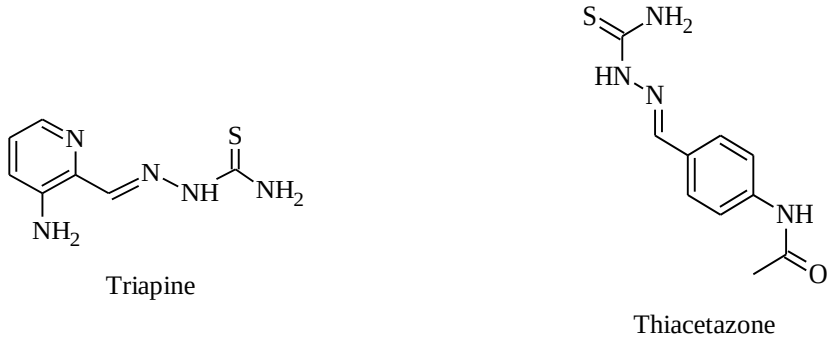

Figure 10: Structure of triapine and thiacetazone

Methisazone is an effective compound against variola and vaccinia viruses (Pandeya *et al*., 2005). In the treatment of smallpox, 1-methylisatin-3-thiosemicarbazone was discovered to be effective (Khan *et al*., 2016). Inhibitors of types 1 and 2 of the *herpes simplex* virus were tested using a variety of thiosemicarbazones synthesized from 2-

acetylpyridine, 2-acetylquinoline, and l-acetylquinoline, some of which were very active (Haribabu *et al*., 2016). Isatin-β-thiosemicarbazones selectively kill multidrug resistant P-glycoprotein over expressing tumor cells (Balachandran *et al*., 2018).

Amino substituted pyridine-2-carboxaldehyde thiosemicarbazones (5-AP) were tested for their ability to inhibit ribonucleotide reductase activity as well as growth in culture and *in vivo* in the L-1210 leukemia with IC_{50} value 3.0 ± 0.6 μM (Cory *et al*., 1995). The ability of 5-AP to obstruct the thymidine and uridine incorporations into DNA and RNA was examined.

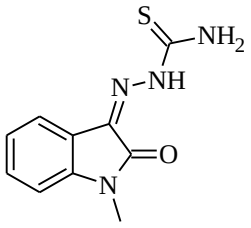

Methisazone

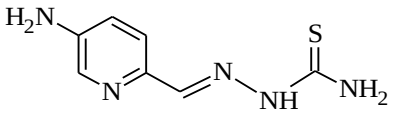

5-AP

Figure 11: Structure of methisazone, and 5-AP

Di-2-pyridylketone-4,4-dimethyl-3-thiosemicarbazone (Dp44mT) has been found to exhibit a paradoxical hypertoxicity against the P-gp-overexpressing cervix carcinoma cell line KB-V1 as compared to parental cell line KB-3-1 (Pape *et al*., 2016). Compared to non-Pgp-expressing tumors in mice, Dp44mT more effectively targeted chemotherapy-resistant human Pgp-expressing xenografted tumors *in vivo*. Additionally, human tumor in mice demonstrated that Dp44mT had substantial anti-cancer effect when applied to Pgp-expressing MDR cells as opposed to drug-sensitive cells (Jansson *et al*., 2015). 6-methoxycarbonyl-substituted indolinones were identified potent inhibitors of VEGFR-2 related endothelial cell proliferation with efficacy on pericyctes and smooth muscle cells with IC_{50} value 36 ± 36 nM (Roth *et al*., 2009).

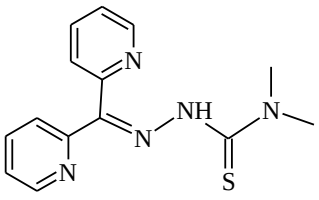

Dp44mT

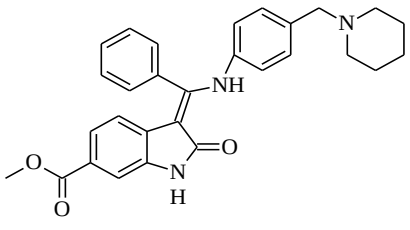

6-methoxycarbonyl substituted indolinone

Figure 12: Structure of Di-2-pyridylketone-4,4-dimethyl-3-thiosemicarbazone and 6-methoxycarbonyl substituted indolinone

At lower doses, α-heterocyclic thiosemicarbazones and copper complexes were reported to catalytically suppress topoisomerase-IIα (0.3-7.2 μM) and lowering the

proliferation of breast cancer cells expressing excessive quantities of topoisomerase-IIα (SK-BR-3). Micromolar GI_{50} was found in antiproliferation assays with the breast cancer cell lines SK-BR-3 (1.9 ± 0.3 μM) and MCF-7 (2.0 ± 0.2 μM), which express high and low levels of Topo-IIα, respectively (Zeglis *et al*., 2011). Histone deacetylase (HDAC) inhibitors and anti-proliferative efficacy against cervical carcinoma cell lines have been described for 5-chloroisatin capped hydroxamic acid, with IC_{50} = 0.97± 0.26 μM (Singh *et al*., 2017). The cytotoxicity of isatin-β-thiosemicarbazones is increased due to the presence of thiosemicarbazone part, a hydrogen bond acceptor atom and a hydrophobic/aromatic moiety on the hydrazinic part. The methoxy group or halogenic group increase the electron density of aromatic ring system which helps to enhance reactivity. As MDRI inhibitors, compounds missing any of the parts (acceptor, hydrophobic, aromatic ring, or thiosemicarbazone portion) are ineffective (Pelosi, 2010).

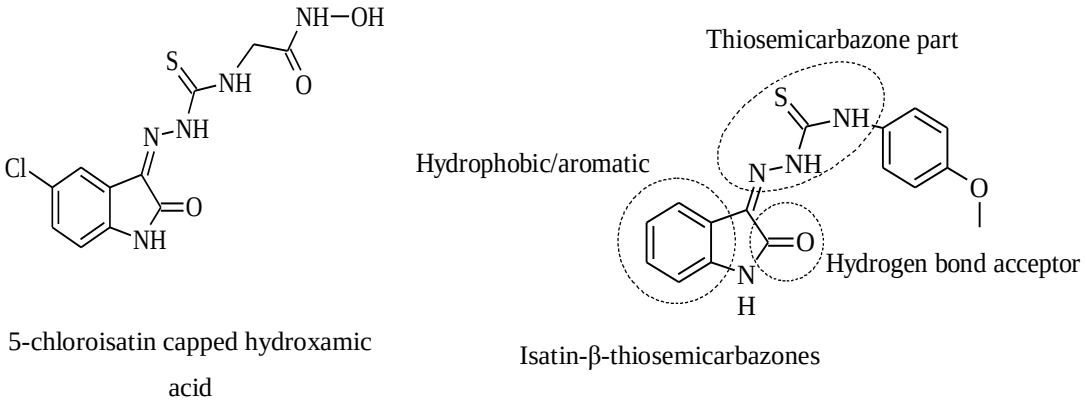

Figure 13: Structure of 5-chloroisatin capped hydroxamic acid and isatin-β-thiosemicarbazone and key part shows cytotoxicity

2.2 Isatin

Isatin (1H-indole-2,3-dione) and its derivatives have a wide range of biological activities and play an important role in medicine. Due to their biological activity, isatin derivatives are synthetic substrates employed in the synthesis of a wide range of heterocyclic compounds as well as being used as medicinal raw materials (Muğlu *et al*., 2019).

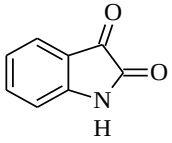

Figure 14: Structure of isatin (1H-indole-2,3-dione)

Isatin was first produced in 1841 by Erdman and Laurent from oxidizing indigo dye with nitric acid and chromic acids (Vandana *et al*., 2017). It has been identified in plants Isatis genus (*Isatis tinctoria*) (**B**), in the fruit of the cannon ball tree, *Couroupita guianensis* Aubl (**A**), and *Calanthe discolor* Lindl, but in animals, parotid gland of the Bufo frog (**D**) (Ibrahim & Elsaman, 2018). These plants can be found in northern and central China, and are used in traditional Chinese medicine (Khan & Maalik, 2015). It is also found in mammalian brain, peripheral tissues, and body fluids. The investigation of isatin levels in conventional and germ-free rats revealed a significant decrease in urine isatin, but not tissue isatin, suggesting that gut flora mainly contributes to urinary isatin (Medvedev *et al*., 2018). Its derivatives are also identified in fungi, *Dicathais orbita*, an Australian marine mollusc (**E**) (Vine *et al*., 2012). It has also been found in coal tar (Da Silva *et al*., 2001). It takes part in many synthetic reactions and play main role of starting molecules in medical application.

Figure 15: *Couroupita guianensis* Aubl (A) *Isatis tinctoria* (B) Bufo frog (D) The marine mollusc (E)

The recent approval of a number of medicines that target tyrosine kinases has rekindled interest in the development of synthetic protein kinase inhibitors as anticancer medications. The USFDA has approved isatin-based compounds, compounds undergoing various clinical trials, and several synthetic analogs substituted in their place to block a variety of RTKs (Prakash & Raja, 2012). Isatin and its derivatives have

various biological properties like antifungal, anti-inflammatory and analgesic; antimicrobial; antiviral; antiasthmatic; antioxidant; herbicide; anticancer, among others (Britto *et al*., 2020). The biological properties of isatin have increased by the modification at position N-1, C-3, C-4, C-5, and C-7 of the isatin ring. Some anticancer medicines that contain isatin, including indirubin, sunitinib, semaxanib, nintedanib, and hesperidin, have the potential to treat a variety of cancers, including tumors that are resistant to treatment (Hou *et al*., 2020).

2.3 Reactivity of isatin

Isatin showed various reaction like addition, substitution, chemoselective reductions, oxidations, ring-expansions and spiro annulations at different position. Nucleophilic addition at 3rd position, aromatic substitution at 5th and 7th position in aryl ring, nucleophilic addition and N-derivatization reaction at 2nd position (Chauhan *et al.*, 2020).

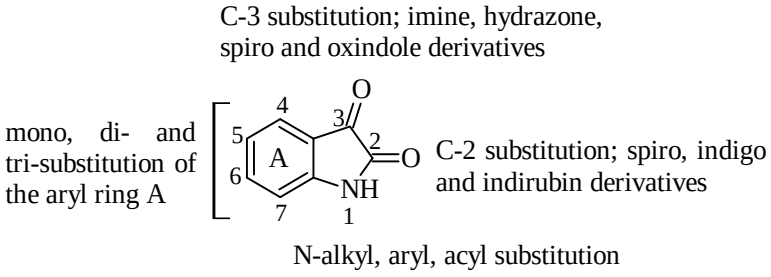

Figure 16: Various substitution patterns for the development of different isatin analogues

N-alkylated isatins are thought to react more quickly than non-N-alkylated isatins. Even though the nitro group has a meta interaction with the ketone carbonyl group, it was revealed that the existence of a nitro group resulted in shorter reaction times (Garden & Skakle, 2002). By increasing the number of electron-withdrawing groups on the ring to produce combinations of dibromo-, tribromo-, iodo-, and nitroisatin derivatives, the overall activity against a panel of human cancer cell lines was increased by up to 100-fold. In the H1299 lung cancer cell line, O-acyl oximes suppressed neuronal ubiquitin C-terminal hydrolase (UCH-L1) at sub-micromolar concentrations. After 48 hours, human colon (DLD-1) and ovarian (PA-1) cancer cell lines exposed to C3-substituted aminomethylene-lysine indolinone demonstrated cytotoxicity (IC_{50} values varied from 10-17 μM) (Vine *et al*., 2013). In U937 cells, Vine *et al*. reported that 5,6,7-tribromoisatin is anti-proliferative (and induces apoptosis) at low concentrations (4 μM), but cytotoxic (and induces necrosis) at high concentrations (130 μM) (Vine *et al.*,

2007). In DAG-1 and RT112 bladder tumor cell lines, the most active compound, azaaurone, suppressed proliferation and caused mortality via a fibroblast growth factor receptor-3 (FGFR)-dependent mechanism (Gerby *et al*., 2007).

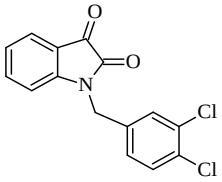

O-acyl oximes

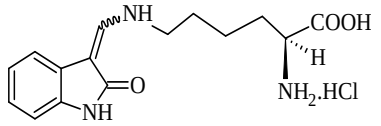

Aminomethylene-lysine indolinone

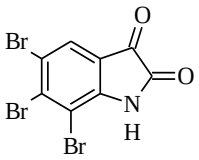

5,6,7-tribromoisatin

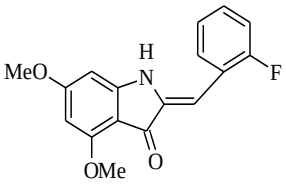

Azaaurone

Figure 17: Structure of O-acyl oximes, aminomethylene-lysine indolinone, 5, 6, 7-tribromoisatin, azaaurone

2.4 Cytotoxic effects of isatin

Isatin was revealed to be a crucial part of tribulin, an endogenous monoamine oxidase type B selective inhibitor. It causes a lowering in food consumption by boosting serotonin levels and directly altering the medial hypothalamus in the brain (Glover *et al*., 1998). Higher levels of isatin have been observed in the cerebral fluid of people suffering from bulimia nervosa (Brewerton *et al*., 1995). Isatin was evaluated against a number of human cancer cell lines, such as HL60 (promyelocytic), PC12 (pheochromocytoma), and N1E-115 (neuroblastoma), and shown to be a cell proliferation inhibitor in all of them. At a concentration of 100 μM, isatin induced DNA disintegration and chromatin condensation during apoptosis, reducing cell proliferation by 80% compared with controls. Only 20% of cells died at 10 μM, indicating that the impact was concentration dependent (Cane *et al*., 2000). The efficacy of isatin on cell growth was dose and time dependent, according to further research utilizing human neuroblastoma SH-SY5Y cells with lower concentrations of isatin commenced to apoptose after 48 h, whereas cells with higher concentrations of isatin displayed a late apoptotic/necrotic response. With an apoptotic response of 82 %, cells having 400 μM of isatin showed the most cell death (Igosheva *et al*., 2005).

2.5 Cytotoxic effect of isatin derivatives

Tyrindoleninone (6-bromo-2-methylthio-3H-indol-3-one), was evaluated towards U937 cells with IC_{50} = 4 μM by using human monocyte-like, histiocytic lymphoma cells. The 6-bromoisatin was more stable and showed minimal cytotoxic against U937 cells with IC_{50} = 74.8 μM (Vine *et al*., 2007). At an IC_{50} of 223 μM (0.05 mg/mL), 6-bromoisatin prevented HT29 cells from proliferating while also inducing apoptosis without raising caspase 3/7 activity. 6-bromoisatin was observed to substantially increase the apoptotic index ($p \leq 0.001$) and decrease cell proliferation ($p \leq 0.01$) in the distal colon when treated *in vivo* at a concentration of 0.05 mg/g. However, 6-bromoisatin led to a drop in plasma potassium levels, indicating a diuretic action. Muricidae isolates include 6-bromoisatin, a good approach for the treatment of colorectal cancer (Esmaeelian *et al*., 2014). N-phenethyl derivatives were found to have moderate to sub-micromolar cytotoxic effects towards U937 cells (IC_{50} = 0.78 μM), with the most active compounds containing a hydrophobic bromo substituent in the meta or para position.

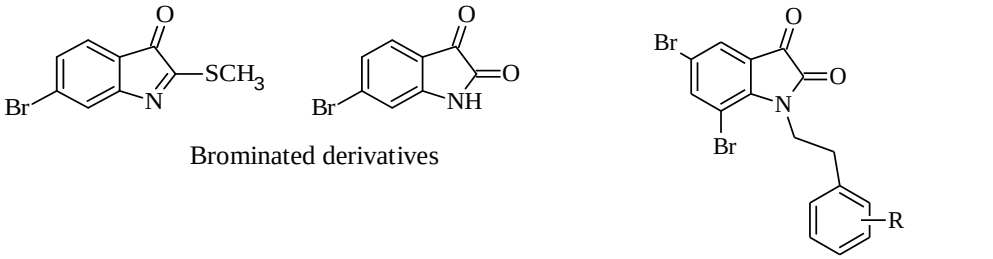

Figure 18: Highly cytotoxic brominated derivatives and structure of N-phenethyl derivative

Furthermore, the tumor cells exhibited elongated cell shape after exposure to these substances, indicating that these analogues affect microtubule dynamics (Matesic *et al*., 2008).

Isatin derivative (isatin-benzothiazole) had good action against MDA-MB-231, MDA-MB-468 and MCF-7 cancer cells, with IC_{50} values of 14.99, 5.26, and 4.23 mM, respectively (Eldehna *et al*., 2015). Isatin-benzothiazole may allow us to efficiently control tumors with few adverse effects and could destroy cancer cells 10-15 times more effectively than non-cancer cells (Solomon *et al*., 2009). The non-small cell lung cancer cell line HOP-92, the colon cancer cell line HCT-116, the CNS cancer cell line SNB-75, the ovarian cancer cell line OVCAR-3, and the renal cancer cell line RXF 393 were all discovered to be highly active growth inhibitors of the 5-bromoisatin derivative

with GI_{50}; 0.01 µM, 0.018 µM, 0.0159 µM, and 0.0197 µM, respectively. The SAR investigation showed that, in compared to 5-unsubstituted isatin analogs, attaching a halogen (Br or Cl) to the 5-position of the isatin scaffold allowed for a gain of one log unit of activity (GI_{50} level) (Havrylyuk *et al*., 2012). Significant activity was demonstrated by 5-chloroisatin with a 3,4-dimethoxy substitution in the aryl ring, with GI_{50} values of 8.54, 4.16, and 3.59 µM against MDA-MB-231, MDA-MB-4468, and MCF-7, respectively. Due to their excellent electron-donating properties, the ketonic groups of isatin is crucial. Potent activity was seen in the 3,4-disubstituted-isatin ring, but not for bulky groups. A slight increase in potency against the cancer cell line MDA-MB-231 was seen when chlorine was substituted at the 5th position of the isatin ring (Nath *et al*., 2020).

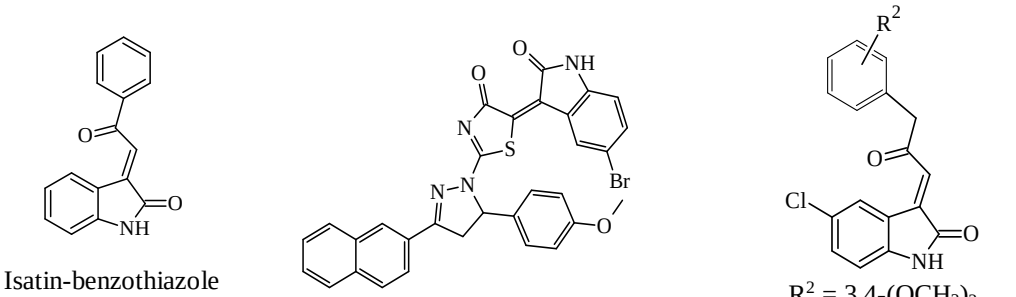

Figure 19: Structure of isatin-benzothiazole, 5-bromoisatin derivative and 5-chloroisatin derivative

2.6 Biological activities of isatin thiosemicarbazones derivatives

The antituberculosis activities of 5-fluoro-isatin-3-thiosemicarbazones and 5-fluoro-1-morpholino/piperidinomethyl-isatin-3-thiosemicarbazones were screened against *Mycobacteriumtuberculosis* H37Rv using the microplate alamar blue assay (MABA) or the BACTEC 460 radiometric system in BACTEC 12B (Özkütük *et al*., 2010). *In vitro* antiproliferative activity of (*Z*)-2-(5-fluoro-2-oxoindolin-3-ylidene)-N-phenylhydrazinecarbothioamide against human colon cancer cell line (HCT 116) with IC_{50} = 31.4 µM was observed.

Figure 20: Structure of 5-fluoro-isatin-3-thiosemicarbazone and (Z)-2-(5-fluoro-2-oxoindolin-3-ylidene)-N-phenylhydrazinecarbothioamide

It is evident that the compound interfered with the cells of the group of ability to divide, causing the majority of the cells to lose their pseudopodial extensions and viability while only cellular debris remained in the growing media (Qasem *et al*., 2014).

With an *in vitro* PLA2 (~50% inhibition at ~200 mg/mL concentration) inhibition assay and an *in silico* molecular docking analysis, 5-methoxyisatin-3-thiosemicarbazone was explored *in vitro* antioxidant behavior and cytotoxicity against MCF-7 (50% inhibition at 100 mg/mL). As evidenced by multiple hydrogen bonding and hydrophobic interactions, *in silico* molecular docking investigations of the compounds at the active region of PLA2 demonstrated the binding potential of the compounds (Saranya *et al*., 2019).

N(4)-substituted 5-nitroisatin-3-thiosemicarbazones (**a**-**c**) have been found to be effective antileishmanial agents with IC_{50} values 1.78 ± 0.35, 0.44 ± 0.02, 1.91 ± 0.04 μg/mL respectively, outperforming the conventional medication pentamidine in terms of leishmanicidal effectiveness. While the para-substituted drug (**b**) demonstrated outstanding leishmanicidal action (IC_{50} = 0.44 ± 0.02 mg/mL), the ortho-substituted molecule (**a**) indicated substantial activity with an IC_{50} value of 1.78 ± 0.35 mg/mL. With IC_{50} values of 1.91 ± 0.04 mg/mL, the monofluoro-substituted compounds (**c**), on the other hand, exhibited significant activity (Pervez *et al*., 2014).

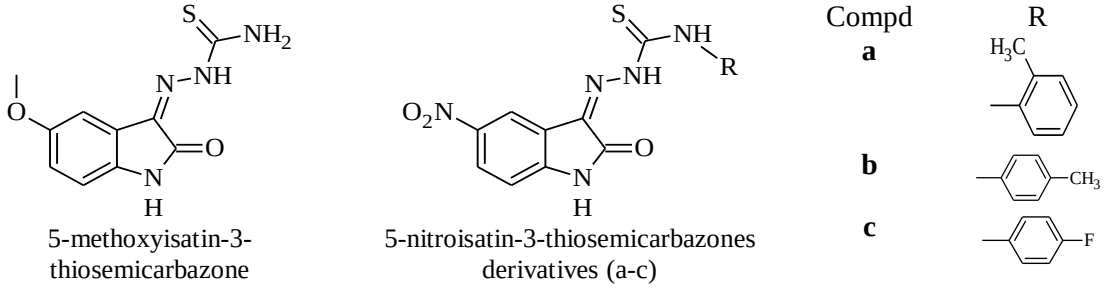

Figure 21: Structure of 5-methoxyisatin-3-thiosemicarbazone and 5-nitroisatin-3-thiosemicarbazones derivatives (a-c)

5-chloro-1*H*-indole-2,3-dione 3-thiosemicarbazones were investigated against several DNA and RNA viruses in CRFK, HeLa, HEL, MDCK and Vero cells. An inhibition percentage of 50.41% was found for ethyl substituted. Methyl and n-butyl substitutes had inhibitory rates of 38.19% and 40.55%, respectively. When compared to the alkyl substituted compounds, the activity was much lower in the benzyl and 4-nitro-phenyl substituted derivatives (Ermut *et al*., 2013).

Using the MTT assay, Juranic *et al*., found that isatin-β-thiocarbohydrazone and N-ethylisatin-β-thiocarbohydrazone exhibit cytotoxic effects on B16 (murine melanoma), HeLa (human cervical cancer), and human peripheral blood mononuclear cell (PBMC) lines. N-ethylisatin-β-thiocarbohydrazone was three times more effective than isatin-β-thiocarbohydrazone against both neoplastic cell lines (IC_{50} = 10.4 μM *vs.* 34.2 μM for B16 and IC_{50} = 21.9 μM *vs*. 61.7 μM for HeLa). The isatin-β-thiocarbohydrazone has a higher cytotoxicity against non-stimulated human blood mononuclear cells (IC_{50} = 17.6 μM *vs.*> 47.0 μM, respectively) than N-ethylisatin-β-thiocarbohydrazone (Vine *et al*., 2012). HeLa cells were the most resistant to the cytostatic isatin-β-thiocarbohydrazone activity, whereas non-stimulated human PBMC appeared to be the most sensitive. When compared to HeLa or PBMC cells, N-ethylisatin-β-thiocarbohydrazone had an antiproliferative effect that was more than 2 to 5 times stronger for B16 cells, and it was more than three times as intense as isatin-β-thiocarbohydrazone for melanoma cell growth suppression (Juranic *et al*., 1999).

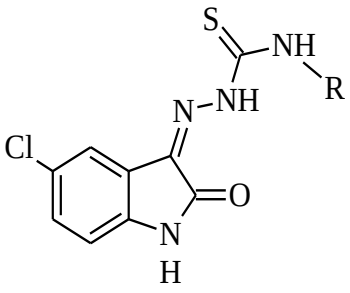

(R = CH_3, C_2H_5, CH_2-CH=CH_2, n-C_4H_9, $CH_2C_6H_5$, 4-FC_6H_4, 4-$NO_2C_6H_4$)
5-chloro-1*H*-indole-2,3-dione 3-thiosemicarbazones

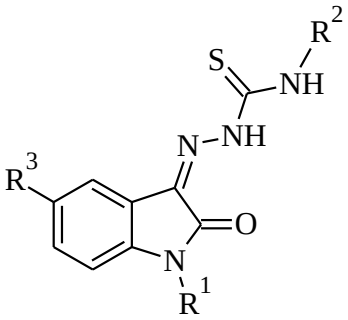

Isatin-β-thiocarbohydrazone**:**
R^1 = H, R^2 = NH_2, R^3 = H and
N-ethylisatin-β-thiocarbohydrazone**:**
R^1 = Et, R^2 = NH_2, R^3 = H)

Figure 22: Structure of 5-chloro-1H-indole-2,3-dione 3-thiosemicarbazones derivatives and isatin-β-thiosemicarbazones

It has been reported using a single dosage of 1-(4-dimethylamino) benzylidene)-5-(2-oxoindolin-3-ylidene)thiocarbohydrazone with IC_{50} value 1500 mg/kg, and test doses of 50 and 100 mg/kg were used to assess hepatotoxicity in rats. As evidenced by the existence of mild to moderate hepatic cords, lack of necrosis, and decreased fatty infiltration, it demonstrated considerable dose dependent liver protection against the toxicant (Tejasree *et al*., 2013).

Anticancer activity of 5-nitroisatin-4-thiomorpholinyl-3-thiosemicarbazone against MCF-7, MDA-MB-231, A431 and PNT2 was investigated *in vitro* with IC_{50} value 1.53

μM, 0.71 μM, 1.34 μM and 0.38 μM respectively. When compared to alkyl groups, the substitution of the N(4) position by a heterocyclic group, thiomorpholinyl group, had more anticancer activity (Singh *et al*., 2021).

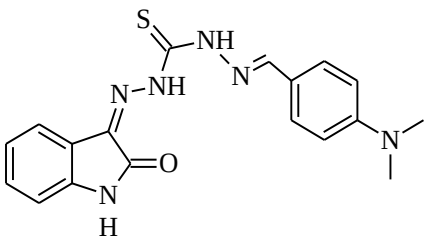

1-(4-dimethylamino) benzylidene)-5-(2-oxoindolin-3-ylidene) thiocarbohydrazone

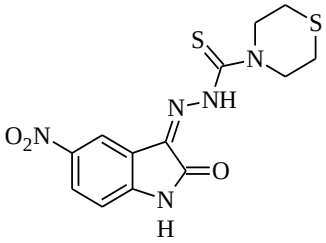

5-nitroisatin-4-thiomorpholinyl-3-thiosemicarbazone

Figure 23: Structure of 1-(4-dimethylamino) benzylidene)-5-(2-oxoindolin-3-ylidene) thiocarbohydrazone and 5-nitroisatin-4-thiomorpholinyl-3-thiosemicarbazone

A series of 5-chloroisatin derivatives with piperazine moiety have been shown to have anti-proliferative effects against two human cancer cell lines. Those compounds were particularly effective against A549 lung cancer cells, with IC_{50} values of 3.59 and 5.58 μM, respectively, and shown high activity against HCT-116 colon cancer cells with IC_{50} values of 4.57 and 3.49 μM. The antiproliferative activity was influenced by the presence of a substituent at the 5-position, with 5-chloro substituted compounds being the most effective with IC_{50} values of 3.49 μM against HCT-116 cells. The insertion of a phenyl group attached to the piperazine ring as a substituent at position 2 was helpful in maintaining the activity, and the steric effect of substituents was more significant for potency than the electronic effect (Lin *et al*., 2013).

Solomon *et al*. examined a variety of 4-piperazinylquinoline-isatin-thiosemicarbazone derivatives for their cytotoxic effects on the MDA-MB-468 (GI_{50}; 15.88 ± 0.15 – 28.41 ± 1.21μM) and MCF-7 (GI_{50}; 15.12 ± 0.34 – 16.93 ± 0.68 μM) human breast cancer cell lines, as well as the 184B5 (GI_{50}; 49.02 ± 1.68 – 47.43 ± 1.23 μM) and MCF10A (GI_{50}; 65.62 ± 1.68 – 24.03 ± 1.02 μM) non-cancer breast epithelial cell lines. In comparison to isatin ring systems with 4-chloro or 6-chloro substitution, 7-chloro substitution on 4-piperazinylquinoline ring systems hybridized with 4-bromo substituted isatin ring systems showed an increased cytotoxic effect on MDA-MB-468 and MCF-7 cells. In comparison to isatin ring systems with 4-chloro or 6-chloro substitution, 7-trifluoromethyl substitution on 4-piperazinylquinoline ring systems hybridized with 4-bromo or 6-bromo substituted isatin ring systems showed less cytotoxicity on two breast cancer cell lines studied. This finding makes it abundantly

evident that a substantial steric bulk (CF_3) substitution on the 4-piperazinylquinoline ring system's 7th position is not advantageous for increasing cytotoxicity on breast cancer cells (Solomon *et al*., 2010).

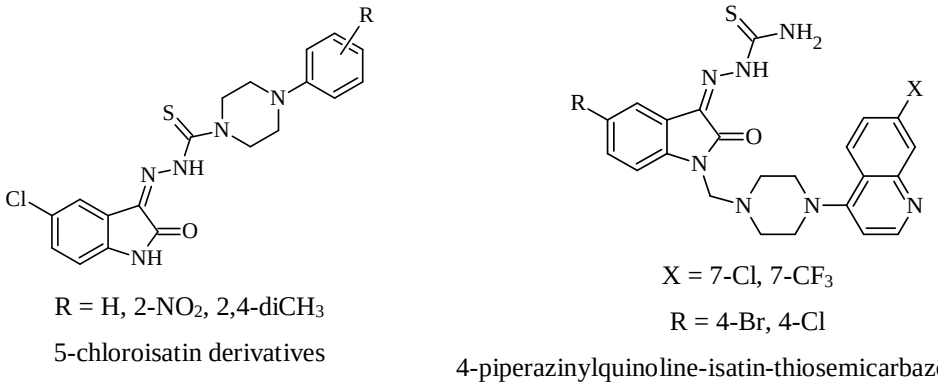

Figure 24: Structure of 5-chloroisatin derivatives and 4-piperazinylquinoline-isatin-thiosemicarbazone

The antiproliferative effects against cervical cancer (HeLa) and kidney fibroblast carcinoma (COS-7) cell lines were assessed by Gabr *et al*., using synthetic isatin-β-thiocarbohydrazone derivatives with IC_{50} values of 1.51 and 2.19 μM. The anticancer activity against Hela and COS-7 cell lines was significantly increased by adding a 2,6-dihalogen substituted phenyl ring to isatin-β-thiocarbohydrazones. Additionally, compared to its 2,6-dichlorophenyl analog, the inclusion of a 2-chloro-6-fluorophenyl moiety showed increased activity (Gabr *et al*., 2017).

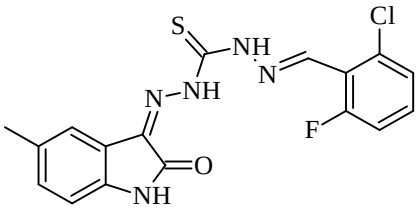

Figure 25: Structure of isatin-β-thiocarbohydrazone

2.7 Biological importance of 5-methoxyisatin

In addition to its anticancer properties, carboxyethenyl isatin derivatives are made using 5-methoxyisatin. 5-Methoxyisatin is also exploited in the CoMFA and CoMSIA procedures for 3D-QSAR study of anti-cancer drugs with IC_{50} value 3.74 and 3.45 μM (Pourbasheer & Amanlou, 2014). SU9516 (5-methoxyisatin derivative) is a possible CDK inhibitor that has the ability to cause apoptosis in colon cancer cells (Pakravan *et al*., 2013). Cyclin-dependent kinase (cdk) inhibitor SU9516 had reported IC_{50} values for cdk2, cdk1, cdk4, and cdk9 of 0.02, 0.04, 0.2, and 0.9 μM, respectively. It promoted G1 and G2-M cell cycle arrest and inhibited pRb phosphorylation, which increased the

development of the pRB/E2F complex. It was a strong cdk2 inhibitor, and compared to cdk4 and cdk1, it was 1.8 and 9 times more selective for cdk2 (Lane *et al*., 2001).

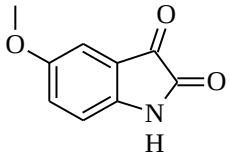

5-methoxyisatin

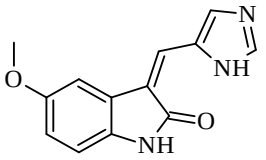

SU9516

Figure 26: Structure of 5-methoxyisatin and its derivative (SU9516)

2.8 Biological importance of 5-hydroxyisatin

Medvedev *et al*., investigated a number of isatin derivatives for their ability to inhibit human MAO A (IC_{50}; 8.4 ± 1.4 μM) and B (IC_{50}; >100 μM) *in vitro*. 5-Hydroxyisatin inhibits MAO A more effectively and selectively than isatinic acid , with an IC_{50} of 8.4 μM (Medvedev *et al*., 1992). Treatment with 5-hydroxyisatin dramatically reduced the endogenous activity of ERK. It was more effective than isatin at preventing the phosphorylation of ERK2. Due to the fact that neither substance affected the phosphorylation of ERK1, these effects seem to be very selective (Medvedev *et al*., 2007). With regard to the proliferation of the BALB/c3T3, BBC, and N1E-115 cell lines, the EC_{50} of 5-hydroxyisatin was 15–25 μM; comparable efficacy was also attained with the PC12, HL60, and NIH 3T3 cells (EC_{50} values of 54.7 ± 6.3.6, 58.2 ± 11.7, and 34.8 ± 6.3.2 μM, respectively). In comparison to the C-3 ketone function (isatin), the presence of a hydroxyl radical at the C-5 position (5-hydroxyisatin) appeared to confer increased potency (Cane *et al*., 2000).

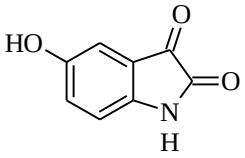

5-hydroxyisatin

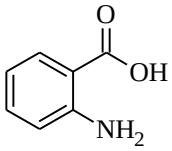

Isatinic acid

Figure 27: Structure of 5-hydroxyisatin and isatinic acid

The cytotoxic activities of 5-hydoxyisatin were evaluated on human promyelocytic leukemia HL60 cell which were lower than 2,6-di(tert-butyl)-4-hydroxytoluene (BHT) as well as screened towards rat liver microsome/tert-butylhydroperoxide system-induced lipid peroxidation and hydrogen peroxide-induced intracellular oxidative stress. It was evaluated 15.7-times stronger DPPH radical scavenging activity than uric acid, and having lower cytotoxicity in HL60 cells (Yasuda *et al*., 2013).

2.9 Biological importance of 5, 7-dibromoisatin analogue

The cytotoxicity of 5,7-dibromoisatin analogue was investigated towards four human cancer cell lines: colon HT29 (IC_{50}; >50 μM), breast MCF-7 (IC_{50}; 22.45 ± 1.12 μM), lung A549 (IC_{50}; >50 μM), and melanoma UACC903 (IC_{50}; 26.5 ± 1.8 μM) (Bheemappa, 2021). The N-benzylation analogue of 5,7-dibromoisatin enhanced apoptosis in lymphoma cells by inducing microtubules and was effective against a variety of human cancer cell lines, as well as a metastatic breast adenocarcinoma cell line (MDA-MB-231 with IC_{50}; 1.91 μM) (Krishnegowda *et al*., 2011). The cytotoxic effect of 5,7-dibromoisatin was tested against U937 cells (IC_{50} = 10.5 μM), whereas the nitro (5-nitroisatin with IC_{50}; 132 μM) and methoxy (5-methoxyisatin with IC_{50}; 420 μM) substituents at position 5 of isatin reduced cytotoxic activity against U937 cells. The activity of isatin was significantly boosted by the addition of electron-withdrawing groups at positions 5, 6, and 7, with substitution at position 5 being the most advantageous (Vine *et al*., 2007).

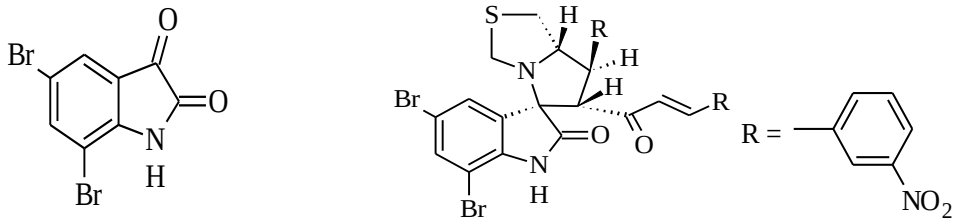

Figure 28: Structure of 5,7-dibromoisatin and its hybrid

CHAPTER 3

3. MATERIALS AND METHODS

3.1 Materials

5-methoxyisatin (98%), 5,7-dibromoisatin (98%), thiomorpholine (98%), morpholine (98%), 2,6-dimethylmorpholine (98%), 1-(2-pyridyl)piperazine (98%), hexamethyleneimine (98%), hydro bromic acid (HBr) (48%), and N-methyl aniline (98%) were purchased from Alfa Aesar. Piperidine, pyrrolidine, 4-methyl-3-thiosemicarbazide (98%) and 4-ethyl-3-thiosemicarbazide (98%) were purchased from Sigma-Aldrich. Carbon disulphide (99%) (Qualigens fine chemicals), sodium chloroacetate (98%) (Chemical center, India), hydrazine hydrate (98%) (Fisher scientific), dimethylamine (Sod Fine Chemical Limited, SDFL), acetonitrile (99%) (Merck), methyl alcohol (99%) (Merck), ethyl alcohol (99.9%) (Analytical CS reagent), diethyl ether (99%) (Merck), glacial acetic acid (99%) (Fisher scientific), concentrated hydrochloric acid (Merck), sodium hydroxide (98%) (Fisher Scientific), Ethyl acetate (98%) (Qualigens Fine Chemicals), Sodium sulphate (98%) (Fisher Scientific) and used as received. Solvents were purified according to the standard procedures.

3.1.1 Cell lines of compounds (1 – 6)

A549, MCF-7 and A431 cell lines were cultured in complete DMEM media.

3.1.2 Cell viability assay

Cell viability of A431, MCF-7, and A549 cells were assessed by crystal violet assay. Approximately 5×10^3 cells were seeded in each well of 96 wells plate. Cells were treated with different concentration of compounds and incubated for 48 h. After 48 h, the media was discarded. Cells were stained with 80 mL (0.4%) crystal violet that is prepared in 50% methanol and incubated for 30 minutes on a bench rocker with 20 oscillations per minute. After that, cells were washed by dipping in a beaker filled with tap water; this prevents the washout of cells. Culture plates were kept overnight for air dry at room temperature. Next day, 150 µL of methanol was added in each well and kept on a rocker for 30 minutes. Finally, optical density was measured in micro-plate reader at 570 nm.

3.1.3 Colony formation assay

A431 cells were analyzed to form colonies. 1000 cells were seeded in each well of six-well plates and incubated for 24 hrs. The cells were treated with the respective compounds in different concentration (0.1 % DMSO as a control, 0.3 µM, 1 µM, 3 µM, and 10 µM). Fresh media was added by replacing the used one in every 72 h, followed by the treatment with respective concentration of compounds. The cell culture was maintained for 10 days with change of media after every two days. After 10 days colonies were washed with DPBS, fixed with methanol and stained with 0.4% crystal violet which was prepared in 50% methanol. The culture plate was air dried and colonies were counted using Image J software.

3.1.4 Propidium iodide staining

Around 1.5×10^5 cells/well were seeded in a six-well plate and after 24 h, treated with different concentration of compound (0.1 % DMSO as a control, 0.3 µM, 1µM, 3 µM, 10 µM). Cells were incubated for 48 h. The cell along with media from the same tube was harvested after 48 hours in 1.5 mL micro-centrifuge tubes. Micro-centrifuge tubes were centrifuged at 3000 rpm for 5 minutes and washed with DPBS twice. Immediately after that, 80% ice-cold ethanol was added while vertexing the tube to minimize the clumping of cells. After that samples were centrifuged and given a DPBS wash twice. After adding PI, cells were incubated at 40º C for 30 minutes. The cells were then analyzed with Flow Cytometry.

3.1.5 Cell cycle analysis

For cell cycle analysis, around 1.5×10^5 cells/well were seeded in a six-well plate and were harvested after 48 hours of treatment. After three PBS washes, cells were fixed with 80% ice-cold ethanol. After incubation with RNase and PI stain for 30 minutes, cells were analyzed by FACS machine and cells in different phase were quantified. The percentage of cell with G0/G1 DNA content was used as a measure of apoptosis.

3.1.6 Cell lysate preparation

After 48 hours incubation, cells were washed with DPBS and 50-80 µL of 2X SDS lysis buffer was added (depends upon confluence of cells). The cells were collected with the help of cell scrapper and collected into the MCT. After that cell were sonicated at 30% of amplification for 10 seconds with 10 seconds interval for three cycles. Sonication

was done by keeping MCT in a 50 mL beaker filled with ice to avoid protein degradation. Samples were centrifuged at 16000 g for 20 minutes at 40º C. Supernatant was collected in fresh MCT and kept at -80º C.

3.1.7 Protein estimation by BCA kit

Pierce ™ BCA protein assay kit was used to know the total protein concentration in the samples. BCA reagent A and reagent B were mixed in 50:1 ratio respectively. Then, 200 µL mixtures were added in each well containing 25 µL of protein samples (Protein samples can be diluted by adding PBS). After that, plate was incubated for 30 minutes at 37º C. The absorbance was taken at 562 nm. After plotting the absorbance (Y-axis) *vs* concentration graph (X-axis), an equation was obtained. From that equation the concentration of protein samples was calculated. To see the expression of particular protein, in each well of SDS gel, add equal amount (25 µg) of total protein. Thus, while dividing 25µg with concentration of protein each MCT gives the volume of protein should be withdrawn for one well. Protein concentration and loading dye should be in 1:0.25.

3.1.8 SDS gel running

According to the molecular weight of protein that is of interest, the percentage of gel is determined. For higher molecular weight protein gel with lower percentage of gel is prepared and vice-versa. After transferring the gel into running buffer and then samples were loaded into the separate well.

3.1.9 Transferring proteins from gel to PVDF membrane

1X transfer buffer was prepared and kept in ice to chill down. Foam pads and filter paper was soaked in 1X transfer buffer. Polyvinylidene difluoride (PVDF) membrane was taken the same size of the gel and activated by dipping it in Methanol for 2 minutes. On a transfer cassette, the gel sandwich was prepared in the order: Sponge, filter paper, gel, PVDF membrane, filter paper, and sponge. While putting PVDF membrane above gel, 1X transfer buffer was flooded to avoid the bubbles in between. The transfer cassette was then arranged in a transfer apparatus, which was kept on the gel tank filled with 1X transfer buffer. Ice-pack is kept inside the tank and tank is kept on the ice box. Transfer was done at 90 volt for 2 hours.

3.1.10 Blocking the membrane

After the transfer is over, the PVDF membrane is kept in 5% skimmed milk for one hour for the blocking of unspecific proteins. 5% skimmed milk was prepared in TBST. 3% BSA is also used as a blocking agent.

3.2 Biological screening of compounds (7-26)

3.2.1 Materials

Human cancer cell line MCF-7, and MDA-MB-231 (breast cancer), A431 (epidermoid carcinoma), A549 and, NCIH-460 (Lung Cancer), PC-3 prostate cancer cell lines were purchased from National Center for Cell Science, Pune, India and PNT-2 prostate normal epithelial cell lines were received from Seoul National University, South Korea. Cells were cultured in DMEM media, purchased from Invitrogen (California, USA) supplemented with 10,000 units/mL, penicillin and 10 mg/mL streptomycin in 0.9% normal saline, purchased from HIMEDIA and 10% heat-inactivated fetal calf serum purchased from Invitrogen (California, USA). Cell culture grade DMSO and Crystal Violet reagents were purchased from Sigma Aldrich (USA).

3.2.2 Cell culture and treatment

MCF-7, MDA-MB-231, A431, A549, NCIH-460, PC-3 and PNT-2 cells were cultured in DMEM medium supplemented with 10% fetal bovine serum and penicillin-streptomycin at 37° C in 5% CO_2 incubator. Cells were treated with 10 µM synthetic thiosemicarbazones for 72 h for screening and compared cell viability with PNT-2 cells.

3.2.3 Cell viability assay

Preparation of 0.5% Crystal violet: For 100 mL CV solution – 0.5 g of methyl violet added in100 mL Milli-Q water.

Cell viability was assessed with Crystal Violet Assay; 3000 of each MCF-7, MDA-MB-231, A431, A549, NCIH-460, PC-3 and PNT-2 2500 cells per 100 µL of medium per well in 96-well plate. After attachment of cells to the surface treatment with different concentration of NP-4301 was done including control (DMSO), further incubated for next 72h. Then removed the medium and added 50 µL of 0.5% Crystal Violet solution to each well, incubated at room temperature on a bench rocker with a frequency of 20 oscillations per minute for 20 minutes. Appropriately washed and kept for drying, then added 200 µL of methanol to each dried well and again kept on bench rocker at room

temperature for 20 minutes. Utilize a microplate reader to determine the optical density (OD570) of each well at 570 nm.

3.3 Instrumentation

The synthesized compounds were characterized by Elemental analysis, FT-IR, NMR, HR-MS, UV-Vis and single crystal X-ray analysis.

3.3.1 Melting point determination

Melting point of synthesized compound were determined by using Philip Haris Melting apparatus at Central Department of Chemistry (CDC), Nepal.

3.3.2 Elemental analysis

Elemental analysis was performed by using a LECO Truspec Micro analyzer at IIT Madras, India.

3.3.3 Infrared Spectroscopy

IR spectra were measured in the range of 4000-400 cm^{-1} by using a SHIMADZU, Tracer 100 FTIR spectrometer at Central Department of Chemistry (CDC), Nepal. The neat samples were used and the data collection was made by using Origin software version 9.0.

3.3.4 Nuclear Magnetic Resonance Spectroscopy (NMR)

NMR spectra were collected in DMSO-d_6 at room temperature on 400 MHz by using TMS as an internal standard on a Bruker advance III HD NMR spectrometer at IISc, Bangalore, India. The magnetic properties of deuterium atoms are sufficiently different from those of ordinary hydrogen that they do not exhibit peaks in the region of the spectrum.

3.3.5 High Resolution Mass Spectroscopy (HRMS)

Mass spectra were recorded in the range 600-200 *m/z* using a LC-QTOF-HRMS Mass Spectrometer at IIT, Madras, India.

3.3.6 UV-Visible Spectroscopy

UV-Visible spectra were recorded in the range of 600-200 nm using a SPECORD®200 PLUS UV-visible spectrophotometer in the solvent EtOH, MeOH and $CHCl_3$ solution at Tribhuvan University, Central Department of Chemistry (CDC), Nepal.

3.3.7 Single Crystal X-ray Crystallography Study

The single crystal of some synthesized thiosemicarbazones were recorded by using Bruker D8 VENTURE diffractometer with PHOTON II detector diffractometer at IIT Madras, India. The single crystal diffraction data were collected at 298 K on Bruker D8 VENTURE diffractometer with PHOTON II detector with Mo/K_α radiation (λ = 0.71073 Å). The data were corrected for Lorentz and polarization effects. Multi-scan absorption correction was applied. The structure was solved by direct methods using ShelXT (Sheldrick, 2015) and refined by full-matrix least-squares refinement techniques on F^2, using ShelXL-2018/3 (Sheldrick, 2015). All calculations were done with the help of OLEX^2 version 1.5 crystallographic software (Dolomanov *et al*., 2009). For the molecular graphics, the programme OLEX^2 (Dolomanov *et al*., 2009) and Mercury (Macrae *et al*., 2020) were used. All non-hydrogen atoms were refined anisotropically. All hydrogen atoms were fixed geometrically with U_{iso} values of 1.2 times the U_{iso} values of their respective carrier atoms. The hydrogen on lattice water were located from difference fourier map and refined using the riding model.

3.4 Synthesis of thiosemicarbazones precursors

3.4.1 Synthesis of N-substituted carbothiohydrazide

The required N-substituted carbothiohydrazide were synthesized by the method described by El-Sawaf (El-Sawaf *et al*., 2018). The synthesis of N-substituted carbothiohydrazide may be depicted as follows:

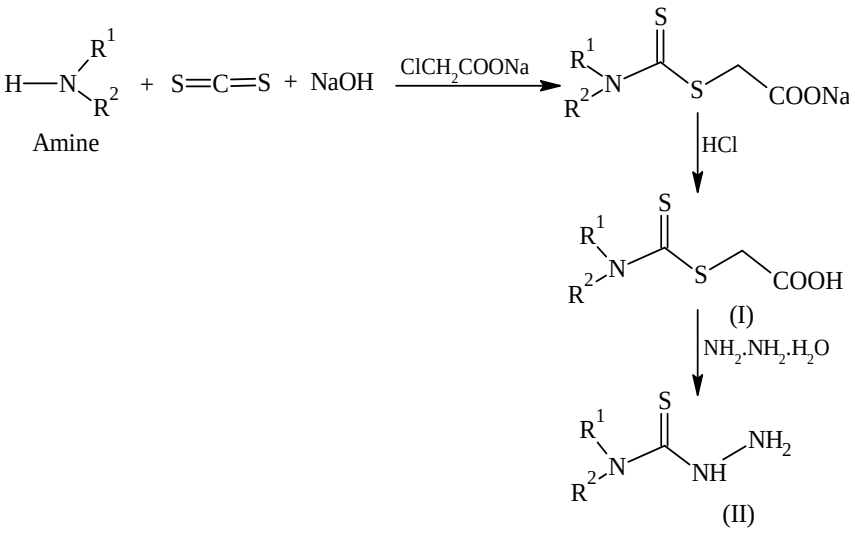

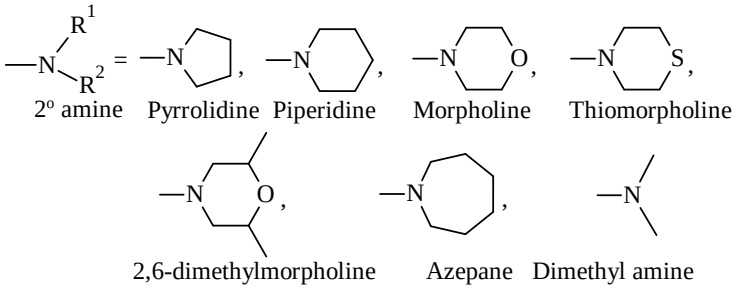

Figure 29: Systematic scheme for N-substituted carbothiohydrazide

To a solution of N-substituted amine (100 mmol) was added sodium hydroxide (100 mmol) and carbon disulphide (100 mmol). The reaction mixture was stirred overnight (17 h) allowing to disappear organic layer. Freshly prepared sodium chloroacetate (100 mmol) was added and the solution was stirred at room temperature for 1 hour. To the yellow solution conc. HCl (10 mL) was added dropwise and white solid product of S-carboxymethyl N-substituted dithiocarbamate (I) was precipitated out. (**Scheme-1**)

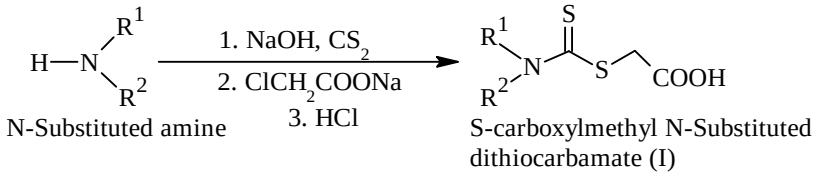

Scheme 1: Synthesis of S-carboxymethyl N-substituted dithiocarbamate (I)

S-carboxymethyl N-substituted dithiocarbamate (500 mmol) was dissolved in 30 mL hydrazine monohydrate (98% pure) in 100 mL round bottom flask and refluxed at 40° C for 20 min with stirring. The resulting mixture was diluted by adding 10 mL water. The white precipitate of N-substituted carbothiohydrazide (II) was collected by filtration and washing with cold water. The white solid was re-crystallized with EtOH and dried. (**Scheme-2**)

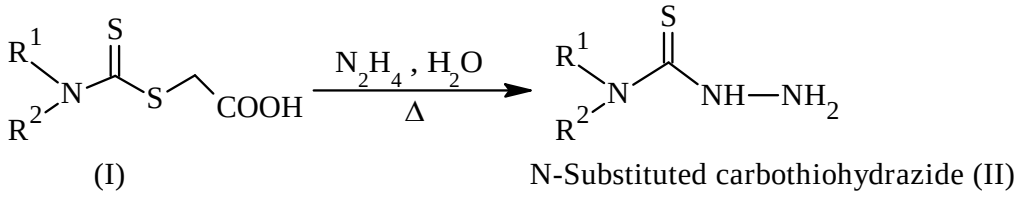

Scheme 2: Synthesis of N-substituted carbothiohydrazide (II)

Table 1: N-substituted carbothiohydrazide

Name and Structure	M.P.	Yield	References
Pyrrolidine-1-carbothiohydrazide 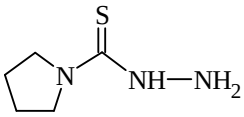	184° C	51%	(Dayal *et al*., 2011) (Muralisankar *et al*., 2016)
Piperidine-1-carbothiohydrazide 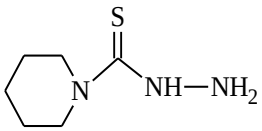	94° C	44%	(Krause *et al.*, 2020) (Kang *et al*., 2011)
Morpholine-4-carbothiohydrazide 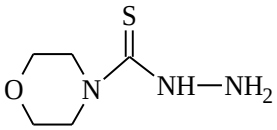	182° C	71%	(El-Sawaf *et al.*, 2018) (Kang *et al*., 2011) (Bala & Mishra, 2014) (Hu *et al*., 2017)
Thiomorpholine-4-carbothiohydrazide 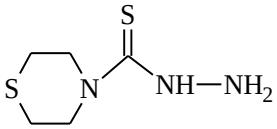	162° C	87%	(Yadav *et al*., 2022)
2,6-dimethylmorpholine-4-carbothiohydrazide 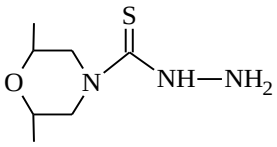	120° C	41%	(De Sousa *et al*., 2006)
Azepane-1-carbothiohydrazide 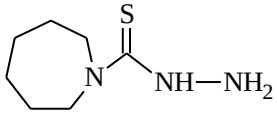	114° C	55%	(Scovill, 1991)
***N, N*-dimethylhydrazinecarbothioamide** 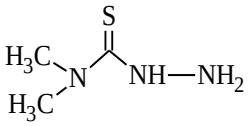	155° C	58%	(Bisceglie *et al*., 2016) (Kang *et al*., 2011)

3.4.2 4-(pyridin-2-yl)piperazine-1-carbothiohydrazide (Scovill, 1991)

Step 1:

Preparation of carboxymethyl-N-methyl-N-phenyldithiocarbamate (I)

A mixture of 12 mL (200 mmol) of CS_2 and 21.6 mL (200 mmol) of N-methylaniline was treated with 250 mL of NaOH solution (8.4 g, 210 mmol) and the solution was stirred at room temperature for 4 hours until the organic layer was disappeared. The straw colour solution was then treated with sodium chloroacetate (23.2 g, 200 mmol) and allowed to stand for 17 hours at room temperature. The solution was acidified with conc. HCl (25 mL) to yield the buff-coloured precipitate of carboxy methyl-N-methyl-N-phenyldithiocarbamate (I). (Yield = 60%, M.P. = 198° C) (**Scheme-3**)

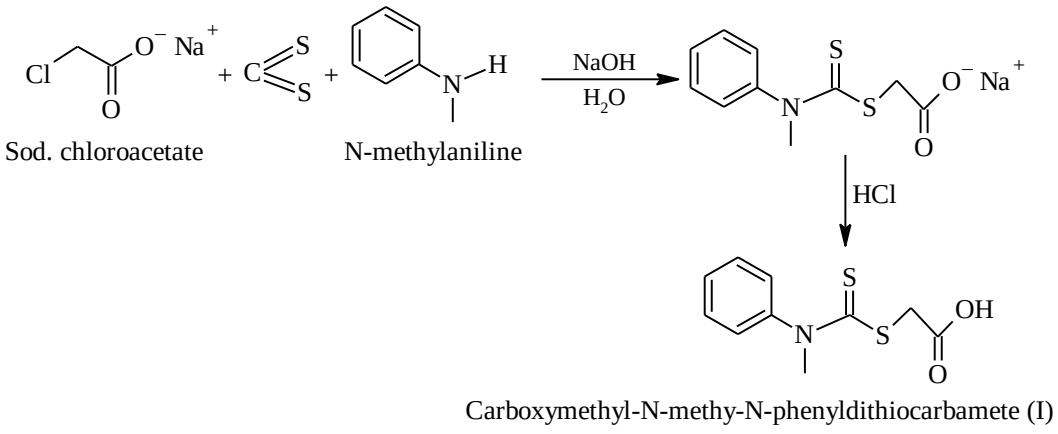

Sod. chloroacetate N-methylaniline

Carboxymethyl-N-methy-N-phenyldithiocarbamete (I)

Scheme 3: Synthesis of carboxy methyl-N-methyl-N-phenyldithiocarbamate (I)

Step 2:

Preparation of 4-methyl-4-phenyl-3-thiosemicarbazide (4-mpt) (II)

A mixture of 17.8 g of carboxymethyl-N-methyl-N-phenyl dithiocarbamate (I), 20 mL of hydrazine hydrate and 10 mL of water was heated on the rings of the water bath for 22 minutes. The N-methyl-N-phenyl-3-thiosemicarbazide (II) separated was filtered, washed with water, dried and recrystallized from EtOH. (Yield = 78%, M.P. =124-125° C). (**Scheme-4**)

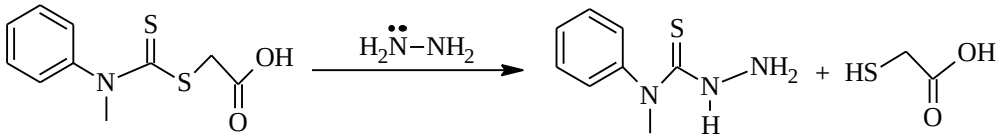

Carboxymethyl-N-methyl-N-phenyldithiocarbamate (I)

N-methyl-N-phenyl-3-thiosemicarbazide (II)

Scheme 4: Synthesis of N-methyl-N-phenyl-3-thiosemicarbazide (II)

Step 3:

Preparation of 4-(pyridin-2-yl) piperazine-1-carbothiohydrazide (III)

A solution of 2.77 g 4-mpt (15 mmol) in 15 mL acetonitrile was treated with 2.5 g 1-(2-pyridyl)piperazine (15 mmol). The mixture was refluxed at 80° C for 40 minutes. The solution was chilled (overnight) and fine colourless crystals were separated out. The solution was filtered and washed with cold acetonitrile (MeCN). The white crystals of 4-(pyridin-2-yl)piperazine-1-carbothiohydrazide (III) was re-crystallized with EtOH. (M.P. = 198° C, Yield = 52%) (**Scheme-5**)

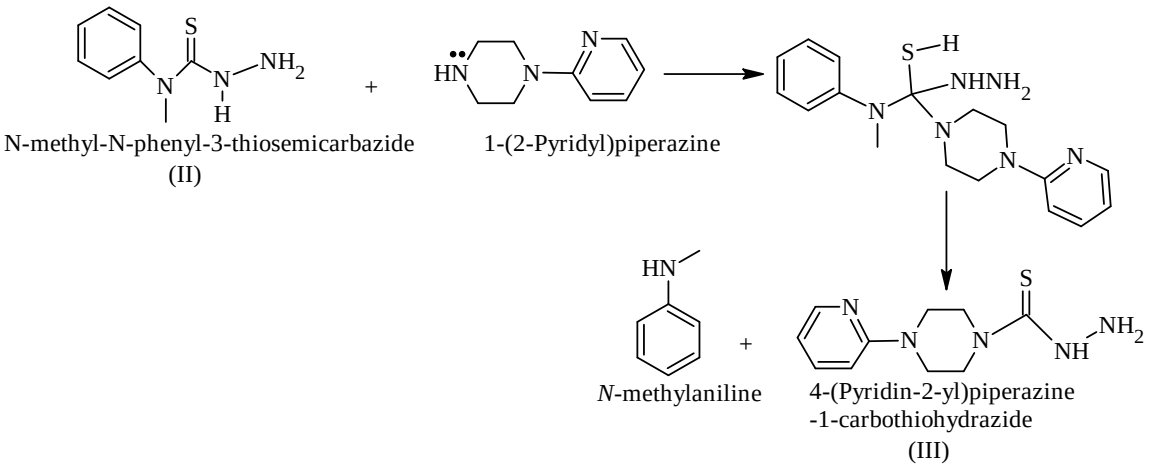

Scheme 5: Synthesis of 4-(pyridin-2-yl)piperazine-1-carbothiohydrazide (III)

3.5 General procedure for the synthesis of 5-methoxyisatin N (4)-substituted thiosemicarbazones (1-6)

A solution of 5-methoxyisatin (2.82 mmol) and 20 mL ethyl alcohol was taken in 250 mL round bottom flask. The mixture was stirred by adding 3 drops of glacial acetic acid as a catalyst about 10 minutes at room temperature. N-substituted carbothiohydrazide (2.82 mmol) was added and the mixture was refluxed at 80° C for 6 h. After cooling at room temperature, the coloured product was filtered, washed with EtOH and dried. The product was re-crystallized with EtOH to get 5-methoxyisatin N(4)-substituted thiosemicarbazone.

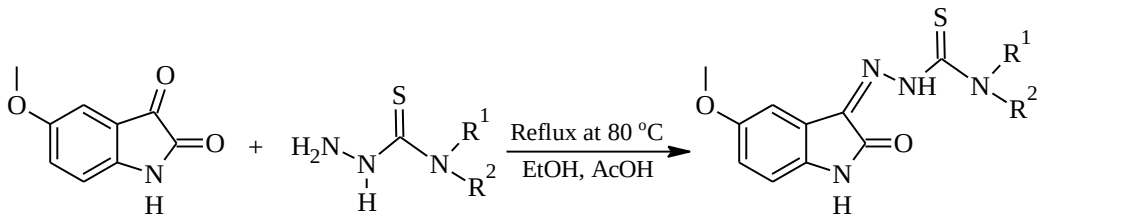

5-methoxyisatin Thiosemicarbazide N(4)-substituted thiosemicarbazone (1-6)

Where,

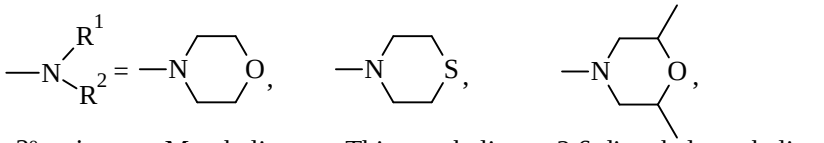

2° amine Morpholine (1) Thiomorpholine (2) 2,6-dimethylmorpholine (3)

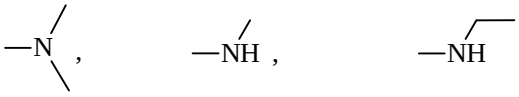

Dimethyl amine (4) Methyl amine (5) Ethyl amine (6)

Figure 30: General structure of synthesized thiosemicarbazones

3.6 Synthesis of 5-hydroxyisatin (Yasuda *et al*., 2013)

A solution of 5-methoxyisatin 1 g (5.6 mmol) and 10.21 mL HBr (48%) were refluxed for 3 h. The solution was diluted by adding water and extracted with ethyl acetate. The organic layers were separated and dried with anhydrous sodium sulphate. The dark brown solid of 5-hydroxyisatin was re-crystallized with MeOH (**Scheme-6**).

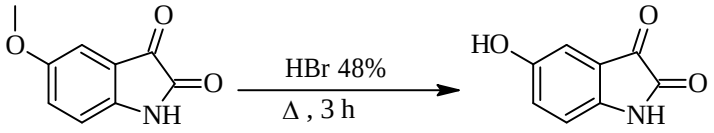

5-methoxyisatin 5-hydroxyisatin

Scheme 6: Synthesis of 5-hydroxyisatin

3.7 General procedure for the synthesis of 5-hydroxyisatin N(4)-substituted thiosemicarbazones (7-16)

A solution of 5-hydroxyisatin (3 mmol) and 20 mL ethyl alcohol was taken in round bottom flask. The mixture was stirred by adding 3 drops of glacial acetic acid as catalyst about 10 minutes at room temperature. N-substituted carbothiohydrazide (3 mmol) was added to the flask. The mixture was refluxed at 80° C for 6 h. After cooling at room temperature, coloured product was filtered, washed with EtOH and dried. The product

was re-crystallized with EtOH to get 5-hydroxyisatin N(4)-substituted thiosemicarbazone.

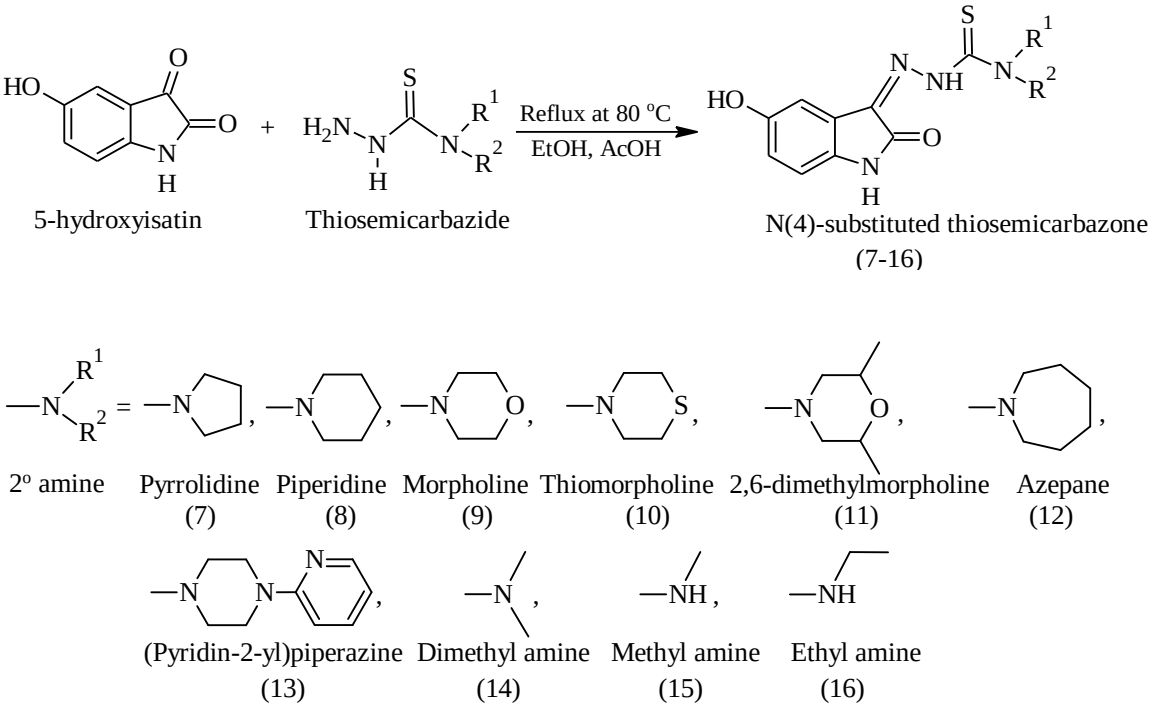

Figure 31: Systematic scheme of 5-hydroxyisatin N(4)-substituted thiosemicarbazones

3.8 General procedure for the synthesis of 5,7-dibromoisatin N(4)-substituted thiosemicarbazones (17-26)

5,7-dibromoisatin (0.82 mmol) and 20 mL ethyl alcohol was taken in 250 mL round bottom flask. The mixture was stirred by adding 3 drops of glacial acetic acid about 10 minutes at room temperature. N-substituted carbothiohydrazide (0.82 mmol) was added to the round bottom flask. The mixture was refluxed at 80° C for 6 h. After cooling at room temperature, yellow product was filtered, washed with EtOH and dried. The product was re-crystallized with EtOH to get 5,7-dibromoisatin N(4)-substituted thiosemicarbazone.

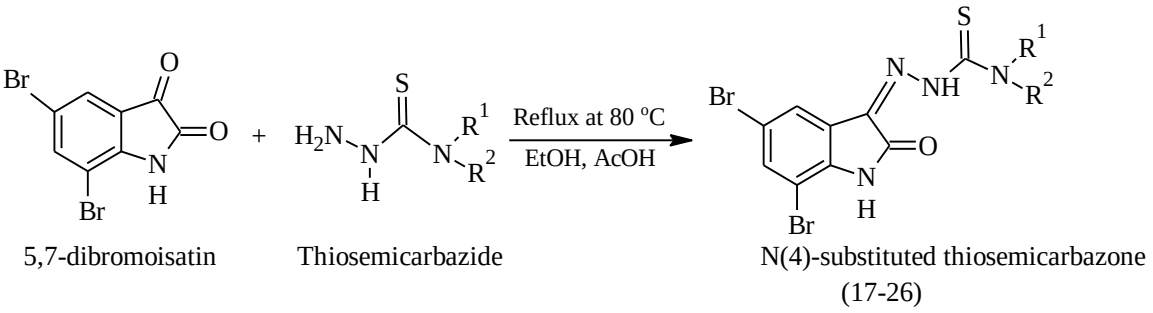

Where,

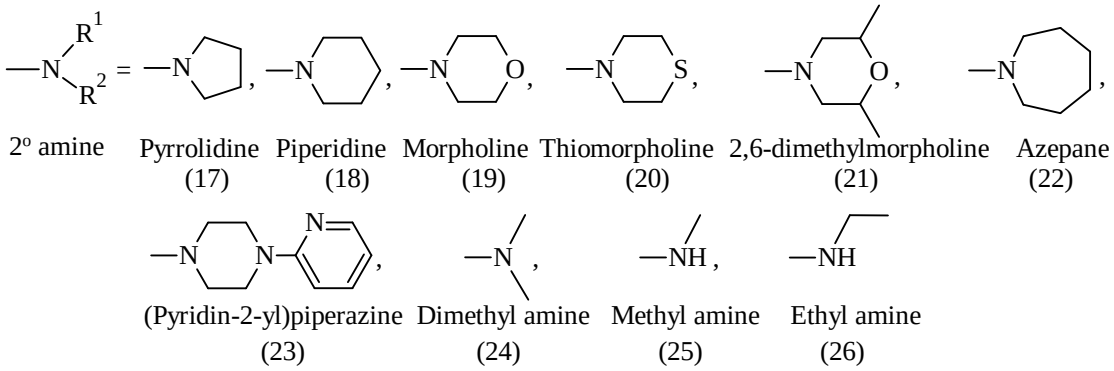

Figure 32: Systematic scheme of 5,7-dibromoisatin N(4)-substituted thiosemicarbazones

CHAPTER 4

4. RESULTS AND DISCUSSION

4.1 SYNTHESIS, CHARATERIZATION AND ANTICANCER ACTIVITY OF N(4)-SUBSTITUTED 5-METHOXYISATIN THIOSEMICARBAZONES

4.1.1 General discussion

The N-substituted carbothiohydrazide were synthesized by the method of El-Sawaf (El-Sawaf *et al*., 2018) and Scovill (Scovill, 1991). 5-Methoxyisatin thiosemicarbazones were synthesized by refluxing 5-methoxyisatin with N-substituted carbothiohydrazide in the presence of absolute ethanol and few drops of glacial acetic acid for 6 h (Singh *et al*., 2021).

Table 2: The physical properties of N(4)-substituted 5-methoxyisatin thiosemicarbazones (1-6)

Compd	Mol. Formula (Mol. Weight)	Melting point (ºC)	Colour	Yields (%)
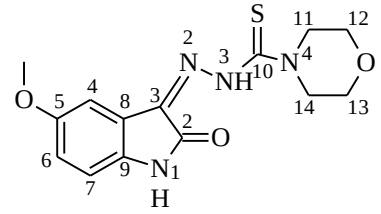 (**MeOIstMor/1**)	$C_{14}H_{16}N_4O_3S$ (320.36)	202º C	Red	51%
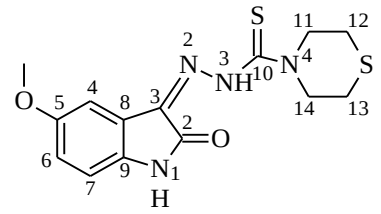 (**MeOIstTmor/2**)	$C_{14}H_{16}N_4O_2S_2$ (336.4324)	198º C	Orange	56%
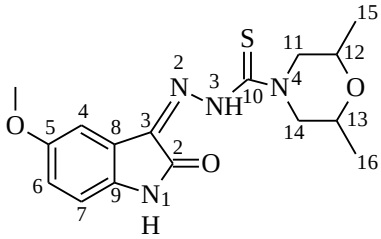 (**MeOIstDmMor/3**)	$C_{16}H_{20}N_4O_3S$ (348.42)	206º C	Red	79%

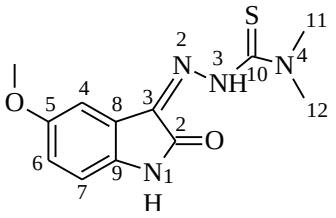 (**MeOIstDm/4**)	$C_{12}H_{14}N_4O_2S$ (278.33)	224° C	Orange	65%
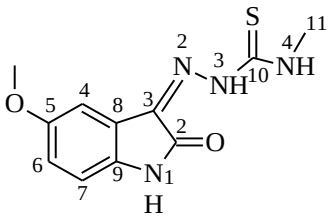 (**MeOIstMet/5**)	$C_{11}H_{12}N_4O_2S$ (264.30)	282° C	Brown	86 %
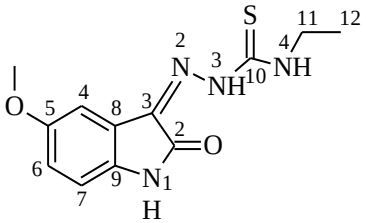 (**MeOIstEth/6**)	$C_{12}H_{14}N_4O_2S$ (278.33)	250° C	Brown	59%

The thiosemicarbazones were obtained in low to moderated yield % (51-86) having melting point in the range of 198-282° C. The thiosemicarbazones were stable in air at room temperature. They were highly soluble in Me_2CO, $CHCl_3$, MeOH, EtOH, DCM, DMSO and DMF. They were insoluble in water. The synthesized compounds were characterized by FT-IR, NMR, UV-Vis Spectroscopic technique. The molecular mass was confirmed by ESI-HRMS mass spectrometry.

The elemental analysis results of compounds (**1-6**) revealed that the experimental data agree with the calculated data within the margins of experimental error.

Table 3: Elemental analysis data of N(4)-substituted 5-methoxyisatin thiosemicarbazones (1-6)

Compd	C	H	N
1	52.55 (52.49)	4.98 (5.03)	17.26 (17.49)
2	49.42 (49.98)	4.60 (4.79)	16.26 (16.65)
3	55.11 (55.16)	5.54 (5.79)	16.04 (16.08)
4	51.87 (51.78)	4.97 (5.07)	20.02 (20.13)
5	50.58 (49.99)	4.44 (4.58)	21.15 (21.20)
6	51.65 (51.75)	5.04 (5.07)	20.05 (20.13)

4.1.2 Spectral studies

4.1.2.1 IR spectra

The assignment of IR spectral bands is most useful in identifying the functional group in the synthesized compound (**1-6**) and are listed in the Table 4.

The symmetric and asymmetric stretching vibrations of indole N-H and azomethine N-H exhibited broad spectral information in the range of 3313-3037 cm^{-1} in the thiosemicarbazones (Swathy *et al.*, 2016). The slight shift to higher wavenumbers in indole N-H (3313 cm^{-1}) is probably a consequence of changes in hydrogen bonding (Casas *et al*., 2000). The stretching vibrations of the *ν*(C=O) and (C=N) groups of thiosemicarbazones exhibited significant spectral bands in the regions 1696-1681 cm^{-1} and 1575-1529 cm^{-1}, respectively. The lack of an IR band at 2600-2500 cm^{-1}, which is distinctive of the S-H group, proved that the solid form of thiosemicarbazones persisted in thione form (Türkkan *et al*., 2017). The significant IR bands in the 1155-1126 cm^{-1} range were ascribed to the thiosemicarbazone moiety of *ν*(N-N) stretching vibration (Joseph *et al*., 2006). In the range of 1196-1168 cm^{-1} and 783-697 cm^{-1}, strong absorption bands due to the stretching vibration of *ν*(C=S) of thiosemicarbazones were seen (Sagdinc *et al*., 2009). This is based on by vibrations involving interactions between C=S stretching and C-N stretching of the C=S group coupled to a nitrogen atom. The stretching vibration of the methoxy group *ν*(-OCH_3) isatin moieties of thiosemicarbazones represents a substantial absorption band in the region 1300-1251 cm^{-1} (Esme *et al*., 2014). The broad stretching vibrations of compound **4**, **5**, **6** (N-H indole and N-H azomethine) were found in the range 3267-3313 cm^{-1}. This is owing to the presence of an alkyl group at the N(4) position of thiosemicarbazones, whereas the compound **1**, **2**, **3** was found in the 3172-3178 cm^{-1} range. This is due to the presence of a heterocyclic substituent at the N(4) position of thiosemicarbazone. When compared to compound (**2**), the methoxy (-OCH_3) stretching vibration in compound (**1**) was downfield *i.e.*, 1294 cm^{-1}. The variation in electronegativity in the heterocyclic ring connected to the thiosemicarbazone moieties is to account for this. In the case of compound (**3**), the methoxy (-OCH_3) stretching vibration (1251 cm^{-1}) found downfield than rest of compound. This is caused by the morpholinyl moieties in the thiosemicarbazone having two methyl substituents at positions 2 and 6.

Table 4: Diagnostic bands in the IR spectra (cm^{-1}) of compounds (1-6)

Compd	ν (N–H)	ν (C=O)	ν (C=N)	ν (C=S)	ν (-OCH_3)	ν (N–N)
1	3178 (br) 3055 (m)	1693 (s)	1575 (s)	1168 (s) 722 (m)	1294 (s)	1126 (s)
2	3172 (br) 3037 (m)	1685 (s)	1539 (s)	1174(s) 783 (m)	1282 (s)	1155 (s)
3	3176 (br) 3064 (m)	1681 (s)	1568 (s)	1179 (s) 697 (m)	1251 (s)	1151 (s)
4	3267 (br) 3176 (m)	1691 (s)	1537 (s)	1182 (s) 775 (m)	1300 (s)	1126 (s)
5	3303 (br) 3233 (m)	1696 (s)	1555 (s)	1196 (s) 745 (m)	1291 (s)	1132 (s)
6	3313 (br) 3257 (m)	1683 (s)	1529 (s)	1184 (s) 783 (m)	1288 (s)	1139 (s)

s = strong, m = medium, br = broad

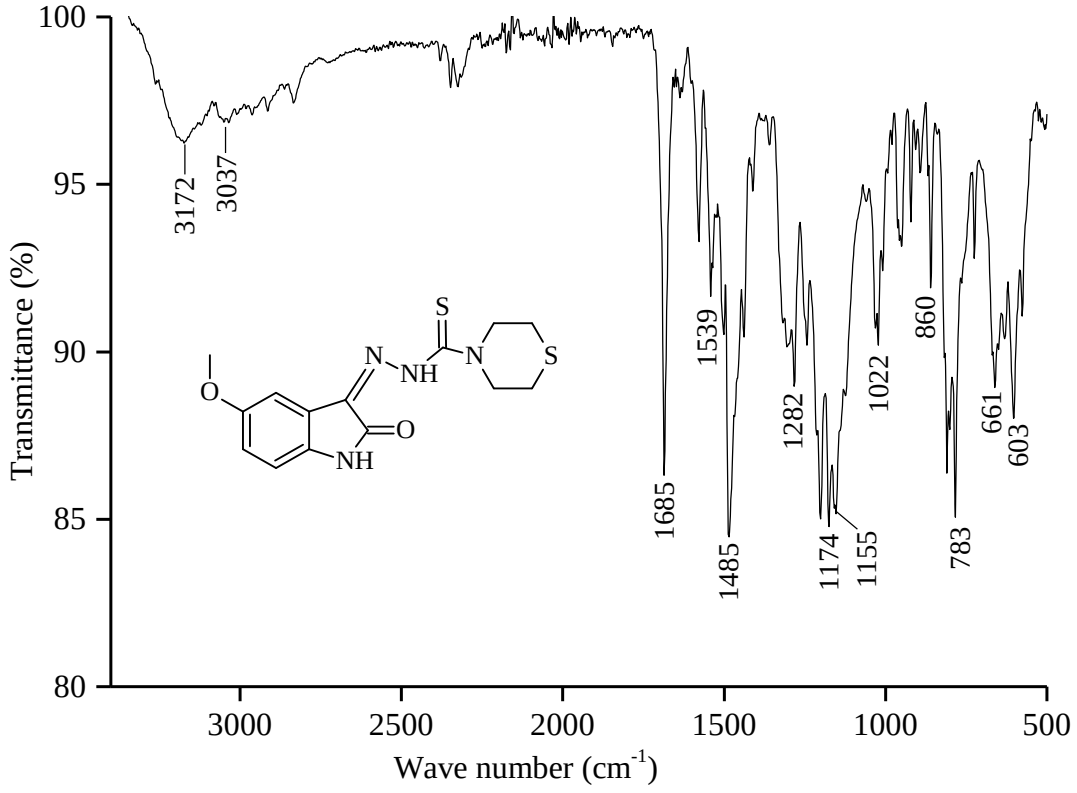

Figure 33: IR spectrum of compound (2)

4.1.2.2 NMR spectra

The ^{1}H NMR spectral values (δ, ppm) of the synthesized compounds (**1, 2, 3, 4, 5, 6**) are enumerated in Table 5.

The ^{1}H-NMR (400 MHz) spectrum that didn't exhibit any peak at δ 4 ppm assigned to thiol (-SH) proton (Jouad *et al*., 2001) and revealed distinct singlet peaks in the range of δ 13.48-12.58 ppm attributable to protons attached to the most polar group; N(3)H of thiosemicarbazone moiety, indicating that Schiff's base ligands exist in solution as neutral thione tautomeric form (Munikumari *et al*., 2019). The Sharp singlet peaks attributed to indole N-H protons were detected in the range of δ 11.10-11.01 ppm (Labisbal *et al*., 2000). Due to their increased external magnetic field, which causes a chemical shift toward downfield (δ13.48-11.01 ppm), these protons require a higher frequency to achieve resonance (Yadav *et al*., 2022). The isatin C(6)-H was deshielded due to the electron-releasing inductive effect of the methoxy group (-OMe) at position-5, and appeared as a doublet at 7.13-6.83 ppm, whereas the isatin C(7)-H appeared as a doublet at δ 7.87-7.01 ppm. Due to the electron-releasing methoxy group and C=N function, the C(4)-H had a significant deshielding effect and resonated further downfield as a doublet at δ 7.75-6.89 ppm (Pervez *et al*., 2010). Due to CH_2 coupling, in the thiosemicarbazone (**5**) N(4)-H resonance was detected as a triplet at δ 9.26-9.24 ppm (Pervez *et al*., 2012). All the aromatic protons (isatin) of the ligands were recorded doublet peak at the region δ 7.87–6.83 ppm (Balachandran *et al*., 2018). The singlet signals of methoxy proton (-OCH_3) was recorded in the region δ 3.79-3.73 ppm (Britto *et al*., 2020). While C(11) & C(14) proton nearer nitrogen displayed a triplet peak at δ 3.99 ppm, C(12) & C(13) proton nearer oxygen resonated to create a broad peak at δ 3.43 ppm in morpholine ring. Due to differences in electronegativity, the thiomorpholine ring proton C(11) & C(14) displayed a triplet peak at δ 4.24 ppm while the C(12) & C(13) proton displayed a triplet peak at δ 2.81 ppm. Compound (**4**) included two methyl proton whose appearance at δ value as multiplet of δ 3.75 ppm demonstrated magnetic equivalency. In the case of the thiosemicarbazone (**6**), CH_2 of the N(4)-ethyl substituent reverberated as a quartet peak at about δ 3.84 ppm and CH_3 of the N(4)-ethyl substituent resonated as a triplet peak at around δ 1.35 ppm (Kassab *et al*., 2010).

Table 5: ^{1}H NMR spectral assignments (δ ppm) of compounds (1-6) (400 MHz)

Compd→	**1**	**2**	**3**	**4**	**5**	**6**
Solvent→	DMSO-d6	DMSO-d6	DMSO-d6	DMSO-d6	DMSO-d6	$CDCl_3$
Proton↓						
-N(1)H	11.10(s)	11.10(s)	11.04(s)	11.07(s)	11.01(s)	-
-N(3)H	13.27(s)	13.23(s)	13.19(s)	13.48(s)	12.58(s)	12.69(s)
-N(4)H	-	-	-	-	9.26(s)	7.26(s)
-H(4)	6.94(d)	6.92(d)	6.90(d)	6.89(d)	7.25(d)	7.75(d)
-H(6)	6.92(d)	6.86(d)	6.88(d)	6.83(d)	6.94(d)	7.13(d)
-H(7)	7.04(d)	7.01(d)	6.94(d)	7.06(d)	6.94(d)	7.87(d)
-H(11)	3.99(t)	4.24(t)	3.68(t)	3.75(m)	3.76(m)	3.84(q)
-H(12)	3.43(t)	2.81(t)	2.94(t)	3.75(m)	-	1.35(t)
-H(13)	3.43(t)	2.81(t)	2.94(t)	-	-	-
-H(14)	3.99(t)	4.24(t)	3.68(t)	-	-	-
-H(15)	-	-	1.16(m)	-	-	-
-H(16)						
3H(OCH_3)	3.76(s)	3.76(s)	3.74(s)	3.73(s)	3.76(s)	3.79(s)

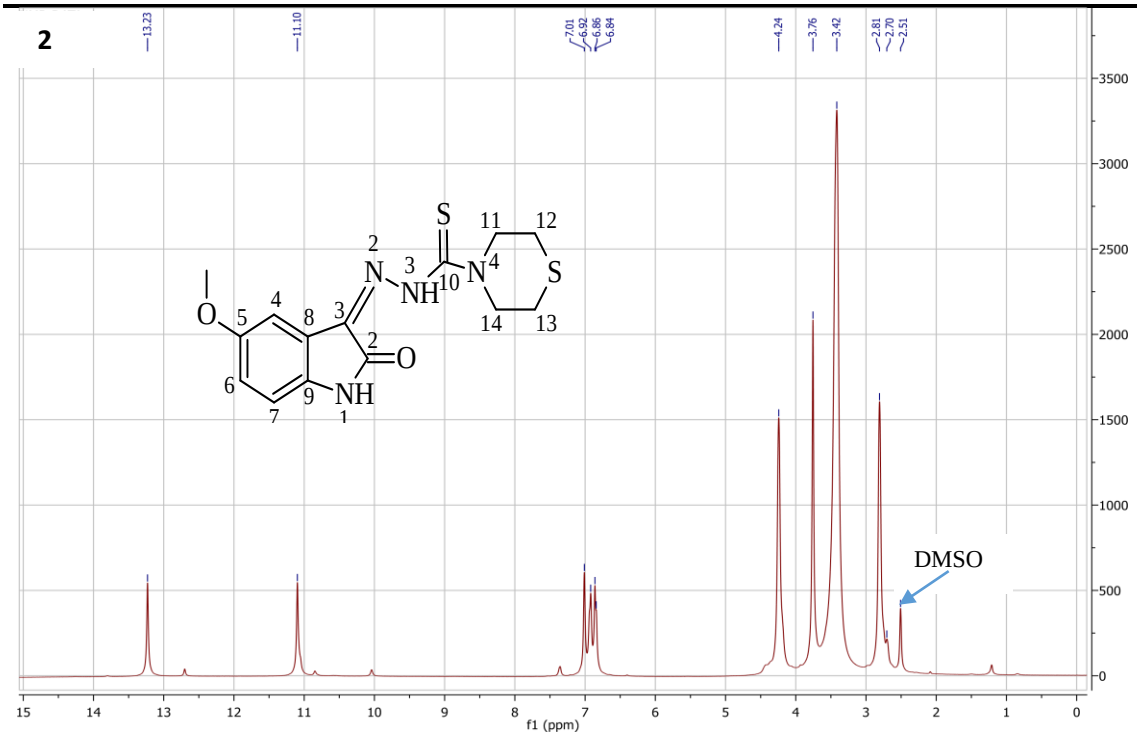

Figure 34: ^{1}H NMR spectrum (400 MHz, DMSO-d6) of compound (2)

The compound (**2)** displayed the doublet signals of aromatic protons at δ 7.01 - 6.86 ppm and two separate singlets for N-NH of thiosemicarbazone and indole N-H moiety at δ 13.23 ppm and δ 11.10 ppm respectively. The triplet signals of thiomorpholinyl protons in compound (**2)** were observed at δ 4.24-2.81 ppm. The singlet signals of methoxy proton (-OCH_3) were seen at δ 3.76 ppm.

The ^{13}C NMR (400 MHz) spectral values (δ, ppm) of the compounds (**1, 2, 3, 4, 5, 6**) are recorded in Table 6.

Chemical shift values for ^{13}C NMR spectra of synthesized compounds were found to be quite similar to those of related N(4) substituted thiosemicarbazones. The magnetically non-equivalent carbon atoms of the thiosemicarbazones had ^{13}C NMR spectra at δ 179.93-177.16 ppm, δ 163.39-163.18 ppm, and δ 136.82-133.86 ppm, which were ascribed to the π bonded carbon atoms of the C=S, C=O, and C=N groups, respectively (Akinchan *et al*., 2002). The chemical shift of C(3) carbon revealed the difference in the spectra of mono- and di-alkyl substituted thiosemicarbazones, with the former appearing 2-3 ppm farther downfield (δ 136.37) than the latter (δ 133.86) (Bain *et al*., 1997). The sharp peaks of the sp^2 hybridized carbon atoms, *i.e*., aromatic carbon atoms of isatin, were found around δ 156.64-105.65 ppm (Çavuş *et al*., 2020). Due to the presence of mono- and di-/cycloalkyl thiosemicarbazones, the chemical shift of C(9) carbon was seen to differ by 2-3 ppm; the former was downfield (δ 135.04 ppm) than the latter (δ 132.29 ppm). In addition, aliphatic carbon atoms (-CH_2) were allocated broad signals in the downfield region δ 71.43-27.04 ppm (Al-Sanea *et al*., 2021), while aliphatic carbon atoms (-CH_3) were assigned broad signals in the upfield region δ 39.90-14.48 ppm (Saranya *et al*., 2019). Chemical shift (δ) values for C(12) and C(13) of compound (**2**) were found to be significantly lower than those for compound (**1**) because of the difference in electronegativity.

Table 6: ^{13}C NMR spectral assignments (δ ppm) of compounds (1-6) (400 MHz)

Compd→	**1**	**2**	**3**	**4**	**5**	**6**
Solvent→ **Carbon↓**	DMSO-d6	DMSO-d6	DMSO-d6	$CDCl_3$	DMSO-d6	DMSO-d6
C=O *viz.* C(2)	163.27	163.25	163.18	163.39	163.21	163.20
C=N *viz.* C(3)	136.04	136.08	136.82	133.86	136.21	136.37

-C(4)	105.94	105.95	105.65	106.56	106.43	106.60
-C(5)	155.82	155.80	155.75	156.64	155.77	155.75
-C(6)	112.41	112.43	112.36	111.68	112.27	112.24
-C(7)	121.20	121.20	121.18	121.59	121.27	121.21
-C(8)	117.66	117.63	117.53	-	117.65	117.62
-C(9)	135.04	134.96	134.80	133.86	132.29	132.38
C=S *viz.* C(10)	179.93	179.80	179.58	180.37	178.17	177.16
-C(11)	66.17	53.36	71.43	29.92	31.78	39.90
-C(12)	50.50	27.04	55.97	29.92	-	14.48
-C(13)	50.50	27.04	55.97	-	-	-
-C(14)	66.17	53.36	71.43	-	-	-
-C(15)	-	-	18.85	-	-	-
-C(16)	-	-	18.85	-	-	-
-C(OCH_3)	56.08	56.07	55.97	56.26	56.08	56.09

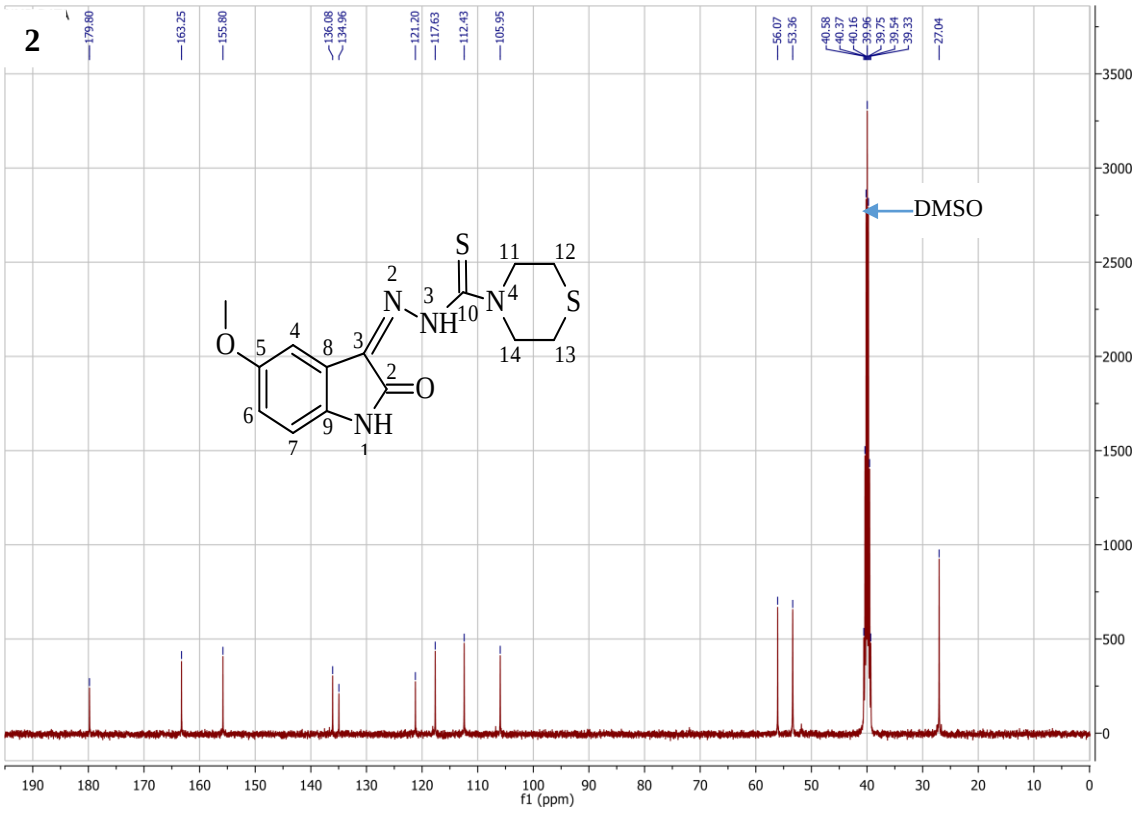

Figure 35: ^{13}C NMR spectrum (400MHz, DMSO-d6) of compound (2)

The Compound (**2)** exhibited ^{13}C NMR spectra at δ 179.80, δ 163.25 and δ 136.08 ppm attributed to C=S, C=O and C=N groups respectively. The chemical shift (δ) values of aromatic carbons were observed in the region δ 155.80-105.95 ppm. The spectra of thiomorpholine carbons were observed at δ 53.36-27.04 ppm. The chemical shift (δ) values of methoxy carbons of the synthesized thiosemicarbazone was observed at δ 56.07 ppm (Çavuş *et al*., 2020).

4.1.2.3 Mass spectroscopy

Positive mode and negative mode in mass spectrometry both relate to the ionization polarity employed during the investigation. In positive mode, the analyte molecules are ionized by losing one or more electrons from them, resulting in the creation of positively charged ions (cationic species). In negative mode, the analyte molecules are ionized by gaining one or more electrons, which results in the creation of negatively charged ions (anionic species). The precursor ion, which stands in for the entire analyte molecule, is responsible for the mass spectrum's most strong peak.

Table 7: The mass spectral data of the synthesized compounds (1-6)

	***m/z* [M+H]$^+$**		***m/z* [M+Na]$^+$**	
Compd ↓	**Found**	**Calculated**	**Found**	**Calculated**
1	321.1016	321.1015	343.0838	343.0835
2	337.0789	337.0787	359.0611	359.0606
3	349.1332	349.1330	371.1150	371.1149
4	279.0910	279.0910	301.0734	301.0729
5	265.0766	265.0753	287.0569	287.0573
6	279.0910	279.0910	301.0733	301.0729

In order to better understand the behavior and structures of synthesized compounds in solutions, high resolution electron spray ionization mass spectrometry (ESI-HRMS) investigation was done in positive mode. Both protonated molecular ion peak $[M+H]^+$ and alkali adduct analyte molecular ion peak $[M+Na]^+$ were found in all of the compounds, indicating the positive fragmentation mode (Matesic *et al.*, 2008). The compound (**1, 2, 3, 4, 5, 6**) exhibited mass spectral peaks at *m/z* (amu): 321.1016(calc., 321.1015), 337.0789 (calc., 337.0787), 349.1332 (calc., 349.1330), 279.0910 (calc., 279.0910), 265.0766 (calc., 265.0753), and 279.0910 (calc., 279.0910) respectively

thus by showing the existence of $[M+H]^+$ (Pawar *et al*., 2021). The compound (**1, 2, 3, 4, 5, 6**) exhibited the peaks at *m/z* (amu): 343.0838 (calc., 343.0835), 359.0611(calc., 359.0606), 371.1150 (calc., 371.1149), 301.0734 (calc., 301.0729), 287.0569 (calc., 287.0573) and 301.0733 (calc., 301.0729) respectively indicating the presence of the sodium ion $[M+Na]^+$. Because numerous alkali salts are employed in the manufacturing of glass, the alkali metals detected in mass spectra of thiosemicarbazones could have come from glassware. Na^+ can originate from the laboratory glassware. Moreover, Na^+ can be found in H_2O (water). As a result, in LC-ESI-MS investigations utilizing both organic and aqueous (H_2O-based) solvents, there is a greater probability of Na^+ forming adducts with molecules, resulting in peaks in the mass spectra corresponding to $[M + Na]^+$ (Arafa & Badry, 2016). The sample is dissolved in a solvent containing sodium ions (Na^+) during electrospray ionization (ESI). The ions of the organic compound may form adducts with the sodium ions when the sample solution is sprayed into the mass spectrometer. As a result, the sodium molecular ion (Na^+) and other fragment ions can be seen in the mass spectrum.

The compound (**1**), which contains the fragment N(4) morpholinyl $[C_{14}H_{16}N_4O_3 + H]^+$ ion, is the cause of the notable peak at *m/z* 289.1297 (calc., 289.3097). In the compound (**2**), the fragment N(4) thiomorpholinyl $[C_{14}H_{15}N_4SO_2 + H]^+$ ion was responsible for the prominent peak at *m/z* 304.3006 (calc.,304.3675). Due to the existence of the fragment N(4) 2,6-dimethylmorpholinyl $[C_{16}H_{20}N_4O_3 + H]^+$ ion, the major peak for compound (**3**) was found at *m/z* 317.1606 (calc., 317.3630). Because of the presence of the fragment N(4) dimethylamine $[C_{12}H_{14}N_4O_2 + H]^+$ ion, the compound (**4**) exhibits a prominent peak at *m/z* 247.1185 (calc., 247.2731). Since the fragment N(4) methyl $[C_{11}H_{12}N_4O + H]^+$ ion was present, in the compound (**5**), major peak at *m/z* 217.1040 (calc., 217.2471) was identified (El-Saied *et al*., 2019). When the fragment N(4) ethyl $[C_{12}H_{14}N_4O_2 + H]^+$ ion is present, the compound (**6**) has a strong peak at *m/z* 247.1195 (calc., 247.2731). All fragmentation is characterized by loss of an one sulfur atom, abbreviated SH (*m/z*; 33 amu). (Almeida *et al*., 2020, El-Saied *et al*., 2019). However, the fragments matching to the thiosemicarbazone portion that were produced when N-N and NH-CS bonds were broken provided evidence of their structural integrity (Pervez *et al.*, 2011).

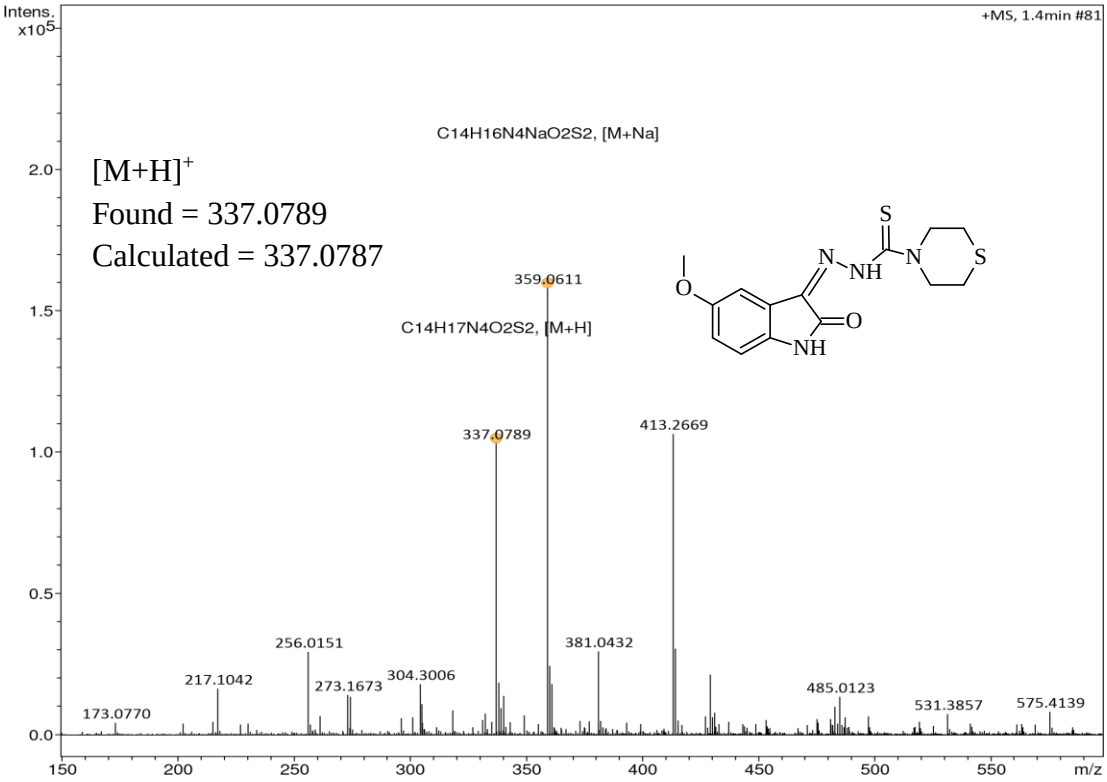

Figure 36: ESI-HRMS of compound (2)

All of the mass spectral data acquired for compounds (**1, 2, 3, 4, 5, 6**) agree with the calculated data for those compounds with the postulated molecular structures.

4.1.2.4 UV-Visible spectroscopy

The UV-Visible spectra of the synthesized compounds (**1, 2, 3, 4, 5, 6**) are listed in Table 8.

The electronic spectra of compound were recorded in $CHCl_3$ and MeOH (25 μM) solutions in the region of 600-200 nm to verify the distinct absorptions of non-bonded electrons and aromatic ring electrons. Because of the electronic transitions π→π*, n→π*, the synthesized compounds showed broad absorption bands in the UV-Visible region (Netalkar *et al*., 2015).

The absorption bands caused by the n→π* electronic transitions of >C=O, >C=N, and –NH-C=S were found as two strong peaks in thiosemicarbazones (Türkkan *et al*., 2017). Since they are covered by the more intense π→π* type, in the case of thiosemicarbazone portion of the molecule did not show any transitions that could be classified as an n→π* type (Kandemirli *et al*., 2009).

The bands due to the n→π* electronic transitions were found in higher wavelength than that in π→π* electronic transitions because the former transitions absorb lower energy than that of later transitions. When compared to N-alkyl thiosemicarbazone, it was reported that the absorption peak of *N*,*N*-dialkyl substituted thiosemicarbazone was smaller (350 nm). The compound (**1**) was revealed to have a smaller absorption peak than compound (**2**) because of the difference in electronegativity between oxygen and sulphur atoms. Nearly identical absorption broad shoulder and sharp peaks were observed for all produced thiosemicarbazones at 350 nm and 284 nm, respectively. This is due to the electronic transition of n→π* and π→π*.

Table 8: UV-Visible spectroscopic data of compounds (1-6)

Solvent	**$CHCl_3$**				**MeOH**	
Compd→ $\lambda_{max(nm)}\downarrow$	**1**	**2**	**3**	**4**	**5**	**6**
π → π*	284 nm	283 nm	284 nm	284 nm	282 nm	283 nm
n → π*	353 nm	356 nm	355 nm	350 nm	356 nm	358 nm

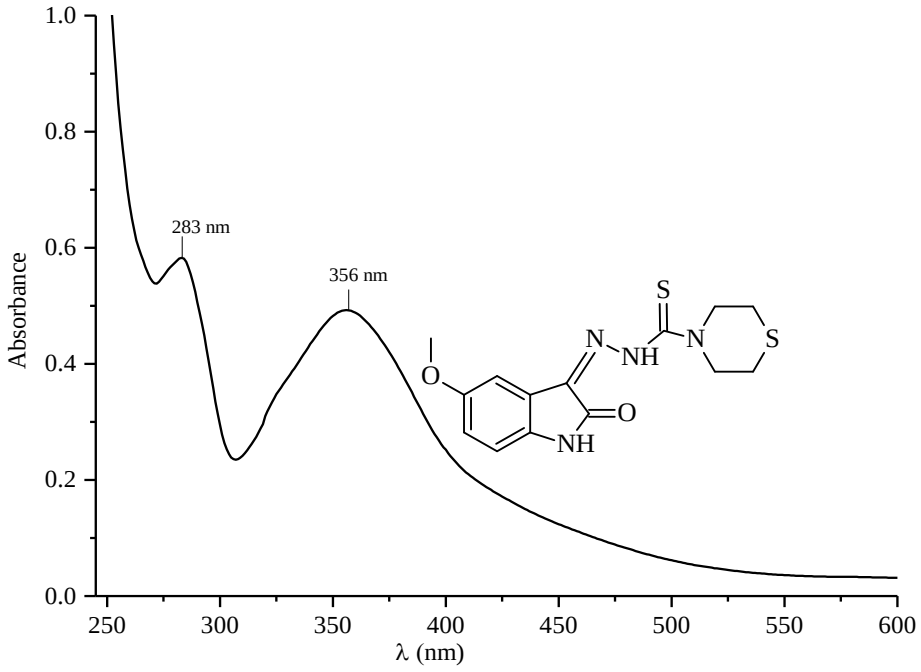

Figure 37: UV-Visible spectra of compound (2)

In the compound (**2**), the electronic one absorption band at 356 nm was assigned to the n→π* transition of the C=N, C=O and (-NH-C=S) groups, while the other absorption band at 283 nm was attributed to the π→π* transitions of π-electrons of aromatic benzene ring (Hussain, 2015).

4.1.2.5 Single crystal X-ray crystallographic study

Single crystals of **MeOIstDm** and **MeOIstDmMor** suitable for X-ray diffraction studies were grown by slow evaporation in $CHCl_3$ and EtOH (1:4). For **MeOIstDm**, a total of 47022 reflections were measured of which 4418 were unique and 3148 were considered observed ($I > 2\sigma(I)$]. The final residual index is; $R_1 = 0.0646$, $wR_2 = 0.1546$ for the observed and $R_1 = 0.1035$, $wR_2 = 0.1768$ for all reflections using 175 parameters. For **MeOIstDmMor**, a total of 74084 reflections were measured of which 6574 were unique and 5048 were considered observed ($I > 2\sigma(I)$]. The final residual index is; *R* 0.0997, *R*w 0.1943 for the observed and *R* 0.1280, *R*w 0.2063 for all reflections using 467 parameters 25 restraints.

4.1.2.6 Crystal structure description

The structure of compound **MeOIstDm** and **MeOIstDmMor** together with the atom labelling scheme is shown in Fig. 38 and Fig. 39 respectively. The compound **MeOIstDm** crystallizes in monoclinic space group *P21/c* (P = Primitive lattice, 21 = two fold rotation along axis, /c = mirror place perpendicular along axis) with one molecule in the asymmetric unit (Fig. 38). In compound (**MeOIstDm**), the comparison of C-N and N-N bond distances with typical single and double bond lengths [C(9)-N(4) 1.358, C(10)-N(2) 1.378, C(10)-N(3) 1.335, C(11)-N(3) 1.467, C(12)-N(3) 1.448, C(8)-N(1) 1.293, N(1)-N(2)1.354 Å] also indicates that charge delocalization is widespread throughout the thiosemicarbazone skeleton (Matesanz *et al*., 2016). The compound **MeOIstDmMor** crystallizes in orthorhombic *P na2₁* (P = Primitive lattice, na = Lattice number absent, 21 = two fold rotation along c-axis) space group with two molecule of compound and with two lattice water molecules in the asymmetric unit (Fig. 38). The quality of data for **MeOIstDmMor** is not very good. The value of R_{int} is 13.2% and the Poor Data/Parameter Ratio of 7.21 The crystal is a weak diffractor and diffract very weakly beyond $2\theta = 42^0$. In compound **MeOIstDmMor**, a comparison of C-N and N-N bond distances with typical single and double bond lengths [C(9)-N(1) 1.322, C(5)-N(1) 1.405, C(10-N(3) 1.358, C(10)-N(4) 1.334, C(16)-N(4) 1.473, C(11)-N(4) 1.428, C(8)=N(2) 1.279, N(2)-N(3)1.354 Å] indicates that charge delocalization is widespread throughout the thiosemicarbazone skeleton. All bond distances are normal in the 5-methoxyisatin moiety in the compound (**MeOIstDmMor**), except for the elongated C(9)-C(8) single bond is 1.525 Å whereas in compound (**MeOIstDm**) C(9)-C(8) single

bond is 1.518 Å. In 5-methoxyisatin moiety C(9)-O(2) distance for studied **MeOIstDmMor** crystal structure is 1.242 Å whereas in (**MeOIstDm**) C(9)-O(2) bond distance is 1.228 Å (Kandemirli *et al*., 2009). In comparison to the 5-methoxyisatin derivative (*Z*)-*N*-(5-methoxy-2-oxoindolin-3-ylidene) pyrrolidine-1-carbothiohy drazide, the bond lengths C-N, N-N, C(9)-C(8), and C(9)-O(2) of the compounds **MeOIstDmMor** and **MeOIstDm** are similar (Aneesrahman *et al*., 2019). Indole-3-thiosemicarbazone, {1.696 (3) Å}, and 5-bromo indole-3-thiosemicarbazone, {1.699(2) Å} have identical C=S bond lengths of 1.679(9) Å in **MeOIstDmMor** and 1.6735(19) Å in **MeOIstDm** (Khan *et al*., 2018). The bond angle of N2-N1-C8-C6 is 179.62° (19), indicating that **MeOIstDm** of the imine N2 atom undergone sp^2 hybridization whereas the torsion angle C5-C4-C8-N2 is 179.11°(9), indicating that the compound **MeOIstDmMor** has an *E* (trans) configuration, resulting in the double bond character of C=N (Arafath *et al*., 2017).

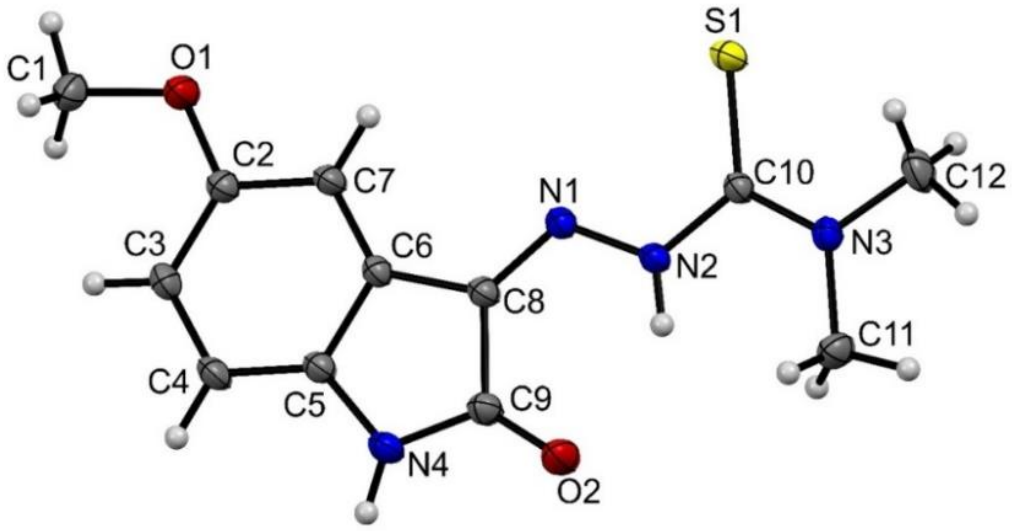

Figure 38: ORTEP diagram of compound MeOIstDm drawn in 30% thermal probability ellipsoids showing atomic numbering scheme.

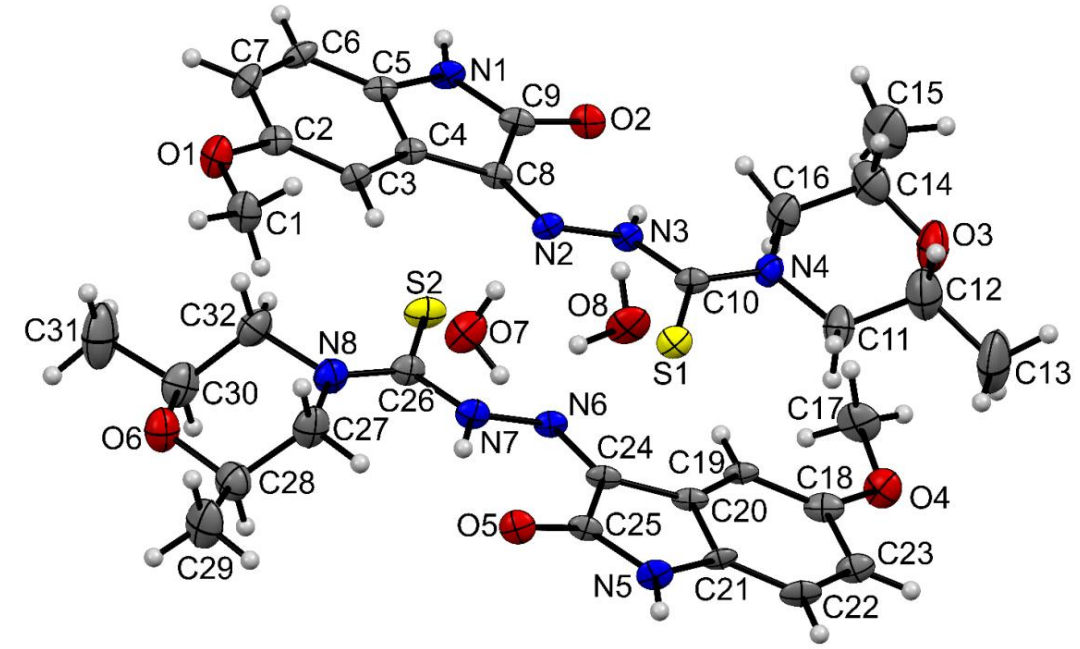

Figure 39: ORTEP diagram of MeOIstDmMor drawn in 20% thermal probability ellipsoids showing atomic numbering scheme. The asymmetric unit contains two crystallographically independent units and two water molecules in the crystal lattice.

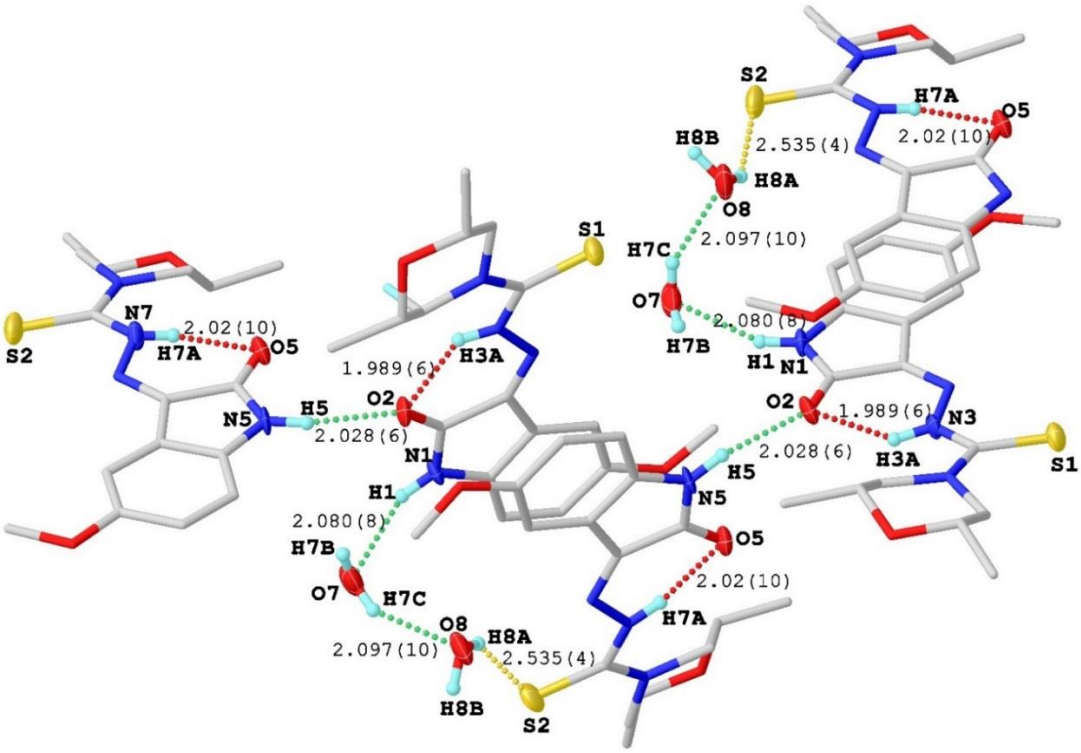

Figure 40: Hydrogen bonding interactions in the crystal lattice of MeOIstDmMor viewed along the crystallographic c-axis (Hydrogen bonding interactions with max D–A distance 2.9 Å and minimum angle 120°).

The two molecules in the asymmetric unit of **MeOIstDmMor** are involved in intra as well as intermolecular H-bonding *via* two lattice water molecules (Fig. 40). The Sulphur atom S2 shows H-bonding with hydrogen atom H8A of lattice water molecule (O8–H8A……S2 = 2.535(4) Å), this water molecule further involved in H-bonding with second water molecule (O7–H7C……O8 = 2.097(10) Å), and oxygen atom (O7) of this water molecule involved in H-bonding with hydrogen atom attached to ring nitrogen (N1) of neighboring molecule (N1–H1……O7 = 2.080(8) Å). The oxygen atom on this molecule involved in intra as well as intermolecular H-bonding, it shows intramolecular H-bonding with hydrogen (H3A) attached to nitrogen (N3–H3A……O2 = 1.989(6) Å) and intermolecular H-bonding with hydrogen H5 attached to the ring nitrogen (N5) of neighboring molecule (N5–H5……O2 = 2.028(6) Å) forming a two-dimensional H-bonding network (Fig. 41).

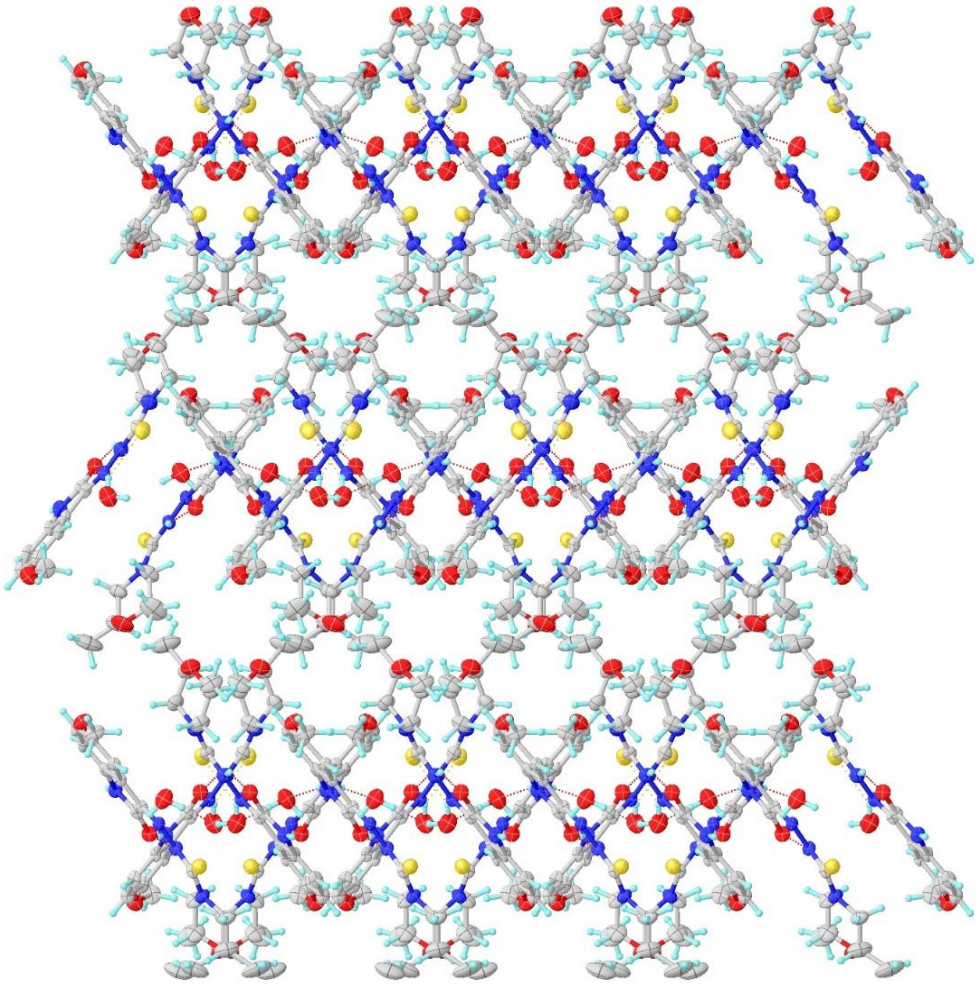

Figure 41: Two-dimensional hydrogen bonding networks in the crystal lattice of MeOIstDmMor viewed along crystallographic a-axis. (Hydrogen bonding interactions with max D–A distance 2.9 Å and minimum angle 120°).

4.1.3 Anticancer activity

Breast cancer is the major largest risk factor for mortality among women from cancer. Breast cancer is a multi-step process that includes various cell types, and prevention is still difficult around the world. Every year, about 1.5 million women worldwide (25%) are diagnosed with breast cancer (Sun *et al*., 2017). One of most active compound was 5-chloro-3-(2-(3,4-dimethoxyphenyl)-2-oxoethylidene)indolin-2-one, which had GI_{50} values of 8.54, 4.76, and 3.59 against many breast cancer MDA-MB-231, MDA-MB-468, and MCF-7 cells, respectively (Karthikeyan *et al*., 2013).The cytotoxic activity of 4-bromo-1-diethylaminomethyl-1H-indole-2,3-dione was identified 10–15 times more effective on cancer cells than non-cancer cells, can be very successful for the treatment of breast cancer with few side effects, and exhibited efficient cytotoxicity on MCF-7 cells, arresting them at G2/M at normal doses (Solomon *et al*., 2009). Benzoxazole combined with benzofuran and 1,2,4-oxadiazole exhibited cytotoxic efficacy towards human breast cancer (MCF-7), lung (A549), melanoma (A375), and colon (HT-29) cell lines (Ghoshal & Patel, 2020). *In vitro* antiproliferative activities of 2-(phenyl)-3H-benzo[d]imidazole-5-carboxylic acids against three breast cancer cell lines (MDA-MB-231, MDA-MB-468 and MCF-7) were investigated (Karthikeyan *et al*., 2017). The MTT assay method was used to test 7-azaisatin derivatives for their *in vitro* cytotoxic effects against MCF-7, A549, and HEPG2 cell lines, respectively (Rekulapally *et al*., 2015).The antiproliferative effect of 3-hydroxypyridine thiosemicarbazone was discovered in MCF-7 and MDA-MB-231 cell lines (Shahi *et al*., 2021). The anti-proliferative effect of isatin-pyridine hybrids was tested *in vitro* against three human cancer cell lines: HepG2 hepatocellular carcinoma, A549 lung cancer, and MCF-7 breast cancer (Eldehna *et al*., 2015). Spirocyclic tetrahydrofuran- and isoxazolidine-2-oxindole collections ability to inhibit lung adenocarcinoma (A549), hepatocellular carcinoma (HepG2), and MCF-7 human breast cancer cell line growth (Peddibhotla, 2009).

Skin cancer accounts for 30% of all newly diagnosed cancers worldwide, and around 1.2 million new skin cancer cases are in the USA each year whereas in India, skin cancer accounts for 1–2%. Skin cancer can be caused by oxidative stress in the skin, which causes DNA damage , protein-DNA crosslinking, and single and double strand DNA breaks (Nirmala *et al*., 2017). Lung cancer is the most frequent cancer worldwide, and it may be substantially avoided by quitting smoking (Ferkol & Schraufnagel, 2014). *In*

vitro cytotoxicity of 3-hydroxy-3-(2-imino-3-methyl-5-oxoimidazolidin-4-yl)indolin-2-one analogs towards A549/ATTC non-small cell lung cancer and LOX IMVI melanoma cell lines was investigated (Penthala *et al*., 2010). Sparfloxacin-isatin hybrids showed anticancer activity against SW480 (human colon adenocarcinoma cells), HeLa (human cervical cancer cells), A549 (human lung carcinoma cells), and HepG2 (human hepatic carcinoma cells) with an IC_{50} of 18.31–>50 μg/mL (Xu *et al*., 2019).

4.1.3.1 Anticancer activity of 5-methoxyisatin N(4)-substituted thiosemicarbazones

Breast cancer cells (MCF-7), Lung cancer cells (A549), and Skin cancer cells (A431) were cultured in 96 well plates in DMEM medium for 12 hours and treated cells with different concentration *i.e.*, 1, 3, 10, and 30 μM of **MeOIstTmor**, **MeOIstDmMor, MeOIstMor, MeOIstDm**, **MeOIstMet** and **MeOIstEth** respectively and incubated for 72 h as shown in Fig. 42 A, B, C and D respectively. All the synthesized compounds showed high to moderate inhibitory effects toward cell viability. Table 9, shows the IC_{50} value of different synthetic compounds against different cell lines, the compound **MeOIstDmMor** has exhibited broad spectrum activity towards A549 with IC_{50} value 2.52 μM than rest of compounds whereas the compound **MeOIstTmor** has exhibited high anticancer activity against MCF-7 with IC_{50}; 2.93 μM. All the compounds have shown moderate activity towards A431 with IC_{50} ranging from 4.80 to 36.49 μM.

Table 9: Cell viability (μM) against cancer cell lines for 72 h.

Compd↓ Cell lines→	Cancer cell lines (IC_{50}) in μM		
	MCF-7	**A431**	**A549**
1	5.41 μM	6.84 μM	5.64 μM
2	2.93 μM	5.29 μM	6.81 μM
3	4.41 μM	4.80 μM	2.52 μM
4	7.41 μM	7.25 μM	3.55 μM
5	8.26 μM	8.09 μM	14.54 μM
6	6.66 μM	36.49 μM	6.54 μM

Cells were seeded at a density of 3000-4000 cells/well in a 96 well plate and incubated at 37˚C for 24 h. Then, the medium was removed, and freshly prepared solutions of the compounds were added (Control, 0.3 μM, 1μM, 3μM, and 10 μM). After a 72h

treatment, crystal violet assay was performed. A, B, C, D shows the effect of **MeOIstTmor**, **MeOIstDmMor**, **MeOIstMor** and **MeOIstDm** on different cell lines respectively. Data are represented as mean ± SD of three independent experiments. With an IC_{50} of 2.93 µM compared to other compounds, the compound **MeOIstTmor** demonstrated strong anticancer activity against MCF-7.

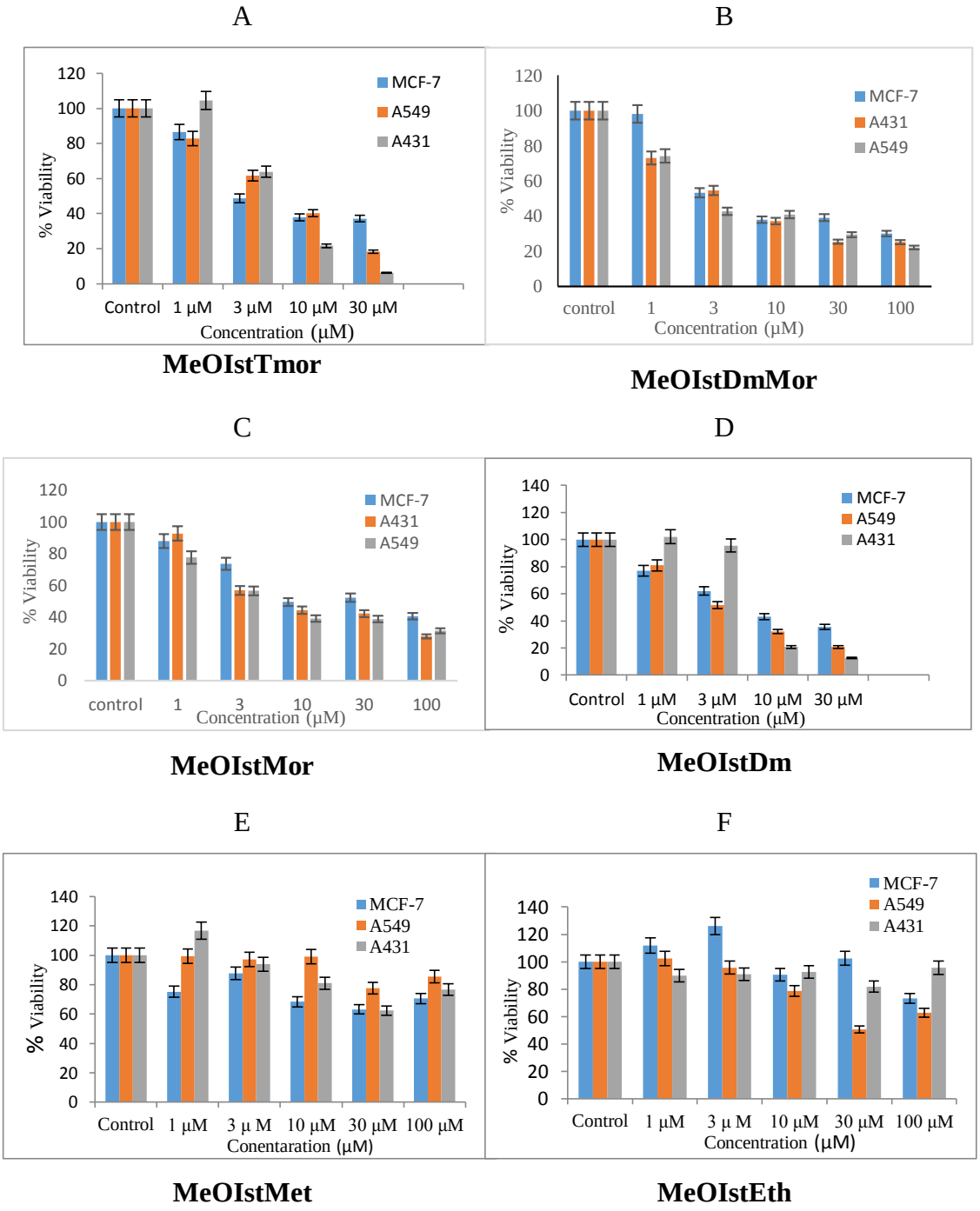

Figure 42: Cell viability assay synthetic compounds with different concentration.

Out of screened compounds for their effects in cell viability in different cancer cell lines **MeOIstDmMor** showed a better antiproliferative effects against the A431 cell line, it

was selected for further studies. To determine the ability of the cells to form colonies in presence of **MeOIstDmMor** in a dose dependent manner. A431 cells were seeded in six well plates with low numbers of 3000 cells/well and treated compound in different concentrations (C, 0.3, 1, 3, and 10 µM), every after 72 h fresh media was added with compound. After two weeks of incubation, it is observed that **MeOIstDmMor** inhibit the size and number of colonies in dose dependent manner (Fig. 43 A and B). The colonization of cell was inhibited 100% above 3 µM as compared to control after two weeks.

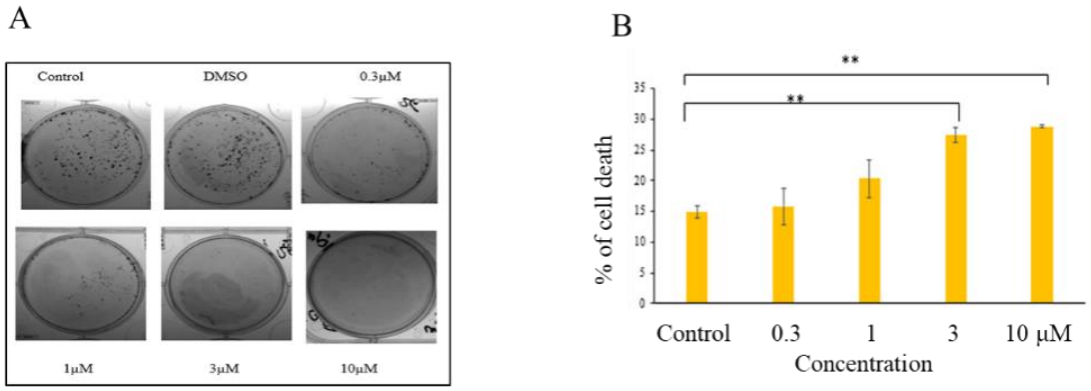

Figure 43: Colony formation assay and flow cytometric analysis of apoptosis by propidium iodide (PI) staining.

The number of colonies drastically decrease as compare to that of control with compound treatment, however the ability to formed colony has completely inhibited in 3 µM and 10 µM of concentration.

To analyze the effect on cell death of A431 cells by flow cytometry assay using propidium iodide staining, cells were treated in different concentrations, *i.e.*, control, 0.3 µM, 1µM, 3µM, and 10 µM of **MeOIstDmMor**. As shown in Fig. 43, in comparison with the control, treatment with **MeOIstDmMor** led to an increase in apoptotic cell population significantly in a concentration dependent manner, which might be due to DNA damage or other survival stresses induced by **MeOIstDmMor** similar to many other thiosemicarbazone derivatives (Shakya *et al.*, 2019). Furthermore, the effect **MeOIstDmMor** in cell cycle was evaluated, A431cells were treated with a lower dose of **MeOIstDmMor** *i.e.*, control, 0.3 µM, and 1µM. Compared to control significant percentage of cells were arrested in the G0/G1 phase treated with 0.3 µM, and 1µM (Fig. 44 A, B, C, D). It was found that **MeOIstDmMor** changed the profile of the cell cycle with an increase in G0/G1 cell population associated with decline G2/M and S

cell population. This increase in percentage of cells in S-phase arrest might be attributed to irreparable DNA damage (Zhang *et al*., 2008).

A431 cells were seeded in six well plates with low numbers of 3000 cells/well and treated compound in different concentrations (C, 0.3, 1, 3, and 10 µM), every after 72 h fresh media was added with compound for 14 days and crystal violet staining was performed B. A431 cells were seeded at a density of 30,000 cells/well in a 12-well plate and incubated at 37˚ C for 24 h and treated compound in different concentrations of **MeOIstDmMor** (C, 0.3, 1, 3, and 10 µM). After a 72 h PI staining was performed. Data represented as mean ± SD of three independent experiments p**< 0.01, *p<0.05. Bar graph showing the percentage of cell death compared to vehicle control (DMSO).

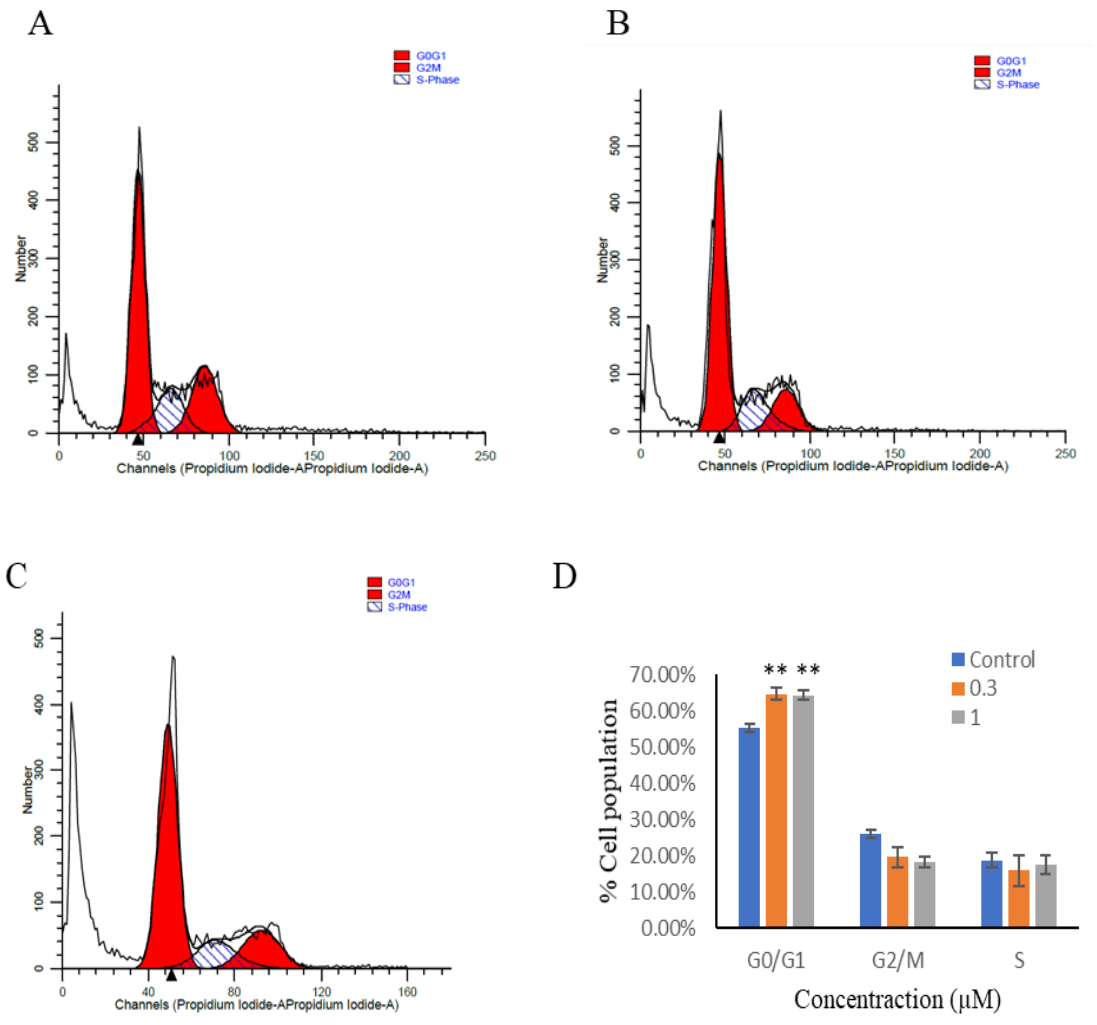

Figure 44: MeOIstDmMor causes G0/G1 cell cycle arrest in A431 cell line (A) control (DMSO). Hectograph representing PI area *vs* number of cells when treated with 0.3 µM (B) and 1 µM (C) of **MeOIstDmMor** were fixed and permeabilized with 80% chilled ethanol and stored for overnight at 4º C. Then cells were washed and subjected to RNase

treatment and PI staining for 30 min at room temperature for flow cytometry to analyze DNA content.

To identify the mechanism of action affected by treatment of **MeOIstDmMor** in skin cancer cell line, examine downstream molecules associated with MAPK signaling path ways that regulate major cellular events including cell proliferation, survival and migration. Improper functioning of MAPK pathways leads to the development and progression of cancer (Shahi *et al*., 2021). Treat **MeOIstDmMor** in A431 skin cancer cell line, downregulate the expression of MAPK pathway molecules c-jun. Where in cancer condition, the highly express c-Jun are associated with cell proliferation and angiogenesis (Shakya *et al*., 2019). **MeOIstDmMor** induced cell death and apoptosis in A431 cells significantly, to understand its effects in the expression of proteins which are responsible for cancer cell proliferation by performing western blot analysis. As shown in Fig. 45 A, the expression level of β-catenin, C-Jun and Akt significantly inhibited after the treatment of cells with **MeOIstDmMor** in concentration dependent manner. It shows that compound **MeOIstDmMor** induce cytotoxic activity with the regulation of β-catenin, C-Jun and Akt which are responsible for cell proliferation, migration and apoptosis in cancer.

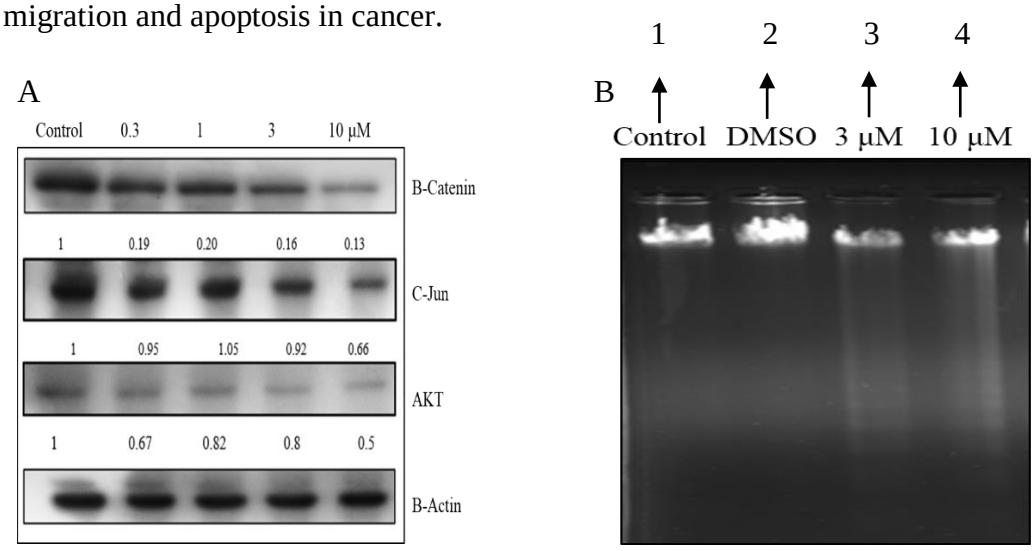

Figure 45: A Western blotting analysis of compound MeOIstDmMor in A431 cell line.

Cleavage of chromosomal DNA into oligonucleosomal size fragment is an integral part of apoptosis. So, to evaluate the role of compound **MeOIstDmMor** in A431cell, DNA fragmentation assay was conducted. As shown in Fig. 45 B that uncut DNA that is control as well as drug control shows distinct band of DNA. However, typical ladder DNA fragments of 180-200 base pairs and multiples thereof on an agarose gel should

be present as the concentration of the drugs increases but, in our experiment, only the formation of DNA smear has been observed as concentration of drugs has increases.

A431 cells were treated with different concentrations of the **MeOIstDmMor** (Control, 0.3 µM, 1 µM, 3 µM and 10 µM) and β-actin was used as loading control. **MeOIstDmMor** inhibit β-Catenin, C-Jun and AKT protein expression in dose dependent manner. **B** Agarose gel showing fragmentation of DNA, Lane 1 contains control DNA sample while lane 2 contain drug control *i.e.*, DMSO. Lane 3 and 4 contain samples for **MeOIstDmMor** 3 µM and 10 µM respectively.

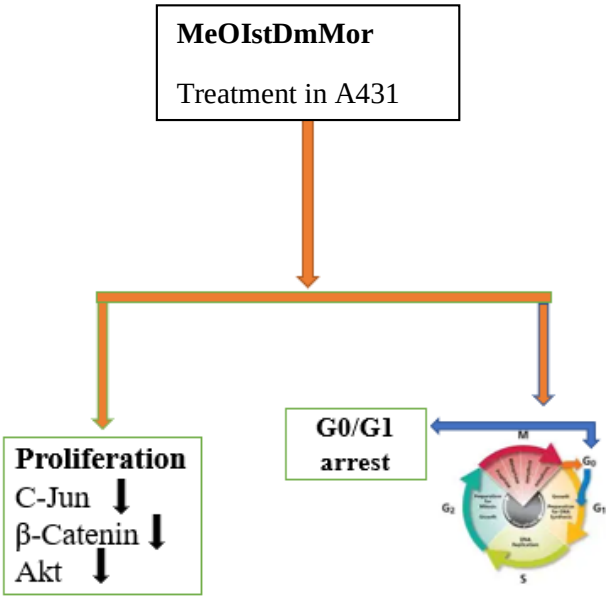

Figure 46: Graphical abstract of MeOIstDmMor mediated anticancer activity in A431 cells lines

4.1.3.2 Molecular docking of compound MeOIstDmMor

Molecular docking studies were carried out by using Molecular Operating Environment (MOE) software package. Three-dimensional (3D) crystal structure of VEGFR2 was obtained from Protein Data Bank (PDB). The accession code for the downloaded enzyme was 4ASD. Before docking studies, the docking protocol was validated by using re-dock method. Native co-crystallized ligand sorafenib was re-docked into the binding site of prepared enzyme. Comparison of the binding orientation was carried out between the re-docked ligand and experimental ligand. The validated protocol with root-mean square deviation less than 2 Å was used for further docking simulations. The 3-D / 2-D interaction plots of native ligand sorafenib are shown in Fig. 47 (a-b). Native

ligand sorafenib forms hydrogen bond interactions with Asp1044, Cys919 and Cys919. While a π-π stacking interaction was also observed between Phe1047 and Phenyl ring of sorafenib. Trifluoromethyl (CF_3) group forms halogen interactions with Ile1044. The synthesized 5-methoxyisatin derivative was also docked into the binding site of VEGFR2 enzyme. Its 3-D / 2-D dimensional interaction plots are shown in Fig. 48 (a-b). The synthesized compound interacts with Asp1046 and Lys868 *via* hydrogen bond interactions. The strength of ligand-enzyme complex was computed in terms of binding energy of the docked poses. The computed binding energy value for native sorafenib was -9.0855 kCal mol^{-1}. While for isatin derivative, it was -6.4015 kCal mol^{-1}. The interaction plots of 5-methoxyisatin derivative are shown in Fig. 49 (a-b). The compound forms two hydrogen bond interactions with Ile1025 and Arg1027.The computed binding energy value for **MeOIstDmMor**, it was -6.3185 kCal mol^{-1}.

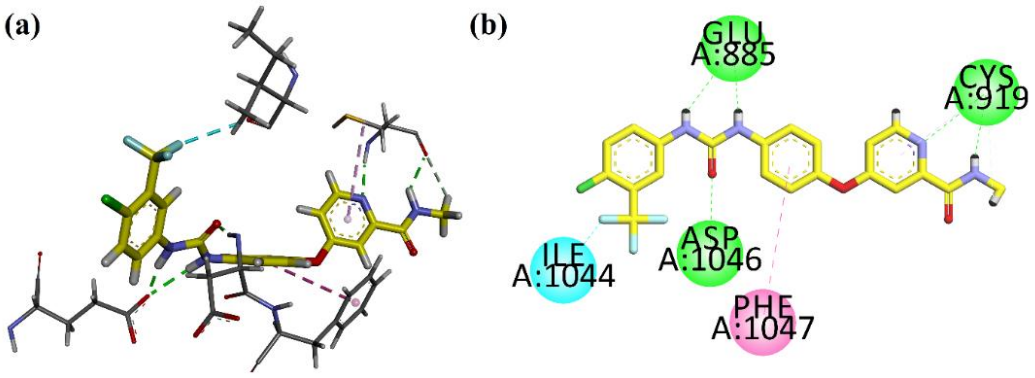

Figure 47: (a-b) 3D and 2D interaction plots of native ligand sorafenib into the binding site of VEGFR2 enzyme (PDB ID = 4ASD)

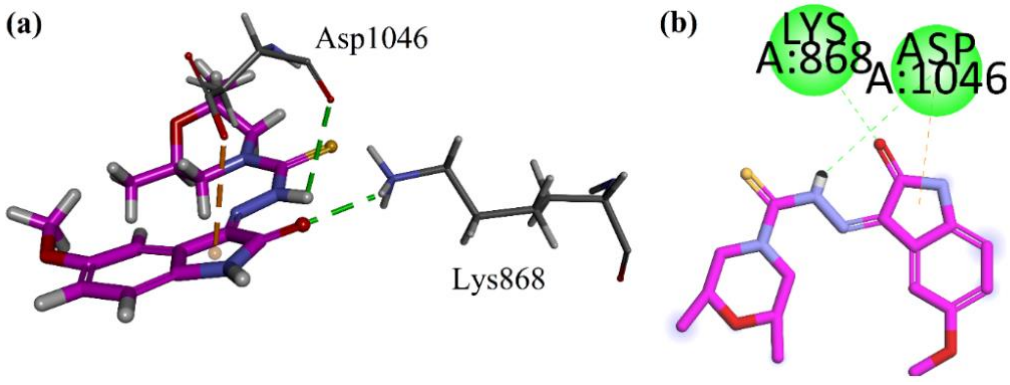

Figure 48: (a-b) 3D and 2D interaction plots of MeOIstDmMor into the binding site of VEGFR2 enzyme (PDB ID = 4ASD)

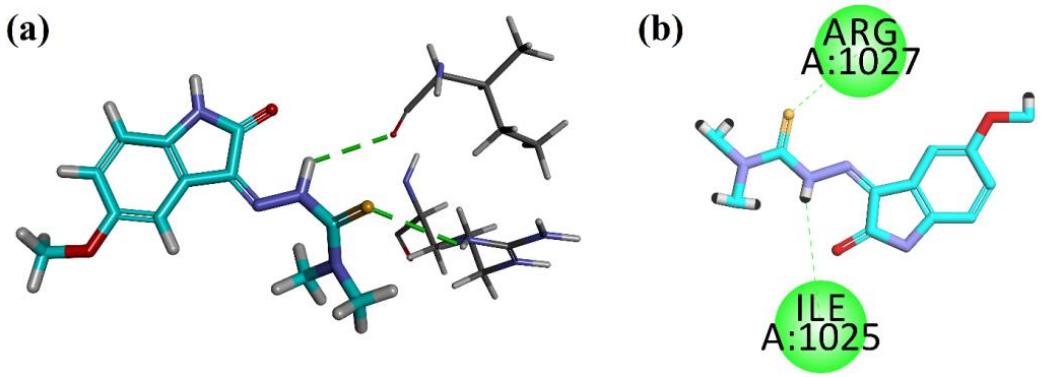

Figure 49: (a-b) 3D and 2D interaction plots of MeOIstDmMor into the binding site of VEGFR2 enzyme (PDB ID = 4ASD)

4.1.4 Molecular docking of compounds MeOIstEth and MeOIstMet

4.1.4.1 Density functional theory

Quantum mechanical calculations in the frame work of density functional theory (DFT) as implemented in an open-source software suite, CP2K was used (Kühne *et al*., 2020). The molecular geometry of the studied compounds was calculated and models were proposed for molecular docking studies. BFGS optimizer was employed in locating the global minima of the molecules. Localized basis sets (DZVP-MOLOPT-SR-GTH) and exchange-correlation functional (BLYP) were used with 300 Ry cutoff of kinetic energy in minimizing the molecular structure up to the energy convergence of 1.0×10^{-6} Ry and the force convergence (MAX and gradient) of 1.0×10^{-4} Ry/Bohr.

4.1.4.2 Molecular docking

ADFR suite was used in accessing the best docked pose of the small molecules with the receptor proteins (Ravindranath *et al*., 2015) The active site was located by an option in the molecular docking program and also from the protein database. In some cases, CASTp server results were also considered for unanimous inferences (Tian *et al*., 2018). The number of independent GA searches were set to 50 with each using up to 10,000,000 evaluations of the scoring functions. This high value ensured that the chances of capturing the best possible docked pose was maximized and instead of local minima of the scoring function, a global minima was reached in a solvated environment. The water map setting with the default weight of 0.60 and entropy of -0.20 were chosen for hydrated docking. The amino acids residues (up to 15) of the receptors at the orthosteric site were assigned to be flexible and the small molecule possessed rotational degrees of freedom during the docking process by default. The box sizes for different

proteins had large variations depending upon the size of the active site. The largest box of size 22 × 28 × 19 points was chosen for the protein with PDB ID of 7BJ6 as an example. The padding of 2.00, grid spacing of 0.375 Å and smoothing of 0.500 were adopted for all the receptors.

Different clusters of docking results related to different searches were obtained and the pose with best affinity was taken for further analysis. The reference ligand was not provided and consequently the RMSD value of each distinct output was not obtained. As a representative case, one of the receptors with its active site occupied by a small molecule ligand is depicted in Fig. 50.

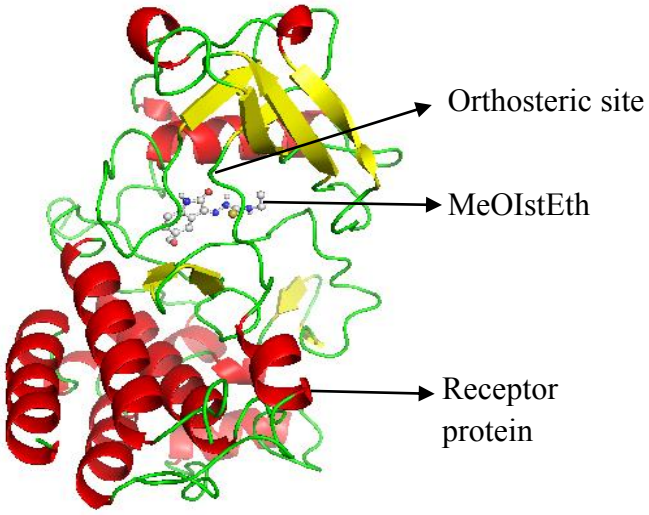

Figure 50: Cartoon representation of a docked pose of MeOIstEth in the active site of protein with PDB ID: 4ASD (carbon gray, nitrogen blue, oxygen red, sulfur yellow, hydrogen cream spheres)

4.1.4.3 Target proteins

The various proteins represented as different PDB ID as receptors of the ligands are tabulated in Table 10. The search for alternate prophylactics of cancerous cell addressing different types of growth factors and other enzymes were considered for spanning a broad range of possible targets. Here, *in silico* approach addresses targeted therapy that deals with the treatment of specific cancer by obstructing the pathways or mutations causing tumor cell proliferation. The receptor with maximum amino acid residue count of 1014 and minimum of 98 were used in this work and the PDB structures were retrieved from RCSB website (rcsb.org) (Berman *et al.*, 2000). The protein structures were cleaned by removing water molecules, ions, metals, ligands and other small molecules. The polar hydrogens were added along with Gasteiger charges.

4ASD is a vascular endothelial growth factor receptor (VEGFR2) with 353 residue count. It is a protein tyrosine kinase receptor that regulate tumor-induced blood vessels formation. 3VHE is a similar target with 359 residue count. 3MJG is a platelet-derived growth factor receptor (PDGFR) and is involved in the development of different types of cancerous cells (Board & Jayson, 2005). Its antagonist could be a good therapeutic candidate. 3MJK is a protein associated with platelet-derived growth factor precursor with 1014 residues. Only A and B chains were considered for molecular docking. 7BJ6 is a murine double minute 2 protein and is considered vital in p53 regulation and cancer cell suppression. 2VTA has been top ranked (fit score of 2.488) by an online program PharmMapper (http://59.78.96.61/pharmmapper) (Wang *et al*., 2017) as potential target (cell division protein kinase 2) in cancer treatment. It consists of a single chain with 298 residues and ligands based on its docking have been currently subjected to clinical trials (Wyatt *et al*., 2008). 6LVK is a fibroblast growth factor receptor 3 used in specially the therapeutics of bladder cancer has been shown to have significant results over VEGFR2 proteins (Kuriwaki *et al*., 2020). This protein is a monomer with 626 residues. These target proteins were selected from different domains and class to encompass broad spectrum in the development of therapeutics against different types of cancer by computational methods. The evaluation of protein structure was performed by Protein Structure Analysis and Verification Server (Mazumder *et al*., 2022) using ERRAT (Colovos & Yeates, 1993) and PROCHECK (Mohan, *et al*., 2013) programs. The results showed acceptable quality of the deposited structures that could be used for molecular docking studies without any additional corrections or modifications.

Table 10: Short details of receptors used in molecular docking

PDB ID ↓	**Receptor class**	**Feature**	**Overall Quality Factor (Disallowed %)**
4ASD	VEGFR2	A monomer with 353 residues	98.64 (0.4%)
3MJG	PDGFR	A hetero-4-mer with 922 residues	82.25 (0%)
3MJK	PDGF precursor	A homo-2-mer with 1014 residues	85.96 (0%)
7BJ6	MDM2 protein	A monomer with 98 residues	100.00 (0%)
2VTA	Cyclin dependent kinase 2	A monomer with 298 residues	88.02 (0%)
3VHE	VEGFR2 kinase domain	A monomer with 359 residues	97.25 (0%)
6LVK	FGFR3	A monomer with 626 residues	98.49 (0%)

4.1.4.4 Test compounds and control drugs

Thiosemicarbazones and their derivatives are nitrogen and sulfur containing compounds having diverse biological and therapeutic values (Sibuh *et al*., 2021). Herein, specifically their anti-cancer potentials have been explored by using computational methods. The molecular structures (ball and stick models) of these two compounds obtained from DFT calculations are shown in Fig. 51. In order to compare the performances of the test compounds, some FDA drugs (Imatinib, Ruxolitinib and Lenalidomide) have also been considered as references (Kim *et al*., 2021). The structures were optimized by molecular mechanics using conjugate gradient algorithm with Newton's method as line search technique. Universal force field was used for the atoms with energy convergence of 10^{-7} units. The molecular structures were obtained as PDB files and the minimization was performed by Avogadro software (Hanwell *et al*., 2012) without any constraints. Their druglikeness, pharmacodynamics and pharmacokinetics have also been studied by computational methods. Imatinib and Ruxolitinib are anti-cancer drugs of class tyrosine kinase inhibitor (antineoplastic agent). Lenalidomide is an immunomodulatory drug used in the treatment of various types of cancer and is an angiogenesis inhibitor. The list of compounds is given in Table 11.

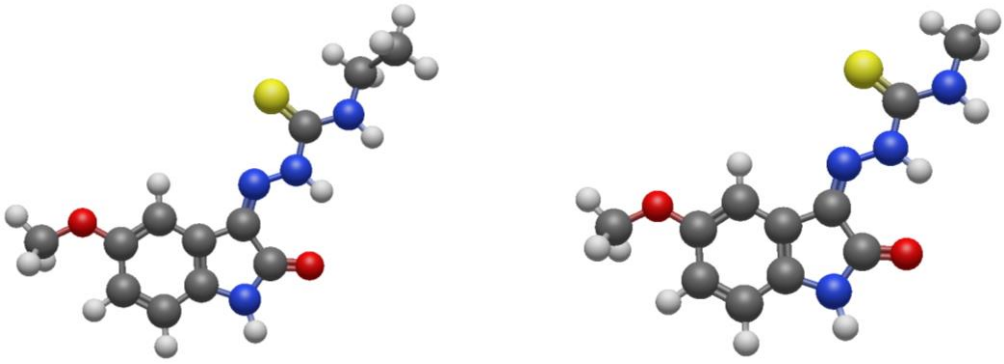

(**a**) (**b**)

Figure 51: Geometry optimized molecular structure of (a) MeOIstEth and of (b) MeOIstMet (Oxygen in red, carbon in gray, sulfur in yellow, nitrogen in blue and hydrogen in shaded white)

Table 11: Short details of compounds and FDA approved drugs2

Compounds↓	Short description, molecular formula
MeOIstEth	Test compound, $C_{12}H_{14}N_4O_2S$
MeOIstMet	Test compound, $C_{11}H_{12}N_4O_2S$
Imatinib	A benzamide, tyrosine kinase inhibitor and apoptosis inducer, $C_{29}H_{31}N_7O$
Ruxolitinib	A pyrrolopyrimidine, Janus kinase inhibitor modulating the immune response, $C_{17}H_{18}N_6$
Lenalidomide	A thalidomide analog blocking the formation of neoplasms, $C_{13}H_{13}N_3O_3$

4.1.4.5 Computational resources

All the codes used were open-source software in this computational work. The visualization and interpretation were also performed using free software (Avogadro and PyMol) easily available in the internet (Hanwell *et al*., 2012, Schiffrin *et al*., 2020). A multi core Intel CPU machine with 256 GB of memory and 6 TB of storage was used in the calculations. The operating system was Ubuntu 20.04 and Windows 8.1 version.

4.1.5 Results and discussion

4.1.5.1 Druglikeness and pharmacology studies

In order to determine the druglike properties and for ADMET prediction of the test compounds, various parameters were calculated using ADMETlab 2.0 server (Xiong *et al*., 2021). The physicochemical properties are shown as radar plots in Fig. 52 and are self-explanatory. All the parameters lie within the acceptable range (between upper and lower limits) and Lipinski's rule of five is not violated. This verifies the drug likeness and its safety.

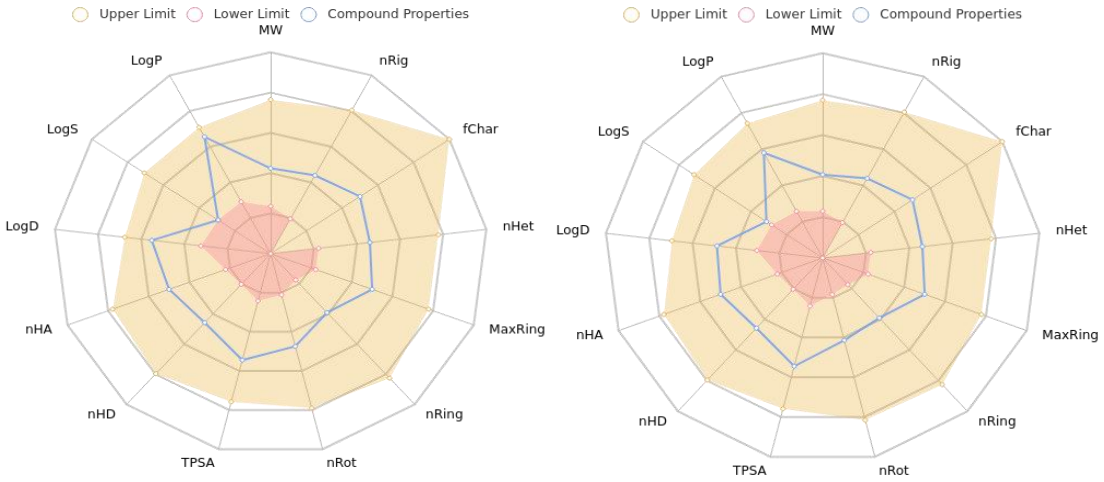

(a) **(b)**

Figure 52: Radar plots of (a) MeOIstEth and of (b) MeOIstMet showing physicochemical data

The selected properties pertaining to adsorption, distribution, metabolism, excretion and toxicity of the drug candidates are shown in Table 12.

Table 12: Adsorption, distribution, metabolism, excretion and toxicity of the drug candidates

Properties	**MeOIstEth**	**MeOIstMet**
Adsorption		
Caco-2 permeability (log cm/s)	-4.78	-4.90
Pgp-inhibitor	Very low probability	Very low probability
Pgp-substrate	Very low probability	Very low probability
Human intestinal absorption	10% probability	10% probability
Distribution		
Plasma protein binding	0.999	0.995
VD (L/Kg)	3.84	1.34
BBB Penetration	Low	Low
Metabolism		
CYP1A2 inhibitor	High	High
CYP1A2 substrate	High	High
CYP2C9 inhibitor	Medium	Medium
CYP2C9 substrate	High	High
Excretion		
Clearance (mL/min/Kg)	5.95	7.26
$T_{1/2}$	Long	Long

Toxicity		
HERG blockers	Low probability	Low probability
Human hepatotoxicity	70% probability of being toxic	70% probability of being toxic
AMES toxicity	Low probability	Low probability
Skin sensitization	Low probability	Low probability
Carcinogenicity	High probability	High probability
Eye irritation	Low probability	Low probability
Respiratory Toxicity	High probability	High probability

The different parameters show that the test compounds do not possess extreme toxicity and have moderate ADME (Absorption, distribution, metabolism and excretion) profile. This suggests that these compounds could be used as potential drug candidates with caution (carcinogenicity and respiratory toxicity) in further clinical trials.

4.1.5.2 Anticancer properties by graph-based signatures

In order to find biologically active compounds having anti-cancer capability, an online program pdCSM (http://biosig.unimelb.edu.au/pdcsm-cancer) was used (Al-Jarf *et al*., 2021). The smiles notations of the test compounds were taken for job submission and no actual three-dimensional molecular geometry were required. The graph-based signatures as implemented in the algorithm predicts the anti-cancer activity (GI_{50}) against 74 cancer cell lines.

It was found that the test compound **MeOIstEth** was active against breast (MCF-7, MDA-MB-468), leukemia (K-562, P388-ADR), ovarian (OVCAR-4), renal (SN12K1) and small cell lung (DMS-273) cancer cell lines. For **MeOIstMet**, breast (MCF-7, MDA-MB-468, T47D), leukemia (CCRF-CEM, K-562, P388-ADR), ovarian (OVCAR-3, OVCAR-4), renal (SN12K1) and small cell lung (DMS-273) cancer cell lines. Surprisingly, the second compound showed activity in larger number of cases than the first compound despite having lower molecular weight.

It was found that **MeOIstEth** is a potent CDK2 inhibitor with IC_{50} of less than 10 μM and pK_i of 6.11 (CDK2-ligand binding affinity) from kinCSM predictor (https://biosig.lab.uq.edu.au/kin_csm/). **MeOIstMet** is also a potent CDK2 inhibitor with IC_{50} of less than 10 μM and pK_i of 6.099. These findings hint that the test

compounds possess anti-cancer notable properties that is worthwhile for further investigation. Fragmentation of molecules that affects protein phosphorylation is studied by this online program and it has been found that the potential type of inhibition is I for both the compounds.

4.1.5.3 Flexible receptor molecular docking

The data obtained from the flexible receptor molecular docking in hydrated environment of two test molecules two test molecules and three approved drugs (controls) on to various proteins has been tabulated in Table 13. In almost all the cases, the control drugs showed better binding affinities than the two thiosemicarbazones (**MeOIstEth** and **MeOIstMet**). Only in case of the receptor with PDB ID: 2VTA, **MeOIstEth** showed better binding affinity than Lenalidomide. In comparing the binding affinities of **MeOIstMet** with that of **MeOIstEth**, it can be inferred that the former almost always results in weaker binding and thus may not be distinctly favored in the inhibition of protein functioning. Apparently, the molecular weight of ligand seems to be a major factor in determining the interaction strength with the amino acid residues with the minor ones being the type, proximity and frequency of non-covalent interactions. A thorough analysis at the atomic level would ultimately provide exact description of the inherent phenomenon.

Table 13: Binding affinities (kCal/mol) of various chemical compounds and drugs against different receptor proteins (PDB ID) related to malignant tumors

	Mol. Wt.	4ASD	3MJG	3MJK	7BJ6	2VTA	3VHE	6LVK
MeOIstEth	278.33	-8.8	-8.2	-7.4	-6.8	-9.7	-8.7	-8.2
MeOIstMet	264.30	-8.7	-8.1	-7.4	-6.5	-9.1	-8.5	-7.9
Imatinib	493.60	-15.7	-14.9	-9.0	-11.1	-13.1	-13.9	-13.2
Ruxolitinib	306.40	-10.6	-10.1	-8.7	-8.8	-11.4	-10.4	-9.7
Lenalidomide	259.26	-9.7	-9.2	-8.2	-7.8	-9.2	-9.2	-8.4

4.1.5.4 Interactions at the atomic-level

The frequency and proximity of different types of non-covalent interactions between the amino acid residues at the orthosteric site of the protein and the docked ligand determines the strength of the protein-ligand complex. Better binding results in stable complex and the protein would be effectively inhibited resulting in the treatment of the

disease. Hence, the pose of the ligand that forms strong bonding with the residues is the ultimate quest in structure-based drug design strategy (Blaney, 2012) that is cost effective. Many drugs have been discovered using this technique and have circumvented the expensive experimental high-throughput screenings (Batool *et al*., 2019). The receptor flexibility incorporated into the calculation along with that of the ligand's provides the closest resemblance to the realistic models as in biological systems. Fig. 53-59 show the best docked pose of **MeOIstEth** at the active site of the receptor molecules. The plots on the left are 3D representations while those at the right are the 2D projections. The pocket areas with hydrogen bonding donors are purple while the acceptors are green. Since, **MeOIstMet** did not yield distinctly better binding affinities than **MeOIstEth**, its atomic level interactions are not presented in the figures.

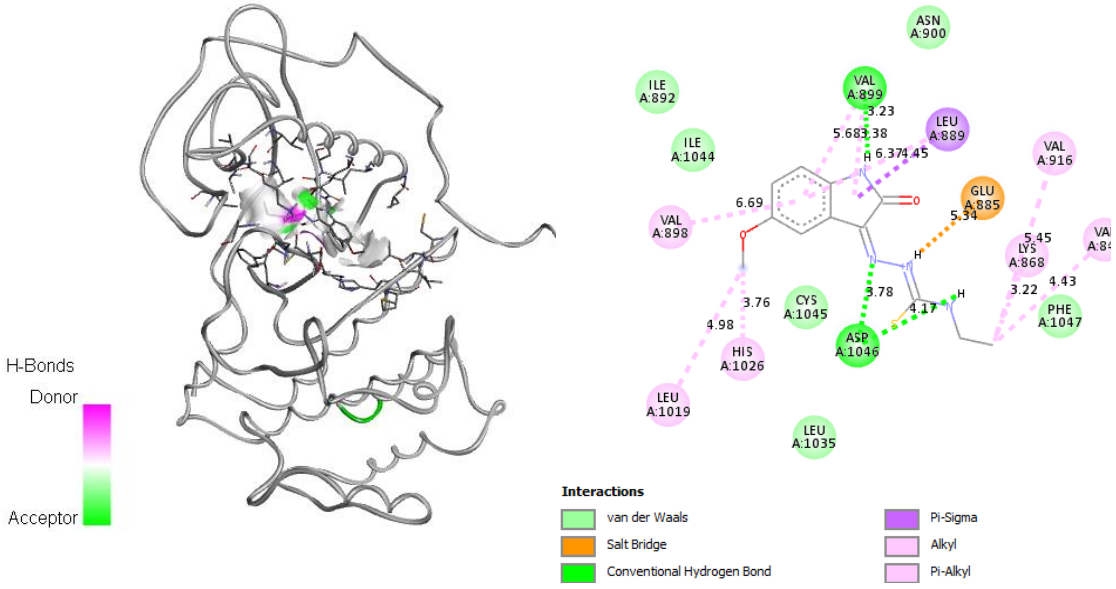

(**a**) (**b**)

Figure 53: Best docked pose of MeOIstEth with 4ASD as (a) 3D with H-bond surface and (b) 2D plots

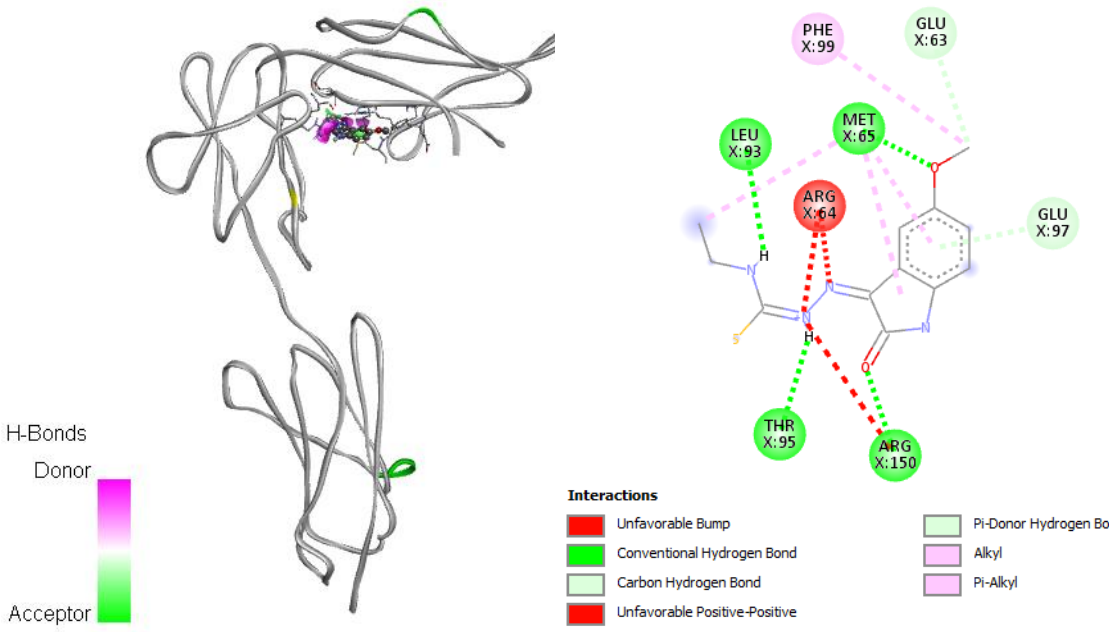

(**a**) (**b**)

Figure 54: Best docked pose of MeOIstEth with 3MJG as (a) 3D with H-bond surface and (b) 2D plots

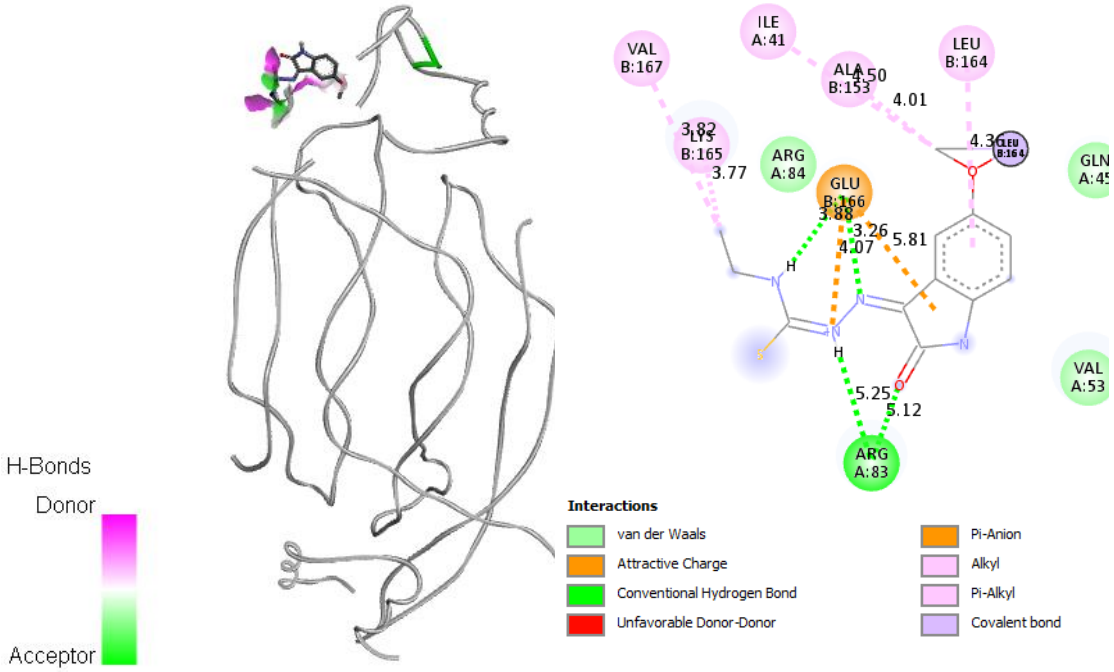

(**a**) (**b**)

Figure 55: Best docked pose of MeOIstEth with 3MJK as (a) 3D with H-bond surface and (b) 2D plots

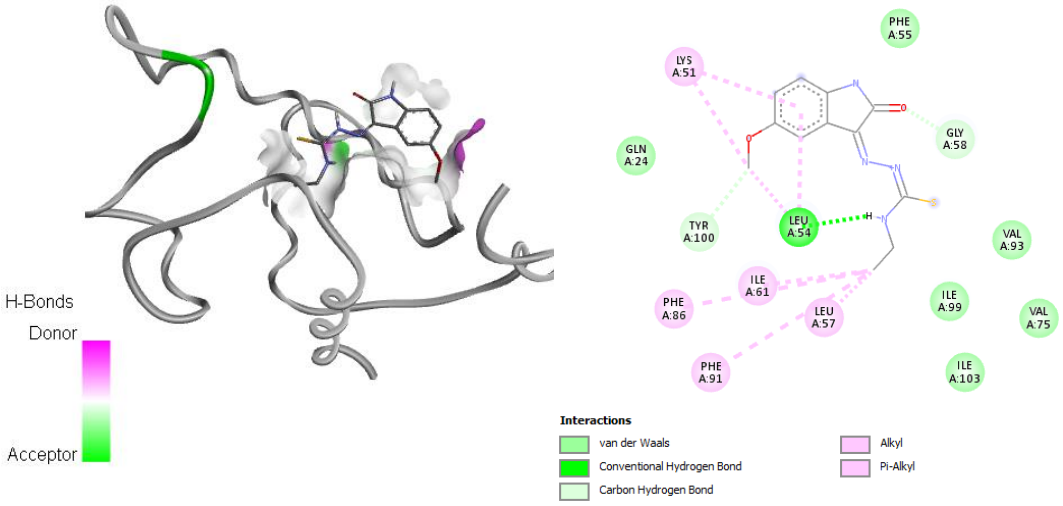

(**a**) (**b**)

Figure 56: Best docked pose of MeOIstEth with 7BJ6 as (a) 3D with H-bond surface and (b) 2D plots

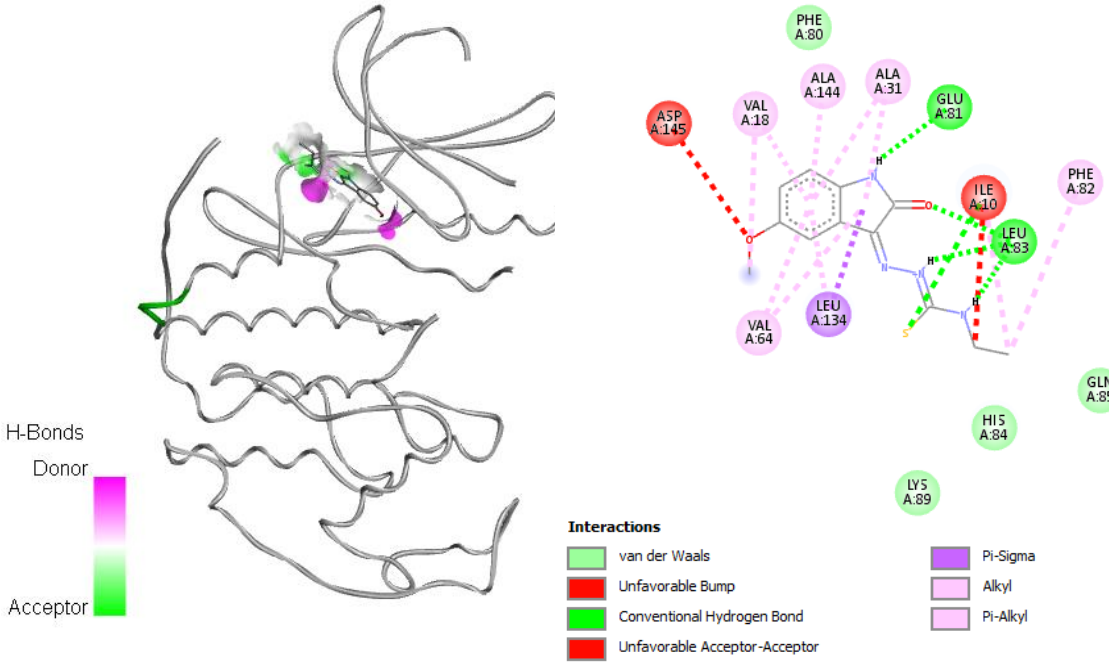

(**a**) (**b**)

Figure 57: Best docked pose of MeOIstEth with 2VTA as (a) 3D with H-bond surface and (b) 2D plots

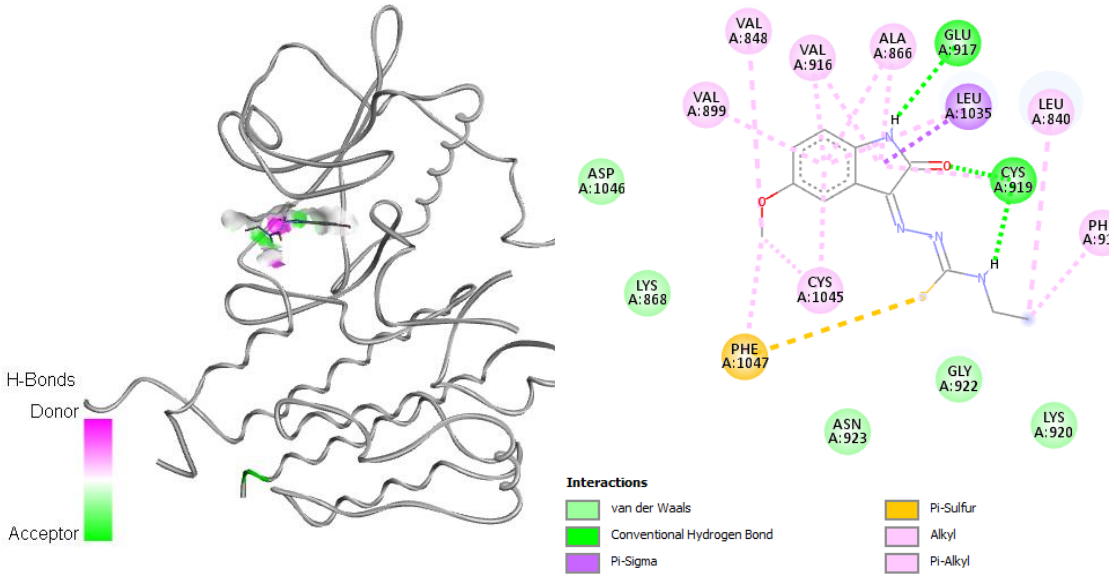

(**a**) (**b**)

Figure 58: Best docked pose of MeOIstEth with 3VHE as (a) 3D with H-bond surface and (b) 2D plots

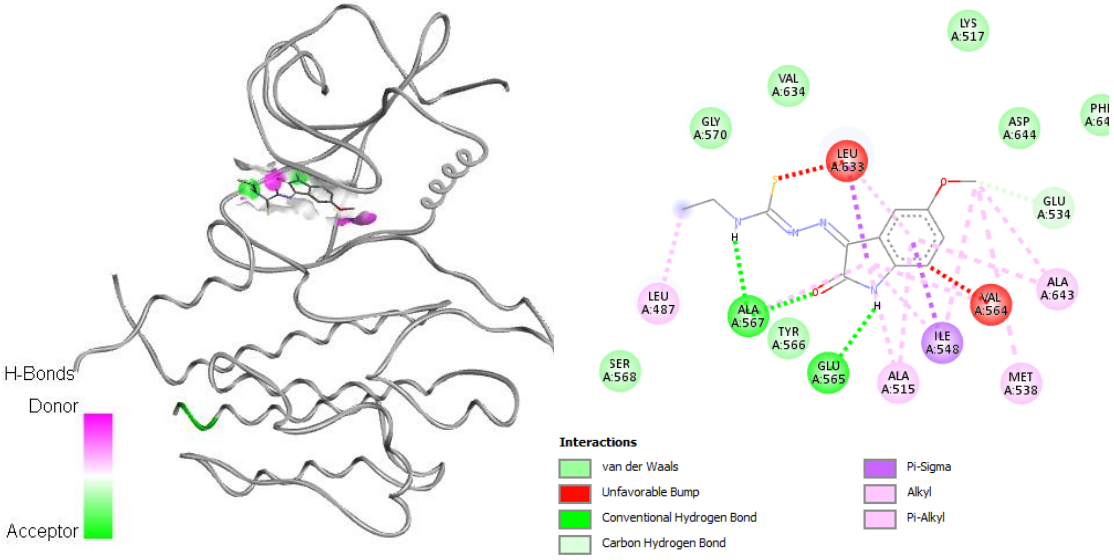

(**a**) (**b**)

Figure 59: Best docked pose of MeOIstEth with 6LVK as (a) 3D with H-bond surface and (b) 2D plots

The occurrences of hydrogen bonding, ionic, unfavorable, pi related and alkyl related interactions with different amino acid residues of various proteins are presented in Table 14. In case of hydrogen bonding, the distances are also shown. Even though some interactions are unfavorable, the presence of other strong non-covalent interactions makes the complex stable in nature. In case of 4ASD, the key amino acid residues

ASP1046, VAL899, LYS868 and GLU885 are involved and have also been reported in case of docking with compounds derived from well-known drugs (Aziz *et al*., 2022) for cancer. In case of 3MJG protein the major interaction is with the residues MET65, LEU93, THR95 and ARG150 with short hydrogen bonding distances. Other key residues THR86 and THR88 have been reported to be involved in interaction with a different compound, indigocarpan (Paramashivam *et al*., 2015). 3MJK protein involves a residue ARG83 with weak hydrogen bonding and other interactions with GLU166, LYS165 and VAL167. However, CYS96, LYS97, SER143, HIS146, ARG148, GLU176 and CYS177 are the key residues reported with Litreol. With titerpenes the key residues are ILE38, HIS39, VAL95, LYS97, THR98, TRP120, PRO121, VAL124, ARG148, VAL152 and VAL160 (Mahajanakatti *et al*., 2014). None of the residues match thus pointing towards different site for docking of the small molecule. The key residue in case of 7BJ6 are LEU54, PHE86, PHE91 and LEU57 as shown in Fig. 56. But other set of key residues GLN72, MET62, GLY58, GLN59 and VAL93 have been reported (Chessari *et al*., 2021) for its native ligand, an isoindolinone. This is due to slight shifting of docking position by the compound. The protein 2VTA has been found to interact with the test compound with the residues VAL18, GLU81, LEU83, ILE10, ASP145, LEU134 and ALA31. All the residues are same as in its native ligand except PHE80, PHE82 and ALA144. 3VHE protein has residues CYS919 and GLU917 involved in weaker hydrogen bonding. CYS919 and LYS920 have been reported as key residues while interacting with Indigocarpan in other studies (Paramashivam *et al*., 2015). In case of 6LVK, there are two amino acid residues GLU565 and ALA567 with strong hydrogen bonding (short distances) with **MeOIstEth** and similar residues have been reported with the native ligand. In most of the cases the involvement of the same amino acid residues suggests that the test compound is bound at the vicinity of the active site of the protein and thus may lead to its effective inhibition.

Table 14: Residues involved in major interactions with MeOIstEth and distances (Å)

PDB ID	Hydrogen-bonds	Salt-bridge/others	Pi related	Alkyl related
4ASD	ASP1046 (4.17, 3.78), VAL899 (3.23)	GLU885	LEU889	LYS868, HIS1026
3MJG	MET65 (1.77), LEU93 (1.95), THR95 (1.88), ARG150 (1.83)	ARG64	GLU63, GLU97	MET65, PHE99
3MJK	ARG83 (5.12, 5.25)	LEU164	GLU166	LYS165, VAL167
7BJ6	LEU54 (2.14)	-	PHE86, PHE91	LEU57

2VTA	GLU81 (4.80), LEU83 (4.23, 5.33), ILE10 (4.32)	ILE10, ASP145	LEU134	ALA31, VAL18
3VHE	CYS919 (3.66), GLU917 (4.03)	PHE1047	LEU1035	ALA866
6LVK	GLU565 (1.88), ALA567 (1.84, 2.08)	VAL564, LEU633	ILE548, LEU633	ALA643, LEU487

Based on the observation of interactions at the methoxy end of the compound, it can be inferred that its replacement with other larger functional groups like butoxy or phenyl rings with diverse substituents (electron withdrawing or even electron donating) may lead to stronger binding at the active pocket. The presence of donors for hydrogen bond formation from the residues of the protein in most of the cases suggests the inclusion of functional group with electronegative elements. This proposition is in accordance to the composition of the FDA approved drug Imatinib which contains multiple nitrogen atoms and has long molecular structure. A trial-and-error method or virtual screening of a library of compounds with multiple types of substituents that may fulfill these criteria may usher to a better lead candidate (also with higher molecular weight) than the control drugs.

4.1.5.5 Future work

The anti-cancer properties of two test compounds (**MeOIstEth** & **MeOIstMet** were investigated by various computational methods using either free software or online servers. One of these compounds hint of being biologically active and showed better binding affinity than one FDA approved drug from flexible receptor molecular docking calculations in a hydrated environment. Atomic level non-covalent interactions were determined in the receptor-ligand complexes and druglikeness along with ADMET predictions made using different programs showed acceptable properties. The compounds require further *in vitro* experiments and could be subjected to further *in vivo* trials.

Further functionalization of the test compounds with suitable groups leading to even better binding with the target receptor may help in improving the efficacy and effectiveness of the proposed compound as a good cancer drug. In order to determine the stability of the complex, the trajectory of the ligand inside the active site, its RMSD and free energy needs to be analyzed. This requires molecular dynamics simulation of the complex with production run of 200 nanoseconds or longer. In other words, the

deviation of docked molecule from the original position with time at certain temperature would help in understanding the change in binding strength and ultimately the efficacy of the proposed drug in inhibiting the regular functioning of the targeted protein.

4.1.5.6 Conclusion

Because of the varying substituents on the N(4)-position of thiosemicarbazone moieties, the anticancer effectiveness of investigated compounds against cancer cell lines MCF-7, A431 and A549 varied slightly.

The synthesized compounds inhibited cell proliferation in the **MCF-7** cell line in the following order:

Compound **2** > Compound **3** > Compound **1** > Compound **6** > Compound **4** > Compound **5**

The synthesized compounds inhibited cell proliferation in the **A431** cell line in the following order:

Compound **3** > Compound **2** > Compound **1** > Compound **4** > Compound **5** > Compound **6**

The synthesized compounds inhibited cell proliferation in the **A549** cell line in the following order:

Compound **3** > Compound **4** > Compound **1** > Compound **2** > Compound **6** > Compound **5**

In both MCF-7 and A549 cancer cell lines, all of the compounds had stronger antiproliferative activity than the positive control (DMSO) but the compound (**3**) and (**2**) showed the best antiproliferative activity against A549 (IC_{50}; 2.52 μM) and MCF-7 (IC_{50}; 2.93 μM) cell lines respectively. Our investigation displayed promising anticancer activity of **MeOIstTmor**, **MeOIstDmMor**, **MeOIstMor** and **MeOIstDm** with IC_{50} of 2.52 to 7.41 μM respectively, which may serve as anticancer drugs for skin cancer in the future. **MeOIstDmMor** significantly inhibit cancer cell proliferation in low dose and inhibited A431 cancer cell colony formation, PI staining was conducted and found to undergo apoptosis in a dosage dependent, with G0/G1 phase cell cycle arrest. Western blotting analysis of **MeOIstDmMor** treated skin cancer cell lines shows

that downstream molecules of MAPK (C-Jun), β-catenin and Akt. Experimental data obtained suggest that **MeOIstDmMor** has a significant cytotoxic effect on skin cancer cell viability, and we conclude that this compound can be used as a therapeutic agent for the treatment of cancer in future.

4.2 SYNTHESIS, CHARACTERIZATION AND ANTICANCER ACTIVITY OF 5-HYDROXYISATIN N(4)-SUBSTITUTED THIOSEMICARBAZONES

4.2.1 IR spectra of 5-hydroxyisatin

The stretching vibrations of the hydroxyl group (-OH) in 5-hydroxyisatin caused broad spectral bands to appear at 3285 cm^{-1}. At 1782 cm^{-1}, stretching vibrations of isatin moeity's *ν*(C=O) groups revealed strong spectral bands. The single and double bond stretching vibrations of the *ν*(C=C) and *ν*(C-C) groups were 1616 and 1491 cm^{-1}, respectively. The C-H bending vibrations were responsible for the absorption peak between 697 and 881 cm^{-1} (Manda, 2013).

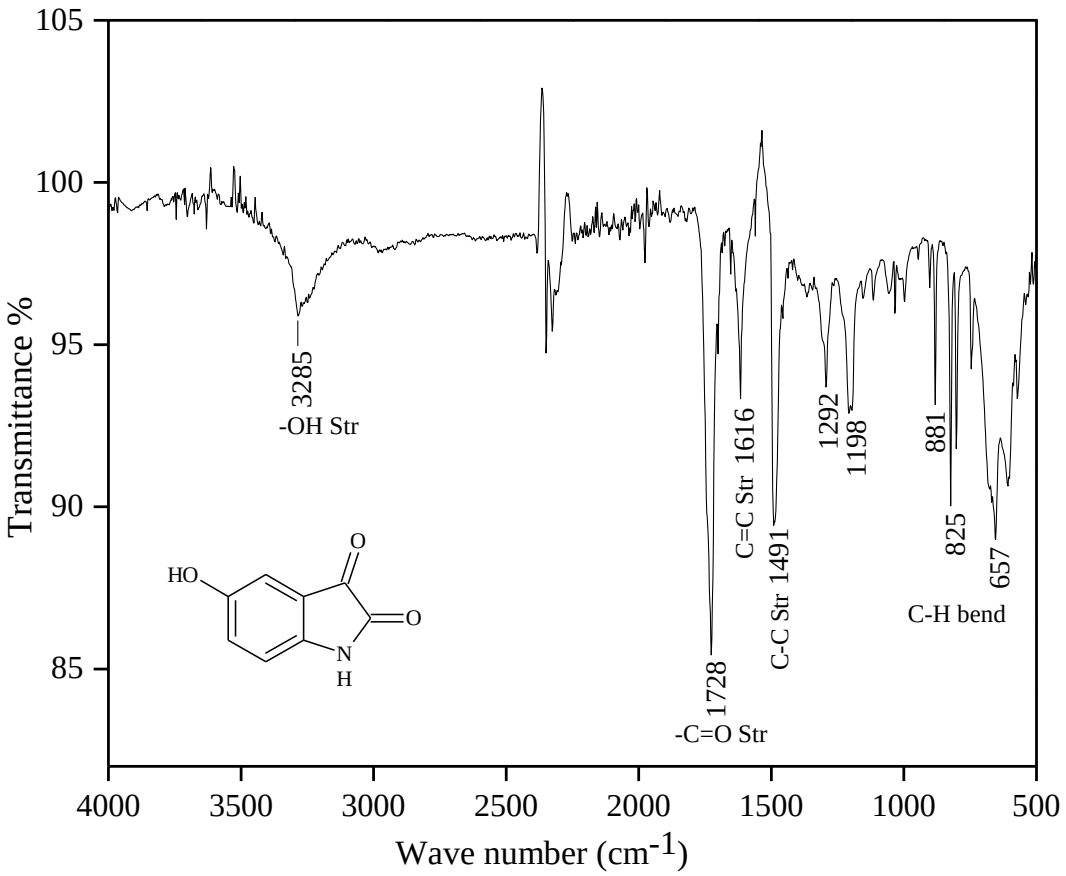

Figure 60: IR spectrum of 5-hydroxyisatin

4.2.2 ESI-HRMS spectra of 5-hydroxyisatin

5-Hydroxyisatin has mass spectral peaks at *m/z* (amu): 164.0351 (164.1382), indicating the presence of $[M+H]^+$, as well as peaks at *m/z* (amu): 186.0170 (186.1102), indicating the presence of $[M+Na]^+$.The fragment ion peak at *m/z*; 130.1594 and *m/z*;116.1184 were detected due to a loss of H_2O_2 and O_2CH_3 group from the 5-hydroxyisatin respectively (Mahmoud *et al*., 2008).

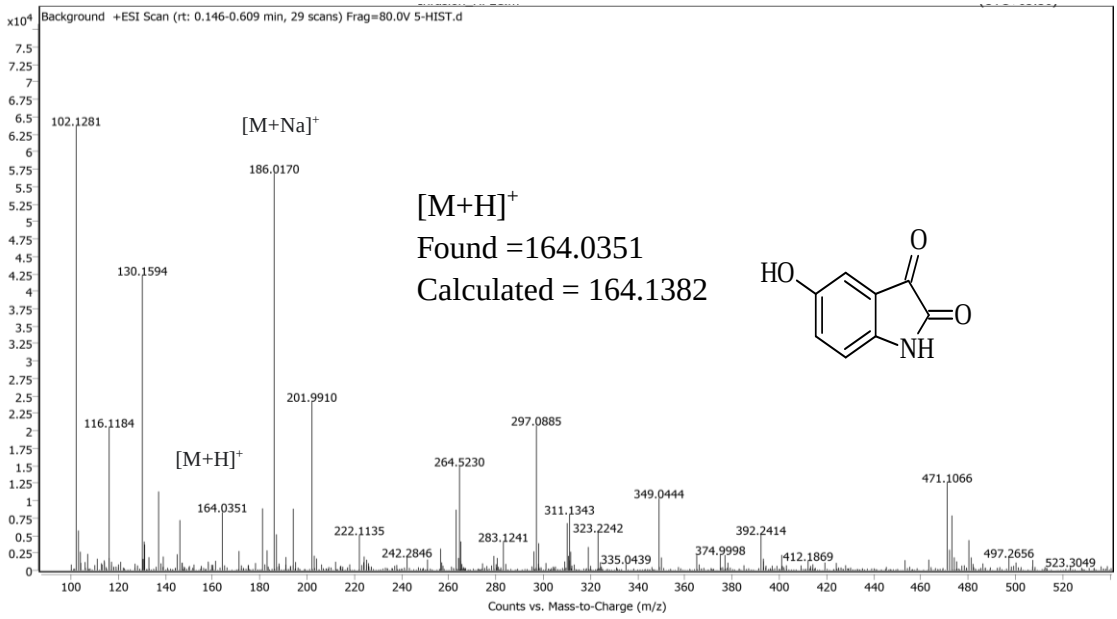

Figure 61: Mass spectrum of 5-hydroxyisatin

4.2.3 General discussion

The N-substituted carbothiohydrazide were synthesized by the method El-Sawaf (El-Sawaf *et al*., 2018) and Scovill (Scovill, 1991). 5-Hydroxyisatin thiosemicarbazones were synthesized by refluxing 5-hydroxyisatin with respective N-substituted carbothiohydrazide in the presence of absolute EtOH and glacial acetic acid (Pervez *et al*., 2018).

Table 15: Physical properties of 5-hydroxyisatin N(4)-substituted thiosemicarbazones (7-16)

Compd	Mol. Formula (Mol. Weight)	Melting point (°C)	Colour	Yields (%)
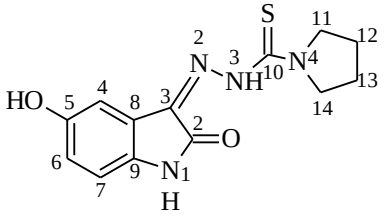	$C_{13}H_{14}N_4O_2S$ (290.34)	170° C	Orange	81%

(**HydIstPyrl/7**)	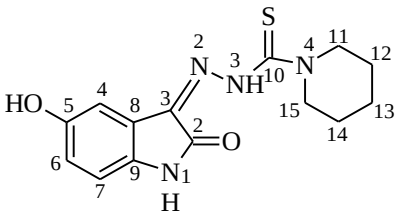	$C_{14}H_{16}N_4O_2S$ (304.36)	248° C	Orange	47%
(**HydIstPip/8**)	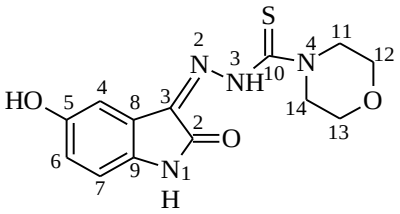	$C_{13}H_{14}N_4O_3S$ (306.34)	270° C	Orange	76%
(**HydIstMor/9**)	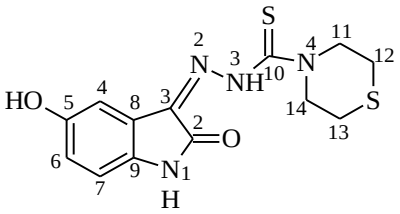	$C_{13}H_{14}N_4O_2S_2$ (322.40)	244° C	Orange	56%
(**HydIstTmor/10**)	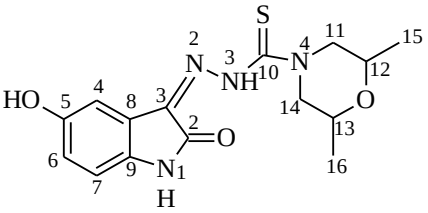	$C_{15}H_{18}N_4O_3S$ (334.39)	266° C	Orange	53%
(**HydIstDmMor/11**)	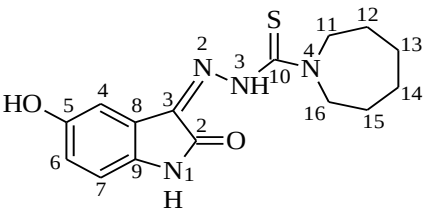	$C_{15}H_{18}N_4O_2S$ (318.39)	268° C	Orange	59%
(**HydIstAzep/12**)					

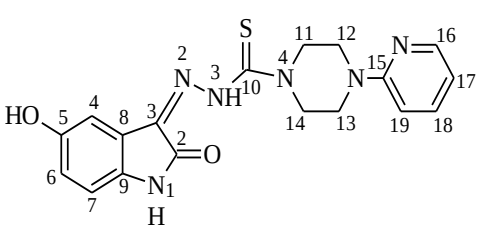 (**HydIstPypz/13**)	$C_{18}H_{18}N_6O_2S$ (382.43)	170° C	Orange	41%
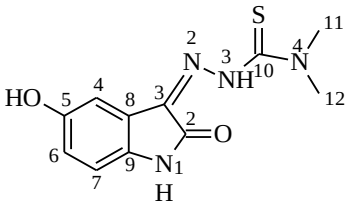 (**HydIstDm/14**)	$C_{11}H_{12}N_4O_2S$ (264.30)	254° C	Orange	85%
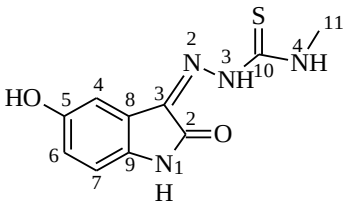 (**HydIstMet/15**)	$C_{10}H_{10}N_4O_2S$ (250.27)	290° C	Orange	72%
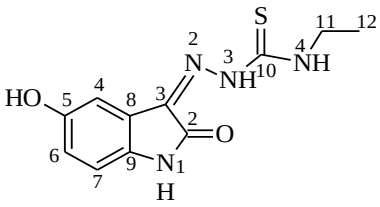 (**HydIstEth/16**)	$C_{11}H_{12}N_4O_2S$ (264.30)	270° C	Orange	49%

The percentage yield (41-85 %) of 5-hydroxyisatin N(4)-substituted thiosemicarbazones were obtained. They were stable in air at room temperature and showed the range of melting point 170-290°C. The thiosemicarbazones **(7, 8, 9, 10, 11, 12, 13, 14, 15, 16)** were slightly soluble in $CHCl_3$; and highly soluble in Me_2CO, EtOH, MeOH, DMF and DMSO. Elemental analysis, FT-IR, NMR, UV-Visible spectroscopy methods, and single crystal x-ray analysis were used to characterize the synthesized thiosemicarbazones. ESI-HRMS mass spectrometry was used to confirm the molecular structures of thiosemicarbazones.

The results of elemental analysis of compounds (7-16) revealed that the experimental data agree with the estimated data within the limits of experimental error.

Table 16: Elemental analysis data of 5-hydroxyisatin N(4)-substituted thiosemicarbazones (7-16)

Compd	C	H	N
7	53.50 (53.78)	4.66 (4.86)	19.23 (19.30)
8	55.26 (55.25)	5.41 (5.30)	18.30 (18.41)
9	50.88 (50.97)	4.74 (4.61)	18.27 (18.29)
10	48.31 (48.43)	4.46 (4.38)	17.39 (17.38)
11	53.68 (53.88)	5.53 (5.43)	16.62 (16.75)
12	56.48 (56.58)	5.77 (5.70)	17.72 (17.60)
13	56.61 (56.53)	4.62 (4.74)	21.86 (21.97)
14	49.88 (49.99)	4.43 (4.58)	21.28 (21.20)
15	47.80 (47.99)	4.01 (4.03)	22.27 (22.39)
16	50.07 (49.99)	4.67 (4.58)	21.18 (21.20)

4.2.4 Spectral studies

4.2.4.1. IR spectra

IR bands of selected functional groups of synthesized compounds **(7, 8, 9, 10, 11, 12, 13, 14, 15, 16)** and are shown in Table 17.

The broad spectral bands due to the intermolecular hydrogen bonded vibrations of hydroxyl group (-OH) of 5-hydroxyisatin were appeared at the region of 3354-3203 cm^{-1} (El-Sharief *et al*., 2019).The symmetric and asymmetric stretching vibrations of indole N-H and azomethine N-H exhibited broad spectral bands in the range of 3189-3103 cm^{-1} in the thiosemicarbazones (Pervez *et al*., 2010).The stretching vibrations of the *v*(C=O) and *v*(C=N) groups of thiosemicarbazones revealed prominent spectral bands in the regions 1697-1668 cm^{-1} and 1548-1531 cm^{-1}, respectively (Balachandran *et al*., 2018). The absence of an IR band at 2600-2500 cm^{-1}, which is indicative of the S-H group, showed that the solid form of thiosemicarbazones existed in thione form (Ramadan *et al*., 2019). Strong IR bands in the 1172-1118 cm^{-1} region were attributed

to the *v*(N-N) stretching vibration of the thiosemicarbazone molecule (Zhang *et al*., 2015). In the range of 1239-1159 cm^{-1} and 792-732 cm^{-1}, two strong absorption bands due to the stretching vibration of *v*(C=S) of thiosemicarbazones were seen (Prabhakaran *et al*., 2008). This is due to the stretching and bending vibration of *v*(C=S). Along with the proton detachment, the CS linkage weakens and the nearby CN and NN bonds get stronger (Sagdinc *et al*., 2009). In the synthesized compounds (**15** and **16**), the stretching vibrations of *v*(C=N) and *v*(C=S) displayed comparable peaks. The stretching vibrations of *v*(O-H) and *v*(N-H) have nearly identical intensities in the compounds (**9** and **10**). The difference in electronegativity made them into insignificant vibrations.

Table 17: Diagnostic bands in the IR spectra (cm^{-1}) of compounds (7-16)

Compd	ν **(O-H)**	ν **(N-H)**	ν **(C=O)**	ν **(C=N)**	ν **(N-N)**	ν **(C=S)**
7	3209 (br)	3123 (m)	1685 (s)	1539 (s)	1157 (s)	1195 (s), 786 (s)
8	3252 (br)	3178 (s)	1683 (s)	1541 (s)	1157 (s)	1203 (s), 785 (s)
9	3211 (br)	3103 (m)	1685 (s)	1544 (s)	1118 (s)	1159 (s), 786 (s)
10	3319 (br)	3172 (s)	1668 (s)	1533 (s)	1153 (s)	1193 (s), 792 (s)
11	3354 (br)	3180 (s)	1670 (s)	1531 (s)	1172 (s)	1239 (s), 771 (s)
12	3211 (br)	3123 (m)	1683 (s)	1535 (s)	1157 (s)	1195 (s), 792 (s)
13	3220 (br)	3151 (m)	1692 (s)	1548 (s)	1159 (s)	1203 (s), 786 (s)
14	3203 (br)	3154 (m)	1695 (s)	1544 (s)	1136 (s)	1172 (s), 786 (s)
15	3282 (br)	3189 (m)	1697 (s)	1544 (s)	1122 (s)	1199 (s), 740 (s)
16	3273 (br)	3149 (s)	1685 (s)	1544 (s)	1130 (s)	1199 (s), 732 (s)

s = strong, m = medium, br = broad

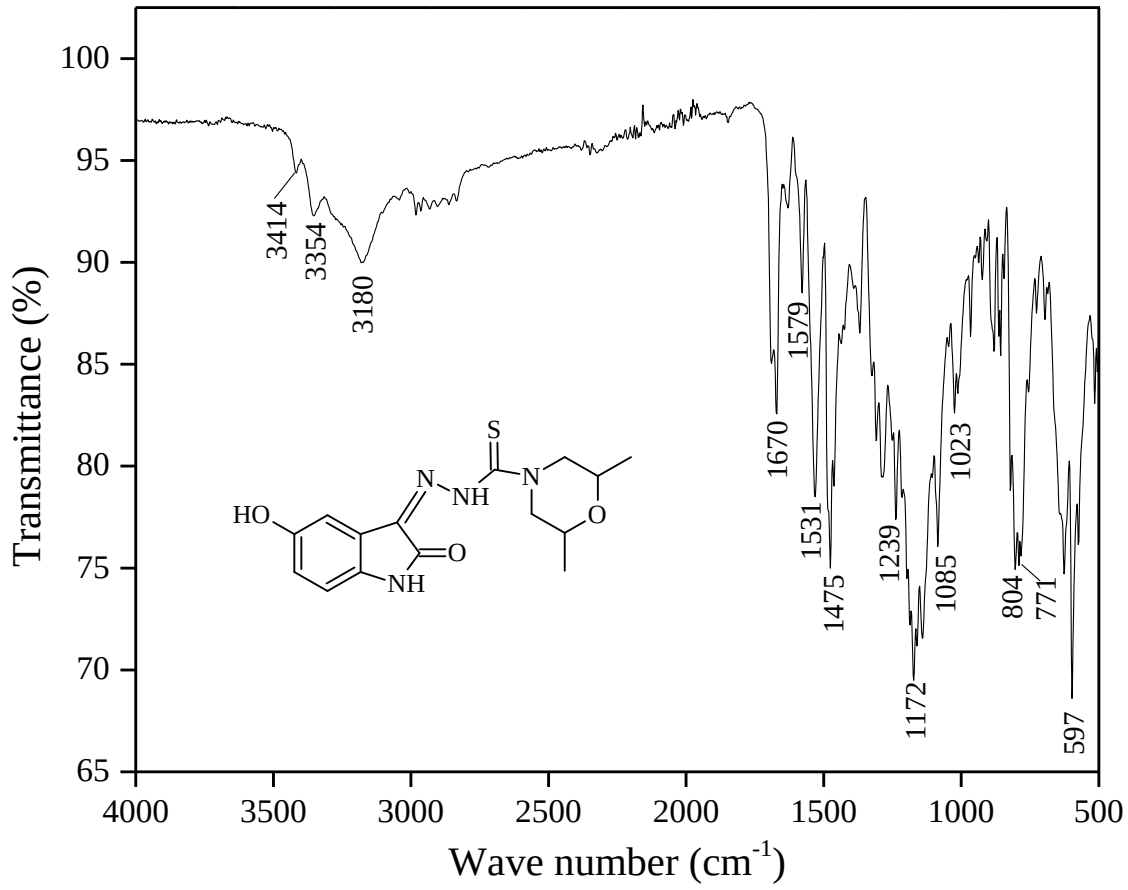

Figure 62: IR spectrum of compound (11)

4.2.4.2 NMR spectra

The ^{1}H NMR spectral values (δ, ppm) of the synthesized compounds (**7, 8, 9, 10, 11, 12, 13, 14, 15, 16**) are tabulated in Table 18

The sharp singlet peaks in the region of δ 13.54-12.59 ppm were attributed to the protons bonded to the most polar group in the spectrum; N(3)H of the thiosemicarbazone moiety suggests that the compounds exist in solution as neutral thione tautomeric form (Muralisankar *et al*., 2017). The peak assigned as N(3)H because of its lower field location (which indicates an intramolecular hydrogen-bonded proton) and because its position is more dependent on the type of N(4) substituent (Konstantinović *et al*., 2008). The sharp singlet peaks attributed to indole N(1)H protons were found in the range of δ 10.99-10.95 ppm (Pervez *et al*., 2017). The synthesized compound's ^{1}H NMR spectra in DMSO-d_6 solution revealed a signal in the δ 9.33–9.25 ppm region that is indicative of an intramolecularly hydrogen-bonded -OH proton (Swathy *et al*., 2016). The isatin C(6)-H was deshielded as a result of the electron-withdrawing inductive effect of the hydroxy group (-OH) at position-5, and

appeared as a doublet at δ 6.94–6.71 ppm, whereas the isatin C(7)–H appeared as a doublet at δ 7.57–6.69 ppm. Due to its electron withdrawing hydroxy group and C=N function, the C(4)-H had a strong deshielding effect and resonated as a doublet at δ 6.94–6.75 downfield. Due to CH_2 coupling, in the thiosemicarbazones N(4)H resonance was detected as a triplet at around δ 9.30 ppm in the compound (**15** and **16**). (Pervez *et al*., 2012). Aromatic protons were detected as doublet peaks in the δ 7.57-6.71 ppm range (Rai *et al*., 2005). The signals of aliphatic C(13)H *i.e.*, (-CH_2) protons were recorded as a triplet toward the downfield region of δ 3.71-1.53 ppm in the compound (**7**-**13**), whereas aliphatic (-CH_3) protons' signals were recorded as a multiplet in the same region δ 1.20-1.15 ppm in the compound (**11** and **16**) (Lahari & Sundararajan, 2020). Due to their involvement in intramolecular hydrogen bonding and consequently low tolerance to solvent interaction, the ^{1}H-NMR values for N(1)H and N(4)H correspond well with the observed values in the compounds (**15** and **16**) (Kohli *et al*., 2014). When compared to compounds (**15**) and (**16**), the N(4) methyl proton as multiplet in compound (**14**) was a little more downfield (δ 3.36 ppm). The morphine C(11,14)H emerged as a triplet at δ 3.97 ppm, while C(12,13)H did the same at around δ 3.71 ppm (El-Sawaf *et al*., 2018). Due to interaction with a nearby CH_2 proton, the CH_2 protons close to the ring nitrogen created a triplet at δ 3.93 ppm (**8**), δ 4.24 ppm (**10**), δ 4.09 ppm (**12**), and δ 4.12 ppm (**13**). The triplet resonance of the CH_2 proton due to coupling with neighboring CH_2 proton was shown at δ 1.88 ppm (**7**), δ 1.66 ppm (**8**), and δ 1.53 ppm (**12**). Due to differences in electronegativity, the CH_2 proton coupling in compounds (**9**) and (**10**) resonated as a triplet at δ 3.71 and δ 2.82 ppm.

Table 18: ^{1}H NMR spectral assignments (δ ppm) of compounds (7-16) (400 MHz, DMSO-d6)

Compd→ Proton↓	**7**	**8**	**9**	**10**	**11**	**12**	**13**	**14**	**15**	**16**
-N(1)H	10.97(s)	10.95(s)	10.98(s)	10.97(s)	10.96(s)	10.96(s)	10.99(s)	10.98(s)	10.89(s)	10.89(s)
-N(3)H	13.33(s)	13.15(s)	13.24(s)	13.13(s)	13.20(s)	13.54(s)	13.26(s)	13.48(s)	12.60(s)	12.59(s)
-N(4)H	-	-	-	-	-	-	-	-	6.76(d)	6.76(d)
-H(4)	6.75(d)	6.75(d)	6.75(d)	6.75(d)	6.76(d)	6.75(d)	6.94(d)	6.76(d)	6.78(d)	6.78(d)
-H(6)	6.75(d)	6.74(d)	6.75(d)	6.75(d)	6.75(d)	6.75(d)	6.94(d)	6.76(d)	6.71(d)	6.71(d)
-H(7)	6.94(d)	6.69(d)	6.91(d)	6.91(d)	6.89(d)	6.93(d)	7.57(d)	6.94(d)	7.07(d)	7.10(d)

-H(11)	3.75(t)	3.93(t)	3.97(t)	4.24(t)	3.68(t)	4.09(t)	4.12(t)	3.36(m)	3.07(m)	3.66(t)
-H(12)	1.88(t)	1.66(t)	3.71(t)	2.82(t)	2.96(t)	1.81(t)	3.71(t)	3.36(m)	-	1.20(m)
-H(13)	1.88(t)	1.66(t)	3.71(t)	2.82(t)	2.96(t)	1.53(t)	3.71(t)	-	-	-
-H(14)	3.75(t)	1.66(t)	3.97(t)	4.24(t)	3.68(t)	1.53(t)	4.12(t)	-	-	-
-H(15)	-	3.93(t)	-	-	1.15(m)	1.81(t)	-	-	-	-
-H(16)	-	-	-	-	1.15(m)	4.09(t)	8.15(d)	-	-	-
-H(17)	-	-	-	-	-	-	6.65(d)	-	-	-
-H(18)	-	-	-	-	-	-	7.75(d)	-	-	-
-H(19)	-	-	-	-	-	-	6.68(d)	-	-	-
-OH	9.29(s)	9.25(s)	9.30(s)	9.30(s)	9.33(s)	9.30(s)	9.30(s)	9.31(s)	9.28(s)	9.26(s)

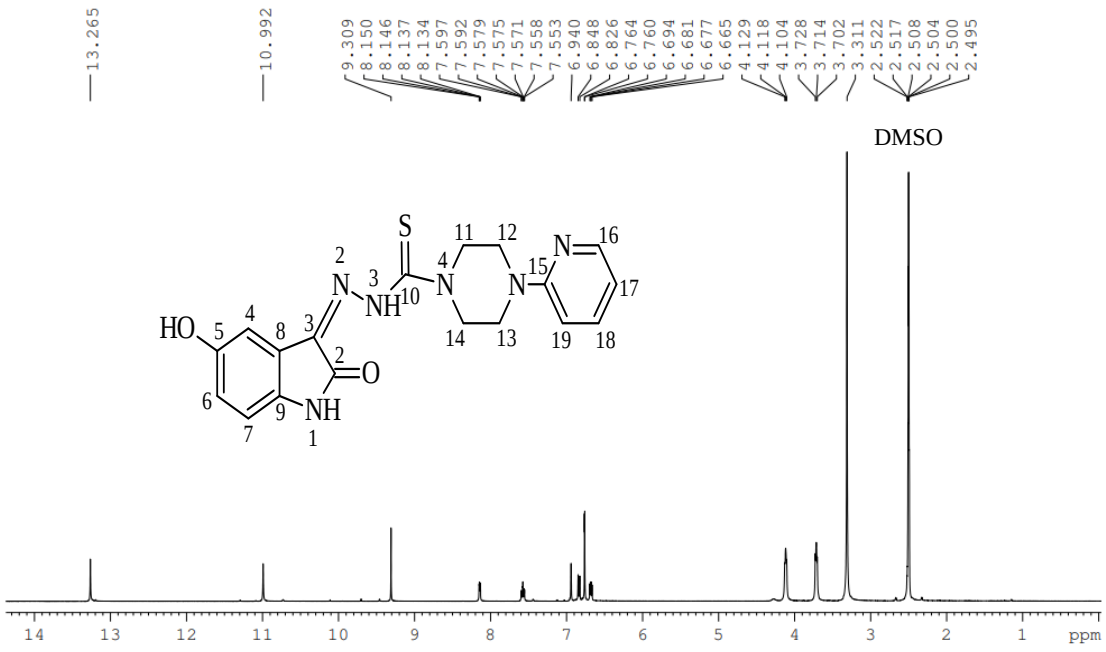

Figure 63: [1]H NMR spectrum (400 MHz, DMSO-d6) of compound (13)

The aromatic protons H (C(4)H, C(6)H, C(7)H, C(16)H, C(17)H, C(18)H, C(19)H) have [1]H NMR signals in the range of δ 8.15-6.65 ppm in compound (**13**). At δ 13.26 ppm and δ 10.99 ppm, it showed two distinct singlets for N-NH of thiosemicarbazone and indole N-H moiety, respectively. Due to CH_2 coupling, N4-H resonance was detected as a triplet at around δ 9.30 ppm. Proton signals of H (C11, C12, C13, C14) in N(4) piperazinyl were detected at the range δ 4.12- 3.71 ppm. In [1]H NMR spectroscopy, pure deuterated DMSO exhibits no peaks. Unfortunately, commercially available

samples are not completely pure, and a residual DMSO-d_5 quartet ^{1}H NMR signal of 2.50 ppm (q) was seen. The ^{1}H NMR results of the synthesized compounds match those of their equivalent counterparts (Singh *et al*., 2021).

The ^{13}C NMR (400 MHz, DMSO-*d6*) spectral values (δ, ppm) of the compounds (**7, 8, 9, 10, 11, 12, 13, 14, 15, 16**) are recorded in Table 19.

The chemical shift values for ^{13}C NMR spectra of synthesized compounds were observed to be quite similar to those of related N(4) substituted thiosemicarbazones. Those thiosemicarbazones had ^{13}C NMR spectra of magnetically non-equivalent carbon atoms at δ 179.53-175.36 ppm, δ 162.91-162.64 ppm, and δ 135.29-134.12 ppm, which were ascribed to the π bonded carbon atoms of C=S, C=O, and C=N groups, respectively (Çavuş *et al*., 2020). The sharp peaks of the sp^2 hybridized carbon atoms, *i.e.* aromatic carbon atoms of isatin and 1-(2-pyridyl) piperazinyl moieties, were found in compounds (**13**) and in compounds (**7, 8, 9, 10, 11, 12, 13, 14, 15, 16**) at δ 153.16-107.07 ppm and δ 153.18-106.87 ppm, respectively (Singh *et al*., 2021). Furthermore, aliphatic carbon atoms (-CH_2) were found to have broad signals in the up field region between δ 65.67 and 23.58 ppm, whereas signals of aliphatic carbon atoms (-CH_3) were found in the range δ 31.30-13.97 ppm (Kopylovich *et al*., 2011). The pyrrolidine ring carbons C(12) & C(13) in the compound (**7**) appeared at δ 25.93 ppm and C(11) & C(14) at δ 53.21 ppm respectively (Muralisankar *et al*., 2016). The ethyl carbons were given credit for two sharp peak (13.97 and 40.13 ppm) in the spectra of compound (**16**) (Balachandran *et al*., 2018). Two methyl carbons C(11) & C(12) in compound (**14**) appeared at a δ value of 40.13 ppm showing magnetically equivalent. The 2,6-dimethyl morpholine ring carbons C (11) & C (14) nearer to the nitrogen appeared at δ 70.91 ppm whereas the carbon C (12) & C (13) nearer to the oxygen appeared at δ 54.81 ppm. In comparison with morpholine and thiomorpholine ring carbons, the carbon nearer to the oxygen were downfield (δ 50.03 ppm) whereas the carbon nearer to the sulphur were upfield (δ 26.54 ppm).

Table 19: ^{13}C NMR spectral assignments (δ ppm) of compounds (7-16) (400 MHz, DMSO-d6)

Compd→	**7**	**8**	**9**	**10**	**11**	**12**	**13**	**14**	**15**	**16**
Carbon↓										
-C(2) *viz.* C=O	162.85	162.72	162.73	162.68	162.72	162.85	162.74	162.91	162.70	162.69
-C(3) *viz.* C=N	134.46	134.12	134.73	134.59	134.63	135.27	134.63	135.29	134.59	134.60
-C(4)	106.94	106.87	107.07	107.06	106.96	106.95	107.07	107.02	107.85	107.97
-C(5)	153.14	153.12	153.16	153.15	153.18	153.15	153.16	153.17	153.05	153.05
-C(6)	111.79	111.81	111.86	111.87	111.90	111.84	113.14	111.86	111.63	111.60
-C(7)	120.86	120.83	120.69	120.68	120.70	120.91	120.73	120.85	120.77	120.76
-C(8)	117.52	117.61	117.82	117.83	117.85	117.54	117.79	117.63	117.84	117.83
-C(9)	133.96	134.09	134.25	134.29	134.28	134.01	134.24	134.04	132.15	132.20
-C(10) *viz* C=S	175.36	178.64	179.53	179.50	179.20	178.42	179.35	178.97	177.65	176.67
-C(11)	53.21	51.01	65.67	52.89	70.91	40.13	49.01	40.13	31.30	40.13
-C(12)	25.93	25.51	50.03	26.54	54.81	26.58	43.68	40.13	-	13.97
-C(13)	25.93	23.58	50.03	26.54	54.81	26.58	43.68			
-C(14)	53.21	25.51	65.67	52.89	70.91	26.58	49.01			
-C(15)	-	51.01	-	-	18.37	26.58	158.26			
-C(16)	-	-	-	-	18.37	40.13	147.49			
-C(17)	-	-	-	-	-	-	111.86			
-C(18)	-	-	-	-	-	-	137.61			
-C(19)	-	-	-	-	-	-	106.93			

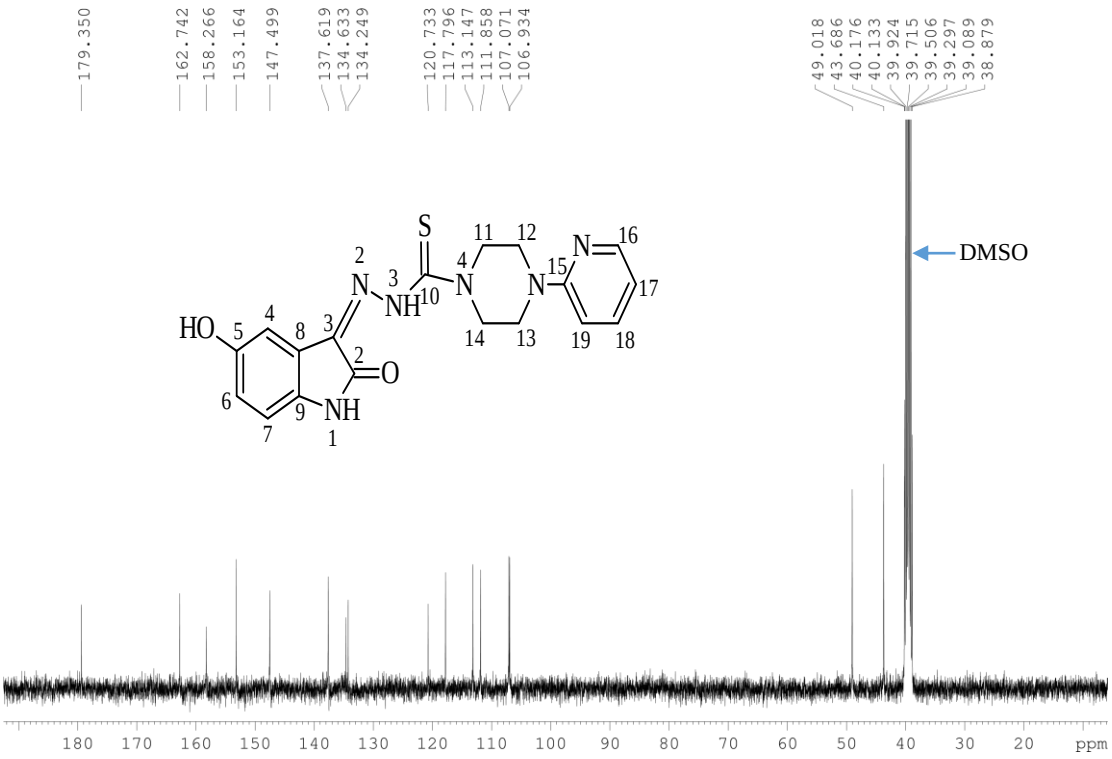

Figure 64: ^{13}C NMR spectrum (400 MHz, DMSO-d6) of compound (13)

In Compound (**13**), the ^{13}C NMR signals present at δ 179.35, δ 162.74 and δ 134.63 ppm were ascribed to sp^2 hybridized carbon atoms of C=S, C=O and C=N groups, respectively. The signals of aromatic carbons (sp^2) were observed in the region δ 153.16-106.93 ppm. The spectra of -CH_2 carbons (sp^3-C) of N(4) substituent were appeared at δ 49.01-43.68 ppm.

4.2.4.3 Mass spectrometry

High-resolution mass spectrometry uses mass spectrometers with high mass accuracy and resolution (HRMS). These instruments can be used to determine elemental compositions, identify unknowns, and distinguish between various compounds having the same nominal mass. By using HRMS, the mass to charge ratio (*m/z*) can be calculated to several significant digits. The protonated molecular ion $[M+H]^+$ peak of the synthesized molecules was verified by high resolution mass spectroscopy. The "improved" resolution makes it possible to measure "exact masses" as opposed to nominal masses. The main clinical uses for high resolution mass spectrometry have been Time-of-Flight (TOF) mass spectrometers and Orbitrap mass spectrometers. To achieve high mass resolution, TOF devices precisely measure the time it takes for ions to go down a flight tube and hit a detector (Crutchfield & Clarke, 2014).

The mass spectral data of the synthesized compounds **(7, 8, 9, 10, 11, 12, 13, 14, 15, 16)** obtained by the high-resolution electron spray ionization mass spectrometry (ESI-HRMS) measurements are summarized in Table 20.

In the mass spectrometry the formation of positive or negative ions as the fragments of the compounds depend on the sign of the applied electrical field. High resolution MS can offer *m/z* peak up to 4 decimal digits. The thiosemicarbazones **(7, 8, 9, 10, 11, 12, 13, 14, 15, 16)** exhibited mass spectral peaks at *m/z* (amu): 291.3438 (calc., 291.3488), 305.3634 (calc., 305.3753), 307.3479 (calc., 307.3482), 323.4084 (calc., 323.4138), 335.3912 (calc., 335.4013), 319.3995 (calc., 319.4019), 383.4323 (calc., 383.4474), 265.3033 (calc., 265.3115), 251.2752 (calc., 251.2849) and 265.3099 (calc., 265.3115) respectively thus by showing the existence of $[M+H]^+$ (Singh *et al*., 2021).

Table 20: Mass spectrometric data of compounds (7-16)

	***m/z* $[M+H]^+$**	
Compd	**Found**	**Calculated**
7	291.3438	291.3488
8	305.3634	305.3753
9	307.3479	307.3482
10	323.4084	323.4138
11	335.3912	335.4013
12	319.3995	319.4019
13	383.4323	383.4474
14	265.3033	265.3115
15	251.2752	251.2849
16	265.3099	265.3115

All the obtained mass spectral data of compounds **(7, 8, 9, 10, 11, 12, 13, 14, 15, 16)** are in agreement with the calculated spectral data of those compounds of proposed molecular structures.

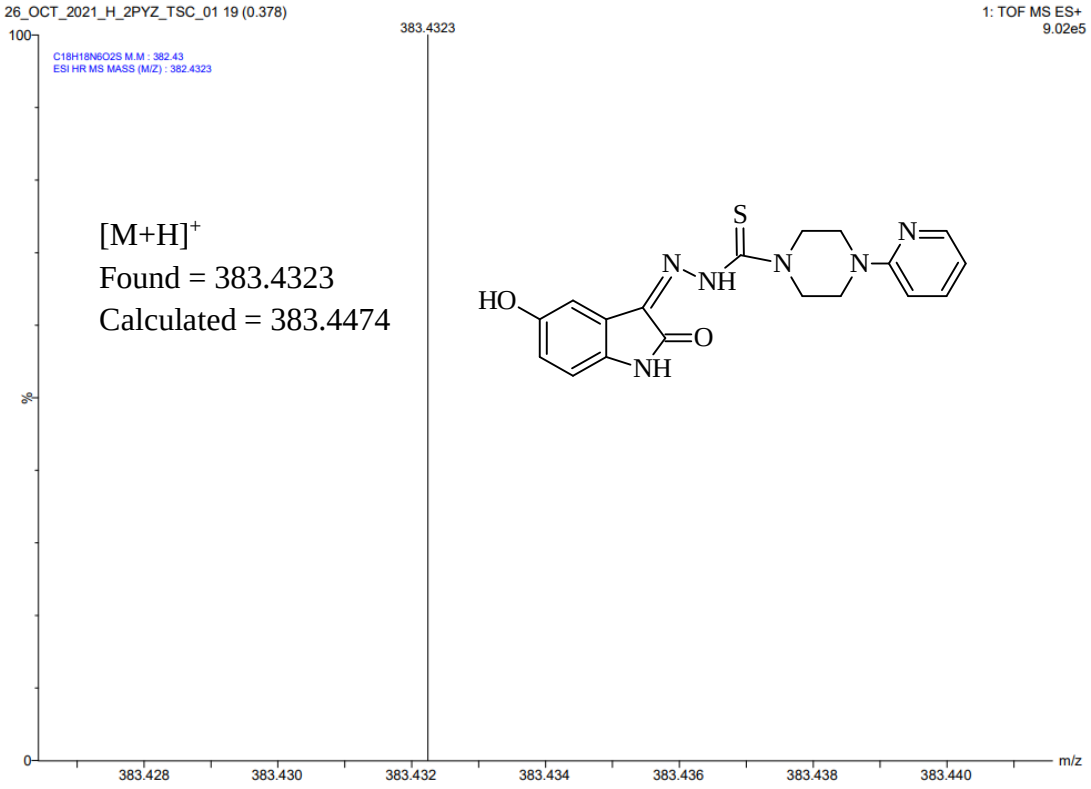

Figure 65: ESI-HRMS of compound (13)

4.2.4.4 UV-Visible spectra

The electronic spectra of the compounds **(7, 8, 9, 10, 11, 12, 13, 14, 15, 16)** were recorded in EtOH and MeOH solutions at the range of 600-200 nm to give the confirmations for the characteristic absorptions of non-bonded electrons and π electrons of aromatic rings. The synthesized compounds showed the broad absorption bands in the UV-Visible region due to the electronic transitions of π→π*, n→π*. In thiosemicarbazones the absorption bands resulted due to the n→π* electronic transitions of >C=O, >C=N and –NH-C=S were observed as two prominent peaks (range 282-286 nm and 348-359 nm) (Türkkan *et al.*, 2017). Since the thiosemicarbazone portion of the molecule is covered by the more intense π→π* type, no transitions that could be classified as an n→π* type were seen in the spectra (Kandemirli *et al*., 2009).

The bands due to the n→π* electronic transitions were found in higher wavelength than that in π→π* electronic transitions because the former transitions absorb lower energy than that of later transitions. In the compounds **(7, 8, 9, 10, 11, 12, 13, 14, 15, 16)** absorption band appeared in the wavelengths region 348-359 nm ascribed to then n→π* electronic transitions of >C=O and >C=N groups (Konakanchi & Gondru, 2019). Due

to the electronic transition of C=O, C=S, and C=N, there was no discernible difference in the absorption band, and they exhibited as shoulder peaks in the same location.

Table 21: UV-Visible spectroscopic data of compounds (7-16)

Solvent	**MeOH**	**EtOH**	**MeOH**	**EtOH**	**MeOH**	**MeOH**	**EtOH**	**MeOH**	**MeOH**	**MeOH**
Compd→ $\lambda_{max(nm)}\downarrow$	**7**	**8**	**9**	**10**	**11**	**12**	**13**	**14**	**15**	**16**
n→π* (nm)	350	351	351	354	355	350	355	348	357	359
π→π* (nm)	285	286	286	283	285	287	284	286	285	284

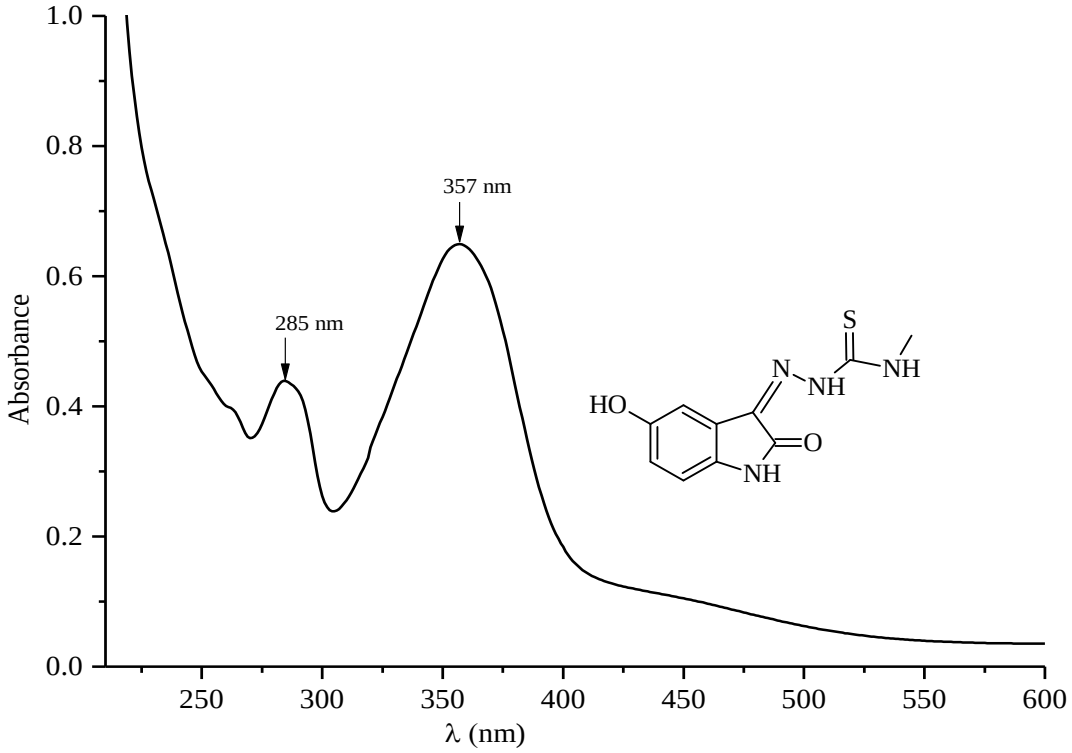

Figure 66: UV-Visible spectra of compound (15)

The compound (**15**) showed the absorption band at 285 nm attributed to the π→π* transition of aromatic rings but that at 357 nm attributed to n→π* electronic transitions of azomethine (>C=N), carbonyl (>C=O) and thioamide (-NH-C=S) groups. The sharp broad peak at 357 nm appeared due to the presence of methyl group at N(4)-position in thiosemicarbazones (Muralisankar *et al*., 2017).

4.2.4.5 Single crystal X-ray crystallographic study

Using single crystal X-ray diffraction, the crystal structure of (Z)-N-(5-hydroxy-2-oxoindolin-3-ylidene)morpholine-4-carbothiohydrazide (**HydIstMor/9**) was established. The orthorhombic Pbca space group promoted the compound (**9**).

A total of 17616 compound (9) reflections were recorded, of which 2433 were declared to be noticed ($I > 2\sigma(I)$). The residual values that generated are as follows: For all 195 parameters, R_1 = 0.0553, wR_2 = 0.1480, and R_1 = 0.0998, wR_2 = 0.1779. The C-S bond length of 1.677 (3) Å indicates that the deprotonated thiosemicarbazone structure evolves considerably from thione to thiol. A correlation of C-N and N-N bond length with typical single and double bond lengths [C(1)-N(1) 1.356 (4) , C(2)-N(1) 1.431 (4), C(8)=N(2) 1.289 (4), C(9)-N(3) 1.359 (4), C(9)-N(4) 1.344 (4), C(10)-N(4) 1.469 (4), N(2)-N(3)1.361(4) Å] exposes that charge transfer of electrons occurs throughout the thiosemicarbazone skeleton (Matesanz *et al.*, 2016). The crystal structures of compound (**9**) revealed an intramolecular hydrogen link between N-H and carbonyl oxygen. The compound (**9**) contains an intramolecular hydrogen bond between the N(1)-H(1) proton and O1 [2.896 (4) Å], generating a six-membered ring and preferring the Z-isomer over the imine C=N bond. The presence of 109.2° bond angle confirms the sp^3 hybridization of morpholinyl oxygen (C12-O3-C11). The torsional angles in (**9**) are 0.5 (7) O1-C1-C8-N2, 179.2 (4) N1-C1-C8-N2, 4.5 (4) N2-N3-C9-S1, -174.9(3) N2-N3-C9-N4, -179.9(3) C10-N4-C9-S1 (Muralisankar *et al.*, 2016).

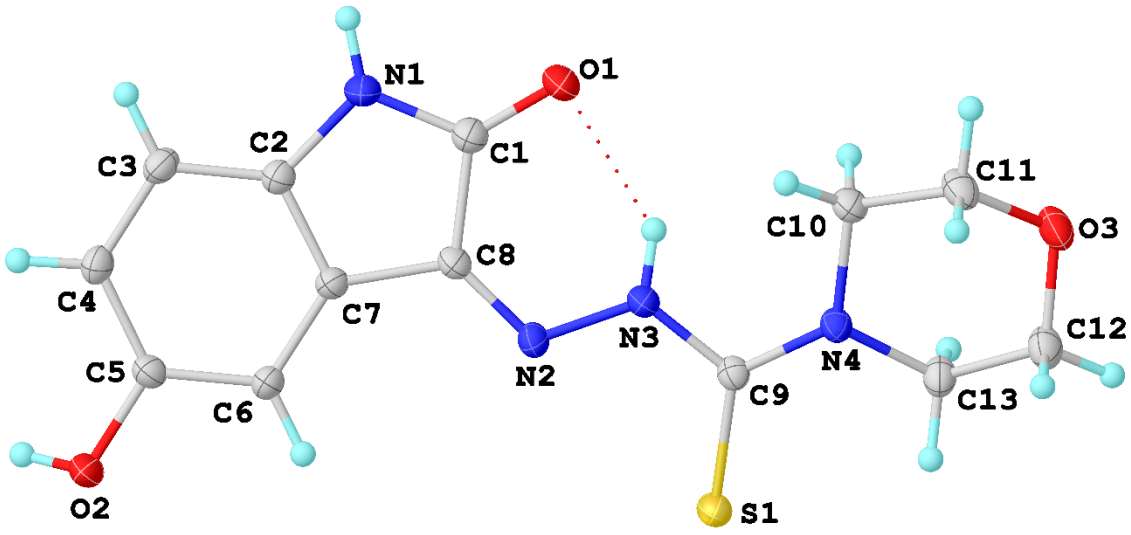

Figure 67: ORTEP diagram of compound (9) drawn in 20% thermal probability ellipsoids showing atomic numbering scheme.

Single crystals of (*Z*)-*N*-(5-hydroxy-2-oxoindolin-3-ylidene)azepane-1-carbothiohydrazide (**HydIstAzep/12**) were selected and analyzed on a Bruker D8 VENTURE diffractometer with PHOTON II detector diffractometer.

For compound (**12**), a total of 35687 reflections were recorded, of which 3870 were declared to be seen ($I > 2\sigma(I)$). 5455 of them were unique. The resulting residual indices are as follows: $R_1 = 0.0880$, $wR_2 = 0.2245$ for the observed, and $R_1 = 0.1333$, $wR_2 = 0.2487$ for all reflections with 409 parameters.

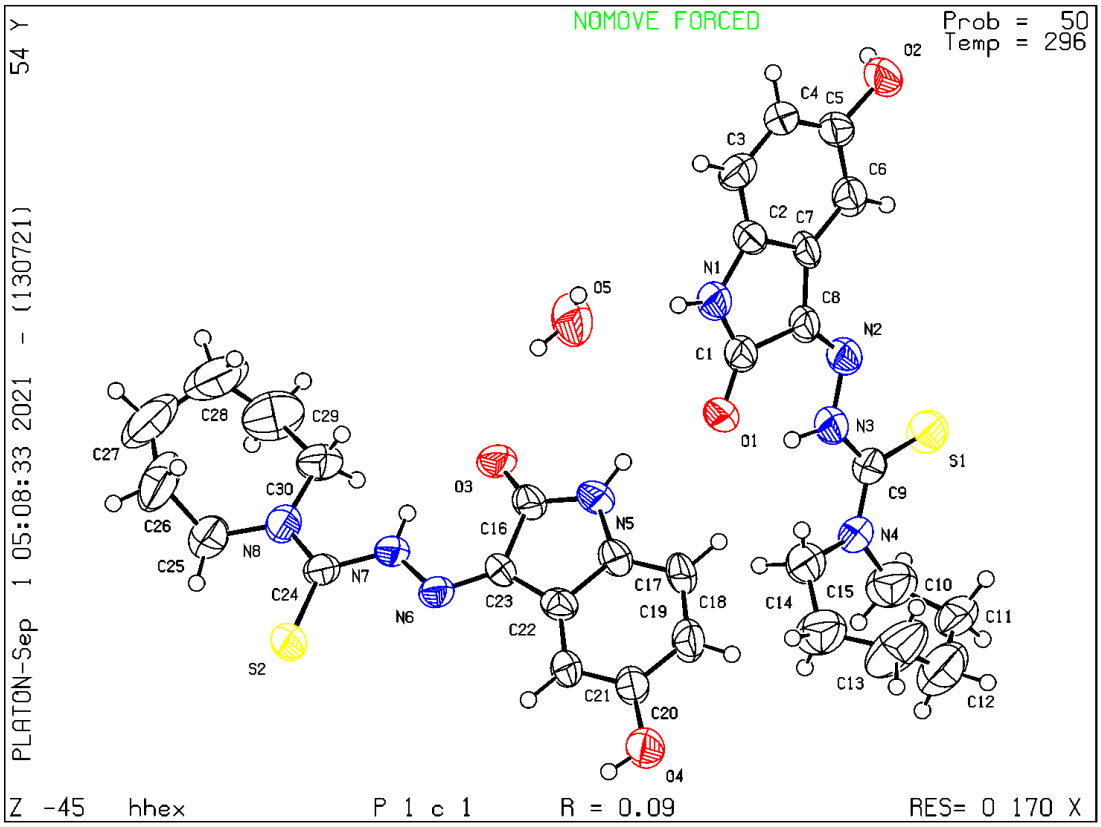

Figure 68: ORTEP diagram of compound (12) drawn in 30% thermal probability ellipsoids showing atomic numbering scheme. The asymmetric unit contains two crystallographically independents units and a water molecule in the crystal lattice.

A suitable cell was found and refined by nonlinear least squares and Bravais lattice procedures. The C(9)=S(1) bond length (1.663 Å) confirms the existence of thiosemicarbazone in thione form and the crystal structure identified the existence of an intra-molecular hydrogen bond between N-H and the carbonyl oxygen (Muralisankar *et al*., 2016). The presence of thiocarbonyl (C=S) and hydrazinic (N-N) part in opposite sites confirms their existence in trans form. In the thiosemicarbazone, the bonds appeared in –C(8)=N(2)–N(3)-C(9)(=S)-N(4) skeleton possess partial single

and double bonds character (1.262-1.347 Å) thereby confirming the delocalization of π electrons on that skeleton (Aneesrahman *et al*., 2019). X-ray values of bond angles such as N1-C1-C8, O1-C1-C8, O1-C1-N1, C3-C2-C7, C3-C2-N1, N1-C2-C7, C2-C3-C4, C5-C4-C3, C4-C5-C6, O2-C5-C6, C7-C6-C5 were found at 106.4°, 124.8°, 128.8°, 120.8°, 130.5°, 108.6°, 117.4°, 122.8°, 122.8°, 117.0°, 117.9° respectively. The crystal structures showed dimeric form associated with one water molecule. The intramolecular hydrogen bond between N3H3O1(0.86°) indicated the for the existence of *Z* configuration. In the crystal structure, the intermolecular hydrogen bond was also observed between the N1H1 and O5 of water molecule and bond angel was found at N1H1O5 (0.86°).

Using single crystal X-ray diffraction, the crystal structure of (Z)-N-ethyl-2-(5-hydroxy-2-oxoindolin-3-ylidene) hydrazine-1-carbothioamide (**HydIstEth/16**) was found. The orthorhombic $P2_12_12_1$ space group supported the compound (**16**).

A total of 7274 reflections were measured for compound (**16**), with 2254 declared to be noticed ($I > 2\sigma(I)$). The residual values that result are as follows: For all reflections with 166 values, $R_1 = 0.0467$, $wR_2 = 0.1122$, and $R_1 = 0.0738$, $wR_2 = 0.1245$. The deprotonated thiosemicarbazone structure transforms significantly from thione to thiol, as demonstrated by a C-S distance of 1.682 (5). A comparison of C-N and N-N bond distances with normal single and double bond lengths [C(1)-N(1) 1.339 (6) , C(2)-N(1) 1.412 (6), C(8)=N(2) 1.288 5), C(9)-N(3) 1.366 (5), C(9)-N(4) 1.310 (6), C(10)-N(4) 1.465 (6), N(2)-N(3)1.356 Å] clearly shows that charge delocalization takes place throughout the thiosemicarbazone skeleton (Matesanz *et al*., 2016). The crystal structures of compound (**16**) revealed an intramolecular hydrogen bond between N-H and carbonyl oxygen. The compound (**16**) contains an intramolecular hydrogen bond between the N(3)-H(3) proton and O1 [2.766 (5) Å], forming a six-membered ring and preferring the Z-isomer over the imine C=N bond. The torsional angles in (**16**) are 179.9(4) O1-C1-C8-N2, -177.4 (4) N1-C1-C8-N2, 173.5 (3) N2-N3-C9-S1, 177.5(4) C2-C7-C8-N2, -2.8(7) C10-N4-C9-S1 (Muralisankar *et al*., 2016).

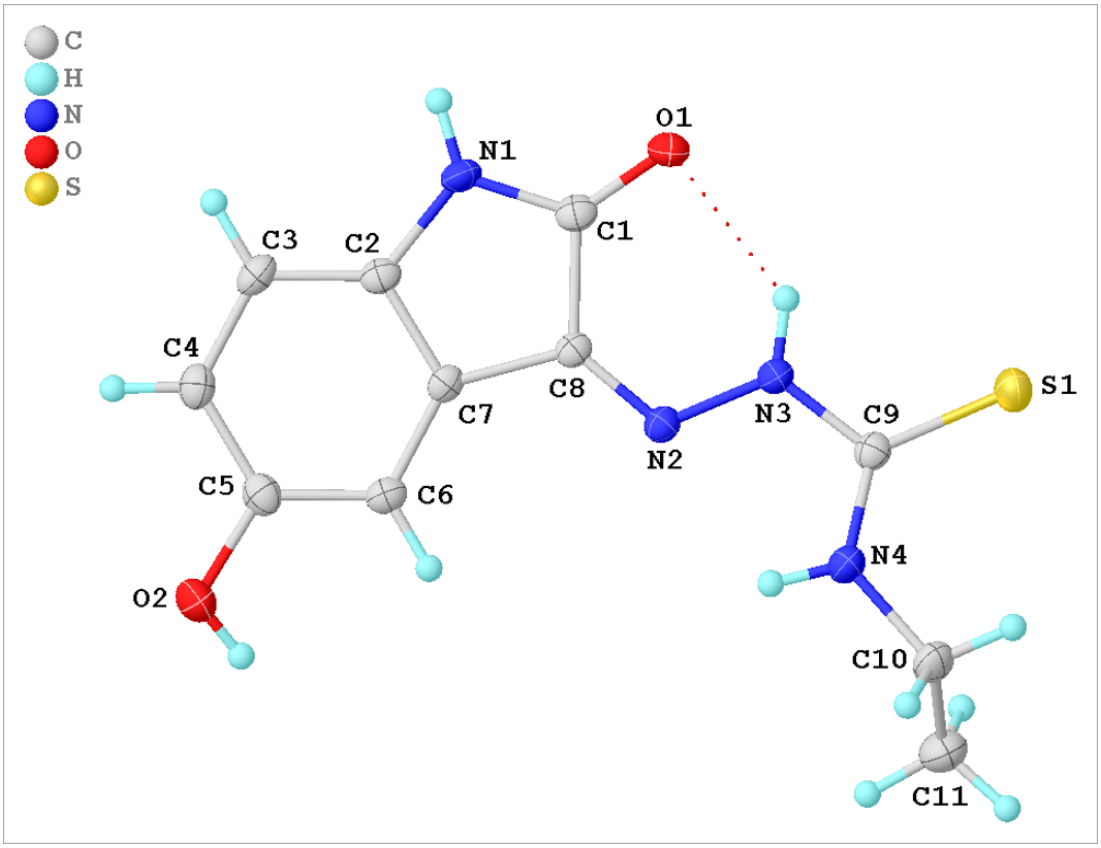

Figure 69*:* ORTEP diagram of compound (16) drawn in 20% thermal probability ellipsoids showing atomic numbering scheme.

4.2.4.6 Anticancer activity of 5-hydroxyisatin N(4)-substituted thiosemicarbazones (7 – 16)

Breast cancer cells (MCF-7, MDA-MB-231), Lung cancer cells (A549), Skin cancer cells (A431), Hypotriploid human cell (NCIH-460), Human prostate cancer cell (PC-3), and Prostate epithelial cell (PNT-2) 2500 cells were grown on 96 well plates in control (DMSO), then treated with different concentrations (1, 3, 10, and 30 μM) for 72 hours. PNT-2 is non-cancerous cell line. It was derived from normal human prostate tissue. It acts as reference cell line for comparison with cancer cell line.

Due to the presence of methyl and ethyl groups that are linked to the N(4) position of the thiosemicarbazone. The cancer cell lines MCF-7, A431, A549, MDA-MB-231, PNT-2, and NCIH-460 showed the lowest anticancer effectiveness for compounds (**15**) and (**16**). The compound (**8**) showed a mild antiproliferative effect on PNT-2 cell lines. This is caused by the heterocyclic piperidinyl ring on the N(4) position of thiosemicarbazones. The heterocyclic azepane ring on the N(4) position of the

thiosemicarbazone moiety caused compound (**12**) to have the lowest anticancer efficacy against A549.

The thiomorpholinyl group of the thiosemicarbazone moiety improved the anticancer potency against most cancer cell lines, whereas the two methyl groups on the N(4) position of the thiosemicarbazone increased the anticancer activity against two cell lines, PC-3 and A431.

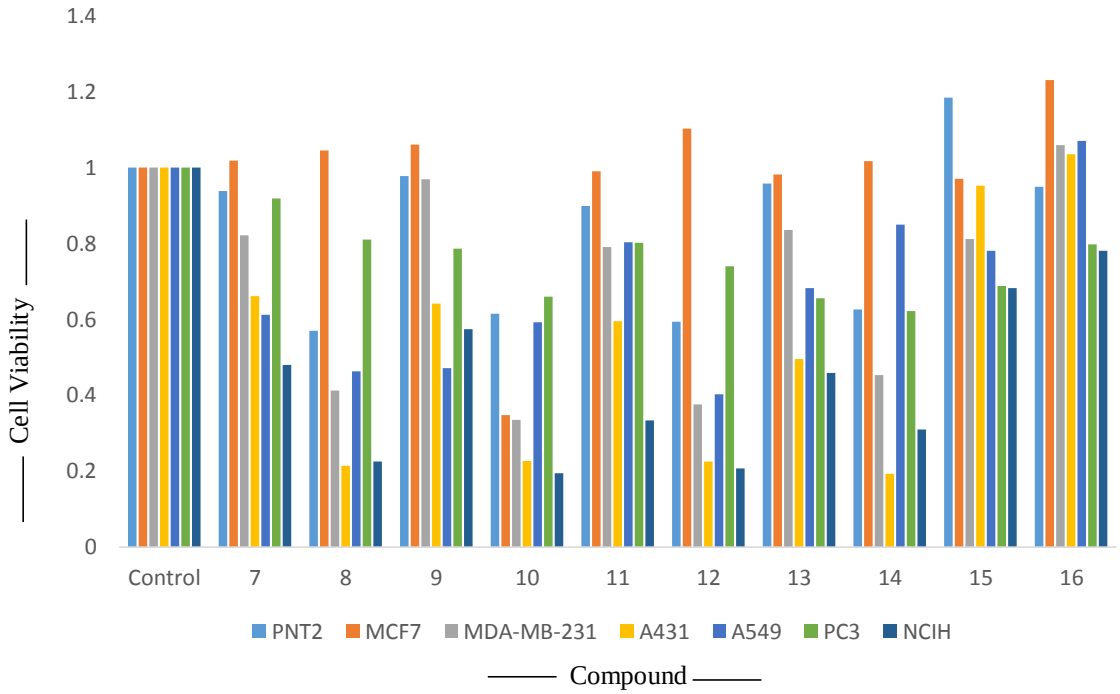

Figure 70: Cell viability assay of synthetic compounds with different concentration in different cell lines (7-16)

4.2.4.7 Conclusion

Because of the different substituents on the N(4)-position of thiosemicarbazone moieties, the anticancer efficiency of the examined compounds against cancer cell lines MCF-7, MDA-MB-231, A549, A431, NCIH-460, PC-3 and PNT-2 slightly differ. In terms of most cancer cell lines, the heterocyclic ring, methyl, and ethyl substituted group on N(4) position of thiosemicarbazones demonstrated the moderate to strong anticancer efficacy.

The synthesized compounds inhibited cell proliferation in the **MCF-7** cell line in the following order:

Compound **10** > Compound **15** > Compound **13** > Compound **11** > Compound **14** > Compound **7 >** Compound **8 >** Compound **9 >** Compound **12 >** Compound **16**

The synthesized compounds inhibited cell proliferation in the **A431** cell line in the following order:

Compound **14** > Compound **8** > Compound **10** > Compound **12** > Compound **13** > Compound **11 >** Compound **9 >** Compound **7 >** Compound **15 >** Compound **16**

The synthesized compounds inhibited cell proliferation in the **A549** cell line in the following order:

Compound **12** > Compound **8** > Compound **9** > Compound **10** > Compound **7** > Compound **13** > Compound **16** > Compound **11** > Compound **14** > Compound **15**

The synthesized compounds inhibited cell proliferation in the **MDA-MB-231** cell line in the following order:

Compound **10** > Compound **12** > Compound **8** > Compound **14** > Compound **11** > Compound **15** > Compound **7** > Compound **13** > Compound **9** > Compound **16**

The synthesized compounds inhibited cell proliferation in the **PNT-2** cell line in the following order:

Compound **8** > Compound **12** > Compound **10** > Compound **14** > Compound **11** > Compound **7** > Compound **16** > Compound **13** > Compound **9** > Compound **15**

The synthesized compounds inhibited cell proliferation in the **PC-3** cell line in the following order:

Compound **14** > Compound **13** > Compound **10** > Compound **15** > Compound **12** > Compound **9** > Compound **16** > Compound **11** > Compound **8** > Compound **7**

The synthesized compounds inhibited cell proliferation in the **NCIH-460** cell line in the following order:

Compound **10** > Compound **12** > Compound **8** > Compound **14** > Compound **11** > Compound **13** > Compound **7** > Compound **9** > Compound **15** > Compound **16**

Compounds (**10**) displayed more antiproliferative activity than the positive control (DMSO) in MCF-7, MDA-MB-231, and NCIH-460 cancer cell lines, but compound (**14**) had better anticancer potency than other compounds in PC-3 and A431 cell lines.

The beneficial effect on cancer of compound (**16**) was lowest in the MCF-7, A431, MDA-Mb-231, and NCIH-460 cell lines.

4.3 SYNTHESIS, CHARACTERIZATION AND ANTICANCER ACTIVITY OF 5,7-DIBROMOISATIN N(4)-SUBSTITUTED THIOSEMICARBAZONES

4.3.1 General discussion

The N-substituted carbothiohydrazide were synthesized by the method El-Sawaf (El-Sawaf *et al*., 2018) and Scovill (Scovill, 1991). 5,7-Dibromoisatin thiosemicarbazones were synthesized by refluxing 5,7-dibromoisatin with N-substituted carbothiohydrazide in the presence of absolute ethanol and few drops of glacial acetic acid for 6 h (Balachandran *et al.*, 2018).

Table 22: Physical properties of 5, 7-dibromoisatin N(4)-substituted thiosemicarbazones (17-26)

Compd	Mol. Formula (Mol. Weight)	Melting point (ºC)	Colour	Yields (%)
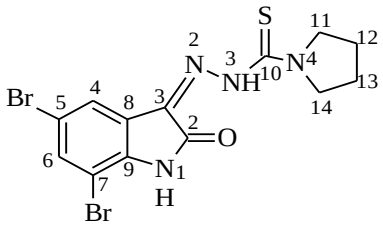 (**DiBrIstPyrl/17**)	$C_{13}H_{12}Br_2N_4OS$ (432.13)	290º C	Yellow	88%
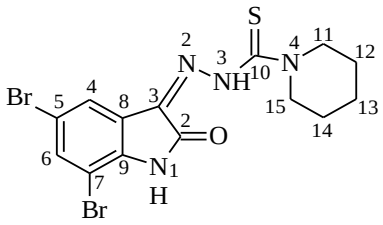 (**DiBrIstPip/18**)	$C_{14}H_{14}Br_2N_4OS$ (446.16)	268º C	Yellow	89%
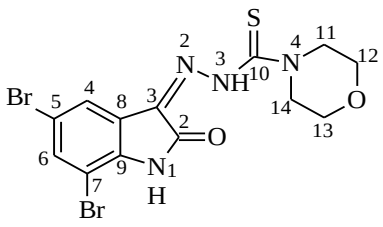 (**DiBrIstMor/19**)	$C_{13}H_{12}Br_2N_4O_2S$ (448.13)	254º C	Yellow	80%

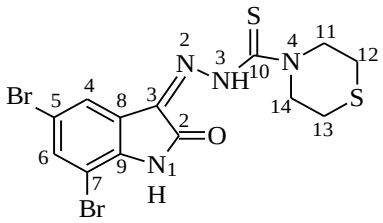 (**DiBrIstTmor/20**)	$C_{13}H_{12}Br_2N_4OS_2$ (464.19)	262° C	Yellow	92%
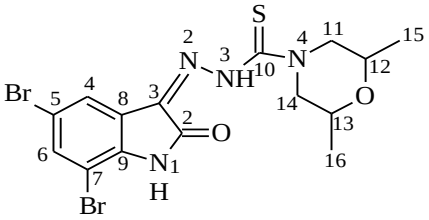 (**DiBrIstDmMor/21**)	$C_{15}H_{16}Br_2N_4O_2S$ (476.18)	236° C	Yellow	87%
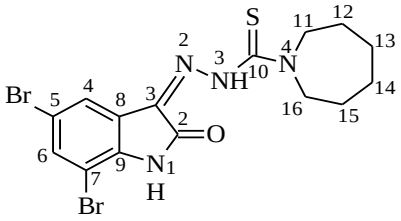 (**DiBrIstAzep/22**)	$C_{15}H_{16}Br_2N_4OS$ (460.18)	260° C	Yellow	71%
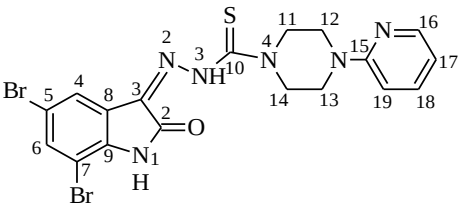 (**DiBrIstPypz/23**)	$C_{18}H_{16}Br_2N_6OS$ (524.23)	262° C	Yellow	81%
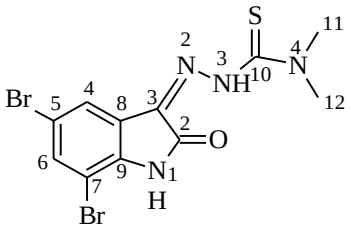 (**DiBrIstDm/24**)	$C_{11}H_{10}Br_2N_4OS$ (406.09)	260° C	Yellow	77%

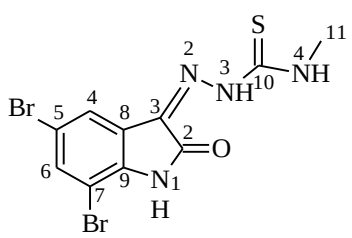 (**DiBrIstMet/25**)	$C_{10}H_8Br_2N_4OS$ (392.06)	296° C	Yellow	76%
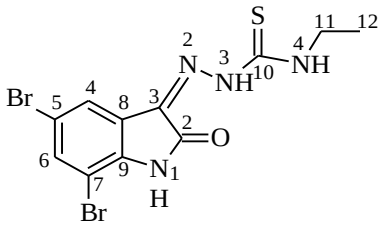 (**DiBrIstEth/26**)	$C_{11}H_{10}Br_2N_4OS$ (406.09)	264° C	Yellow	56%

The high yield (56-89%) of 5,7-dibromoisatin N(4)-substituted thiosemicarbazones were obtained in the laboratory. They were stable in air at room temperature and showed the range of melting point 254-296° C. The thiosemicarbazones (**17, 18, 19, 20, 21, 22, 23, 24, 25, 26**) were slightly soluble in Et_2O, MeCN, CH_2Cl_2; and highly soluble in $CHCl_3$, DMF, EtOH, Me_2CO and DMSO. Elemental analysis, FT-IR, ^1H and ^{13}C NMR, UV-Visible spectroscopy methods, and single crystal X-ray analysis were used to characterize the synthesized thiosemicarbazones. ESI-HRMS mass spectrometry was used to confirm the molecular structures of thiosemicarbazones.

The results of elemental analysis of compounds (**17-26**) revealed that the experimental data agree with the calculated data within the margins of error.

Table 23: Elemental analysis data of 5,7-dibromoisatin N(4)-substituted thiosemicarbazones (17-26)

Compd	C	H	N
17	36.07(36.13)	2.67 (2.80)	12.88 (12.97)
18	37.77 (37.69)	3.17 (3.16)	12.58 (12.56)
19	34.77 (34.84)	2.57 (2.70)	12.40 (12.50)
20	33.77 (33.64)	2.57 (2.61)	12.10 (12.07)
21	37.77 (37.83)	3.57 (3.39)	11.60 (11.77)

22	39.17 (39.15)	3.57 (3.50)	12.60 (12.17)
23	41.17 (41.24)	3.07 (3.08)	16.06 (16.03)
24	32.47 (32.53)	2.37 (2.48)	13.76 (13.80)
25	30.57 (30.63)	2.07 (2.06)	14.26 (14.29)
26	32.57 (32.53)	2.37 (2.48)	13.66 (13.80)

4.3.2 Spectral studies

4.3.2.1 IR spectra

The infrared bands of particular functional groups of synthesized compounds (**17-26**) are displayed in Table 24.

The thiosemicarbazones displayed broad spectral bands in the range of 3143−3196 cm^{-1} attributed to the stretching vibrations of indole N-H and azomethine N-H which are involved in hydrogen bonding (Wiles & Suprunchuk, 1969). The strong broad spectral bands due to the stretching vibrations of *v*(C=O) and *v*(C=N) groups of thiosemicarbazones were seen in the region 1685-1705 cm^{-1} and 1533-11610 cm^{-1} respectively (Dileepan *et al*., 2018). The solid form of thiosemicarbazones existed in thione form which was confirmed by the absence of IR band at 2600-2500 cm^{-1}, characteristics of S-H group (Osman *et al*., 2020). The medium IR bands present in the range of 1186-1143 cm^{-1} attributed to *v*(N-N) stretching vibration of thiosemicarbazone moiety (Vineetha & Kurup, 2013). The strong broad absorption bands due to the stretching vibration of *v*(C=S) of thiosemicarbazones were seen in the range of 1292-1183 cm^{-1} and 792-713 cm^{-1} (Khan *et al*., 2018). This is caused by vibrations involving interactions between C-N stretching of the C=S group connected to a nitrogen atom and C=S stretching of the group. Despite the fact that the thione group (C=S) has been reported to be particularly unstable in the monomeric state and to frequently transform into a stable C-SH single bond (Ali, 2016). The strong spectral bands due to the stretching vibration of *v*(C-Br) were seen in the region 557-628 cm^{-1} (Sridhar & Ramesh, 2001). The stretching vibration of the compound (**24**, **25** and **26**) with *v*(C=S) was lower than that of the other heterocyclic thiosemicarbazones due to the presence of a N(4)-alkyl group, but that of *v*(C=N) showed a greater frequency. Due to the existence

of heterocyclic, N(4)-alkyl, and 5,7-dibromo substitutions, the N-H vibration of indole and azomethine had little to no effect.

Table 24: Diagnostic bands in the IR spectra (cm^{-1}) of compounds (17-26)

Compd	*ν* (N-H)	*ν* (C=O)	*ν* (C=N)	*ν* (N-N)	*ν* (C=S)	*ν* (C-Br)
17	3178 (br) 3053 (m)	1685 (s)	1543 (s)	1159 (s)	1201 (s) 785 (s)	594 (s)
18	3157 (br) 3052 (m)	1691 (s)	1543 (s)	1186 (s)	1234 (s) 713 (s)	561 (s)
19	3149 (br) 3051 (m)	1687 (s)	1527 (s)	1157 (s)	1292 (s) 719 (s)	557 (s)
20	3157 (br) 3064 (m)	1689 (s)	1543 (s)	1170 (s)	1219 (s) 713 (s)	561 (s)
21	3153 (br) 3047 (m)	1693 (s)	1533 (s)	1170 (s)	1240 (s) 721 (s)	563 (s)
22	3313 (br) 3174 (m)	1668 (s)	1529 (s)	1151 (s)	1193 (s) 792 (s)	592 (s)
23	3161 (br) 3062 (m)	1689 (s)	1568 (s)	1172 (s)	1196(s) 759 (s)	563 (s)
24	3196 (br)	1687 (s)	1541 (s)	1165 (s)	1196 (s)) 763 (s)	594 (s)
25	3176 (br) 3049 (m)	1705 (s)	1602 (s)	1143 (s)	1207 (s) 726 (s)	561 (s)
26	3350 (s) 3143(br) 3045 (m)	1685 (s)	1610 (s)	1143 (s)	1183 (s) 786 (s)	628 (s)

s = strong, m = medium, br = broad

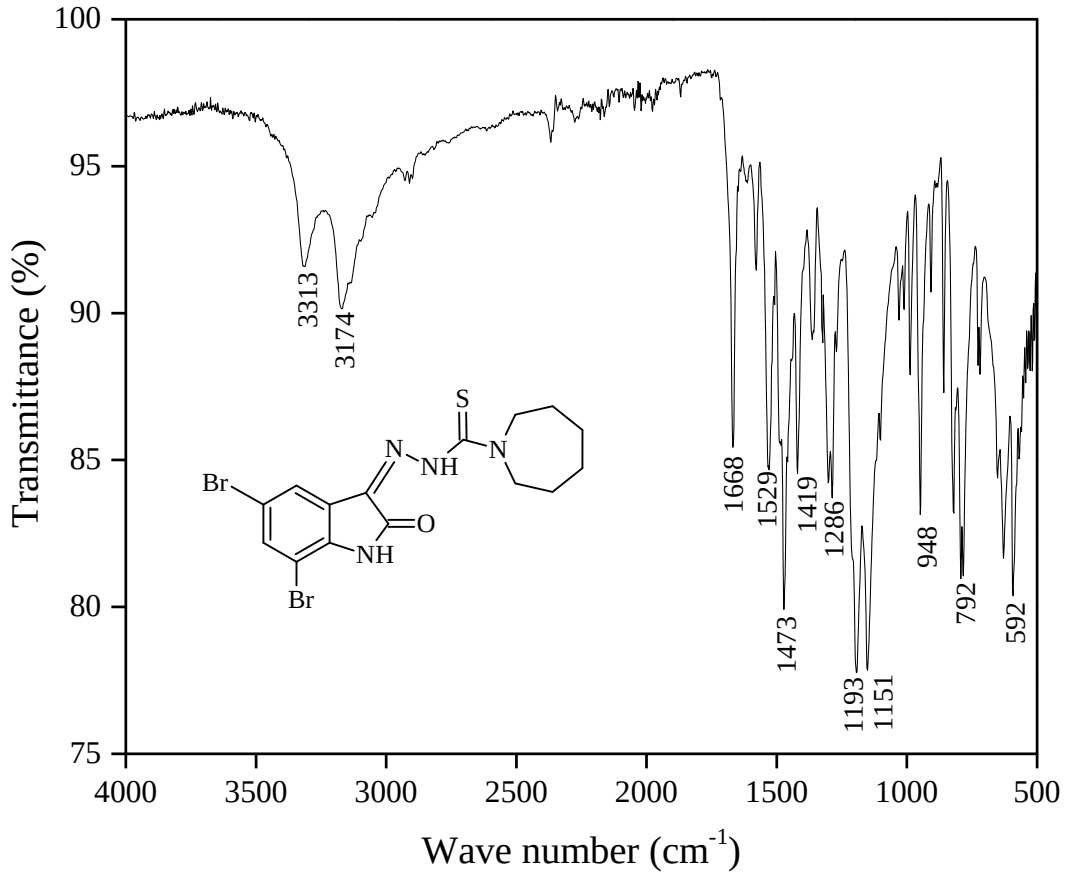

Figure 71: IR spectrum of compound (22)

4.3.2.2 NMR spectra

The ^{1}H NMR spectral values (δ, ppm) of the synthesized compounds (**17, 18, 19, 20, 21, 22, 23, 24, 25, 26**) are enumerated in Table 25.

The sharp singlet peaks in the range of δ 13.38-12.32 ppm attributed to the protons bonded to the N(3)H of thiosemicarbazone moiety indicates that the Schiff's base ligands exist as neutral thione tautomeric form in solution (Aneesrahman *et al*., 2019). The appearance of the NH signal in this region demonstrates that the (*Z*)-form of an intramolecular hydrogen bond exists. The sharp singlet peaks ascribed to the protons of indole N-H were reported in the region δ 11.71-11.62 ppm (Czele, 2022, Khan *et al*., 2016). The existence of intramolecular hydrogen bonds between the N(3)H and C(2)O atoms and between N(4)H and N(2) can be used to explain the occurrence of three distinct N-H in the ^{1}H-NMR of compound (**25** and **26**) (Althagafi *et al*., 2019). All the aromatic protons of isatin moiety were seen as singlet or doublet signals at δ 8.14-7.56 ppm (Dzulkifli *et al*., 2015). The signals of aliphatic (-CH_2) protons were recorded as a triplet toward the downfield region of δ 3.70 ppm (Ibrahim *et al*., 2018), whereas

aliphatic (-CH_3) protons' signals were recorded as a multiplet in the same region 1.15 ppm in the compound (**21**) (Netalkar *et al*., 2015). Due to the overall loss in electron density, compound (**21** and **26**) saw a little downfield shift to aliphatic protons. The aliphatic protons of azepane were detected as three signals at δ 4.07, δ 3.30, and δ 1.54 ppm, which were ascribed to positions C(11), C(12), and C(13), respectively (Muralisankar *et al*., 2019). Due to interaction with surrounding CH_2 *i.e*., (C(12,15) protons), the CH_2 *i.e*., (C(11,16) protons) close to the ring nitrogen created a triplet at δ 4.07 ppm in compound (**22**). Due to coupling with CH_2 *i.e*., C(11,16) and CH_2 *i.e.*, C (13,14) protons, the CH_2 *i.e.*, C(12,15) protons resonate as the triplet seen at δ 3.30 ppm and the CH_2 *i.e.*, C(13,14) protons also resonated as the triplet at δ l.54 ppm. The pyrrolidinyl ring protons (**17**) away from the electronegative nitrogen were identified as the cause of the triplet at δ 1.89 ppm, demonstrating that the protons at C(12) and C (13) were magnetically equivalent. It can be seen that C(11) and C(14) were magnetically equivalent by the triplet at δ 3.76 ppm, which was identified as the ring proton closer to electronegative nitrogen. The morpholinyl proton C(12) & C(13) near the oxygen resonated to give a broad triplet peak at δ 3.35 ppm whereas C(11) & C(14) proton near the nitrogen showed a triplet peak at δ 4.02 ppm. Thiosemicarbazone (**26**) CH_2 of N(4)-ethyl substituent resonated as quartet peak at 3.68 ppm and CH_3 of N(4)-ethyl substituent resonated as triplet peak at 1.21 ppm (Kassab *et al*., 2010). A multiplet signal corresponding to the methyl group appeared in the range of δ 3.38 to 3.39 ppm in the spectra of N-methyl derivatives (**24**, **25**) (Emami *et al*., 2021).

Table 25: ^{1}H NMR spectral assignments (δ ppm) of compounds (17-26) (400 MHz, DMSO-d6)

Compd→ Proton↓	**17**	**18**	**19**	**20**	**21**	**22**	**23**	**24**	**25**	**26**
-N(1)H	11.70(s)	11.68(s)	11.71(s)	11.70(s)	11.70(s)	11.69(s)	11.71(s)	11.71(s)	11.62(s)	11.62(s)
-N(3)H	13.12(s)	12.96(s)	13.01(s)	12.99(s)	12.99(s)	13.38(s)	13.04(s)	13.25(s)	12.34(s)	12.32(s)
-N(4)H	-	-	-	-	-	-	-	-	7.84(m)	7.88(m)
-H(4)	7.79(d)	7.56(d)	7.79(d)	7.80(d)	7.80(d)	7.80(d)	8.14(d)	7.80(d)	9.42(d)	9.45(d)
-H(6)	7.65(d)	7.79(d)	7.63(d)	7.60(d)	7.58(d)	7.58(d)	8.13(d)	7.63(d)	9.41(d)	9.44(d)
-H(11)	3.76(t)	3.95(t)	4.02 (t)	4.26(t)	3.70(d)	4.07(t)	4.16(t)	3.39(m)	3.38(m)	3.68(q)
-H(12)	1.89(t)	1.67(t)	3.35 (t)	2.81(t)	3.01(t)	3.30(t)	3.30(t)	3.39(m)	-	1.21(t)

-H(13)	1.89(t)	1.67(t)	3.35 (t)	2.81(t)	3.01(t)	1.54(t)	3.30(t)
-H(14)	3.76(t)	1.67(t)	4.02 (t)	4.26(t)	3.70(d)	1.54(t)	4.16(t)
-H(15)	-	3.95(t)	-	-	1.15(m)	3.30(t)	-
-H(16)	-	-	-	-	1.15(m)	4.07(t)	8.14(d)
-H(17)	-	-	-	-	-	-	6.84(d)
-H(18)	-	-	-	-	-	-	7.66(d)
-H(19)	-	-	-	-	-	-	6.66(d)

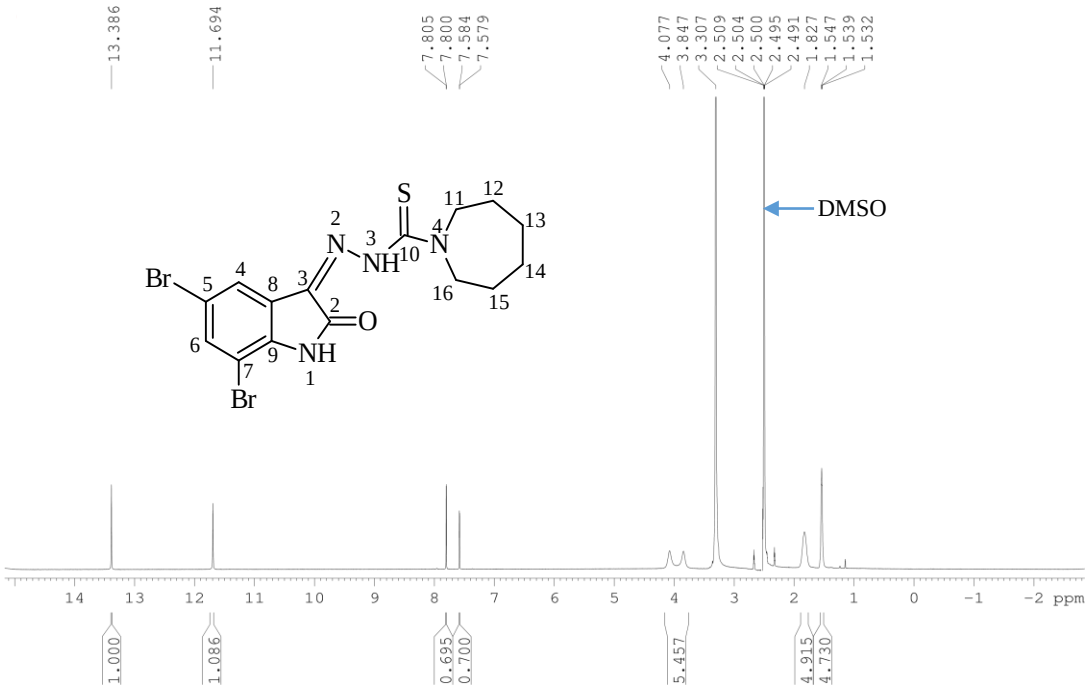

Figure 72: ^{1}H NMR spectrum (400 MHz, DMSO-d6) of compound (22)

In compound (**22**), ^{1}H NMR signals of aromatic protons *viz.* H(C(4), C(6)) were observed in the region δ 7.80-7.58 ppm. It displayed two separate singlets for N=N-H of thiosemicarbazone and indole N-H moiety at δ 13.38 ppm and δ 11.69 ppm respectively. The signals of N(4)-cyclohexyl protons *viz.* H(C (11), C(12), C(13), C (14), C(15), C(16)) were observed at δ 4.07- 1.54 ppm.

The ^{13}C NMR (400 MHz, DMSO-*d6*) spectral values (δ, ppm) of the compounds (**17-26**) are recorded in Table 26.

Chemical shift values for ^{13}C NMR spectra of synthetic compounds were found to be very similar to those of related N(4) substituted thiosemicarbazones of isatin. The magnetically non-equivalent carbon atoms of those thiosemicarbazones had ^{13}C NMR

spectra at δ 179.30-177.53 ppm, δ 163.59-162.33 ppm, and δ 134.67-134.41 ppm, which were ascribed to the π bonded carbon atoms of C=S, C=O, and C=N groups, respectively (Muğlu, 2020). The sharp peaks of sp^2 hybridized carbon atoms, *i.e.*, aromatic carbon atoms of isatin moieties, were found around δ 140.51-104.14 ppm (Akinchan *et al*., 2002). The morpholinyl ring carbon C(11) & C(14) were appeared at 65.71 ppm whereas C(12) & C(13) ring carbon showed at δ 50.51 ppm. In thiomorpholinyl ring carbon, the carbon nearer to the sulphur appeared upfield δ 26.59 ppm whereas the carbon nearer to the nitrogen showed downfield δ 53.20 ppm. 2,6-Dimethyl morpholinyl ring carbon C(11) & C(14) near to nitrogen appeared downfield 70.91 ppm whereas the carbon C(12) & C(13) near to the oxygen appeared upfield δ 55.07 ppm. At a δ value of 40.13 ppm, two methyl carbons C(11) and C(12) in compound (**24**) appeared to be magnetically equivalent. At a value of δ 24.00 ppm, the pyrrolidinyl ring carbon C(12) and C(13) emerged, displaying magnetic equivalence. The presence of the bromine group in the synthesized thiosemicarbazones prompted the C(5) (about 104 ppm) and C(7) (about 120 ppm) carbon atoms to migrate downfield (higher values of δ).

Table 26: ^{13}C NMR spectral assignments (δ ppm) of compounds (17-26) (400 MHz, DMSO-d6)

Compd→ Carbon↓	**17**	**18**	**19**	**20**	**21**	**22**	**23**	**24**	**25**	**26**
-C(2) *viz.* C=O	163.05	162.47	162.48	162.43	162.44	-	-	162.59	162.33	162.33
-C(3) *viz.* C=N	134.85	134.43	134.67	134.66	134.61	-	134.65	134.41	134.43	134.44
-C(4)	-	131.70	132.25	132.20	132.24	-	-	132.72	129.76	129.84
-C(5)	104.78	104.30	104.32	104.30	104.32	-	106.89	104.30	104.17	104.14
-C(6)	124.26	123.73	123.60	123.55	123.60	-	-	123.70	123.76	123.74
-C(7)	121.95	121.29	121.64	121.56	121.45	-	121.59	121.43	122.06	122.16
-C(8)	115.04	114.47	114.60	114.54	114.55	-	113.05	114.52	114.32	114.31
-C(9)	-	140.06	140.22	140.23	140.18	-	-	139.95	140.51	140.51
-C(10) *viz.* C=S	-	178.39	179.25	179.30	179.06	-	-	178.76	177.53	176.55
-C(11)	54.32	51.36	65.71	53.20	70.91	-	49.45	40.13	31.27	40.13
-C(12)	24.00	25.53	50.51	26.59	55.07	-	43.55	40.13	-	13.88
-C(13)	24.00	23.52	50.51	26.59	55.07	-	43.55			
-C(14)	54.32	25.53	65.71	53.20	70.91	-	49.45			
-C(15)	-	51.36	-	-	18.33	-	-			
-C(16)	-	-	-	-	18.33	-	-			

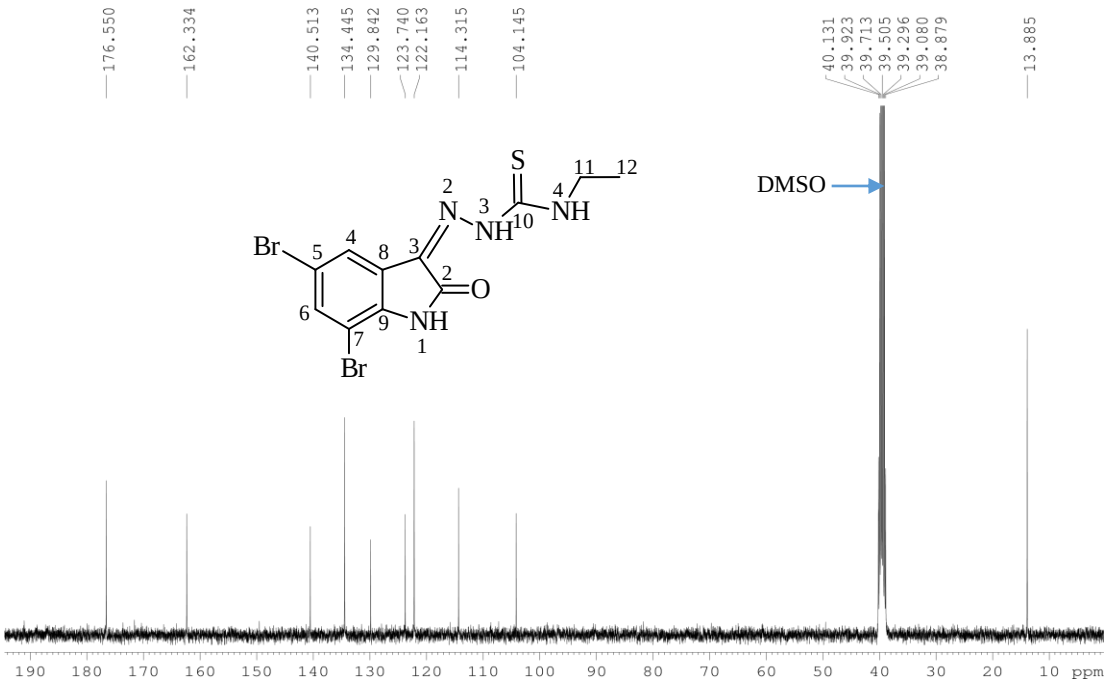

Figure 73: ^{13}C NMR spectrum (400 MHz, DMSO-d6) of compound (26)

In Compound (**26)**, the ^{13}C NMR signals present at δ 176.55, δ 162.33 and δ 134.44 ppm were ascribed to sp^2 hybridized carbon atoms of C=S, C=O and C=N groups, respectively. The signals of aromatic carbons (sp^2-C) were observed in the region δ 140.51-104.14 ppm. The spectra of aliphatic (–CH_2) carbons (sp^3-C) of N(4)-substituent were appeared at δ 40.13 whereas the methyl carbon (-CH_3) was seen at δ 13.88 ppm (Güzel *et al*., 2008).

4.3.2.3 Mass spectrometry

Mass spectrometers with high resolution and high mass accuracy are used in high-resolution mass spectrometry (HRMS). These tools can be used to differentiate distinct compounds with the same nominal mass, identify unknowns, and establish elemental compositions. The mass to charge ratio (*m/z*) can be measured by HRMS to multiple decimal places. The protonated molecular ion $[M+H]^+$ peak of the synthesized molecules was verified by high resolution mass spectroscopy. Because of the "better" resolution, "precise masses" may be measured as opposed to nominal masses. Time-of-Flight (TOF) mass spectrometers and Orbitrap mass spectrometers have been the main clinical applications for high resolution mass spectrometry. The time it takes for ions to go down a flight tube and strike a detector is carefully measured by TOF devices to achieve high mass resolution (Crutchfield & Clarke, 2014). TOF-MS has various

advantages over conventional MS, including quick acquisition rates, high precision in mass measurements, and a wide mass range.

The mass spectral data of the synthesized compounds (**17, 18, 19, 20, 21, 22, 23, 24, 25, 26**) obtained by the high-resolution electron spray ionization mass spectrometry (LC-QTOF-HRMS) measurements are summarized in Table 27.

Table 27: Mass spectrometric data of compounds (17-26)

	***m/z* [M+H]$^+$**	
Compd	**Found**	**Calculated**
17	433.1301	433.138
18	447.1624	447.168
19	449.1331	449.138
20	465.1921	465.198
21	477.1833	477.188
22	461.1794	461.188
23	525.2350	525.238
24	407.0908	407.098
25	393.0672	393.068
26	407.0954	407.098

All the obtained mass spectral data of compounds (**17, 18, 19, 20, 21, 22, 23, 24, 25, 26**) are in agreement with the calculated spectral data of those compounds of proposed molecular structures.

In the mass spectrometry the formation of positive or negative ions as the fragments of the compounds depend on the sign of the applied electrical field. High resolution MS can offer *m/z* peak up to 4 decimal digits. The thiosemicarbazones (**17, 18, 19, 20, 21, 22, 23, 24, 25, 26**) exhibited mass spectral peaks at *m/z* (amu): 433.1301 (calc., 433.138), 447.1624 (calc., 447.168), 449.1331 (calc., 449.138), 465.1921 (calc., 465.198), 477.1833 (calc., 477.188), 461.1794 (calc., 461.188), 525.2350 (calc., 525.238), 407.0908 (calc., 407.098), 393.0672 (calc., 393.068) and 407.0954 (calc., 407.098) respectively thus by showing the existence of $[M+H]^+$ (Swathy *et al*., 2016).

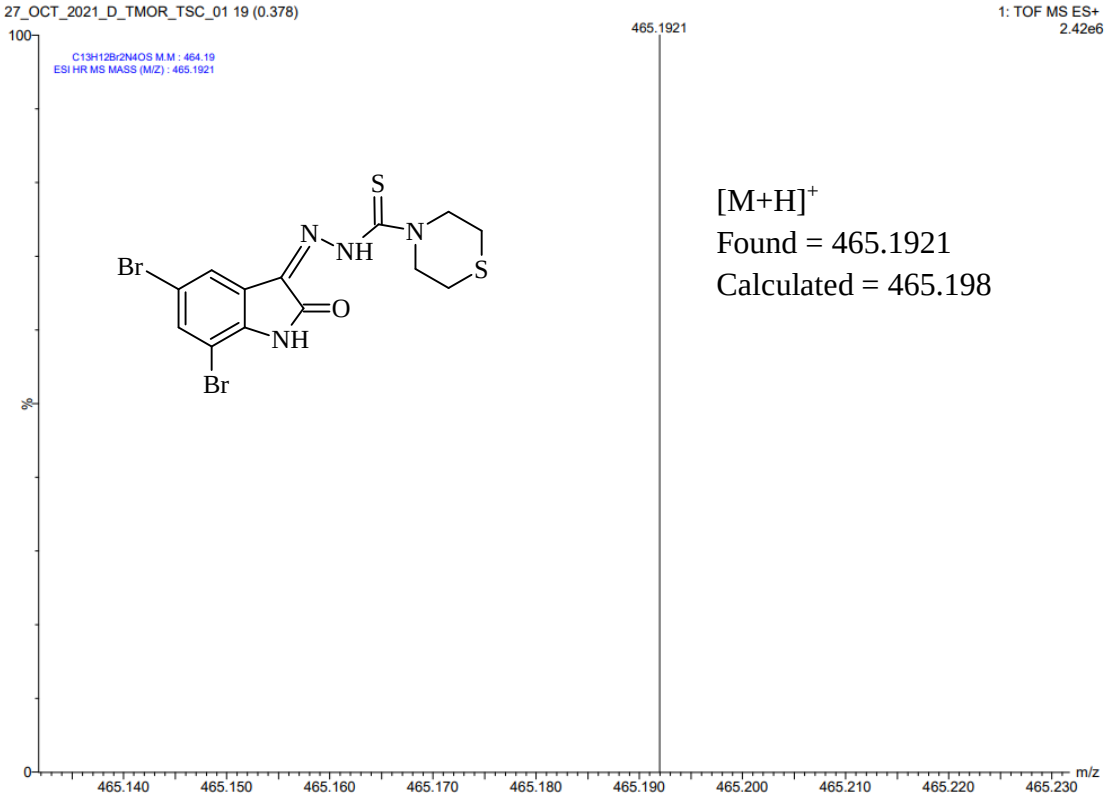

Figure 74: ESI-HRMS of compound (20)

4.3.2.4 UV-Visible spectra

The UV-Visible spectral data of the synthesized compounds (**17, 18, 19, 20, 21, 22, 23, 24, 25, 26**) are summarized in Table 28.

The electronic spectral data of the thiosemicarbazones were recorded in the region 600-250 nm using dilute solution of $CHCl_3$ (25µM).

In all the compounds the absorption bands in the region 283-286 nm corresponding to $\pi \rightarrow \pi^*$ electronic transitions of aromatic ring and thiosemicarbazone moiety were not seen in distinct manner possibly due to the solvent cutoff (the wavelength below which the solvent itself absorbs all of the light, ($CHCl_3$; 245 nm) and low concentration of compound solutions (Lu *et al*., 2006). The broad shoulder peak appeared around 365 nm due to the $n \rightarrow \pi^*$ transitions of thiosemicarbazones moiety (C=S) in the synthesized compounds whereas the sharp shoulder peak appeared around 285 nm due to the azomethine C=N double bond. Due to the presence of a N(4)-alkyl substituent in the compound (**25** and **26**), the absorption bands of thiosemicarbazones with heterocyclic groups appeared at a higher wavelength. The absorption band of thiosemicarbazones

containing N(4)-alkyl group and heterocyclic group did not significantly differ from one another.

Table 28: UV-Visible spectroscopic data of compounds (17-26)

$CHCl_3$ (25 µM) Solvent										
Compd→	**17**	**18**	**19**	**20**	**21**	**22**	**23**	**24**	**25**	**26**
λ_{max}↓										
n→π* (nm)	360	362	363	363	362	361	360	359	365	367
π→π* (nm)	285	284	285	283	284	285	285	285	286	286

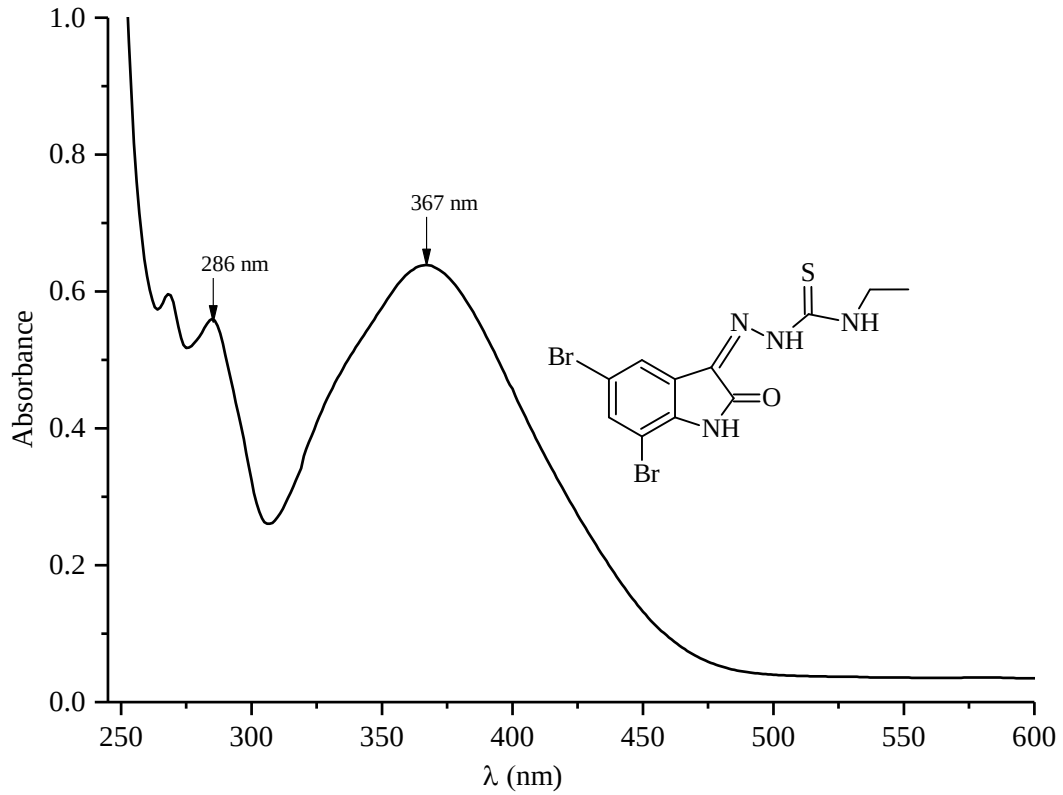

Figure 75: UV-Visible spectra of compound (26)

The compound **(26)** showed the absorption band at 286 nm attributed to the π→π* transition of aromatic rings but that at 367 nm attributed to n→π* electronic transitions of azomethine (>C=N) and carbonyl (>C=O) and thioamide (-NH-C=S) groups. The broad sharp peak at 367 nm appeared due to the presence of ethyl group at N(4) position in thiosemicarbazone.

4.3.2.5 Single crystal X-ray crystallographic study

The crystal structure of (*Z*)-*N*-(5,7-dibromo-2-oxoindolin-3-ylidene)azepane-1-carbothiohydrazide (**DiBrIstAzep/22**) was determined using single crystal X-ray diffraction. The compound **22** grew in the monoclinic P21/c space group.

A total of 26380 reflections for compound (**22**) were measured, of which 3512 were considered to be observed ($I > 2\sigma(I)$). The resulting residual indices are as follows: $R_1 = 0.0498$, $wR_2 = 0.1171$, and $R_1 = 0.0815$, $wR_2 = 0.1428$ for all reflections with 209 parameters.

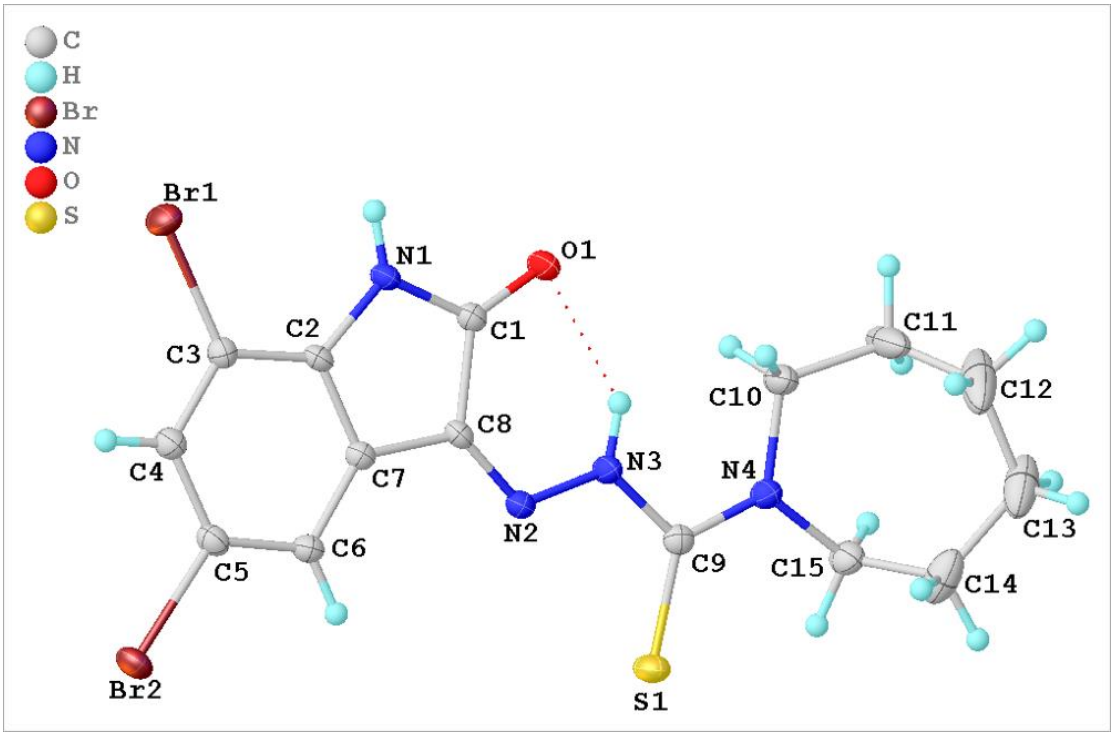

Figure 76: ORTEP diagram of compound (22**)** drawn in 20% thermal probability ellipsoids showing atomic numbering scheme.

The deprotonated thiosemicarbazone structure evolves significantly from thione to thiol, as evidenced by a C-S distance of 1.674. (5). A comparison of C-N and N-N bond distances with normal single and double bond lengths [C(1)-N(1) 1.373, C(2)-N(1) 1.399, C(8)=N(2) 1.296, C(9)-N(3) 1.391, C(9)-N(4) 1.342, C(10)-N(4) 1.469, N(2)-N(3)1.331Å] reveals that charge delocalization occurs throughout the thiosemicarbazone skeleton (Matesanz et al., 2016). The torsional angles in compound (**22)** are 178.6(5) (Br1−C3−C4−C5), 178.9(4) (Br2−C5−C6−C7), -0.9(10)

(O1−C1−C8−C7), 5.4(7) (N2−N3−C9−S1), 177.7(5) (C3−C2−C7−C8) and 1.8(9)° (C7−C2−C3−C4) (Muralisankar *et al*., 2016).

The crystal structure of (*Z*)-*2*-(5,7-dibromo-2-oxoindolin-3-ylidene)-*N*-ethylhydrazine-1-carbothioamide (**DiBrIstEt/26**) crystallizes in the monoclinic P21/c space group and single crystal X-ray diffraction analysis.

A total of 50738 reflections for compound (**26**), of which 1688 were deemed to be observed ($I > 2\sigma(I)$), were measured. Of these, 3130 were unique. The resultant residual indices are as follows: for the observed, R_1 = 0.0461, wR_2 = 0.1099, and for all reflections with 173 parameters, R_1 = 0.0691, wR_2 = 0.1211.

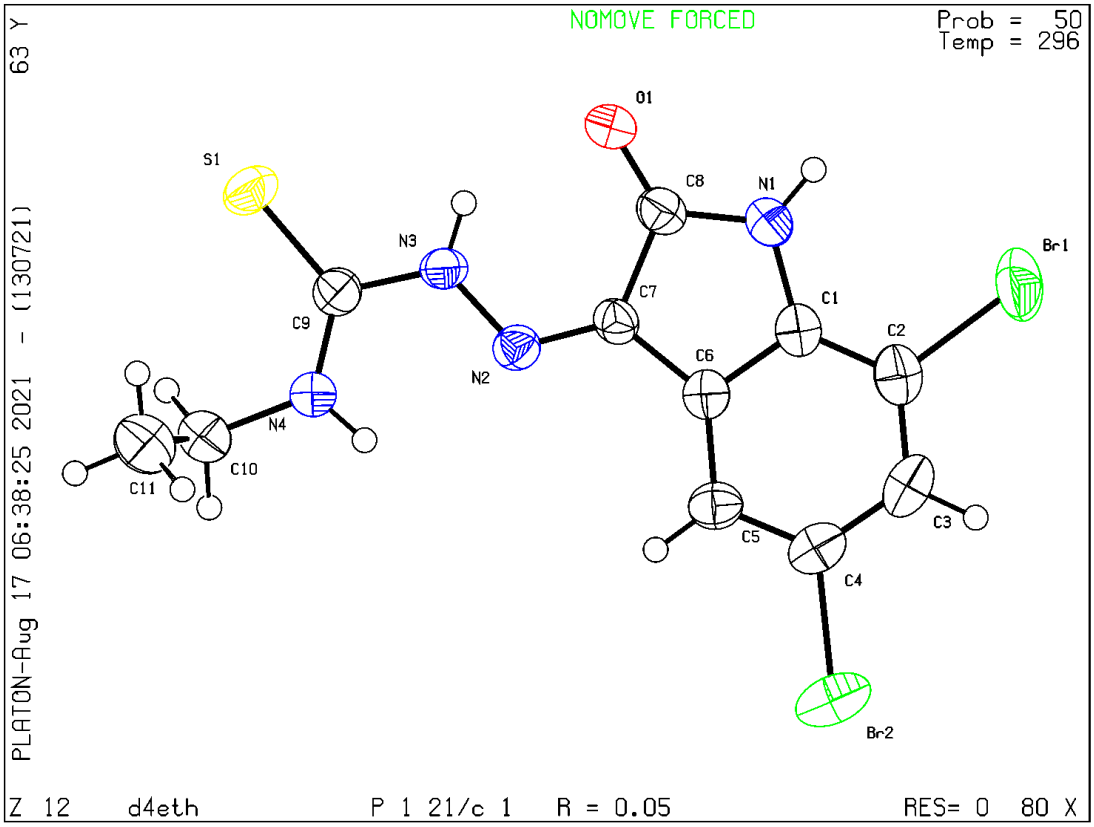

Figure 77: The ORTEP diagram of compound (26) showing the thermal ellipsoid at 30% probability level.

The deprotonated thiosemicarbazone skeleton undergoes significant evolution from the thione to the thiol form which is reflected in a C-S distance of 1.668(4). A comparison of C-N and N-N bond distances with typical single and double bond lengths [C(8)-N(1) 1.353, C(1)-N(1) 1.398, C(7)=N(2) 1.291, C(9)-N(3) 1.376, C(9)-N(4) 1.318, C(10)-N(4) 1.468, N(2)-N(3)1.341 Å] indicates that charge delocalization is widespread throughout the thiosemicarbazone skeleton (Matesanz *et al*., 2016). This suggests that

the S1=C9-N4-N2=C7 sequence in both residues has an all-trans conformation, as evidenced by the torsion angles of the C9-N4-N2 and C7-N2-N3 chains, which are 120.3(3)° and 118.1(3)°, respectively (Osman, *et al*., 2020).

4.3.3 Anticancer activity of 5,7-dibromoisatin N(4)-substituted thiosemicarbazones (17 – 26)

Breast cancer cells (MCF-7, MDA-MB-231), Lung cancer cells (A549), Skin cancer cells (A431), Hypotriploid human cell (NCIH-460), Human prostate cancer cell (PC-3), and Prostate epithelial cell (PNT-2) 2500 cells were grown on 96 well plates in control (DMSO), then incubated for 72 hours with varied concentrations of 1, 3, 10, and 30 μM. As cell viability, the anticancer effects of the synthesized compounds were tested against breast cancer (MDA-MB-231) and normal prostate epithelial cell (PNT-2). In micromolar concentrations, the compounds exhibited significant anticancer efficacy (IC_{50}; 2.47 to >10 μM). The compound **DiBrIstTmor** has higher anticancer potency in MDA-MB-231 (IC_{50}; 2.74 μM) and PNT-2 (IC_{50}; 2.54 μM) compared to the other compounds. At the highest concentration of 10 μM the PNT-2 cells showed 82% viability in the compound **DiBrIstMor**. So, the upper limit of 10 μM is considered as IC_{50} value for the same compound.

The compound (**21**) shown to be effective against the majority of cancer cell lines, including A431, A549, MDA-MB-231, and PC-3, due to two methyl groups in the 2 and 6 positions of the morpholine ring. The substance (**25**) had a somewhat effective influence on the cancer cell lines A431, MDA-MB-231, and PNT-2. This is caused by the methyl group that is present at the thiosemicarbazone moiety's N(4) position. The modest anticancer activity of compound (**24**) was demonstrated by the two methyl groups at the N(4) position.

Table 29: Cell viability (μM) against cancer cell lines for 72 h.

Compd↓ Cell lines→	Cancer cell lines (IC_{50}) in μM	
	MDA-MB-231	**PNT-2**
19	2.49 μM	>10 μM
20	2.47 μM	2.54 μM
21	7.26 μM	9.08 μM
24	2.57 μM	8.26 μM

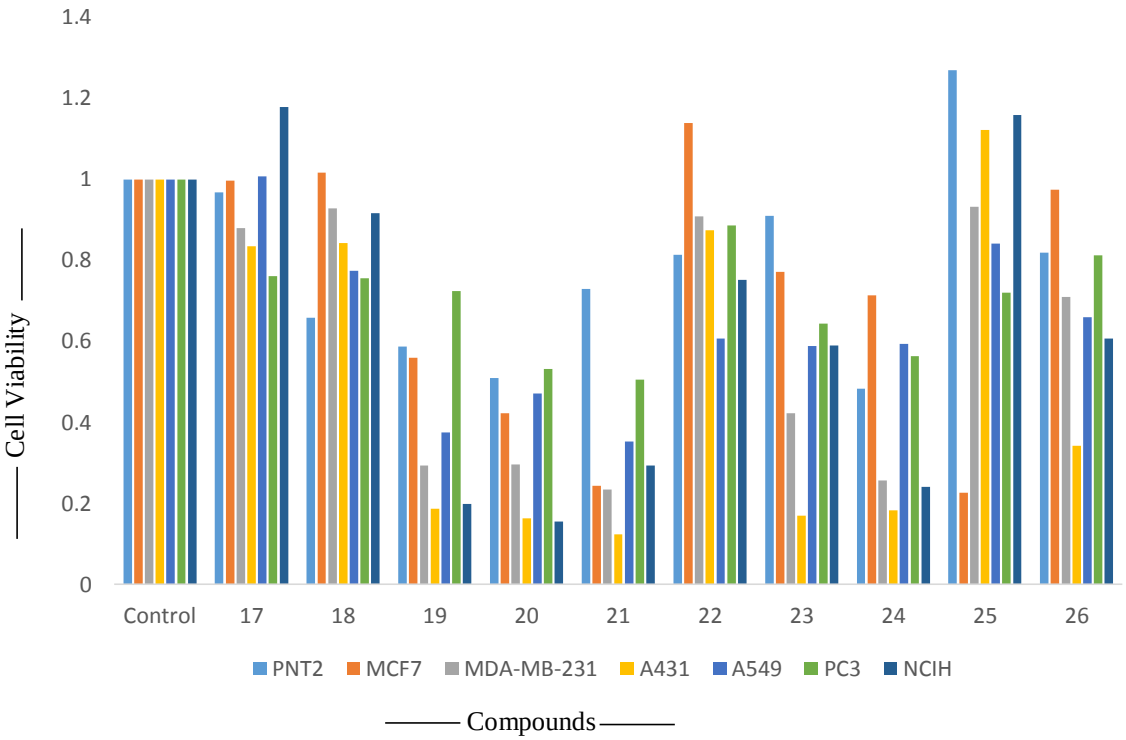

Figure 78: Cell viability assay of synthetic compounds with different concentration in different cell lines (17-26)

4.3.3.1 Conclusion

The anticancer activity of examined compounds against cancer cell lines MCF-7, MDA-MB-231, A549, A431, NCIH-460, PC-3 and PNT-2 differed slightly due to altering substituents on the N (4)-position of thiosemicarbazone moieties.

The synthesized compounds inhibited cell proliferation in the **MCF-7** cell line in the following order:

Compound **25** > Compound **21** > Compound **20** > Compound **19** > Compound **24** > Compound **23** > Compound **26** > Compound **17** > Compound **18** > Compound **22**

The synthesized compounds inhibited cell proliferation in the **A431** cell line in the following order:

Compound **21** > Compound **20** > Compound **23** > Compound **19** > Compound **24** > Compound **26** > Compound **17** > Compound **18** > Compound **22** > Compound **25**

The synthesized compounds inhibited cell proliferation in the **A549** cell line in the following order:

Compound **21** > Compound **19** > Compound **20** > Compound **23** > Compound **24** > Compound **22** > Compound **26** > Compound **18** > Compound **25** > Compound **17**

The synthesized compounds inhibited cell proliferation in the **MDA-MB-231** cell line in the following order:

Compound **21** > Compound **24** > Compound **20** > Compound **19** > Compound **23** > Compound **26** > Compound **17** > Compound **22** > Compound **18** > Compound **25**

The synthesized compounds inhibited cell proliferation in the **PNT-2** cell line in the following order:

Compound **24** > Compound **20** > Compound **19** > Compound **18** > Compound **21** > Compound **22** > Compound **26** > Compound **23** > Compound **17** > Compound **25**

The synthesized compounds inhibited cell proliferation in the **PC-3** cell line in the following order:

Compound **21** > Compound **20** > Compound **24** > Compound **23** > Compound **25** > Compound **19** > Compound 1**7** > Compound **18** > Compound **26** > Compound **22**

The synthesized compounds inhibited cell proliferation in the **NCIH-460** cell line in the following order:

Compound **20** > Compound **19** > Compound **24** > Compound **21** > Compound **23** > Compound **26** > Compound **22** > Compound **18** > Compound **25** > Compound 1**7**

Compounds (**21**) demonstrated more antiproliferative activity than the positive control (DMSO) in the cancer cell lines A431, A549, MDA-MB-231, and PC-3, whereas compound (**20**) had better anticancer potency than other compounds in the cell lines NCIH-460.

4.3.4 Molecular docking of compound HydIstAzep and DiBrIstEth

4.3.4.1 Density functional theory approximations

Quantum-chemical calculations in the realm of density functional theory (DFT) was employed for determining various quantities (Burke & Wagner, 2013). For this, an open-source program, CP2K was chosen for its versatility and user friendliness (Kühne *et al.*, 2020). The molecular structure of the test compounds was modeled and were proposed for molecular docking studies. An iterative search algorithm, BFGS (quasi

Newton) which approximates the inverse Hessian was employed in locating the global minima of the molecules without constraining any atoms or symmetry elements (Broyden, 1970). DZVP-MOLOPT-SR-GTH as localized basis set and BLYP as exchange-correlation functional were used with 500 Ry cutoff of kinetic energy in minimizing the molecular structures up to 1.0×10^{-6} Ry in energy and 1.0×10^{-4} Ry/Bohr in force (MAX and gradient) (Vondele & Hutter, 2007).

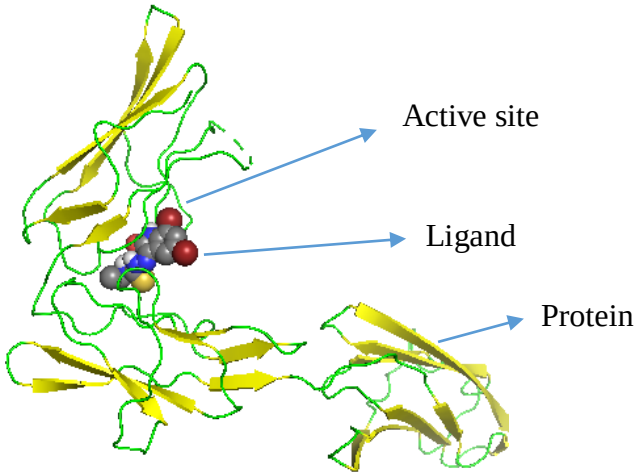

Figure 79: Illustration of a ligand (DiBrIstEth) docked in the active site of protein with PDB ID: 3MJG (carbon gray, nitrogen blue, oxygen red, sulfur yellow, hydrogen cream spheres, beta sheet yellow, loops green)

4.3.4.2 Molecular docking calculations

The best docked pose of the small molecule with the receptor protein was found by using ADFR software suite and its graphics user interface, AGFR (Ravindranath *et al.*, 2015). The orthosteric site in the protein was identified from the AutoSite sub-program and verified from the literature. Additionally, CASTp server was also used for locating the active site (Tian *et al.*, 2018). The number of independent searches were set to 48 with each GA using up to 10 million evaluations of the scoring functions. The high value ensured that the best possible docked pose was captured using different clusters and a global minimum resulted in a hydrated environment. The water map setting with default parameters in weight and entropy were chosen. Up to 15 amino acid residues at the active site were considered to be flexible and by default the small molecule possessed rotational degrees of freedom during the search. The box sizes for different proteins had large variations depending upon the size of the active site. The protein 7BJ6, with largest box (22 × 28 × 19 points) was chosen as an example and with slight

variation in others. The same padding (2.00), grid spacing (0.375 Å) and smoothing (0.500) were adopted for all the receptors and no flexible residues lied outside the box.

The pose with the best binding affinity obtained from the search in case of each receptor was considered for further analysis. A reference ligand was not chosen in any of the cases and RMSD value of each distinct output could not be calculated. Fig. 79 is an illustration of a docking pose of a ligand, **DiBrIstEth** in the active site of a protein with PDB ID of 3MLG.

4.3.4.3 Receptor proteins

Seven different proteins with their PDB ID and receptor classes that are considered as anti-cancer targets are tabulated in Table 30. The search for alternate prophylactics of cancerous cell addressing different types of growth factors and other enzymes were considered for spanning a broad range of possible targets. Here, *in silico* approach addresses targeted therapy that deals with the treatment of specific cancer by obstructing the pathways or mutations causing tumor cell proliferation. The receptor with maximum amino acid residue count of 1014 and minimum of 98 were used in this work and the PDB structures were retrieved from RCSB website (rcsb.org) (Berman *et al*., 2000). The protein structures were cleaned by removing water molecules, ions, metals, ligands and other small molecules. The polar hydrogens were added along with Gasteiger charges ensuring electro-neutrality of the target.

4ASD is a vascular endothelial growth factor receptor (VEGFR2) protein with 353 amino acid residue count. It is a protein tyrosine kinase receptor that regulates tumor-induced blood vessels formation, endothelial migration and proliferation (Miettinen *et al*., 2012). 3VHE is a similar target with 359 residue count. 3MJG is a platelet-derived growth factor receptor (PDGFR) and is involved in the development of different types of cancerous cells (Board & Jayson, 2005). Its antagonist could be a good therapeutic candidate. 3MJK is a protein associated with platelet-derived growth factor precursor with 1014 residues. Only A and B chains were considered for molecular docking. 7BJ6 is a murine double minute 2 protein and is considered vital in p53 regulation and cancer cell suppression. 2VTA has been top ranked (highest fit score) by an online program PharmMapper (http://59.78.96.61/pharmmapper) (Wang *et al*., 2017) as potential target (cell division protein kinase 2) in cancer treatment. It consists of a single chain with 298 residues and ligands based on its docking have been currently under clinical trials

(Wyatt *et al*., 2008). 6LVK is a fibroblast growth factor receptor 3 used in specially the therapeutics of bladder cancer has been shown to have significant results over VEGFR2 proteins (Kuriwaki *et al*., 2020). This protein in a monomer with 626 residues. These target proteins were selected from different domains and class to encompass broad spectrum in the development of therapeutics against different types of cancer by computational methods. The evaluation of protein structure was performed by Protein Structure Analysis and Verification Server (Mazumder *et al*., 2022) using ERRAT (Colovos & Yeates, 1993) and PROCHECK (Laskowski *et al*., 1993) programs. The results showed acceptable quality of the published structures that could be used for molecular docking calculations without any further fixation or revision.

Table 30: Brief details of receptors taken for molecular docking calculations

Receptor class	PDB ID ↓	Feature (residues)	Overall Quality Factor (Disallowed %)
VEGFR2	4ASD	A monomer (353)	98.64 (0.4%)
PDGFR	3MJG	A hetero-4-mer (922)	82.25 (0%)
PDGF precursor	3MJK	A homo-2-mer (1014)	85.96 (0%)
MDM2 protein	7BJ6	A monomer (98)	100.00 (0%)
Cyclin dependent kinase 2	2VTA	A monomer (298)	88.02 (0%)
VEGFR2 kinase domain	3VHE	A monomer (359)	97.25 (0%)
FGFR3	6LVK	A monomer (626)	98.49 (0%)

4.3.4.4 Test compounds, control drugs and ADMET prediction

Thiosemicarbazones (-NNC=SN-) and their derivatives are the compounds having significant biological and therapeutic values (Sibuh *et al.*, 2021). This work encompasses specifically a search for their anti-cancer activity by *in silico* methods. This includes stand alone computer programs and online servers. The geometry (ball and stick model) of the test compounds as obtained from DFT calculations are shown in Fig. 80. In order to compare the performances of the test compounds, two FDA drugs, Ruxolitinib and Lenalidomide have also been considered. Their structures (sdf format) and other information were obtained from PubChem database (https://pubchem.ncbi.nlm.nih.gov/) (Kim *et al*., 2021). The molecular structures were optimized by molecular mechanics using conjugate gradient algorithm with Newton's

method as line search technique (> 200 structures). Universal force field was used for the atoms with energy convergence of 10^{-7} units. The molecular structures were obtained as pdb files and the minimization was performed by Avogadro software (Hanwell *et al*., 2012) without any structural constraints. Their drug likeness, pharmacodynamics and pharmacokinetics were studied by computational methods using various online servers like Pro Tox II (https://tox-new.charite.de/protox_II/) (Banerjee *et al*., 2018) and pkCSM (https://biosig.lab.uq.edu.au/pkcsm/) (Pires *et al*., 2015).

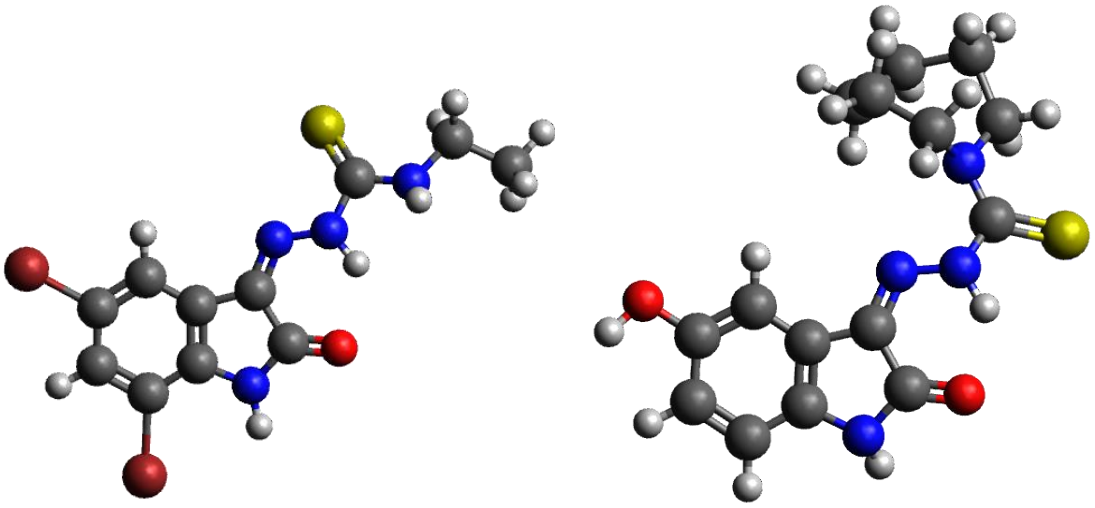

(**a**) (**b**)

Figure 80: Geometry optimized molecular structure of (a) DiBrIstEth and of (b) HydIstAzep (Oxygen in light red, carbon in gray, sulfur in yellow, nitrogen in blue, bromine in dark red and hydrogen in shaded white)

Ruxolitinib is an approved anti-cancer drug of class tyrosine kinase inhibitor (antineoplastic agent) and Lenalidomide is an immunomodulatory drug used in the treatment of various types of cancer. It is an angiogenesis and metastasis inhibitor that stops endothelial cell migration. The list of the compounds is provided in Table 31.

Table 31: Short details of the test compounds and two FDA approved drugs; Isomeric/canonical SMILES

Compounds	**Molecular formula**	**Short description**
DiBrIstEth	$C_{11}H_{10}N_4OSBr_2$	A test compound, a halogenated thiosemicarbazone; [H]N2c1c([Br])c([H])c([Br])c([H])c1/C(=N/[N]([H])C(=[S])N([H])C([H])([H])C([H])([H])[H])C2=O

HydIstAzep	$C_{15}H_{18}N_4O_2S$	A test compound, a thiosemicarbazone; O=C2N([H])c1c([H])c([H])c(O[H])c([H])c1/C2=N/[N]([H])C(=[S])N3C([H])([H])C([H])([H])C([H])([H])C([H])([H])C([H])([H])C3([H])[H]
Ruxolitinib	$C_{17}H_{18}N_4$	A reference drug, a pyrrolopyrimidine, Janus kinase inhibitor modulating the immune response; C1CCC(C1)[C@@H](CC#N)N2C=C(C=N2)C3=C4C=CNC4=NC=N3
Lenalidomide	$C_{13}H_{13}N_3O_3$	A reference drug, a thalidomide analog blocking the formation of neoplasms; C1CC(=O)NC(=O)C1N2CC3=C(C2=O)C=CC=C3N

4.3.4.5 Computational resources

Readily available free software and free servers were used throughout the computational work. The binaries of Avogadro, PyMol (Rayan & Rayan, 2017) and Biovia discovery studio visualizer (Khan *et al*., 2020) programs were downloaded from the internet and used without compilation. An Intel CPU desktop with 256 GB of memory and 6 TB of storage was used for the calculations. Ubuntu 20.04 and Windows 8.1 operating systems were used depending upon the compatibility of the programs.

4.3.5 Results and discussion

4.3.5.1 Physicochemical properties of test molecules

Some important physicochemical properties of two synthesized molecules calculated by Pro tox II and pdCSM servers (https://biosig.lab.uq.edu.au/pdcsm_cancer/) (Al-Jarf *et al*., 2021) are shown in Table 32. **DiBrIstEth** is comparably more lipophilic than **HydIstAzep** as suggested by their partition coefficients and that the later has more polarizability than the former as shown by their refractivity values. All the parameters lie between the acceptable limits and thus can be considered as good candidates for additional analysis.

Table 32: Physicochemical properties of two test molecules

Properties	**DiBrIstEth**	**HydIstAzep**
Molecular refractivity	88.64	96.38
Octanol/water partition coefficient (logP)	2.35	1.80
Surface area ($Å^2$)	132.02	133.74

4.3.5.2 Druglikeness and pharmacology studies

In order to find the druglikeness and ADMET properties of the test compounds, various parameters were determined using pkCSM servers and Pro Tox II. The ADMET predictions are shown in Table 33. The data show that majority of the parameters lie within the acceptable range (between upper and lower limits) and Lipinski's rule of five were not violated. Both the test compounds fall under class 5 of toxicity which implies that it may be harmful if swallowed according to the relation $2000 < LD50 \leq 5000$ (units mg/Kg). This suggests an administration of smaller doses of compounds for safety measures.

Table 33: ADMET predicted by pkCSM server

Model Name	Unit	Predicted Value	
		DiBrIstEth	HydIstAzep
Absorption			
Water solubility	Numeric (log mol/L)	-4.46	-4.2
Caco2 permeability	Numeric (log Papp in 10^{-6} cm/s)	1.04	0.87
Intestinal absorption (human)	Numeric (% Absorbed)	87.83	93.32
Skin Permeability	Numeric (log Kp)	-2.95	-3.00
P-glycoprotein substrate	Categorical (Yes/No)	No	Yes
P-glycoprotein I inhibitor	Categorical (Yes/No)	No	No
P-glycoprotein II inhibitor	Categorical (Yes/No)	No	No
Distribution			
VDss (human)	Numeric (log L/kg)	0.03	-0.13
Fraction unbound (human)	Numeric (Fu)	0.40	0.39
BBB permeability	Numeric (log BB, <-0.30)	-0.12	-0.93
CNS permeability	Numeric (log PS, <-2.00)	-3.00	-3.37
Metabolism			
CYP2D6 substrate	Categorical (Yes/No)	No	Yes
CYP3A4 substrate	Categorical (Yes/No)	No	No
CYP1A2 inhibitior	Categorical (Yes/No)	Yes	No
CYP2C19 inhibitior	Categorical (Yes/No)	Yes	No
CYP2C9 inhibitior	Categorical (Yes/No)	No	No
CYP2D6 inhibitior	Categorical (Yes/No)	No	No
CYP3A4 inhibitior	Categorical (Yes/No)	No	No

Excretion			
Total Clearance	Numeric (log mL/min/kg)	-0.41	-0.14
Renal OCT2 substrate	Categorical (Yes/No)	No	No
Toxicity			
AMES toxicity	Categorical (Yes/No)	No	No
Max. tolerated dose (human)	Numeric (log mg/kg/day)	0.66	-0.36
hERG I inhibitor	Categorical (Yes/No)	No	No
hERG II inhibitor	Categorical (Yes/No)	No	Yes
Oral Rat Acute Toxicity (LD50)	Numeric (mol/kg)	2.9	2.61
Oral Rat Chronic Toxicity (LOAEL)	Numeric (log mg/kg_bw/day)	1.76	1.64
Hepatotoxicity	Categorical (Yes/No)	No	Yes
Skin Sensitization	Categorical (Yes/No)	No	No
T.Pyriformis toxicity	Numeric (log ug/L)	1.2	0.4
Minnow toxicity	Numeric (log mM)	1.25	1.99

The test compounds have better VDss relative to Ruxolitinib but their total clearance is lower. The oral rat toxicities are also relatively better and the drug shows hepatotoxicity. A quick comparative analysis shows that the test compounds have acceptable properties that may be subjected to further studies. This verifies the drug likeness and the toxicity profile is shown in Table 34.

Table 34: Toxicity profile of two test compounds by Pro Tox II server

Classification, Target		**DiBrIstEth**		**HydIstAzep**	
		Prediction	Probability	Prediction	Probability
Organ toxicity	Hepatotoxicity	Inactive	0.53	Inactive	0.61
Toxicity end points					
Carcinogenicity		Active	0.55	Active	0.51
Immunotoxicity		Inactive	0.84	Active	0.57
Mutagenicity		Inactive	0.5	Inactive	0.55
Cytotoxicity		Inactive	0.65	Inactive	0.64

Tox21-Nuclear receptor signalling pathways				
Aryl hydrocarbon Receptor (AhR)	Active	0.51	Inactive	0.84
Androgen Receptor (AR)	Inactive	0.96	Inactive	0.93
Androgen Receptor Ligand Binding Domain (AR-LBD)	Inactive	0.96	Inactive	0.97
Aromatase	Inactive	0.91	Inactive	0.94
Estrogen Receptor Alpha (ER)	Inactive	0.85	Inactive	0.85
Estrogen Receptor Ligand Binding Domain (ER-LBD)	Inactive	0.97	Inactive	0.97
Peroxisome Proliferator Activated Receptor Gamma (PPAR-Gamma)	Inactive	0.81	Inactive	0.86
Tox21-Stress response pathways				
Nuclear factor (erythroid-derived 2)-like 2/antioxidant responsive element (nrf2/ARE)	Inactive	0.94	Inactive	0.87
Heat shock factor response element (HSE)	Inactive	0.94	Inactive	0.87
Mitochondrial Membrane Potential (MMP)	Inactive	0.68	Inactive	0.79
Phosphoprotein (Tumor Supressor) p53	Inactive	0.89	Inactive	0.91
ATPase family AAA domain-containing protein 5 (ATAD5)	Inactive	0.94	Inactive	0.95

Both the compounds show activeness (probability of slightly more than 0.50) in two of the cases and hint at the cautionary proposition for further trials. Surprisingly, Ruxolitinib and Lenalidomide both show class 4 toxicity (LD50 of 800 and 700 mg/Kg respectively) despite being FDA approved drugs. Their borderline carcinogenicity shows that the test compounds require proper *in vivo* assay for correct prediction of toxicity.

4.3.5.3 Anticancer properties by graph-based signatures

The compounds with anti-cancer properties were analyzed using pdCSM, a server-based approach. The input parameter as smiles notation was used for the job submission

as 3D crystal geometry was not required. The fragment and graph-based signatures in the algorithm predicts the anti-cancer activity (GI_{50}) of small molecules against 74 cancer cell lines. It was observed that the test compound **DiBrIstEth** was active against breast (MCF7, MDA-MB-231, ATCC, MDA-MB-468, T-47D), CNS (SF-295, U251), leukemia (CCRF-CEM, K-562, P388-ADR), non-small cell lung (NCIH-460), ovarian (OVCAR-4, SK-OV-3), prostate (PC-3), and renal (SN12K1) cancer cell lines. **HydIstAzep** was active against breast (MDA-MB-231, ATCC, MDA-MB-468, T-47D), colon (COLO-205), leukemia (CCRF-CEM, HL-60TB, K-562, P388-ADR, P388, SR), melanoma (MDA-MB-435), non-small cell lung (NCIH-460), ovarian (NCI-ADR-RES, OVCAR-4), prostate (DU-145, PC-3), renal (SN12C, SN12K1), and small cell lung (DMS-273) cancer cell lines.

It was determined that the molecule **DiBrIstEth** is a potent CDK2 inhibitor (IC_{50} < 10 μM) and the value of pK_i equal to 5.803 (CDK2-ligand binding affinity, non-allosteric) from kinCSM predictor be (https://biosig.lab.uq.edu.au/kin_csm/). Similarly, **HydIstAzep** was also found to be a potent CDK2 inhibitor (IC_{50} < 10 μM) with pK_i of 5.718. These findings hint that the test compounds possess anti-cancer properties that are worthwhile to be studied at the next level of experimental investigation. Fragmentation of compounds that affects protein phosphorylation was explored by this server and it was deduced that the potential type of inhibition was type I1/2 and type I for the two thiosemicarbazones respectively.

The pharmacokinetic and toxicity properties as calculated by graph-based signatures show that the compound, **DiBrIstEth** possesses fully acceptable values. However, in case of the compound, **HydIstAzep**, some parameters (reaction with P-gp, hERG II inhibition and liver toxicity) point towards its unacceptability as a drug. After additional experimental confirmations only then, true nature can be established.

4.3.5.4 Flexible receptor molecular docking

The binding affinities of various compounds with different receptors in hydrated environment are shown in Table 35. In all the cases, compound **HydIstAzep** display better values than the compound **DiBrIstEth** and the control drug Lenalidomide. The other control drug Ruxolitinib, however show better binding than **HydIstAzep** in five cases. It yielded stronger interaction in all the seven cases than **DiBrIstEth**. In case of the receptors with PDB ID: 4ASD and 7BJ6, **HydIstAzep** showed better binding

affinity than Ruxolitinib. Apparently, the molecular mass may be a major factor in determining the interaction strength with the amino acid residues along with the type and frequency of non-covalent interactions. Atomic level analysis would shed some light on the true nature of various types of interactions and is presented in the next section.

Table 35: Binding affinities (kCal/mol) of two test compounds and two drugs against different receptor proteins (PDB ID) related to malignant tumors

	Mol. Mass	4ASD	3MJG	3MJK	7BJ6	2VTA	3VHE	6LVK
DiBrIstEt	406.09	-10.4	-9.3	-8.4	-7.9	-10.0	-9.4	-8.3
HydIstAzep	318.39	-11.1	-9.6	-8.6	-9.0	-10.4	-10.1	-9.0
Ruxolitinib	306.40	-10.6	-10.1	-8.7	-8.8	-11.4	-10.4	-9.7
Lenalidomide	259.26	-9.7	-9.2	-8.2	-7.8	-9.2	-9.2	-8.4

4.3.5.5 Non-covalent interactions present in adduct

The different types of non-covalent interactions and its frequency between the amino acid residues at the active site of the protein and the docked ligand determines the strength of the protein-ligand binding. Only those protein and ligand interactions with binding affinities of less than or equal to -10.0 kCal/mol are considered (corresponding to the top five cases) for analysis and are shown in Fig. 81-85. Stronger binding results in a stable complex and the protein would be inhibited of its regular functioning resulting in the treatment of the disease. Hence, the pose of the ligand that forms strong and effective bonding with the residues at the active site is the desired goal in cost-reduced structure-based drug design strategy (Blaney, 2012). Many formulations like Zanamivir (Hentabli *et al*., 2016) and Nelfinavir (Kaldor *et al*., 1997) have been discovered using this technique and many others have circumvented the expensive experimental high-throughput screenings (Batool *et al*., 2019).

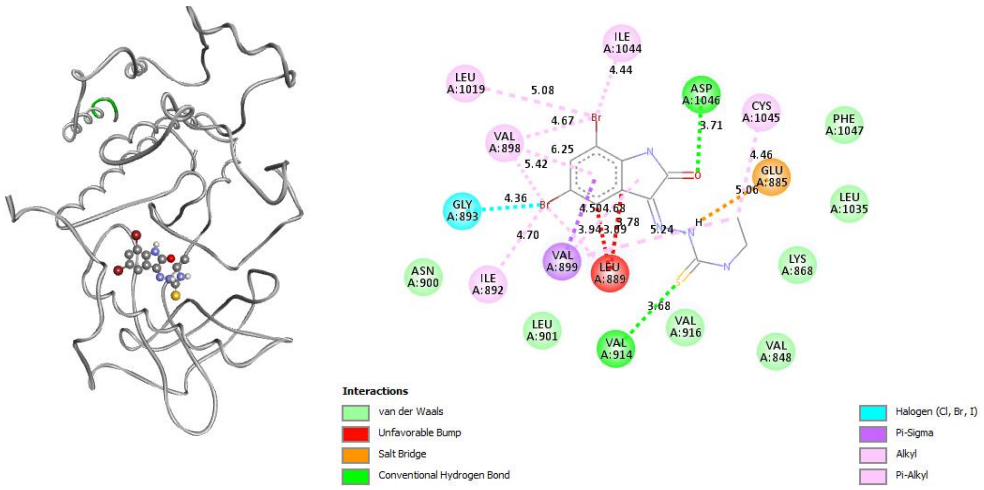

(**a**) (**b**)

Figure 81: Best docked pose of DiBrIstEth with receptor 4ASD as (a) 3D and (b) 2D plot with different types of interactions

The receptor flexibility incorporated into the modelling along with that of the ligand's with solvation provides the closest resemblance to the realistic models as in biological systems. Fig. 81-85 show the top five best docked poses of thiosemicarbazones at the active site of the proteins.

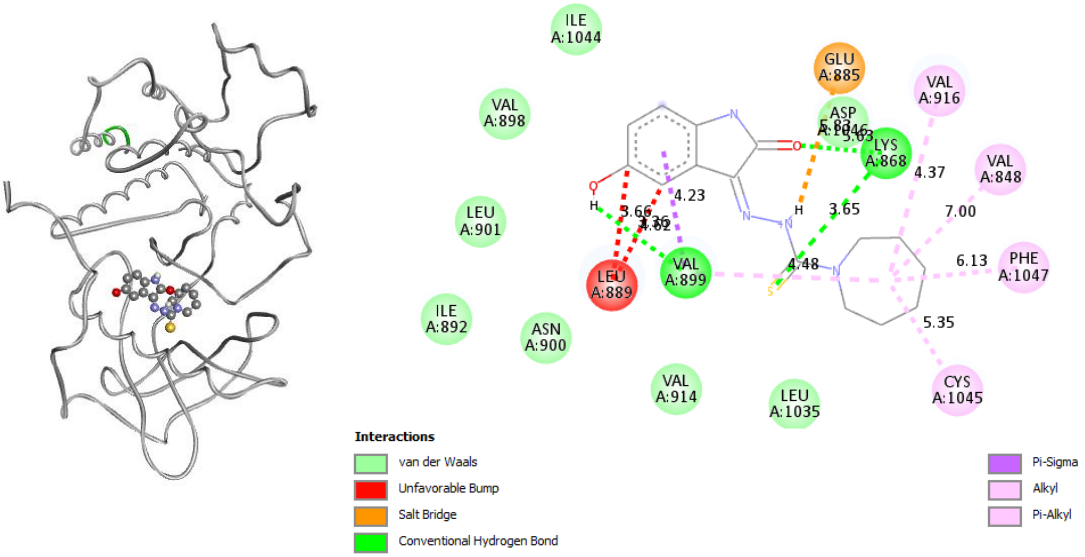

(**a**) (**b**)

Figure 82: Best docked pose of HydIstAzep with 4ASD as (a) 3D and (b) 2D plot with different types of interactions

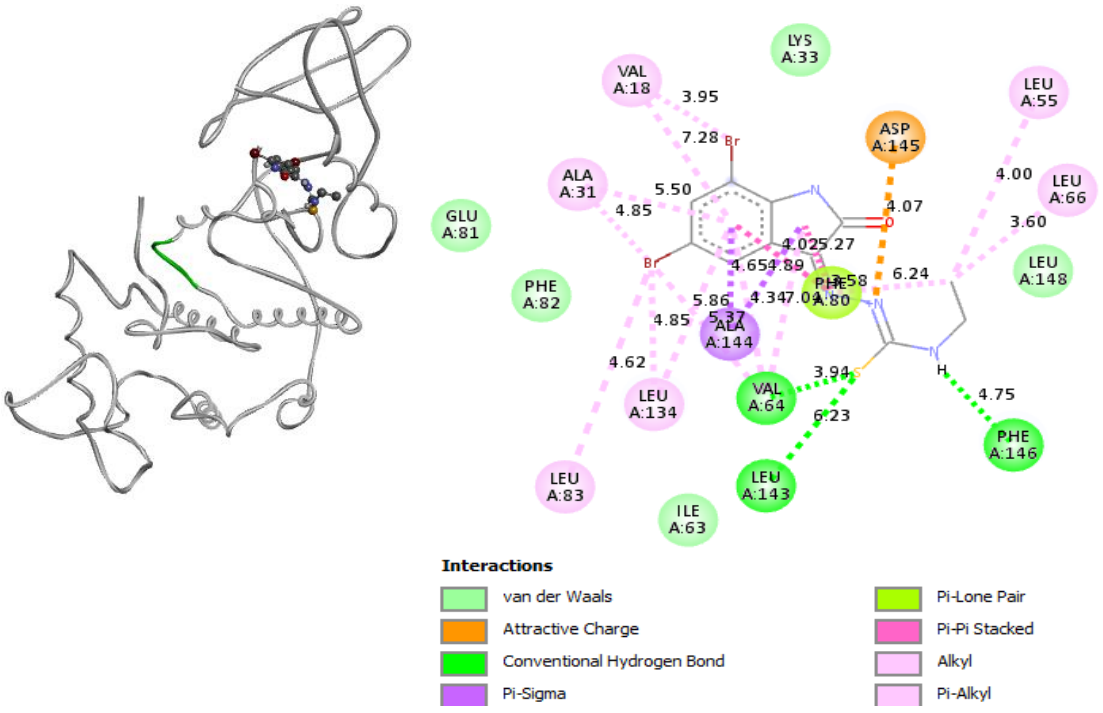

(**a**) (**b**)

Figure 83: Best docked pose of DiBrIstEth with 2VTA as (a) 3D and (b) 2D plot with different types of interactions

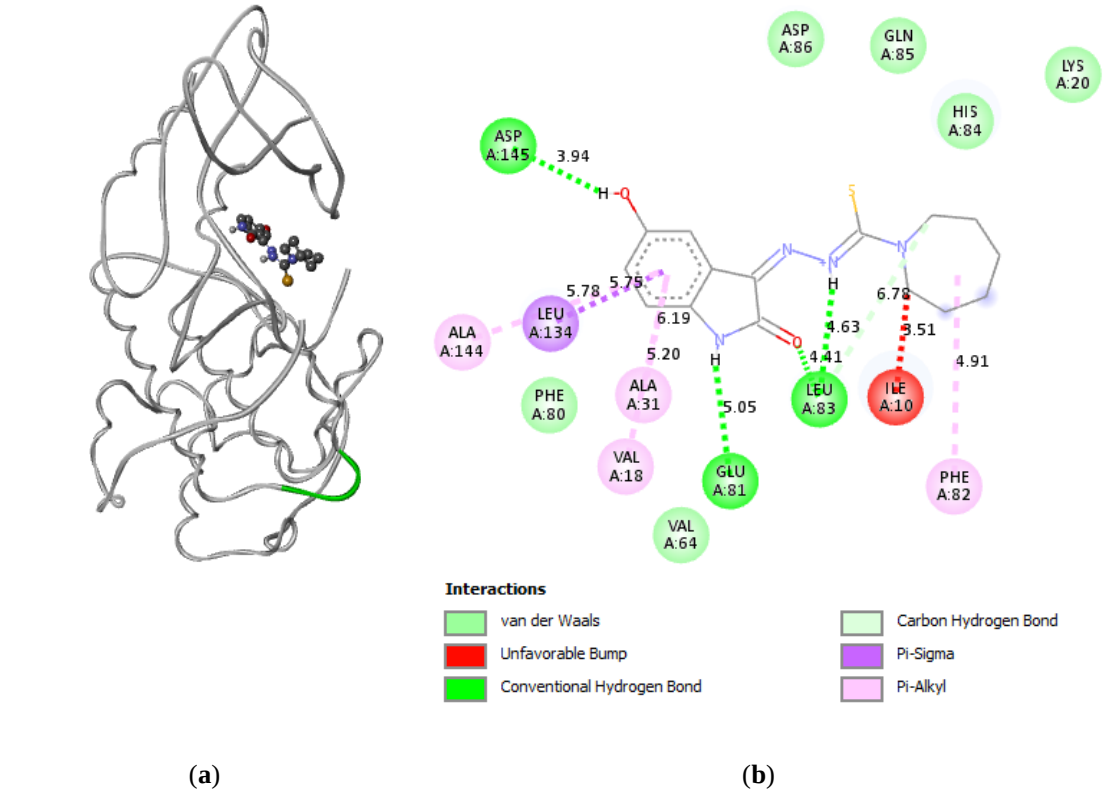

(**a**) (**b**)

Figure 84: Best docked pose of HydIstAzep with 2VTA as (a) 3D and (b) 2D plot with different types of interactions

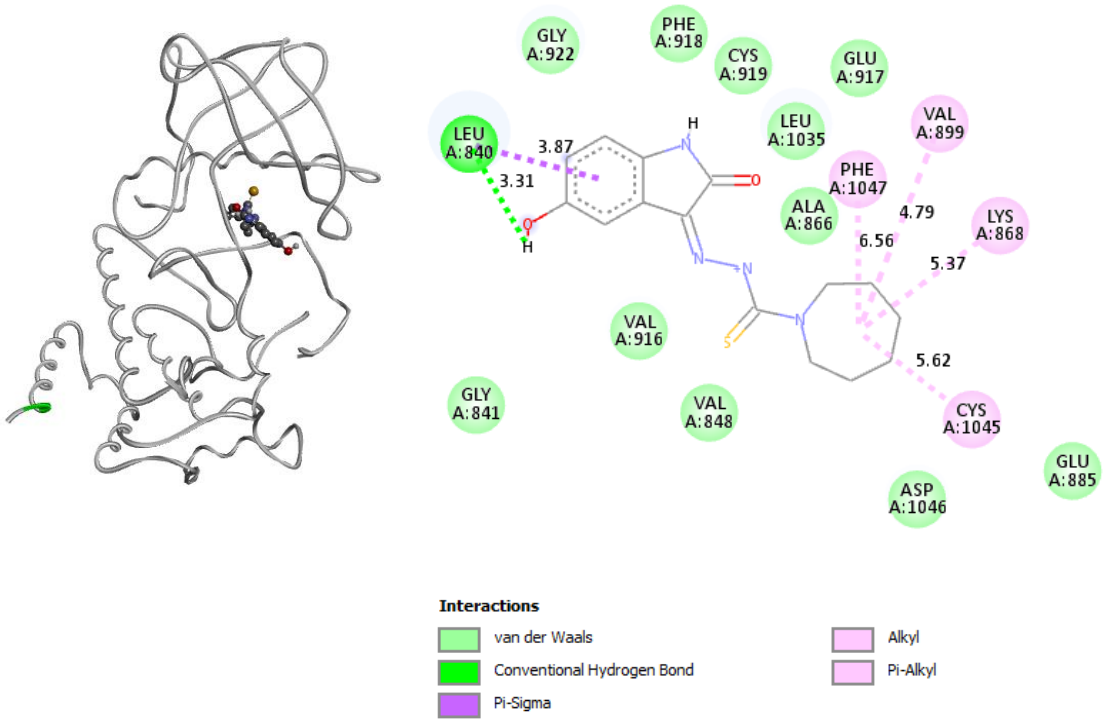

(**a**) (**b**)

Figure 85: Best docked pose of HydIstAzep with 3VHE as (a) 3D and (b) 2D plot with different types of interactions

The presence of different types of non-covalent interactions (hydrogen bonding, ionic, unfavorable, pi, halogen and alkyl related) between different amino acid residues of various proteins and the ligands are shown in Table 36. The hydrogen bonding distances show that majority of these are moderately strong. Even though some unfavorable interactions are present, all the other non-covalent interactions make the complex stable. In case of 4ASD-**DiBrIstEth** complex, the key amino acid residues VAL914, ASP1046, GLU885, LEU889, ILE892, VAL899, VAL898, LEU1019, ILE1044, CYS1045, and GLY893 are involved and have also been reported for other cancer drugs (Naithani, 2021). In case of 4ASD-**HydIstAzep** complex, the major interactions are with the key residues LYS868, VAL899, GLU885, LEU889, VAL899, VAL848, VAL916, CYS1045, AND PHE1047. Comparing the two cases with the same receptor, it can be inferred that the residues involved in interactions except hydrogen bonding are nearly the same (Ahmed *et al*., 2021). This can be attributed to different functional groups or atoms present in the ligands that participate in the interactions.

The receptor 2VTA, has been found to interact with the first test compound through the residues VAL64, LEU143, PHE146, ASP145, VAL18, ALA31, LEU55, LEU66, PHE80, LEU83, ALA144, and LEU134. In case of second test compound, the residues are GLU81, LEU83, ASP145, ILE10, VAL18, ALA31, PHE82, ALA144, and LEU134. All the residues are the same as in its native ligand considering the two cases (Wyatt *et al*., 2008).

The complex of 3VHE with **HydIstAzep** involves the residues LEU840, LEU840, LYS868, VAL899, CYS1045, and PHE1047 interacting with the ligand. For this receptor, different amino acid residues GLU917 and LYS920 have been reported in case of Indigocarpan in other studies (Paramashivam *et al*., 2015). A formation of three covalent bonds has been reported in the docked structure by a ligand 1, 3, 4 Oxadiazoles with the involvement of different residues like HIS1024, ILE1044, and CYS1045 in this receptor (Holmes *et al*., 2015). This suggests a possibility of even stronger binding of the ligand at this active site. Moreover, LEU840 has been shown to be a key amino acid residue in chrysoeriol compound docked with 3VHE receptor (Lai *et al*., 2018). However, ASP1046 and CYS919 are two new amino acid residues reported at the binding site. LEU840, LYS868, and PHE1047 are the three residues that are common in many of these complexes. Furthermore, valine and leusine (non-polar residues) seem to be the common ones that are involved in non-covalent interactions with the ligands. Considering all the above cases, the involvement of some common amino acid residues suggests that the test compounds are bound at the vicinity of the active site of the protein and thus suggests its effective inhibition.

Table 36: Key amino residues involved in major interactions in different complexes

Complexes	Hydrogen-bonds (Distance, Å)	Salt-bridge/others	Pi, alkyl and halogen related
4ASD-**DiBrIstEt**	VAL914 (3.68), ASP1046 (3.71)	GLU885, LEU889	ILE892, VAL899, VAL898, LEU1019, ILE1044, CYS1045, GLY893
4ASD-**HydIstAzep**	LYS868 (3.65, 5.63), VAL899 (3.66)	GLU885, LEU889	VAL899, VAL848, VAL916, CYS1045, PHE1047
2VTA-**DiBrIstEth**	VAL64 (3.94), LEU143 (6.23), PHE146 (4.75)	ASP145	VAL18, ALA31, LEU55, VAL64, LEU66, PHE80, LEU83, ALA144, LEU134
2VTA-**HydIstAzep**	GLU81 (5.05), LEU83 (4.41, 4.63), ASP145 (3.94)	ILE10	VAL18, ALA31, PHE82, ALA144, LEU134
3VHE-**HydIstAzep**	LEU840 (3.31)	-	LEU840, LYS868, VAL899, CYS1045, PHE1047

The ethyl end of the compound **DiBrIstEth**, has at most three interactions (no hydrogen bonds) with the residues and hence do not provide stronger interactions required for the stability of the adduct. Its substitution with other hetero-atom (electron donating, hydrogen acceptor) or with polar hydrogen containing functional groups (hydrogen donor) capable of forming hydrogen bonds may lead to stronger binding at the active pocket. The presence of hydrogen bond acceptors (HBA) and hydrogen bond donors (HBD) that actually form well orientated strong hydrogen bonds tend to facilitate protein-ligand binding (Chen *et al*., 2016). The other extreme of the molecule indeed has many interactions and hence this rationale for substituent exploration is justified. Hence there are numerous possibilities of generating compounds with different functional groups that may be better in the formation of a stable complex with a receptor. A virtual screening of thousands of molecules from a database constructed using criteria based on optimum pharmacophoric features seems to be an interesting avenue to pursue in the quest for alternate anti-cancer drug. This proposition is based on the presence of multiple nitrogen atoms in Ruxolitinib where stronger hydrogen bonding is feasible at different parts of the structure. To be more specific, the pharmacophoric feature consisting of hetero aromatic ring, linker (spacer), HBA-HBD and a hydrophobic tail in the structure of an effective drug like molecule has been published (Elkaeed *et al*., 2022, Aziz *et al*., 2022) which could be applied in same or modified conditions. The lack of strong hydrogen bonding at the HBD-HBA part of the molecules in majority of the cases studied points towards the change in one or more groups in the molecular structure. The test molecules do follow this feature and alternate designs exploring its multiple groups would be even more interesting to carry out as future research.

4.3.5.6 Conclusion and prospective

Different computational methods were applied in the assessment of anti-cancer properties of two thiosemicarbazones, **DiBrIstEth** and **HydIstAzep** and were found to be biologically active. It showed better protein-ligand binding affinity than a control drug from molecular docking calculations in a solvated environment. Molecular level analysis of poses and different interactions in receptor-ligand complexes revealed the participation of key amino acid residues as in other systems with the functional groups or atoms of the ligands. The druglikeness along with ADMET predictions showed that

the compounds require further *in vitro* assays and *in vivo* trials to confirm their toxic properties.

In order to expand the search space of thiosemicarbazones for developing drugs with higher efficacy and specificity, functionalization at different parts of the structure seems to be an appropriate design strategy. In order to determine the stability of a protein-ligand complex in physiological conditions, molecular dynamics simulation (200 ns production run) and free energy calculations are required. Appropriate steps are being carried out in this direction in the quest for better alternate formulation of an anti-cancer drug.

CHAPTER 5

5. CONCLUSION AND RECOMMENDATIONS

5.1. Conclusion

The simultaneous occurrence of condensation between isatin derivative and NH; of the thiosemicarbazide moiety and transamination, in which the N-methylaniline from 4-methyl-4-phenyl thiosemicarbazide (4mpt) is replaced by the amine present in the solution, is required for the preparation of the thiosemicarbazones from respective thiosemicarbazides in a single step. N-methylaniline behaves as a good leaving group in the reaction since the outcome of the reaction is dependent on the strength of the bases. The solvent is essential to the process as well. Acetonitrile (MeCN) is employed as the solvent in this instance, and a modest refluxing condition is applied. The *in vitro* cytotoxic study of synthesized 5-substituted (-OMe, -OH) and 5,7-disubstituted (-Br) isatin thiosemicarbazones showed that most of the compounds experience significant cytotoxic activity toward breast cancer (MCF-7), skin cancer (A431) and lung cancer (A549). The potency of the tested compounds against these cell lines were found to vary slightly with the variation in N(4) substitution and substitution at the parent isatin ring at C5 and C7-postion. There are numerous derivatives with higher biological activity as a result of the structural changes made to the isatin ring at the locations C5, and C7. Hybridization is a promising approach for drug development since hybrid molecules have the potential to increase specificity, increase effectiveness, and overcome drug resistance. Many hybrid compounds are now through various phases of clinical trials. Mono- and di-substitution are permitted for the phenyl ring's substitutes at positions C5, and C7, and the addition of an electron-donating or electron-withdrawing group at position C5 is helpful for regulating the electronic effect, lipophilicity, and physicochemical property. Through improved recognition by important biomolecules (DNA and proteins), thiosemicarbazone moieties appear to improve their antiproliferative effects.

5.2. Recommendation for further work

The recommendation for further research concerning its impact gives new directions in the field of research. This dissertation work has been established that 5-substituted (-OMe, -OH) and 5,7-disubstited (-Br) isatin thiosemicarbazones has been showed highest to moderate anticancer potency towards different cancer cell lines. The mechanisms that affect anticancer efficacy can be discovered through mechanism analysis, and these aspects can be taken into account when designing more effective molecules. The substitution at C5 or C5 & C7 position of isatin ring leads to considerable anticancer activity. Therefore, anticancer activity of 5-substituted (-OMe, -OH) and 5,7-disubstituted (-Br) isatin thiosemicarbazones and modification at N(4) position should explore.

CHAPTER 6

6. SUMMARY

The thesis is divided into four chapters. The theoretical underpinnings for this research are described in a compact fashion in the first two chapters, and the rest of the chapter discusses the experiments and findings.

Chapter 1

This chapter gives a brief review of thiosemicarbazones, including their types (mono and bis), generic thiosemicarbazone synthesis processes, and the condensation of aldehydes or ketones with N-substituted thiosemicarbazides to generate thiosemicarbazones. It provides an introduction to the stereochemistry and bonding of thiosemicarbazones. It also explains the anticancer drug's mode of action. The anticancer activity of N(4)-substituted thiosemicarbazones and the reported considerable effects on the activity with structural alterations serve as the basis for the study's justification. The study's goals are the synthesis, characterization, and assessment of anticancer activity. Chemotherapy drugs can: prevent the creation of precursor DNA molecules, directly harm the DNA in the cell's nucleus, influence the formation or destruction of the mitotic spindles. The study is motivated by the anticancer activity of 5-substituted (-OMe, -OH) and 5,7-disubstituted (-Br) isatin thiosemicarbazones, as well as the considerable effects of structural alterations on activity. The goal of study is to synthesize, characterize, and test the anticancer activity of 5-substituted (-OMe, -OH) and 5,7-disubstituted (-Br) isatin thiosemicarbazones.

Chapter 2

This chapter contains a comprehensive overview of the literature on the biological action of thiosemicarbazones. According to research, thiosemicarbazones have a wide range of biological properties, including antibacterial, antiviral, antioxidant, antitubercular, and anticancer action. The strongest inhibitors of RR activity are thiosemicarbazones, which bind iron at the enzyme's active site or create an iron chelate that inhibits the enzyme by obliterating the tyrosyl radical in the R2 subunit of RR. Therefore, the goal of the current research is to generate novel thiosemicarbazones and assess their anticancer efficacy. Among the thiosemicarbazones, triapine (3-aminopyridine-2-carboxaldehyde thiosemicarbazone, 3-AP) is the most promising

molecule undergoing clinical phase II studies. A series of thiosemicarbazones derived from 2-acetylpyridine, 2-acetylquinoline and l-acetylquinoline was evaluated as inhibitors of type l and type 2 herpes simplex virus and some of them were highly active. Isatin-β-thiosemicarbazones selectively kill multidrug resistant P-glycoprotein over expressing tumor cells. The overall activity against a panel of human cancer cell lines was improved by up to 100-fold by increasing the number of electron-withdrawing groups on the ring to generate combinations of dibromo-, tribromo-, iodo-, and nitro-isatin derivatives. Tyrindoleninone (6-bromo-2-methylthio-3H-indol-3-one), was evaluated towards U937 cells with IC_{50} = 4 µM by using human monocyte-like, histiocytic lymphoma cells. The non-small cell lung cancer cell line HOP-92, the colon cancer cell line HCT-116, the CNS cancer cell line SNB-75, the ovarian cancer cell line OVCAR-3, and the renal cancer cell line RXF 393 were all discovered to be highly active growth inhibitors of the 5-Bromoisatin derivative with GI_{50}; 0.01 µM, 0.018 µM, 0.0159 µM, and 0.0197 µM, respectively.

Chapter 3

The synthesis of carbothiohydrazides and thiosemicarbazones are discussed in this chapter. **El-Sawaf** and **Scovill's** method of condensation reaction was used to synthesis the thiosemicarbazides with the N-substitution. The condensation of 5-substituted (-OMe, -OH) and 5,7-disubstituted (-Br) isatin with desired carbothiohydrazide in absolute alcohol using a catalytic quantity of glacial acetic acid resulted in N(4) substituted thiosemicarbazones. The thiosemicarbazones synthesized are:

- 5-Methoxyisatin derived thiosemicarbazones (**1-6**)
- 5-Hydroxyisatin derived thiosemicarbazones (**7-16**)
- 5,7-Dibromoisatin derived thiosemicarbazones (**17-26**)

Chapter 4

The results and discussion of the synthesized thiosemicarbazones (**1-26**); six 5-methoxyisatin derived TSCs (**1-6**), ten 5-hydroxyisatin derived TSCs (**7-16**) and ten 5,7-dibromoisatin derived TSCs (**17-26**) are presented in this chapter. All of them were characterized by NMR, FT-IR, ESI-HRMS, Electronic spectral studies (UV-Vis), single crystal X-ray analysis and molecular docking.

IR study

The synthesized compounds exhibited characteristic bands corresponding to the various functional groups. In the synthesized compounds, the broad band around 3313-3103 cm^{-1} were assigned to the symmetrical stretching mode of *ν*(N-H) from indole N-H and azomethine N-H in the spectra of the thiosemicarbazones. The absence of band around 2570 cm^{-1}, specific to *ν*(S-H) confirmed the existence of thiosemicarbazones in thione tautomeric form in the solid state. The strong bands around 1490-1431 cm^{-1}, and 833-763 cm^{-1} (*ν*(C=S)), 1705-1668 cm^{-1} *ν*(C=O) and 1610-1527 cm^{-1} and *ν*(C=N) confirmed the formation of thiosemicarbazones. It was discovered that the type of substituent at the N (4) position affected the peak location of various functionality.

NMR Study

The **^{1}H-NMR** spectra of the compounds were consistent with the analogous thiosemicarbazones and confirmed that it exists as neutral molecule in solution. N(3)H has an intramolecular hydrogen bond with the nitrogen of pyrrolidine in the *Z* isomer. When N(4) was substituted with a bulky group, a significant downfield shift of roughly δ12 ppm was seen for the N(3)H proton. The absence of a signal around δ 4 ppm corresponding to thiol (-SH) proton also confirmed that thiosemicarbazones exists as thione tautomer in solution. All aromatic protons of compounds appeared at δ 7.84 to 6.71 ppm, with calculated multiplicity.

The **^{13}C-NMR** spectra for the aromatic carbon atoms of the compounds were observed around δ 155.80-104.14 ppm. The **^{13}C-NMR** spectra for chemically non-equivalent; C=S, C=O and C=N carbon atoms of thiosemicarbazones showed the chemical shift values toward downfield at about δ180.37-175.36, δ163.39-162.33 and δ136.82-133.86 ppm respectively. It was found from ^{13}C-NMR spectra that the type of N(4)-substituent has no discernible impact on the position of the carbon peak. In the synthesized thiosemicarbazones, the chemical shift values of all aromatic as well as aliphatic carbons/protons were observed in the expected region of the proposed structure.

Mass spectrometry

The high resolution electron spray ionization mass spectrometry (**ESI-HRMS**) analysis of synthesized compounds confirmed the molecular structures with the presence of

expected molecular ion $[M+H]^+$ and/or alkali adduct analyte molecular ion peak $[M+Na]^+$ with the value of *m/z* peak up to 4-5 decimal digits.

UV-Visible study

The UV-Visible bands appeared due to π→π* and n→π* electronic transition confirmed the proposed structure of synthesized thiosemicarbazones. The absorption bands of >C=O, >C=N and -NH-C=S in thiosemicarbazones resulted due to the n→π* electronic transitions. The bands due to the n→π* transitions were found to higher wavelength than electronic transition of π→π*.

Single crystal X-ray crystallographic study

Seven thiosemicarbazones were identified by their single crystal data, which proved that they were formed from the corresponding thiosemicarbazides and carbonyl compounds. The ORTEP view of the structure refinement parameters and their thione tautomeric form verified their existence, and the molecular packing view along the a, b, and c axis demonstrated the presence of intramolecular and intermolecular hydrogen bonding. The seven single crystals of synthesized compound were published in Cambridge Crystallographic Data Center (CCDC) in United Kingdom. The CCDC reference number of synthesized compound were tabulated as:

Sample code/Number	CCDC reference number
MeOIstDmMor/3	2194145
MeOIstDm/4	2194144
HydIstMor/9	2245790
HydIstAzep/12	2245783
HydIstEth/16	2245789
DiBrIstAzep/22	2245786
DiBrIstEt/26	2245787

Anticancer screening and molecular docking

All the synthesized compounds identified stronger antiproliferative activity than that of the positive control (DMSO) against MCF-7, A431, A549, MDA-MB-231, NCIH-460, PC-3 and PNT-2 cancer cell lines. The molecular docking was studied for the molecule having single X-ray crystals with the goal of predicting the ligand-receptor complex structure using computational methods.

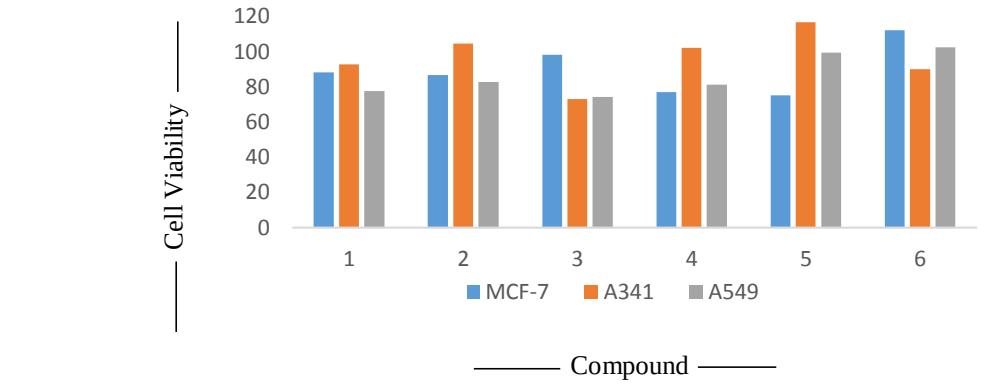

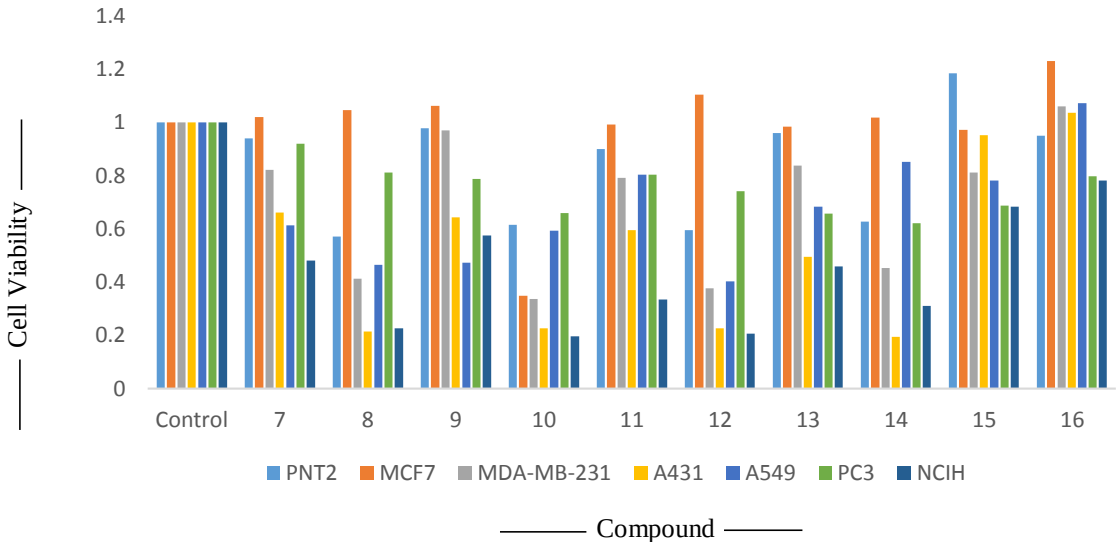

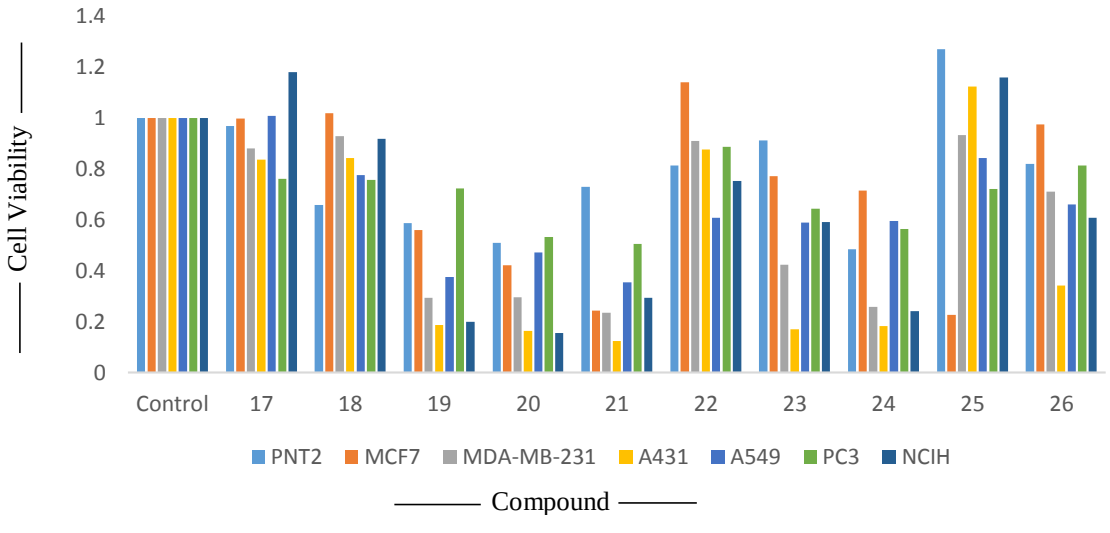

REFERENCES

Abbas, Z., & Rehman, S. (2018). An Overview of Cancer Treatment Modalities. *Neoplasm*, **6**(1): 140–157. DOI: 10.5772/intechopen.76558

Abdulghani, A. J. & Hussain, R. K. (2015). Synthesis and Characterization of Schiff Base Metal Complexes Derived from Cefotaxime with 1H-indole-2,3-dione (Isatin) and 4-N,N-dimethyl-aminobenzaldehyde. *Scientific Research Publishing*, **5**(6): 88–101. DOI: 10.4236/ojic.2015.54010

Agarwal, R. K., Singh, L., & Sharma, D. K. (2006). Synthesis, Spectral, and Biological Properties of Copper(II) Complexes of Thiosemicarbazones of Schiff Bases Derived from 4-aminoantipyrine and Aromatic Aldehydes. *Bioinorganic Chemistry and Applications*, **2006**(2): 1–10. DOI: 10.1155/BCA/2006/59509

Ahmed, M. F., Santali, E. Y., & El-Haggar, R. (2021). Novel Piperazine–Chalcone Hybrids and Related Pyrazoline Analogues Targeting VEGFR-2 Kinase; Design, Synthesis, Molecular Docking Dtudies, and Anticancer Evaluation. *Journal of Enzyme Inhibition and Medicinal Chemistry*, **36**(1): 307–318. DOI: 10.1080/14756366.2020.1861606

Akinchan, N. T., Drozdzewski, P. M., & Holzer, W. (2002). Syntheses and Spectroscopic Studies on Zinc(II) and Mercury(II) Complexes of Isatin-3-thiosemicarbazone. *Journal of Molecular Structure*, **641**(1): 17–22. DOI: 10.1016/S0022-2860(02)00134-5

Al-Jarf, R., de Sá, A. G. C., Pires, D. E. V., & Ascher, D. B. (2021). pdCSM-cancer: Using Graph-Based Signatures to Identify Small Molecules with Anticancer Properties. *Journal of Chemical Information and Modeling*, **61**(7): 3314–3322. DOI: 10.1021/acs.jcim.1c00168

Al-Sanea, M. M., Obaidullah, A. J., Shaker, M. E., Chilingaryan, G., Alanazi, M. M., Alsaif, N. A., Alkahtani, H. M., Alsubaie, S. A., & Abdelgawad, M. A. (2021). A New CDK2 Inhibitor with 3-hydrazonoindolin-2-one Scaffold Endowed with Anti-breast Cancer Activity: Design, Synthesis, Biological Evaluation, and in Silico Insights. *Molecules*, **26**(2): 412. DOI: 10.3390/molecules26020412

Alahari, A., Trivelli, X., Guérardel, Y., Dover, L. G., Besra, G. S., Sacchettini, J. C.,

Reynolds, R. C., Coxon, G. D., & Kremer, L. (2007). Thiacetazone, an Antitubercular Drug that Inhibits Cyclopropanation of Cell wall Mycolic Acids in Mycobacteria. *PLoS ONE*, **2**(12): 1343. DOI: 10.1371/journal.pone.0001343

Ali, A. Q. (2016). Synthesis , Spectroscopic , Thermal Studies of Nickel (II) and Palladium (II) Complexes of Tridentate Ligand and Their DNA Cleavage Activity Synthesis of Schiff Base Ligand. *Journal of Sebha University*, **15**(2): 36–53.

Ali, A. Q., Teoh, S. G., Eltayeb, N. E., Ahamed, M. B. K., & Majid, A. A. (2014). Synthesis of nickel(II) Complexes of Isatin Thiosemicarbazone Derivatives: *In Vitro* Anti-cancer, DNA Binding, and Cleavage Activities. *Journal of Coordination Chemistry*, **67**(20): 3380–3400. DOI: 10.1080/00958972.2014.959943

Almeida, C. M., de Carvalho, J. G. M., Fujimori, M., França, E. L., Honorio-França, A. C., Parreira, R. L. T., Orenha, R. P., & Gatto, C. C. (2020). Structural Investigation of Group 10 Metal Complexes with Thiosemicarbazone: Crystal Structure, Mass Spectrometry, Hirshfeld Surface and *in Vitro* Antitumor Activity. *Structural Chemistry*, **31**(5): 2093–2103. DOI: 10.1007/s11224-020-01564-2

Althagafi, I. I., Abouzied, A. S., Farghaly, T. A., Al-Qurashi, N. T., Alfaifi, M. Y., Shaaban, M. R., & Abdel Aziz, M. R. (2019). Novel Nano-sized Bis-indoline Derivatives as Antitumor Agents. *Journal of Heterocyclic Chemistry*, **56**(2): 391–399. DOI: 10.1002/jhet.3410

Aly, M. M., Mohamed, Y. A., El-Bayouki, K. A. M., Basyouni, W. M., & Abbas, S. Y. (2010). Synthesis of Some New 4(3H)-quinazolinone-2-carboxaldehyde Thiosemicarbazones and Their Metal Complexes and a Study on Their Anticonvulsant, Analgesic, Cytotoxic and Antimicrobial Activities-Part-1. *European Journal of Medicinal Chemistry*, **45**(8): 3365–3373. DOI: 10.1016/j.ejmech.2010.04.020

Aneesrahman, K. N., Ramaiah, K., Rohini, G., Stefy, G. P., Bhuvanesh, N. S. P., & Sreekanth, A. (2019). Synthesis and Characterisations of Copper(II) Complexes of 5-Methoxyisatin Thiosemicarbazones: Effect of N-terminal Substitution on DNA/Protein Binding and Biological Activities. *Inorganica Chimica Acta*,

492(3): 131–141. DOI: 10.1016/j.ica.2019.04.019

Arafa, W. A. A., & Badry, M. G. (2016). Facile Synthesis of Bis-thiosemicarbazone Derivatives as Key Precursors for the Preparation of Functionalised Bis-thiazoles. *Journal of Chemical Research*, **40**(7): 385–392. DOI: 10.3184/174751916X14639296902648

Arafath, M. A., Adam, F., Al-Suede, F. S. R., Razali, M. R., Ahamed, M. B. K., Abdul Majid, A. M. S., Hassan, M. Z., Osman, H., & Abubakar, S. (2017). Synthesis, Characterization, X-ray Crystal Structures of Heterocyclic Schiff Base Compounds and *in Vitro* Cholinesterase Inhibition and Anticancer Activity. *Journal of Molecular Structure*, **1149**(1): 216–228. DOI: 10.1016/j.molstruc.2017.07.092

Arora, S., Agarwal, S., & Singhal, S. (2014). Anticancer Activities of Thiosemicarbazides/Thiosemicarbazones: A Review. *International Journal of Pharmacy and Pharmaceutical Sciences*, **6**(9): 34–41.

Arruebo, M., Vilaboa, N., Sáez-Gutierrez, B., Lambea, J., Tres, A., Valladares, M., & González-Fernández, Á. (2011). Assessment of the Evolution of Cancer Treatment Therapies. *Cancers*, **3**(3): 3279–3330. DOI: 10.3390/cancers3033279

Aung, T. N., Qu, Z., Kortschak, R. D., & Adelson, D. L. (2017). Understanding the Effectiveness of Natural Compound Mixtures in Cancer through Their Molecular Mode of Action. *International Journal of Molecular Sciences*, **18**(3): DOI: 10.3390/ijms18030656

Aziz, N. A. A. M., George, R. F., El-Adl, K., & Mahmoud, W. R. (2022). Design, Synthesis, *in Silico* Docking, ADMET and Anticancer Evaluations of Thiazolidine-2,4-diones Bearing Heterocyclic Rings as Dual VEGFR-2/EGFRT790M Tyrosine Kinase Inhibitors. *RSC Advances*, **12**(20): 12913–12931. DOI: 10.1039/d2ra01119k

Bain, G. A., West, D. X., Krejci, J., Valdcs-, J., Hernbndez-ortega, S., & Toscanob, R. A. (1997). Synthetic and Spectroscopic Investigations of N(4)-Substituted Isatin Thiosemicarbazones and Their Copper (II) Complexes. *Polyhedron*, **16**(5): 855–862.

Bala, M., & Mishra, L. K. (2014). Complexing Behaviour and Antifungal Activity of N-[(1E)-1-(1H-Benzimidazol-2-yl)ethylidene]morpholine-4-carbothiohydrazide and Related Ligand with Metal Ions. *International Journal of Inorganic Chemistry*, **2014**(2): 1–10. DOI: 10.1155/2014/902575

Balachandran, C., Haribabu, J., Jeyalakshmi, K., Bhuvanesh, N. S. P., Karvembu, R., Emi, N., & Awale, S. (2018). Nickel(II) Bis(isatin thiosemicarbazone) Complexes Induced Apoptosis through Mitochondrial Signaling Pathway and G0/G1 Cell Cycle Arrest in IM-9 cells. *Journal of Inorganic Biochemistry*, **182**(10): 208–221. DOI: 10.1016/j.jinorgbio.2018.02.014

Banerjee, P., Eckert, A. O., Schrey, A. K., & Preissner, R. (2018). ProTox-II: A Webserver for the Prediction of Toxicity of Chemicals. *Nucleic Acids Research*, **46**(1): 257–263. DOI: 10.1093/nar/gky318

Batool, M., Ahmad, B., & Choi, S. (2019). A Structure-Based Drug Discovery Paradigm. *International Journal of Molecular Sciences*, **20**(11): 2783. DOI: 10.3390/ijms20112783

Berman, H.M., Westbrook, J., Feng, J., Gilliland, G., Bhat, T.N., Weissig, H., Shindyalov, I. N. & Bourne, P. E. (2000). The Protein Data Bank. *Nucleic Acids Research*, **28**(1): 235–242.

Bharathi Dileepan, A. G., Daniel Prakash, T., Ganesh Kumar, A., Shameela Rajam, P., Violet Dhayabaran, V., & Rajaram, R. (2018). Isatin Based Macrocyclic Schiff base Ligands as Novel Candidates for Antimicrobial and Antioxidant Drug Design: *In Vitro* DNA Binding and Biological Studies. *Journal of Photochemistry & Photobiology*,***183***(4): 191-200. DOI: 10.1016/j.jphotobiol.2018.04.029

Bheemappa, M. (2021). Analysis of Pharmacological , Biological Deeds of Isatin and Its Derivatives. *International Journal of Scientific Research in Engineering & Technology*, **01**(01): 95–113.

Bisceglie, F., Alinovi, R., Pinelli, S., Galetti, M., Pioli, M., Tarasconi, P., Mutti, A., Goldoni, M., & Pelosi, G. (2016). Autophagy and Apoptosis: Studies on the Effects of Bisthiosemicarbazone Copper(II) Complexes on p53 and p53-null Tumour Cell Lines. *Metallomics*, **8**(12): 1255–1265. DOI: 10.1039/c6mt00170j

Blaney, J. (2012). A very Short History of Structure-Based Design: How did We get Here and Where do We Need to go? *Journal of Computer-Aided Molecular Design*, **26**(1): 13–14. DOI: 10.1007/s10822-011-9518-x

Board, R., & Jayson, G. C. (2005). Platelet-Derived Growth Factor Receptor (PDGFR): A Target for Anticancer Therapeutics. *Drug Resistance Updates*, **8**(2): 75–83. DOI: 10.1016/j.drup.2005.03.004

Bray, F., Ferlay, J., Soerjomataram, I., Siegel, R. L., Torre, L. A., & Jemal, A. (2018). Global Cancer Statistics 2018: GLOBOCAN Estimates of Incidence and Mortality Worldwide for 36 Cancers in 185 Countries. *CA: A Cancer Journal for Clinicians*, **68**(6): 394–424. DOI: 10.3322/caac.21492

Brewerton, T. D., Zealberg, J. J., Lydiard, R. B., Glover, V., Sandler, M., & Ballenger, J. C. (1995). CSF Isatin is Elevated in Bulimia Nervosa. *Biological Psychiatry*, **37**(7): 481–483. DOI: 10.1016/0006-3223(94)00328-Z

Britto, K. B., Francisco, C. S., Ferreira, D., Borges, B. J. P., Conti, R., Profeti, D., Rodrigues, L. R., Lacerda, V., Morais, P. A. B., & Borges, W. S. (2020). Identifying New Isatin Derivatives with gsk-3β Inhibition Capacity through Molecular Docking and Bioassays. *Journal of the Brazilian Chemical Society*, **31**(3): 476–487. DOI: 10.21577/0103-5053.20190206

Broyden, C. G. (1970). The Convergence of a Class of Double-rank Minimization Algorithms 1. General Considerations. *IMA Journal of Applied Mathematics (Institute of Mathematics and Its Applications)*, **6**(1): 76–90. DOI: 10.1093/imamat/6.1.76

Burke, K., & Wagner, L. O. (2013). DFT in a Nutshell. *International Journal of Quantum Chemistry*, **113**(2): 96–101. DOI:10.1002/qua.24259

Cane, A., Tournaire, M. C., Barritault, D., & Crumeyrolle-Arias, M. (2000). The Endogenous Oxindoles 5-Hydroxyoxindole and Isatin are Antiproliferative and Proapoptotic. *Biochemical and Biophysical Research Communications*, **276**(1): 379–384. DOI: 10.1006/bbrc.2000.3477

Casas, J. S., Castiñeiras, A., Rodríguez-argüelles, M. C., Sánchez, A., Sordo, J., Vázquez-lópez, A., & Vázquez-lópez, E. M. (2000). Reactions of Diorganotin(IV)

Oxides with Isatin 3- and 2-thiosemi-carbazones and with Isatin 2,3-Bis(thiosemicarbazone): Influence of Diphenyldithiophosphinic Acid (isatin = 1H-indole-2,3-dione). *The Royal Society of Chemistry*, **2000**(1): 4056–4063. DOI: 10.1039/b005103i

Çavuş, M. S., Yakan, H., Muğlu, H., & Bakır, T. (2020). Novel Carbohydrazones Including 5-Substituted Isatin: Synthesis, Characterization, and Quantum-Chemical Studies on the Relationship between Electronic and Antioxidant Properties. *Journal of Physics and Chemistry of Solids*, **140**(1): 31907-9. DOI: 10.1016/j.jpcs.2020.109362

Cersosimo, R. J., & Hong, W. K. (1986). Epirubicin: A Review of the Pharmacology, Clinical Activity, and Adverse Effects of an Adriamycin Analogue. *Journal of Clinical Oncology*, **4**(3): 425–439. DOI: 10.1200/JCO.1986.4.3.425

Chauhan, G., Pathak, D. P., Ali, F., Bhutani, R., Kapoor, G., & Khasimbi, S. (2020). Advances in Synthesis, Derivatization and Bioactivity of Isatin: A Review. *Current Organic Synthesis*, **17**(1): 1-38. DOI: 10.2174/1570179417666200924150907

Chen, D., Oezguen, N., Urvil, P., Ferguson, C., Dann, S. M., & Savidge, T. C. (2016). Regulation of Protein-Ligand Binding Affinity by Hydrogen Bond Pairing. *Science Advances*, **2**(3): 1-16. DOI: 10.1126/sciadv.1501240

Chessari, G., Hardcastle, I. R., Ahn, J. S., Anil, B., Anscombe, E., Bawn, R. H., Bevan, L. D., Blackburn, T. J., Buck, I., Cano, C., Carbain, B., Castro, J., Cons, B., Cully, S. J., Endicott, J. A., Fazal, L., Golding, B. T., Griffin, R. J., Haggerty, K., & Zhao, Y. (2021). Structure-Based Design of Potent and Orally Active Isoindolinone Inhibitors of MDM2-p53 Protein-Protein Interaction. *Journal of Medicinal Chemistry*, **64**(7): 4071–4088. DOI: 10.1021/acs.jmedchem.0c02188

Colovos, C., & Yeates, T. (1993). Verification of Protein Structures: Patterns of Nonbonded Atomic Interactions. *Protein Science*, **2**(1): 1511–1519. DOI: 10.1002/pro.5560020916

Conklin, K. A. (2000). Dietary Antioxidants During Cancer Chemotherapy: Impact on Chemotherapeutic Effectiveness and Development of Side Effects. *Nutrition and Cancer*, **37**(1): 1–18. DOI:10.1207/S15327914NC3701_1

Cory, J. G., Cory, A. H., Rappa, G., Lorico, A., Llu, M. C., Lin, T. S., & Sartorelli, A. C. (1995). Structure-Function Relationships for a New Series of Pyridine-2-carboxaldehyde Thiosemicarbazones on Ribonucleotide Reductase Activity and Tumor Cell Growth in Culture and *in Vivo*. *Advances in Enzyme Regulation*, **35**(3): 55–68. DOI: 10.1016/0065-2571(94)00005-N

Crutchfield, C. A., & Clarke, W. (2014). Present and Future Applications of High Resolution Mass Spectrometry in the Clinic. *Discoveries*, **2**(2): 1-12. DOI:10.15190/d.2014.9

Czelen, P., Skotnicka, A., & Szefle, B. (2022). Designing and Synthesis of New Isatin Derivatives as Potential CDK2 Inhibitors. *International Journal of Molecular Sciences*, **23**(1): 8046. DOI: 10.3390/ijms23148046

Da Silva, J. F. M., Garden, S. J., & Pinto, A. C. (2001). The Chemistry of Isatins: A Review from 1975 to 1999. *Journal of the Brazilian Chemical Society*, **12**(3): 273–324. DOI: 10.1590/S0103-50532001000300002

Damaraju, D., Damaraju, V. L., Brun, M., Mowles, D., Kuzma, M., Berendt, R. C., Sawyer, M. B., & Cass, C. E. (2008). Cytotoxic Activities of Nucleoside and Nucleobase Analog Drugs in Malignant Mesothelioma: Characterization of a Novel Nucleobase Transport Activity. *Biochemical Pharmacology*, **75**(10): 1901–1911. DOI: 10.1016/j.bcp.2008.02.006

Dayal, D., Palanimuthu, D., Shinde, S. V., Somasundaram, K., & Samuelson, A. G. (2011). A Novel Zinc Bis(thiosemicarbazone) Complex for Live Cell Imaging. *Journal of Biological Inorganic Chemistry*, **16**(4): 621–632. https://doi.org/10.1007/s00775-011-0764-0

De Oliveira, J. F., Da Silva, A. L., Vendramini-Costa, D. B., Da Cruz Amorim, C. A., Campos, J. F., Ribeiro, A. G., De Moura, R. O., Neves, J. L., Ruiz, A. L. T. G., De Carvalho, J. E., & Alves De Lima, M. D. C. (2015). Synthesis of Thiophene-Thiosemicarbazone Derivatives and Evaluation of their *in Vitro* and *in Vivo* Antitumor Activities. *European Journal of Medicinal Chemistry*, **104**(1): 148–156. DOI: 10.1016/j.ejmech.2015.09.036

De Sousa, G. F., Resck, I. S., Lariucci, C., & Sabino, J. R. (2006). 2,6-Dimethylmorpholin-4-yl 3,5-dimethyl-1H-pyrazole Thioketone. *Acta*

Crystallographica Section E: Structure Reports Online, **62**(8): 3366–3368. DOI: 10.1107/S1600536806026730

Demaria, M., O'Leary, M. N., Chang, J., Shao, L., Liu, S., Alimirah, F., Koenig, K., Le, C., Mitin, N., Deal, A. M., Alston, S., Academia, E. C., Kilmarx, S., Valdovinos, A., Wang, B., De Bruin, A., Kennedy, B. K., Melov, S., Zhou, D., … Campisi, J. (2017). Cellular Senescence Promotes Adverse Effects of Chemotherapy and Cancer Relapse. *Cancer Discovery*, **7**(2): 165–176. DOI: 10.1158/2159-8290.CD-16-0241

Ding, Z., Zhou, M., & Zeng, C. (2020). Recent Advances in Isatin Hybrids as Potential Anticancer Agents. *Archiv Der Pharmazie*, **353**(3): 1–13. DOI: 10.1002/ardp.201900367

Dolomanov, O. V., Bourhis, L. J., Gildea, R. J., Howard, J. A. K., & Puschmann, H. (2009). OLEX2: A Complete Structure Solution, Refinement and Analysis Program. *Journal of Applied Crystallography*, **42**(2): 339–341. DOI: 10.1107/S0021889808042726

Dzulkifli, N. N., Farina, Y., & Yamin, B. M. (2015). Dysprosium (III) Isatin 2-Methyl-3-Thiosemicarbazone: Synthesis, Structural and Characterization. *Malaysian Journal of Analytical Sciences*, **19**(3): 541–549.

El-Saied, F., El-Aarag, B., Salem, T., Said, G., Khalifa, S. A. M., & El-Seedi, H. R. (2019). Synthesis, Characterization, and *in Vivo* Anti-cancer Activity of New Metal Complexes Derived from Isatin-N(4)antipyrinethiosemicarbazone Ligand against Ehrlich Ascites Carcinoma Cells. *Molecules*, **24**(18): 3313. DOI: 10.3390/molecules24183313

El-Sawaf, A. K., El-Essawy, F., Nassar, A. A., & El-Samanody, E. S. A. (2018). Synthesis, Spectral, Thermal and Antimicrobial Studies on Cobalt(II), Nickel(II), Copper(II), Zinc(II) and Palladium(II) Complexes Containing Thiosemicarbazone Ligand. *Journal of Molecular Structure*, **1157**(2): 381–394. DOI: 10.1016/j.molstruc.2017.12.075

El-Sharief, A. M. S., Ammar, Y. A., Belal, A., El-Sharief, M. A. M. S., Mohamed, Y. A., Mehany, A. B. M., Elhag Ali, G. A. M., & Ragab, A. (2019). Design, Synthesis, Molecular Docking and Biological Activity Evaluation of Some Novel

Indole Derivatives as Potent Anticancer Active Agents and Apoptosis Inducers. *Bioorganic Chemistry*, **85**(2): 399–412. DOI: 10.1016/j.bioorg.2019.01.016

Eldehna, W. M., Altoukhy, A., Mahrous, H., & Abdel-Aziz, H. A. (2015). Design, Synthesis and QSAR Study of Certain Isatin-pyridine Hybrids as Potential Anti-proliferative Agents. *European Journal of Medicinal Chemistry*, **90**(1): 684–694. DOI: 10.1016/j.ejmech.2014.12.010

Elkaeed, E. B., Yousef, R. G., Elkady, H., Gobaara, I. M. M., Alsfouk, A. A., Husein, D. Z., Ibrahim, I. M., Metwaly, A. M., & Eissa, I. H. (2022). The Assessment of Anticancer and VEGFR-2 Inhibitory Activities of a New 1H-Indole Derivative: *In Silico* and *In Vitro* Approaches. *Processes*, **10**(7): 1–25. DOI: 10.3390/pr10071391

Emami, S., Valipour, M., Kazemi Komishani, F., Sadati-Ashrafi, F., Rasoulian, M., Ghasemian, M., Tajbakhsh, M., Honarchian Masihi, P., Shakiba, A., Irannejad, H., & Ahangar, N. (2021). Synthesis, *in Silico*, *in Vitro* and *in Vivo* Evaluations of Isatin Aroylhydrazones as Highly Potent Anticonvulsant Agents. *Bioorganic Chemistry*, **112**(4): 104943. DOI: 10.1016/j.bioorg.2021.104943

Ermut, G., Karali, N., Çetin, I., Topçul, M., & Birteksöz, S. (2013). Synthesis and Chemotherapeutic Activities of 5-Chloro-1H-indole-2,3-dione 3-thiosemicarbazones. *Marmara Pharmaceutical Journal*, **17**(2): 147–154. DOI: 10.12991/201317383

Esmaeelian, B., Abbott, C. A., Le Leu, R. K., & Benkendorff, K. (2014). 6-Bromoisatin Found in Muricid Mollusc Extracts Inhibits Colon Cancer Cell Proliferation and Induces Apoptosis, Preventing Early Stage Tumor Formation in a Colorectal Cancer Rodent Model. *Marine Drugs*, **12**(1): 17–35. DOI: 10.3390/md12010017

Esme, A., Sagdinc, S. G., & Yildiz, S. Z. (2014). Experimental and Theoretical Studies on Sudan Red G [1-(2-methoxyphenylazo)-2-naphthol] and Its Cu(II) Coordination Compound. *Journal of Molecular Structure*, **1075**(1): 264–278. DOI: 10.1016/j.molstruc.2014.07.009

Ewesuedo, R.B., & Ratain, M. J. (2003). Principles of Cancer Chemotherapy. *Oncologic Therapies*, **1**(2): 19–66. DOI: 10.1007/978-3-642-55780-4_3

Ferkol, T., & Schraufnagel, D. (2014). The Global Burden of Respiratory Disease. *Annals of the American Thoracic Society*, **11**(3): 404–406. DOI: 10.1513/AnnalsATS.201311-405PS

Ferlay, J., Soerjomataram, I., Dikshit, R., Eser, S., Mathers, C., Rebelo, M., Parkin, D. M., Forman, D., & Bray, F. (2015). Cancer Incidence and Mortality Worldwide: Sources, Methods and Major Patterns in GLOBOCAN 2012. *International Journal of Cancer*, **136**(5): 359–386. DOI: 10.1002/ijc.29210

Ferraz de Paiva, R. E., Vieira, E. G., Rodrigues da Silva, D., Wegermann, C. A., & Costa Ferreira, A. M. (2021). Anticancer Compounds Based on Isatin-Derivatives: Strategies to Ameliorate Selectivity and Efficiency. *Frontiers in Molecular Biosciences*, **7**(2): 1–24. DOI: 10.3389/fmolb.2020.627272

Gabr, M. T., El-Gohary, N. S., El-Bendary, E. R., El-Kerdawy, M. M., & Ni, N. (2017). Isatin-β-thiocarbohydrazones: Microwave-Assisted Synthesis, Antitumor Activity and Structure-Activity Relationship. *European Journal of Medicinal Chemistry*, **128**(1): 36–44. DOI: 10.1016/j.ejmech.2017.01.030

Garden, S. J., & Skakle, J. M. S. (2002). Isatin Derivatives are Reactive Electrophilic Components for the Baylis-Hillman Reaction. *Tetrahedron Letters*, **43**(11): 1969–1972. DOI: 10.1016/S0040-4039(02)00160-0

Gerby, B., Boumendjel, A., Blanc, M., Bringuier, P. P., Champelovier, P., Fortuné, A., Ronot, X., & Boutonnat, J. (2007). 2-Arylidenedihydroindole-3-ones: Design, Synthesis, and Biological Activity on Bladder Carcinoma Cell Lines. *Bioorganic and Medicinal Chemistry Letters*, **17**(1): 208–213. DOI: 10.1016/j.bmcl.2006.09.057

Ghoshal, T., & Patel, T. M. (2020). Anticancer Activity of Benzoxazole Derivative (2015 onwards): A Review. *Future Journal of Pharmaceutical Sciences*, **6**(1): 1-24. DOI: 10.1186/s43094-020-00115-0

Glover, V., Attach, S. K. B. H., & Rya, A. (1998). The Psychopharmacology of Isatin: A Brief Review. *Stress Medicine*, **14**(4): 225–229. DOI: 10.1002/(SICI)1099-1700(1998100)14:4<225::AID-SMI801>3.0.CO;2-P

Güzel, Ö., Karali, N., & Salman, A. (2008). Synthesis and Antituberculosis Activity of

5-methyl/trifluoromethoxy-1H-indole-2,3-dione-3-thiosemicarbazone Derivatives. *Bioorganic and Medicinal Chemistry*, **16**(19): 8976–8987. DOI: 10.1016/j.bmc.2008.08.050

Haiguang, L., Lin, L., & Kai, Y. (2015). Chemotherapy Targeting Cancer Stem Cells. *Am J Cancer Res*, **5**(3): 880–893.

Hande, K. R. (2008). Topoisomerase II Inhibitors. *Update on Cancer Therapeutics*, **3**(1): 13–26. DOI: 10.1016/j.uct.2008.02.001

Hanwell, M.D., Curtis, D.E., Lonie, D.C., Vandermeersch, T., Zurek, E., & Hutchison, G. R. (2012). Avogadro: An Advanced Semantic Chemical Editor, Visualization, and Analysis Platform. *Journal of Cheminformatics*, **4**(17): 1–17. DOI: 10.1186/1758-2946-4-17

Haribabu, J., Subhashree, G. R., Saranya, S., Gomathi, K., Karvembu, R., & Gayathri, D. (2016). Isatin Based Thiosemicarbazone Derivatives as Potential Bioactive Agents: Anti-oxidant and Molecular Docking Studies. *Journal of Molecular Structure*, **1110**(1): 185–195. DOI: 10.1016/j.molstruc.2016.01.044

Harness, R., Robertson, C., & Beckford, F. (2008). Thiosemicarbazone Complexes of Group 12 Elements. An Investigation of the Thiosemicarbazone from p-dimethylaminobenzaldehyde. *Journal of Undergraduate Chemistry Research*, **7**(3): 92–97.

Havrylyuk, D., Zimenkovsky, B., Vasylenko, O., Gzella, A., & Lesyk, R. (2012). Synthesis of New 4-thiazolidinone-, Pyrazoline-, and Isatin-Based Conjugates with Promising Antitumor Activity. *Journal of Medicinal Chemistry*, **55**(20): 8630–8641. DOI: 10.1021/jm300789g

Hentabli, H., Naomie, S., & Faisal, S. (2016). Quantitative Structure Activity Relationships in Computer Aided Molecular Design. *Jurnal Teknologi*, **78**(3): 97–104. DOI: 10.11113/jt.v78.9723

Holmes, L., Lahurd, A., Wasson, E., McClarin, L., & Dabney, K. (2015). Racial and Ethnic Heterogeneity in the Association between Total Cholesterol and Pediatric Obesity. *International Journal of Environmental Research and Public Health*, **13**(1): 1–10. DOI: 10.3390/ijerph13010019

Hou, Y., Shang, C., Wang, H., & Yun, J. (2020). Isatin–Azole Hybrids and Their Anticancer Activities. *Archiv Der Pharmazie*, **353**(1): 1–10. DOI: 10.1002/ardp.201900272

Hu, B., Wang, B., Zhao, B., Guo, Q., Li, Z. H., Zhang, X. H., Liu, G. Y., Liu, Y., Tang, Y., Luo, F., Du, Y., Chen, Y. X., Ma, L. Y., & Liu, H. M. (2017). Thiosemicarbazone-Based Selective Proliferation Inactivators Inhibit Gastric Cancer Cell Growth, Invasion, and Migration. *MedChemComm*, **8**(12): 2173–2180. DOI: 10.1039/c7md00353f

Ibrahim, M. M., Elsaman, T., & Al-Nour, M. Y. (2018). Synthesis, Anti-Inflammatory Activity, and In Silico Study of Novel Diclofenac and Isatin Conjugates. *International Journal of Medicinal Chemistry*, **2018**(1): 1–11. DOI: 10.1155/2018/9139786

Ibrahim, S., & Elsaman, T. (2018). Cytotoxic and Anticancer Activities of Indoline-2,3-dione (Isatin) and Its Derivatives. *Journal of Pharmaceutical Research International*, **21**(2): 1–19. DOI: 10.9734/jpri/2018/39708

Igosheva, N., Lorz, C., O'Conner, E., Glover, V., & Mehmet, H. (2005). Isatin, An Endogenous Monoamine Oxidase Inhibitor, Triggers a Dose- and Time-ependent Switch from Apoptosis to Necrosis in Human Neuroblastoma Cells. *Neurochemistry International*, **47**(3): 216–224. DOI: 10.1016/j.neuint.2005.02.011

Juranic, Z., Anastasova, F., Juranic, I., Stanojkovic, T., Radulovic, S., & Vuletic, N. (1999). Antiproliferative Action of Isatine-beta-thiocarbohydrazone and N-ethylisatine-beta-thiocarbohydrazone on Human PBMC and on Two Neoplastic Cell Lines. *Journal of Experimental & Clinical Cancer Research*, **3**(18): 317–324.

Jansson, P. J., Yamagishi, T., Arvind, A., Seebacher, N., Gutierrez, E., Stacy, A., Maleki, S., Sharp, D., Sahni, S., & Richardson, D. R. (2015). Di-2-pyridylketone 4,4-dimethyl-3-thiosemicarbazone (Dp44mT) Overcomes Multidrug Resistance by a Novel Mechanism Involving the Hijacking of Lysosomal P-Glycoprotein (Pgp). *Journal of Biological Chemistry*, **290**(15): 9588–9603. DOI: 10.1074/jbc.M114.631283

Joseph, M., Kuriakose, M., Kurup, M. R. P., Suresh, E., Kishore, A., & Bhat, S. G.

(2006). Structural, Antimicrobial and Spectral Studies of Copper(II) Complexes of 2-benzoylpyridine N(4)-phenyl Thiosemicarbazone. *Polyhedron*, **25**(1): 61–70. DOI: 10.1016/j.poly.2005.07.006

Jouad, E. M., Larcher, G., Allain, A., Riou, A., Bouet, G. M., Khan, M. A., & Thanh, X. D. (2001). Synthesis, Structure and Biological Activity of Nickel(II) Complexes of 5-Methyl 2-Furfural Thiosemicarbazone. *Journal of Inorganic Biochemistry*, **86**(3): 565–571. DOI: 10.1016/S0162-0134(01)00220-3

Kaldor, S. W., Kalish, V. J., Davies, J. F., Shetty, B. V., Fritz, J. E., Appelt, K., Burgess, J. A., Campanale, K. M., Chirgadze, N. Y., Clawson, D. K., Dressman, B. A., Hatch, S. D., Khalil, D. A., Kosa, M. B., Lubbehusen, P. P., Muesing, M. A., Patick, A. K., Reich, S. H., Su, K. S., & Tatlock, J. H. (1997). Viracept (nelfinavir mesylate, AG1343): A Potent, Orally Bioavailable Inhibitor of HIV-1 Protease. *Journal of Medicinal Chemistry*, **40**(24): 3979–3985. DOI: 10.1021/jm9704098

Kandemirli, F., Arslan, T., Karadayi, N., Ebenso, E. E., & Köksoy, B. (2009). Synthesis and Theoretical Study of 5-Methoxyisatin-3-(N-cyclohexyl)thiosemicarbazone and Its Ni(II) and Zn(II) Complexes. *Journal of Molecular Structure*, **938**(3): 89–96. DOI: 10.1016/j.molstruc.2009.09.009

Kang, I., Wang, L., Hsu, T., Yueh, A., Lee, C., Lee, Y., Lee, C., Chao, Y., Shih, S., & Chern, J. (2011). Isatin-β-thiosemicarbazones as Potent Herpes Simplex Virus Inhibitors. *Bioorganic & Medicinal Chemistry Letters*, **21**(7): 1948–1952. DOI: 10.1016/j.bmcl.2011.02.037

Kaplancikli, Z.A., AltJntop, M. D., Sever, B., Cantürk, Z., & Özdemir A. (2016). Synthesis and *In Vitro* Evaluation of New Thiosemicarbazone Derivatives as Potential Antimicrobial Agents. *Journal of Chemistry*, **2016**(1): 1–7. DOI: 10.1155/2016/1692540

Karthikeyan, C., Solomon, V. R., Lee, H., & Trivedi, P. (2013). Design, Synthesis and Biological Evaluation of Some Isatin-Linked Chalcones as Novel Anti-breast Cancer Agents: A molecular Hybridization Approach. *Biomedicine and Preventive Nutrition*, **3**(4): 325–330. DOI: 10.1016/j.bionut.2013.04.001

Karthikeyan, C., Solomon, V. R., Lee, H., & Trivedi, P. (2017). Synthesis and Biological Evaluation of 2-(phenyl)-3H-benzo[d]imidazole-5-carboxylic Acids

and its Methyl Esters as Potent Anti-breast Cancer Agents. *Arabian Journal of Chemistry*, **10**(1): 1788–1794. DOI: 10.1016/j.arabjc.2013.07.003

Kassab, S. E., Hegazy, G. H., Eid, N. M., Amin, K. M., & El-gendy, A. A. (2010). Synthesis of 1H-Indole-2 , 3-Dione-3- Thiosemicarbazone Ribonucleosides as Antibacterial Agents. *Nucleosides, Nucleotides & Nucleic Acids*, **29**(1): 72–80. DOI: 10.1080/15257770903459267

Keldsen, N., Havsteen, H., Vergote, I., Bertelsen, K., & Jakobsen, A. (2003). Altretamine (hexamethylmelamine) in the Treatment of Platinum-resistant Ovarian Cancer: A Phase II Study. *Gynecologic Oncology*, **88**(2): 118–122. DOI: 10.1016/S0090-8258(02)00103-8

Khan, A., Jasinski, J. P., Smoleaski, V. A., Paul, K., Singh, G., & Sharma, R. (2016). Synthesis, Structure and Cytotoxicity Evaluation of Complexes of N1-substituted-isatin-3-thiosemicarbazone with Copper(I) Halides. *Inorganica Chimica Acta*, **449**(1): 119–126. DOI: 10.1016/j.ica.2016.05.013

Khan, A., Jasinski, J. P., Smolenski, V. A., Hotchkiss, E. P., Kelley, P. T., Shalit, Z. A., Kaur, M., Paul, K., & Sharma, R. (2018). Enhancement in Anti-tubercular Activity of Indole Based Thiosemicarbazones on Complexation with Copper(I) and Silver(I) Halides: Structure Elucidation, Evaluation and Molecular Modelling. *Bioorganic Chemistry*, **80**(1): 303–318. DOI: 10.1016/j.bioorg.2018.06.027

Khan, F. A., & Maalik, A. (2015). Advances in Pharmacology of Isatin and Its Derivatives: A Review. *Tropical Journal of Pharmaceutical Research*, **14**(10): 1937–1942. DOI: 10.4314/tjpr.v14i10.28

Khan, S. L., Sonwane, G. M., Siddiqui, F. A., Jain, S. P., Kale, M. A., & Borkar, V. S. (2020). Discovery of Naturally Occurring Flavonoids as Human Cytochrome P450 (CYP3A4) Inhibitors with the Aid of Computational Chemistry. *Indo Global Journal of Pharmaceutical Sciences*, **10**(4): 58–69. DOI: 10.35652/igjps.2020.10409

Kim, S., Chen, J., Cheng, T., Gindulyte, A., He, J., He, S., Li, Q., Shoemaker, B. A., Thiessen, P. A., Yu, B., Zaslavsky, L., Zhang, J., & Bolton, E. E. (2021). PubChem in 2021: New Data Content and Improved Web Interfaces. *Nucleic Acids Research*, **49**(1): 1388–1395. DOI: 10.1093/nar/gkaa971

Kohli, E., Arora, R., & Kakkar, R. (2014). Theoretical Study of the Stability of Tautomers and Conformers of Isatin-3-Thiosemicarbazone (IBT). *Canadian Chemical Transactions*, **2**(3): 327–342. DOI: 10.13179/canchemtrans.2014.02.03.0112

Konakanchi, R., & Gondru, R. (2019). Palladium (II) Complexes of 5-Substituted Isatin Thiosemicarbazones : Synthesis , Spectroscopic Characterization , Biological Evaluation and *in Silico* Docking Studies. *Synthetic Communications***,** **49**(1): 146-158. DOI: 10.1080/00397911.2018.1546400

Konstantinović, S. S., Kapor, A., Radovanović, B. C., & Deak, A. (2008). Synthesis, X-ray and Antimicrobial Activity of Isatin-3-phenylhydrazone. *Chemical Industry and Chemical Engineering Quarterly*, **14**(1): 27–34. DOI: 10.2298/CICEQ0801027K

Kopylovich, M. N., Nunes, A. C. C., Mahmudov, K. T., Haukka, M., Mac Leod, T. C. O., Martins, L. M. D. R. S., Kuznetsov, M. L., & Pombeiro, A. J. L. (2011). Complexes of Copper(II) with 3-(ortho-substituted phenylhydrazo)pentane-2, 4-diones: Syntheses, Properties and Catalytic Activity for Cyclohexane Oxidation. *Dalton Transactions*, **40**(12): 2822–2836. DOI: 10.1039/c0dt01527j

Krause, M., Foks, H., Ziembicka, D., Augustynowicz-Kopeć, E., Głogowska, A., Korona-Głowniak, I., Bojanowski, K., Siluk, D., & Gobis, K. (2020). 4-Substituted Picolinohydrazonamides as a New Class of Potential Antitubercular Agents. *European Journal of Medicinal Chemistry*, **190**(1): 1-19. DOI: 10.1016/j.ejmech.2020.112106

Krishnegowda, G., Prakasha Gowda, A. S., Tagaram, H. R. S., Carroll, K. F. S. O., Irby, R. B., Sharma, A. K., & Amin, S. (2011). Synthesis and Biological Evaluation of a Novel Class of Isatin Analogs as Dual Inhibitors of Tubulin Polymerization and Akt Pathway. *Bioorganic and Medicinal Chemistry*, **19**(20): 6006–6014. DOI: 10.1016/j.bmc.2011.08.044

Kühne, T. D., Iannuzzi, M., Del Ben, M., Rybkin, V. V., Seewald, P., Stein, F., Laino, T., Khaliullin, R. Z., Schütt, O., Schiffmann, F., Golze, D., Wilhelm, J., Chulkov, S., Bani-Hashemian, M. H., Weber, V., Borštnik, U., Taillefumier, M., Jakobovits, A. S., Lazzaro, A., Pabst, H., Müller, T., Schade, R., Guidon, M., Andermatt, S.,

Holmberg, N., Schenter, G. K., Hehn, A., Bussy, A., Belleflamme, F., Tabacchi, G., Glöß, A., Lass, M., Bethune, I., Mundy, C.J., Plessl, C., Watkins, M., Vondele, J.V., Krack, M., and Hutter, J. (2020). CP2K: An Electronic Structure and Molecular Dynamics Software Package-Quickstep: Efficient and Accurate Electronic Structure Calculations. *Journal of Chemical Physics*, **152**(19): 1–47. DOI: 10.1063/5.0007045

Kuriwaki, I., Kameda, M., Hisamichi, H., Kikuchi, S., Iikubo, K., Kawamoto, Y., Moritomo, H., Kondoh, Y., Amano, Y., Tateishi, Y., Echizen, Y., Iwai, Y., Noda, A., Tomiyama, H., Suzuki, T., & Hirano, M. (2020). Structure-Based Drug Design of 1,3,5-triazine and Pyrimidine Derivatives as Novel FGFR3 Inhibitors with High Selectivity Over VEGFR2. *Bioorganic and Medicinal Chemistry*, **28**(10): 115453. DOI: 10.1016/j.bmc.2020.115453

Labisbal, E., Sousa, A., Castiñeiras, A., García-Vázquez, J. A., Romero, J., & West, D. X. (2000). Spectral and Structural Studies of Metal Complexes of Isatin 3-hexamethyleneiminylthiosemicarbazone Prepared Electrochemically. *Polyhedron*, **19**(10): 1255–1262.DOI: 10.1016/S0277-5387(00)00383-1

Lahari, K., & Sundararajan, R. (2020). Design and Synthesis of Novel Isatin Derivatives as Potent Analgesic, Anti-inflammatory and Antimicrobial Agents. *Journal of Chemical Sciences*, **132**(1): 1–15. DOI: 10.1007/s12039-020-01795-0

Lai, S., Chen, J. N., Huang, H. W., Zhang, X. Y., Jiang, H. L., Li, W., Wang, P. L., Wang, J., & Liu, F. N. (2018). Structure Activity Relationships of Chrysoeriol and Analogs as Dual c-Met and VEGFR2 Trosine Kinase Inhibitors. *Oncology Reports*, **40**(3): 1650–1656. DOI: 10.3892/or.2018.6542

Lane, M. E., Yu, B., Pestell, R. G., Wadler, S., Rice, A., Lipson, K. E., Liang, C., Sun, L., Tang, C., & McMahon, G. (2001). A Novel cdk2-Selective Iinhibitor, SU9516, Induces Apoptosis in Colon Carcinoma Cells. *Cancer Research*, **61**(16): 6170–6177.

Laskowski, R. A., MacArthur, M. W., Moss, D. S., & Thornton, J. M. (1993). PROCHECK: A Program to Check the Stereochemical Quality of Protein Structures. *Journal of Applied Crystallography*, **26**(2): 283–291. DOI: 10.1107/s0021889892009944

Le Bot, M. A., Bégué, J. M., Kernaleguen, D., Robert, J., Ratanasavanh, D., Airiau, J., Riché, C., & Guillouzo, A. (1988). Different Cytotoxicity and Metabolism of Doxorubicin, Daunorubicin, Epirubicin, Esorubicin and Idarubicin in Cultured Human and Rat Hepatocytes. *Biochemical Pharmacology*, **37**(20): 3877–3887. DOI: 10.1016/0006-2952(88)90069-X

Lin, H. H., Wu, W. Y., Cao, S. L., Liao, J., Ma, L., Gao, M., Li, Z. F., & Xu, X. (2013). Synthesis and Antiproliferative Evaluation of Piperazine-1-carbothiohydrazide Derivatives of Indolin-2-one. *Bioorganic and Medicinal Chemistry Letters*, **23**(11): 3304–3307. DOI: 10.1016/j.bmcl.2013.03.099

Lu, Y. H., Lu, Y. W., Wu, C. L., Shao, Q., Chen, X. L., & Bimbong, R. N. B. (2006). UV-visible Spectroscopic Study of the Salicyladehyde Benzoylhydrazone and Its Cobalt Complexes. *Spectrochimica Acta - Part A: Molecular and Biomolecular Spectroscopy*, **65**(4): 695–701. DOI: 10.1016/j.saa.2005.12.032

Luqmani, Y. A. (2005). Mechanisms of Drug Resistance in Cancer Chemotherapy. *Medical Principles and Practice*, **14**(1): 35–48. DOI: 10.1159/000086183

Macrae, C. F., Sovago, I., Cottrell, S. J., Galek, P. T. A., Pidcock, E., Platings, M., Shields, G. P., Stevens, J. S., Towler, M., & Wood, P. A. (2020). Mercury 4 . 0 : from Visualization to Analysis , Design and Prediction. *Journal of Applied Crystallography*, **53**(1): 226–235. DOI: 10.1107/S1600576719014092

Mahajanakatti, A. B., Murthy, G., Sharma, N., & Skariyachan, S. (2014). Exploring Inhibitory Potential of Curcumin Against Various Cancer Targets by i*n Silico* Virtual Screening. *Interdisciplinary Sciences – Computational Life Sciences*, **6**(1): 13–24. DOI: 10.1007/s12539-014-0170-8

Mahmoud, M. E., Yakout, A. A., Ahmed, S. B., & Osman, M. M. (2008). Speciation, Selective Extraction and Preconcentration of Chromium Ions Via Alumina-Functionalized-isatin-thiosemicarbazone. *Journal of Hazardous Materials*, **158**(3): 541–548. DOI: 10.1016/j.jhazmat.2008.01.114

Manda, S., & Konda, S. (2013). Synthesis and Antibacterial Activity of the 5-[2(3)-dialkylamino alkoxy] Isatin-3-thiosemicarbazones and 5-[2(3)-dialkylamino alkoxy] Isatin-3-hydrazone. *International Journal of Pharmaceutical Biological and Chemical Sciences*, **2**(4): 38–42. www.ijpbcs.net or www.ijpbcs.com

Matesanz, A. I., Albacete, P., & Souza, P. (2016). Synthesis and Characterization of a New Bioactive Mono(thiosemicarbazone) Ligand Based on 3,5-diacetyl-1,2,4-triazol diketone and Its Palladium and Platinum Complexes. *Polyhedron*, **109**(1): 161–165. DOI: 10.1016/j.poly.2016.02.008

Matesic, L., Locke, J. M., Bremner, J. B., Pyne, S. G., Skropeta, D., Ranson, M., & Vine, K. L. (2008). N-Phenethyl and N-naphthylmethyl Isatins and Analogues as *in Vitro* Cytotoxic Agents. *Bioorganic and Medicinal Chemistry*, **16**(6): 3118–3124. DOI: 10.1016/j.bmc.2007.12.026

Mazumder, L., Hasan, M. R., Fatema, K., Islam, M. Z., & Tamanna, S. K. (2022). Structural and Functional Annotation and Molecular Docking Analysis of a Hypothetical Protein from Neisseria gonorrhoeae: An *In-Silico* Approach. *BioMed Research International*, **2022**(1): 1–25. DOI: 10.1155/2022/4302625

Medvedev, A., Buneeva, O., & Glover, V. (2007). Biological Targets for Isatin and Its Analogues: Implications for Therapy. *Biologics: Targets and Therapy*, **1**(2): 151–162.

Medvedev, A., Buneeva, O., Gnedenko, O., Ershov, P., & Ivanov, A. (2018). Isatin, An Endogenous Nonpeptide Biofactor: A Review of Its Molecular Targets, Mechanisms of Actions, and Their Biomedical Implications. *BioFactors*, **44**(2): 95–108. DOI: 10.1002/biof.1408

Medvedev, A. E., Goodwin, B., Clow, A., Halket, J., Glover, V., & Sandler, M. (1992). Inhibitory Potency of Some Isatin Analogues on Human Monoamine Oxidase A and B. *Biochemical Pharmacology*, **44**(3): 590–592. DOI: 10.1016/0006-2952(92)90454-Q

Miettinen, M., Rikala, M. S., Rys, J., Lasota, J., & Wang, Z. F. (2012). Vascular Endothelial Growth Factor Receptor 2 as a Marker for Malignant Vascular Tumors and Mesothelioma: An Immunohistochemical Study of 262 Vascular Edothelial and 1640 Nonvascular Tumors. *American Journal of Surgical Pathology*, **36**(4): 629–639. DOI: 10.1097/PAS.0b013e318243555b

Mohan, A., Gangwar, P., & Khan, D. (2013). Structure Prediction and Molecular Docking Studies of "Prostaglandin D synthesis":Inhibition of Hair Growth in a Ndrogenetic Alopecia. *World Journal of Pharmaceutical Research*, **2**(4): 1114–

1121.

Muğlu, H. (2020). Synthesis, Characterization, and Antioxidant Activity of Some New N4-arylsubstituted-5-methoxyisatin-β-thiosemicarbazone Derivatives. *Research on Chemical Intermediates*, **46**(4): 2083–2098. DOI: 10.1007/s11164-020-04079-x

Muğlu, H., Çavuş, M. S., Bakır, T., & Yakan, H. (2019). Synthesis, Characterization, Quantum Chemical Calculations and Antioxidant Activity of New Bis-Isatin Carbohydrazone and Thiocarbohydrazone Derivatives. *Journal of Molecular Structure*, **1196**(1): 819–827. DOI: 10.1016/j.molstruc.2019.07.002

Munikumari, G., Konakanchi, R., Nishtala, V. B., Ramesh, G., Kotha, L. R., Chandrasekhar, K. B., & Ramachandraiah, C. (2019). Palladium(II) Complexes of 5-substituted Isatin Thiosemicarbazones: Synthesis, Spectroscopic Characterization, Biological Evaluation and *in Silico* Docking Studies. *Synthetic Communications*, **49**(1): 146–158. DOI: 10.1080/00397911.2018.1546400

Muralisankar, M., Basheer, S. M., Haribabu, J., Bhuvanesh, N. S. P., Karvembu, R., & Sreekanth, A. (2017). An Investigation on the DNA/protein Binding, DNA Cleavage and *in Vitro* Anticancer Properties of SNO Pincer Type Palladium(II) Complexes with N-substituted Isatin Thiosemicarbazone Ligands. *Inorganica Chimica Acta*, **466**(2): 61–70. DOI: 10.1016/j.ica.2017.05.044

Muralisankar, M., Dheepika, R., Haribabu, J., Balachandran, C., Aoki, S., Bhuvanesh, N. S. P., & Nagarajan, S. (2019). Design, Synthesis, DNA/HSA Binding, and Cytotoxic Activity of Half-Sandwich Ru(II)-Arene Complexes Containing Triarylamine-Thiosemicarbazone Hybrids [Research-article]. *ACS Publications*, **4**(7): 11712–11723. DOI: 10.1021/acsomega.9b01022

Muralisankar, M., Haribabu, J., Bhuvanesh, N. S. P., Karvembu, R., & Sreekanth, A. (2016). Synthesis, X-ray Crystal Structure, DNA/Protein Binding, DNA Cleavage and Cytotoxicity Studies of N(4) Substituted Thiosemicarbazone Based Copper(II)/Nickel(II) Complexes. *Inorganica Chimica Acta*, **449**(4): 82–95. DOI: 10.1016/j.ica.2016.04.043

Muralisankar, M., Sreedharan, R., Sujith, S., Bhuvanesh, N. S. P., & Sreekanth, A. (2017). N(1)-Pentyl Isatin-N(4)-Methyl-N(4)-Phenyl Thiosemicarbazone (PITSc)

as a Corrosion Inhibitor on Mild Steel in HCl. *Journal of Alloys and Compounds*, **695**(4): 171–182. DOI: 10.1016/j.jallcom.2016.10.173

Muralisankar, M., Sujith, S., Bhuvanesh, N. S. P., & Sreekanth, A. (2016). Synthesis and Crystal Structure of New Monometallic and Bimetallic Copper(II) Complexes with N-Substituted Isatin Thiosemicarbazone Ligands: Effects of the Complexes on DNA/Protein-Binding Property, DNA Cleavage Study and *in Vitro* Anticancer Activity. *Polyhedron*, **118**(2): 103–117. DOI: 10.1016/j.poly.2016.06.017

Singh, N. K., Shrestha, S., Shahi, N., Choudhary, R. K., Kumbhar A.A., Pokharek Y. R., & Yadav, P. N. (2021). Enhancement of Anticancer Activity of N(4)1-(2-Pyridyl)piperazinyl 5-Nitroisatin Thiosemicarbazone on Chelation with Copper(II). *Asian Journal of Chemistry*, **33**(3): 557–564. DOI: 10.14233/ajchem.2021.23004

Naithani, M. (2021). Molecular Docking Analysis of Piperlongumine with Different Apoptotic Proteins Involved in Hepatocellular Carcinoma. *Bioinformation*, **17**(9): 829–833. DOI: 10.6026/97320630017829

Nath, R., Pathania, S., Grover, G., & Akhtar, M. J. (2020). Isatin Containing Heterocycles for Different Biological Activities: Analysis of Structure Activity Relationship. *Journal of Molecular Structure*, **1222**(1): 128900. DOI: 10.1016/j.molstruc.2020.128900

Netalkar, P. P., Netalkar, S. P., & Revankar, V. K. (2015). Transition Metal Complexes of Thiosemicarbazone: Synthesis, Structures and *in Vitro* Antimicrobial Studies. *Polyhedron*, **100**(1): 215–222. DOI: 10.1016/j.poly.2015.07.075

Nirmala, J. G., Akila, S., Narendhirakannan, R.T., & Chatterjee, S. (2017). Vitis Vinifera Peel Polyphenols Stabilized Gold Nanoparticles Induce Cytotoxicity and Apoptotic Cell Death in A431 Skin Cancer Cell Lines. *Advanced Powder Technology*, **28**(2017): 1170–1184. DOI: 10.1016/j.apt.2017.02.003

Nutting, C. M., Herpen, C. M. L. Van, Miah, A. B., Bhide, S. A., Machiels, J., Buter, J., Kelly, C., Raucourt, D. De, & Harrington, K. J. (2009). Phase II Study of 3-AP Triapine in Patients with Recurrent or Metastatic Head and Neck Squamous Cell Carcinoma. *Annals of Oncology*, **20**(7): 1275–1279. DOI: 10.1093/annonc/mdn775

Osman, U.M., Silvarajoo, S., Kamarudin, K.H., Mohamed Tahir, M. I., & Chong, K.H. (2020). Ni(II) Complex Containing a Thiosemicarbazone Ligand: Synthesis, Spectroscopy, Single-Crystal X-ray Crystallographic and Conductivity Studies. *Journal of Molecular Structure*, **20**(1): 128994. DOI: 10.1016/j.molstruc.2020.128994

Özkütük, M., Öğretir, C., Arslan, T., Kandemirli, F., & Köksoy, B. (2010). Acid Dissociation Constants of Some Novel Isatin Thiosemicarbazone Derivatives. *Journal of Chemical and Engineering Data*, **55**(8): 2714–2718. DOI: 10.1021/je9009738

Padhye, S. (1985). Transition Metal Complexes of Semicarbazones and Thiosemicarbazones. *Science*, **63**(1): 127–160.

Pakravan, P., Kashanian, S., Khodaei, M. M., & Harding, F. J. (2013). Biochemical and Pharmacological Characterization of Isatin and Its Derivatives: From Structure to Activity. *Pharmacological Reports*, **65**(2): 313–335. DOI: 10.1016/S1734-1140(13)71007-7

Pandeya, S. N., Smitha, S., Jyoti, M., & Sridhar, S. K. (2005). Biological Activities of Isatin and Its Derivatives. *Acta Pharmaceutica*, **55**(1): 27–46.

Pape, V. F. S., Tóth, S., Füredi, A., Szebényi, K., Lovrics, A., Szabó, P., Wiese, M., & Szakács, G. (2016). Design, Synthesis and Biological Evaluation of Thiosemicarbazones, Hydrazinobenzothiazoles and Arylhydrazones as Anticancer Agents with a Potential to Overcome Multidrug Resistance. *European Journal of Medicinal Chemistry*, **117**(1): 335–354. DOI: 10.1016/j.ejmech.2016.03.078

Paramashivam, S. K., Elayaperumal, K., Natarajan, B., Ramamoorthy, M., Balasubramanian, S., & Dhiraviam, K. (2015). *In Silico* Pharmacokinetic and Molecular Docking Studies of Small Molecules Derived from Indigofera Aspalathoides Vahl Targeting Receptor Tyrosine Kinases. *Bioinformation*, **11**(2): 73–84. DOI: 10.6026/97320630011073

Paulmurugan, R. (2012). Introduction to Cancer Biology. In *Molecular Imaging Probes for Cancer Research*, **2012** (1): 3-27. DOI: 10.1142/9789814293686_0001

Pawar, S., Amate, A., Chakravarty, D., Butcher, R. J., & Kumbhar, A. A. (2021). Cu(II) Complexes of 2-indole Thiocarbohydrazones: Synthesis, Characterization and DNA Cleavage Studies. *Journal of Chemical Sciences*, **133**(4): 107. DOI: 10.1007/s12039-021-01962-x

Peddibhotla, S. (2009). 3-Substituted-3-hydroxy-2-oxindole, an Emerging New Scaffold for Drug Discovery with Potential Anti-Cancer and other Biological Activities. *Current Bioactive Compounds*, **5**(1): 20–38. DOI: 10.2174/157340709787580900

Pelosi, G. (2010). Thiosemicarbazone Metal Complexes: From Structure to Activity. *The Open Crystallography Journal*, **3**(2): 16–28. DOI: 10.2174/1874846501003020016

Penthala, N. R., Yerramreddy, T. R., Madadi, N. R., & Crooks, P. A. (2010). Synthesis and *in Vitro* Evaluation of N-alkyl-3-hydroxy-3-(2-imino-3-methyl- 5-oxoimidazolidin-4-yl)indolin-2-one Analogs as Potential Anticancer Agents. *Bioorganic and Medicinal Chemistry Letters*, **20**(15): 4468–4471. DOI: 10.1016/j.bmcl.2010.06.042

Pervez, H., Khan, N., Iqbal, J., Zaib, S., Yaqub, M., Tahir, M. N., & Naseer, M. M. (2018). Synthesis, Crystal Structure, Molecular Docking Studies and Bio-Evaluation of Some N4-benzyl-substituted Isatin-3-thiosemicarbazones as Urease and Glycation Inhibitors. *Heterocyclic Communications*, **24**(1): 51–58. DOI: 10.1515/hc-2017-0148

Pervez, H., Khan, N., Zaib, S., Yaqub, M., Naseer, M. M., Tahir, M. N., & Iqbal, J. (2017). Synthesis, X-ray Molecular Structure, Biological Evaluation and Molecular Docking Studies of Some N4-benzyl Substituted 5-Nitroisatin-3-Thiosemicarbazones. *Bioorganic and Medicinal Chemistry*, **25**(3): 1022–1029. DOI: 10.1016/j.bmc.2016.12.012

Pervez, H., Manzoor, N., Yaqub, M., Khan, A., Khan, K., Nasim, F.-H., & Choudhary, M. (2010). Synthesis and Urease Inhibitory Properties of Some New N4-Substituted 5-Nitroisatin-3-thiosemicarbazones. *Letters in Drug Design & Discovery*, **7**(2): 102–108. DOI: 10.2174/157018010790225840

Pervez, H., Manzoor, N., Yaqub, M., & Khan, K. M. (2014). 5-Nitroisatin-Derived

Thiosemicarbazones: Potential Antileishmanial Agents. *Journal of Enzyme Inhibition and Medicinal Chemistry*, **29**(5): 628–632. DOI: 10.3109/14756366.2013.836641

Pervez, H., Manzoor, N., Yaqub, M., Nasim, F. U. H., & Khan, K. M. (2012). Synthesis and Biological Evaluation of Some N 4-Substituted 5-Nitroisatin-3-thiosemicarbazones. *Medicinal Chemistry Research*, **21**(9): 2251–2262. DOI: 10.1007/s00044-011-9745-7

Pervez, H., Saira, N., Iqbal, M. S., Yaqub, M., & Khan, K. M. (2011). Synthesis and Toxicity Evaluation of Some N4-aryl Substituted 5-trifluoromethoxyisatin-3-thiosemicarbazones. *Molecules*, **16**(8): 6408–6421. DOI: 10.3390/molecules16086408

Pires, D. E. V., Blundell, T. L., & Ascher, D. B. (2015). pkCSM: Predicting Small-Molecule Pharmacokinetic and Toxicity Properties Using Graph-based Signatures. *Journal of Medicinal Chemistry*, **58**(9): 4066–4072. DOI: 10.1021/acs.jmedchem.5b00104

Pourbasheer, E., & Amanlou, M. (2014). 3D-QSAR Analysis of Anti-Cancer Aagents by CoMFA and CoMSIA. *Medicinal Chemistry Research*, **23**(2): 800–809. DOI: 10.1007/s00044-013-0676-3

Prabhakaran, R., Renukadevi, S. V., Karvembu, R., Huang, R., Mautz, J., Huttner, G., Subashkumar, R., & Natarajan, K. (2008). Structural and Biological Studies of Mononuclear Palladium(II) Complexes Containing N-Substituted Thiosemicarbazones. *European Journal of Medicinal Chemistry*, **43**(2): 268–273. DOI: 10.1016/j.ejmech.2007.03.006

Prakash, C. R., & Raja, S. (2012). Indolinones as Promising Scaffold as Kinase Inhibitors: A Review. *Mini-Reviews in Medicinal Chemistry*, **12**(2): 98–119. DOI: 10.2174/138955712798995039

Qasem, A., Guan, S., Salhin, A., & Eltaher, N. (2014). Synthesis of Isatin Thiosemicarbazones Derivatives : *In Vitro* Anti-cancer , DNA Binding and Cleavage. Activities. *Molecular and Biomolecular Spectroscopy*, **125**(1): 440–448. DOI: 10.1016/j.saa.2014.01.086

Rai, A., Sengupta, S. K., & Pandey, O. P. (2005). Lanthanum(III) and Praseodymium(III) Complexes with Isatin Thiosemicarbazones. *Spectrochimica Acta - Part A: Molecular and Biomolecular Spectroscopy*, **61**(12): 2761–2765. DOI: 10.1016/j.saa.2004.09.031

Ralhan, R., & Kaur, J. (2007). Alkylating Agents and Cancer Therapy. *Expert Opinion on Therapeutic Patents*, **17**(9): 1061–1075. DOI: 10.1517/13543776.17.9.1061

Ramadan, E. S., Rasheed, H. A., & El Ashry, E. S. H. (2019). Synthesis and Antimicrobial Screening of Novel 1,3-dioxolanes Linked to N-5 of 5H-1,2,4-triazino[5,6-b]indole-3-thiol. *Journal of the Serbian Chemical Society*, **84**(1): 1–10. DOI: 10.2298/JSC171127067R

Ravindranath, P. A., Forli, S., Goodsell, D. S., Olson, A. J., & Sanner, M. F. (2015). AutoDockFR: Advances in Protein-Ligand Docking with Explicitly Specified Binding Site Flexibility. *PLoS Computational Biology*, **11**(12): 1–28. DOI: 10.1371/journal.pcbi.1004586

Rayan, B., & Rayan, A. (2017). Avogadro Program for Chemistry Education: To What Extent can Molecular Visualization and Three-dimensional Simulations Enhance Meaningful Chemistry Learning? *World Journal of Chemical Education*, **5**(4), 136–141. DOI: 10.12691/wjce-5-4-4

Rekulapally, S., Jarapula, R., Gangarapu, K., Manda, S., & Vaidya, J. R. (2015). *In Silico* and *in Vitro* Studies of Novel 7-azaindole and 7-azaisatin Derivatives as Potent Anticancer Agents. *Medicinal Chemistry Research*, **24**(9): 3412–3422. DOI: 10.1007/s00044-015-1390-0

Roth, G. J., Heckel, A., Colbatzky, F., Handschuh, S., Kley, J., Lehmann-Lintz, T., Lotz, R., Tontsch-Grunt, U., Walter, R., & Hilberg, F. (2009). Design, Synthesis, and Evaluation of Indolinones as Triple Angiokinase Inhibitors and the Discovery of a Highly Specific 6-methoxycarbonyl-substituted Indolinone (BIBF 1120). *Journal of Medicinal Chemistry*, **52**(14): 4466–4480. DOI: 10.1021/jm900431g

Sagdinc, S., Köksoy, B., Kandemirli, F., & Bayari, S. H. (2009). Theoretical and Spectroscopic Studies of 5-fluoro-isatin-3-(N-benzylthiosemicarbazone) and Its Zinc(II) Complex. *Journal of Molecular Structure*, **917**(3): 63–70. DOI: 10.1016/j.molstruc.2008.06.033

Sahasranaman, S., Howard, D., & Roy, S. (2008). Clinical Pharmacology and Pharmacogenetics of Thiopurines. *European Journal of Clinical Pharmacology*, **64**(8): 753–767. DOI: 10.1007/s00228-008-0478-6

Sánchez, J. A., Handal, M. G., Vílchez Rodriguez, J. F., Mejía, S. I., & Pagoaga, A. P. (2019). Time Intervals From Onset of Clinical Manifestations to Treatment in Patients with Cancer at Hospital General San Felipe, Tegucigalpa, Honduras. *Journal of Global Oncology*, **2019**(5): 1–7. DOI: 10.1200/JGO.19.00107

Saranya, S., Haribabu, J., Vadakkedathu Palakkeezhillam, V. N., Jerome, P., Gomathi, K., Rao, K. K., Hara Surendra Babu, V. H., Karvembu, R., & Gayathri, D. (2019). Molecular Structures, Hirshfeld Analysis and Biological Investigations of Isatin Based Thiosemicarbazones. *Journal of Molecular Structure*, **1198**(1): 126904. DOI: 10.1016/j.molstruc.2019.126904

Schiffrin, B., Radford, S. E., Brockwell, D. J., & Calabrese, A. N. (2020). PyXlinkViewer: A Flexible Tool for Visualization of Protein Chemical Crosslinking Data within the PyMOL Molecular Graphics System. *Protein Science*, **29**(8): 1851–1857. DOI: 10.1002/pro.3902

Scovill, J. P. (1991). A Facile Synthesis of Thiosemicarbazides and Thiosemicarbazones by the Transamination of 4-methyl-4-phenyl-3-thiosemicarbazide. *Phosphorus, Sulfur, and Silicon and the Related Elements*, **60**(2): 15–19. DOI: 10.1080/10426509108233920

Shahi, N., Pandey, V., Pathak, A., Thapa, R. S., Pokhrel, P., Pokharel, Y. R., & Yadav, P. N. (2021). Anticancer Potential of 3-hydroxypyridine-2-carboxaldehyde N(4)-methyl and Pyrrolidinylthiosemicarbazones and Their Zn(II) Complexes in Different Cancers via Targeting MAPK Superfamily Signaling Pathway. *Results in Chemistry*, **3**(1):100104. DOI: 10.1016/j.rechem.2021.100104

Shakya, B., Shahi, N., Ahmad, F., Yadav, P. N., & Pokharel, Y. R. (2019). 2-Pyridineformamide N(4)-ring Incorporated Thiosemicarbazones Inhibit MCF-7 Cells by Inhibiting JNK Pathway. *Bioorganic and Medicinal Chemistry Letters*, **29**(13): 1677–1681. DOI: 10.1016/j.bmcl.2019.04.031

Sheldrick, G. M. (2015). Crystal Structure Refinement with SHELXL. *Acta Crystallographica Section C: Structural Chemistry*, **71**(1): 3–8. DOI:

10.1107/S2053229614024218

Sheldrick, G. M. (2015). SHELXT - Integrated Space-group and Crystal-structure Determination. *Acta Crystallographica Section A: Foundations of Crystallography*, **71**(1): 3–8. DOI: 10.1107/S2053273314026370

Shrestha, G., Neupane, P., Lamichhane, N., Acharya, B. C., Siwakoti, B., Subedi, K. P., Pradhananga, K. K., & Mulmi, R. (2020). Cancer Incidence in Nepal: A Three-Year Trend Analysis 2013-2015. *Asian Pacific Journal of Cancer Care*, **5**(3): 145–150. DOI: 10.31557/apjcc.2020.5.3.145-150

Sibuh, B. Z., Gupta, P. K., Taneja, P., Khanna, S., Sarkar, P., Pachisia, S., Khan, A. A., Jha, N. K., Dua, K., Singh, S. K., Pandey, S., Slama, P., Kesari, K. K., & Roychoudhury, S. (2021). Synthesis, *in Silico* Study, and Anti-cancer Activity of Thiosemicarbazone Derivatives. *Biomedicines*, **9**(10): 1–19. DOI: 10.3390/biomedicines9101375

Singh, A., Raghuwanshi, K., Patel, V. K., Jain, D. K., Veerasamy, R., Dixit, A., & Rajak, H. (2017). Assessment of 5-substituted Isatin as Surface Recognition Group: Design, Synthesis, and Antiproliferative Evaluation of Hydroxamates as Novel Histone Deacetylase Inhibitors. *Pharmaceutical Chemistry Journal*, **51**(5): 366–374. DOI: 10.1007/s11094-017-1616-1

Singh, N. K., Shrestha, S., Shahi, N., Choudhary, R. K., Kumbhar, A. A., Pokharel, Y. R., & Yadav, P. N. (2021). Anticancer Potential of N(4)substituted 5-Nitroisatin Thiosemicarbazones and Their Copper(II) Complexes. *Rasayan Journal of Chemistry*, **14**(3): 1600–1610. DOI: 10.31788/RJC.2021.1436341

Solomon, V. R., Hu, C., & Lee, H. (2009). Hybrid Pharmacophore Design and Synthesis of Isatin-benzothiazole Analogs for Their Anti-breast Cancer Activity. *Bioorganic and Medicinal Chemistry*, **17**(21): 7585–7592. DOI: 10.1016/j.bmc.2009.08.068

Solomon, V. R., Hu, C., & Lee, H. (2010). Design and Synthesis of Anti-breast Cancer Agents from 4-piperazinylquinoline: A Hybrid Pharmacophore Approach. *Bioorganic and Medicinal Chemistry*, **18**(4): 1563–1572. DOI: 10.1016/j.bmc.2010.01.001

Sorensen, M., Sehested, M., & Jensen, P. (1995). Characterisation of a Human Small-Cell Lung Cancer Cell Line Resistant to the DNA Topoisomerase I-directed Drug Topotecan. *British Journal of Cancer*, **72**(2): 399–404. DOI: 10.1038/bjc.1995.345

Souza, M. A., Johann, S., dos Santos Lima, L. A. R., Campos, F. F., Mendes, I. C., Beraldo, H., de Souza-Fagundes, E. M., Silva Cisalpino, P., Augusto Rosa, C., de Almeida Alves, T. M., de Sá, N. P., & Zani, C. L. (2013). The Antimicrobial Activity of Lapachol and Its Thiosemicarbazone and Semicarbazone Derivatives. *Memorias Do Instituto Oswaldo Cruz*, **108**(3): 342–351. DOI: 10.1590/S0074-02762013000300013

Sridhar, S. K., & Ramesh, A. (2001). Synthesis and Pharmacological Activities of Hydrazones, Schiff and Mannich Bases of Isatin Derivatives. *Biological and Pharmaceutical Bulletin*, **24**(10): 1149–1152. DOI: 10.1248/bpb.24.1149

Sun, Y. S., Zhao, Z., Yang, Z. N., Xu, F., Lu, H. J., Zhu, Z. Y., Shi, W., Jiang, J., Yao, P. P., & Zhu, H. P. (2017). Risk Factors and Preventions of Breast Cancer. *International Journal of Biological Sciences*, **13**(11): 1387–1397. DOI: 10.7150/ijbs.21635

Suvarapu, L., & Baek, S. O. (2015). Synthesis and Characterization of 4-Benzyloxybenzaldehyde-4-methyl-3-thiosemicarbazone (Containing Sulphur and Nitrogen Donor Atoms) and Its Cd(II) Complex. *Metals*, **5**(4): 2266–2276. DOI: 10.3390/met5042266

Swathy, S. S., Selwin Joseyphus, R., Nisha, V. P., Subhadrambika, N., & Mohanan, K. (2016). Synthesis, Spectroscopic Investigation and Antimicrobial Activities of Some Transition Metal Complexes of a [(2-hydroxyacetophenone)-3-isatin]-bishydrazone. *Arabian Journal of Chemistry*, **9**(1): 1847–1857. DOI: 10.1016/j.arabjc.2012.05.004

Tejasree, C., Kiran, G., Rajyalakshmi, G., & Rama Narsimha Reddy, A. (2013). Hepatoprotective Activity of 1-(4-(Dimethylamino)Benzylidene)-5-(2-Oxoindolin-3-ylidene) Thiocarbohydrazone in Rats. *Toxicological and Environmental Chemistry*, **95**(9): 1589–1594. DOI: 10.1080/02772248.2014.887257

Tian, W., Chen, C., Lei, X., Zhao, J., & Liang, J. (2018). CASTp 3.0: Computed Atlas of Surface Topography of Proteins. *Nucleic Acids Research*, **46**(1): 363–367. DOI: 10.1093/nar/gky473

Türkkan, E., Sayin, U., Erbilen, N., Pehlivanoglu, S., Erdogan, G., Tasdemir, H. U., Saf, A. O., Guler, L., & Akgemci, E. G. (2017). Anticancer, Antimicrobial, Spectral, Voltammetric and DFT Studies with Cu(II) Complexes of 2-hydroxy-5-methoxyacetophenone Thiosemicarbazone and Its N(4)-substituted Derivatives. *Journal of Organometallic Chemistry*, **831**(2): 23–35. DOI: 10.1016/j.jorganchem.2016.12.020

Vandana, K., Marathakam, A., Thushara B. S., & Rajitha, K. (2017). A Review on Isatin Derivatives with Diverse Biological Activities. *World Journal of Pharmaceutical Research*, **6**(16): 318–332. DOI: 10.20959/wjpr201716-10244

Vondele, J.V., & Hutter, J. (2007). Gaussian Basis Sets for Accurate Calculations on Molecular Systems in Gas and Condensed Phases. *Journal of Chemical Physics*, **127**(11): 114105. DOI: 10.1063/1.2770708

Vine, K. L., Locke, J. M., Ranson, M., Benkendorff, K., Pyne, S. G., & Bremner, J. B. (2007). *In Vitro* Cytotoxicity Evaluation of Some Substituted Isatin Derivatives. *Bioorganic and Medicinal Chemistry*, **15**(2): 931–938. DOI: 10.1016/j.bmc.2006.10.035

Vine, K. L., Matesic, L., Locke, J. M., & Skropeta, D. (2013). Recent Highlights in the Development of Isatin-Based Anticancer Agents. In *Advances in Anticancer Agents in Medicinal Chemistry*. **2013**(1): 254-312. DOI: 10.2174/978160805496111302000 8

Vine, K., Matesic, L., Locke, J., Ranson, M., & Skropeta, D. (2012). Cytotoxic and Anticancer Activities of Isatin and Its Derivatives: A Comprehensive Review from 2000-2008. *Anti-Cancer Agents in Medicinal Chemistry*, **9**(4): 397–414. DOI: 10.2174/1871520610909040397

Vineetha, M. C., & Kurup, M. R. P. (2013). Synthesis and Spectral Characterization of Copper (II) and Zinc (II) Complexes of An Acylhydrazone. *Mapana Journals Science*, **2**(2): 67–79. DOI: 10.12723/mjs.25.7

Wang, X., Shen, Y., Wang, S., Li, S., Zhang, W., Liu, X., Lai, L., Pei, J., & Li, H. (2017). PharmMapper 2017 Update: A Web Server for Potential Drug Target Identification with a Comprehensive Target Pharmacophore Database. *Nucleic Acids Research*, **45**(1): 356–360. DOI: 10.1093/nar/gkx374

Wiles, D. M., & Suprunchuk, T. (1969). The Infrared Absorption Spectra of Thiosemicarbazide and Related Compounds: NH_2 and NH Vibrations . *Canadian Journal of Chemistry*, **47**(6): 1087–1089. DOI: 10.1139/v69-173

William D. Graf, M.D., Phillip F. Chance, M.D., M. William Lensch, B.S., Lilly J. Eng, M.D., Hillary P. Lipe, R.N.P., & Thomas D. Bird, M.D. (1996). Severe Vincristine Neuropathy in Charcot-Marie-Tooth Disease Type 1A. *American Cancer Society*, **77**(7): 1356–1362.

Wyatt, P.G., Woodhead, A.J, Berdini, V., Boulstridge, J.A., Carr, M.G., Cross, D.M., Davis, D.J., Devine, L.A., Early, T.R., Feltell, R.E., Lewis, E.J., McMenamin, R.L., Navarro, E.F., O'Brien, M.A., O'Reilly, M., Reule, M., Saxty, G., Seavers, L.C.A., Smith, D.M., Squires, M.S., Trewartha, G., Walker, M.T., and Woolford, A.J.A. (2008). Identification of N-(4-Piperidinyl)-4-(2,6-dichlorobenzoylamino)-1H-pyrazole-3-carboxamide (AT7519), a Novel Cyclin Dependent Kinase Inhibitor Using Fragment. *Journal of Medicinal Chemistry*, **51**(1): 4986–4999. DOI: 10.1021/jm800382h

Xia, C., Dong, X., Li, H., Cao, M., Sun, D., He, S., Yang, F., Yan, X., Zhang, S., Li, N., & Chen, W. (2022). Cancer Statistics in China and United States, 2022: Profiles, Trends, and Determinants. *Chinese Medical Journal*, **135**(5): 584–590. DOI: 10.1097/CM9.0000000000002108

Xiong, G., Wu, Z., Yi, J., Fu, L., Yang, Z., Hsieh, C., Yin, M., Zeng, X., Wu, C., Lu, A., Chen, X., Hou, T., & Cao, D. (2021). ADMETlab 2.0: An Integrated Online Platform for Accurate and Comprehensive Predictions of ADMET Properties. *Nucleic Acids Research*, **49**(1): 5–14. DOI: 10.1093/nar/gkab255

Xu, Z., Zhao, S. J., Lv, Z. S., Gao, F., Wang, Y., Zhang, F., Bai, L., & Deng, J. L. (2019). Fluoroquinolone-isatin Hybrids and Their Biological Activities. *European Journal of Medicinal Chemistry*, **162**(1): 396–406. DOI: 10.1016/j.ejmech.2018.11.032

Yadav, P. N., Singh, N. K., Sharma, S., Krishnakumar, A., Choudhary, R. K., Kumbhar, A. A., Butcher, R. J., & Pokharel, Y. R. (2022). Exploration of Anticancer Potency of N(4) Thiomorpholinyl Isatin/Haloisatin Thiosemcarbazones on Coordination to Cu^{2+} Ion. *Journal of Inorganic Biochemistry*, **4**(1): 109767. DOI: 10.2139/ssrn.4042515

Yakan, H. (2020). Preparation, Structure Elucidation, and Antioxidant Activity of New Bis(thiosemicarbazone) Derivatives. *Turkish Journal of Chemistry*, **44**(4): 1085–1099. DOI: 10.3906/KIM-2002-76

Yasuda, D., Takahashi, K., Ohe, T., Nakamura, S., & Mashino, T. (2013). Antioxidant Activities of 5-Hydroxyoxindole and Its 3-Hydroxy-3-phenacyl Derivatives: The Suppression of Lipid Peroxidation and Intracellular Oxidative Stress. *Bioorganic and Medicinal Chemistry*, **21**(24): 7709–7714. DOI: 10.1016/j.bmc.2013.10.021

Yu, Y., Kalinowski, D. S., Kovacevic, Z., Siafakas, A. R., Jansson, P. J., Stefani, C., Lovejoy, D. B., Sharpe, P. C., Bernhardt, P. V., & Richardson, D. R. (2009). Thiosemicarbazones from the Old to New: Iron Chelators that are more than just Ribonucleotide Reductase Inhibitors. *Journal of Medicinal Chemistry*, **52**(17): 5271–5294. DOI: 10.1021/jm900552r

Zeglis, B. M., Divilov, V., & Lewis, J. S. (2011). Role of Metalation in the Topoisomerase IIα Inhibition and Antiproliferation Activity of a Series of α-heterocyclic-N4-substituted Thiosemicarbazones and Their Cu(II) Complexes. *Journal of Medicinal Chemistry*, **54**(7): 2391–2398. DOI: 10.1021/jm101532u

Zhang, H., Thomas, R., Oupicky, D., & Peng, F. (2008). Synthesis and Characterization of New Copper Thiosemicarbazone Complexes with an ONNS Quadridentate System: Cell Growth Inhibition, S-phase Cell Cycle Arrest and Proapoptotic Activities on Cisplatin-resistant Neuroblastoma Cells. *Journal of Biological Inorganic Chemistry*, **13**(1): 47–55. DOI: 10.1007/s00775-007-0299-6

Zhang, X. M., Guo, H., Li, Z. S., Song, F. H., Wang, W. M., Dai, H. Q., Zhang, L. X., & Wang, J. G. (2015). Synthesis and Evaluation of Isatin-β-thiosemicarbazones as Novel Agents Against Antibiotic-resistant Gram-positive Bacterial Species. *European Journal of Medicinal Chemistry*, **101**(1): 419–430. DOI: 10.1016/j.ejmech.2015.06.047

APPENDICES

Appendix A: IR spectra of TSCs

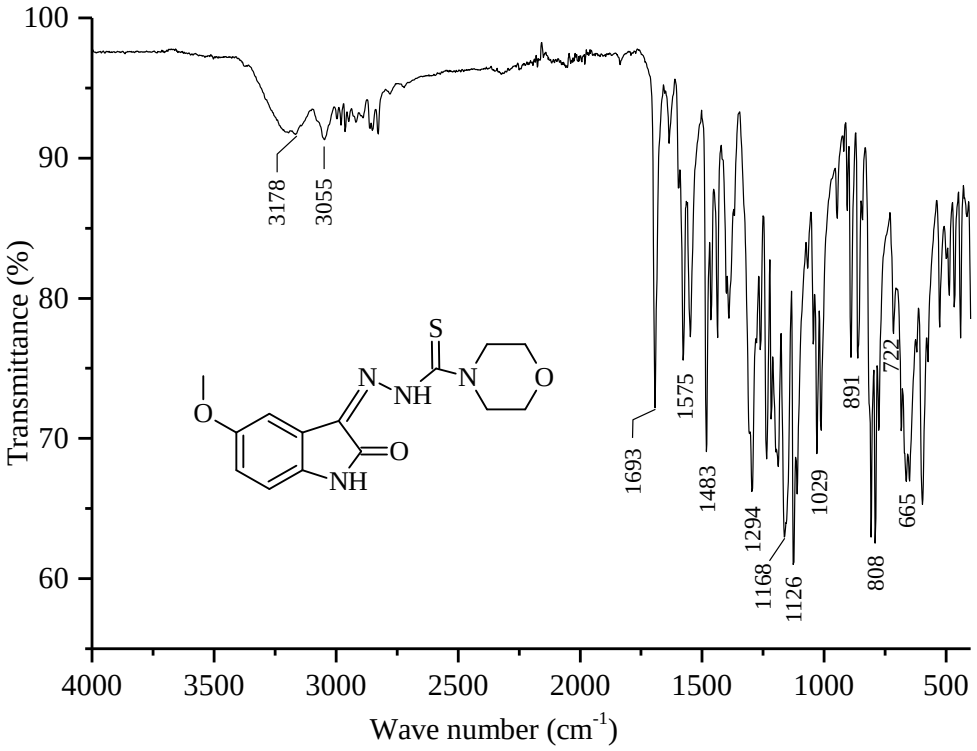

Appendix A1: IR spectrum of compound (***MeOIstMor*/1**)

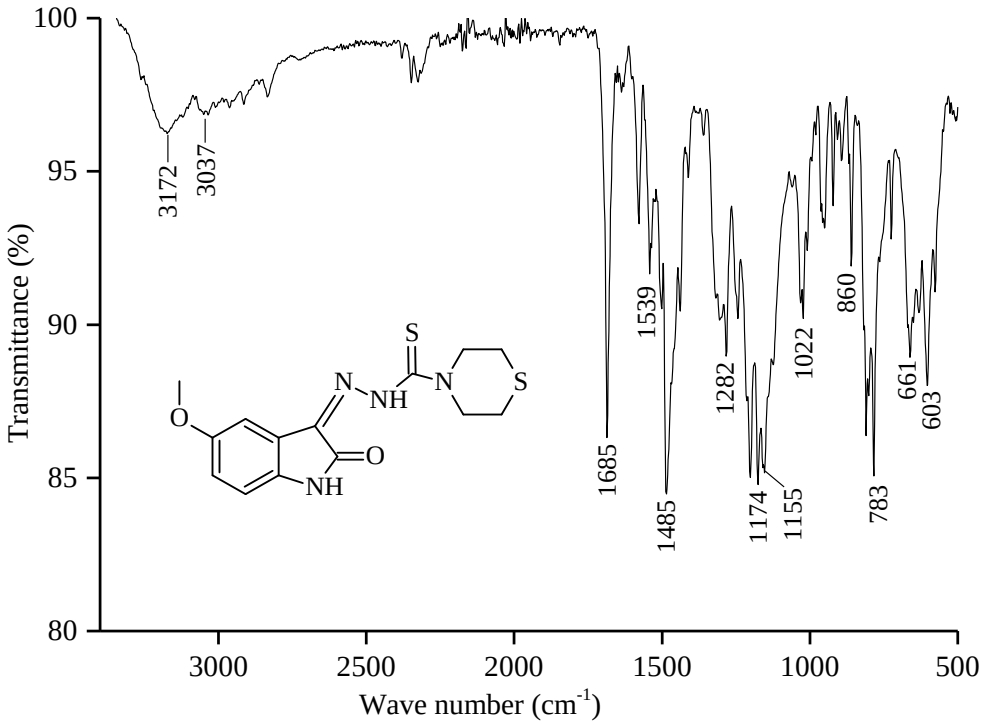

Appendix A2: IR spectrum of compound (***MeOIstTmor*/2)**

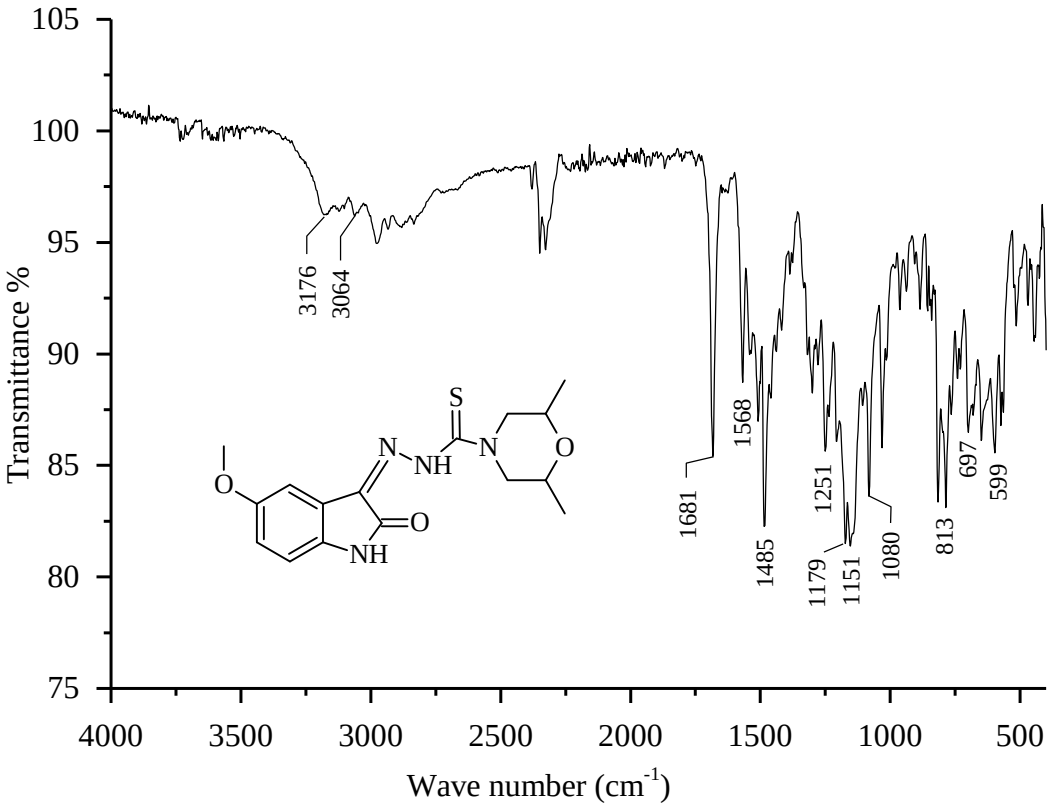

Appendix A3: IR spectrum of compound (***MeOIstDmMor*/3)**

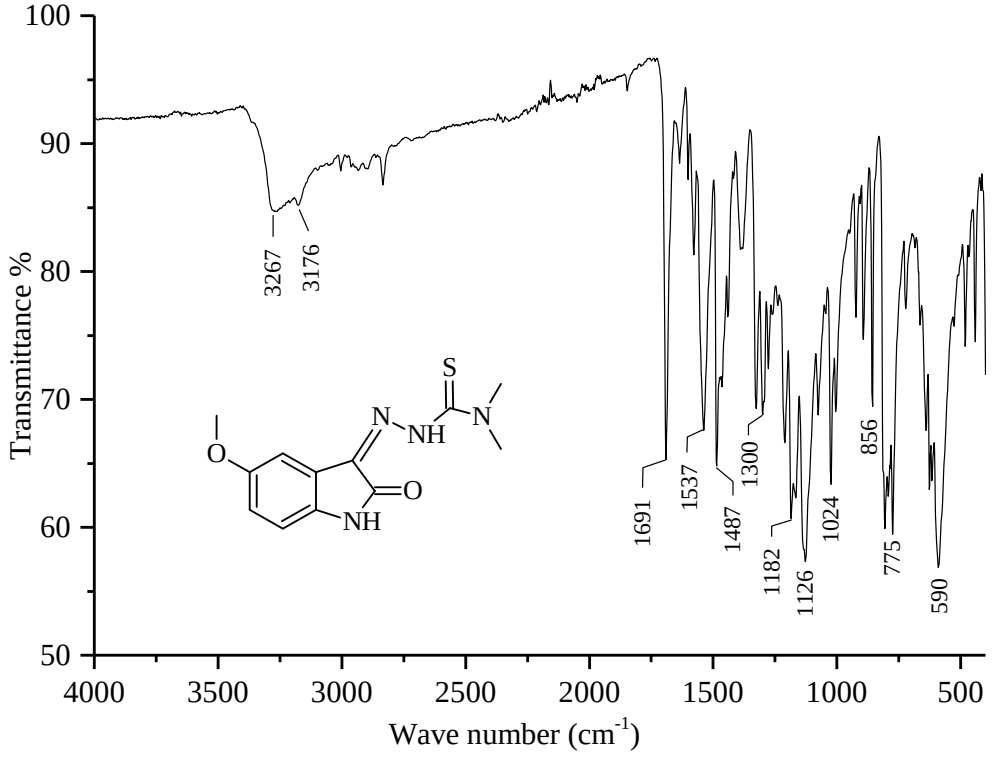

Appendix A4: IR spectrum of compound (***MeOIstDm*/4)**

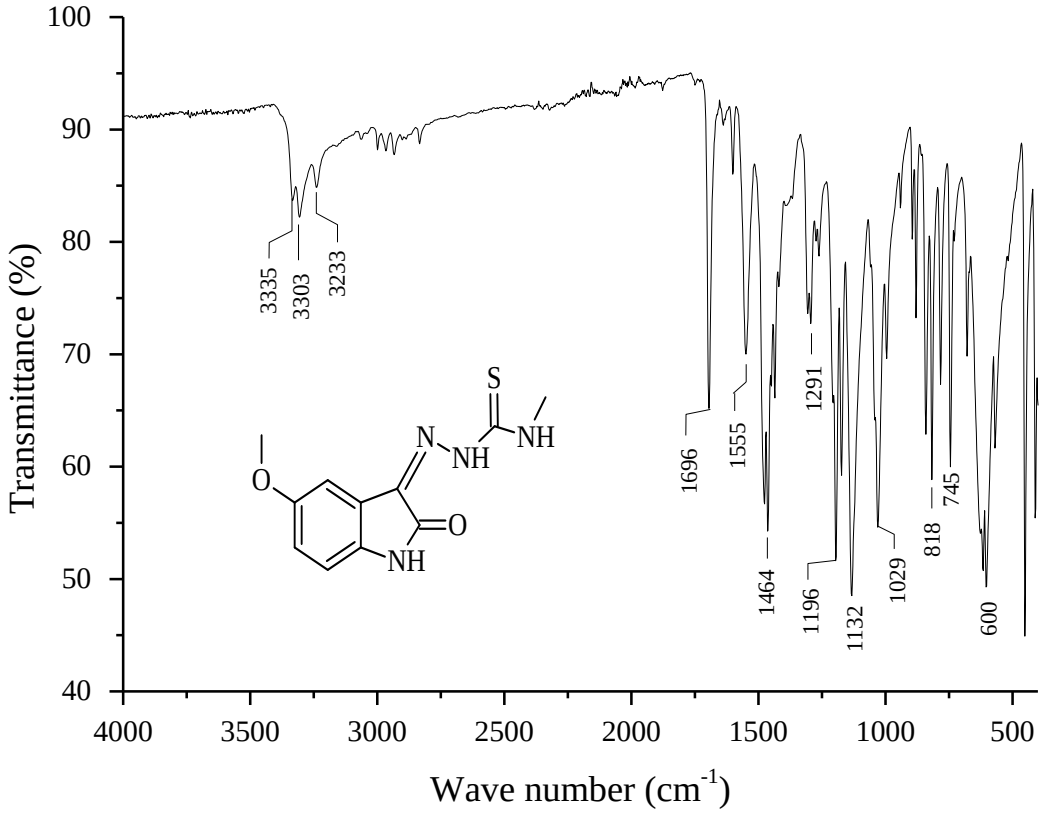

Appendix A5: IR spectrum of compound (***MeOIstMet*/5)**

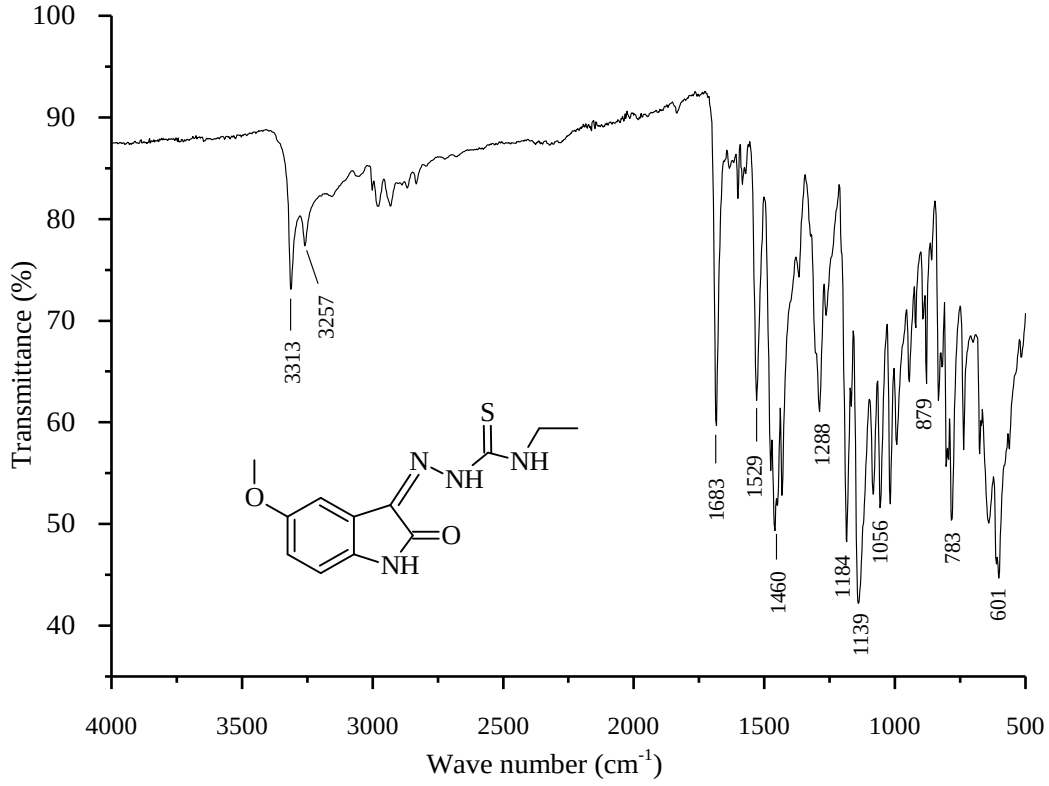

Appendix A6: IR spectrum of compound (***MeOIstEth*/6)**

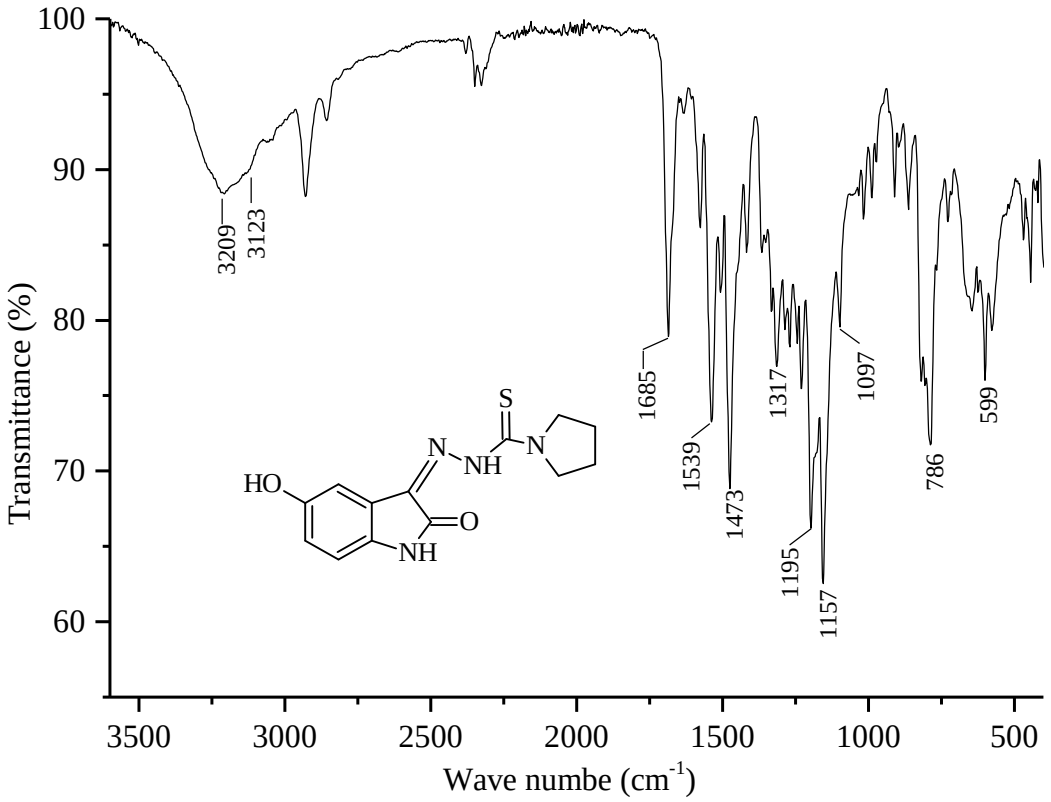

Appendix A7: IR spectrum of compound (***HydIstPyrl*/7)**

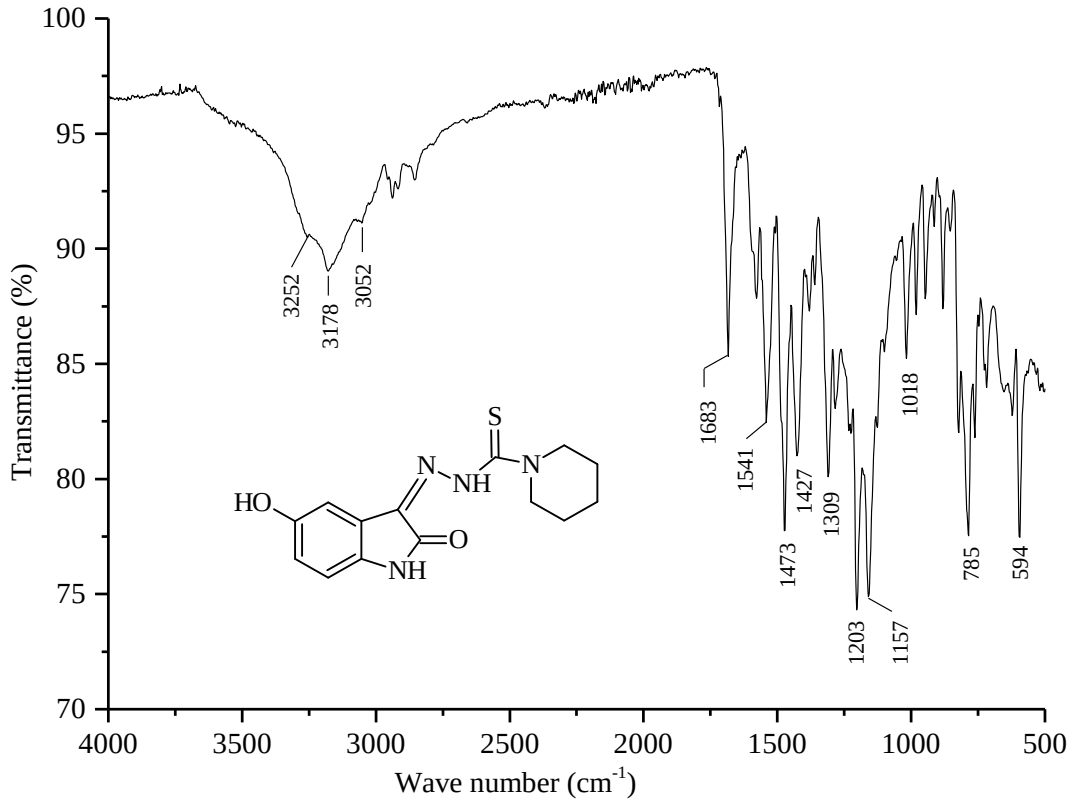

Appendix A8: IR spectrum of compound (***HydIstPip*/8)**

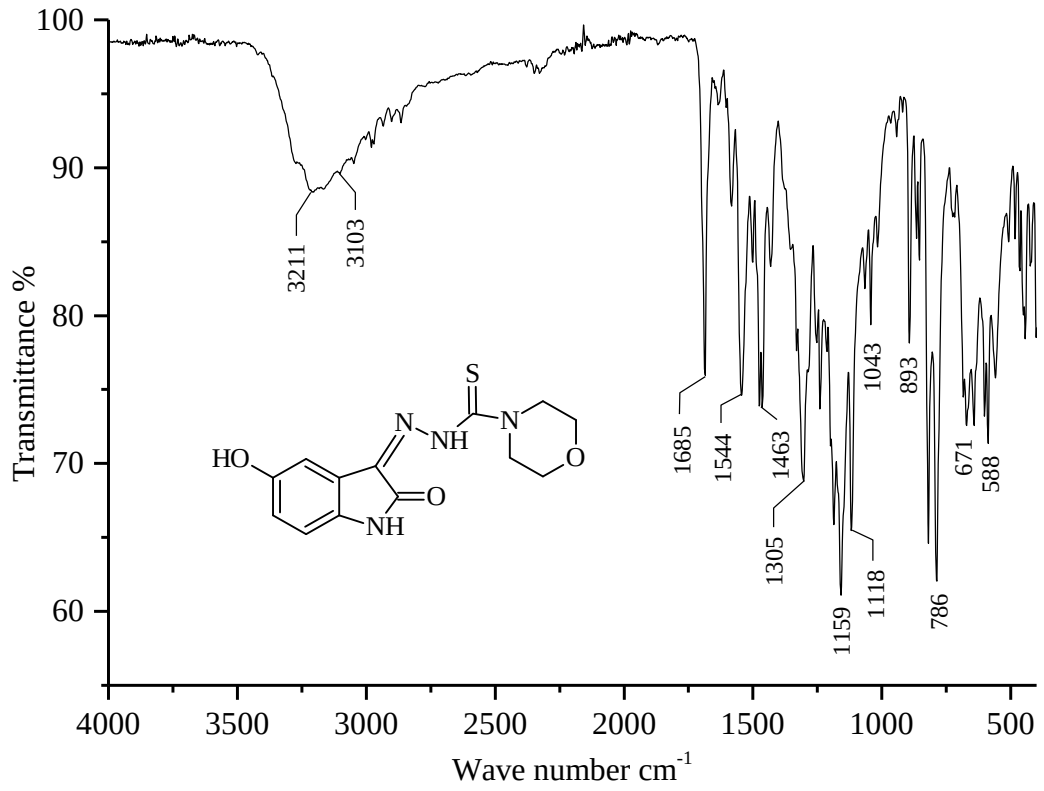

Appendix A9: IR spectrum of compound (***HydIstMor*/9)**

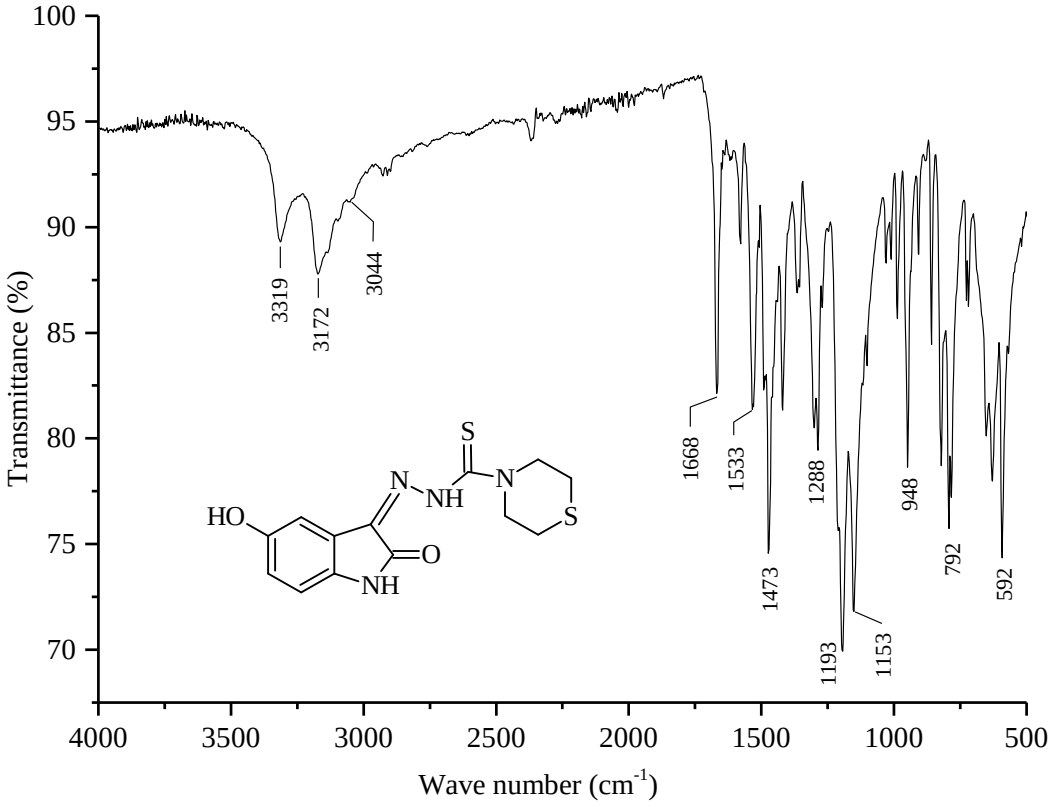

Appendix A10: IR spectrum of compound (***HydIstTmor*/10)**

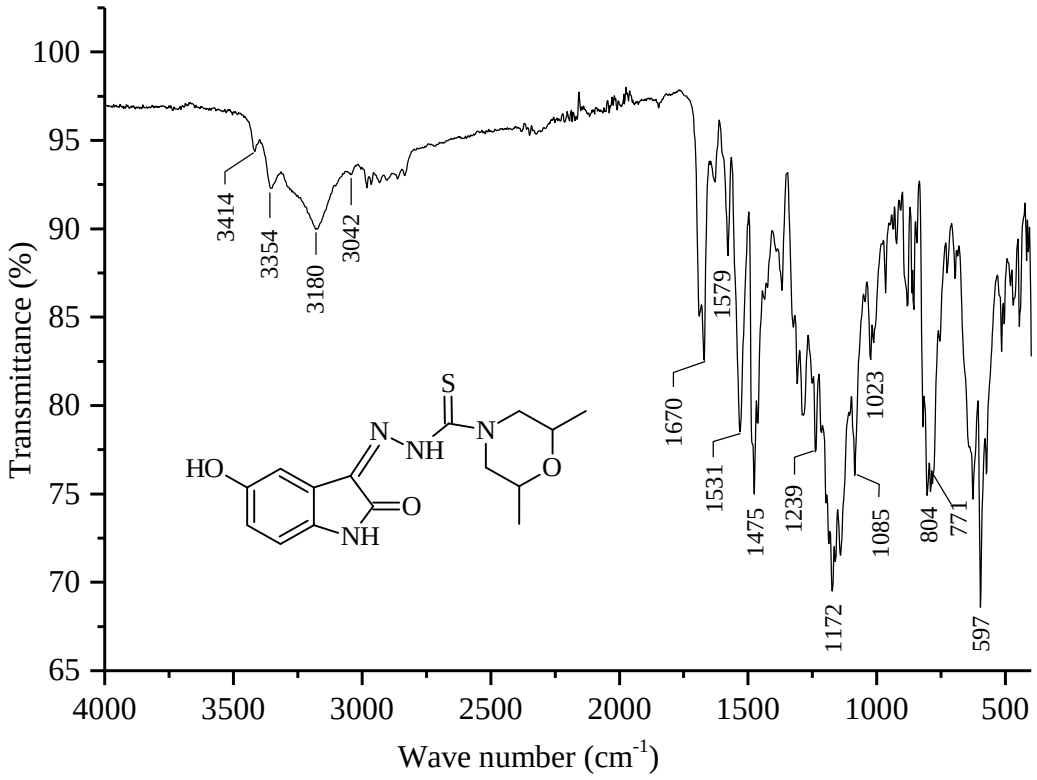

Appendix A11: IR spectrum of compound (***HydIstDmMor*/11)**

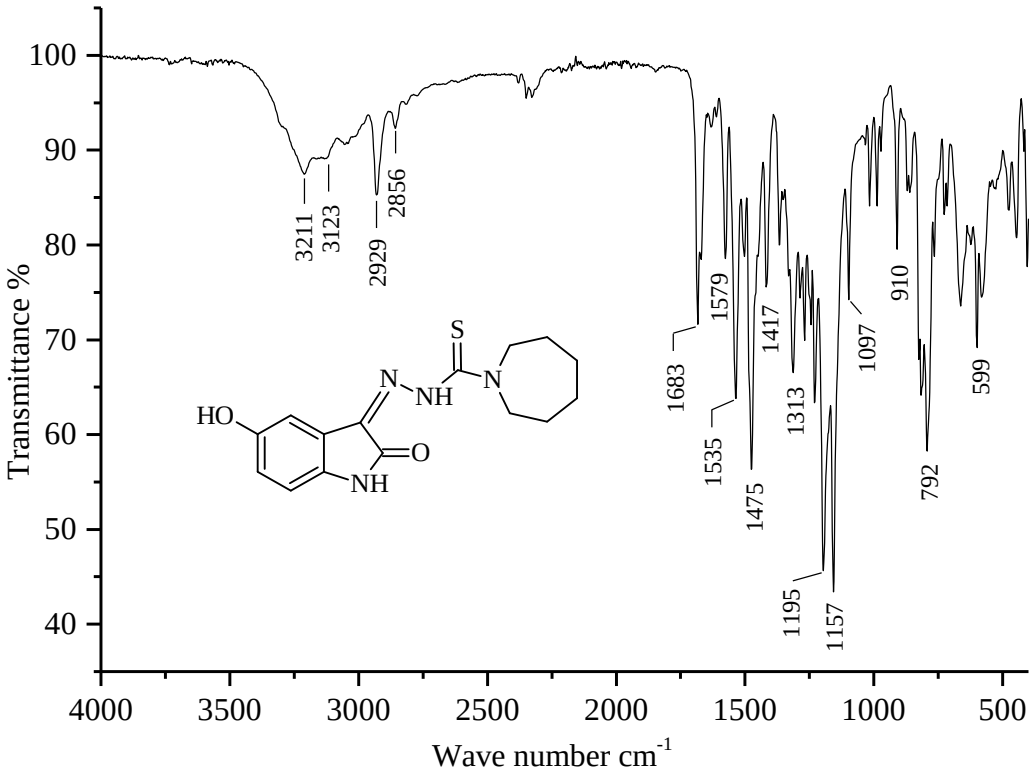

Appendix A12: IR spectrum of compound (***HydIstAzep*/12)**

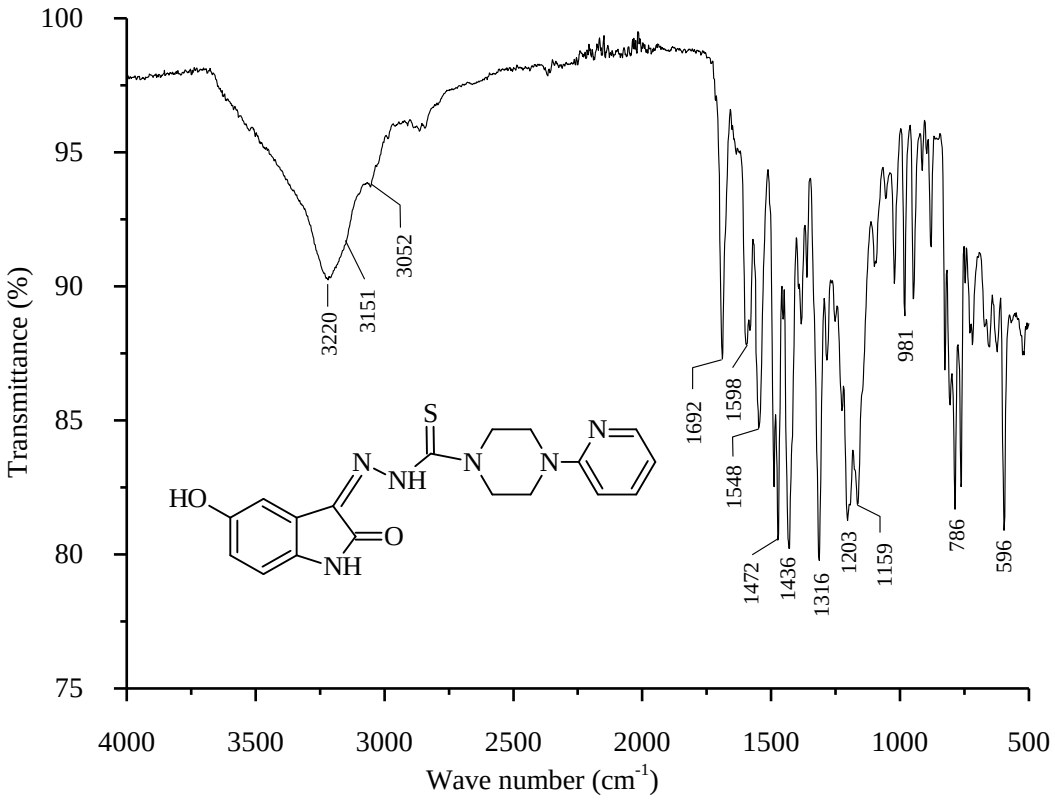

Appendix A13: IR spectrum of compound (***HydIstPypz*/13)**

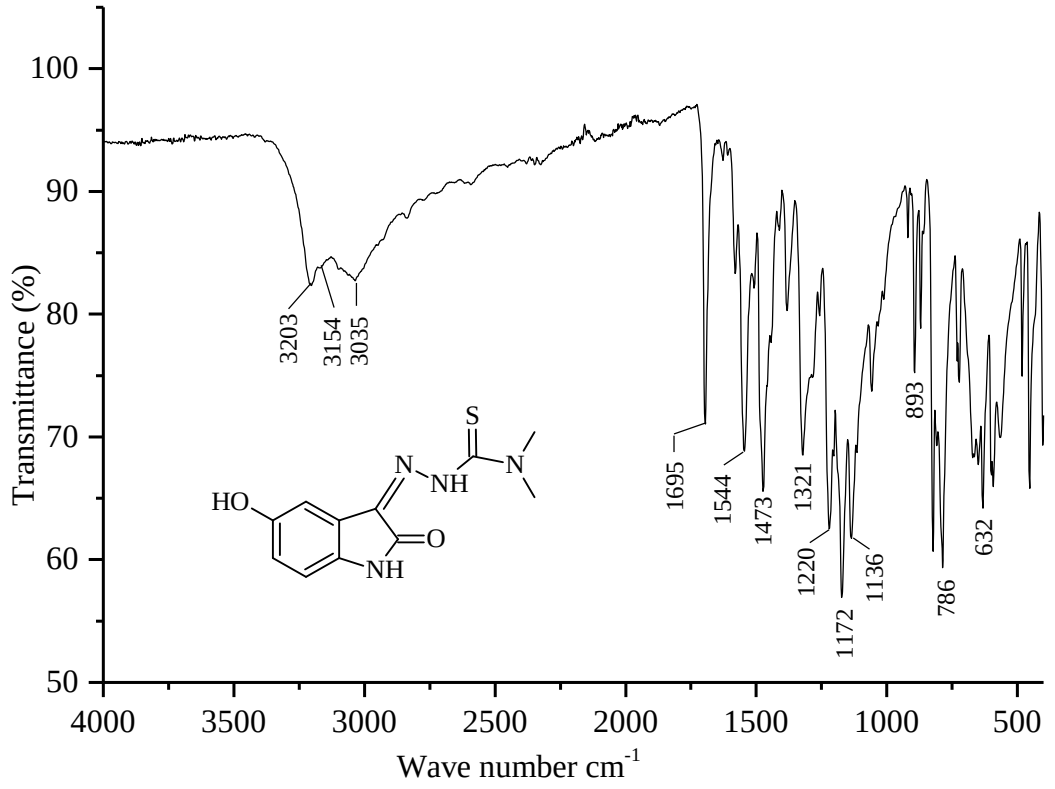

Appendix A14: IR spectrum of compound (***HydIstDm*/14)**

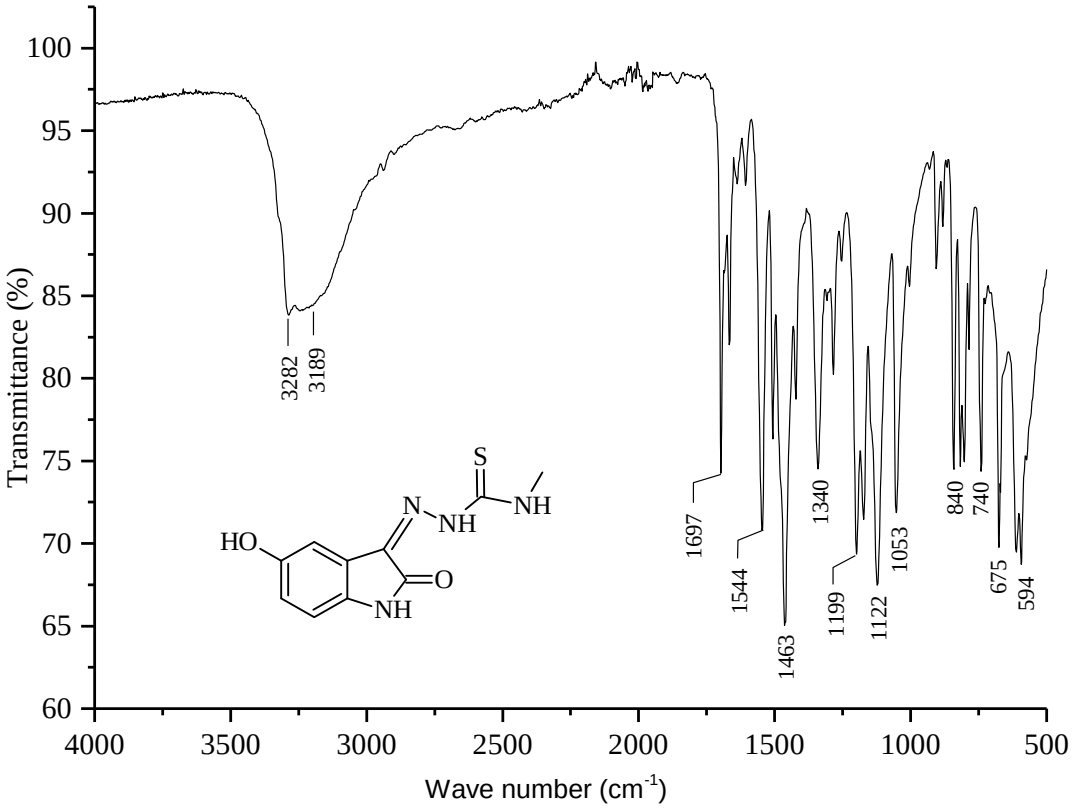

Appendix A15: IR spectrum of compound (***HydIstMet*/15)**

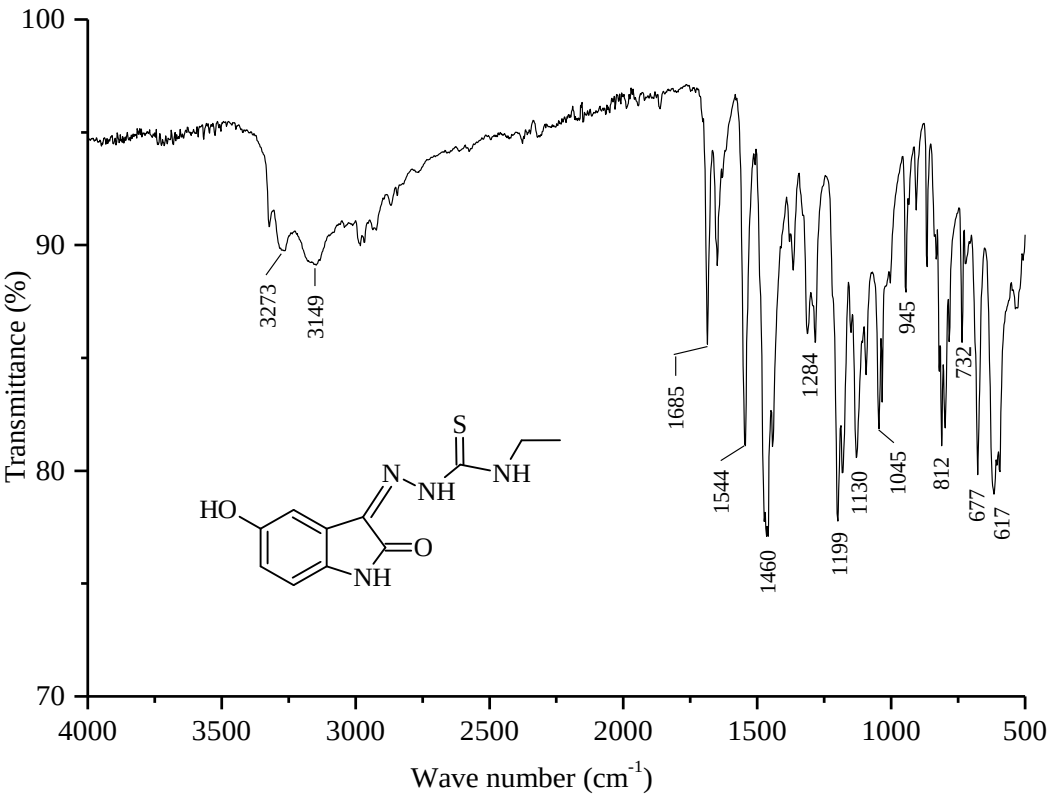

Appendix A16: IR spectrum of compound (***HydIstEth*/16)**

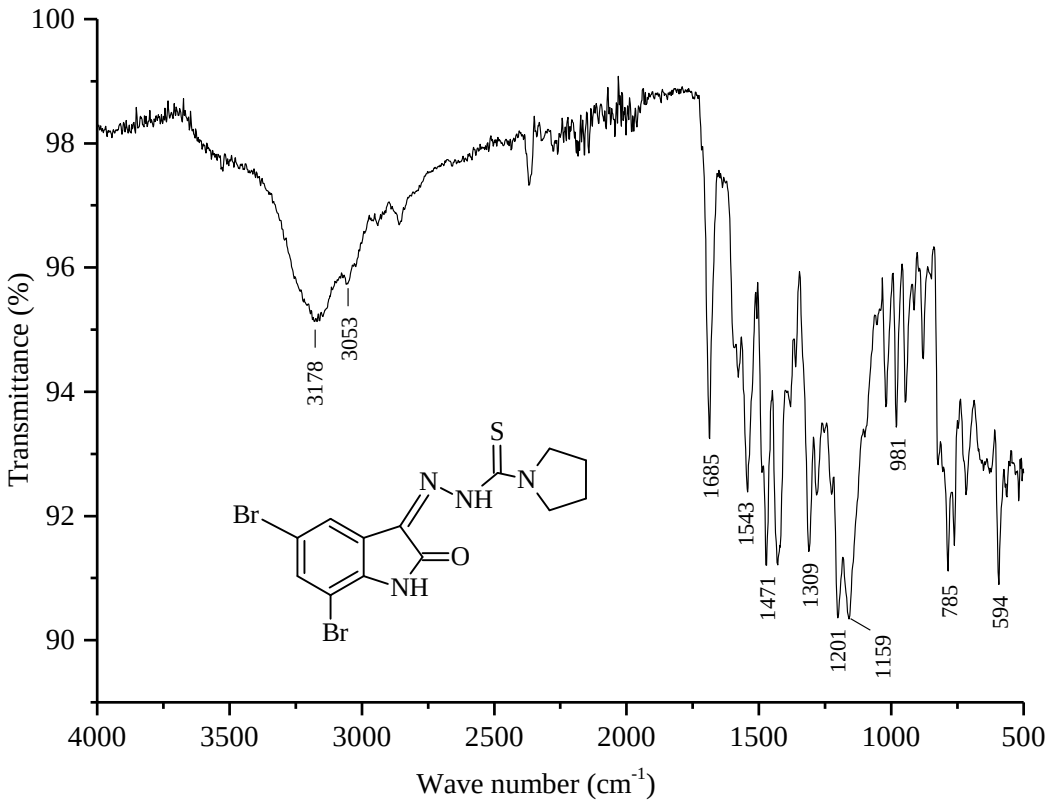

Appendix A17: IR spectrum of compound (***DiBrIstPyrl*/17)**

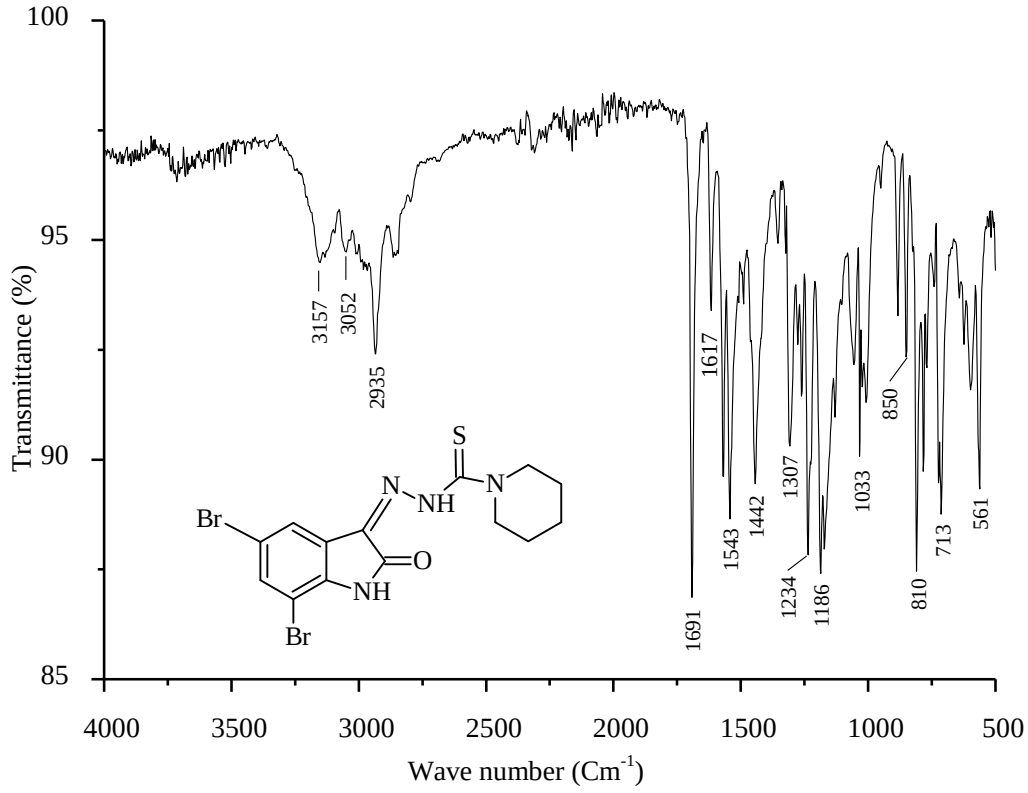

Appendix A18: IR spectrum of compound (***DiBrIstPip*/18)**

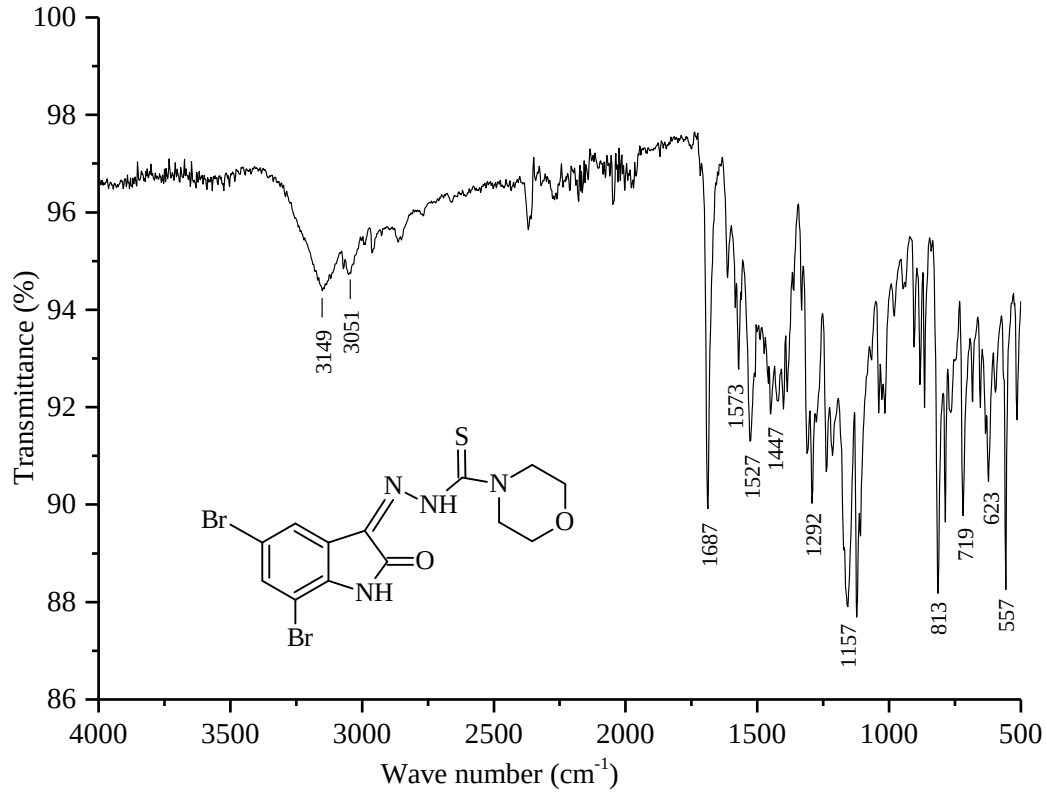

Appendix A19: IR spectrum of compound (***DiBrIstMor*/19)**

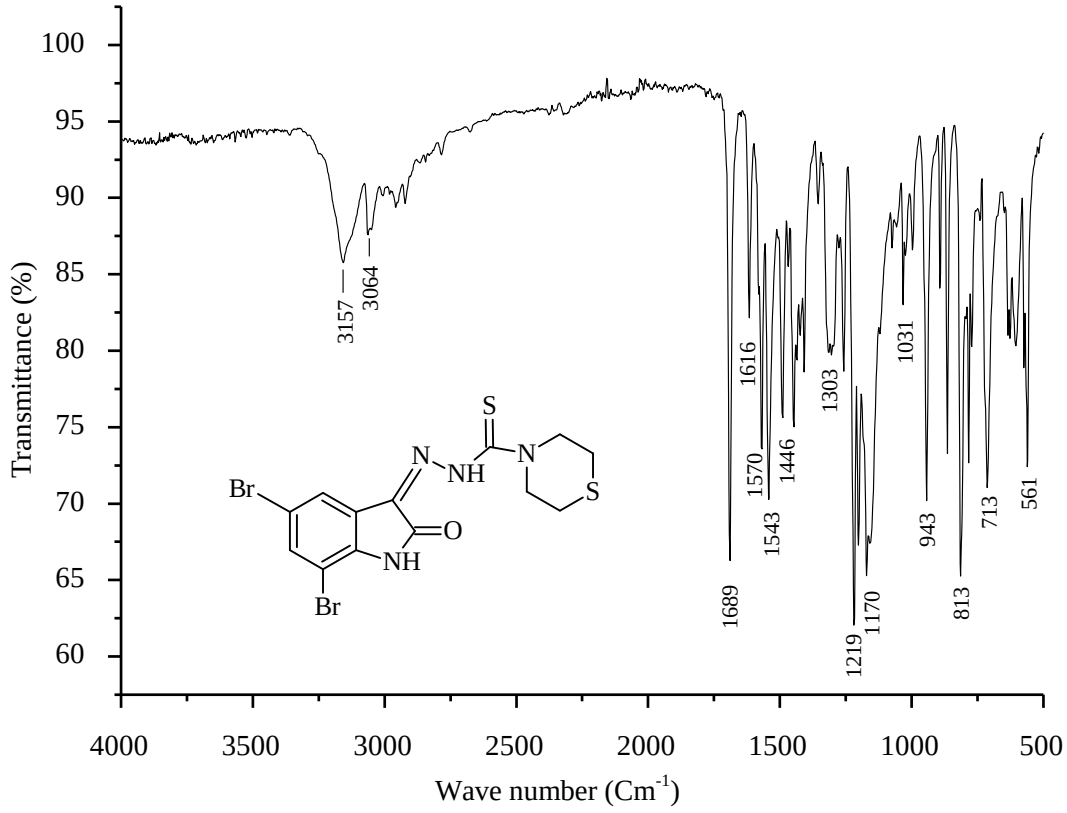

Appendix A20: IR spectrum of compound (***DiBrIstTmor*/20)**

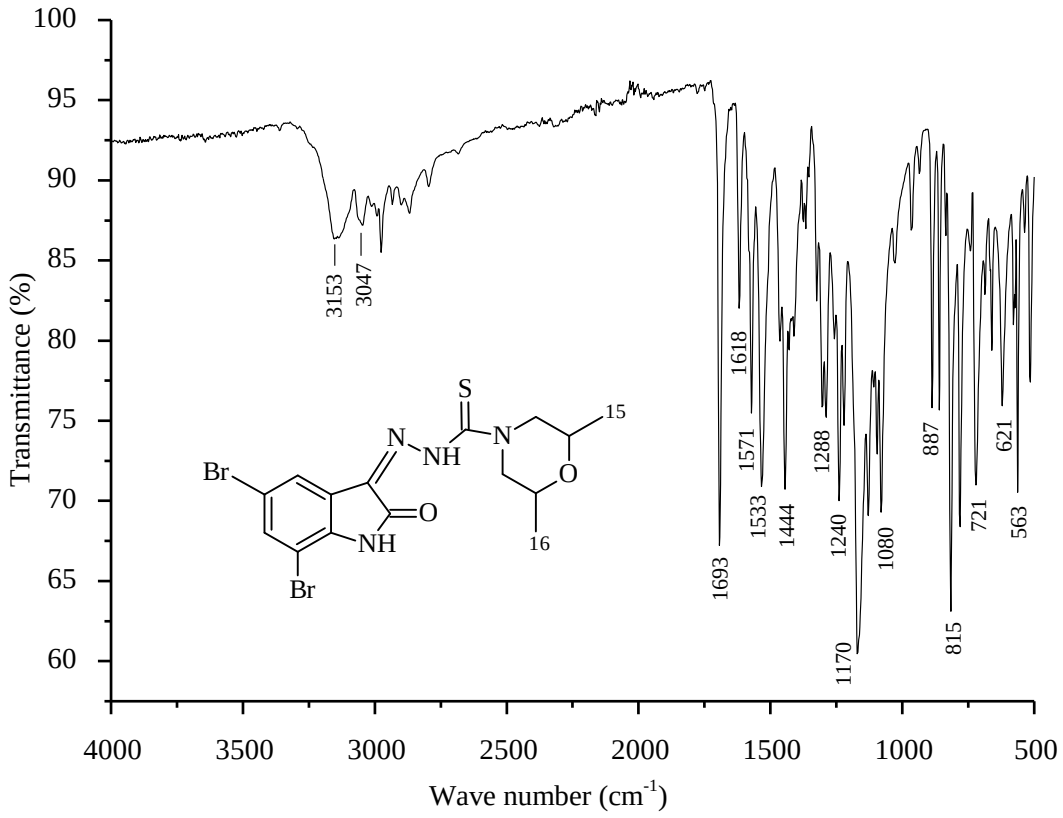

Appendix A21: IR spectrum of compound (***DiBrIstDMor*/21)**

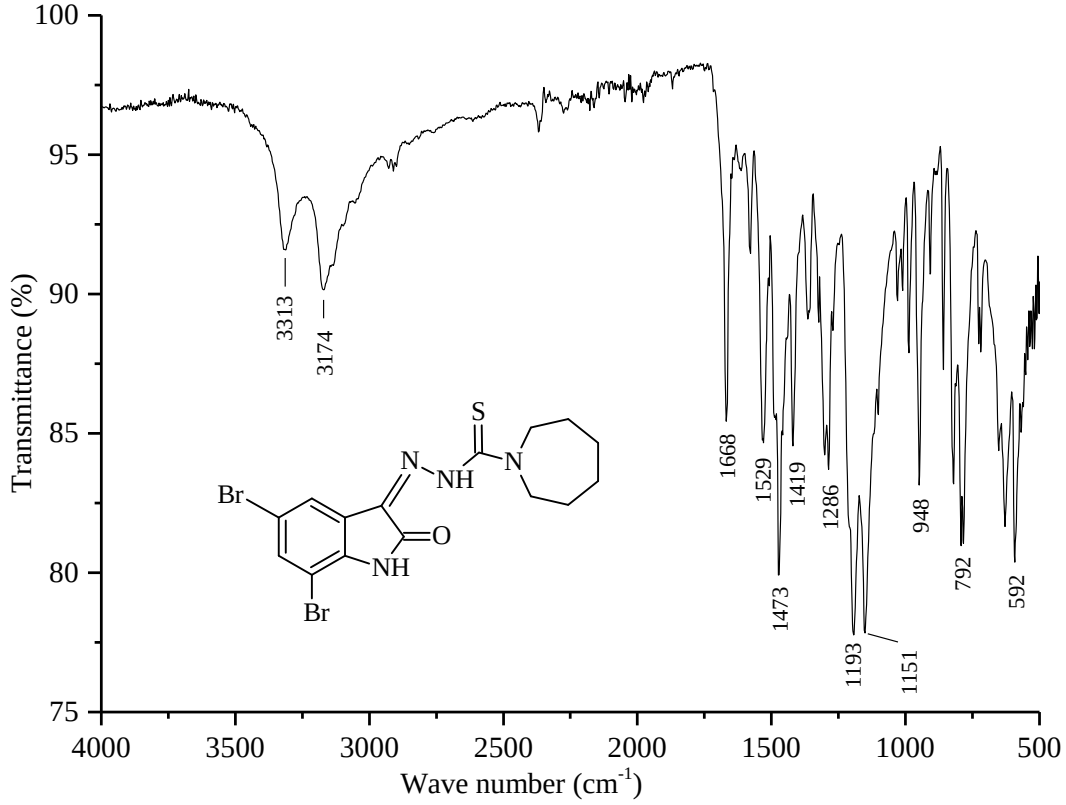

Appendix A22: IR spectrum of compound (***DiBrIstAzep*/22)**

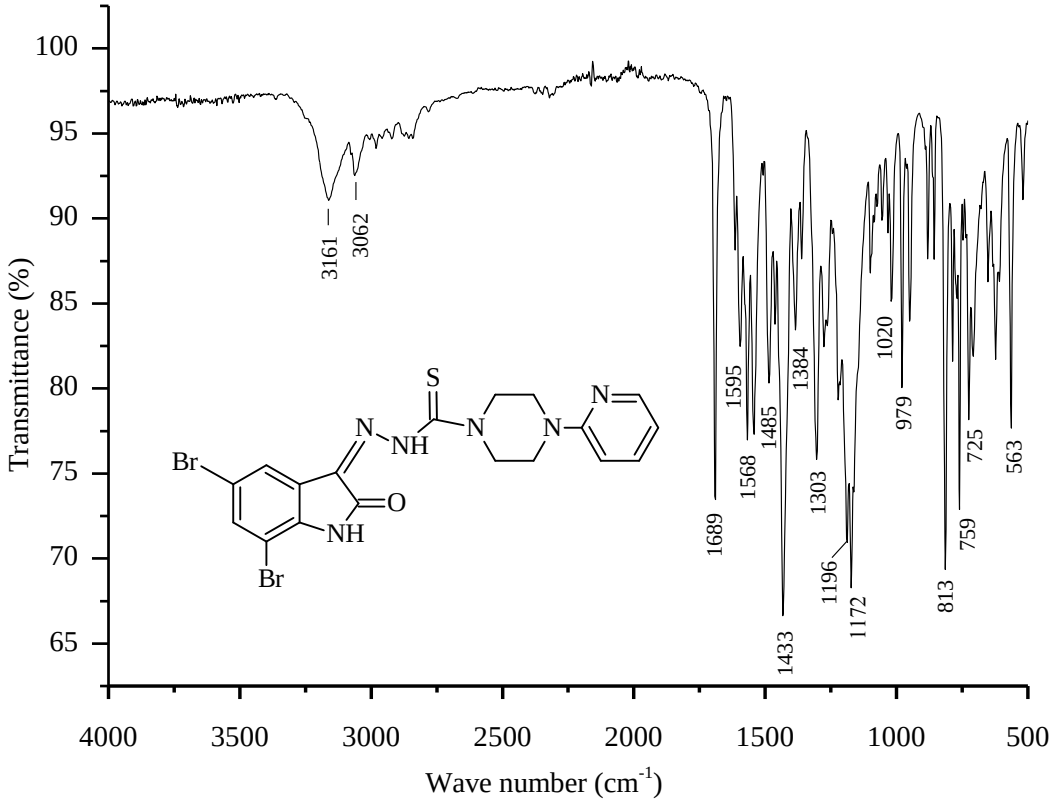

Appendix A23: IR spectrum of compound (***DiBrIstPypz*/23)**

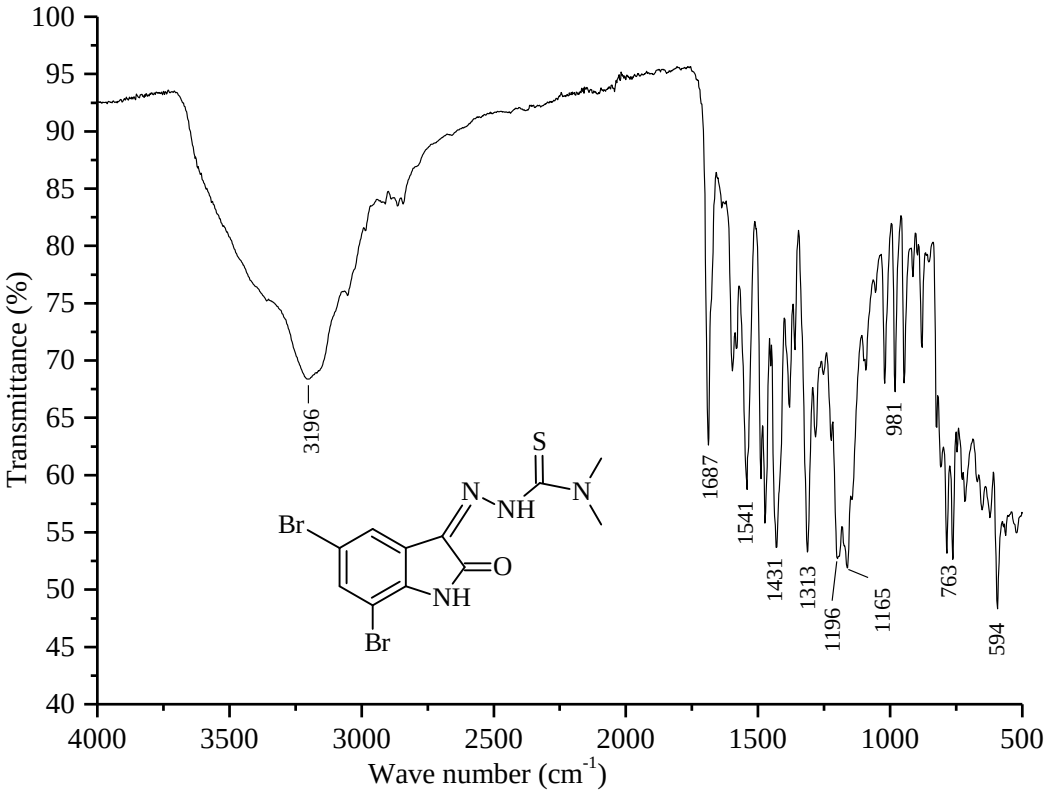

Appendix A24: IR spectrum of compound (***DiBrIstDm*/24)**

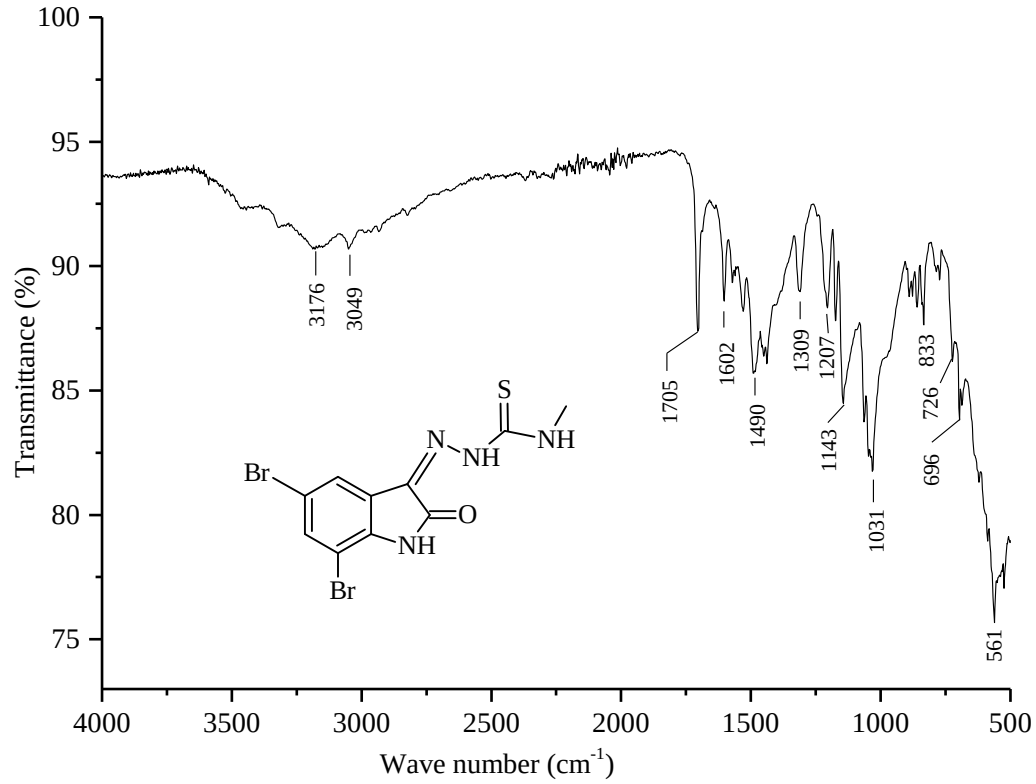

Appendix A25: IR spectrum of compound (***DiBrIstMet*/25)**

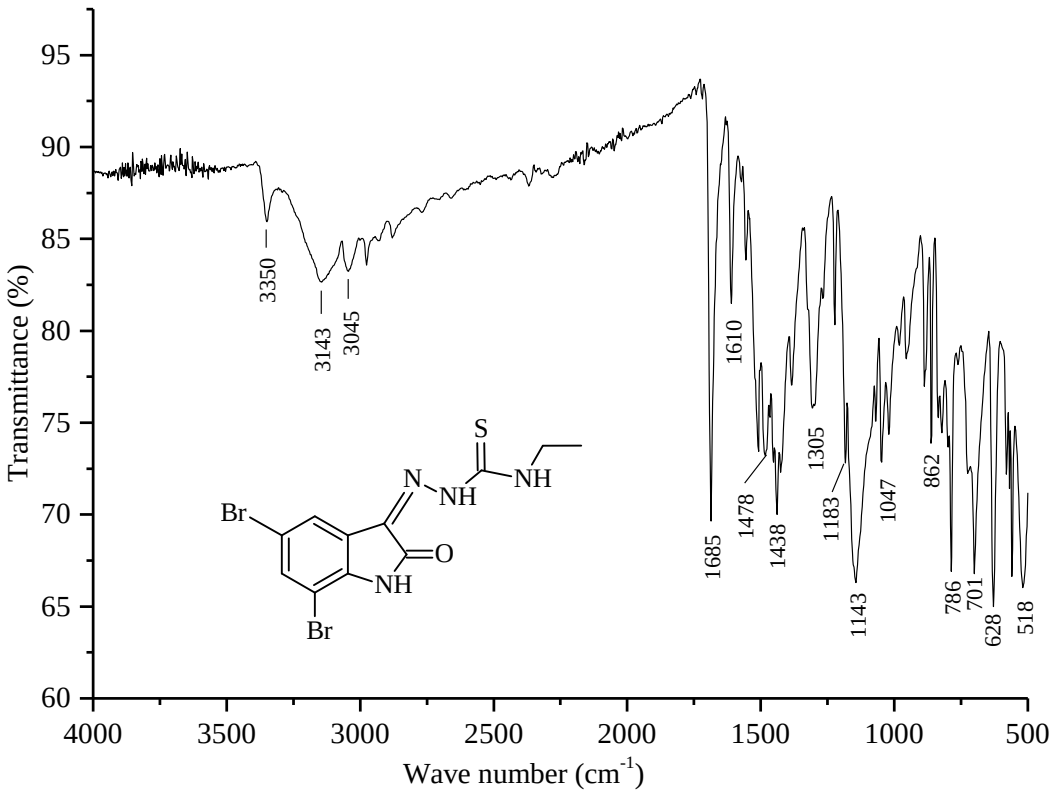

Appendix A26: IR spectrum of compound (***DiBrIstEth*/26)**

Appendix B

NMR spectra of Thosemicarbazones (TSCs) (^{1}H and ^{13}C)

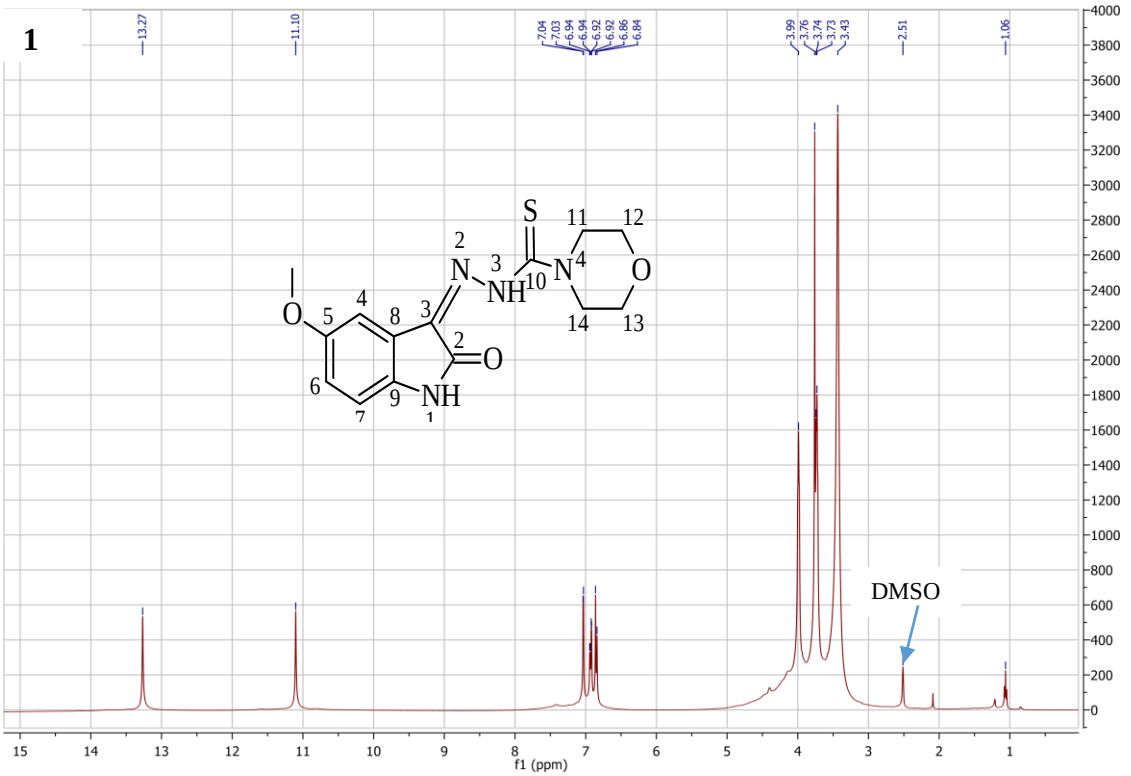

Appendix B1: ^{1}H NMR spectrum (400 MHz, DMSO-*d6*) of compound (***MeOIstMor*/1)**

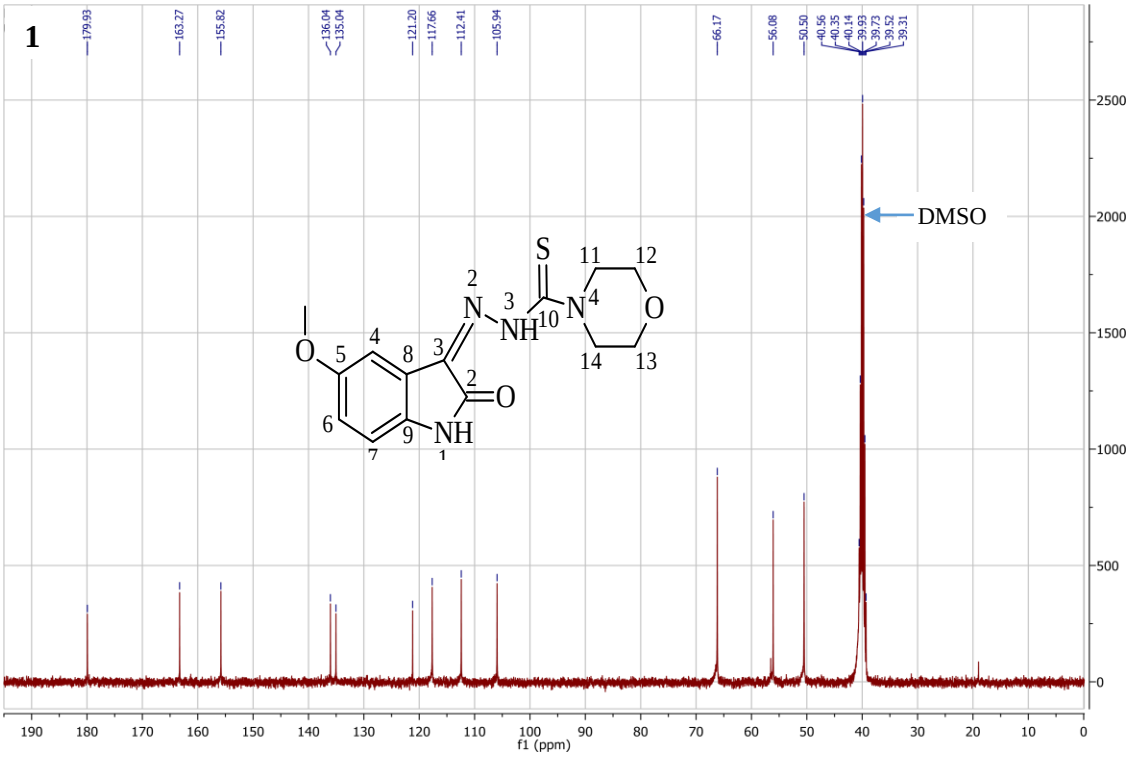

Appendix B1: ^{13}C NMR spectrum (400 MHz, DMSO-*d6*) of compound (***MeOIstMor*/1)**

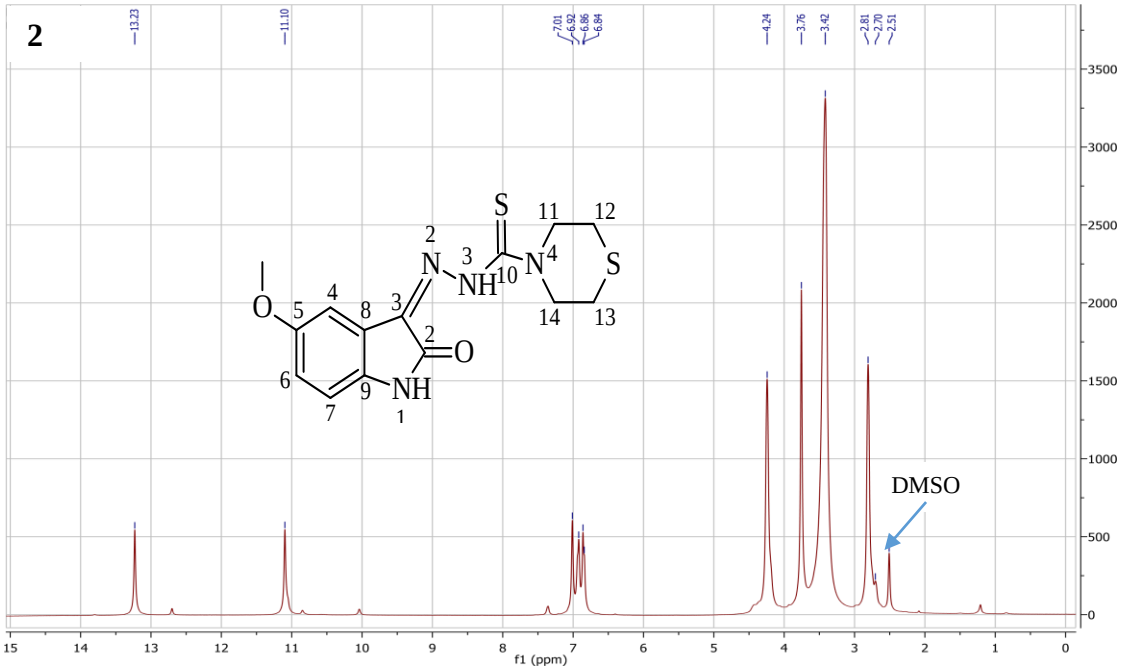

Appendix B2: ^{1}H NMR spectrum (400 MHz, DMSO-*d6*) of compound (***MeOIstTmor*/2**)

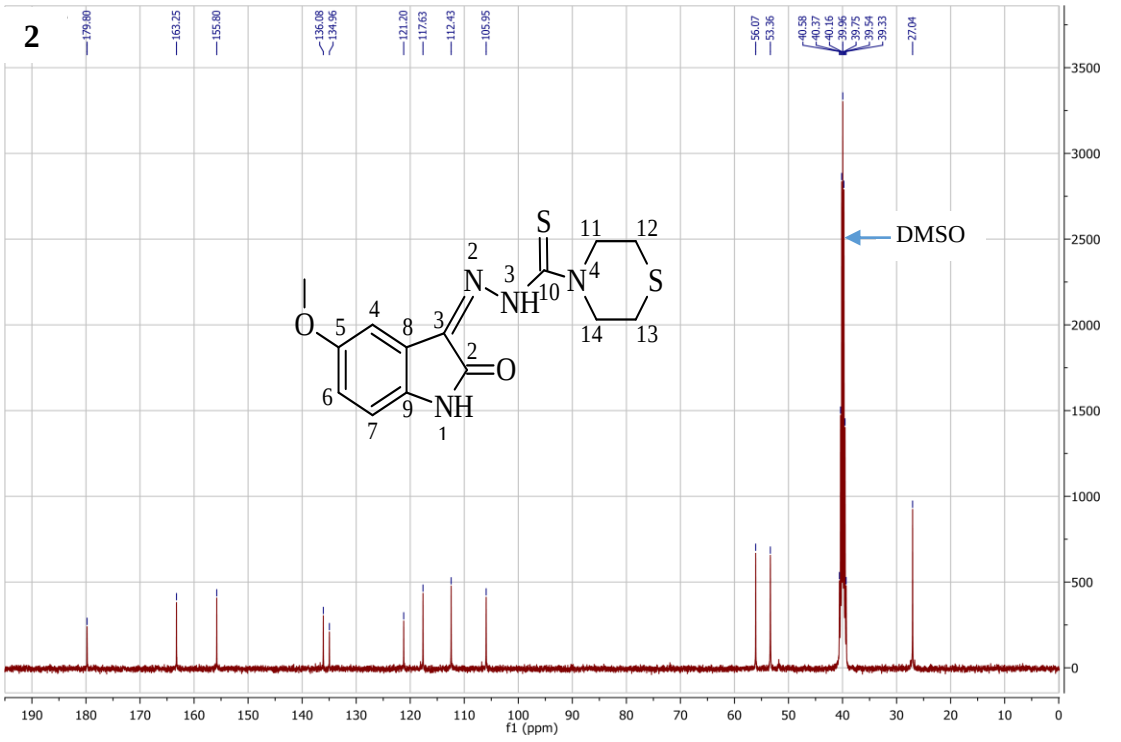

Appendix B2: ^{13}C NMR spectrum (400 MHz, DMSO-*d6*) of compound (***MeOIstTmor*/2**)

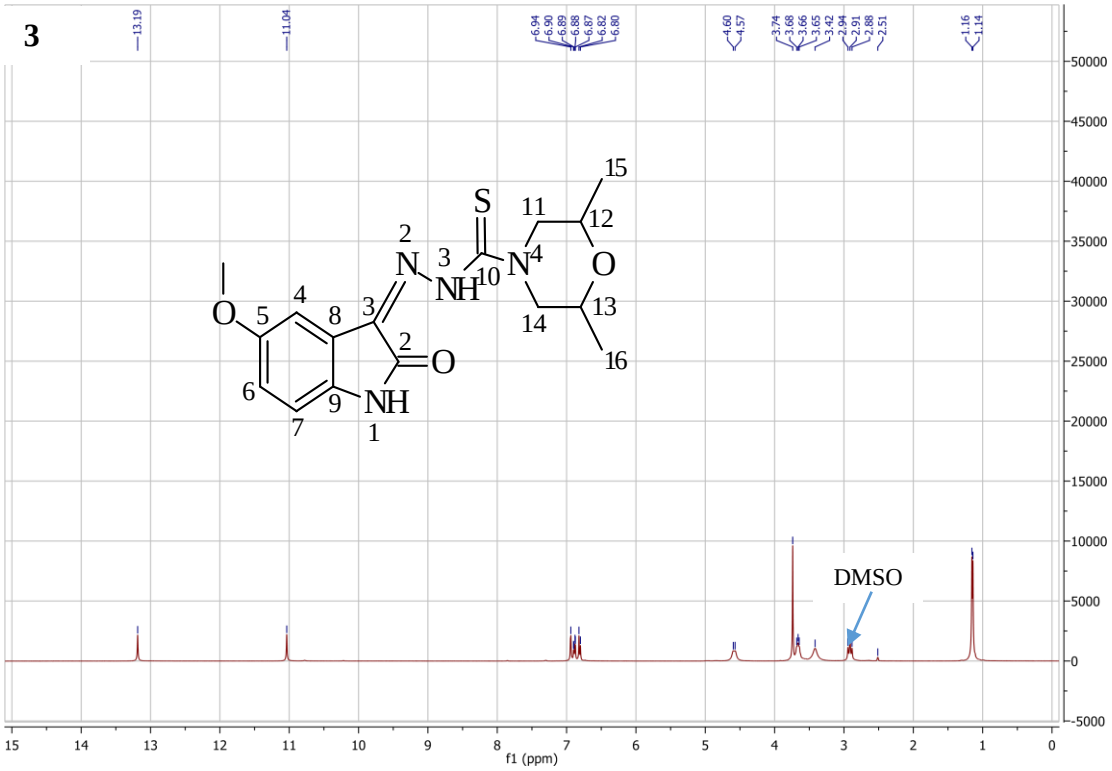

Appendix B3: ^{1}H NMR spectrum (400 MHz, DMSO-*d6*) of compound (***MeOIstDmMor*/3)**

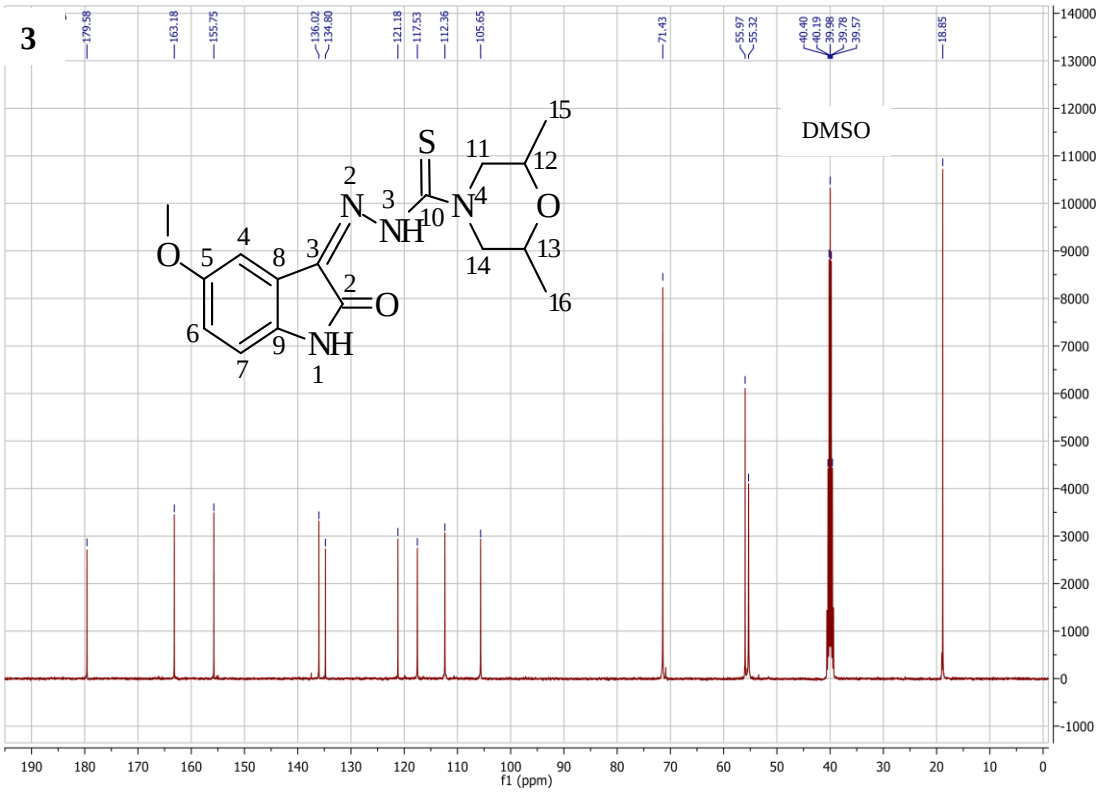

Appendix B3: ^{13}C NMR spectrum (400 MHz, DMSO-*d6*) of compound (***MeOIstDmMor*/3)**

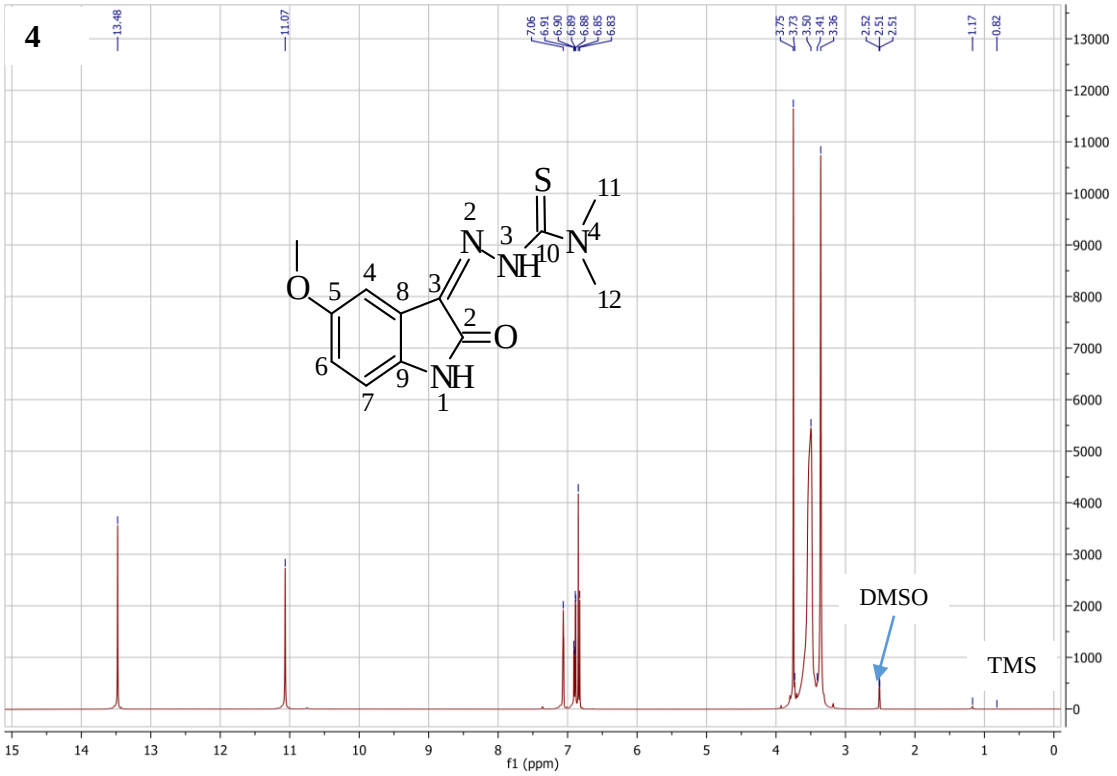

Appendix B4: ^{1}H NMR spectrum (400 MHz, DMSO-*d6*) of compound (***MeOIstDm*/4**)

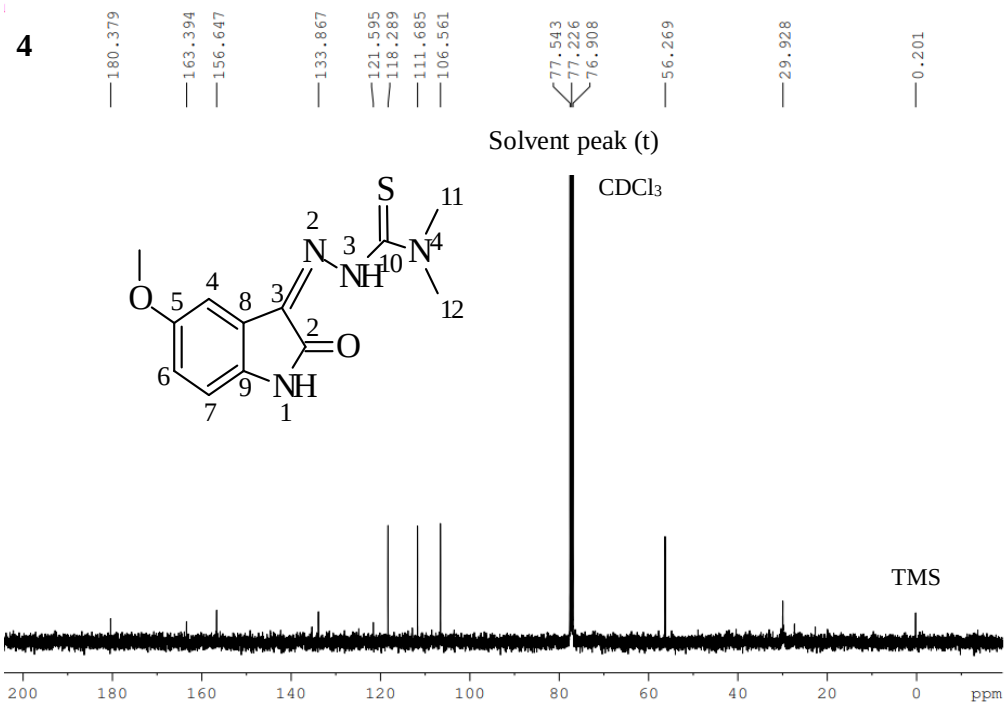

Appendix B4: ^{13}C NMR spectrum (400 MHz, $CDCl_3$) of compound (***MeOIstDm*/4**)

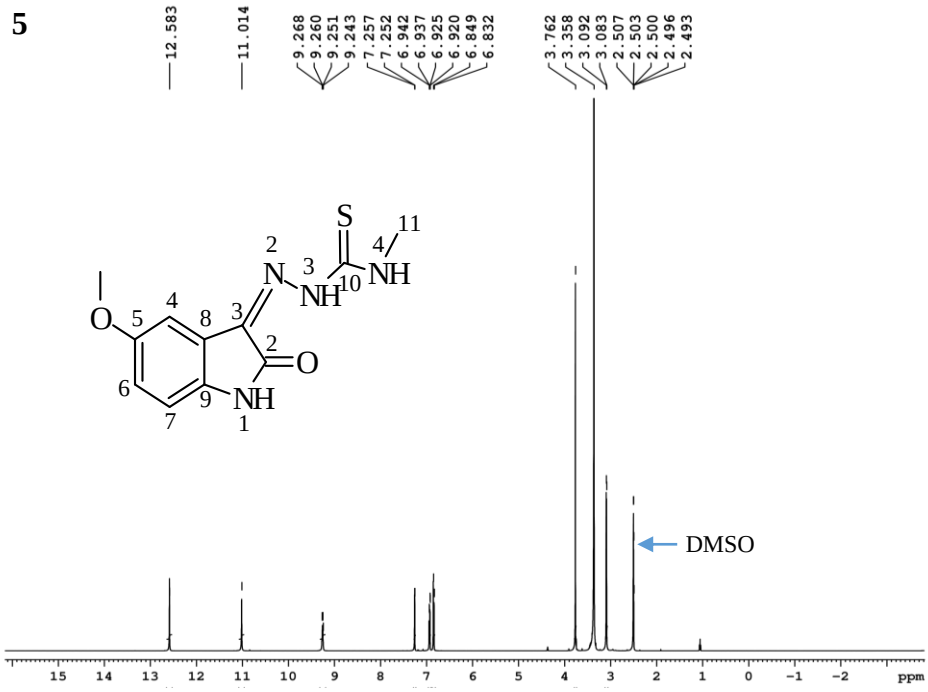

Appendix B5: ^{1}H NMR spectrum (400 MHz, DMSO-*d6*) of compound (***MeOIstMet*/5)**

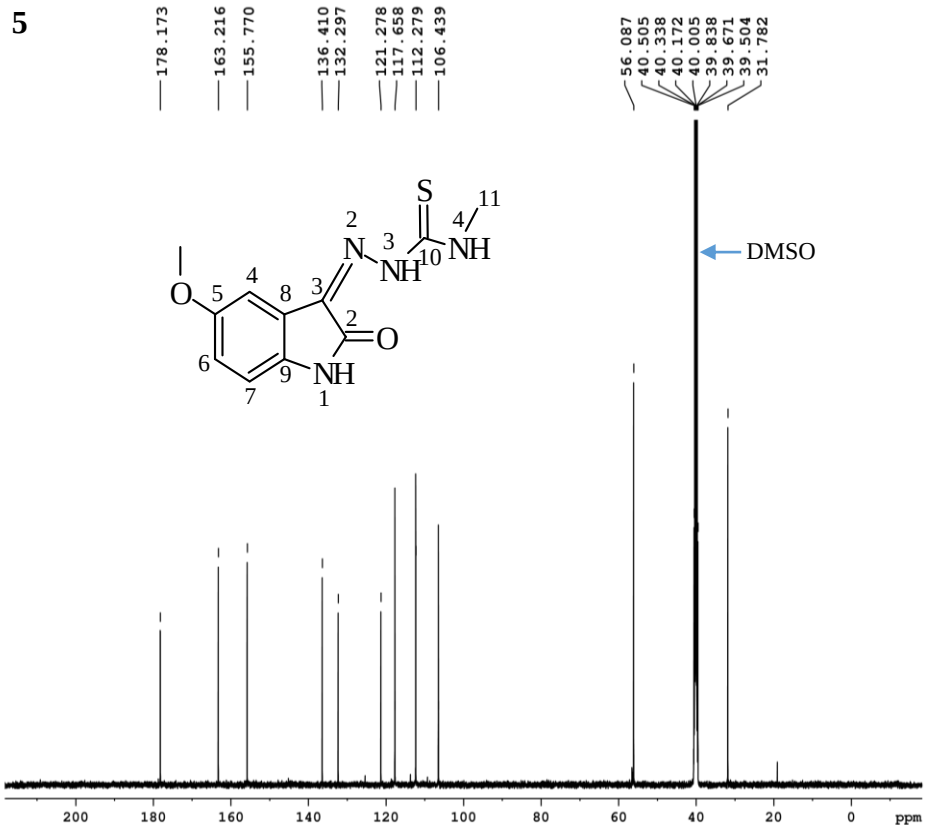

Appendix B5: ^{13}C NMR spectrum (400 MHz, DMSO-*d6*) of compound (***MeOIstMet*/5)**

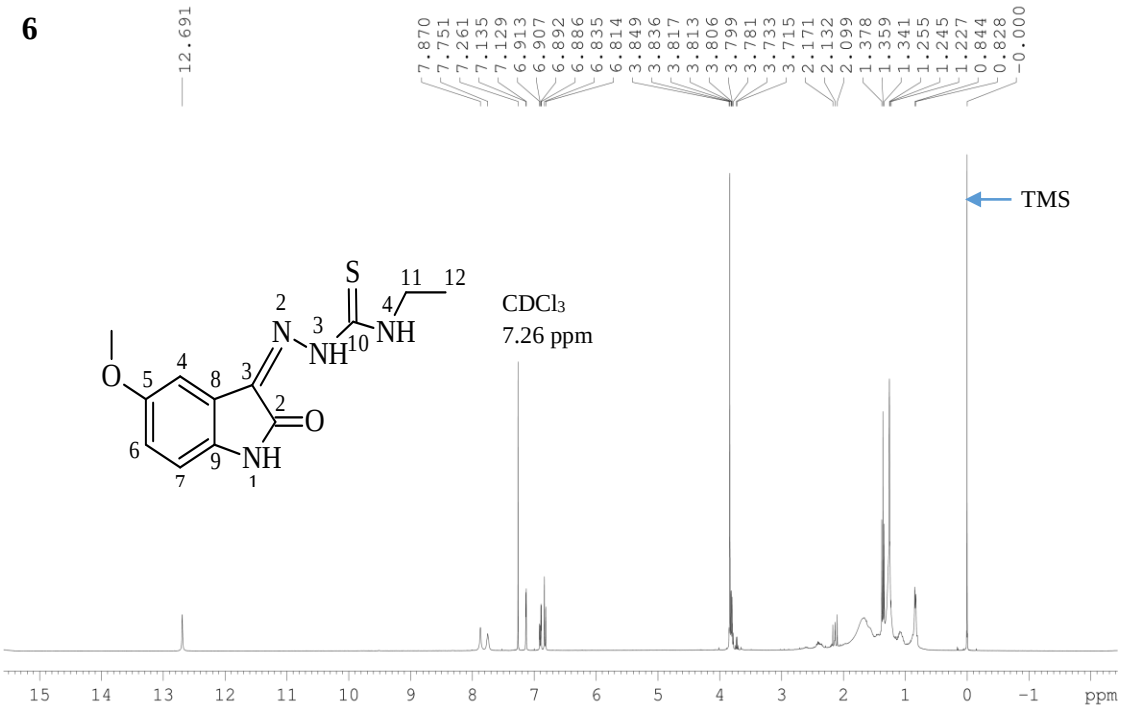

Appendix B6: ^{1}H NMR spectrum (400 MHz, $CDCl_3$) of compound (***MeOIstEth*/6**)

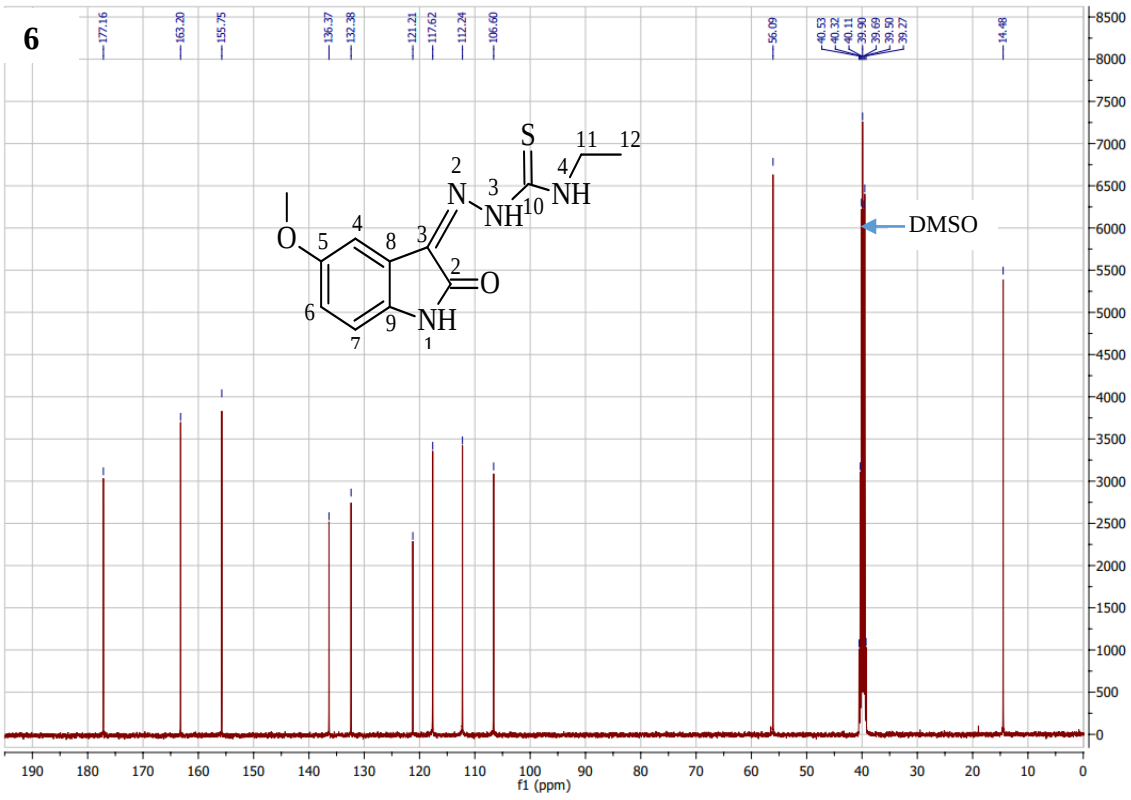

Appendix B6: ^{13}C NMR spectrum (400 MHz, DMSO-*d6*) of compound (***MeOIstEth*/6**)

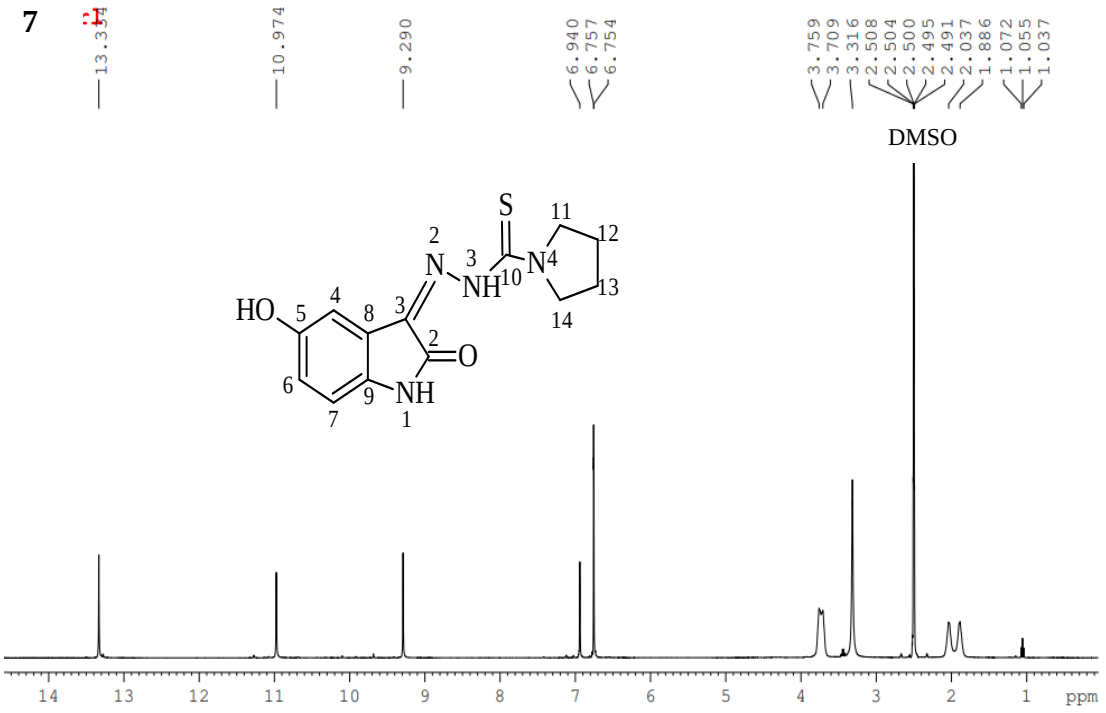

Appendix B7: ^{1}H NMR spectrum (400 MHz, DMSO-*d6*) of compound (***HydIstPyrl*/7**)

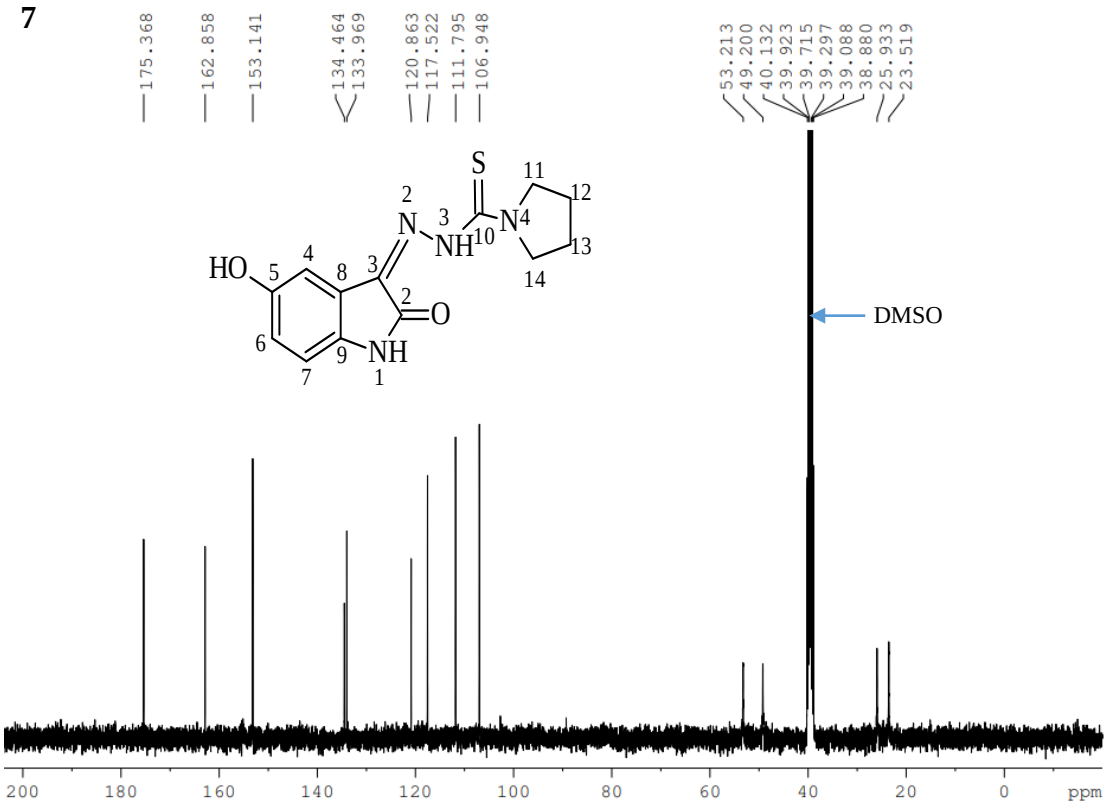

Appendix B7: ^{13}C NMR spectrum (400 MHz, DMSO-*d6*) of compound (***HydIstPyrl*/7**)

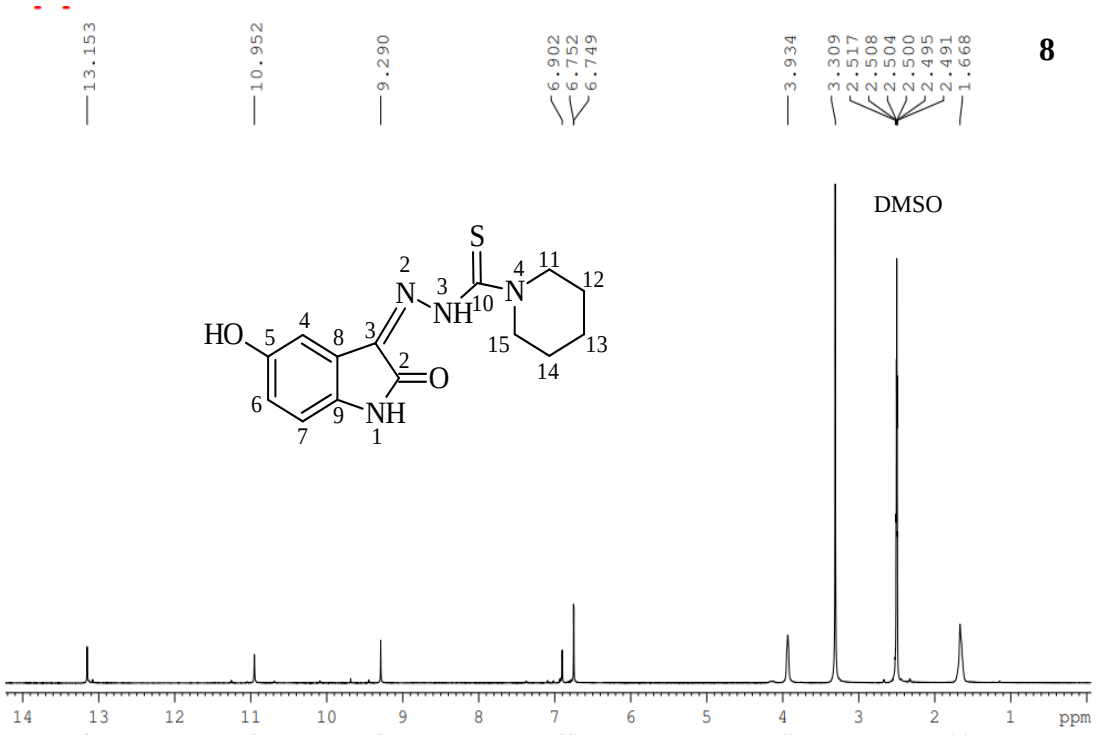

Appendix B8: ^{1}H NMR spectrum (400 MHz, DMSO-*d6*) of compound (***HydIstPip*/8)**

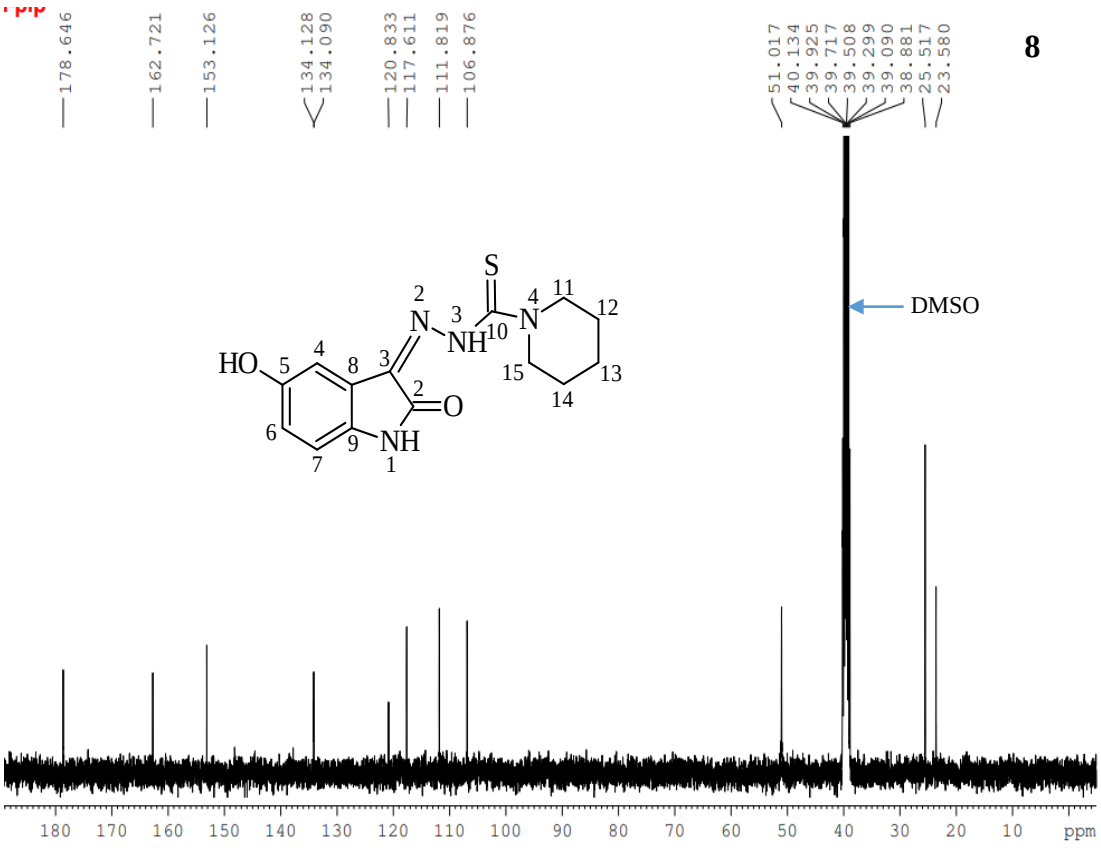

Appendix B8: ^{13}C NMR spectrum (400 MHz, DMSO-*d6*) of compound (***HydIstPip*/8)**

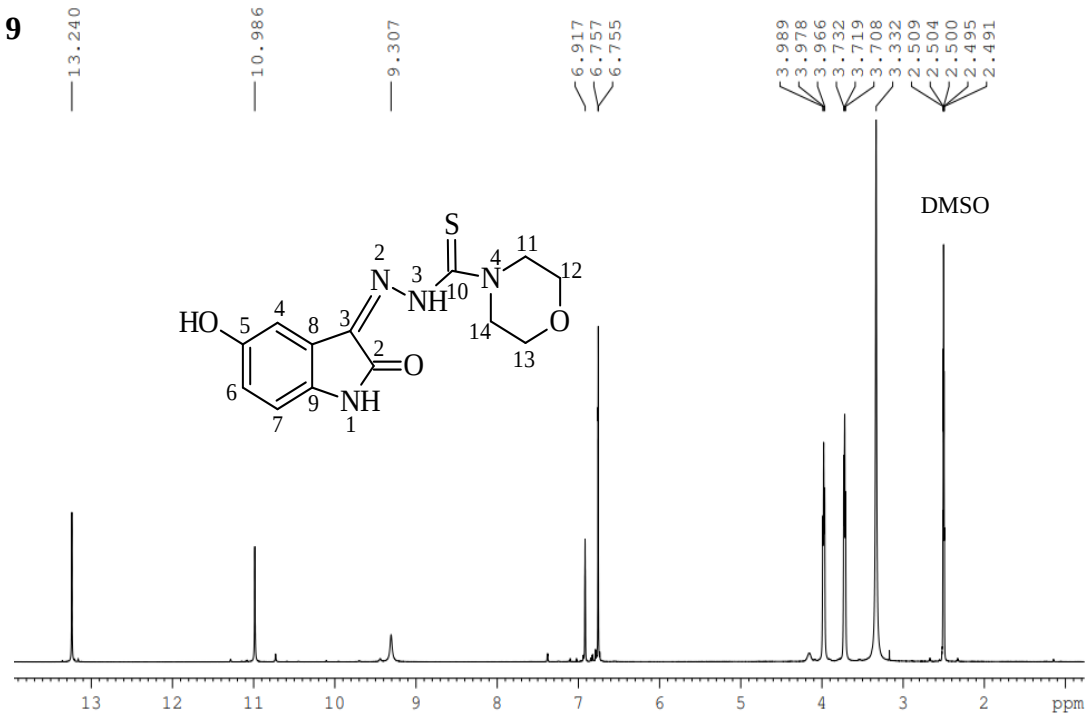

Appendix B9:[1]H NMR spectrum (400 MHz, DMSO-*d6*) of compound (***HydIstMor*/9**)

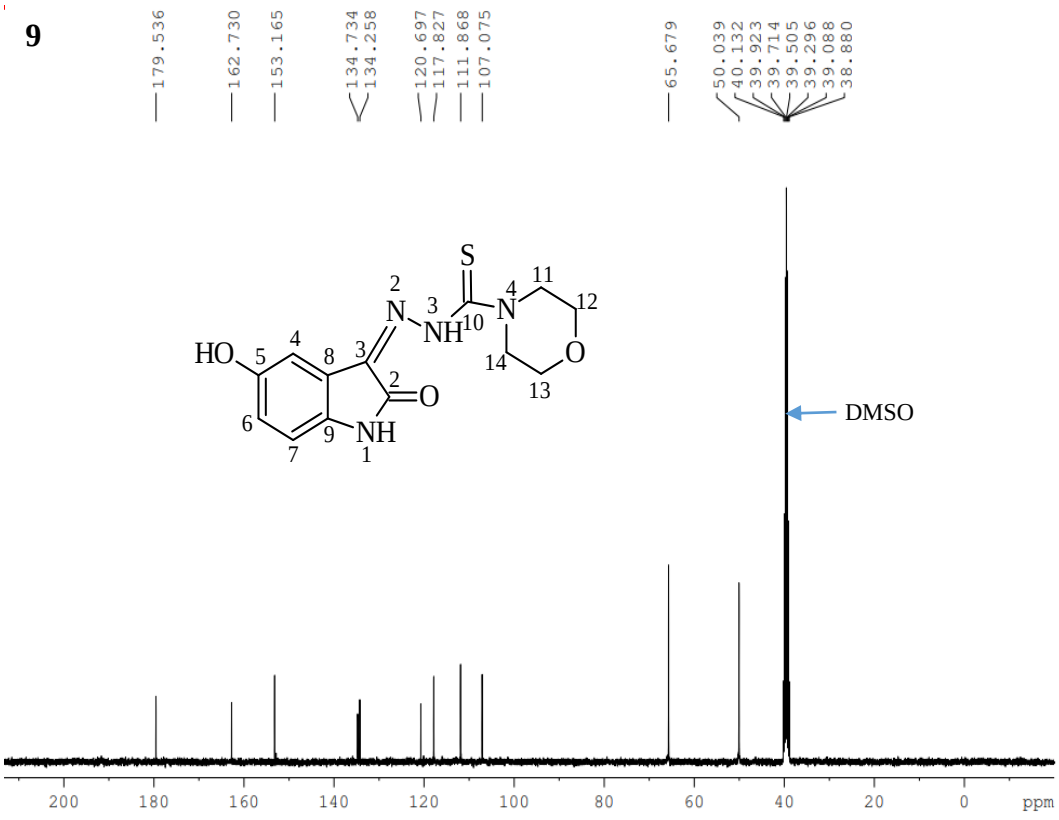

Appendix B9:[13]C NMR spectrum (400 MHz, DMSO-*d6*) of compound (***HydIstMor*/9**)

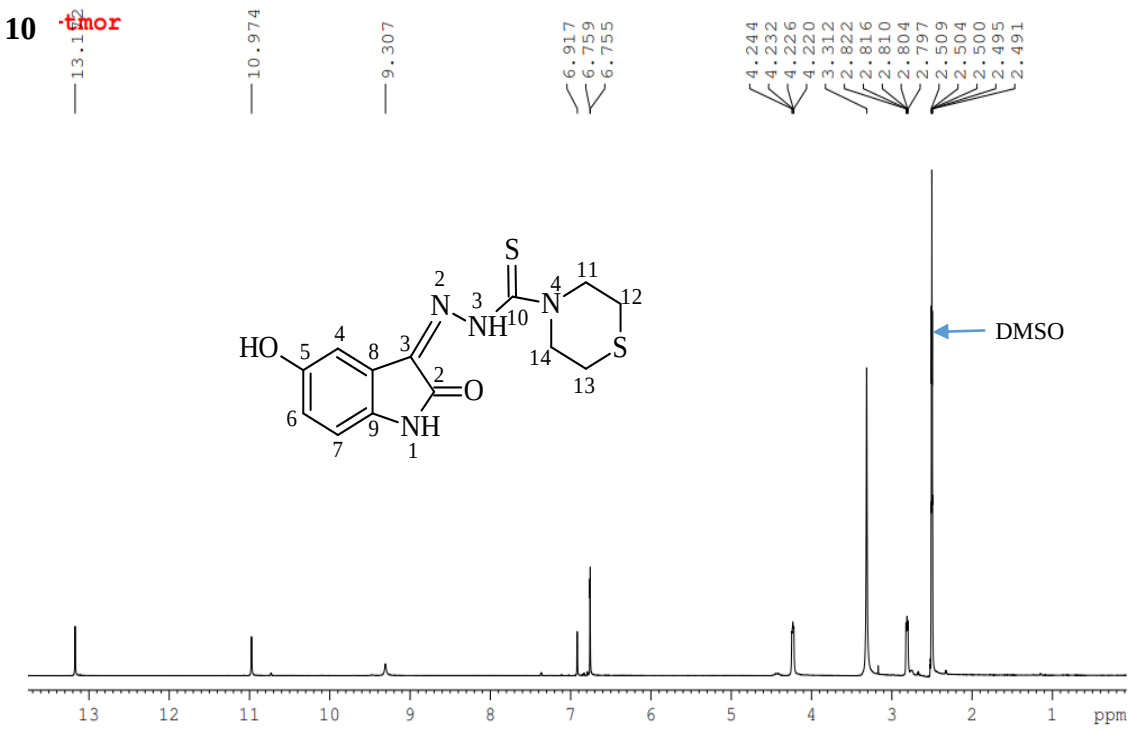

Appendix B10: ^{1}H NMR spectrum (400 MHz, DMSO-*d6*) of compound (***HydIstTmor*/10**)

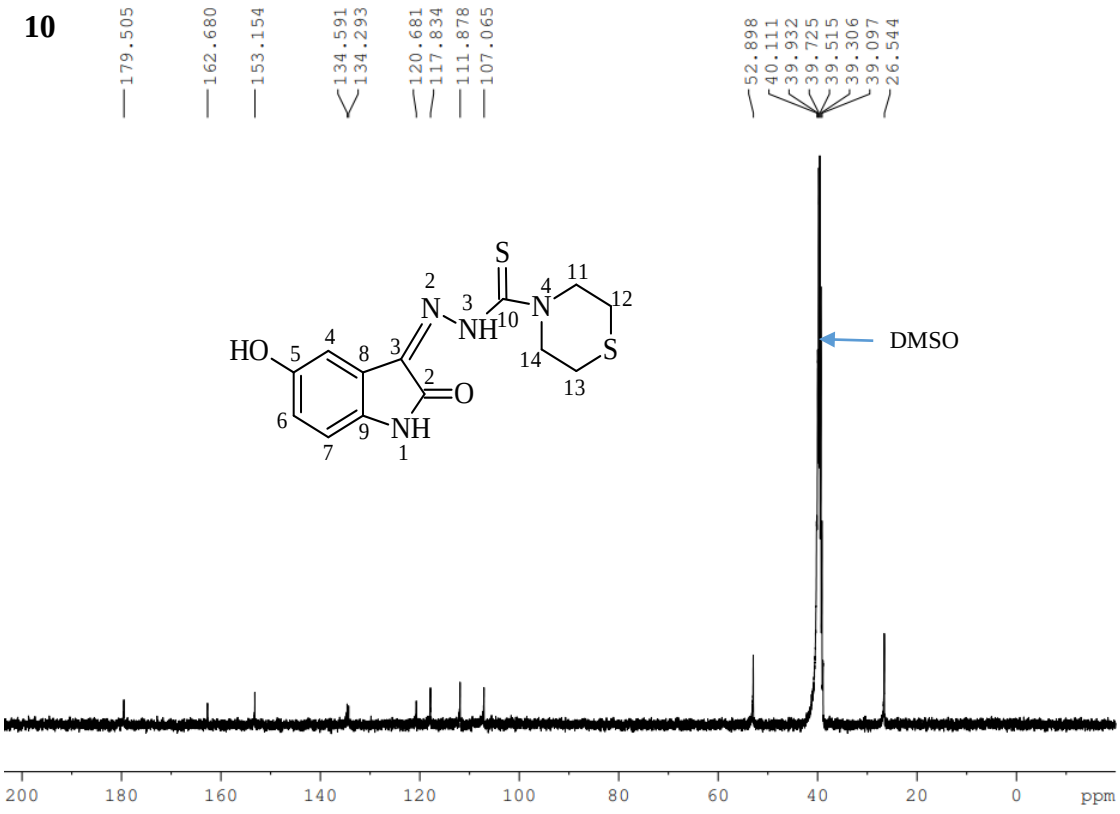

Appendix B10: ^{13}C NMR spectrum (400 MHz, DMSO-*d6*) of compound (***HydIstTmor*/10**)

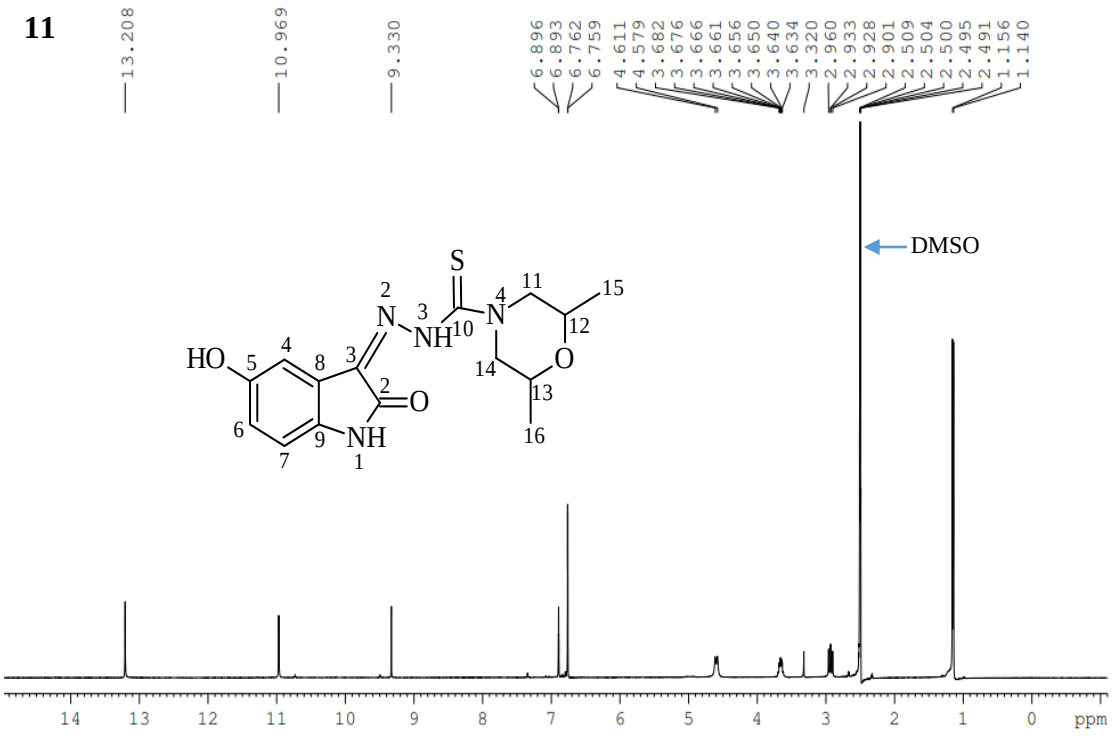

Appendix B11: ^{1}H NMR spectrum (400 MHz, DMSO-*d6*) of compound (***HydIstDmMor*/11**)

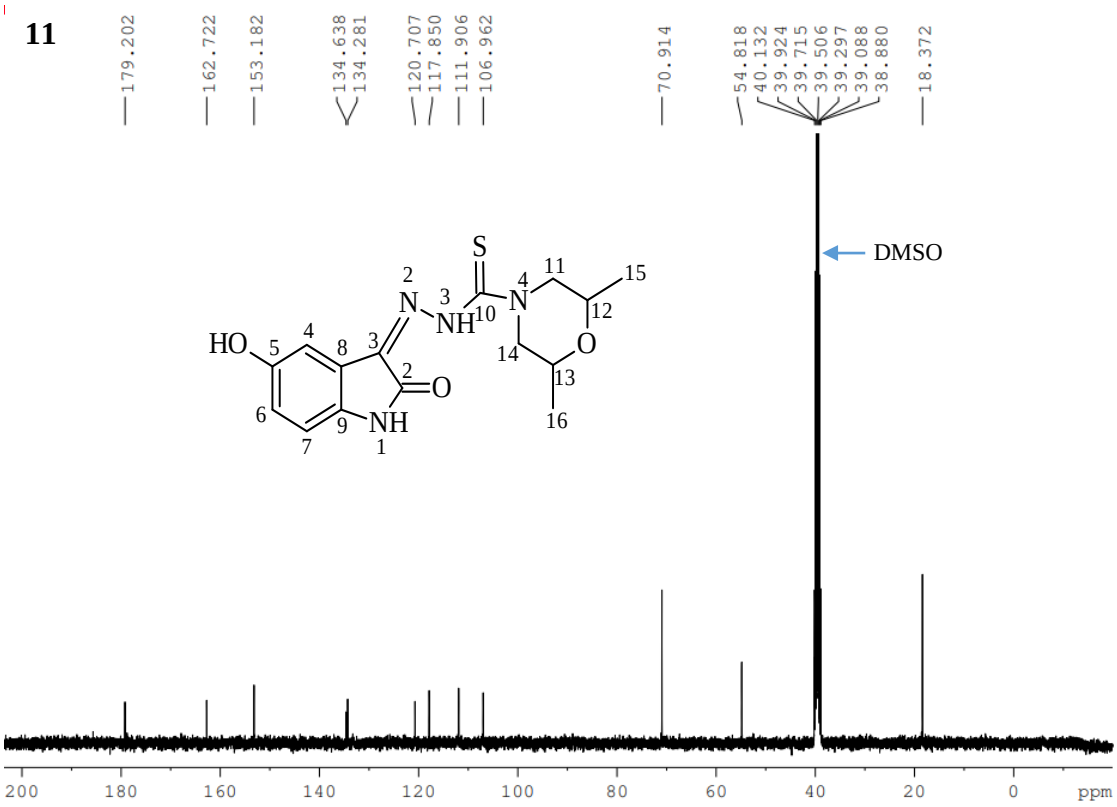

Appendix B11: ^{13}C NMR spectrum (400 MHz, DMSO-*d6*) of compound (***HydIstDmMor*/11**)

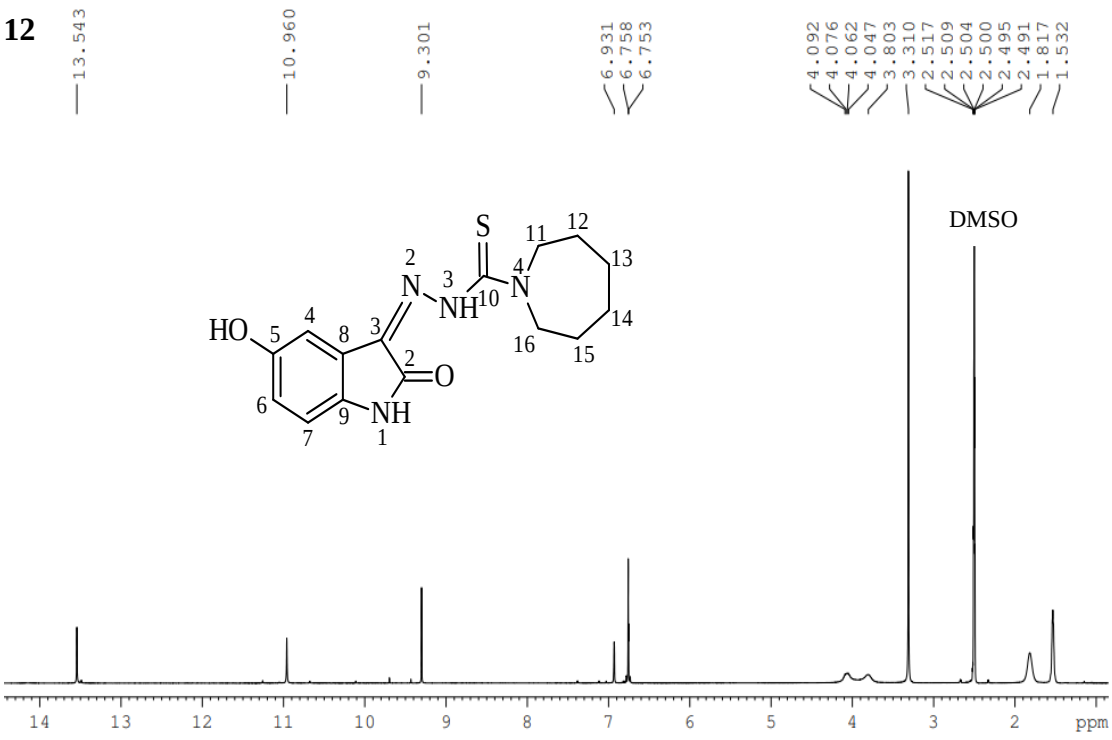

Appendix B12: ^{1}H NMR spectrum (400 MHz, DMSO-*d6*) of compound (***HydIstAzep*/12**)

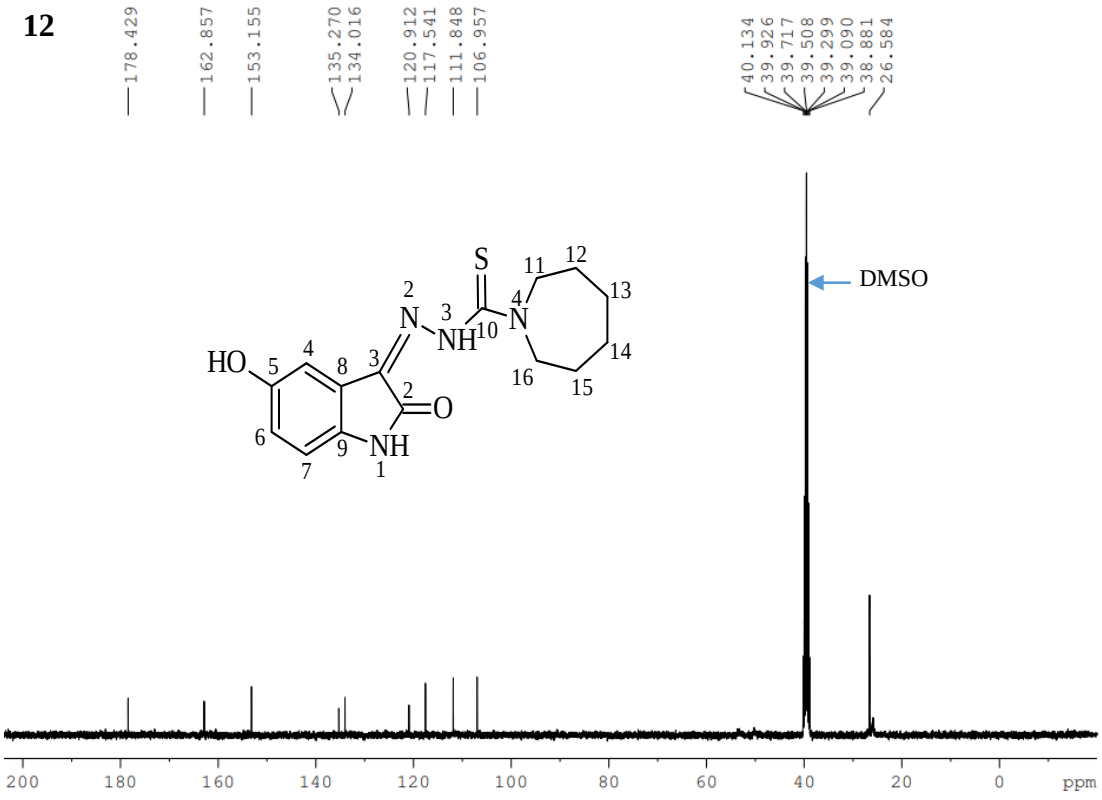

Appendix B12: ^{13}C NMR spectrum (400 MHz, DMSO-*d6*) of compound (***HydIstAzep*/12**)

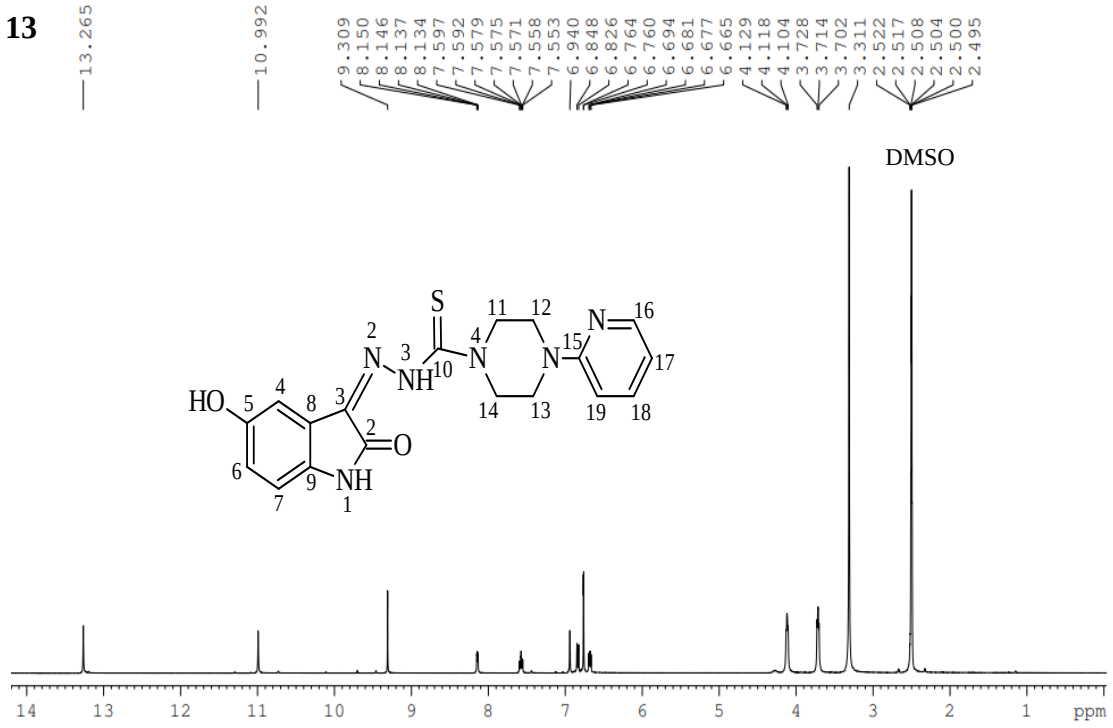

Appendix B13: ^{1}H NMR spectrum (400 MHz, DMSO-*d6*) of compound (***HydIstPypz*/13)**

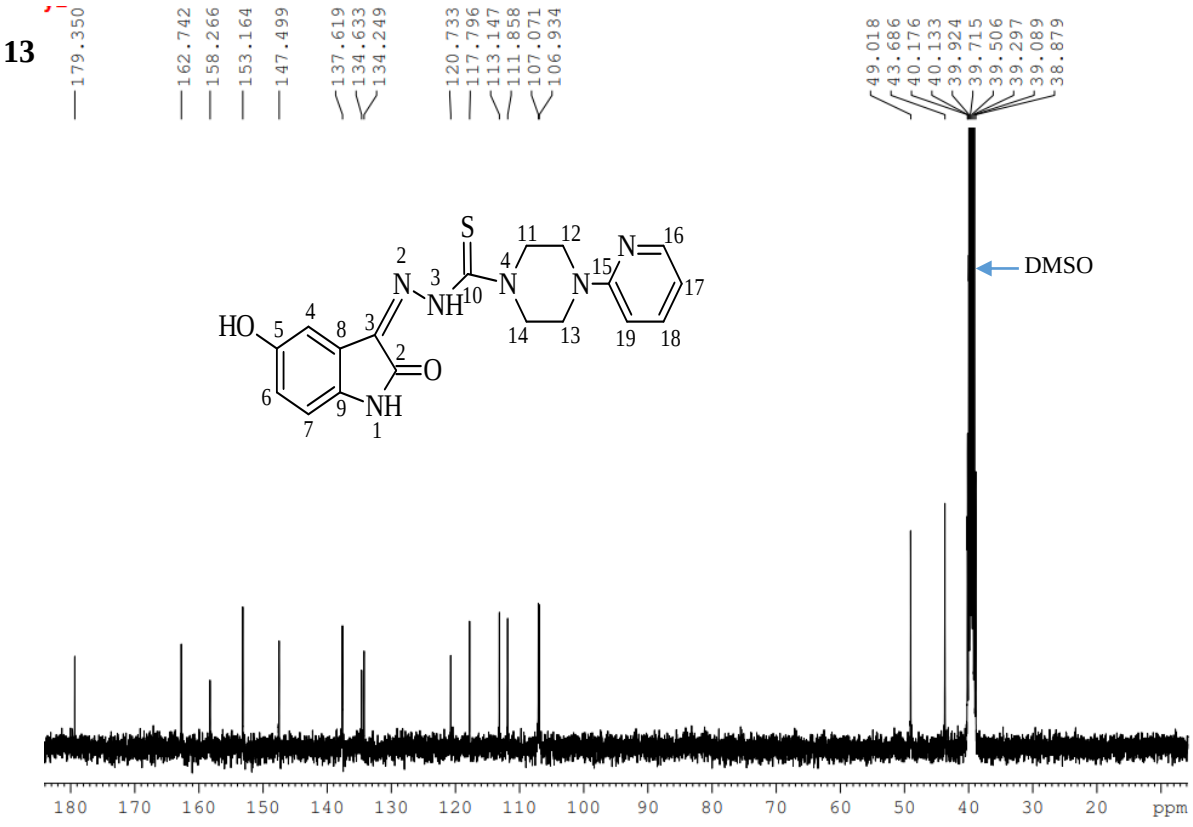

Appendix B13: ^{13}C NMR spectrum (400 MHz, DMSO-*d6*) of compound (***HydIstPypz*/13)**

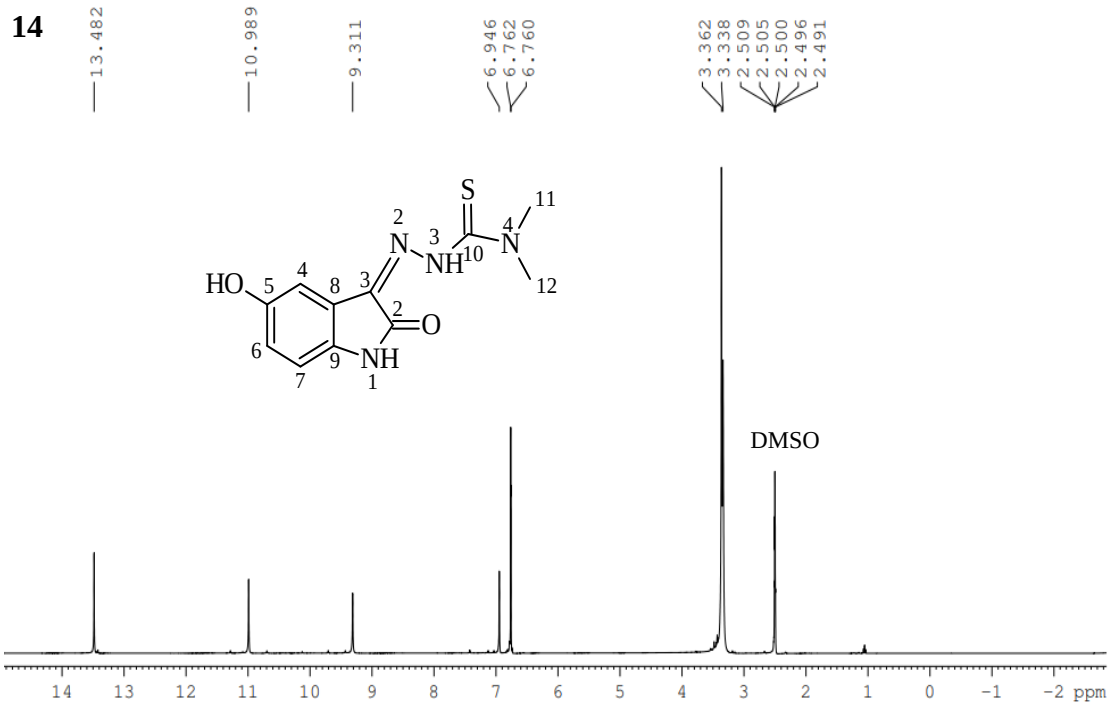

Appendix B14: ^{1}H NMR spectrum (400 MHz, DMSO-*d6*) of compound (***HydIstDm*/14**)

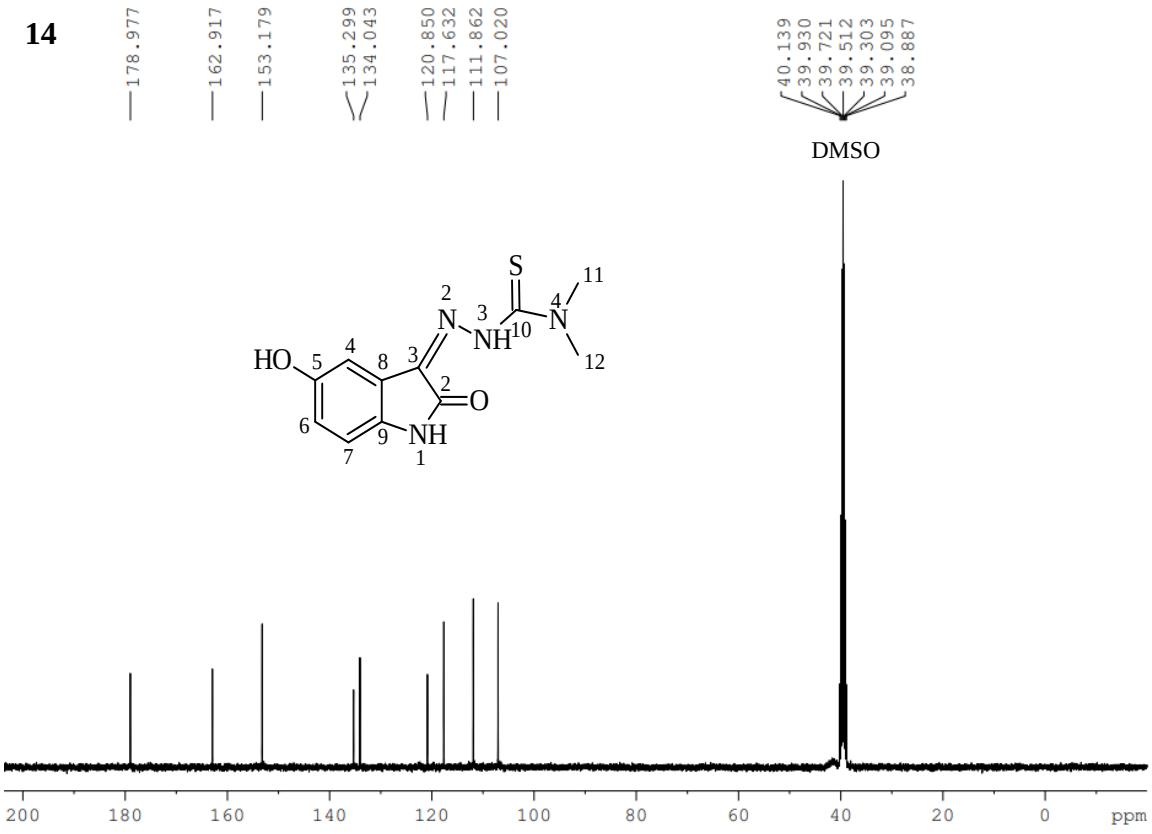

Appendix B14: ^{13}C NMR spectrum (400 MHz, DMSO-*d6*) of compound (***HydIstDm*/14**)

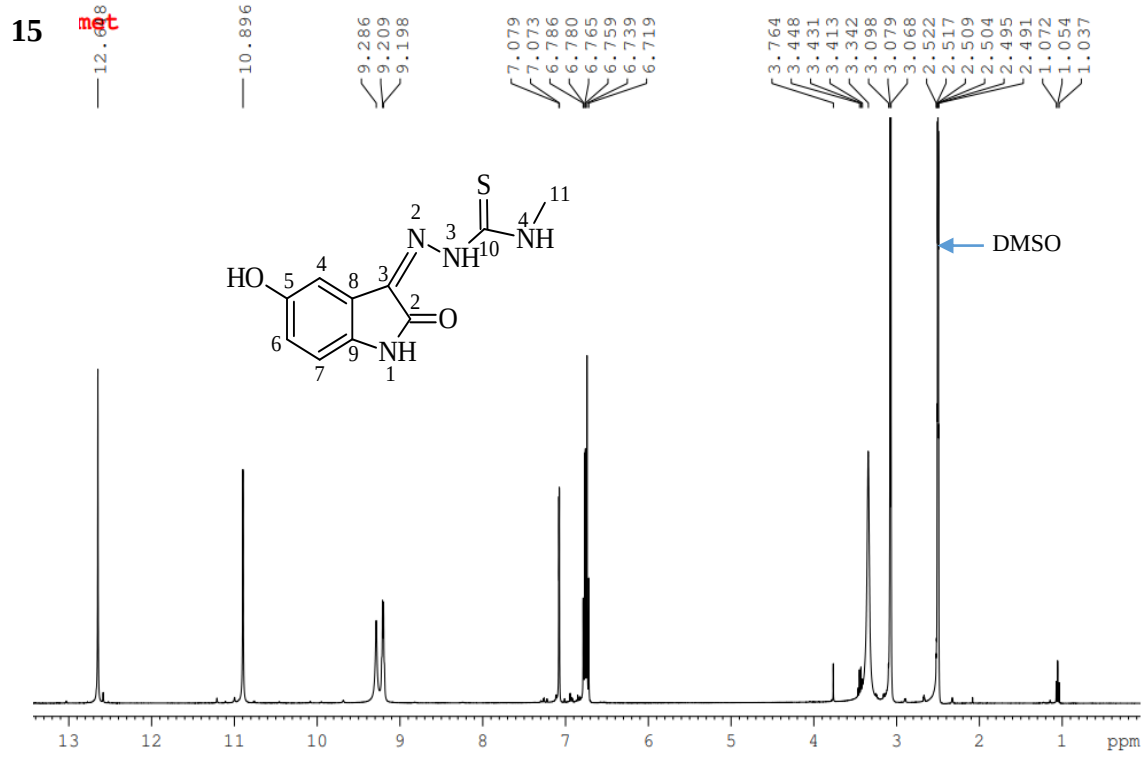

Appendix B15: ^{1}H NMR spectrum (400 MHz, DMSO-*d6*) of compound (***HydIstMet*/15)**

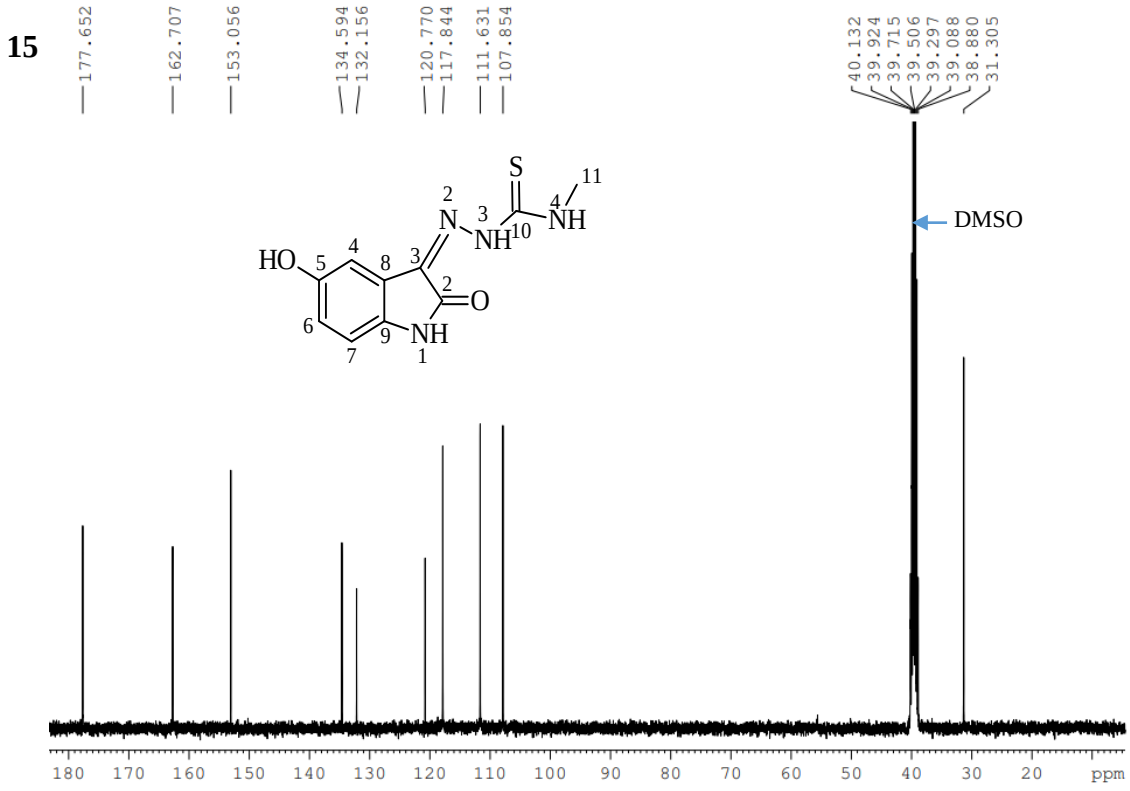

Appendix B15: ^{13}C NMR spectrum (400 MHz, DMSO-*d6*) of compound (***HydIstMet*/15)**

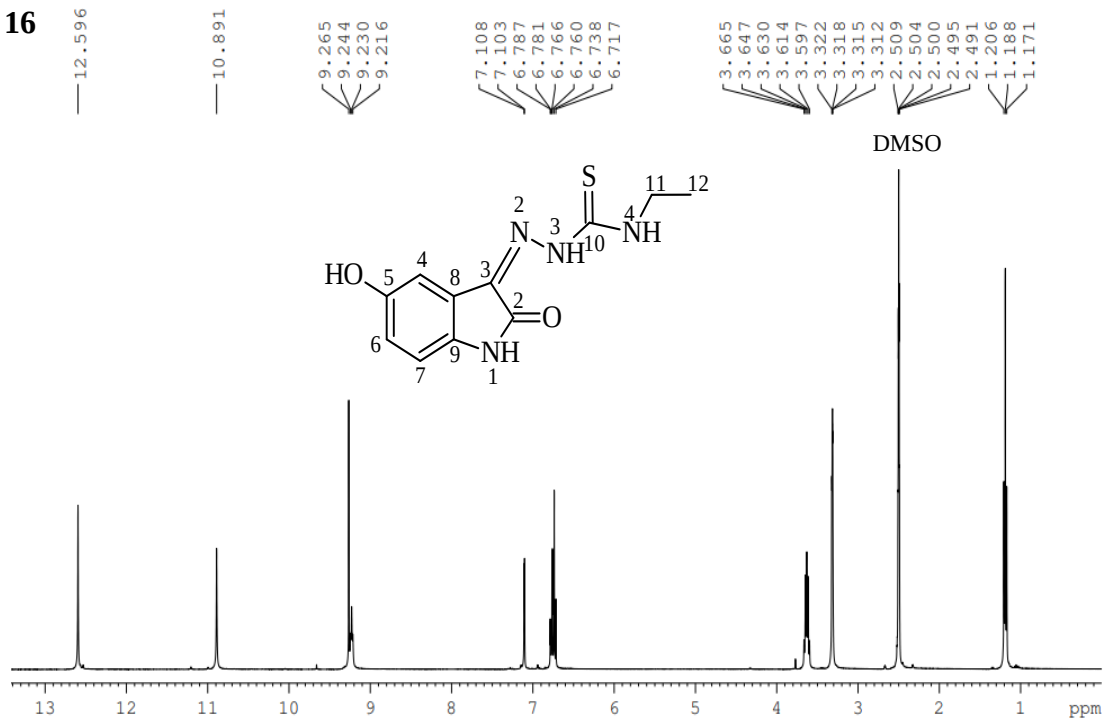

Appendix B16: ^{1}H NMR spectrum (400 MHz, DMSO-*d6*) of compound (***HydIstEth*/16)**

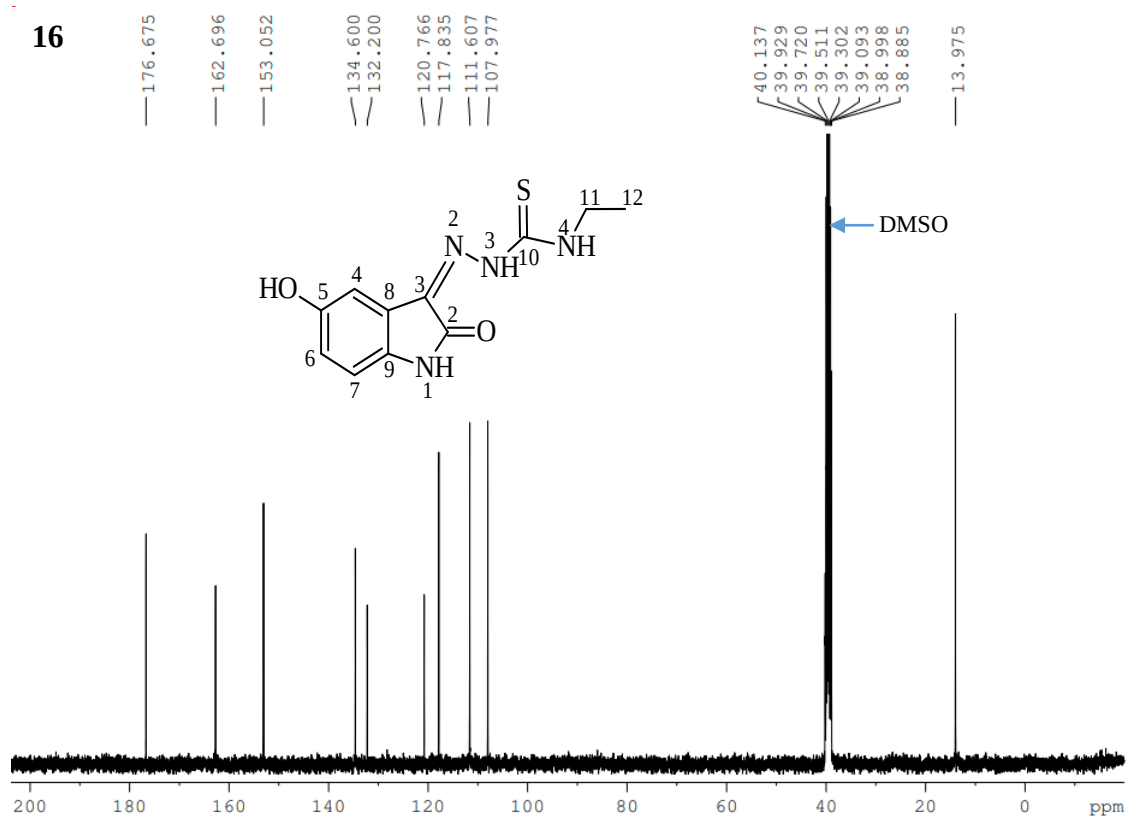

Appendix B16: ^{13}C NMR spectrum (400 MHz, DMSO-*d6*) of compound (***HydIstEth*/16)**

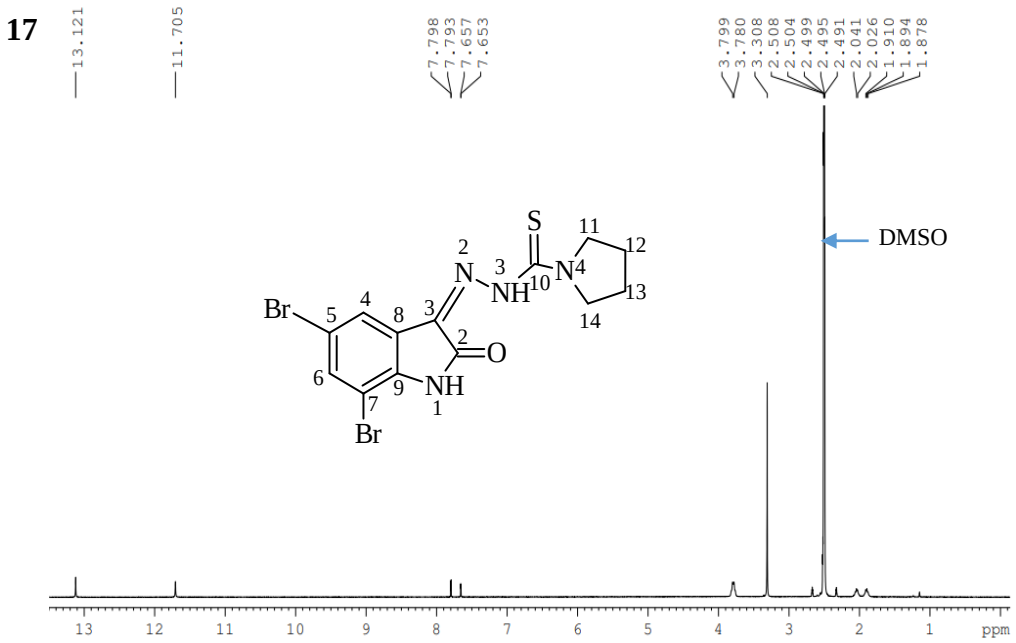

Appendix B17: ^{1}H NMR spectrum (400 MHz, DMSO-*d6*) of compound (***DiBrIstPyrl*/17**)

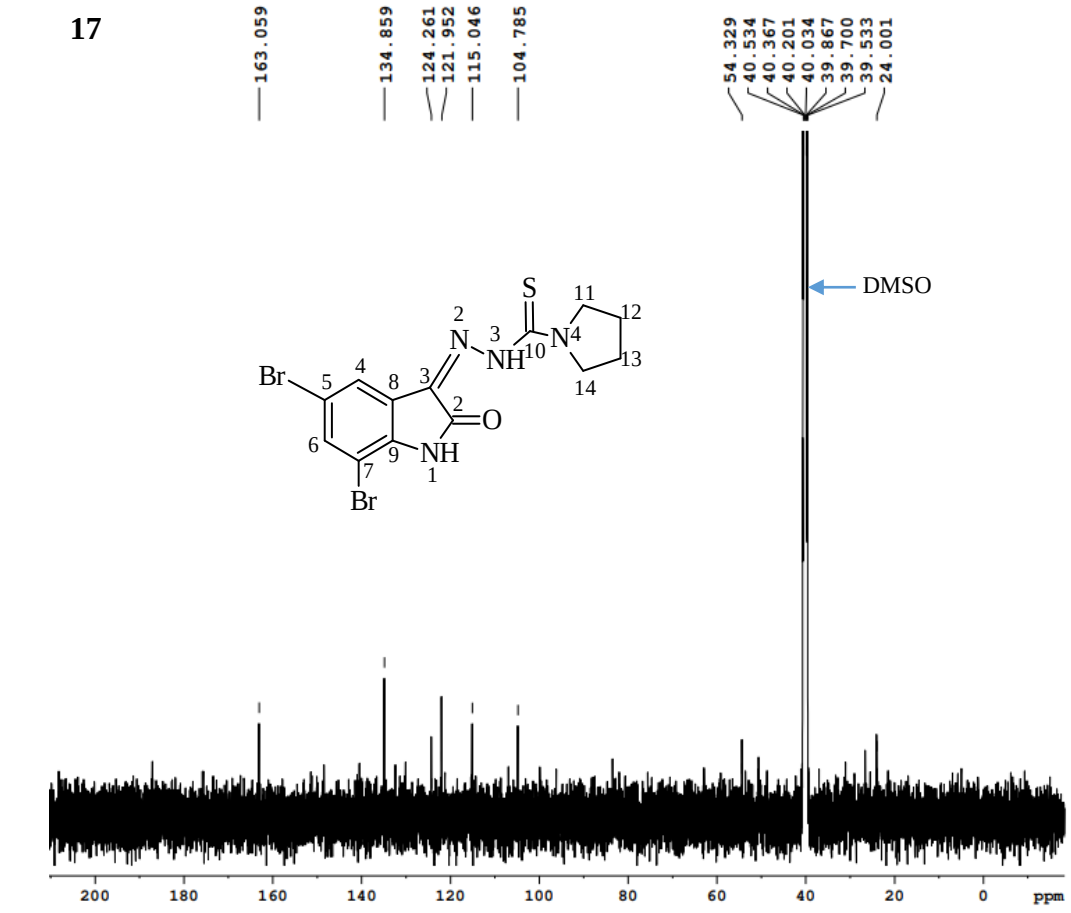

Appendix B17: ^{13}C NMR spectrum (400 MHz, DMSO-*d6*) of compound (***DiBrIstPyrl*/17**)

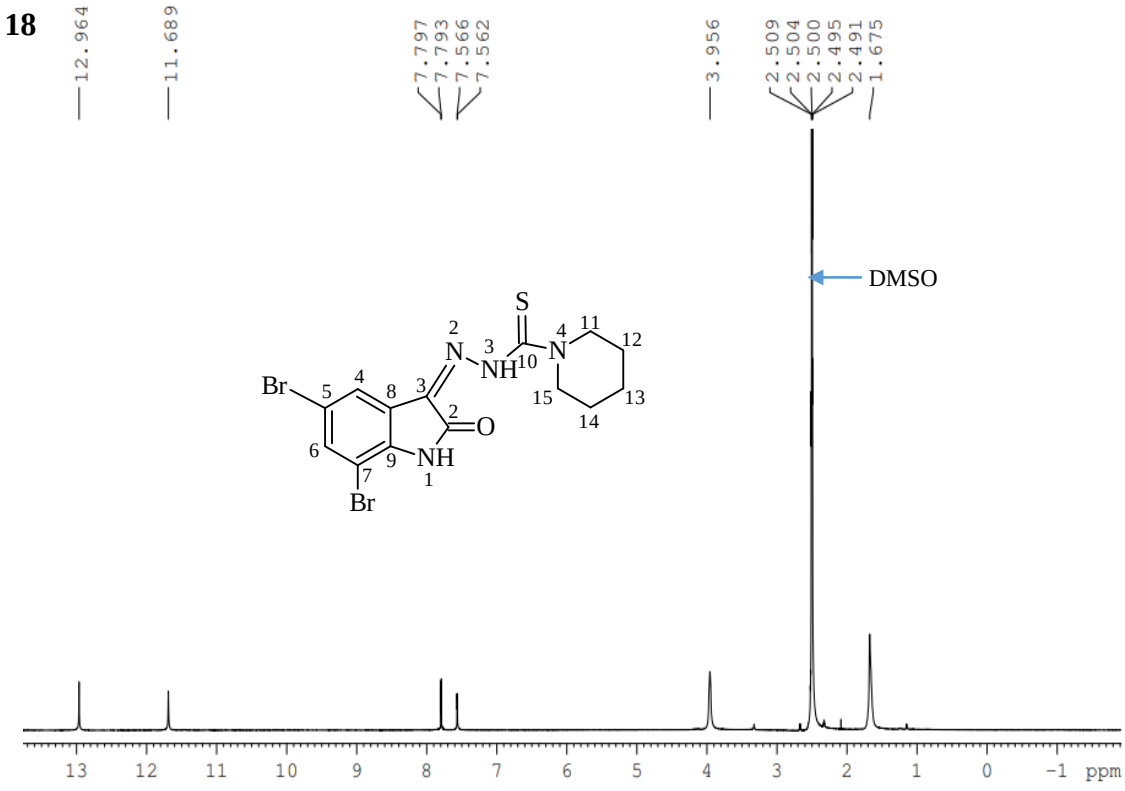

Appendix B18: ^{1}H NMR spectrum (400 MHz, DMSO-*d6*) of compound (***DiBrIstPip*/18)**

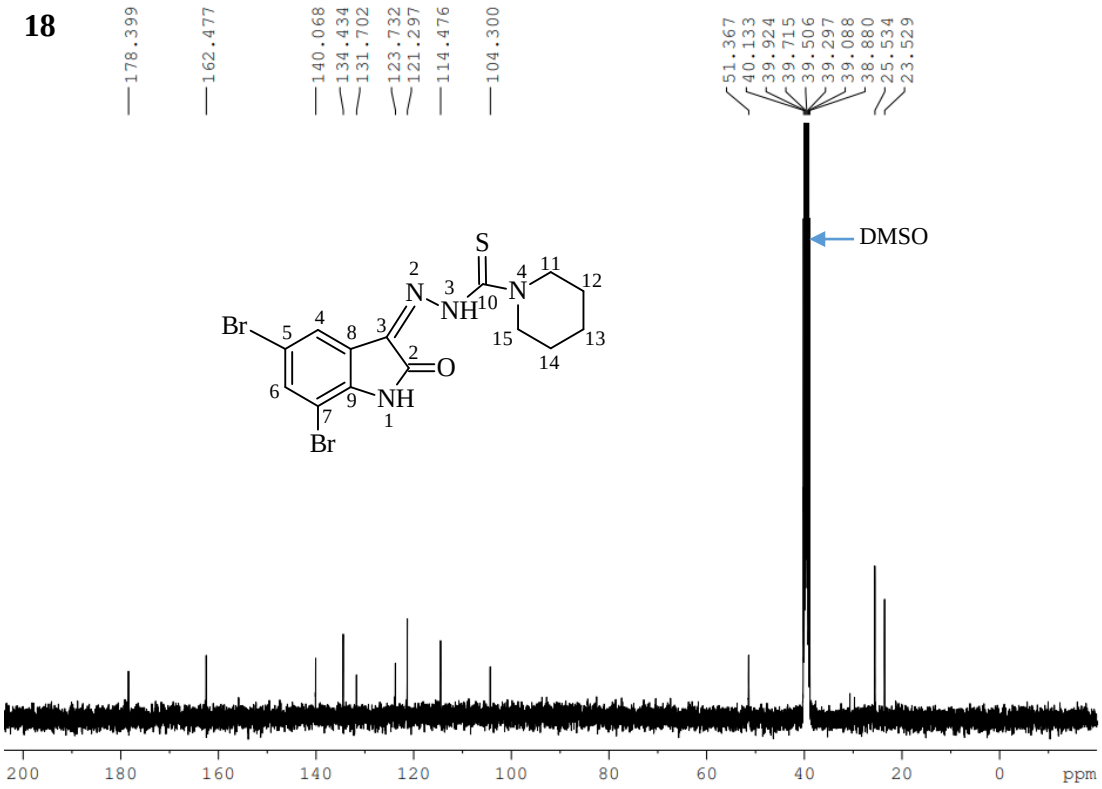

Appendix B18: ^{13}C NMR spectrum (400 MHz, DMSO-*d6*) of compound (***DiBrIstPip*/18)**

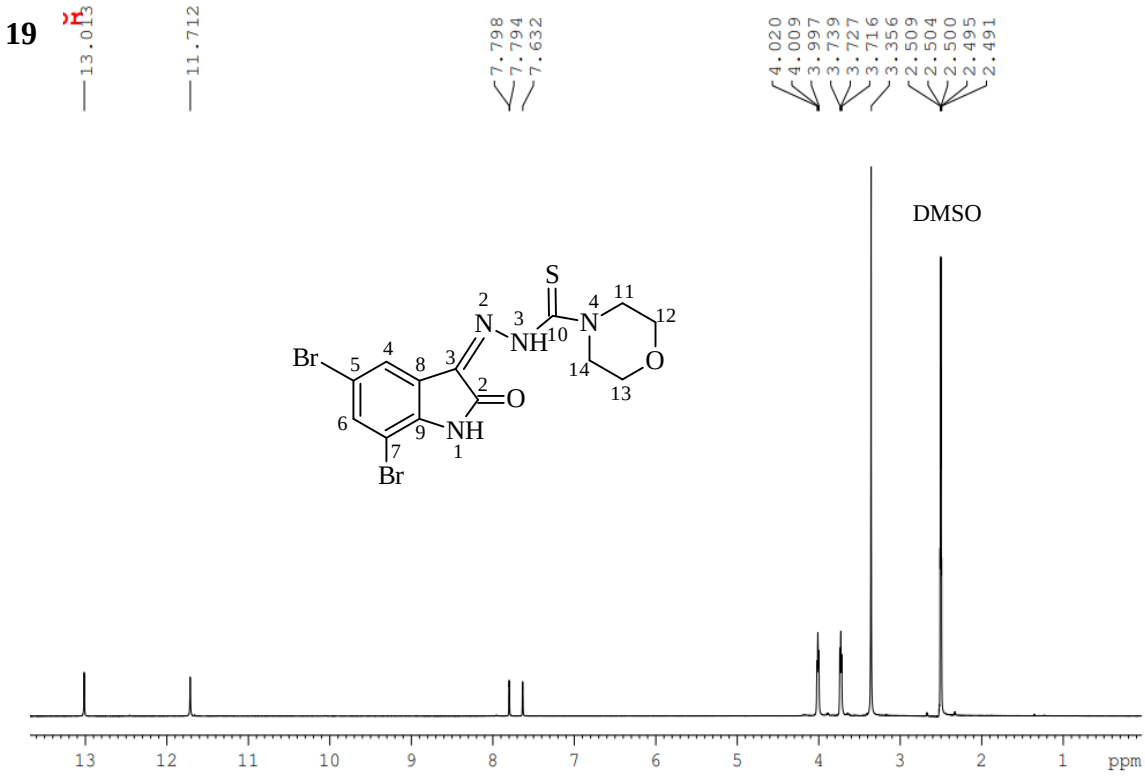

Appendix B19: ^{1}H NMR spectrum (400 MHz, DMSO-*d6*) of compound (***DiBrIstMor*/19)**

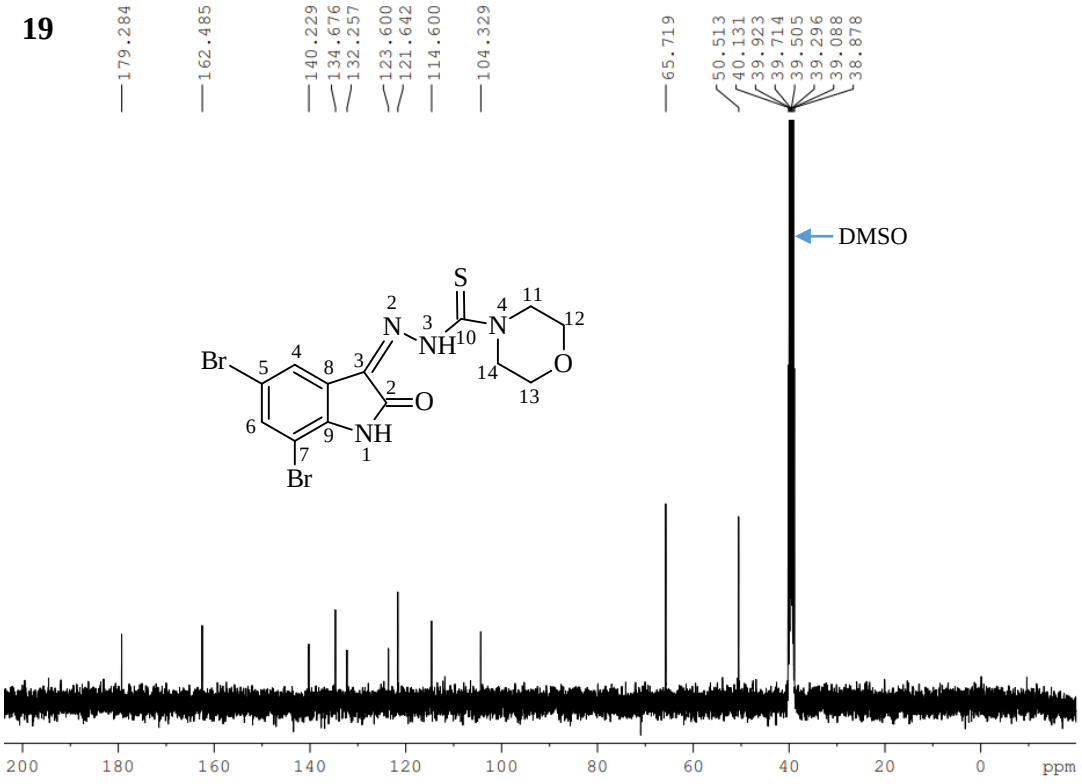

Appendix B19: ^{13}C NMR spectrum (400 MHz, DMSO-*d6*) of compound (***DiBrIstMor*/19)**

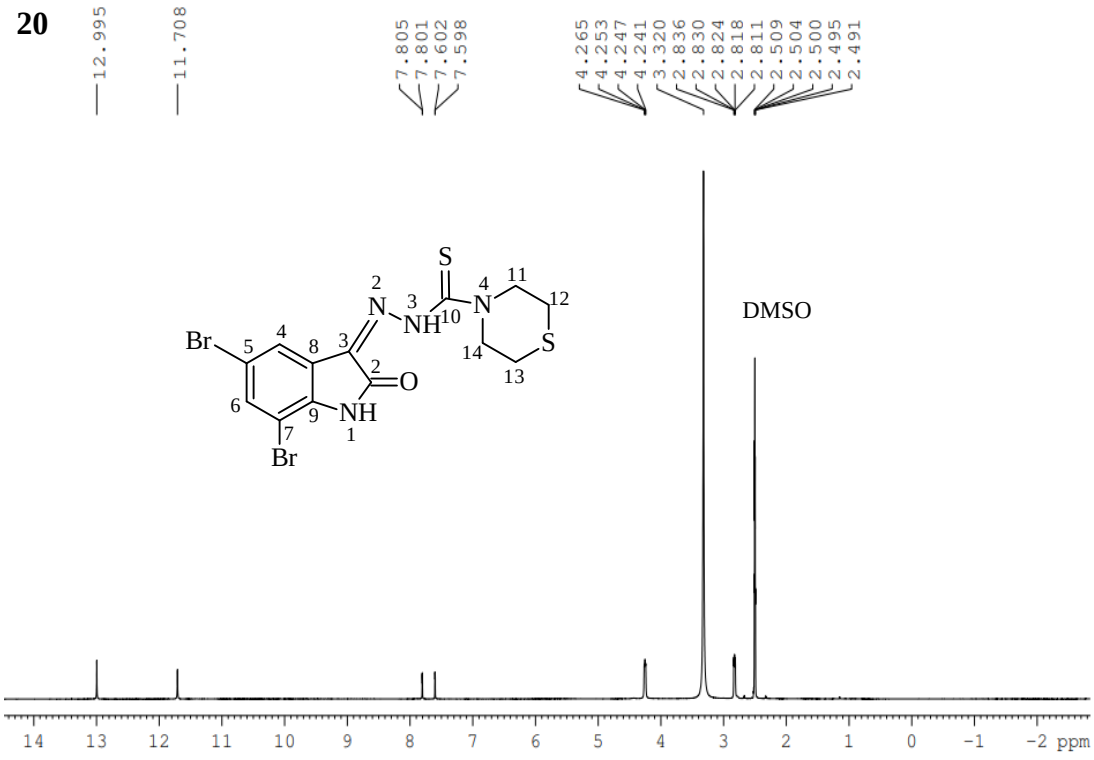

Appendix B20: ^{1}H NMR spectrum (400 MHz, DMSO-*d6*) of compound (***DiBrIstTmor*/20**)

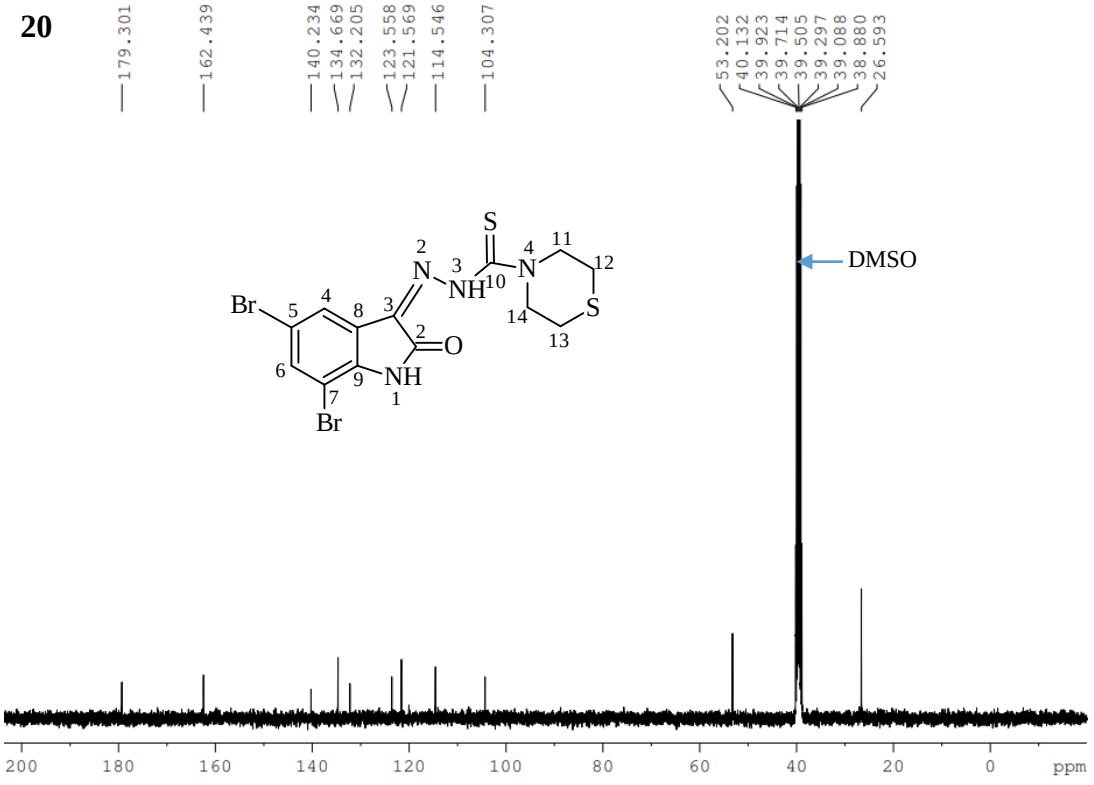

Appendix B20: ^{13}C NMR spectrum (400 MHz, DMSO-*d6*) of compound (***DiBrIstTmor*/20**)

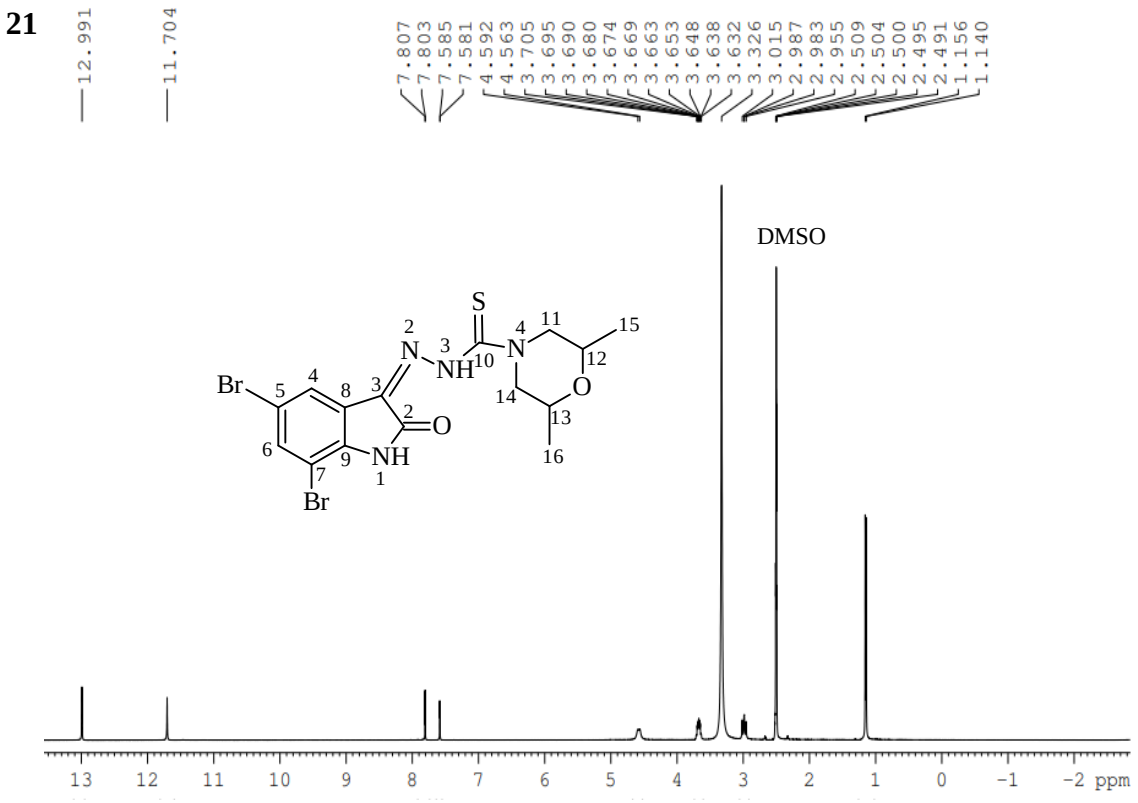

Appendix B21: ^{1}H NMR spectrum (400 MHz, DMSO-*d6*) of compound (***DiBrIstDmMor*/21)**

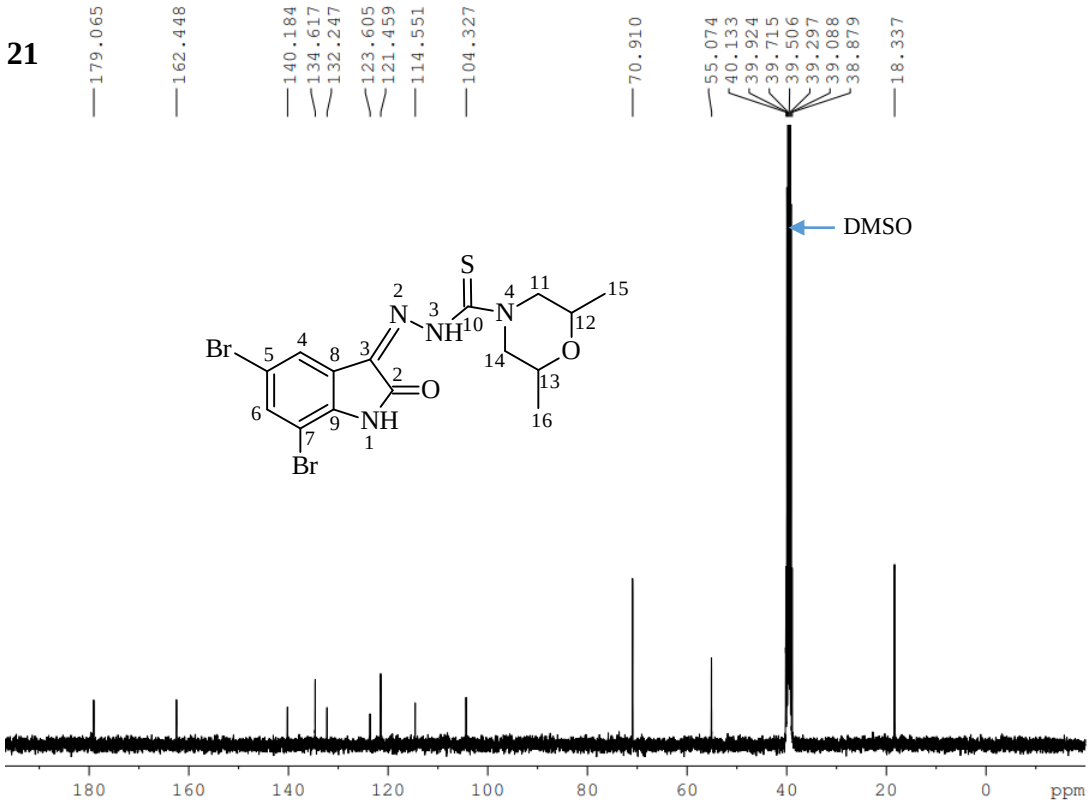

Appendix B21: ^{13}C NMR spectrum (400 MHz, DMSO-*d6*) of compound (***DiBrIstDmMor*/21)**

22

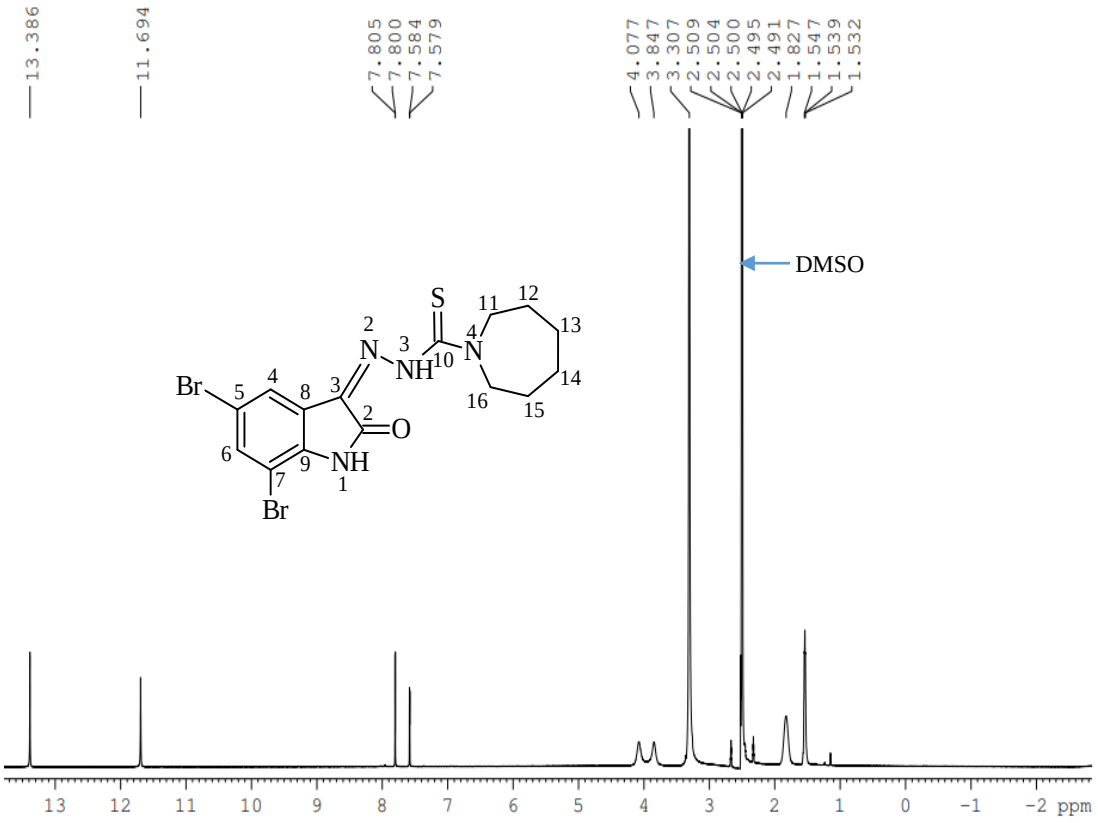

Appendix B22: ^{1}H NMR spectrum (400 MHz, DMSO-*d6*) of compound (***DiBrIstAzep*/22**)

23

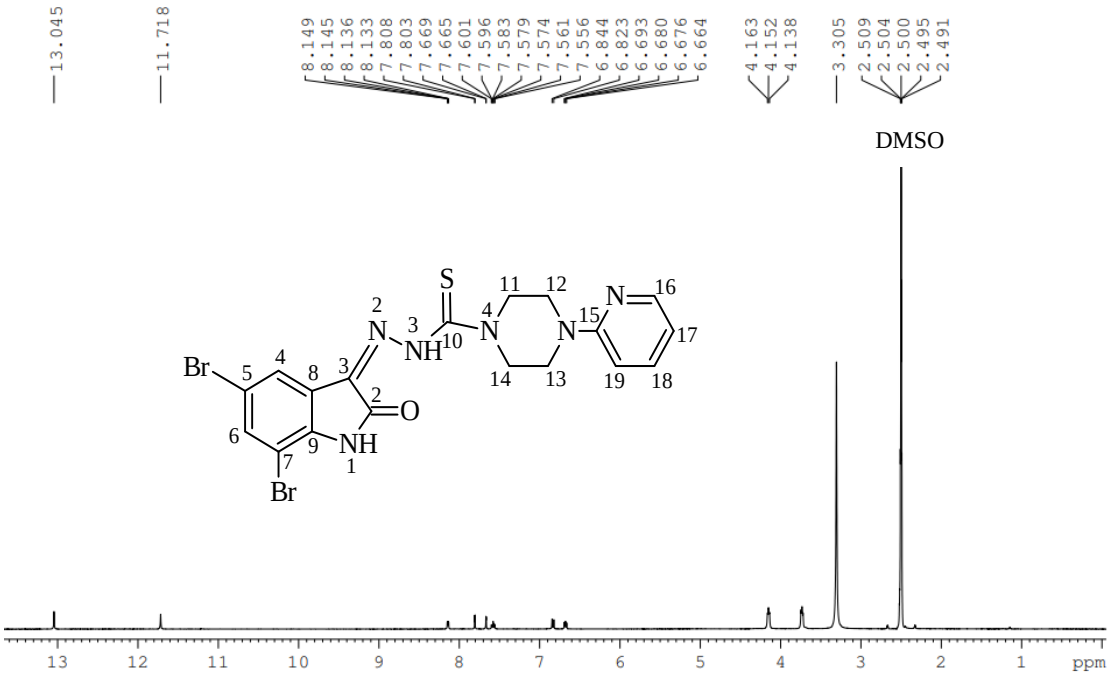

Appendix B23: ^{1}H NMR spectrum (400 MHz, DMSO-*d6*) of compound (***DiBrIstPypz*/23**)

23

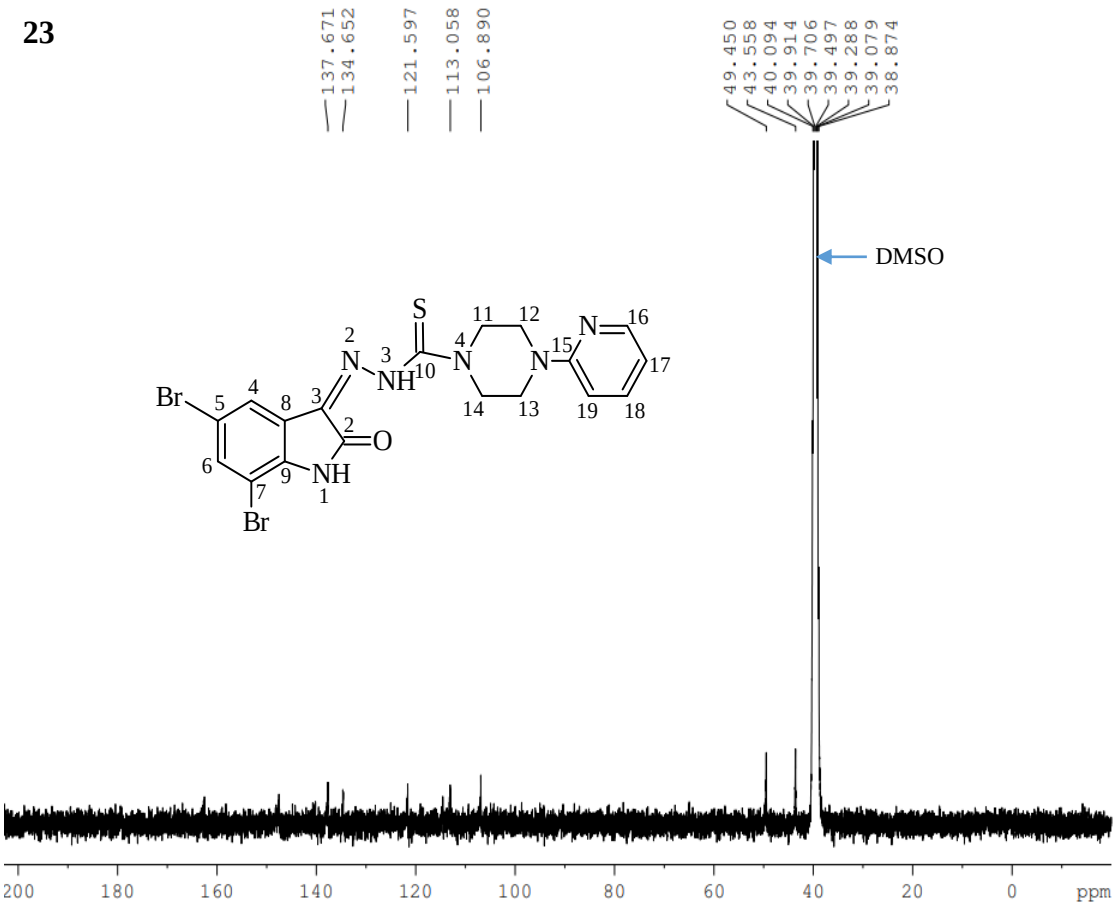

Appendix B23: ^{13}C NMR spectrum (400 MHz, DMSO-*d6*) of compound (***DiBrIstPypz*/23**)

24

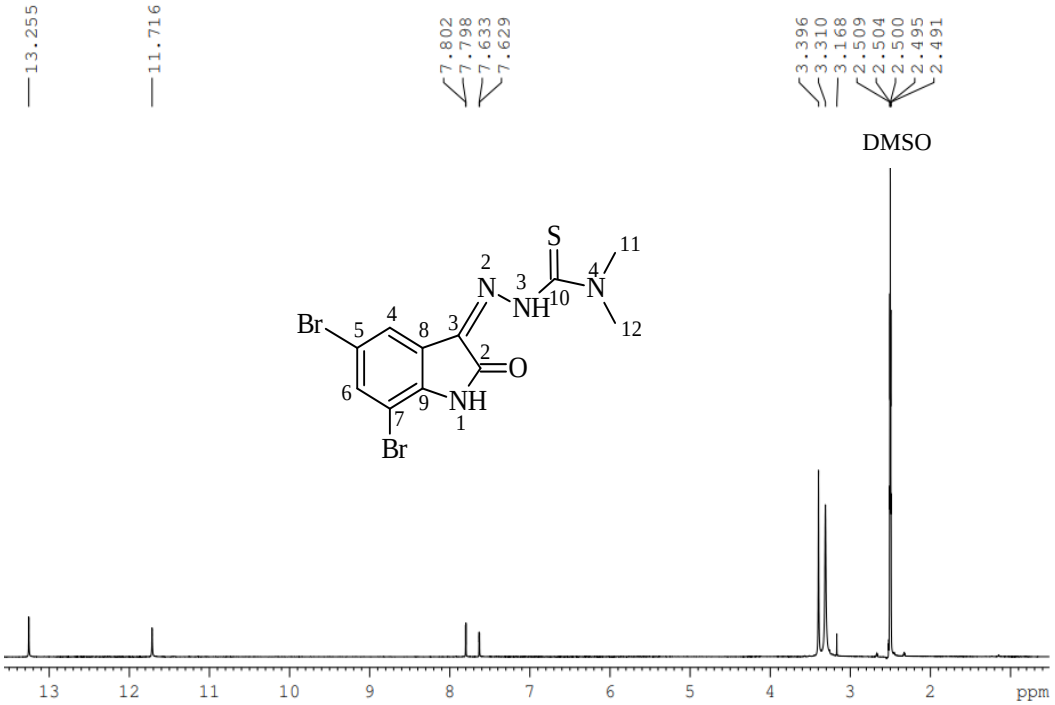

Appendix B24: ^{1}H NMR spectrum (400 MHz, DMSO-*d6*) of compound (***DiBrIstDm*/24**)

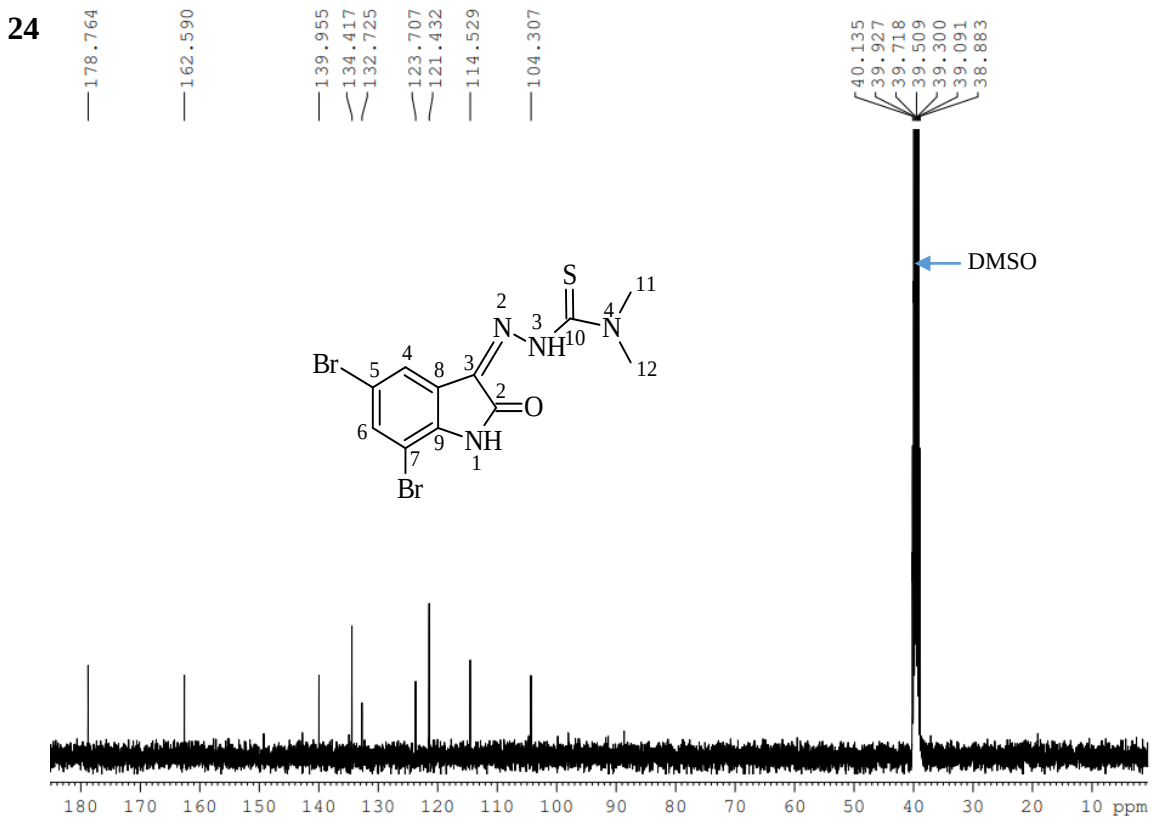

Appendix B24: ^{13}C NMR spectrum (400 MHz, DMSO-*d6*) of compound (***DiBrIstDm*/24**)

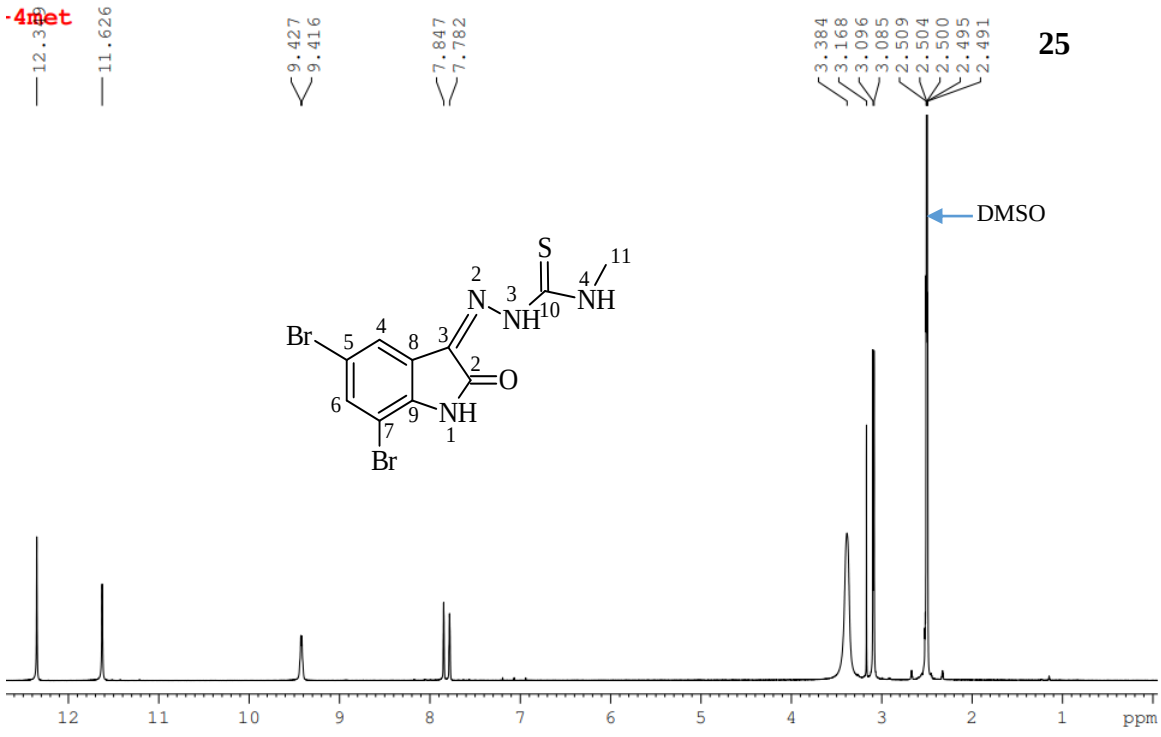

Appendix B25: ^{1}H NMR spectrum (400 MHz, DMSO-*d6*) of compound (***DiBrIstMet*/25**)

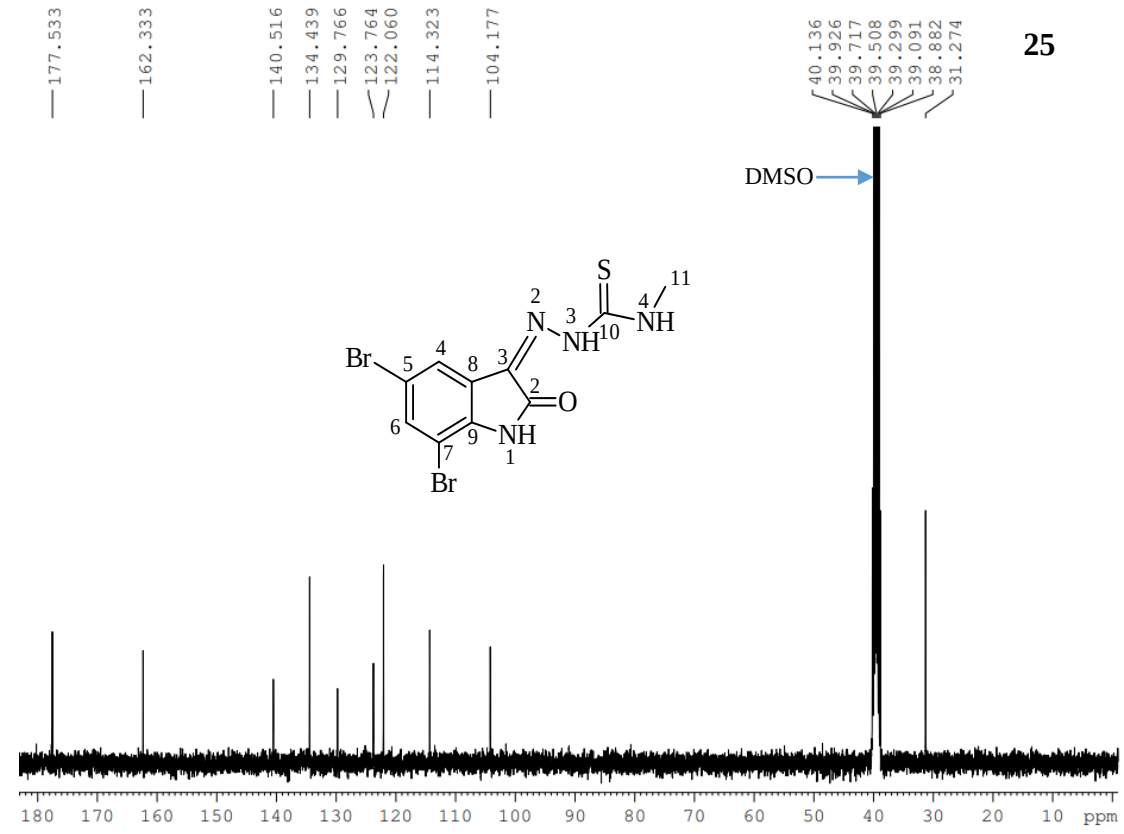

Appendix B25: ^{13}C NMR spectrum (400 MHz, DMSO-*d6*) of compound (***DiBrIstMet*/25**)

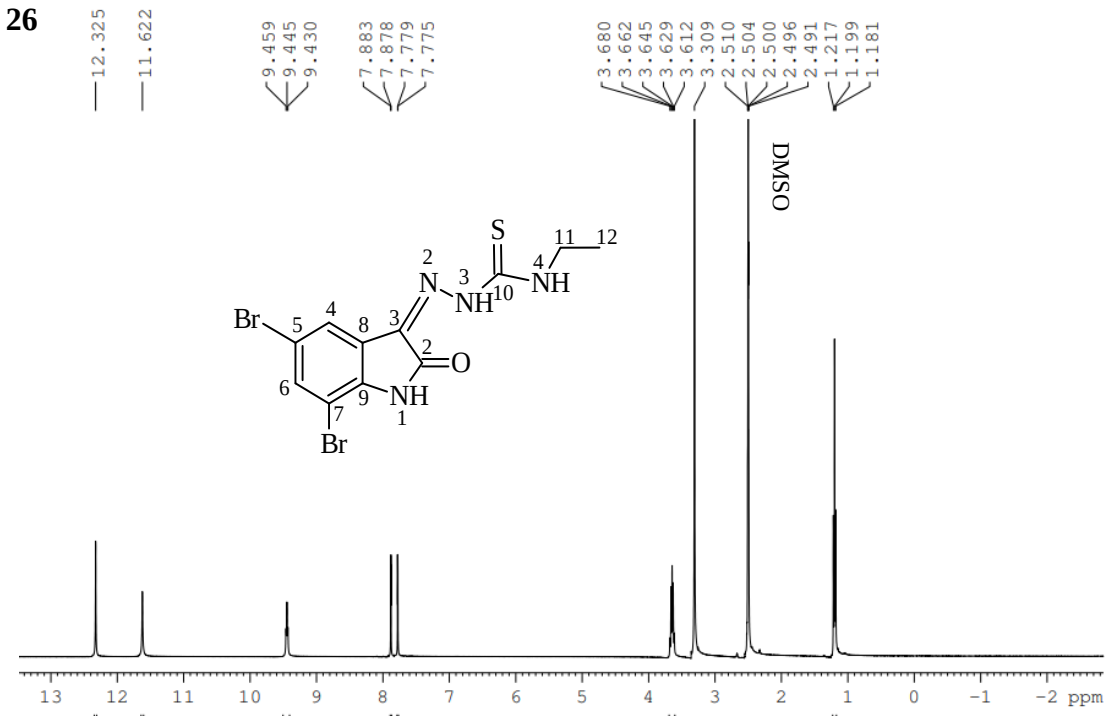

Appendix B26: ^{1}H NMR spectrum (400 MHz, DMSO-*d6*) of compound (***DiBrIstEth*/26**)

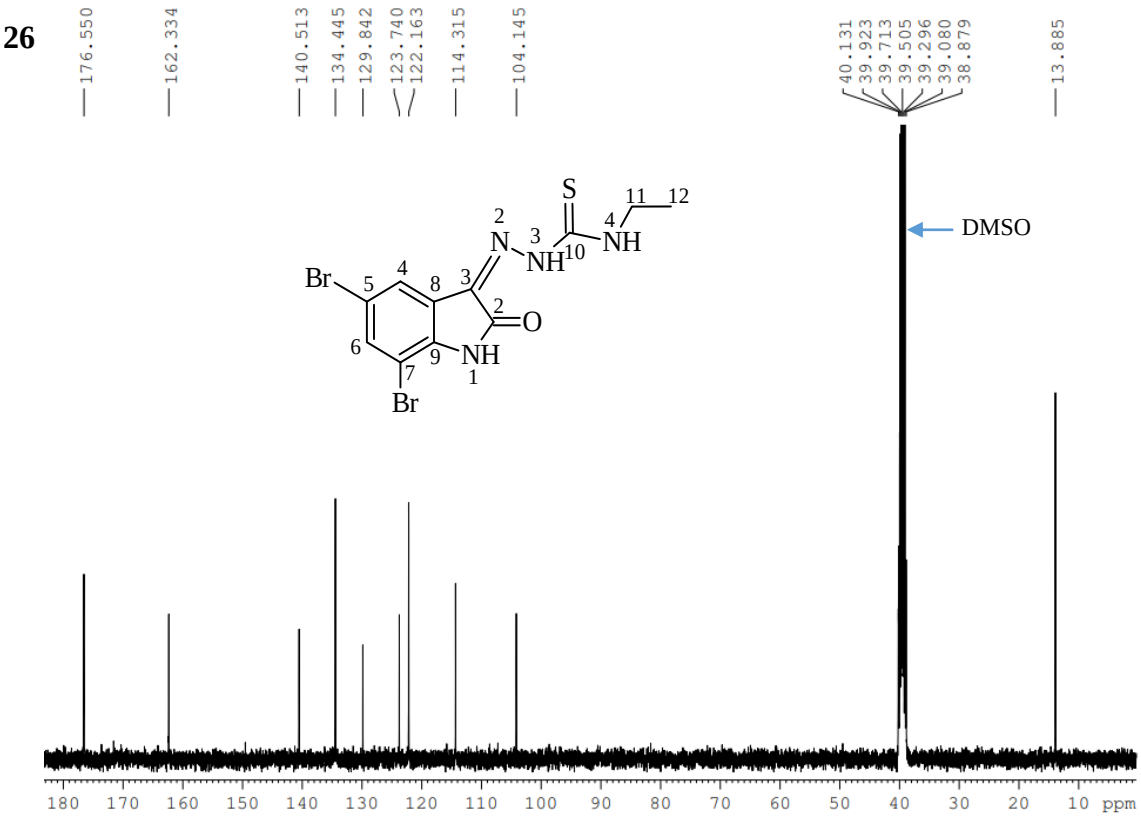

Appendix B26: ^{13}C NMR spectrum (400 MHz, DMSO-*d6*) of compound (***DiBrIstEth*/26)**

Appendix C

ESI-HRMS of TSCs

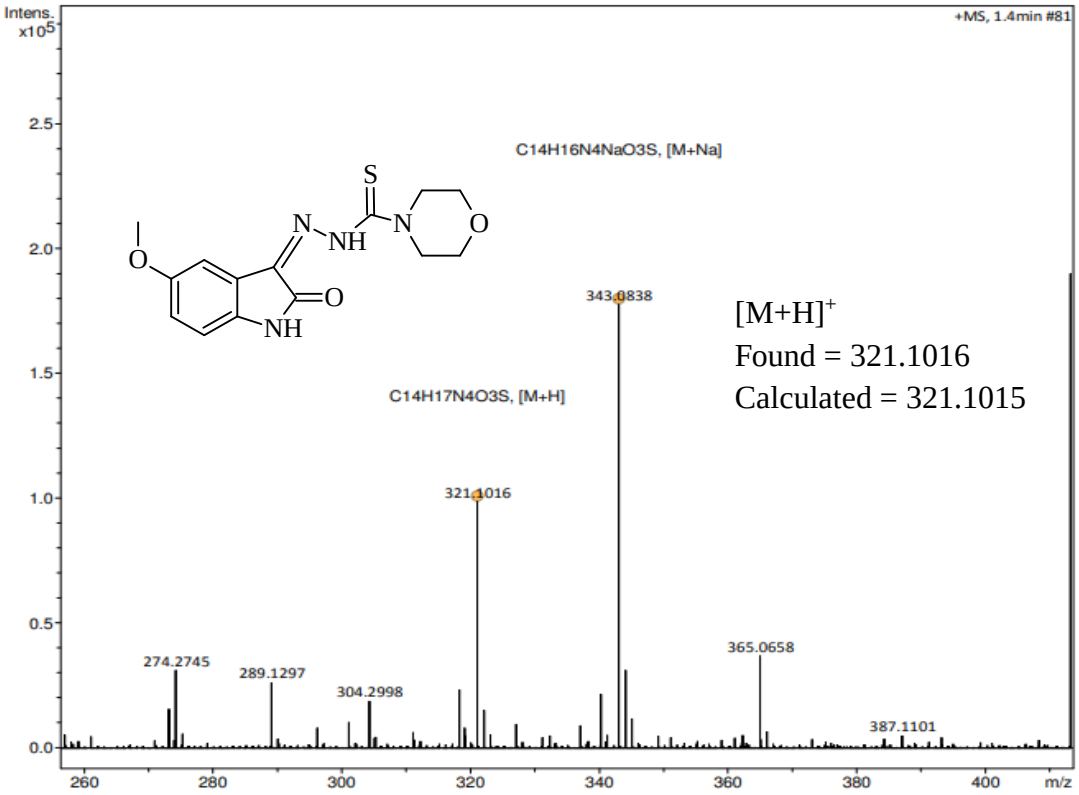

Appendix C1: ESI-HRMS of compound **(*MeOIstMor*/1)**

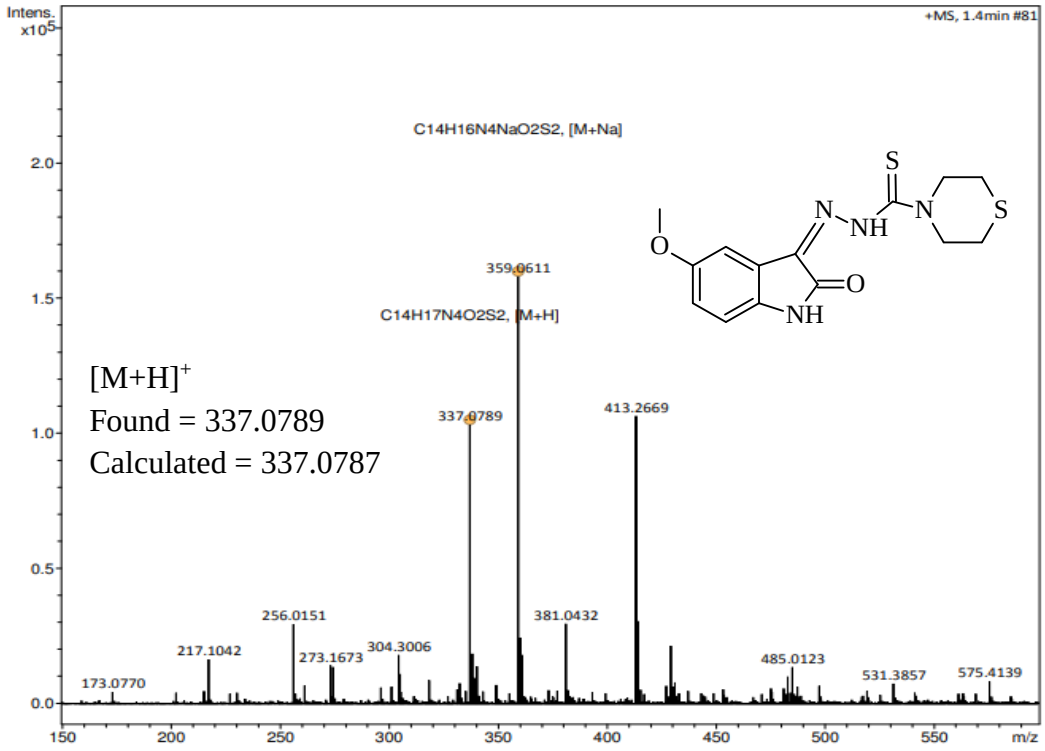

Appendix C2: ESI-HRMS of compound **(*MeOIstTmor*/2)**

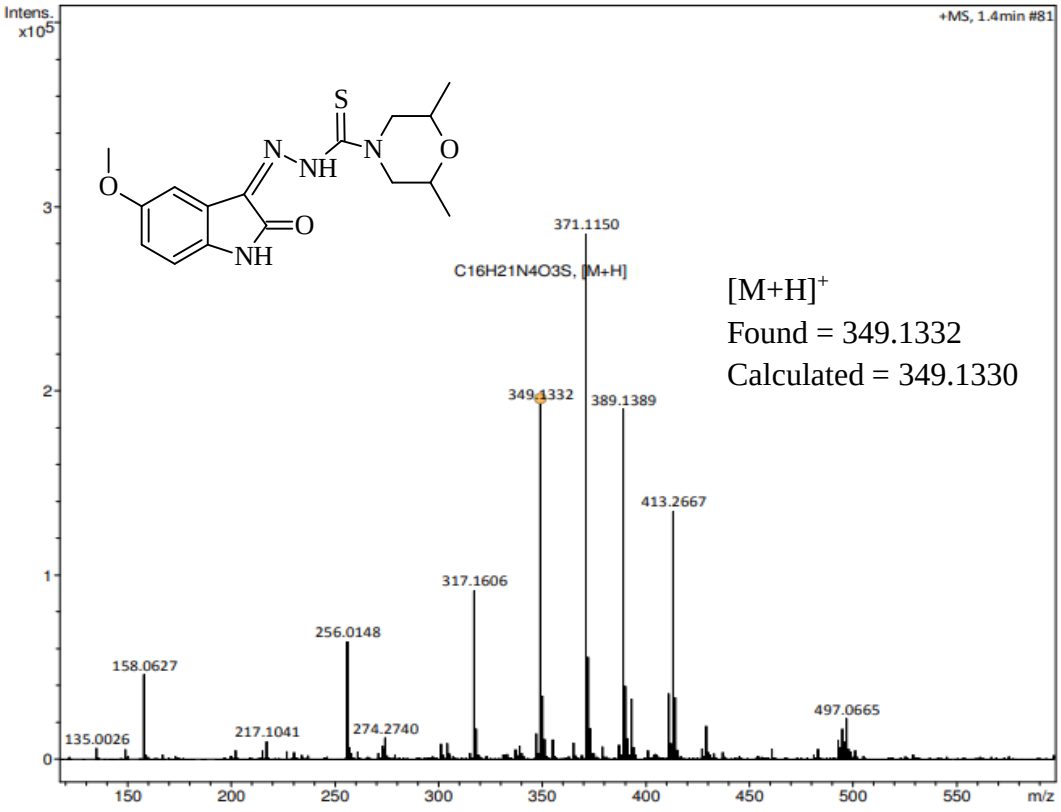

Appendix C3: ESI-HRMS of compound **(*MeOIstDmMor*/3)**

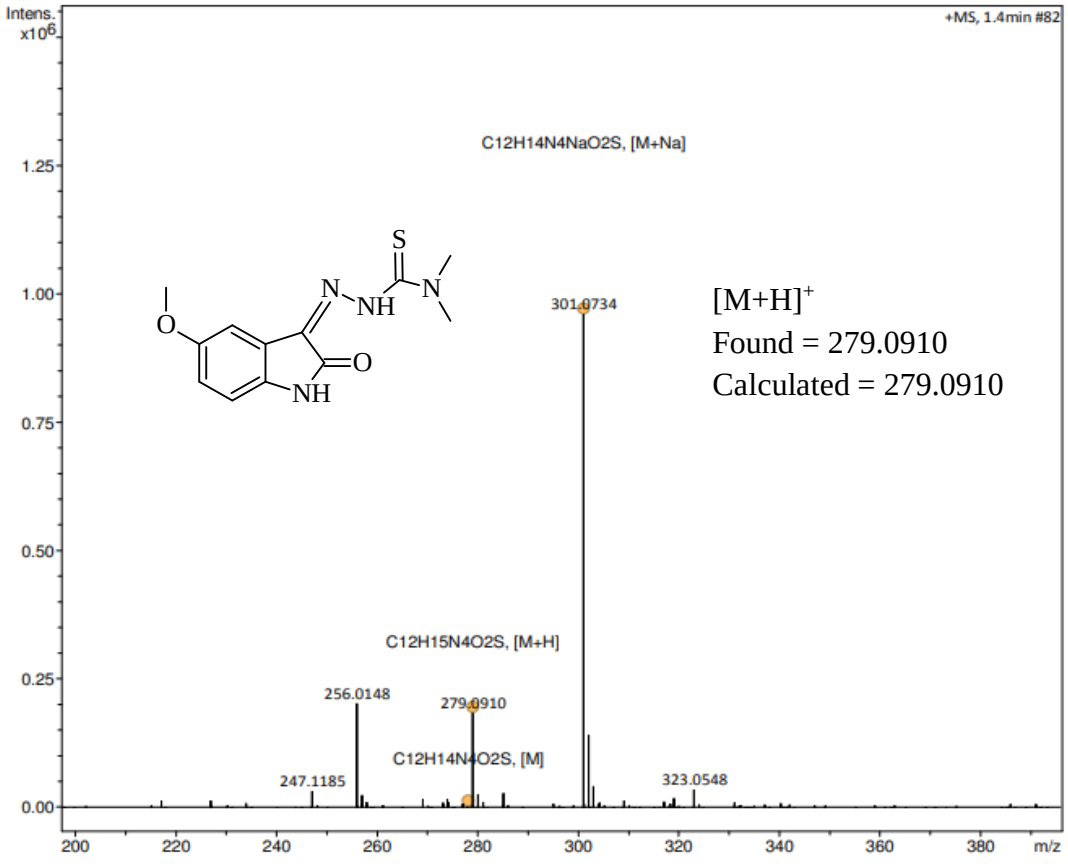

Appendix C4: ESI-HRMS of compound **(*MeOIstDm*/4)**

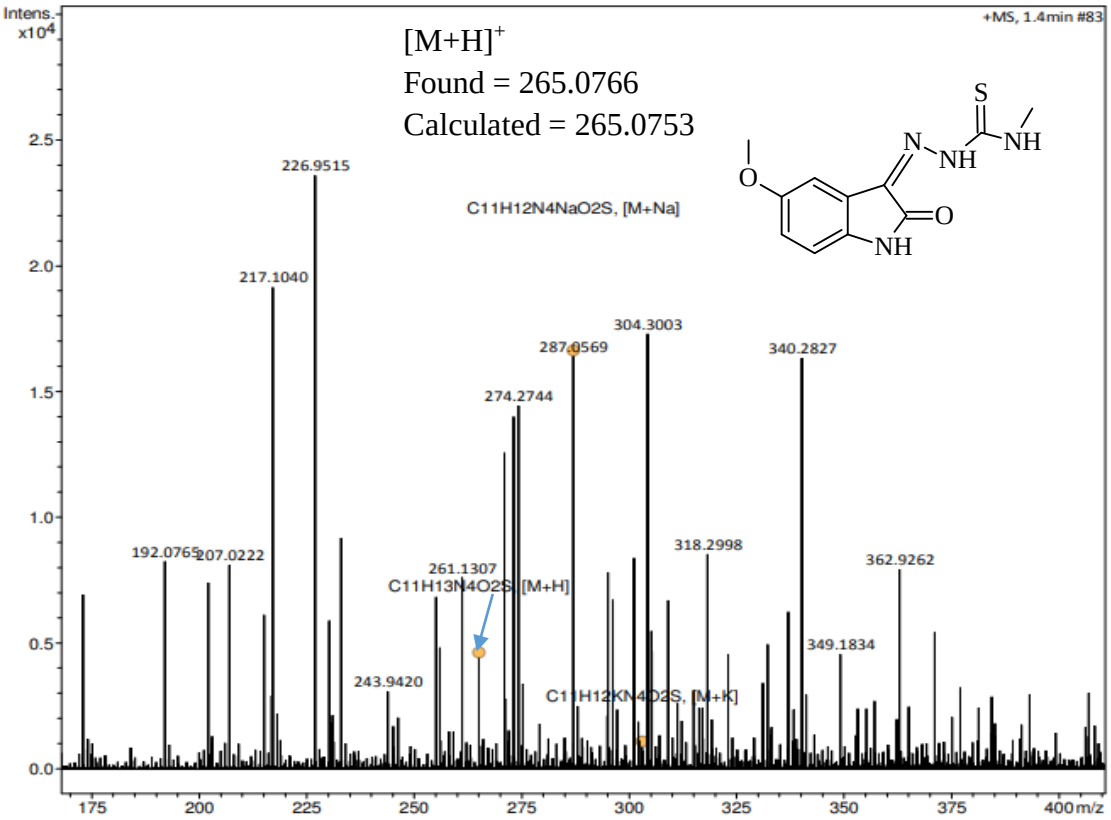

Appendix C5: ESI-HRMS of compound **(*MeOIstMet*/5)**

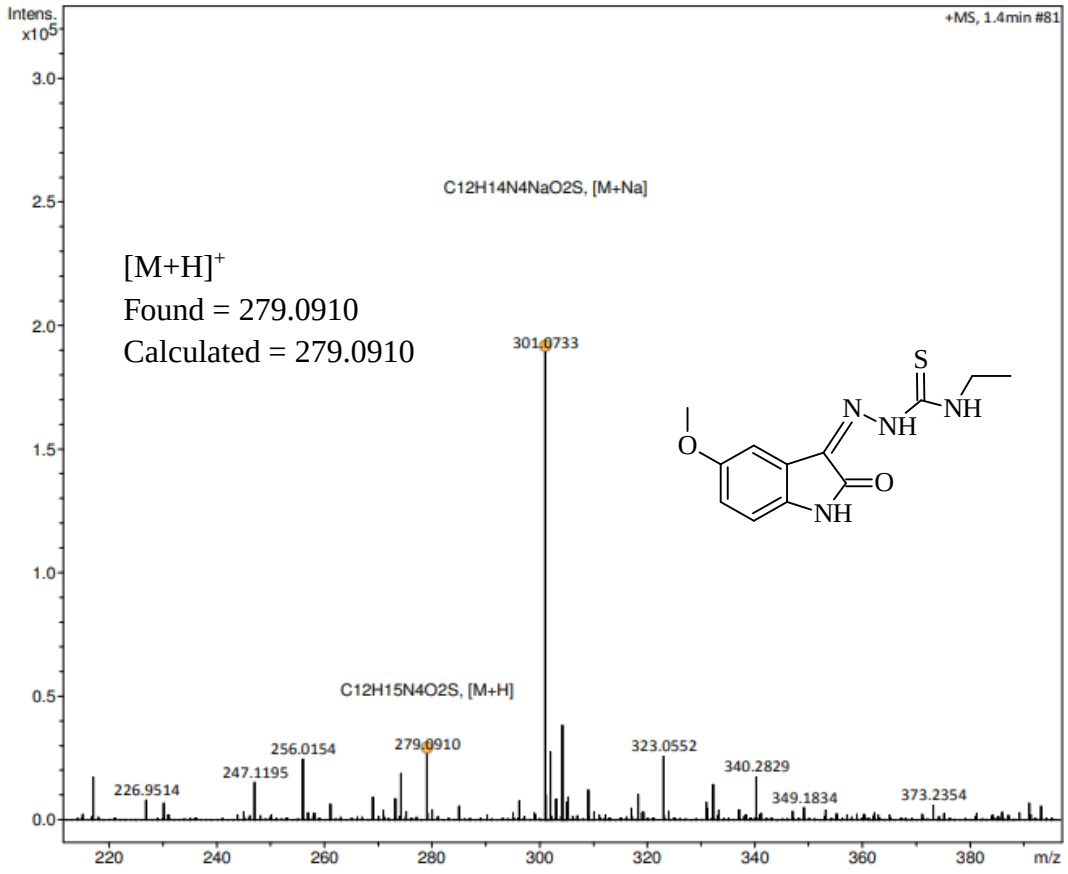

Appendix C6: ESI-HRMS of compound **(*MeOIstEth*/6)**

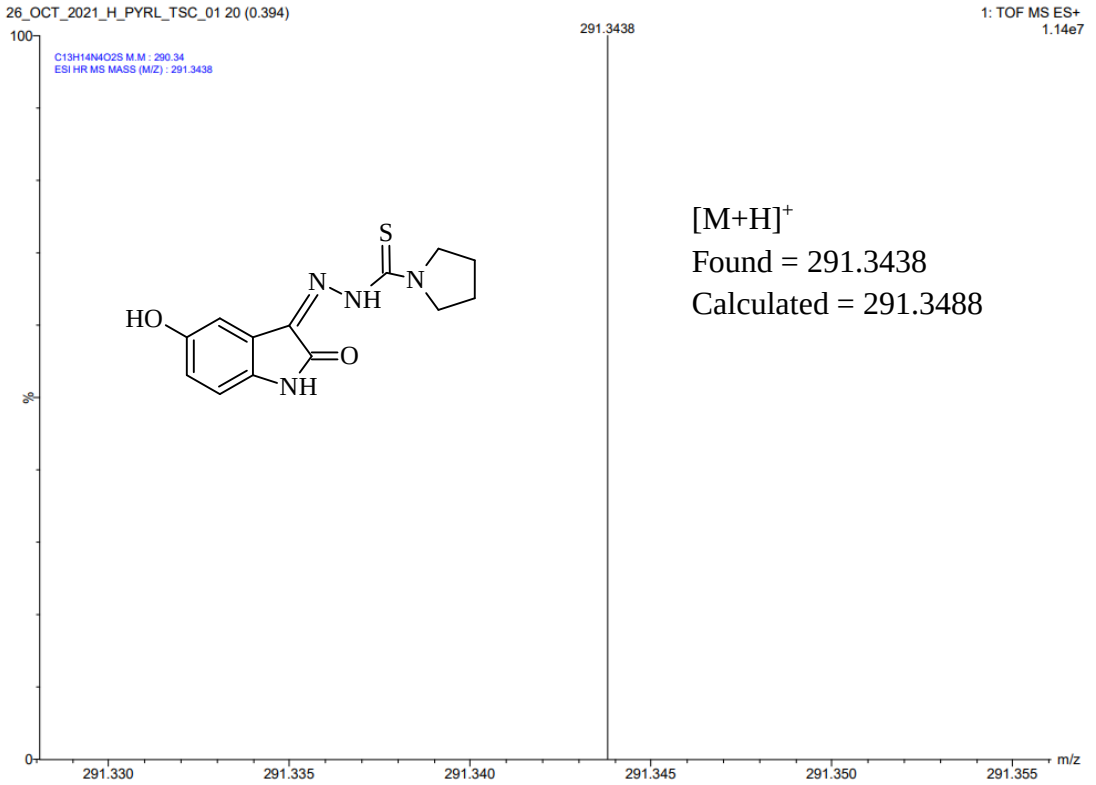

Appendix C7: ESI-HRMS of compound **(*HydIstPyrl*/7)**

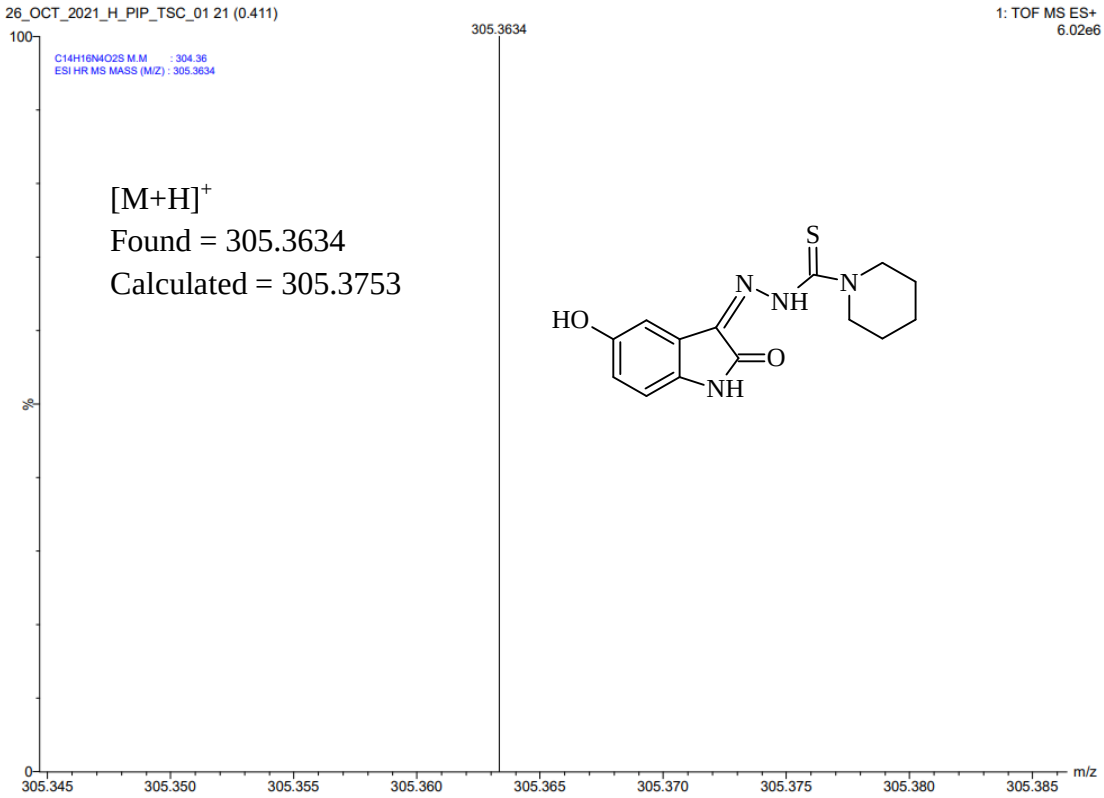

Appendix C8: ESI-HRMS of compound **(*HydIstPip*/8)**

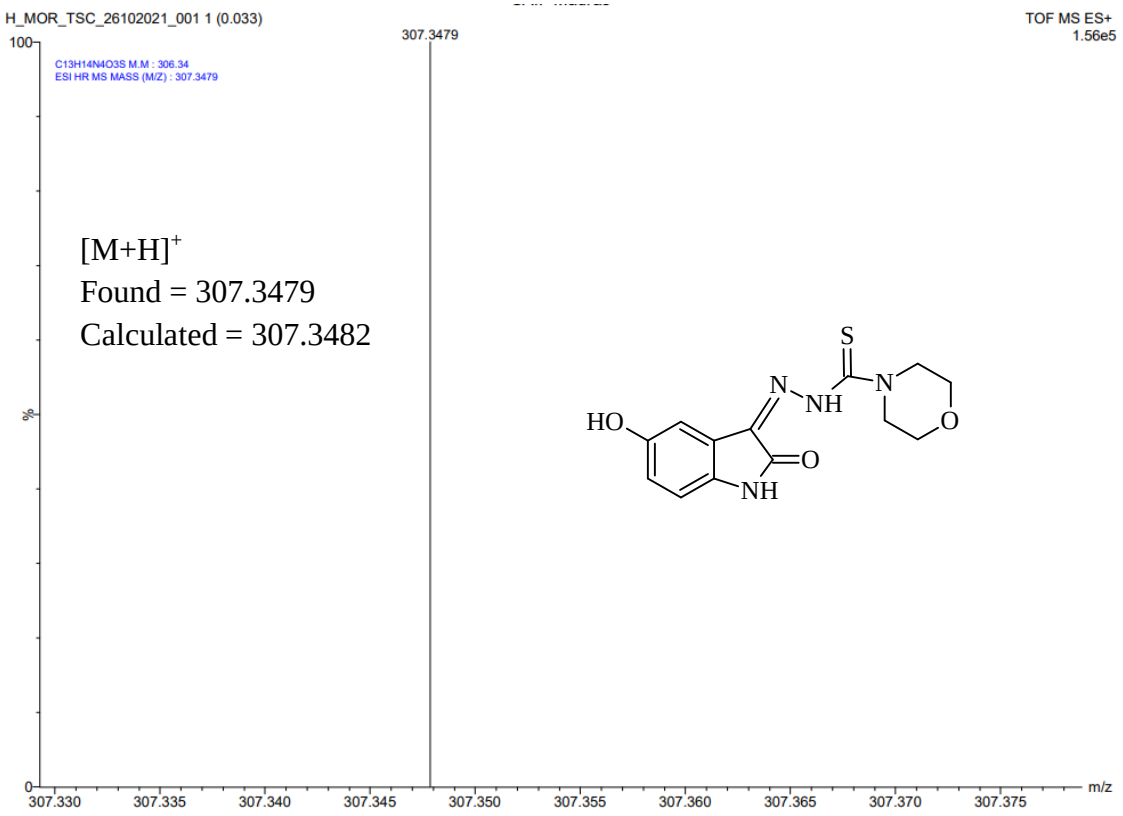

Appendix C9: ESI-HRMS of compound **(*HydIstMor*/9)**

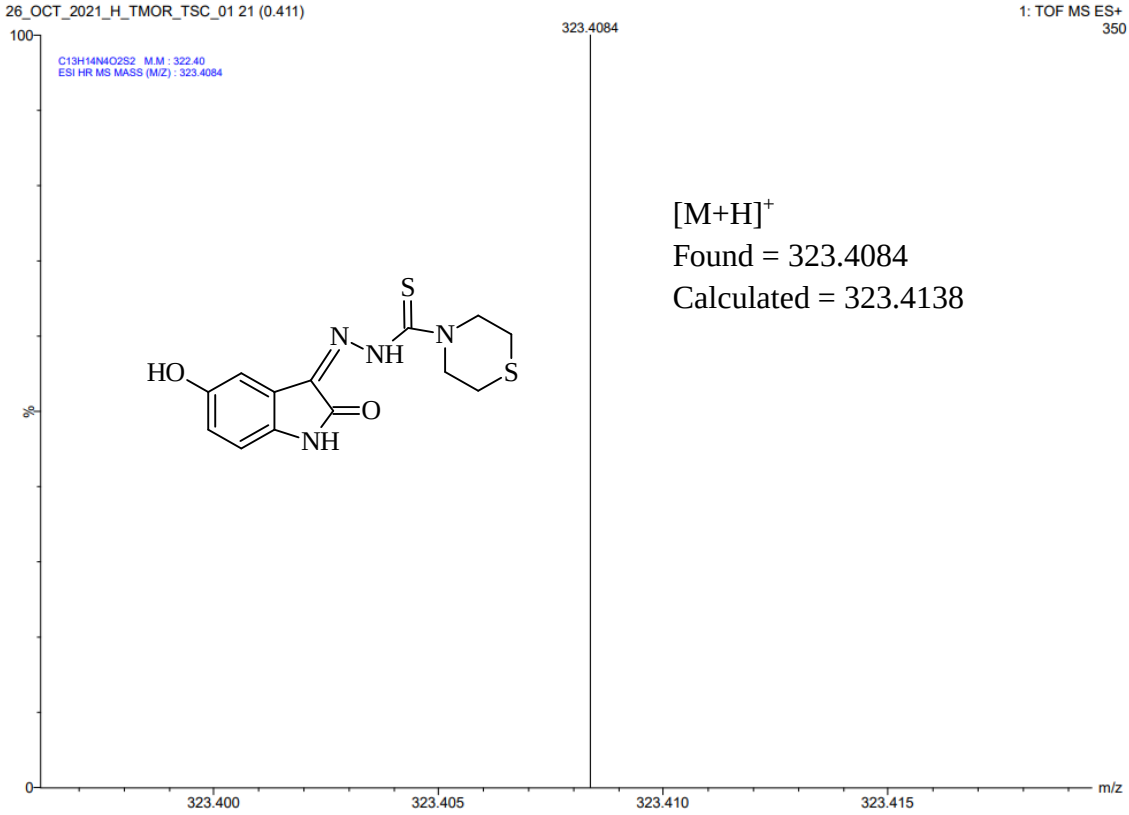

Appendix C10: ESI-HRMS of compound **(*HydIstTmor*/10)**

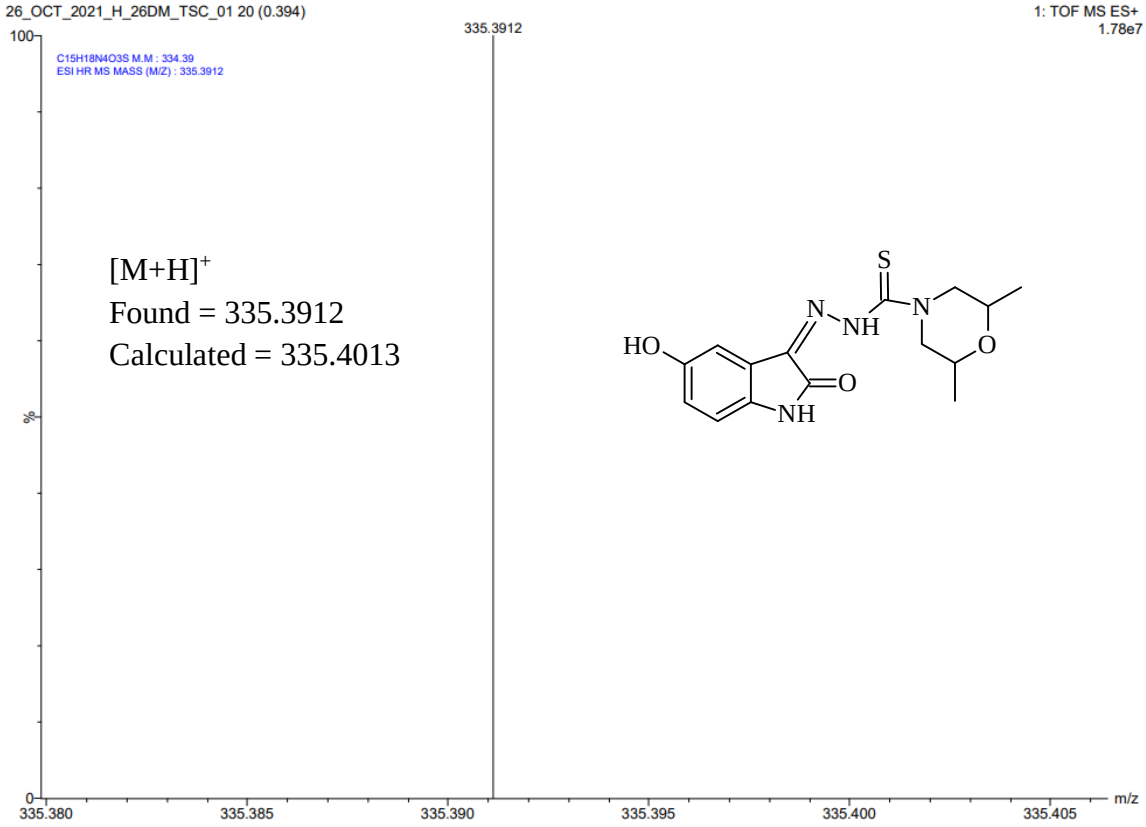

Appendix C11: ESI-HRMS of compound **(*HydIstDmMor*/11)**

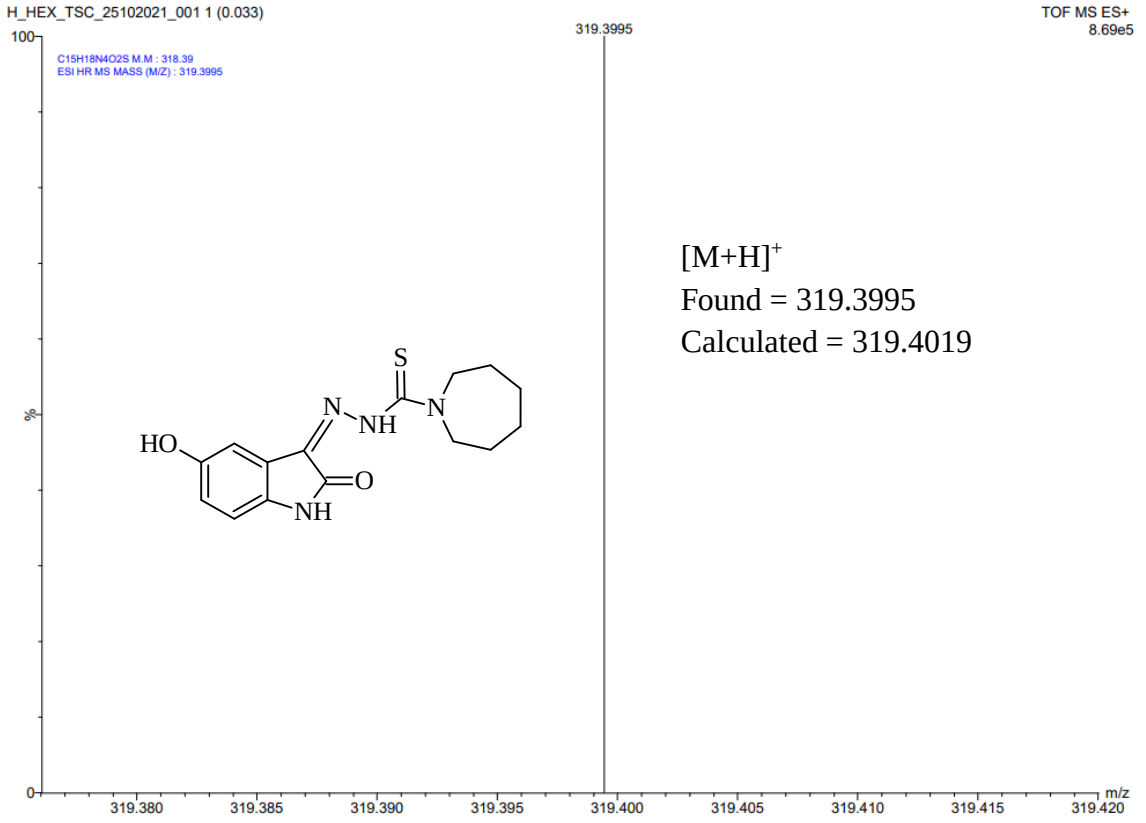

Appendix C12: ESI-HRMS of compound **(*HydIstAzep*/12)**

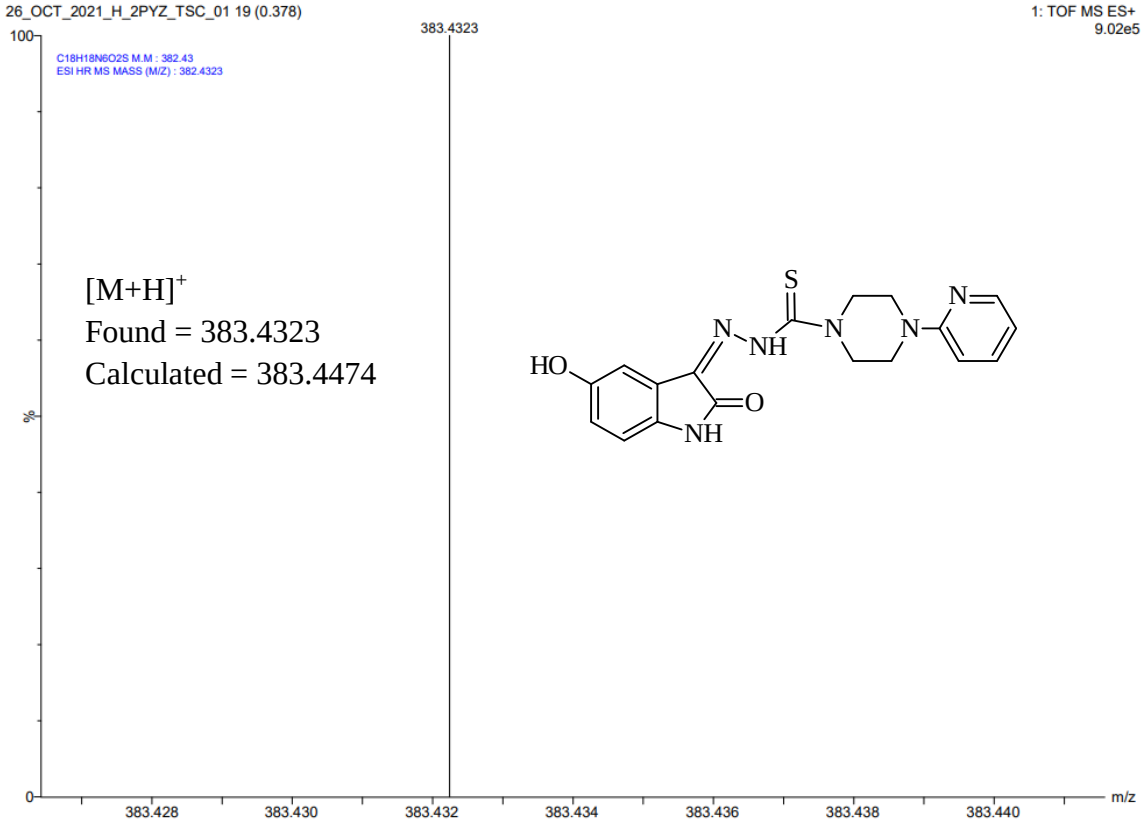

Appendix C13: ESI-HRMS of compound **(*HydIstPypz*/13)**

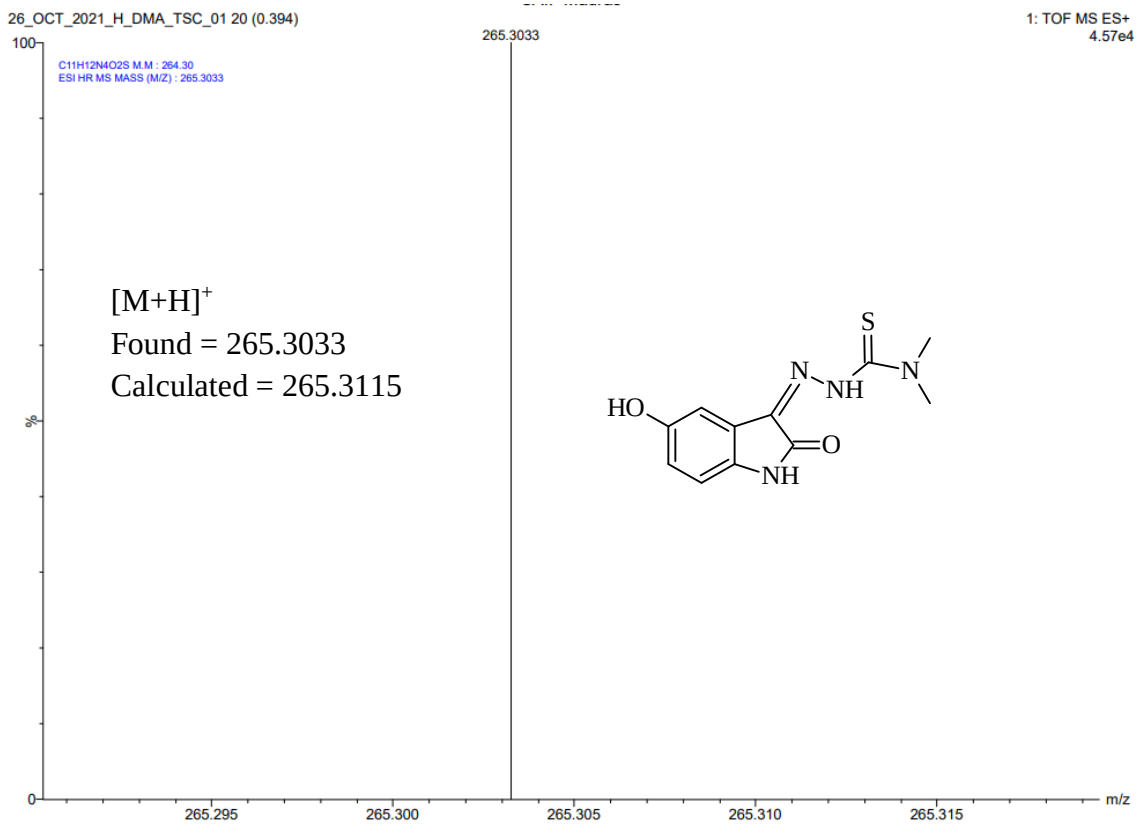

Appendix C14: ESI-HRMS of compound **(*HydIstDm*/14)**

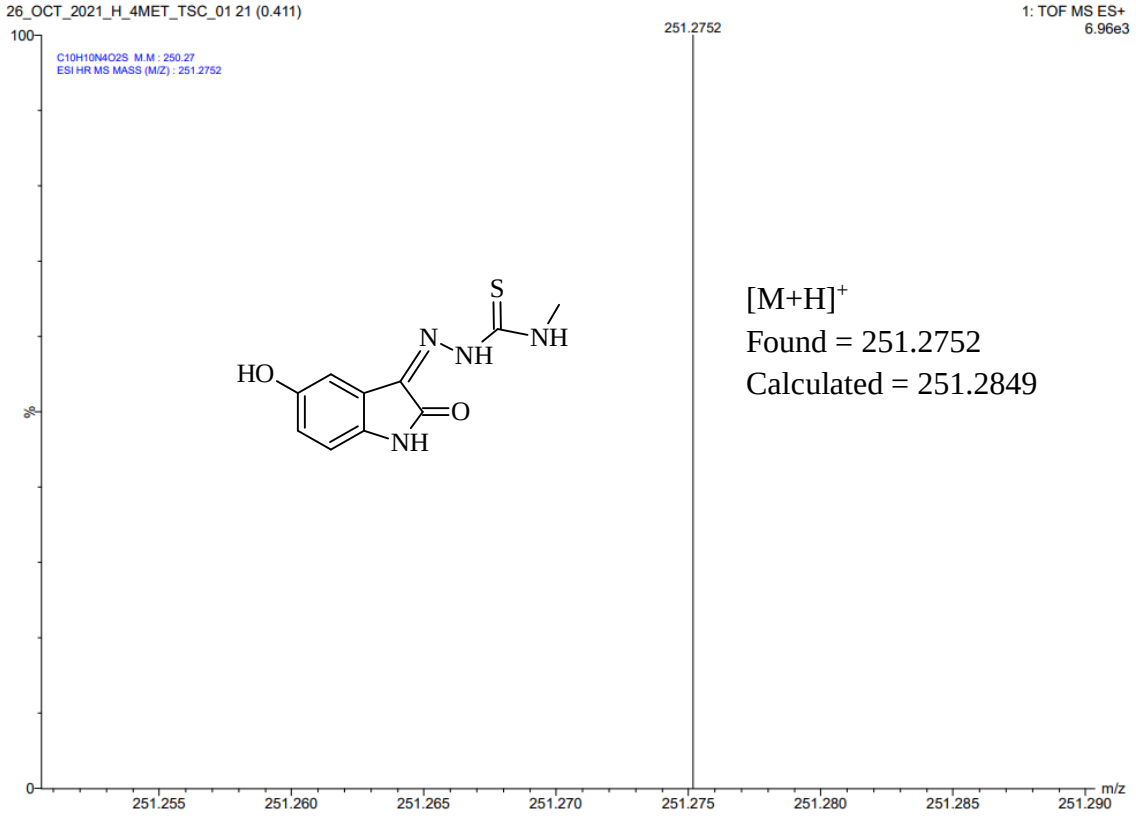

Appendix C15: ESI-HRMS of compound **(*HydIstMet*/15)**

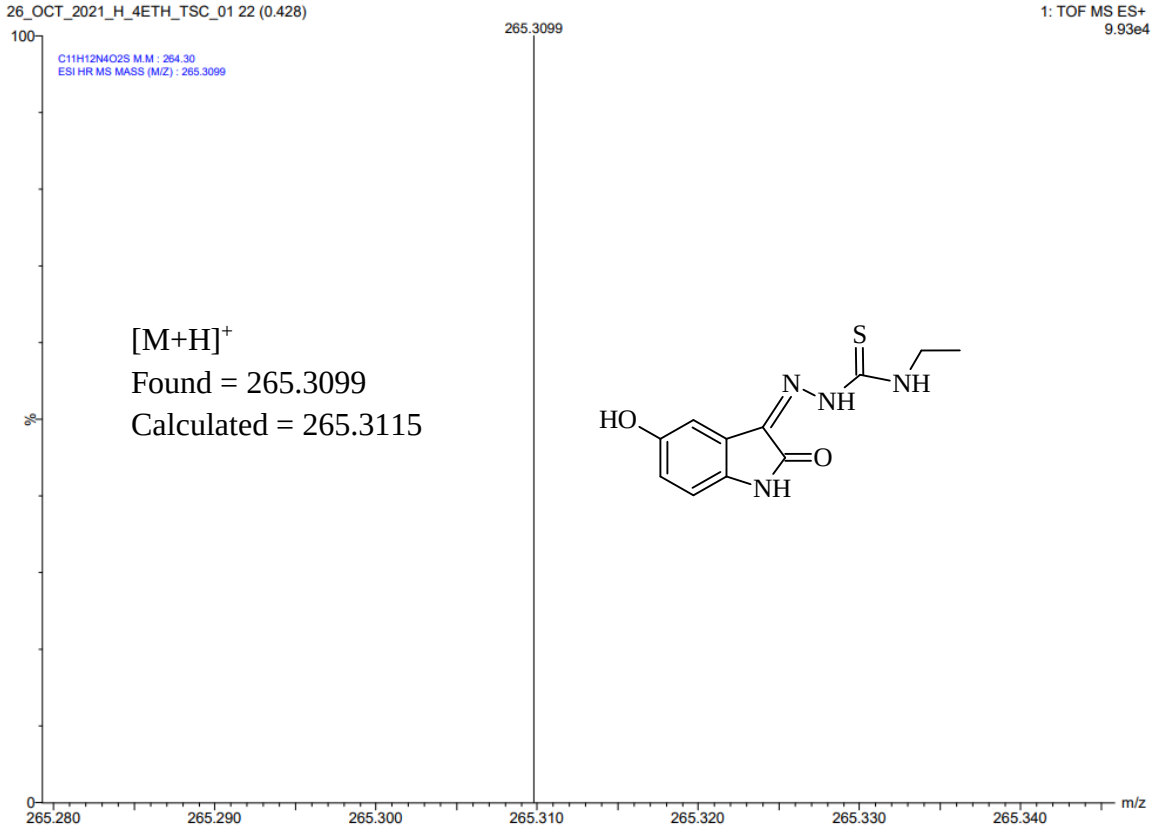

Appendix C16: ESI-HRMS of compound **(*HydIstEth*/16)**

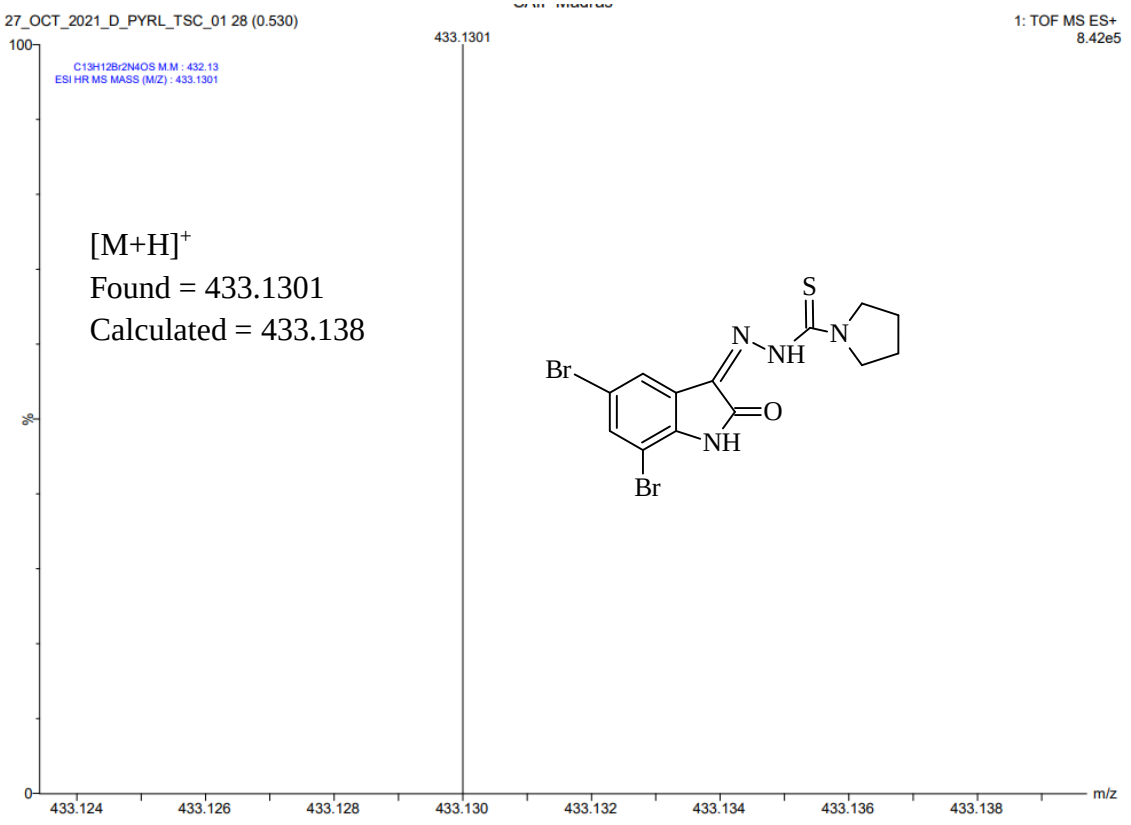

Appendix C17: ESI-HRMS of compound (***DiBrIstPyrl*/17)**

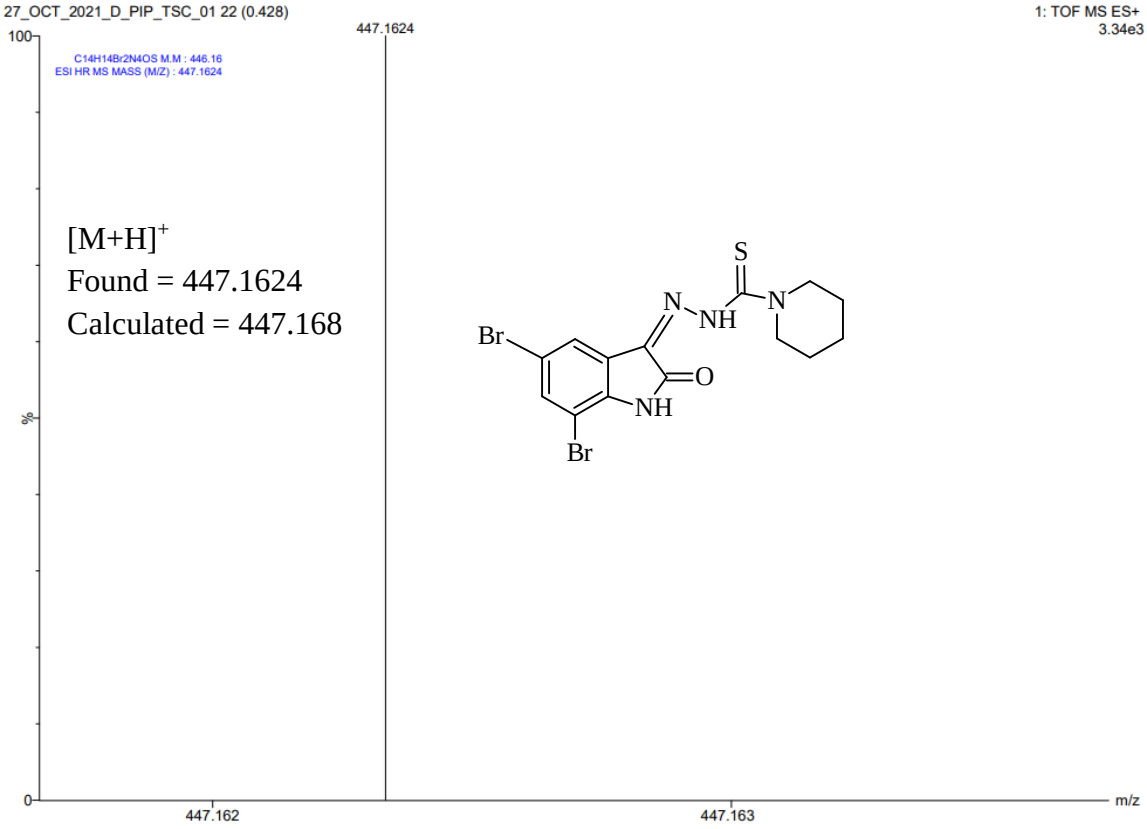

Appendix C18: ESI-HRMS of compound (***DiBrIstPip*/18)**

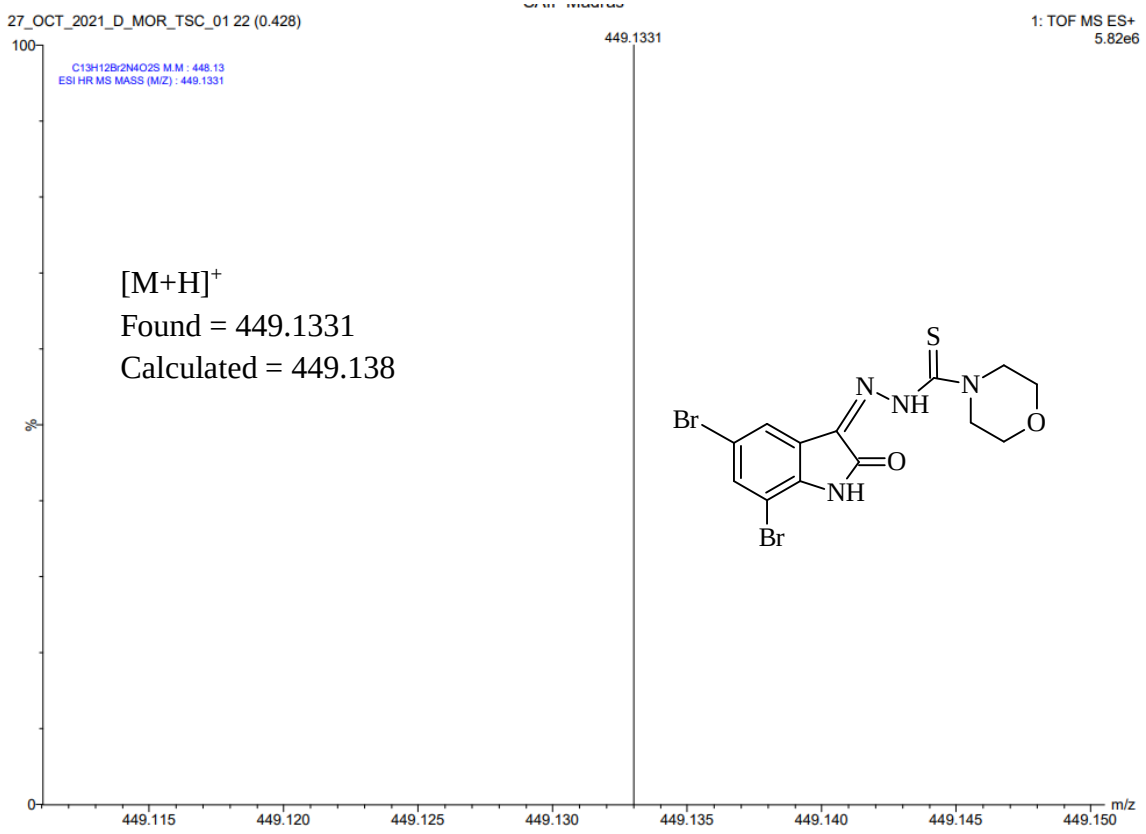

Appendix C19: ESI-HRMS of compound (***DiBrIstMor*/19)**

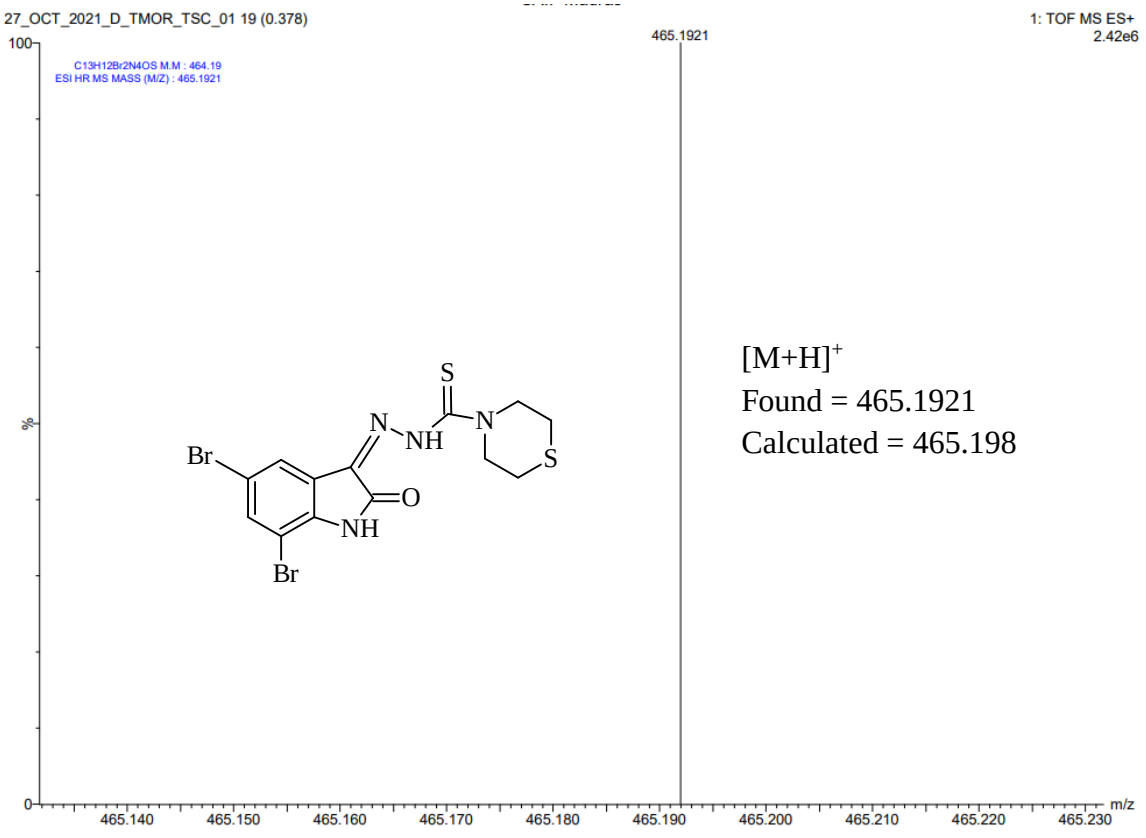

Appendix C20: ESI-HRMS of compound (***DiBrIstTmor*/20)**

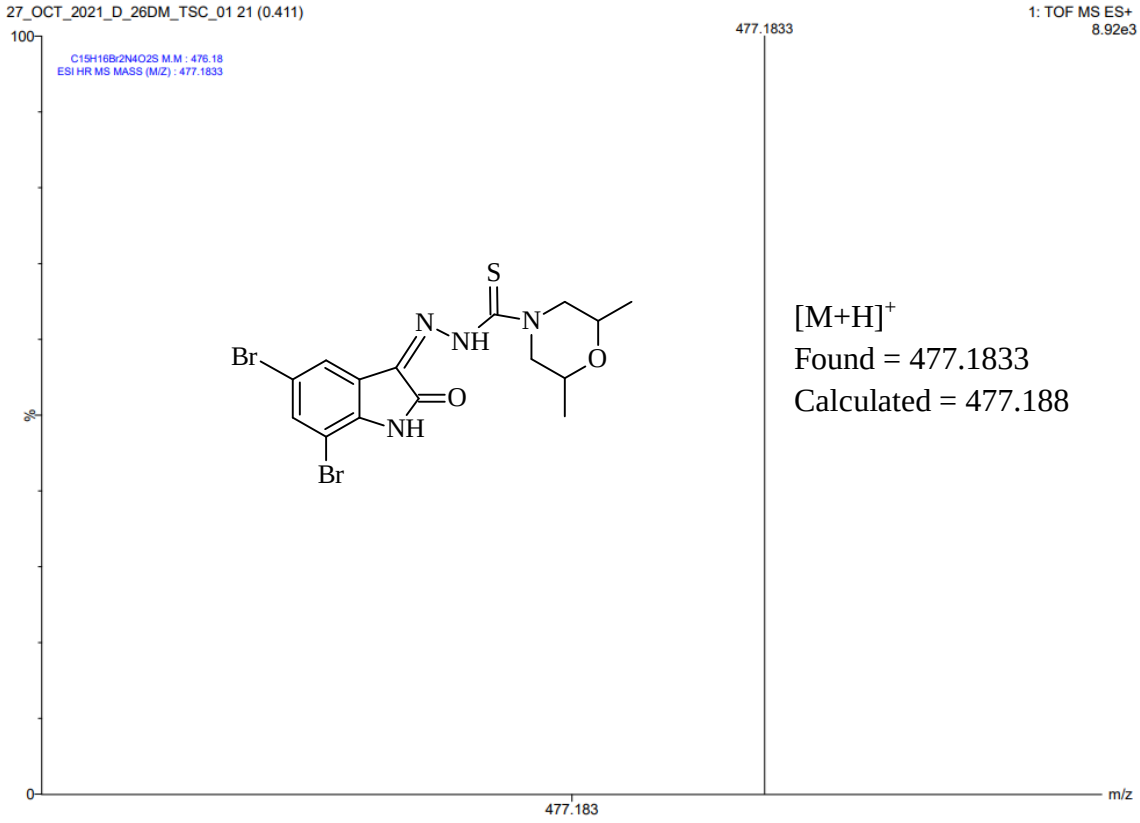

Appendix C21: ESI-HRMS of compound (***DiBrIstDmMor*/21)**

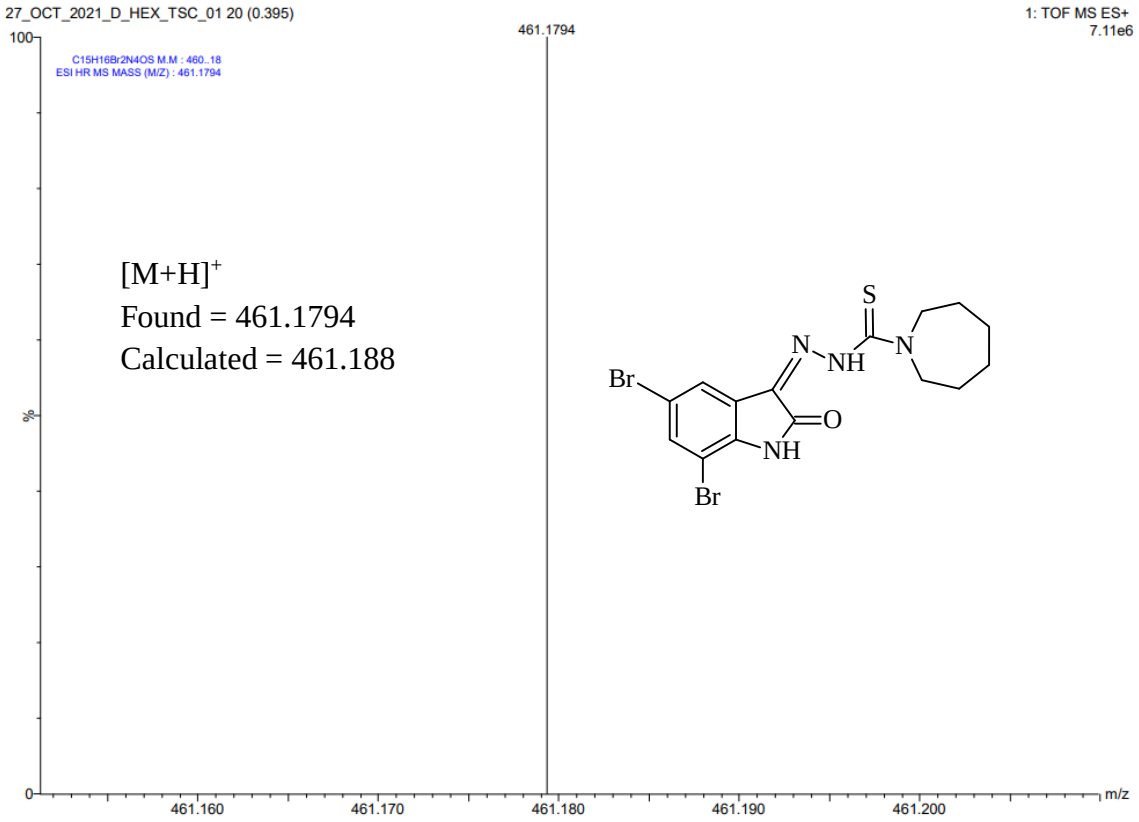

Appendix C22: ESI-HRMS of compound (***DiBrIstAzep*/22)**

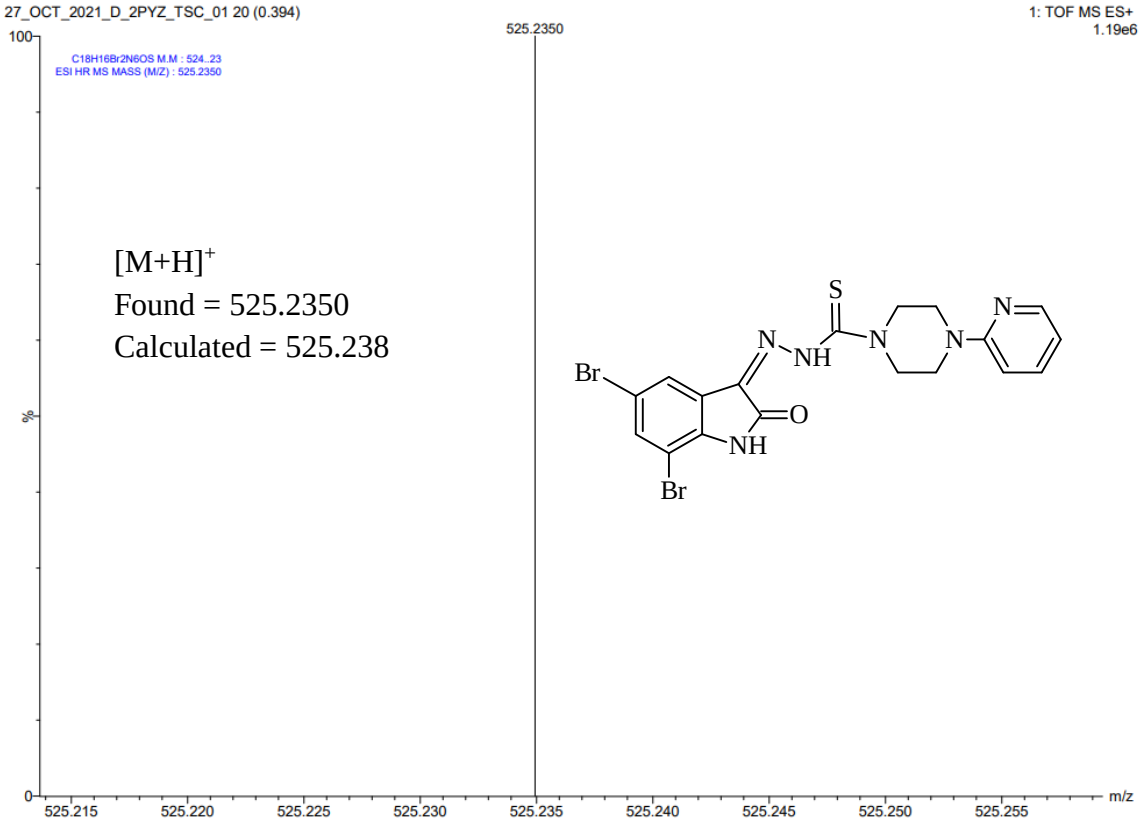

Appendix C23: ESI-HRMS of compound (***DiBrIstPypz*/23)**

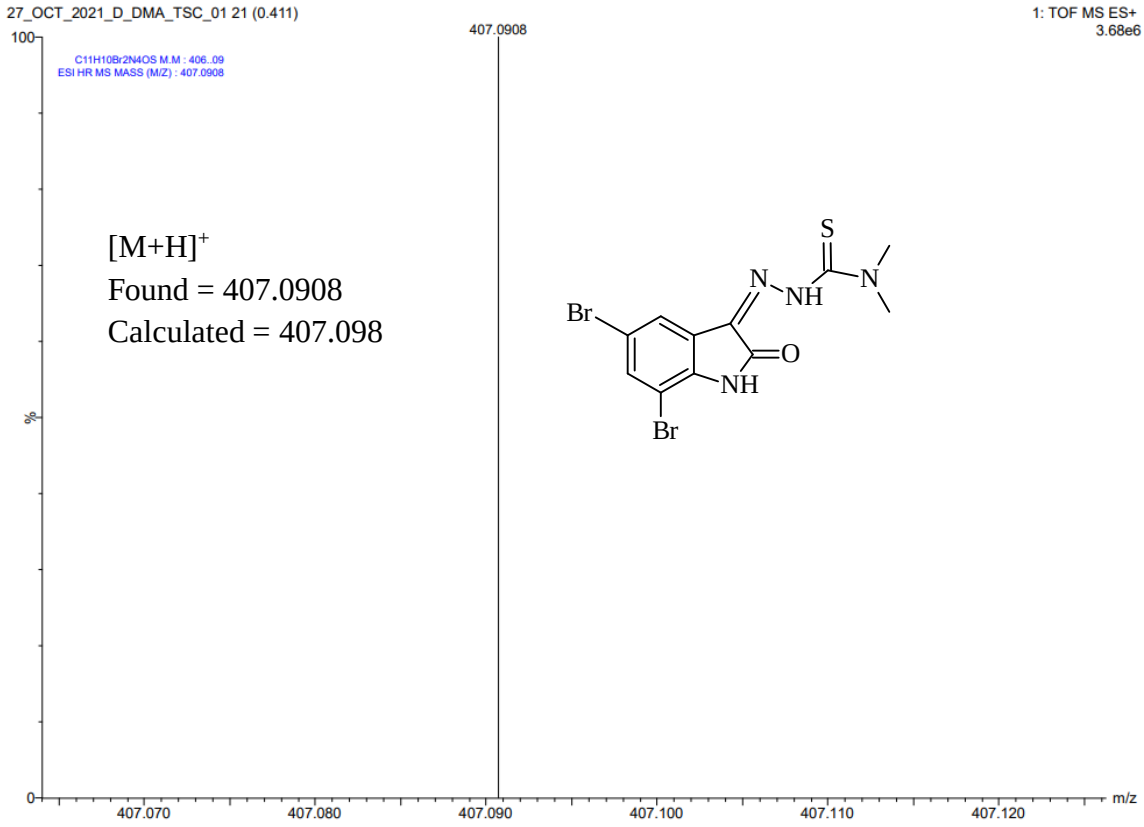

Appendix C24: ESI-HRMS of compound (***DiBrIstDm*/24)**

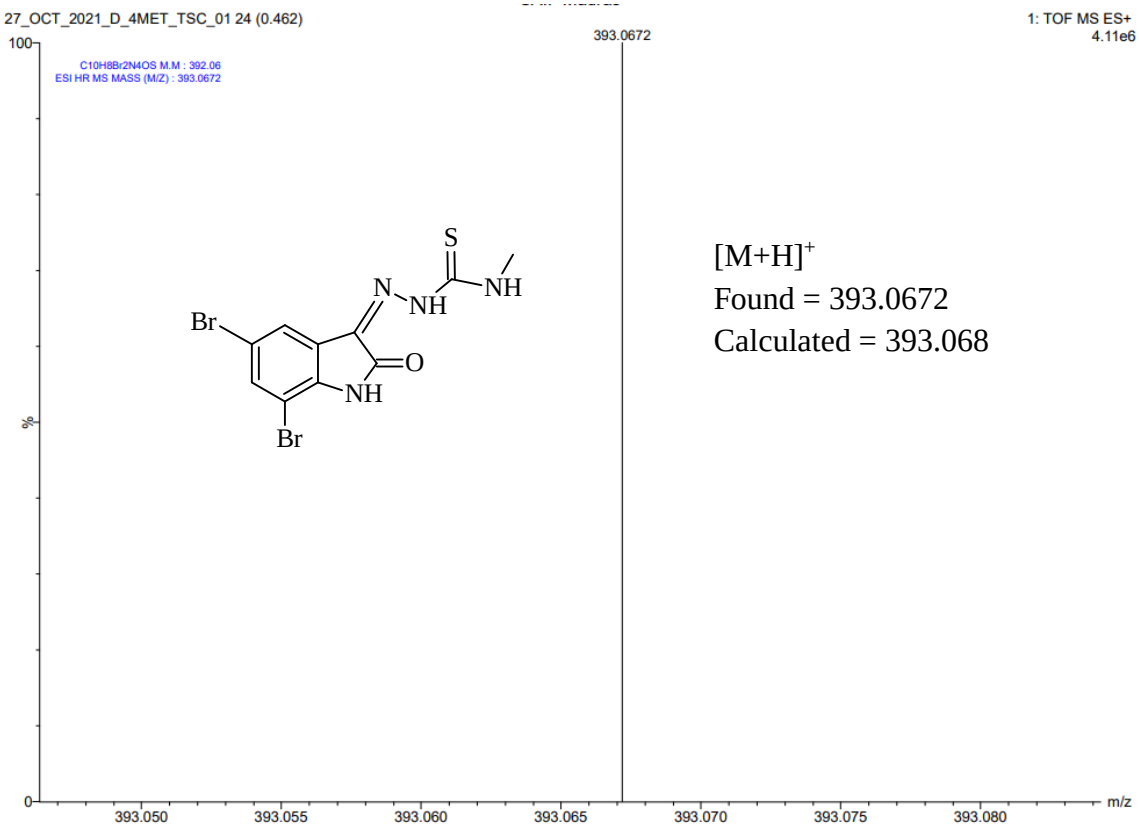

Appendix C25: ESI-HRMS of compound (***DiBrIstMet*/25)**

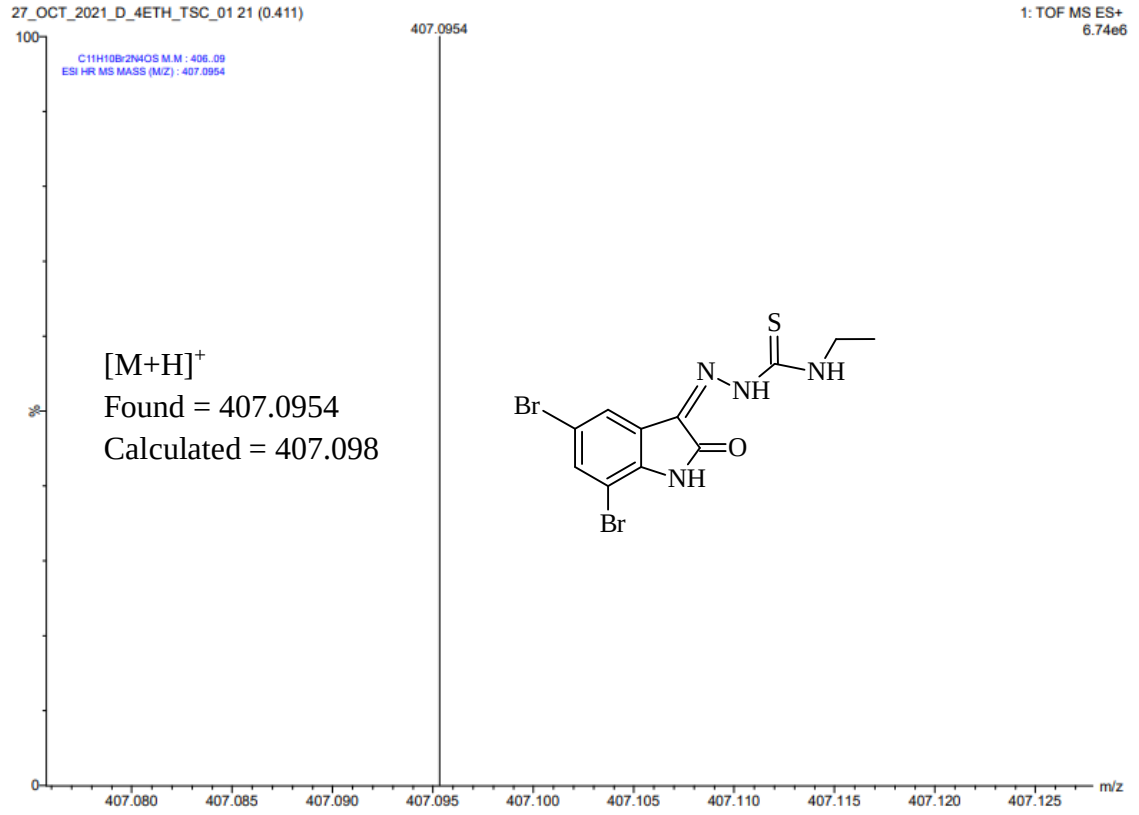

Appendix C26: ESI-HRMS of compound (***DiBrIstEth*/26)**

Appendix D

UV-Visible Spectra of TSCs

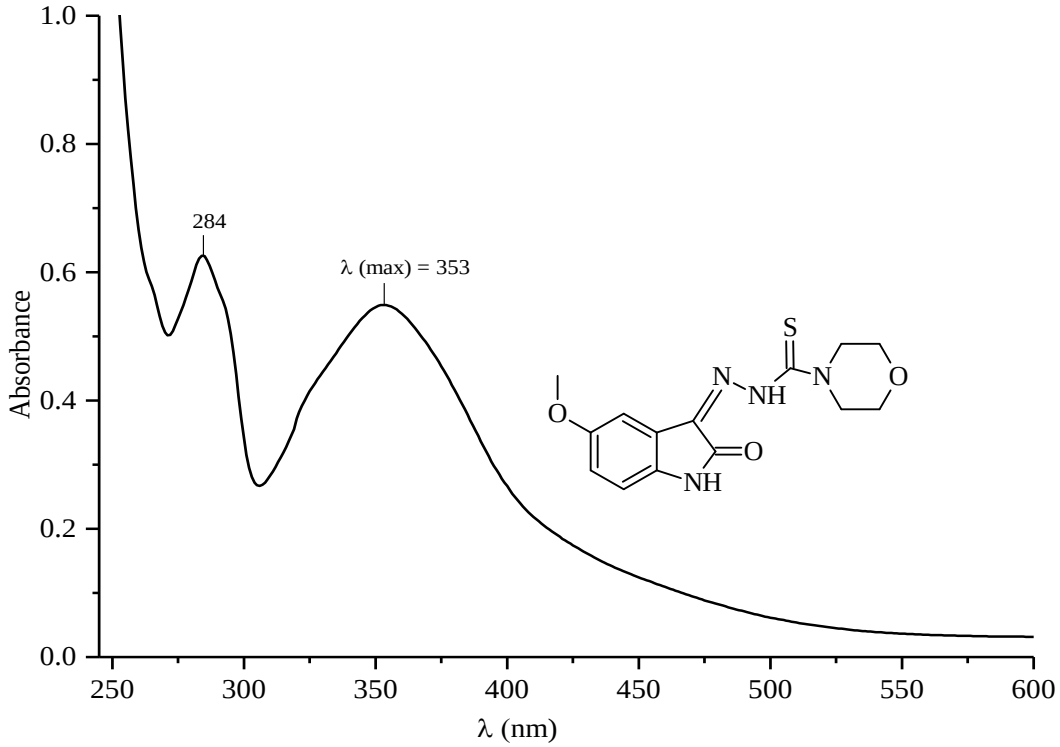

Appendix D1: UV-Visible spectra of compound (***MeOIstMor*/1)**

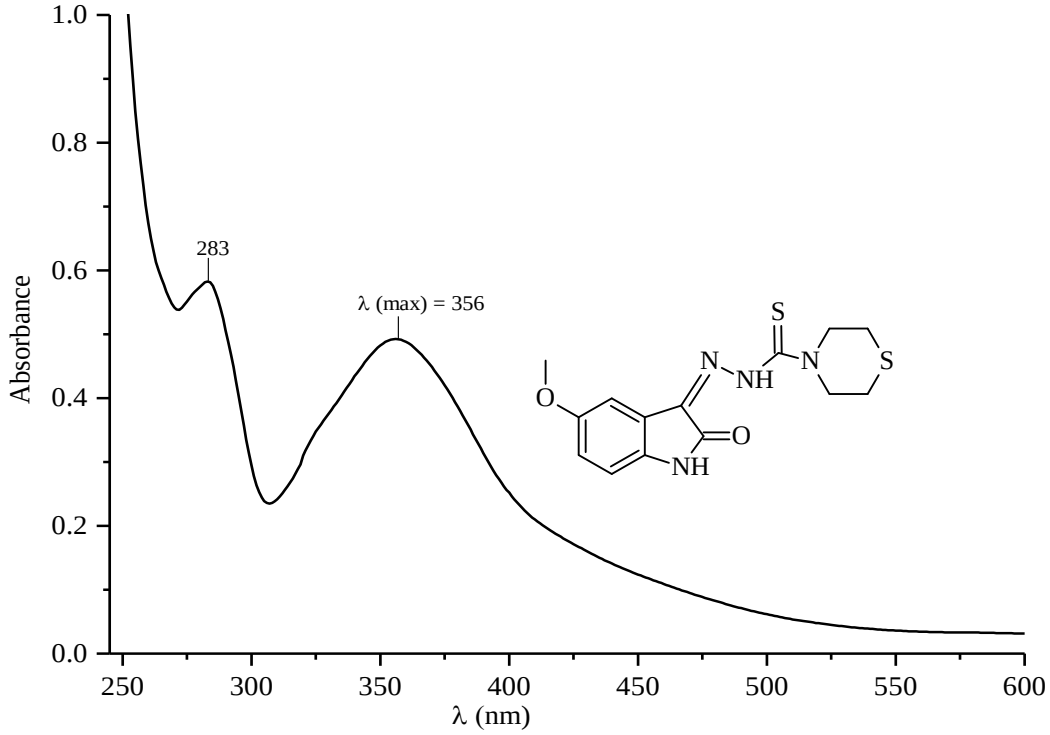

Appendix D2: UV-Visible spectra of compound ***MeOIstTmor*/2)**

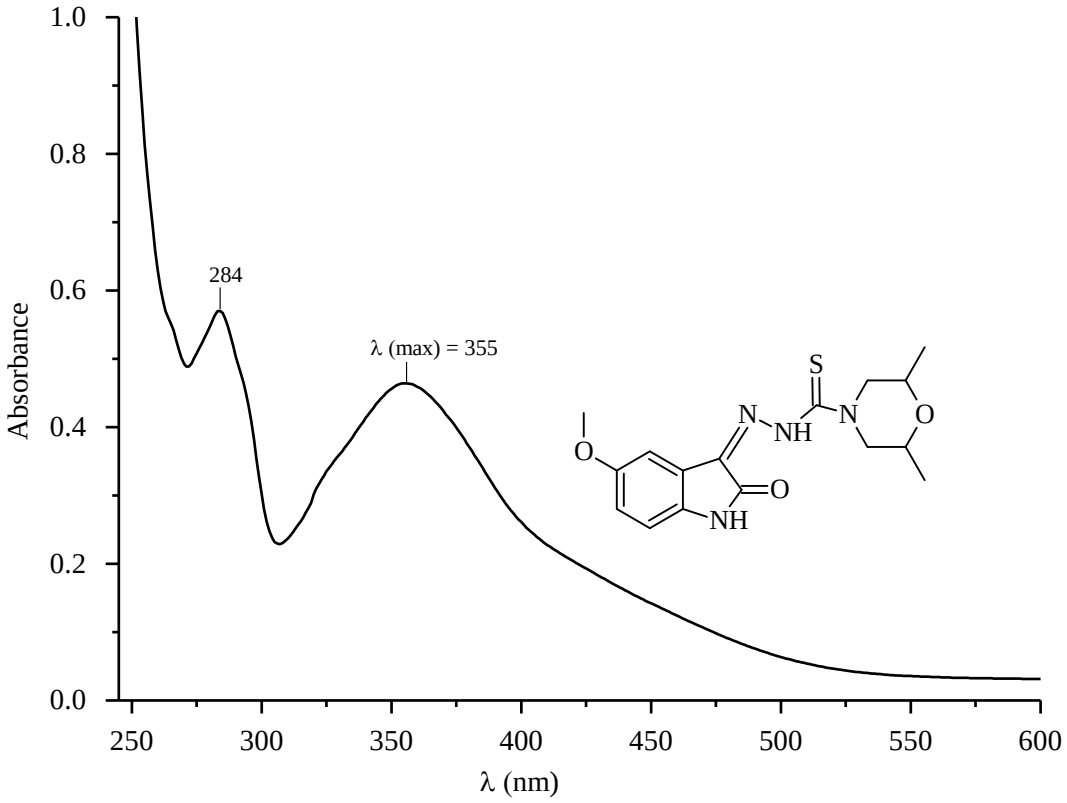

Appendix D3: UV-Visible spectra of compound (***MeOIstDmMor*/3)**

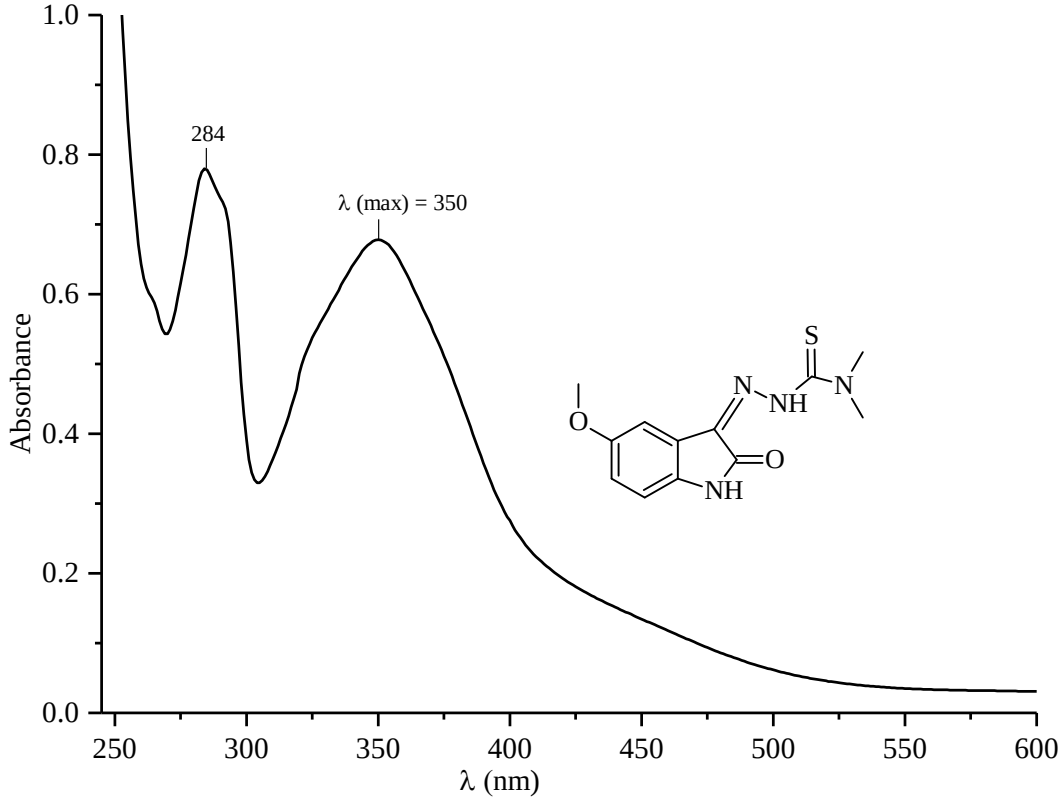

Appendix D4: UV-Visible spectra of compound (***MeOIstDm*/4)**

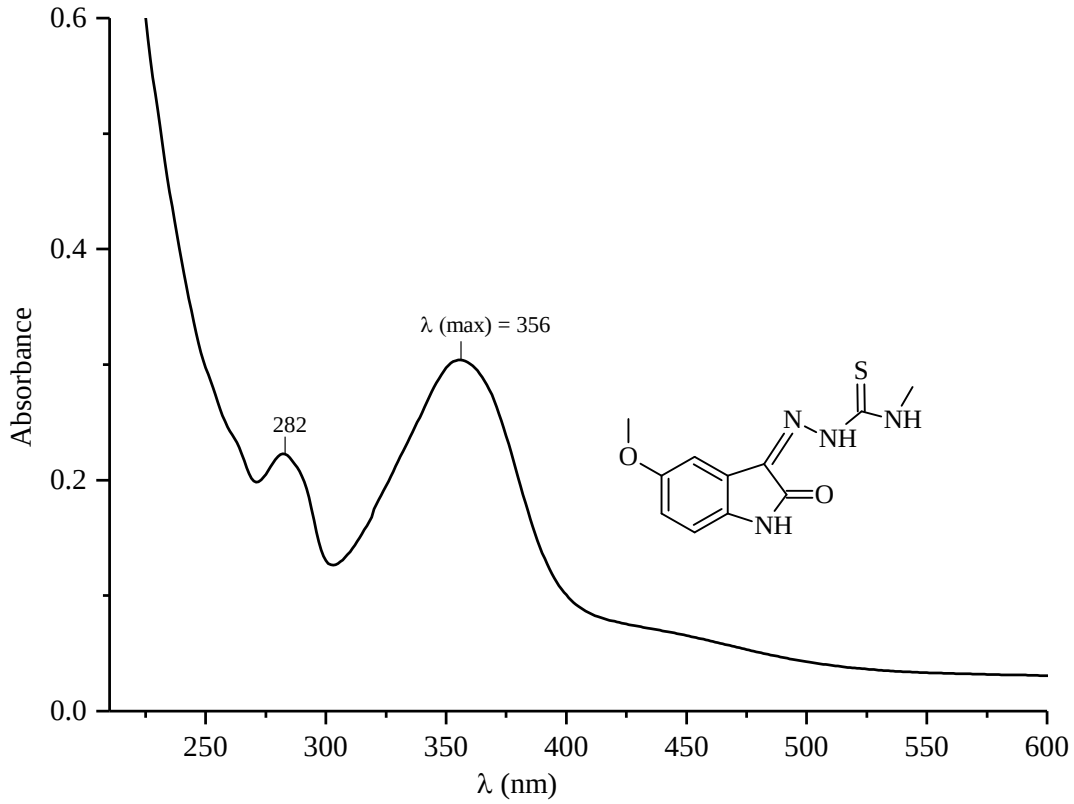

Appendix D5: UV-Visible spectra of compound (***MeOIstMet*/5)**

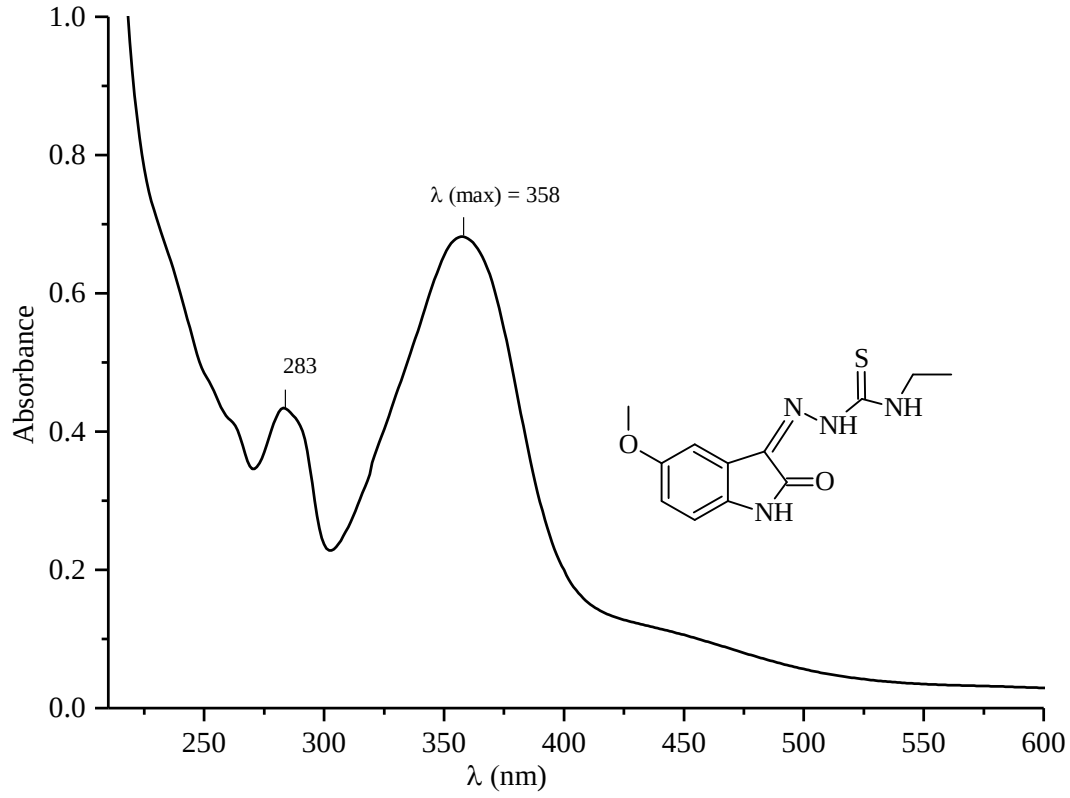

Appendix D6: UV-Visible spectra of compound (***MeOIstEth*/6)**

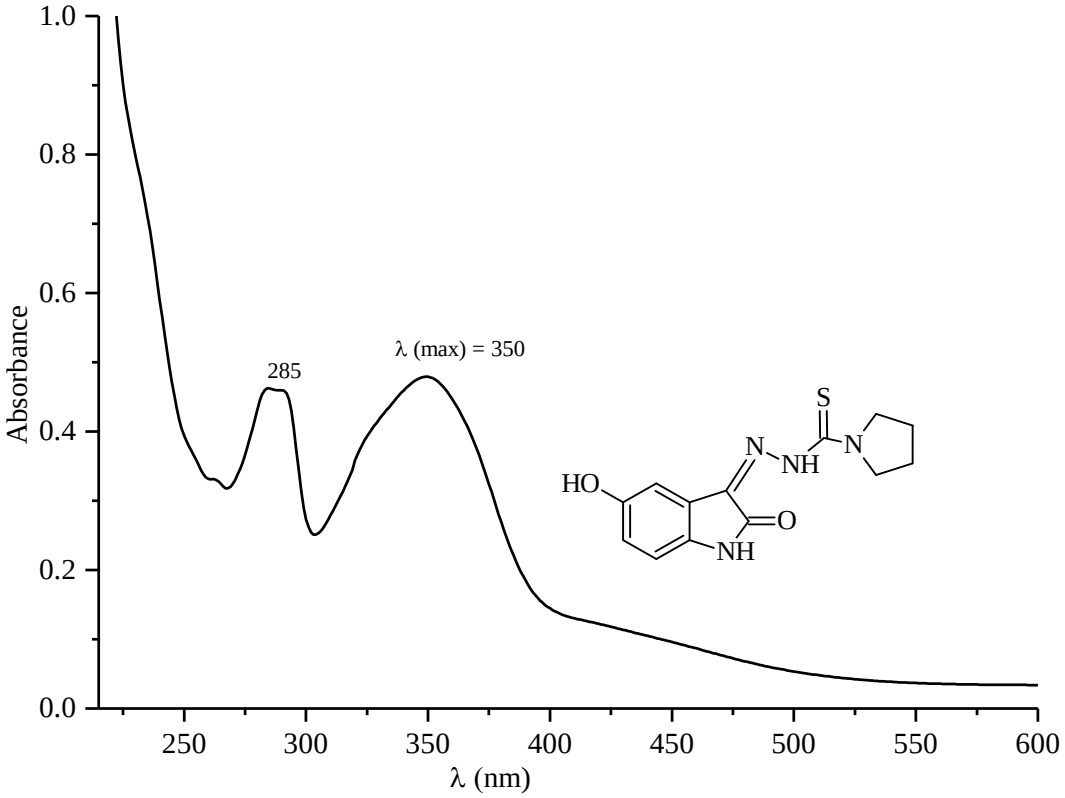

Appendix D7: UV-Visible spectra of compound (***HydIstPyrl*/7)**

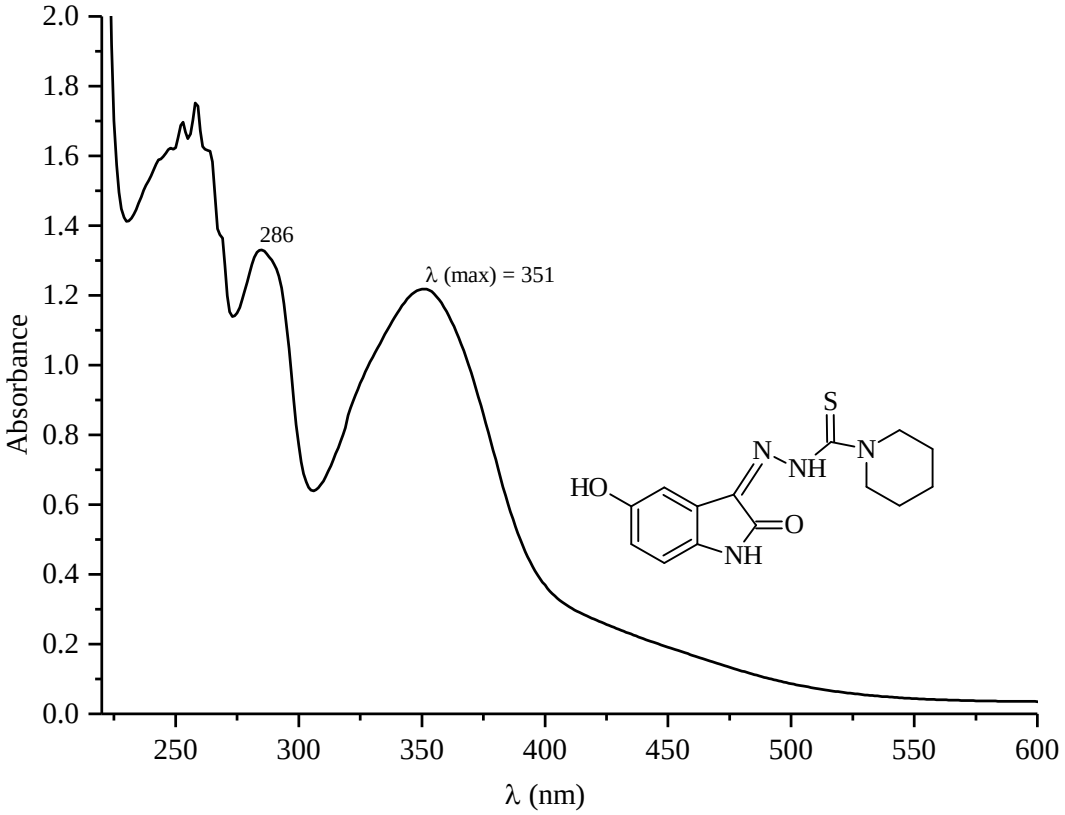

Appendix D8: UV-Visible spectra of compound (***HydIstPip*/8)**

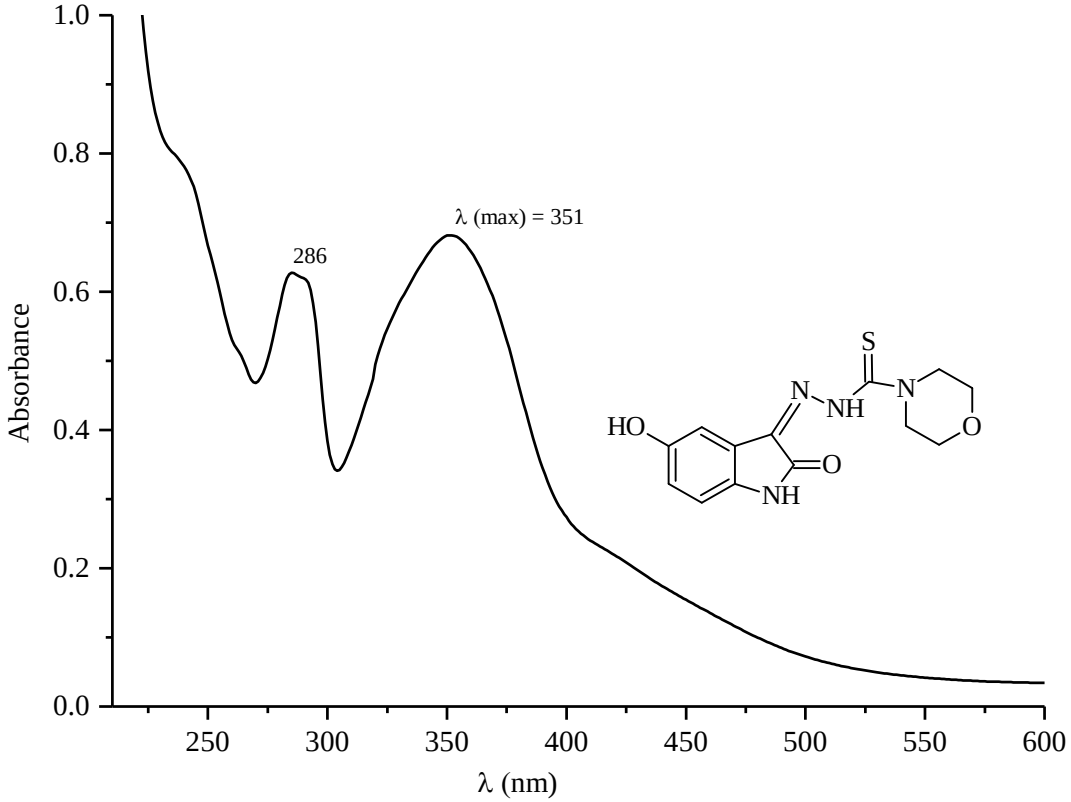

Appendix D9: UV-Visible spectra of compound (***HydIstMor*/9)**

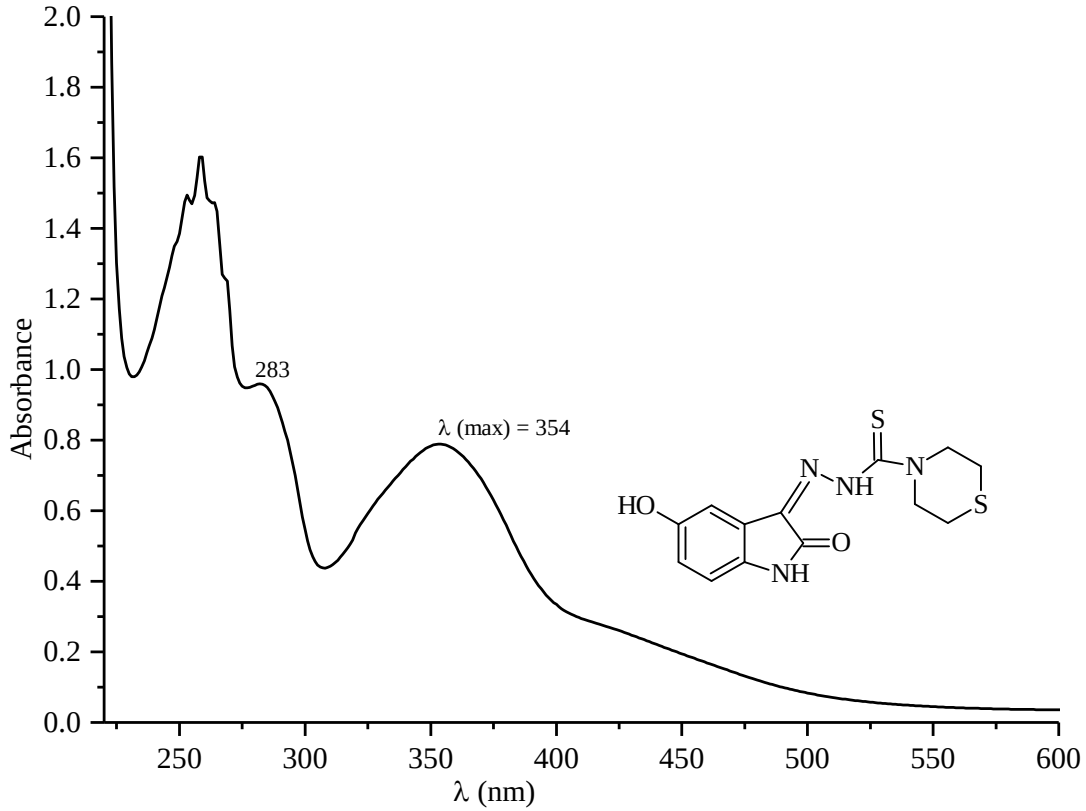

Appendix D10: UV-Visible spectra of compound (***HydIstTmor*/10)**

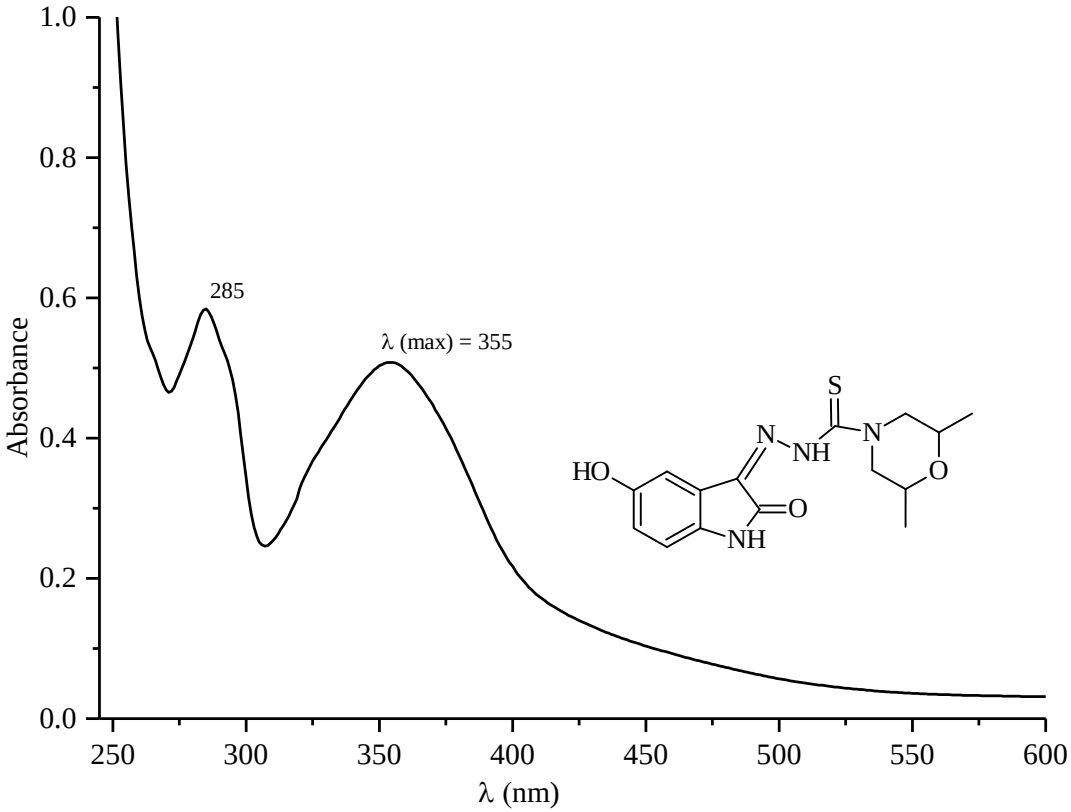

Appendix D11: UV-Visible spectra of compound (***HydIstDmMor*/11)**

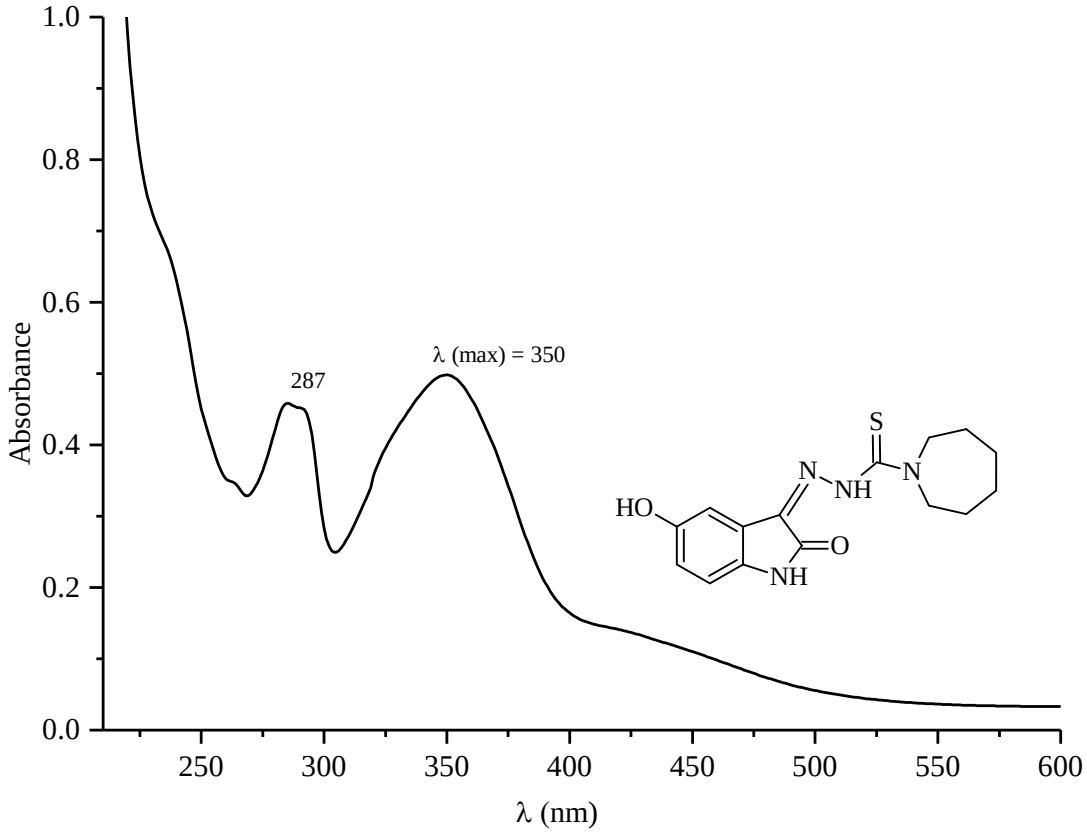

Appendix D12: UV-Visible spectra of compound (***HydIstAzep*/12)**

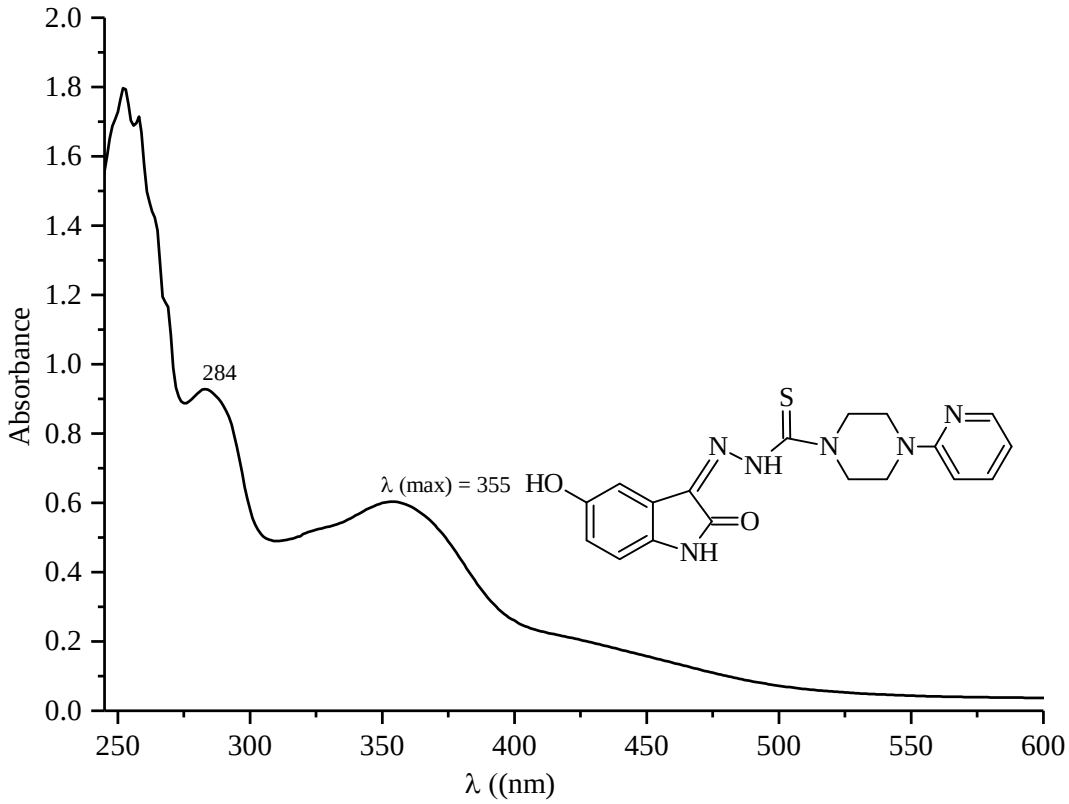

Appendix D13: UV-Visible spectra of compound (***HydIstPypz***/**13)**

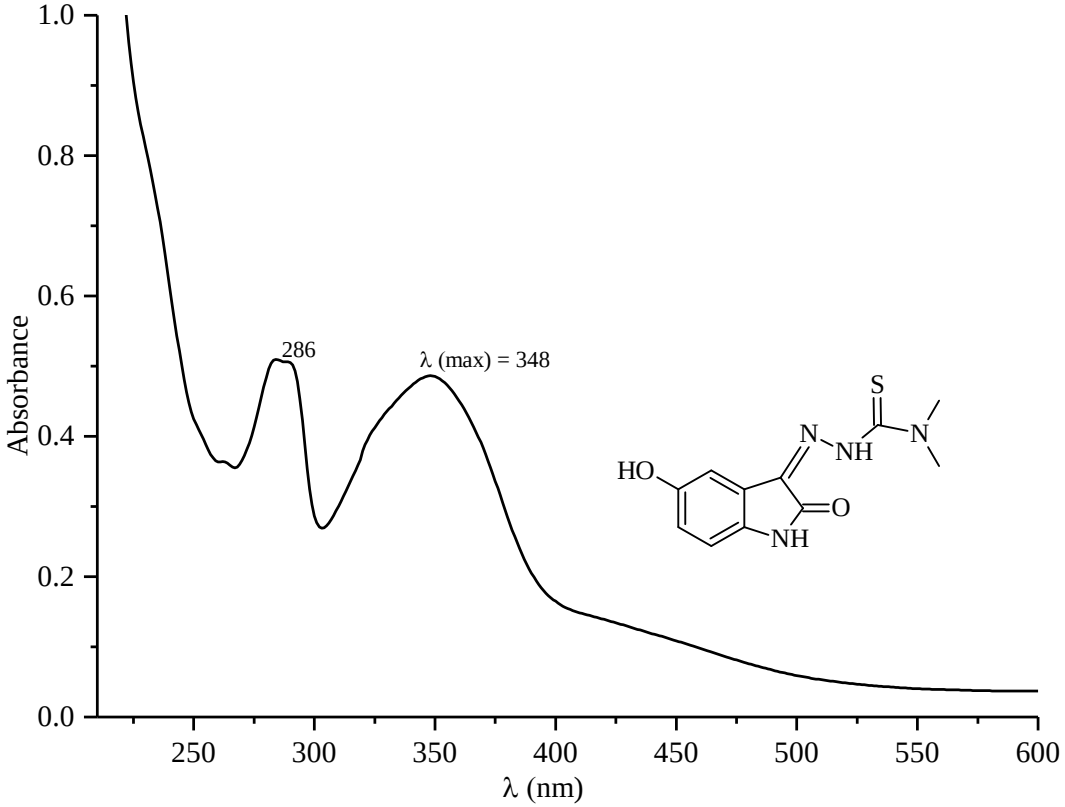

Appendix D14: UV-Visible spectra of compound (***HydIstDm***/**14)**

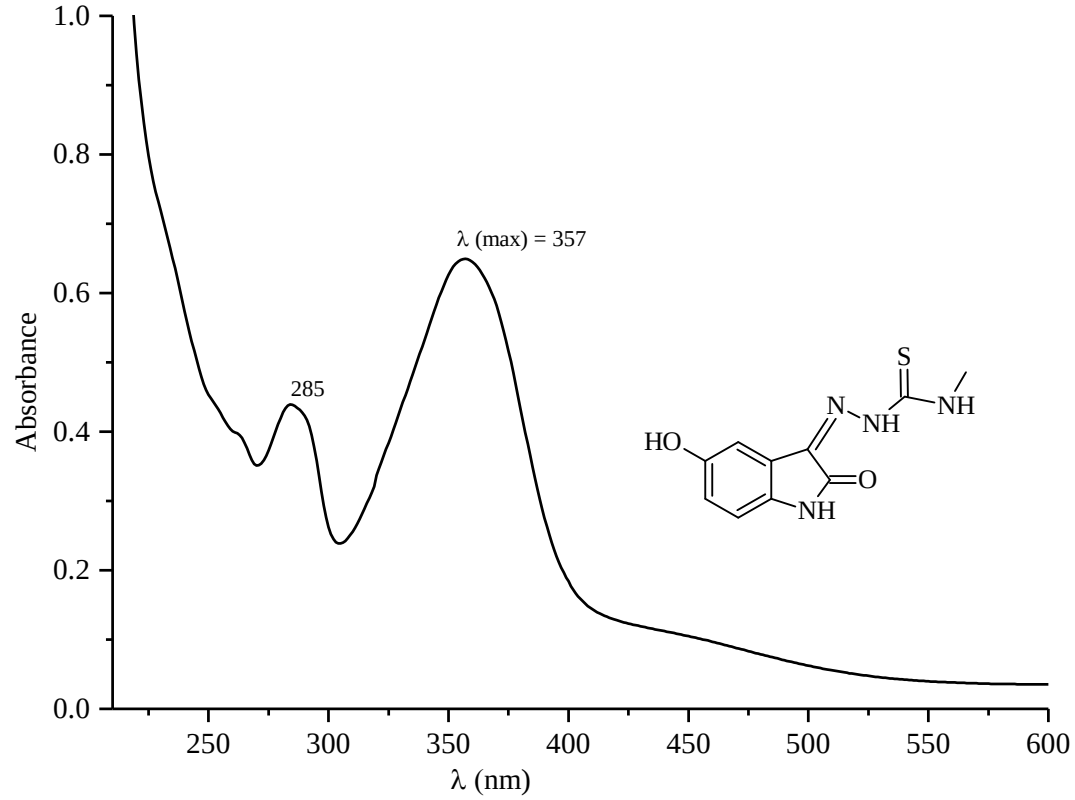

Appendix D15: UV-Visible spectra of compound (***HydIstMet*/15)**

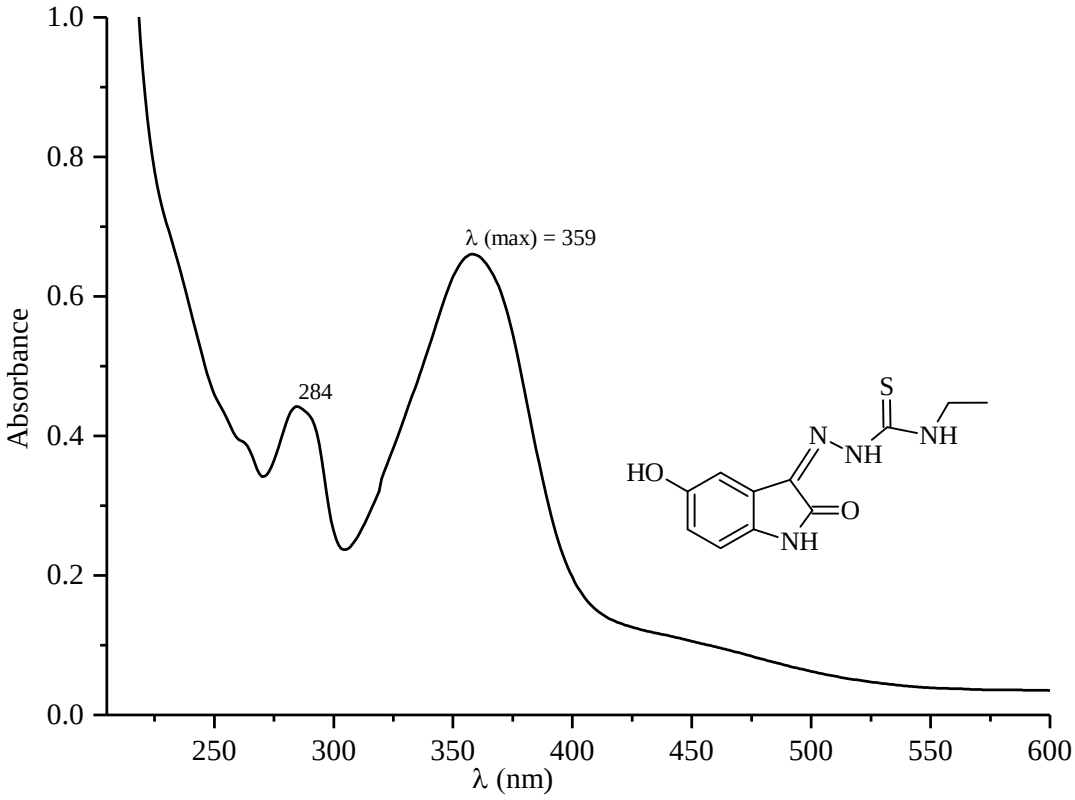

Appendix D16: UV-Visible spectra of compound (***HydIstEth*/16)**

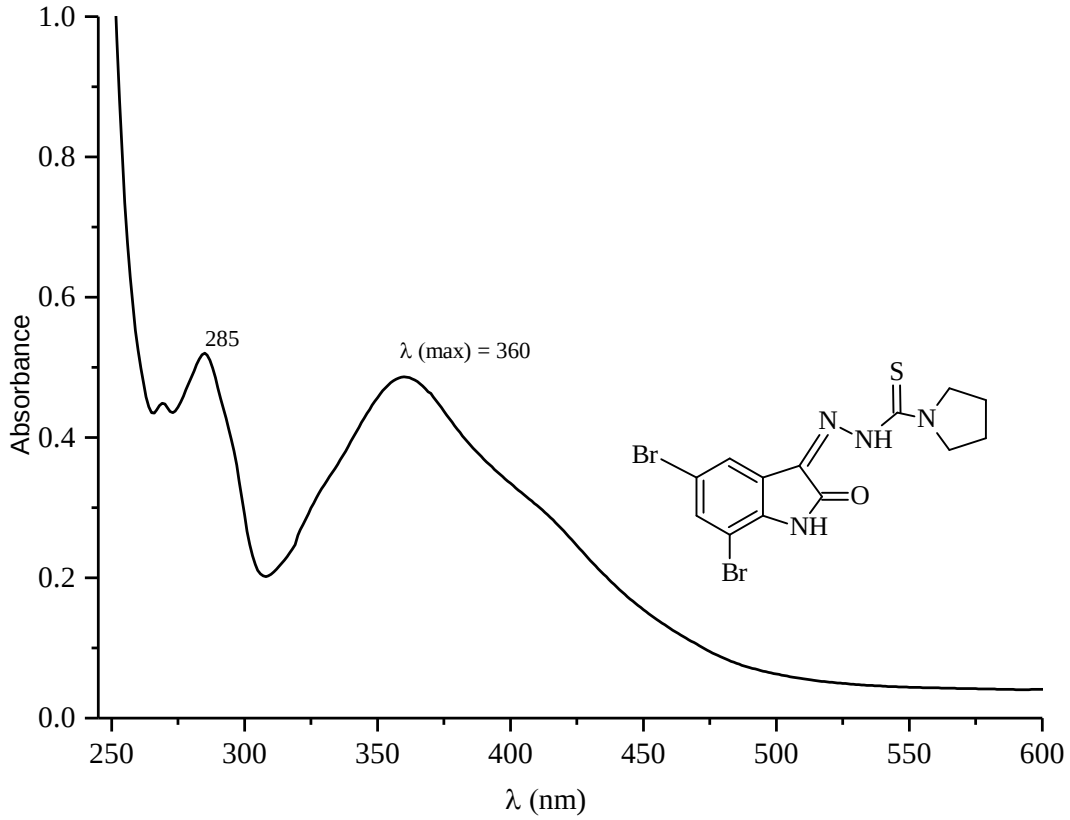

Appendix D17: UV-Visible spectra of compound (***DiBrIstPyrl*/17)**

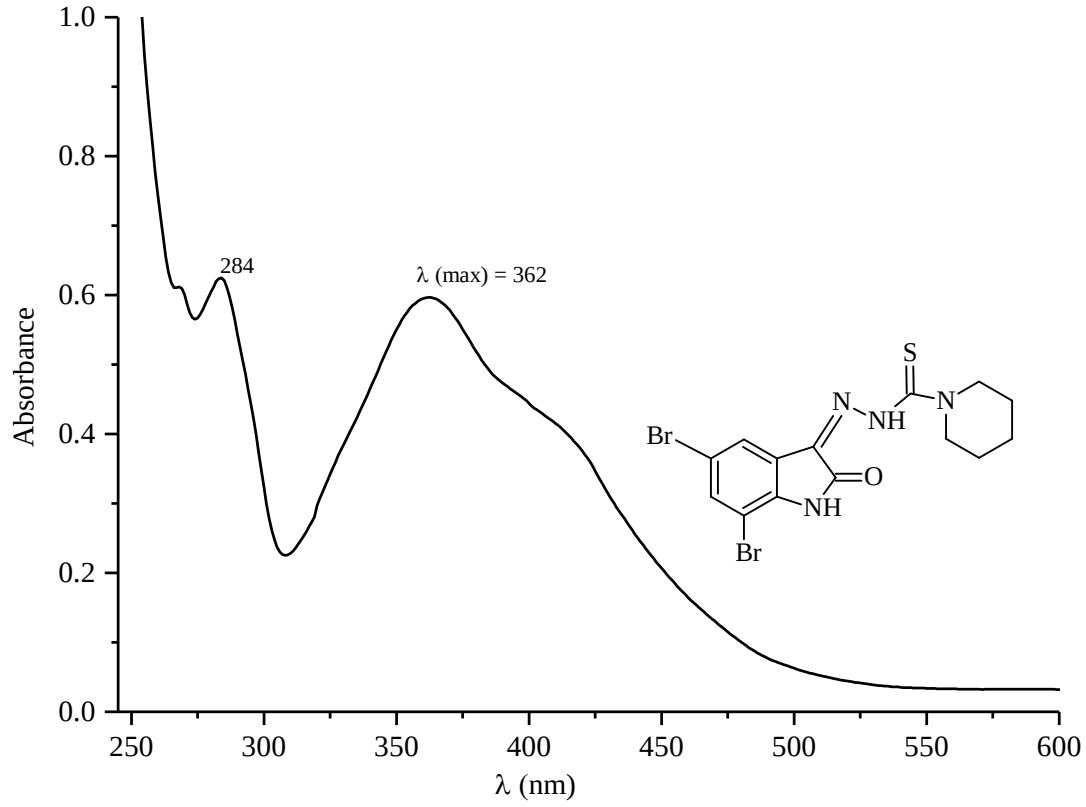

Appendix D18: UV-Visible spectra of compound (***DiBrIstPip*/18)**

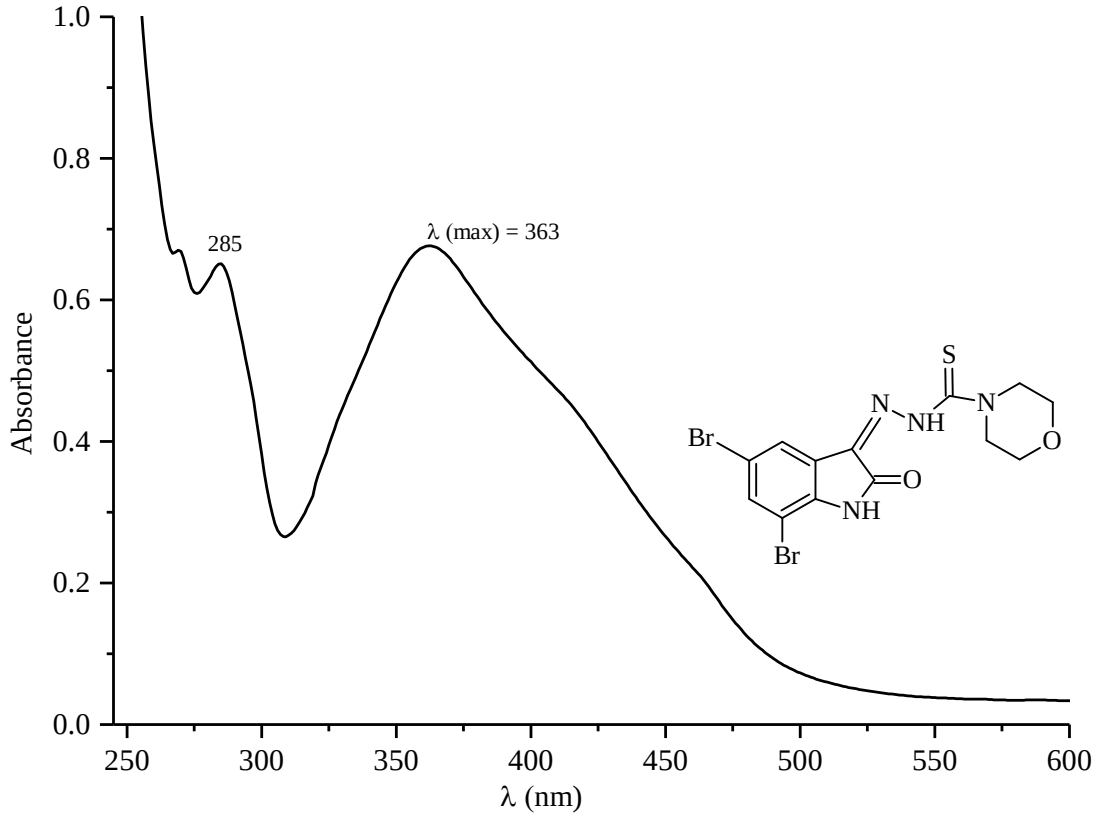

Appendix D19: UV-Visible spectra of compound (***DiBrIstMor*/19)**

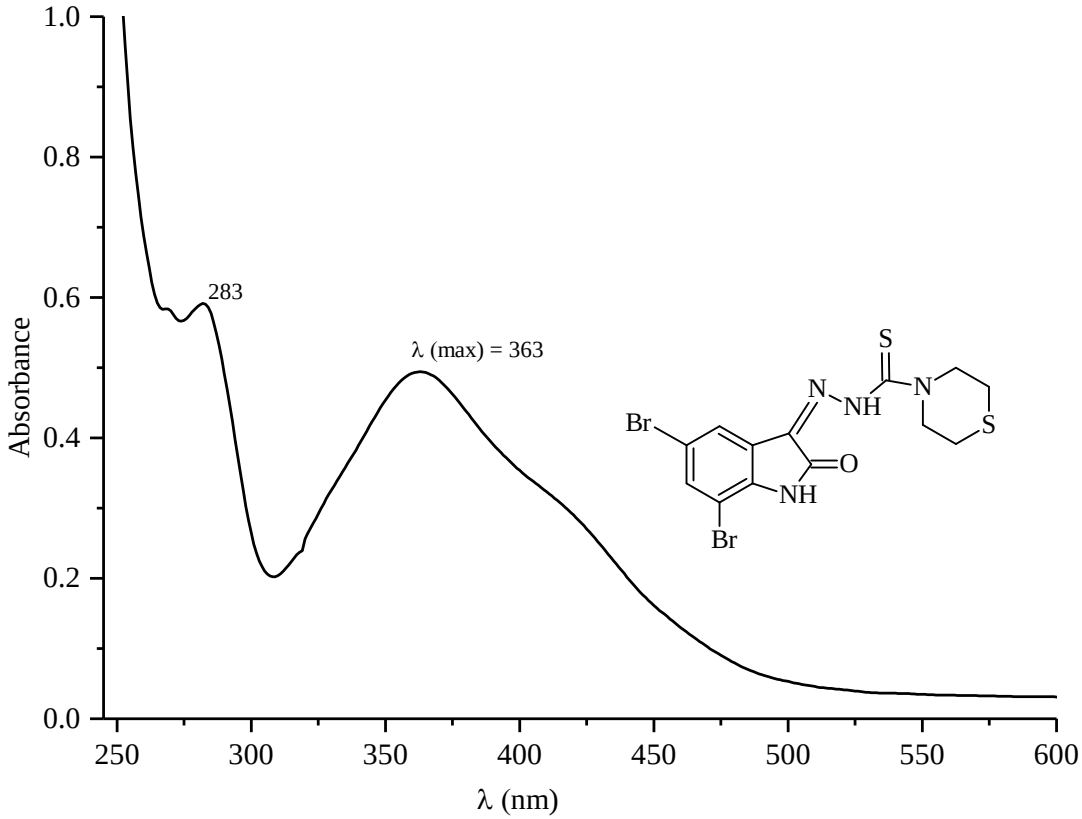

Appendix D20: UV-Visible spectra of compound (***DiBrIstTmor*/20)**

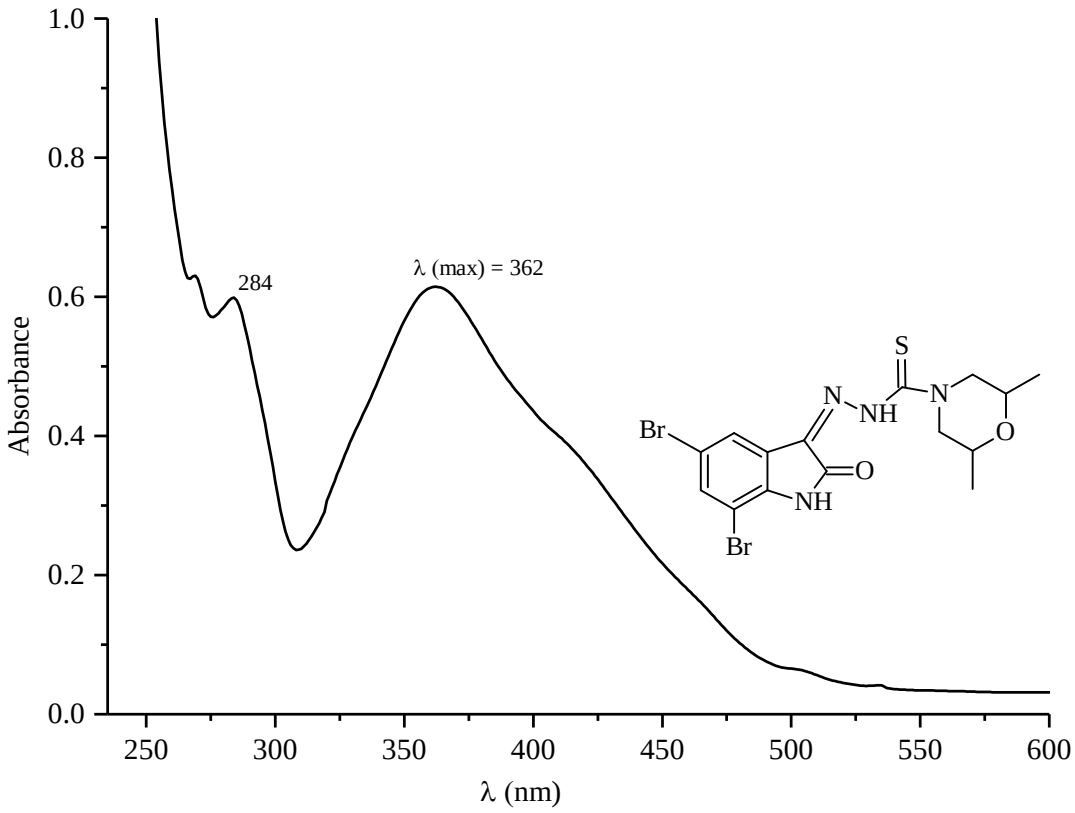

Appendix D21: UV-Visible spectra of compound (***DiBrIstDmMor***/**21)**

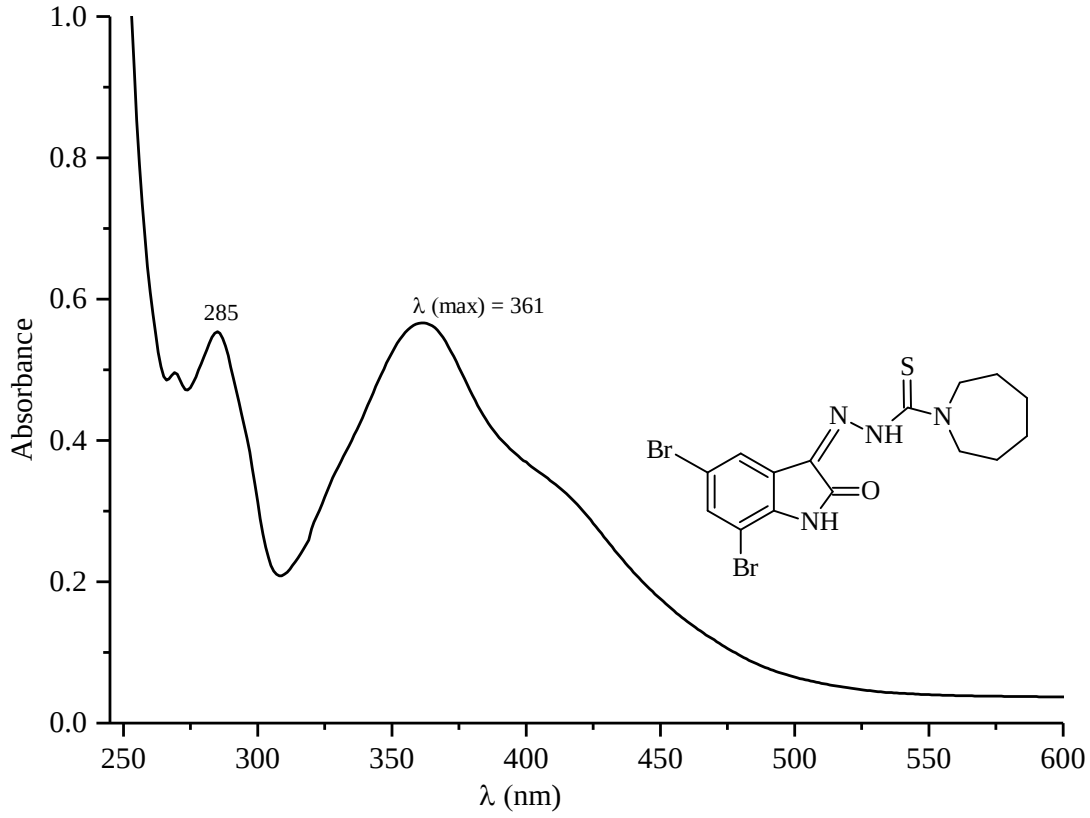

Appendix D22: UV-Visible spectra of compound (***DiBrIstAzep***/**22)**

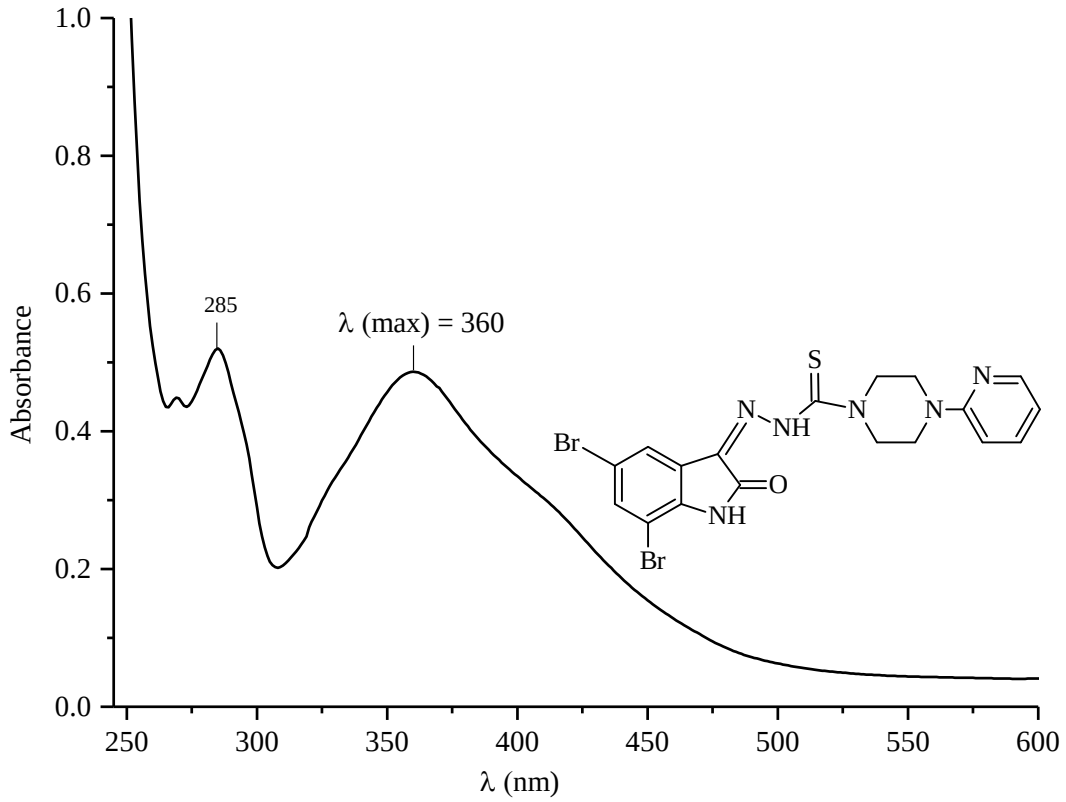

Appendix D23: UV-Visible spectra of compound (***DiBrIstPypz***/**23)**

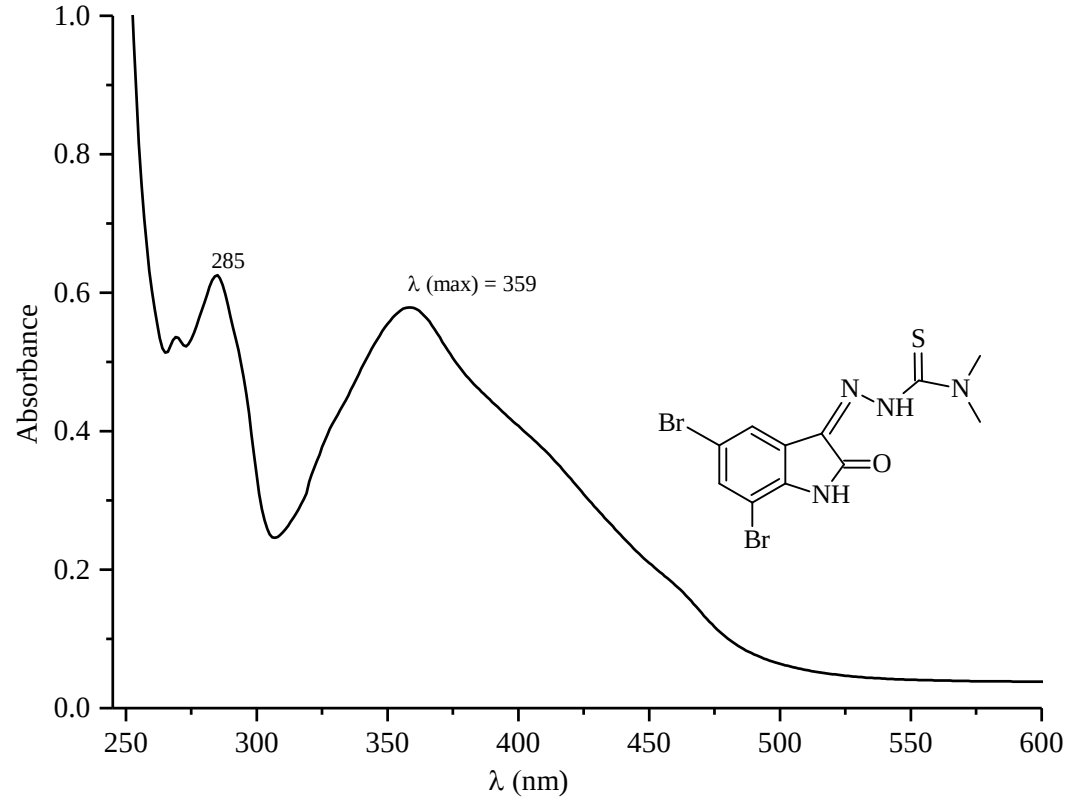

Appendix D24: UV-Visible spectra of compound (***DiBrIstDm***/**24)**

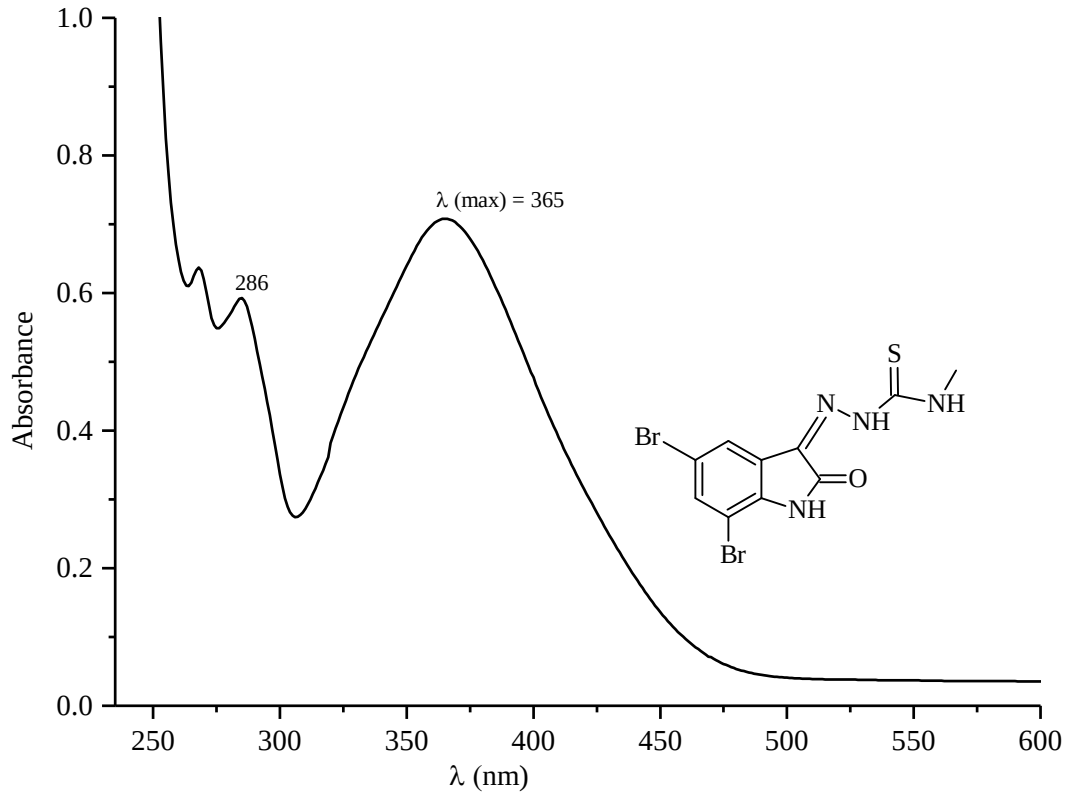

Appendix D25: UV-Visible spectra of compound (***DiBrIstMet*/25)**

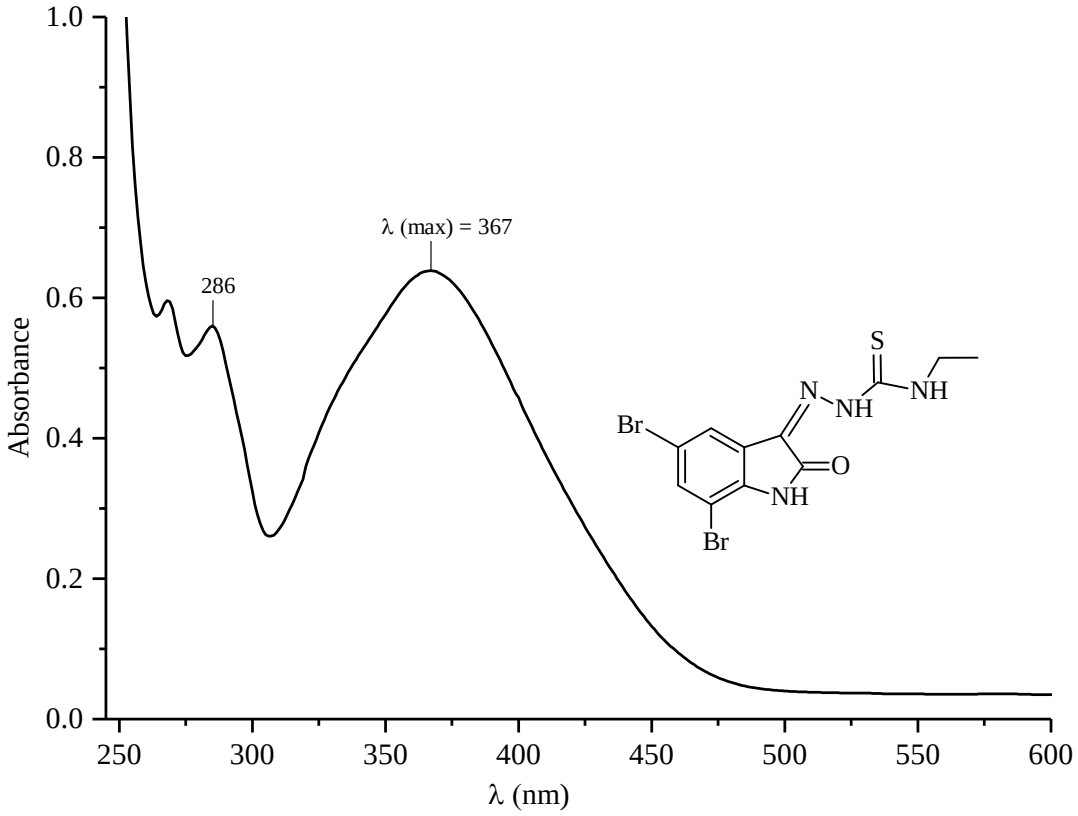

Appendix D26: UV-Visible spectra of compound (***DiBrIstEth*/26)**

Appendix E

Appendix E1

The ORTEP view of compound (***MeOIstDmMor*/3)** [**CCDC** reference No. = 2194145]

Table: Crystal data and structure refinement for compound **3**

Identification code	***MeOIstDmMor***
Empirical formula	$C_{16}H_{22}N_4O_4S$
Formula weight	366.43
Temperature/K	296.15
Crystal system	Orthorhombic
Space group	$Pna2_1$
a/Å	16.091(3)
b/Å	8.6078(14)
c/Å	27.098(5)
α/°	90
β/°	90
γ/°	90
Volume/Å^3	3753.3(11)
Z	8
ρ_{calc}g/cm^3	1.297
μ/mm^{-1}	0.200
F(000)	1552.0
Crystal size/mm^3	0.15 × 0.12 × 0.1

Radiation	MoKα (λ = 0.71073)
2Θ range for data collection/°	6.932 to 49.998
Index ranges	$-19 \leq h \leq 19$, $-10 \leq k \leq 10$, $-32 \leq l \leq 32$
Reflections collected	74084
Independent reflections	6574 [R_{int} = 0.1318, R_{sigma} = 0.0648]
Data/restraints/parameters	6574/25/467
Goodness-of-fit on F^2	1.202
Final R indexes [I>=2σ (I)]	R_1 = 0.0997, wR_2 = 0.1943
Final R indexes [all data]	R_1 = 0.1280, wR_2 = 0.2063
Largest diff. peak/hole / e $Å^{-3}$	0.34/-0.30
Flack parameter	0.10(9)

Table: Bond lengths for compound **3**

Atom	Atom	Length/Å	Atom	Atom	Length/Å
C1	O1	1.411(12)	C18	C19	1.389(14)
C2	C3	1.374(13)	C18	C23	1.415(14)
C2	C7	1.396(14)	C18	O4	1.382(12)
C2	O1	1.378(12)	C19	C20	1.407(12)
C3	C4	1.425(12)	C20	C21	1.391(12)
C4	C5	1.405(12)	C20	C24	1.440(14)
C4	C8	1.424(13)	C21	C22	1.368(14)
C5	C6	1.361(13)	C21	N5	1.396(12)
C5	N1	1.405(12)	C22	C23	1.399(15)

Table: Bond lengths for compound **3**

Atom	Atom	Length/Å	Atom	Atom	Length/Å
C6	C7	1.389(14)	C24	C25	1.504(11)
C8	C9	1.525(11)	C24	N6	1.319(11)
C8	N2	1.279(11)	C25	N5	1.316(12)
C9	N1	1.322(13)	C25	O5	1.235(12)
C9	O2	1.242(12)	C26	N7	1.356(13)
C10	N3	1.358(12)	C26	N8	1.333(14)
C10	N4	1.334(13)	C26	S2	1.688(10)
C10	S1	1.679(9)	C27	C28	1.487(19)
C11	C12	1.435(19)	C27	N8	1.484(14)
C11	N4	1.428(15)	C28	C29	1.524(17)
C12	C13	1.50(2)	C28	O6	1.437(16)
C12	O3	1.449(18)	C30	C31	1.50(2)
C14	C15	1.59(2)	C30	C32	1.458(18)
C14	C16	1.439(19)	C30	O6	1.414(16)
C14	O3	1.377(18)	C32	N8	1.482(15)
C16	N4	1.473(14)	N2	N3	1.354(10)
C17	O4	1.399(14)	N6	N7	1.351(12)

Table: Bond angles for compound **3**

Atom	Atom	Atom	Angle/°	Atom	Atom	Atom	Angle/°
C3	C2	C7	121.0(9)	C22	C21	C20	120.7(9)
C3	C2	O1	125.2(8)	C22	C21	N5	130.1(8)
O1	C2	C7	113.8(9)	C21	C22	C23	120.2(9)
C2	C3	C4	118.4(8)	C22	C23	C18	118.1(11)
C5	C4	C3	118.8(9)	C20	C24	C25	106.5(8)
C5	C4	C8	109.3(8)	N6	C24	C20	126.6(8)
C8	C4	C3	131.8(8)	N6	C24	C25	127.0(9)
C6	C5	C4	122.3(9)	N5	C25	C24	105.8(8)
C6	C5	N1	130.9(9)	O5	C25	C24	126.3(9)
N1	C5	C4	106.8(8)	O5	C25	N5	127.9(8)
C5	C6	C7	118.3(9)	N7	C26	S2	121.0(9)
C6	C7	C2	121.1(9)	N8	C26	N7	115.4(9)
C4	C8	C9	104.5(8)	N8	C26	S2	123.6(9)
N2	C8	C4	128.5(8)	N8	C27	C28	111.6(11)
N2	C8	C9	126.8(9)	C27	C28	C29	111.9(13)
N1	C9	C8	106.3(8)	O6	C28	C27	110.4(12)
O2	C9	C8	124.6(9)	O6	C28	C29	107.2(11)
O2	C9	N1	129.0(8)	C32	C30	C31	112.0(14)
N3	C10	S1	121.7(8)	O6	C30	C31	107.4(12)
N4	C10	N3	113.9(8)	O6	C30	C32	111.7(11)
N4	C10	S1	124.3(8)	C30	C32	N8	111.1(11)

Table: Bond angles for compound **3**

Atom	Atom	Atom	Angle/°	Atom	Atom	Atom	Angle/°
N4	C11	C12	116.3(13)	C9	N1	C5	113.1(7)
C11	C12	C13	114.2(17)	C8	N2	N3	116.6(7)
C11	C12	O3	113.5(13)	N2	N3	C10	123.6(7)
O3	C12	C13	108.3(16)	C10	N4	C11	120.8(9)
C16	C14	C15	109.9(15)	C10	N4	C16	123.4(9)
O3	C14	C15	107.9(13)	C11	N4	C16	114.5(9)
O3	C14	C16	114.3(14)	C25	N5	C21	112.4(7)
C14	C16	N4	112.2(12)	C24	N6	N7	115.2(7)
C19	C18	C23	122.9(10)	N6	N7	C26	122.2(8)
O4	C18	C19	123.9(9)	C26	N8	C27	126.0(10)
O4	C18	C23	113.2(10)	C26	N8	C32	122.3(10)
C18	C19	C20	116.2(8)	C32	N8	C27	111.7(10)
C19	C20	C24	132.1(8)	C2	O1	C1	116.3(8)
C21	C20	C19	121.8(10)	C14	O3	C12	110.2(12)
C21	C20	C24	106.1(7)	C18	O4	C17	115.9(9)
C20	C21	N5	109.2(9)	C30	O6	C28	113.4(10)

Table: Torsion angles for compound **3**

A	B	C	D	Angle/°	A	B	C	D	Angle/°
C2	C3	C4	C5	0.4(13)	C21	C22	C23	C18	-1.2(16)

Table: Torsion angles for compound **3**

A	B	C	D	Angle/°	A	B	C	D	Angle/°
C2	C3	C4	C8	178.7(9)	C22	C21	N5	C25	179.6(10)
C3	C2	C7	C6	-1.7(16)	C23	C18	C19	C20	2.4(14)
C3	C2	O1	C1	3.4(15)	C23	C18	O4	C17	-173.8(11)
C3	C4	C5	C6	-2.1(13)	C24	C20	C21	C22	179.3(9)
C3	C4	C5	N1	178.8(8)	C24	C20	C21	N5	1.0(10)
C3	C4	C8	C9	-178.3(9)	C24	C25	N5	C21	2.4(11)
C3	C4	C8	N2	-2.8(16)	C24	N6	N7	C26	-171.8(9)
C4	C5	C6	C7	1.8(14)	C25	C24	N6	N7	1.2(13)
C4	C5	N1	C9	-0.3(10)	C27	C28	O6	C30	56.5(16)
C4	C8	C9	N1	-0.2(10)	C28	C27	N8	C26	-131.0(13)
C4	C8	C9	O2	177.2(9)	C28	C27	N8	C32	51.1(15)
C4	C8	N2	N3	-178.5(8)	C29	C28	O6	C30	178.6(12)
C5	C4	C8	C9	0.0(9)	C30	C32	N8	C26	130.1(13)
C5	C4	C8	N2	175.6(9)	C30	C32	N8	C27	-51.9(15)
C5	C6	C7	C2	0.1(15)	C31	C30	C32	N8	175.5(13)
C6	C5	N1	C9	-179.4(10)	C31	C30	O6	C28	178.4(14)
C7	C2	C3	C4	1.4(14)	C32	C30	O6	C28	-58.4(16)
C7	C2	O1	C1	-175.8(10)	N1	C5	C6	C7	-179.3(9)
C8	C4	C5	C6	179.3(8)	N2	C8	C9	N1	-175.9(9)
C8	C4	C5	N1	0.2(10)	N2	C8	C9	O2	1.5(15)
C8	C9	N1	C5	0.3(10)	N3	C10	N4	C11	-164.4(9)

Table: Torsion angles for compound **3**

A	B	C	D	Angle/°	A	B	C	D	Angle/°
C8	N2	N3	C10	172.6(9)	N3	C10	N4	C16	1.7(15)
C9	C8	N2	N3	-3.9(13)	N4	C10	N3	N2	-168.4(8)
C11	C12	O3	C14	53(2)	N4	C11	C12	C13	-167.9(15)
C12	C11	N4	C10	-156.3(13)	N4	C11	C12	O3	-43(2)
C12	C11	N4	C16	36.4(18)	N5	C21	C22	C23	179.3(10)
C13	C12	O3	C14	-178.8(15)	N6	C24	C25	N5	177.3(9)
C14	C16	N4	C10	153.6(13)	N6	C24	C25	O5	-0.8(16)
C14	C16	N4	C11	-39.4(17)	N7	C26	N8	C27	-1.3(18)
C15	C14	C16	N4	174.0(13)	N7	C26	N8	C32	176.4(10)
C15	C14	O3	C12	178.3(15)	N8	C26	N7	N6	170.7(9)
C16	C14	O3	C12	-59.1(18)	N8	C27	C28	C29	-171.6(12)
C18	C19	C20	C21	-2.2(13)	N8	C27	C28	O6	-52.3(15)
C18	C19	C20	C24	179.2(10)	O1	C2	C3	C4	-177.8(9)
C19	C18	C23	C22	-0.8(16)	O1	C2	C7	C6	177.5(10)
C19	C18	O4	C17	8.0(15)	O2	C9	N1	C5	-176.9(9)
C19	C20	C21	C22	0.4(14)	O3	C14	C16	N4	52.5(18)
C19	C20	C21	N5	-177.9(8)	O4	C18	C19	C20	-179.6(9)
C19	C20	C24	C25	179.2(9)	O4	C18	C23	C22	-179.0(10)
C19	C20	C24	N6	0.2(16)	O5	C25	N5	C21	-179.5(9)
C20	C21	C22	C23	1.4(15)	O6	C30	C32	N8	55.0(16)
C20	C21	N5	C25	-2.3(11)	S1	C10	N3	N2	11.6(13)

Table: Torsion angles for compound **3**

A	B	C	D	Angle/°	A	B	C	D	Angle/°
C20	C24	C25	N5	-1.7(10)	S1	C10	N4	C11	15.6(14)
C20	C24	C25	O5	-179.8(9)	S1	C10	N4	C16	-178.2(10)
C20	C24	N6	N7	-179.9(9)	S2	C26	N7	N6	-9.1(14)
C21	C20	C24	C25	0.4(10)	S2	C26	N8	C27	178.5(10)
C21	C20	C24	N6	-178.6(9)	S2	C26	N8	C32	-3.8(17)

Molecular structure of Compound 3

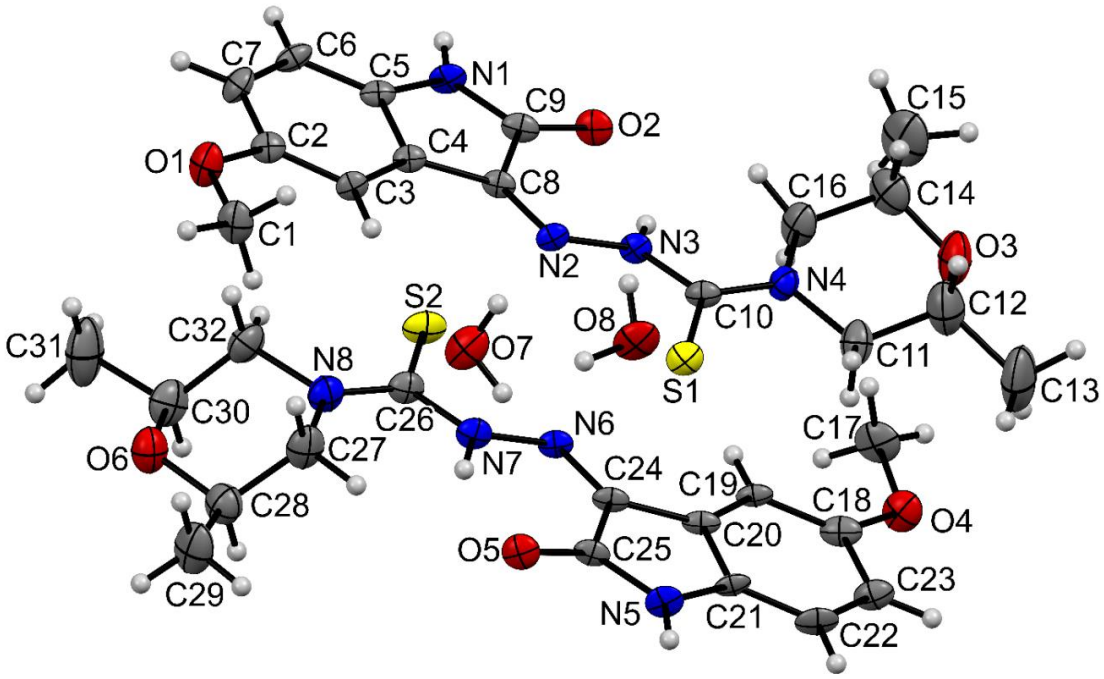

ORTEP diagram of **MeOIstDmMor/3** drawn in 20% thermal probability ellipsoids showing atomic numbering scheme. The asymmetric unit contains two crystallographically independents units and two water molecules in the crystal lattice.

Appendix E2

The ORTEP view of compound (***MeOIstDm*/4)** [**CCDC** reference No. = 2194144]

Table: Crystal data and structure refinement for compound **4**

Identification code	***MeOIstDm***
Empirical formula	$C_{12}H_{14}N_4O_2S$
Formula weight	278.33
Temperature/K	296.15
Crystal system	Monoclinic
Space group	$P2_1/c$
a/Å	9.357(2)
b/Å	9.9370(19)
c/Å	14.207(3)
α/°	90
β/°	104.929(9)
γ/°	90
Volume/Å^3	1276.4(5)
Z	4
ρ_{calc}g/cm^3	1.448
μ/mm^{-1}	0.258
F(000)	584.0
Crystal size/mm^3	0.35 × 0.25 × 0.2
Radiation	MoKα (λ = 0.71073)
2Θ range for data collection/°	5.06 to 64

Index ranges	$-13 \leq h \leq 13$, $-14 \leq k \leq 14$, $-21 \leq l \leq 21$
Reflections collected	47022
Independent reflections	4418 [R_{int} = 0.0439, R_{sigma} = 0.0250]
Data/restraints/parameters	4418/0/175
Goodness-of-fit on F^2	1.096
Final R indexes [I>=2σ (I)]	R_1 = 0.0646, wR_2 = 0.1546
Final R indexes [all data]	R_1 = 0.1035, wR_2 = 0.1768
Largest diff. peak/hole / e $Å^{-3}$	0.64/-0.42

Table: Bond lengths for compound **4**

Atom	Atom	Length/Å	Atom	Atom	Length/Å
S1	C10	1.6735(19)	N4	C5	1.416(3)
O1	C1	1.430(3)	N4	C9	1.358(3)
O1	C2	1.377(2)	C2	C3	1.390(3)
O2	C9	1.228(3)	C2	C7	1.394(3)
N1	N2	1.354(2)	C3	C4	1.398(3)
N1	C8	1.293(2)	C4	C5	1.371(3)
N2	C10	1.378(2)	C5	C6	1.399(3)
N3	C10	1.335(2)	C6	C7	1.380(3)
N3	C11	1.467(3)	C6	C8	1.455(3)
N3	C12	1.448(3)	C8	C9	1.518(3)

Table: Bond angles for compound **4**

Atom	Atom	Atom	Angle/°	Atom	Atom	Atom	Angle/°
C2	O1	C1	117.12(18)	C6	C5	N4	109.37(17)
C8	N1	N2	116.52(17)	C5	C6	C8	106.85(16)
N1	N2	C10	120.44(16)	C7	C6	C5	120.64(17)
C10	N3	C11	122.21(17)	C7	C6	C8	132.50(17)
C10	N3	C12	121.01(18)	C6	C7	C2	118.30(18)
C12	N3	C11	116.73(18)	N1	C8	C6	125.41(18)
C9	N4	C5	111.70(16)	N1	C8	C9	128.01(18)
O1	C2	C3	124.03(19)	C6	C8	C9	106.58(16)
O1	C2	C7	114.97(18)	O2	C9	N4	127.92(19)
C3	C2	C7	121.00(19)	O2	C9	C8	126.58(19)
C2	C3	C4	120.31(19)	N4	C9	C8	105.50(17)
C5	C4	C3	118.51(18)	N2	C10	S1	122.48(14)
C4	C5	N4	129.39(18)	N3	C10	S1	123.48(15)
C4	C5	C6	121.23(18)	N3	C10	N2	114.03(16)

Table: Torsion angles for compound **4**

A	B	C	D	Angle/°	A	B	C	D	Angle/°
O1	C2	C3	C4	179.1(2)	C5	N4	C9	O2	178.4(2)
O1	C2	C7	C6	-179.5(2)	C5	N4	C9	C8	-0.8(3)
N1	N2	C10	S1	3.3(3)	C5	C6	C7	C2	0.5(3)
N1	N2	C10	N3	-177.90(18)	C5	C6	C8	N1	179.5(2)
N1	C8	C9	O2	1.8(4)	C5	C6	C8	C9	0.1(2)
N1	C8	C9	N4	-178.9(2)	C6	C8	C9	O2	-178.8(2)
N2	N1	C8	C6	-179.62(19)	C6	C8	C9	N4	0.4(2)
N2	N1	C8	C9	-0.4(3)	C7	C2	C3	C4	-0.5(4)
N4	C5	C6	C7	-179.76(19)	C7	C6	C8	N1	-1.5(4)
N4	C5	C6	C8	-0.6(2)	C7	C6	C8	C9	179.1(2)
C1	O1	C2	C3	5.3(3)	C8	N1	N2	C10	-175.4(2)
C1	O1	C2	C7	-175.0(2)	C8	C6	C7	C2	-178.4(2)
C2	C3	C4	C5	0.2(4)	C9	N4	C5	C4	-177.8(2)
C3	C2	C7	C6	0.2(3)	C9	N4	C5	C6	0.9(3)
C3	C4	C5	N4	179.2(2)	C11	N3	C10	S1	-176.54(18)
C3	C4	C5	C6	0.5(3)	C11	N3	C10	N2	4.7(3)
C4	C5	C6	C7	-0.9(3)	C12	N3	C10	S1	6.4(3)
C4	C5	C6	C8	178.3(2)	C12	N3	C10	N2	-172.4(2)

Molecular Structure of compound 4

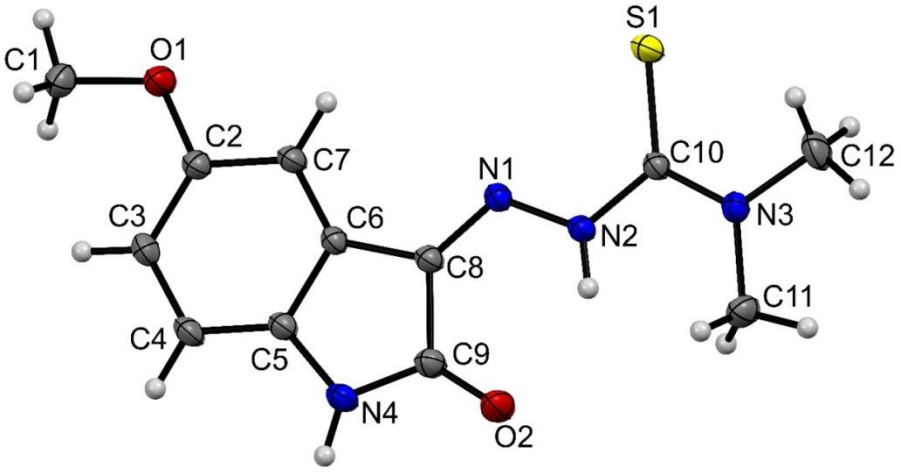

ORTEP diagram of compound **4** drawn in 30% thermal probability ellipsoids showing atomic numbering scheme.

Appendix E3

The ORTEP view of compound (***HydIstMor*/9)** [**CCDC** reference No. = 2245790]

Table: Crystal data and structure refinement for compound **9**.

Identification code	***HydIstMor***
Empirical formula	$C_{13}H_{14}N_4O_3S$
Formula weight	306.34
Temperature/K	301.00
Crystal system	orthorhombic
Space group	Pbca
a/Å	13.6452(9)
b/Å	8.4928(6)
c/Å	24.1431(17)
α/°	90
β/°	90
γ/°	90
Volume/Å^3	2797.8(3)
Z	8
ρ_{calc}g/cm^3	1.455

μ/mm^{-1}	2.217
F(000)	1280.0
Crystal size/mm^3	0.14 × 0.12 × 0.11
Radiation	CuKα (λ = 1.54178)
2Θ range for data collection/°	7.322 to 131.998
Index ranges	$-16 \leq h \leq 16$, $-9 \leq k \leq 10$, $-28 \leq l \leq 28$
Reflections collected	17616
Independent reflections	2433 [R_{int} = 0.0871, R_{sigma} = 0.0454]
Data/restraints/parameters	2433/1/195
Goodness-of-fit on F^2	1.039
Final R indexes [I>=2σ (I)]	R_1 = 0.0553, wR_2 = 0.1480
Final R indexes [all data]	R_1 = 0.0998, wR_2 = 0.1779
Largest diff. peak/hole / e $Å^{-3}$	0.46/-0.33

Table: Bond lengths for compound **9**.

Atom	Atom	Length/Å	Atom	Atom	Length/Å
S1	C9	1.677(3)	N4	C13	1.468(4)
O1	C1	1.229(4)	C1	C8	1.503(4)
O2	C5	1.375(4)	C2	C3	1.376(4)
O3	C11	1.418(4)	C2	C7	1.391(4)
O3	C12	1.412(4)	C3	C4	1.382(5)
N1	C1	1.356(4)	C4	C5	1.389(5)
N1	C2	1.413(4)	C5	C6	1.387(5)
N2	N3	1.361(4)	C6	C7	1.388(4)
N2	C8	1.289(4)	C7	C8	1.451(4)
N3	C9	1.359(4)	C10	C11	1.501(5)
N4	C9	1.344(4)	C12	C13	1.499(5)
N4	C10	1.469(4)			

Table: Bond angles for compound **9**.

Atom	Atom	Atom	Angle/°	Atom	Atom	Atom	Angle/°
C12	O3	C11	109.2(3)	O2	C5	C6	117.2(3)
C1	N1	C2	111.5(3)	C6	C5	C4	121.1(3)
C8	N2	N3	116.0(3)	C5	C6	C7	117.5(3)
C9	N3	N2	120.9(3)	C2	C7	C8	107.0(3)
C9	N4	C10	122.8(3)	C6	C7	C2	120.6(3)
C9	N4	C13	119.8(3)	C6	C7	C8	132.4(3)
C13	N4	C10	114.4(3)	N2	C8	C1	127.5(3)
O1	C1	N1	127.3(3)	N2	C8	C7	125.9(3)
O1	C1	C8	127.0(3)	C7	C8	C1	106.6(3)
N1	C1	C8	105.7(3)	N3	C9	S1	121.7(2)
C3	C2	N1	128.7(3)	N4	C9	S1	124.2(2)
C3	C2	C7	122.2(3)	N4	C9	N3	114.1(3)
C7	C2	N1	109.2(3)	N4	C10	C11	110.5(3)
C2	C3	C4	117.1(3)	O3	C11	C10	111.8(3)
C3	C4	C5	121.6(3)	O3	C12	C13	111.6(3)
O2	C5	C4	121.6(3)	N4	C13	C12	112.2(3)

Table: Hydrogen bonds for compound **9**.

D	H	A	d(D-H)/Å	d(H-A)/Å	d(D-A)/Å	D-H-A/°
N1	H1	O2[1]	0.86	2.07	2.896(4)	161.9

Table: Torsion angles for compound **9**.

A	B	C	D	Angle/°	A	B	C	D	Angle/°
O1	C1	C8	N2	-0.5(7)	C3	C2	C7	C6	1.3(5)
O1	C1	C8	C7	-179.5(4)	C3	C2	C7	C8	-179.2(3)
O2	C5	C6	C7	-179.3(3)	C3	C4	C5	O2	-179.8(3)
O3	C12	C13	N4	-52.0(4)	C3	C4	C5	C6	2.0(6)
N1	C1	C8	N2	179.2(4)	C4	C5	C6	C7	-1.0(5)
N1	C1	C8	C7	0.1(4)	C5	C6	C7	C2	-0.6(5)
N1	C2	C3	C4	178.9(3)	C5	C6	C7	C8	-179.9(4)
N1	C2	C7	C6	-178.1(3)	C6	C7	C8	N2	-0.6(6)
N1	C2	C7	C8	1.4(4)	C6	C7	C8	C1	178.4(4)
N2	N3	C9	S1	4.5(4)	C7	C2	C3	C4	-0.3(5)
N2	N3	C9	N4	-174.9(3)	C8	N2	N3	C9	-172.2(3)
N3	N2	C8	C1	1.2(5)	C9	N4	C10	C11	154.9(3)
N3	N2	C8	C7	-180.0(3)	C9	N4	C13	C12	-155.1(3)
N4	C10	C11	O3	54.7(4)	C10	N4	C9	S1	-179.9(3)
C1	N1	C2	C3	179.3(4)	C10	N4	C9	N3	-0.4(5)
C1	N1	C2	C7	-1.4(4)	C10	N4	C13	C12	44.1(4)
C2	N1	C1	O1	-179.6(4)	C11	O3	C12	C13	61.7(4)
C2	N1	C1	C8	0.7(4)	C12	O3	C11	C10	-63.6(4)
C2	C3	C4	C5	-1.3(5)	C13	N4	C9	S1	20.9(5)
C2	C7	C8	N2	-180.0(3)	C13	N4	C9	N3	-159.6(3)
C2	C7	C8	C1	-0.9(4)	C13	N4	C10	C11	-44.9(4)

Molecular structure of compound 9

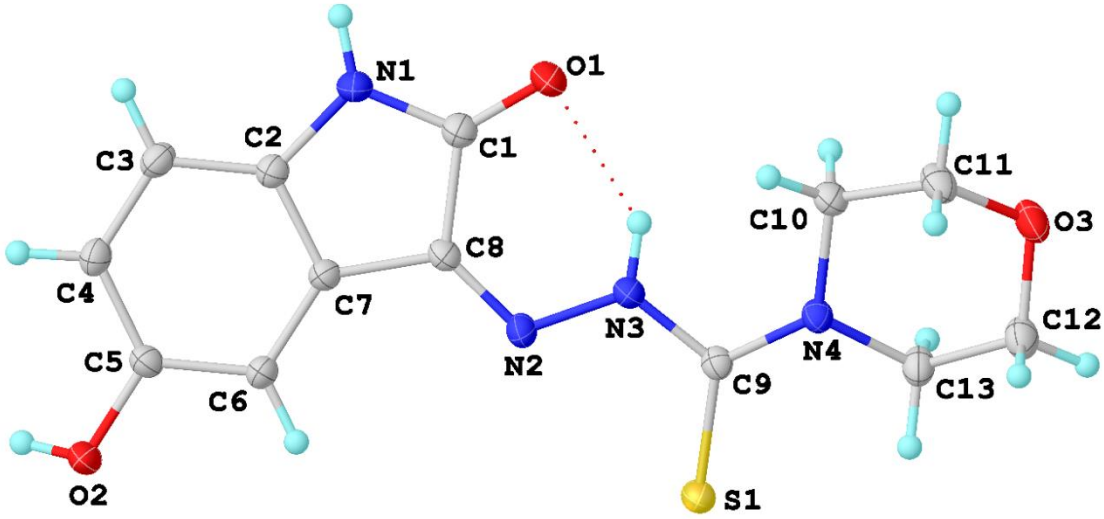

ORTEP diagram of compound (9) drawn in 20% thermal probability ellipsoids showing atomic numbering scheme.

Appendix E4

The ORTEP view of compound (***HydIstAzep*/12)** [**CCDC** reference No. = 2245783]

Table: Crystal data and structure refinement for compound **12**

Identification code	***HydIstAzep***
Empirical formula	$C_{30}H_{38}N_8O_5S_2$
Formula weight	654.80
Temperature/K	296.15
Crystal system	monoclinic
Space group	Pc
a/Å	8.54(2)
b/Å	13.46(3)
c/Å	13.87(3)
α/°	90

β/°	96.04(5)
γ/°	90
Volume/Å^3	1585(7)
Z	2
ρ_{calc}g/cm^3	1.372
μ/mm^{-1}	0.221
F(000)	692.0
Crystal size/mm^3	0.2 × 0.18 × 0.15
Radiation	MoKα (λ = 0.71073)
2Θ range for data collection/°	5.674 to 49.988
Index ranges	-10 ≤ h ≤ 10, -16 ≤ k ≤ 16, -16 ≤ l ≤ 16
Reflections collected	35687
Independent reflections	5455 [R_{int} = 0.1330, R_{sigma} = 0.1048]
Data/restraints/parameters	5455/33/409
Goodness-of-fit on F^2	1.015
Final R indexes [I>=2σ (I)]	R_1 = 0.0880, wR_2 = 0.2245
Final R indexes [all data]	R_1 = 0.1333, wR_2 = 0.2487
Largest diff. peak/hole / e Å^{-3}	1.38/-0.40
Flack parameter	0.00(10)

Table: Bond lengths for compound **12**.

Atom	Atom	Length/Å	Atom	Atom	Length/Å
C1	C8	1.519(14)	C16	N5	1.322(13)
C1	N1	1.310(15)	C16	O3	1.235(13)
C1	O1	1.221(13)	C17	C18	1.389(16)
C2	C3	1.349(15)	C17	C22	1.385(14)
C2	C7	1.400(15)	C17	N5	1.394(14)
C2	N1	1.400(13)	C18	C19	1.413(16)
C3	C4	1.377(15)	C19	C20	1.358(15)
C4	C5	1.355(16)	C20	C21	1.382(14)
C5	C6	1.387(16)	C20	O4	1.358(13)
C5	O2	1.371(13)	C21	C22	1.375(14)
C6	C7	1.359(14)	C22	C23	1.454(15)
C7	C8	1.448(15)	C23	N6	1.283(12)
C8	N2	1.262(13)	C24	N7	1.377(13)
C9	N3	1.347(14)	C24	N8	1.343(13)
C9	N4	1.329(13)	C24	S2	1.671(11)
C9	S1	1.663(11)	C25	C26	1.528(19)
C10	C11	1.48(2)	C25	N8	1.455(15)
C10	N4	1.455(18)	C26	C27	1.40(3)
C11	C12	1.488(19)	C27	C28	1.53(3)
C12	C13	1.45(2)	C28	C29	1.46(3)
C13	C14	1.50(2)	C29	C30	1.47(2)
C14	C15	1.452(19)	C30	N8	1.492(15)
C15	N4	1.454(16)	N2	N3	1.347(13)

Table: Bond lengths for compound **12**.

Atom	Atom	Length/Å	Atom	Atom	Length/Å
C16	C23	1.500(14)	N6	N7	1.335(12)

Table: Bond angles for compound **12.**

Atom	Atom	Atom	Angle/°	Atom	Atom	Atom	Angle/°
N1	C1	C8	106.4(9)	C17	C18	C19	116.3(10)
O1	C1	C8	124.8(10)	C20	C19	C18	121.2(10)
O1	C1	N1	128.8(10)	C19	C20	C21	122.3(10)
C3	C2	C7	120.8(10)	O4	C20	C19	115.8(9)
C3	C2	N1	130.5(10)	O4	C20	C21	122.0(9)
N1	C2	C7	108.6(9)	C22	C21	C20	117.2(9)
C2	C3	C4	117.4(11)	C17	C22	C23	105.2(8)
C5	C4	C3	122.8(11)	C21	C22	C17	121.8(10)
C4	C5	C6	120.0(10)	C21	C22	C23	133.0(9)
C4	C5	O2	122.8(11)	C22	C23	C16	106.2(8)
O2	C5	C6	117.0(11)	N6	C23	C16	127.3(9)
C7	C6	C5	117.9(10)	N6	C23	C22	126.4(8)
C2	C7	C8	106.9(8)	N7	C24	S2	121.8(7)
C6	C7	C2	121.1(10)	N8	C24	N7	113.8(9)
C6	C7	C8	132.0(10)	N8	C24	S2	124.4(8)
C7	C8	C1	105.3(9)	N8	C25	C26	113.9(12)
N2	C8	C1	127.7(10)	C27	C26	C25	114.6(16)
N2	C8	C7	126.9(9)	C26	C27	C28	116.6(17)
N3	C9	S1	121.8(8)	C29	C28	C27	115.7(17)

Table: Bond angles for compound **12.**

Atom	Atom	Atom	Angle/°	Atom	Atom	Atom	Angle/°
N4	C9	N3	113.7(9)	C28	C29	C30	119.0(18)
N4	C9	S1	124.5(8)	C29	C30	N8	115.1(13)
N4	C10	C11	114.6(13)	C1	N1	C2	112.8(9)
C10	C11	C12	113.7(13)	C8	N2	N3	116.4(9)
C13	C12	C11	118.5(14)	N2	N3	C9	122.8(9)
C12	C13	C14	116.7(16)	C9	N4	C10	119.6(10)
C15	C14	C13	117.6(14)	C9	N4	C15	123.2(9)
C14	C15	N4	117.3(11)	C15	N4	C10	117.2(10)
N5	C16	C23	106.6(9)	C16	N5	C17	111.0(8)
O3	C16	C23	125.2(9)	C23	N6	N7	115.3(8)
O3	C16	N5	128.1(9)	N6	N7	C24	120.4(8)
C18	C17	N5	127.9(9)	C24	N8	C25	120.2(10)
C22	C17	C18	121.2(10)	C24	N8	C30	119.4(9)
C22	C17	N5	110.9(9)	C25	N8	C30	120.3(9)

Table: Hydrogen bonds for compound **12**.

D	H	A	d(D-H)/Å	d(H-A)/Å	d(D-A)/Å	D-H-A/°
N1	H1	O5	0.86	2.08	2.881(14)	155.1
N3	H3A	O1	0.86(3)	1.96(7)	2.688(13)	142(10)
N5	H5	O1	0.86	2.06	2.852(12)	152.8
N7	H7	O3	0.86	1.96	2.667(12)	138.4
O4	H4A	$O3^{1}$	0.82	1.89	2.695(12)	168.1

Table: Torsion angles for compound **12**.

A	B	C	D	Angle/°	A	B	C	D	Angle/°
C1	C8	N2	N3	-2.9(15)	C22	C23	N6	N7	179.9(8)
C2	C3	C4	C5	-1.0(18)	C23	C16	N5	C17	3.4(11)
C2	C7	C8	C1	1.0(11)	C23	N6	N7	C24	179.9(9)
C2	C7	C8	N2	177.2(10)	C25	C26	C27	C28	-61(2)
C3	C2	C7	C6	-0.3(16)	C26	C25	N8	C24	116.7(13)
C3	C2	C7	C8	-178.9(10)	C26	C25	N8	C30	-68.2(16)
C3	C2	N1	C1	177.5(11)	C26	C27	C28	C29	58(3)
C3	C4	C5	C6	1.0(17)	C27	C28	C29	C30	-79(3)
C3	C4	C5	O2	-175.0(10)	C28	C29	C30	N8	63(2)
C4	C5	C6	C7	-0.5(15)	C29	C30	N8	C24	179.1(13)
C5	C6	C7	C2	0.2(15)	C29	C30	N8	C25	4.0(18)
C5	C6	C7	C8	178.4(10)	N1	C1	C8	C7	-1.7(11)
C6	C7	C8	C1	-177.4(10)	N1	C1	C8	N2	-177.9(10)
C6	C7	C8	N2	-1.2(18)	N1	C2	C3	C4	-177.9(11)
C7	C2	C3	C4	0.7(16)	N1	C2	C7	C6	178.6(9)
C7	C2	N1	C1	-1.2(12)	N1	C2	C7	C8	0.0(11)
C7	C8	N2	N3	-178.3(9)	N3	C9	N4	C10	177.8(11)
C8	C1	N1	C2	1.8(11)	N3	C9	N4	C15	-1.8(14)
C8	N2	N3	C9	179.8(9)	N4	C9	N3	N2	170.2(9)
C10	C11	C12	C13	-51(2)	N4	C10	C11	C12	72.6(17)
C11	C10	N4	C9	94.3(14)	N5	C16	C23	C22	-3.5(11)
C11	C10	N4	C15	-86.1(15)	N5	C16	C23	N6	172.8(10)
C11	C12	C13	C14	63(3)	N5	C17	C18	C19	-176.3(10)

Table: Torsion angles for compound **12**.

A	B	C	D	Angle/°	A	B	C	D	Angle/°
C12	C13	C14	C15	-80(2)	N5	C17	C22	C21	177.6(9)
C13	C14	C15	N4	40(2)	N5	C17	C22	C23	-0.3(11)
C14	C15	N4	C9	-146.9(13)	N7	C24	N8	C25	178.4(9)
C14	C15	N4	C10	33.5(19)	N7	C24	N8	C30	3.3(14)
C16	C23	N6	N7	4.3(15)	N8	C24	N7	N6	-179.8(8)
C17	C18	C19	C20	-2.6(16)	N8	C25	C26	C27	83.8(18)
C17	C22	C23	C16	2.2(10)	O1	C1	C8	C7	178.9(10)
C17	C22	C23	N6	-174.2(10)	O1	C1	C8	N2	2.7(17)
C18	C17	C22	C21	-1.9(15)	O1	C1	N1	C2	-178.8(11)
C18	C17	C22	C23	-179.7(10)	O2	C5	C6	C7	175.7(9)
C18	C17	N5	C16	177.3(11)	O3	C16	C23	C22	174.1(9)
C18	C19	C20	C21	0.8(18)	O3	C16	C23	N6	-9.6(17)
C18	C19	C20	O4	-179.1(10)	O3	C16	N5	C17	-174.1(10)
C19	C20	C21	C22	0.6(16)	O4	C20	C21	C22	-179.6(9)
C20	C21	C22	C17	0.0(14)	S1	C9	N3	N2	-10.6(14)
C20	C21	C22	C23	177.1(10)	S1	C9	N4	C10	-1.3(14)
C21	C22	C23	C16	-175.3(10)	S1	C9	N4	C15	179.1(9)
C21	C22	C23	N6	8.4(17)	S2	C24	N7	N6	1.6(12)
C22	C17	C18	C19	3.1(15)	S2	C24	N8	C25	-3.1(14)
C22	C17	N5	C16	-2.1(12)	S2	C24	N8	C30	-178.1(8)

Molecular structure of Compound 12

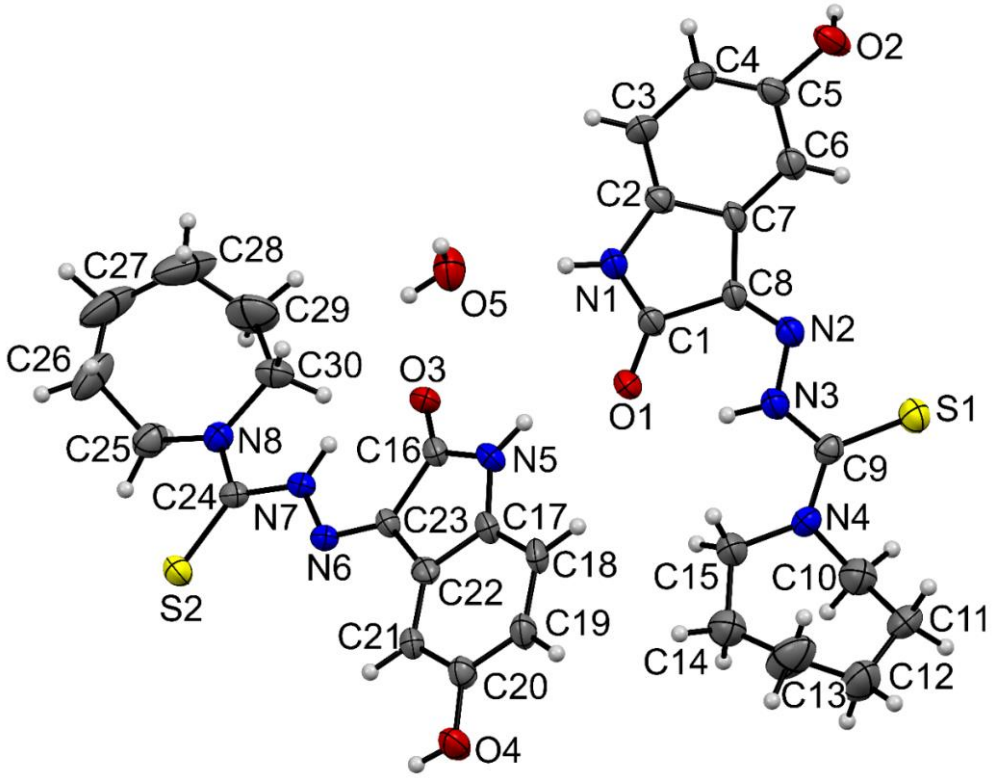

ORTEP diagram of compound **12** drawn in 30% thermal probability ellipsoids showing atomic numbering scheme. The asymmetric unit contains two crystallographically independents units and a water molecule in the crystal lattice.

Appendix E5

The ORTEP view of compound (***HydIstEth*/16)** [**CCDC** reference No.= 2245789]

Table: Crystal data and structure refinement for compound **16**.

Identification code	***HydIstEth***
Empirical formula	$C_{11}H_{12}N_4O_2S$
Formula weight	264.31
Temperature/K	301.00
Crystal system	orthorhombic
Space group	$P2_12_12_1$
a/Å	4.5707(11)
b/Å	11.989(3)
c/Å	22.157(6)

α/°	90
β/°	90
γ/°	90
Volume/Å^3	1214.2(5)
Z	4
ρ_{calc}g/cm^3	1.446
μ/mm^{-1}	2.394
F(000)	552.0
Crystal size/mm^3	0.13 × 0.11 × 0.08
Radiation	CuKα (λ = 1.54178)
2Θ range for data collection/°	7.98 to 141.086
Index ranges	-4 ≤ h ≤ 5, -12 ≤ k ≤ 14, -26 ≤ l ≤ 26
Reflections collected	7274
Independent reflections	2254 [R_{int} = 0.0662, R_{sigma} = 0.0661]
Data/restraints/parameters	2254/0/166
Goodness-of-fit on F^2	1.066
Final R indexes [I>=2σ (I)]	R_1 = 0.0467, wR_2 = 0.1122
Final R indexes [all data]	R_1 = 0.0738, wR_2 = 0.1245
Largest diff. peak/hole / e Å^{-3}	0.63/-0.22
Flack parameter	0.05(5)

Table: Bond lengths for compound **16**.

Atom	Atom	Length/Å	Atom	Atom	Length/Å
S1	C9	1.682(5)	C1	C8	1.505(6)
O1	C1	1.235(6)	C2	C3	1.372(7)
O2	C5	1.373(6)	C2	C7	1.390(6)
N1	C1	1.339(6)	C3	C4	1.390(7)
N1	C2	1.412(6)	C4	C5	1.388(7)
N2	N3	1.356(5)	C5	C6	1.383(7)
N2	C8	1.288(5)	C6	C7	1.390(6)

Table: Bond lengths for compound **16**.

Atom	Atom	Length/Å	Atom	Atom	Length/Å
N3	C9	1.366(5)	C7	C8	1.464(6)
N4	C9	1.310(6)	C10	C11	1.503(8)
N4	C10	1.465(6)			

Table: Bond angles for compound **16**.

Atom	Atom	Atom	Angle/°	Atom	Atom	Atom	Angle/°
C1	N1	C2	111.2(4)	O2	C5	C6	121.8(4)
C8	N2	N3	117.2(4)	C6	C5	C4	121.4(5)
N2	N3	C9	119.6(4)	C5	C6	C7	117.7(4)
C9	N4	C10	126.8(4)	C2	C7	C8	106.5(4)
O1	C1	N1	127.9(4)	C6	C7	C2	120.6(4)
O1	C1	C8	125.3(4)	C6	C7	C8	132.9(4)
N1	C1	C8	106.8(4)	N2	C8	C1	128.8(4)
C3	C2	N1	128.5(4)	N2	C8	C7	125.5(4)
C3	C2	C7	121.7(4)	C7	C8	C1	105.8(4)
C7	C2	N1	109.8(4)	N3	C9	S1	118.2(3)
C2	C3	C4	117.9(4)	N4	C9	S1	125.7(3)
C5	C4	C3	120.7(5)	N4	C9	N3	115.9(4)
O2	C5	C4	116.8(5)	N4	C10	C11	111.9(4)

Table: Hydrogen bonds for compound **16**.

D	H	A	d(D-H)/Å	d(H-A)/Å	d(D-A)/Å	D-H-A/°
N1	H1	O1[1]	0.86	2.03	2.887(5)	172.2
N3	H3	O1	0.86	2.10	2.766(5)	134.3

Table: Torsion angles for compound **16**.

A	B	C	D	Angle/°	A	B	C	D	Angle/°
O1	C1	C8	N2	0.9(8)	C2	C7	C8	N2	177.5(4)
O1	C1	C8	C7	179.9(4)	C2	C7	C8	C1	-1.5(5)
O2	C5	C6	C7	178.9(4)	C3	C2	C7	C6	0.5(7)
N1	C1	C8	N2	-177.4(4)	C3	C2	C7	C8	-179.5(4)
N1	C1	C8	C7	1.6(5)	C3	C4	C5	O2	-178.9(4)
N1	C2	C3	C4	178.8(5)	C3	C4	C5	C6	2.5(8)
N1	C2	C7	C6	-179.0(4)	C4	C5	C6	C7	-2.6(7)
N1	C2	C7	C8	0.9(5)	C5	C6	C7	C2	1.1(6)
N2	N3	C9	S1	173.5(3)	C5	C6	C7	C8	-178.8(5)
N2	N3	C9	N4	-9.8(6)	C6	C7	C8	N2	-2.6(8)
N3	N2	C8	C1	-3.0(7)	C6	C7	C8	C1	178.4(5)
N3	N2	C8	C7	178.3(4)	C7	C2	C3	C4	-0.6(7)
C1	N1	C2	C3	-179.4(5)	C8	N2	N3	C9	179.1(4)
C1	N1	C2	C7	0.1(5)	C9	N4	C10	C11	-106.8(6)
C2	N1	C1	O1	-179.3(5)	C10	N4	C9	S1	-2.8(7)
C2	N1	C1	C8	-1.0(5)	C10	N4	C9	N3	-179.2(4)
C2	C3	C4	C5	-0.8(7)					

Molecular Structure of compound 16

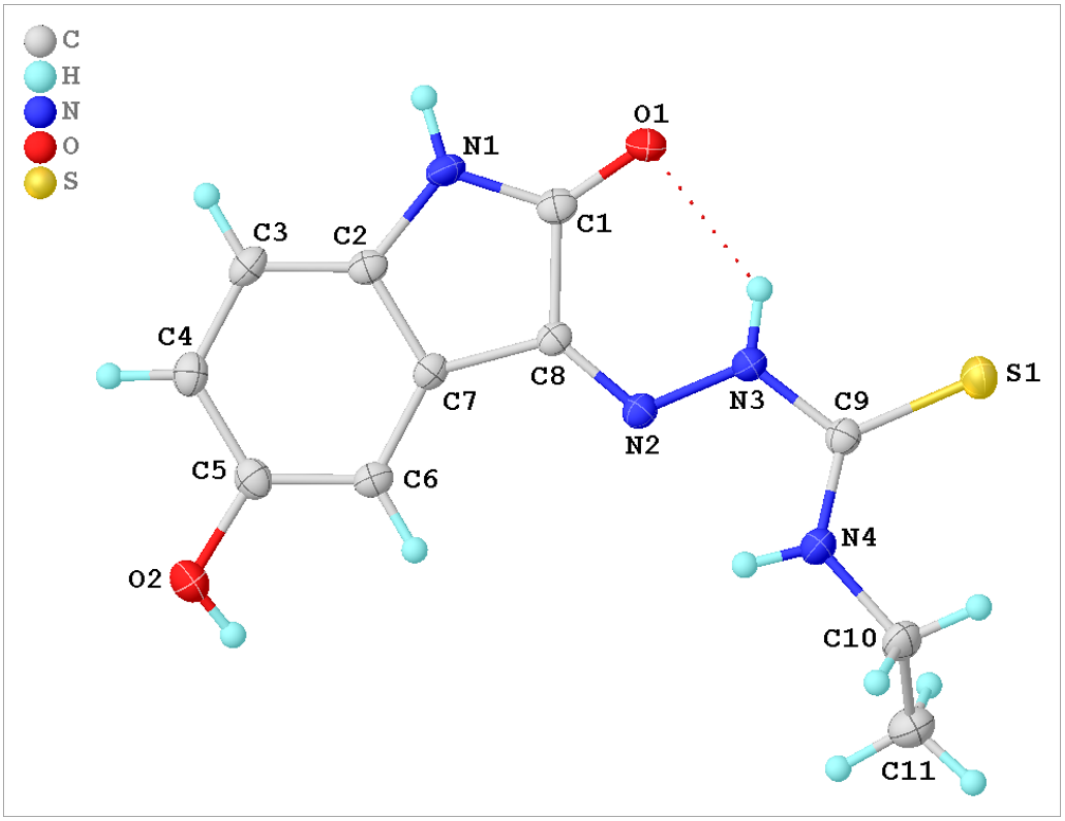

ORTEP diagram of compound (**16**) drawn in 20% thermal probability ellipsoids showing atomic numbering scheme.

Appendix E6

The ORTEP view of compound (***DiBrIstAzep*/22)** [**CCDC** reference No. = 2245786]

Table: Crystal data and structure refinement for compound **22**.

Identification code	***DiBrIstAzep***
Empirical formula	$C_{15}H_{16}Br_2N_4OS$
Formula weight	460.20
Temperature/K	301.00
Crystal system	monoclinic
Space group	$P2_1/c$
a/Å	13.4568(7)
b/Å	15.3218(7)
c/Å	8.4720(4)
α/°	90

β/°	100.286(3)
γ/°	90
Volume/Å^3	1718.70(14)
Z	4
ρ_{calc}g/cm^3	1.778
μ/mm^{-1}	7.197
F(000)	912.0
Crystal size/mm^3	0.13 × 0.11 × 0.1
Radiation	CuKα (λ = 1.54178)
2Θ range for data collection/°	6.676 to 149.762
Index ranges	-16 ≤ h ≤ 16, -19 ≤ k ≤ 19, -10 ≤ l ≤ 9
Reflections collected	26380
Independent reflections	3512 [R_{int} = 0.0737, R_{sigma} = 0.0397]
Data/restraints/parameters	3512/15/209
Goodness-of-fit on F^2	1.051
Final R indexes [I>=2σ (I)]	R_1 = 0.0498, wR_2 = 0.1171
Final R indexes [all data]	R_1 = 0.0815, wR_2 = 0.1428
Largest diff. peak/hole / e Å^{-3}	0.54/-0.91

Table: Bond lengths for compound **22**.

Atom	Atom	Length/Å	Atom	Atom	Length/Å
Br1	C3	1.894(5)	C2	C3	1.376(7)
Br2	C5	1.902(5)	C2	C7	1.395(7)
S1	C9	1.674(5)	C3	C4	1.366(8)
O1	C1	1.230(6)	C4	C5	1.387(8)
N1	C1	1.373(7)	C5	C6	1.381(8)
N1	C2	1.399(6)	C6	C7	1.389(7)
N2	N3	1.331(6)	C7	C8	1.459(7)
N2	C8	1.296(7)	C10	C11	1.497(9)
N3	C9	1.391(7)	C11	C12	1.515(17)

Table: Bond lengths for compound **22**.

Atom	Atom	Length/Å	Atom	Atom	Length/Å
N4	C9	1.342(7)	C12	C13	1.485(14)
N4	C10	1.469(7)	C13	C14	1.516(13)
N4	C15	1.463(7)	C14	C15	1.495(10)
C1	C8	1.498(7)			

Table: Bond angles for compound **22**.

Atom	Atom	Atom	Angle/°	Atom	Atom	Atom	Angle/°
C1	N1	C2	110.4(4)	C6	C5	C4	122.0(5)
C8	N2	N3	116.7(4)	C5	C6	C7	116.9(5)
N2	N3	C9	120.6(4)	C2	C7	C8	106.6(4)
C9	N4	C10	121.4(5)	C6	C7	C2	121.4(5)
C9	N4	C15	120.1(5)	C6	C7	C8	132.0(5)
C15	N4	C10	118.4(5)	N2	C8	C1	128.3(5)
O1	C1	N1	125.7(5)	N2	C8	C7	125.6(4)
O1	C1	C8	127.8(5)	C7	C8	C1	106.1(4)
N1	C1	C8	106.5(4)	N3	C9	S1	120.5(4)
C3	C2	N1	129.6(5)	N4	C9	S1	125.5(4)
C3	C2	C7	120.0(5)	N4	C9	N3	114.0(4)
C7	C2	N1	110.3(4)	N4	C10	C11	114.9(5)
C2	C3	Br1	119.6(4)	C10	C11	C12	116.5(10)
C4	C3	Br1	120.9(4)	C13	C12	C11	115.8(9)
C4	C3	C2	119.4(5)	C12	C13	C14	115.9(8)
C3	C4	C5	120.2(5)	C15	C14	C13	114.4(7)
C4	C5	Br2	117.9(4)	N4	C15	C14	114.4(6)
C6	C5	Br2	120.1(4)				

Table: Torsion angles for compound **22**.

A	B	C	D	Angle/°	A	B	C	D	Angle/°
Br1	C3	C4	C5	178.6(5)	C3	C2	C7	C8	177.7(5)
Br2	C5	C6	C7	178.9(4)	C3	C4	C5	Br2	-178.6(5)
O1	C1	C8	N2	-0.9(10)	C3	C4	C5	C6	0.0(9)
O1	C1	C8	C7	-178.7(6)	C4	C5	C6	C7	0.4(9)
N1	C1	C8	N2	178.0(5)	C5	C6	C7	C2	0.3(8)
N1	C1	C8	C7	0.2(6)	C5	C6	C7	C8	-178.5(6)
N1	C2	C3	Br1	0.2(8)	C6	C7	C8	N2	1.5(10)
N1	C2	C3	C4	179.9(6)	C6	C7	C8	C1	179.3(6)
N1	C2	C7	C6	-179.9(5)	C7	C2	C3	Br1	-177.9(4)
N1	C2	C7	C8	-0.8(6)	C7	C2	C3	C4	1.8(9)
N2	N3	C9	S1	5.4(7)	C8	N2	N3	C9	178.3(5)
N2	N3	C9	N4	-175.4(5)	C9	N4	C10	C11	171.4(8)
N3	N2	C8	C1	2.3(8)	C9	N4	C15	C14	-105.2(7)
N3	N2	C8	C7	179.7(5)	C10	N4	C9	S1	177.6(5)
N4	C10	C11	C12	-60.7(11)	C10	N4	C9	N3	-1.6(8)
C1	N1	C2	C3	-177.3(6)	C10	N4	C15	C14	78.1(8)
C1	N1	C2	C7	0.9(6)	C10	C11	C12	C13	84.0(13)
C2	N1	C1	O1	178.3(5)	C11	C12	C13	C14	-57.6(16)
C2	N1	C1	C8	-0.6(6)	C12	C13	C14	C15	53.8(13)
C2	C3	C4	C5	-1.1(9)	C13	C14	C15	N4	-81.4(8)
C2	C7	C8	N2	-177.5(5)	C15	N4	C9	S1	1.0(8)
C2	C7	C8	C1	0.4(6)	C15	N4	C9	N3	-178.2(5)
C3	C2	C7	C6	-1.4(8)	C15	N4	C10	C11	-11.9(10)

Molecular Structure of compound 22

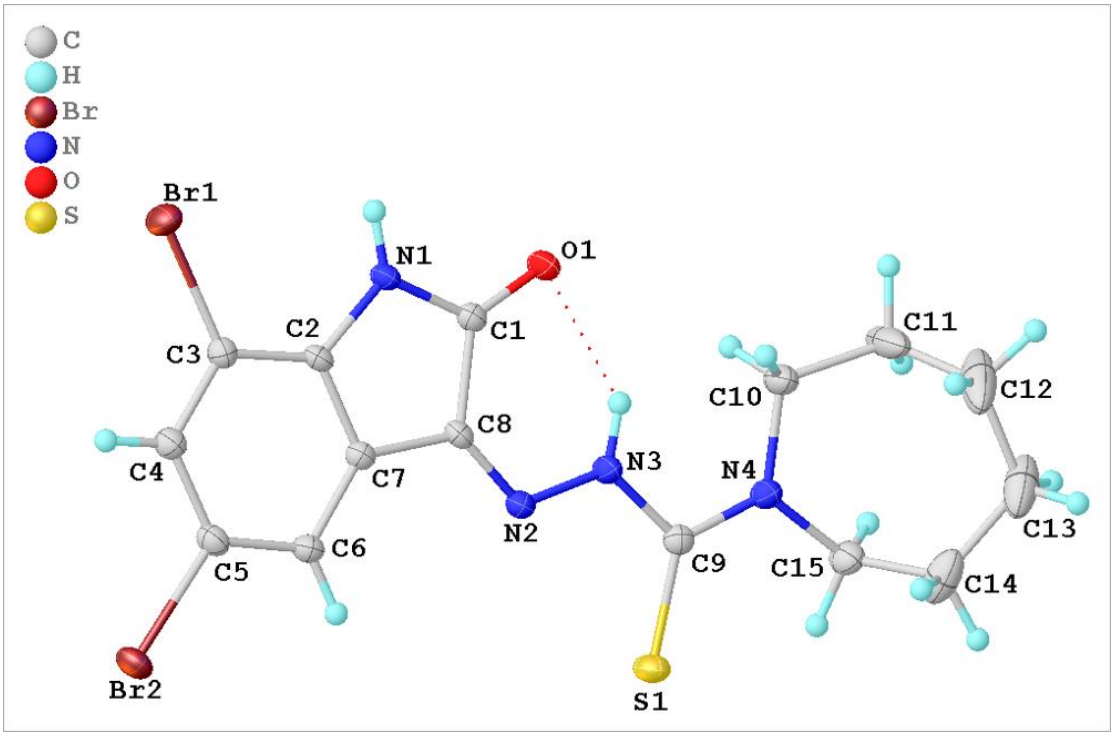

ORTEP diagram of compound (22) drawn in 20% thermal probability ellipsoids showing atomic numbering scheme.

Appendix E7

The ORTEP view of compound (***DiBrIstEt*/26)** [**CCDC** reference No. =2245787]

Table: Crystal data and structure refinement for compound **26**.

Identification code	***DiBrIstEt***
Empirical formula	$C_{11}H_{10}Br_2N_4OS$
Formula weight	406.11
Temperature/K	296.15
Crystal system	Monoclinic
Space group	P21/c
Unit cell dimensions	a = 8.0054(12)Å, α = 90°
	b =16.759(2)Å, β =110.416(5)°

	c = 11.4723(18)Å, γ = 90°
Volume	1442.5(4)$Å^3$
Z	4
Density calculated	1.870 g/cm^3
Absorption coefficient	5.761mm^{-1}
F(000)	792.0
Crystal size	0.15 × 0.12 × 0.1mm^3
Radiation	MoKα (λ = 0.71073)
2Θ range for data collection	6.164 to 53.95°
Index ranges	-10 ≤ h ≤ 10, -21 ≤ k ≤ 21, -14 ≤ l ≤ 14
Reflections collected	50738
Independent reflections	3130 [R_{int} = 0.0775, R_{sigma} = 0.0301]
Data/restraints/parameters	3130/0/173
Goodness-of-fit on F2	1.035
Final R indexes [I>=2σ (I)]	R_1 = 0.0461, wR_2 = 0.1099
Final R indexes [all data]	R_1 = 0.0691, wR_2 = 0.1211
Largest diff. peak/hole	0.60/-0.73e Å-3

Table: Bond lengths for compound **26**

Atom	Atom	Length/Å	Atom	Atom	Length/Å
Br1	C2	1.889(5)	N4	C10	1.468(6)
Br2	C4	1.897(4)	C1	C2	1.366(6)
S1	C9	1.668(4)	C1	C6	1.403(6)
O1	C8	1.234(5)	C2	C3	1.390(7)

Table: Bond lengths for compound **26**

Atom	Atom	Length/Å	Atom	Atom	Length/Å
N1	C1	1.398(5)	C3	C4	1.381(7)
N1	C8	1.353(5)	C4	C5	1.377(6)
N2	N3	1.341(4)	C5	C6	1.393(6)
N2	C7	1.291(5)	C6	C7	1.450(6)
N3	C9	1.376(5)	C7	C8	1.493(6)
N4	C9	1.318(5)	C10	C11	1.480(8)

Table: Bond angles for compound **26**

Atom	Atom	Atom	Angle/°	Atom	Atom	Atom	Angle/°
C8	N1	C1	111.0(3)	C4	C5	C6	117.4(4)
C7	N2	N3	118.1(3)	C1	C6	C7	106.2(3)
N2	N3	C9	120.3(3)	C5	C6	C1	120.1(4)
C9	N4	C10	124.6(4)	C5	C6	C7	133.7(4)
N1	C1	C6	109.8(4)	N2	C7	C6	126.2(4)
C2	C1	N1	129.2(4)	N2	C7	C8	127.3(4)
C2	C1	C6	121.0(4)	C6	C7	C8	106.4(3)
C1	C2	Br1	119.4(4)	O1	C8	N1	126.8(4)
C1	C2	C3	119.4(4)	O1	C8	C7	126.7(4)
C3	C2	Br1	121.2(4)	N1	C8	C7	106.5(4)
C4	C3	C2	119.0(4)	N3	C9	S1	118.5(3)
C3	C4	Br2	118.3(3)	N4	C9	S1	125.7(3)
C5	C4	Br2	118.7(4)	N4	C9	N3	115.8(4)
C5	C4	C3	123.0(4)	N4	C10	C11	111.7(5)

Table: Torsion angles for compound **26**

A	B	C	D	Angle/°	A	B	C	D	Angle/°
Br1	C2	C3	C4	-178.0(3)	C2	C1	C6	C7	-178.7(4)
Br2	C4	C5	C6	177.6(3)	C2	C3	C4	Br2	-178.5(3)
N1	C1	C2	Br1	-4.2(6)	C2	C3	C4	C5	1.2(7)
N1	C1	C2	C3	176.6(4)	C3	C4	C5	C6	-2.0(6)
N1	C1	C6	C5	-177.6(4)	C4	C5	C6	C1	0.5(6)
N1	C1	C6	C7	1.8(4)	C4	C5	C6	C7	-178.7(4)
N2	N3	C9	S1	-177.2(3)	C5	C6	C7	N2	-4.8(7)
N2	N3	C9	N4	3.3(6)	C5	C6	C7	C8	176.8(4)
N2	C7	C8	O1	4.8(7)	C6	C1	C2	Br1	176.5(3)
N2	C7	C8	N1	-176.0(4)	C6	C1	C2	C3	-2.7(6)
N3	N2	C7	C6	-177.9(4)	C6	C7	C8	O1	-176.8(4)
N3	N2	C7	C8	0.3(6)	C6	C7	C8	N1	2.4(4)
C1	N1	C8	O1	177.9(4)	C7	N2	N3	C9	177.0(4)
C1	N1	C8	C7	-1.4(5)	C8	N1	C1	C2	-179.7(4)
C1	C2	C3	C4	1.3(6)	C8	N1	C1	C6	-0.3(5)
C1	C6	C7	N2	175.9(4)	C9	N4	C10	C11	-83.4(6)
C1	C6	C7	C8	-2.6(4)	C10	N4	C9	S1	1.6(7)
C2	C1	C6	C5	1.8(6)	C10	N4	C9	N3	-179.0(4)

Molecular Structure of compound 26

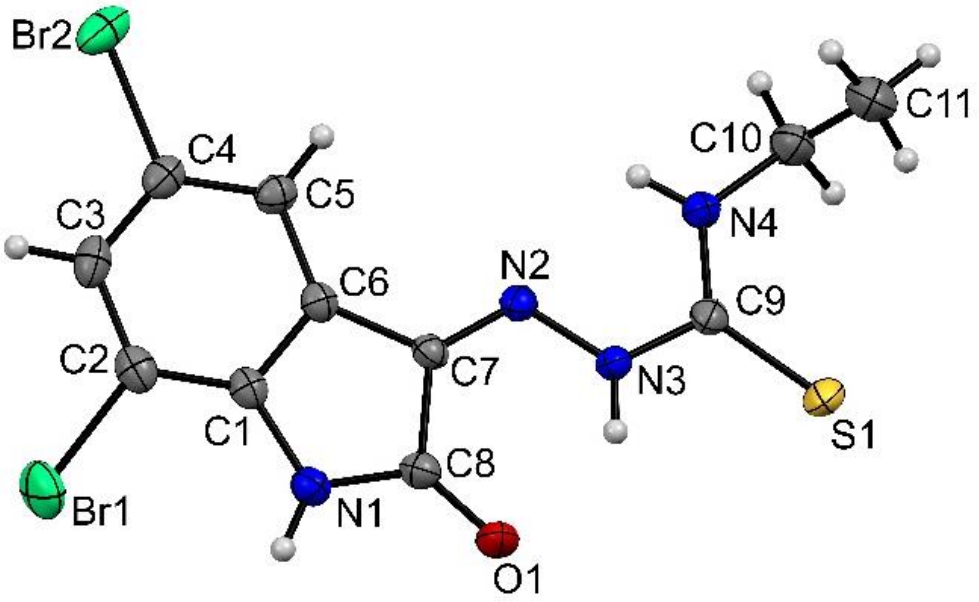

The molecular structure of compound **26**, with displacement ellipsoids drawn in 30% thermal probability level.

LIST OF PUBLICATIONS

1. Chaudhary, U., Dawa, D., Banerjee, I., Sharma, S., Mahiya, K., Rauf, A., Pokharel, Y.R., & Yadav, P.N. (2023). Anticancer Potency of N(4)-ring Incorporated-5-methoxyisatin Thiosemicarbazones. *Journal of Molecular Structure*, **1274**(2): 134549. DOI: 10.1016/j.molstruc.2022.134549

2. Chaudhary, U., Gurung V., Pachakhan, S. T., Subin, J. A., Pokharel, Y. R., & Yadav, P. N. (2023). Evaluation of Anticancer Potential of N(4)-Alkyl Substituted 5-Methoxyisatin Thiosemicarbazones: Synthesis, Characterization and Molecular Docking. *Asian Journal of Chemistry*, **35**(3): 605-616. DOI: 10.14233/ajchem.2023.26967

LIST OF PRESENTATIONS

Oral Presentation

1. Biological Evaluation of N(4)-alkyl Substituted 5-methoxyisatin Thiosemicarbazones. Upendra Chaudhary, Indranil Banerjee, Yuba Raj Pokharel, and Paras Nath Yadav; 9th National Conference on Science and Technology, "Science for Society and Innovation for Prosperity" 26-28 June, 2022, Khumaltar, Lalitpur, Nepal

Journal of Molecular Structure 1274 (2023) 134549

Contents lists available at ScienceDirect

Journal of Molecular Structure

journal homepage: www.elsevier.com/locate/molstr

Anticancer potency of N(4)-ring incorporated-5-methoxyisatin thiosemicarbazones

Upendra Chaudhary[a], Dawa Dawa[b], Indranil Banerjee[b], Shivani Sharma[b], Kuldeep Mahiya[c], Abdur Rauf[d], Yuba Raj Pokharel[b,*], Paras Nath Yadav[a,*]

[a] Central Department of Chemistry, Tribhuvan University, Kirtipur, Kathmandu, Nepal
[b] Faculty of Life Science and Biotechnology, South Asian University, Akbar Bhawan, Chanakyapuri, New Delhi-110021, India
[c] Department of Chemistry, F G M Government College, Adampur, Mandi Adampur, Hisar-125052, Haryana, India
[d] Department of Chemistry, University of Swabi, Anbar-23561, Khyber Pakhtunkhwa, Pakistan

ARTICLE INFO

Article history:
Received 24 August 2022
Revised 6 November 2022
Accepted 12 November 2022
Available online 17 November 2022

Keywords:
Anticancer activities
Breast cancer
Cell cycle arrest
Crystal structure
Lung cancer
5-methoxyisatin, Skin cancer
Thiosemicarbazones

ABSTRACT

(*Z*)-*N*'-(5-methoxy-2-oxoindolin-3-ylidene)thiomorpholine-4-carbothiohydrazide (*MeOIstTmor*), (*Z*)-*N*'-(5-methoxy-2-oxoindolin-3-ylidene)-2,6-dimethylmorpholine-4-carbothiohydrazide (*MeOIstDmMor*), (*Z*)-*N*'-(5-methoxy-2-oxoindolin-3-ylidene)morpholine-4-carbothiohydrazide (*MeOIstMor*) and (*Z*)-2-(5-methoxy-2-oxoindolin-3-ylidene)-*N,N*-dimethylhydrazine-1-carbothioamide (*MeOIstDm*) were synthesized and characterized by elemental analysis, FT-IR, ^{1}H NMR, ^{13}C NMR, UV–Vis, ESI-HRMS and single crystal X-ray analysis. Molecular docking studies showed that compound *MeOIstDmMor* interacted strongly with VEGFR2 *via* hydrogen bonding. The anticancer activities of the synthesized compounds were tested against breast cancer (MCF-7), skin cancer (A431), and lung cancer (A549) for cell viability, cell cycle arrest and western blot analysis. The compounds exhibited significant anticancer potency in micromolar concentration (IC_{50}, 2.52–7.41 μM). The compound *MeOIstDmMor* was found G0/G1 cell cycle arrest in A431 cells and inhibited C-Jun, β-catenin, Akt proteins involve in cell proliferation. Among the four compounds, compound *MeOIstDmMor* exhibited strong anticancer potency in A549 (IC_{50}, 2.52 μM) than rest of the compounds. Similarly, compound *MeOIstMor* exhibited high anticancer activity in MCF-7, IC_{50}; 2.93 μM.

1. Introduction

According to the recently released GLOBOCAN data estimated 2.3 million new cancer cases in 2020. Breast cancer is the most common cancer in women in both developing and developed countries [1]. Isatin and its derivatives such as tryptanthrin, 2-oxindoles, indirubins, sunitinib, isatin thiosemicarbazone and others are pharmacologically active compounds with anticancer, antiviral, antibacterial, anticonvulsant, antituberculosis and antidiabetic activity, as well as other properties [2]. A potent microtubule destabilizing agent 5,7-Dibromo-N-alkylisatins suppress initial tumor growth in vivo, induce apoptosis and depolymerize microtubules [3]. Isatin derivative sparfloxacin showed anticancer potency against HepG2 (human hepatic carcinoma cells), SW480 (human colon adenocarcinoma cells), A549 (human lung carcinoma cells) and HeLa (human cervical cancer cells) with an IC_{50} of 18.31->50 μg/mL [4]. Some cancer cell lines like MGC-803, PC-3 and SW620 were highly sensitive to moxifloxacin/gatifloxacin-1,2,3-triazoleisatin hybrid [5]. One of the derivatives of isatin, Sunitinib (SU011248) prevents many members of the split-kinase domain group of receptor tyrosine kinases (RTKs), such as the vascular endothelial growth factor receptors (VEGFRs) types 1 and type 2 (FLT1 and FLK1/KDR), platelet-derived growth factor receptors (PDGFR-α and PDGFR-β), stem cell factor receptor c-KIT, FLT3 and RET kinases [6]. For the treatment of solid tumors including breast and lung cancer, GlaxoSmithKline (GSK) created the anti-cancer drug Lapatinib, which includes a sulphone moiety. It has been shown to target the epidermal growth factor pathway [7]. Isatin derivatives inhibit tyrosine kinases (TKIs) and cyclin-dependent kinases (CDKs) through binding with ATP pocket as well as inhibiting caspases [8]. Thiosemicarbazones are effective against a variety of tumors, including leukemia, pancreatic cancer, breast cancer, non-small cell lung cancer, cervical cancer, prostate cancer, and bladder cancer [9]. According to SAR investigations of the synthesized thiosemicarbazones, the existence of lipophilic/inductively electron withdrawing groups (Cl, F, F_3CO, NO_2) at position-5 of the isatin moiety had a key role in

* Corresponding authors.
E-mail addresses: yrp@sau.ac.in (Y.R. Pokharel), pnyadav219@gmail.com (P.N. Yadav).

https://doi.org/10.1016/j.molstruc.2022.134549
0022-2860/

causing or boosting various activities, especially urease inhibition [10]. 2-Pyridineformamide thiosemicarbazones exerted a cytotoxic effect on PANC-1 cells in NDM, including apoptosis, in micromolar concentration [11]. By using MTT assay, it was revealed to be more powerful towards MCF-7, A431, A375, and Hela cell lines, with IC_{50} of 0.9 μM for MCF-7 [12]. α-N-Heterocyclic thiosemicarbazones inhibit ribonucleotidereductase (RR) which repair DNA synthesis in cancer chemotherapeutics [13]. Thiosemicarbazones activity is believed to be the result of increased interactions between their hydrophobic substituents and the hydrophobic residues in the TYR cavity *via* van der Waal's force, and even the potential of their N–N–S tridentate scaffold to bind catalytic copper ions in the enzyme [14]. Recently we have reported potent anticancer activity of 5-nitrosatin-4-(1-(2-pyridyl)piperazinyl)−3-thiosemicarbazone, 5-nitroisatin-4-thiomorpholinyl-3-thiosemicarbazone, 5-nitroisatin-4,4-dimethyl-3-thiosemicarbazone and their copper complexes on MCF-7, MDA-MB-231, A431 and PNT2 cells [15,16,17]. Similarly, 3-hydroxypyridine-2-carboxaldehyde N(4)-methyl and pyrrolidinyl thiosemicarbazones and their Zn(II) complexes were investigated from our laboratory for their ability to inhibit cell growth in PC3, HeLa, DU145, A431 and A549 cells [18].

In the present study, 5-methoxyisatin with N(4)-ring substituted thiosemicarbazones were synthesized with the anticipation that such modification could result in significant anticancer activity. The molecular and isomeric structures of *MeOIstDmMor* and *MeOIstDm* were determined by X-ray single crystal diffraction analysis. Anticancer activities of the compounds were evaluated against A549, MCF-7 and A431 cell lines. Additionally, molecular docking study of *MeOIstDmMor* was completed on VEGFR2 enzyme.

2. Experimental

2.1. Materials and methods

5-Methoxyisatin, thiomorpholine, 2, 6-dimethylmorpholine, morpholine, dimethylamine and N-methyl aniline were purchased from Alfa Aesar. Carbon disulphide (Qualigens fine chemicals), sodium chloroacetate (Chemical center, India), hydrazine hydrate, 98% (Fisher scientific), acetonitrile (Merck), methyl alcohol (Fisher scientific), ethyl alcohol (Merk), diethyl ether (Merck), glacial acetic acid (Fisher scientific), concentrated hydrochloric acid (Merck) and sodium hydroxide (Fisher Scientific) were used as obtained.

2.2. Instruments

FT-IR spectra were recorded using SHIMADZU, Tracer 100, melting points were determined on Philip Harris Melting Point Apparatus, and UV–Visible spectra were recorded in the range of 600–200 nm using a SPECORD®200 PLUS UV-visible spectrophotometer in MeOH and in $CHCl_3$ solution at Central Department of Chemistry, Tribhuvan University (TU), Nepal. The elemental analysis was performed using a LECO Truspec Micro analyzer, at IIT Madras, India. NMR spectra were recorded in DMSO-d_6 by using TMS as an internal standard on Bruker advance III HD NMR spectrometer, 400 MHz spectrometer and Mass spectra were recorded using ESI-HRMS on Bruker IMPACT HD liquid chromatography Mass Spectrometer at the Department of Chemistry, Savitribai Phule Pune University, India. Bruker D_8 VENTURE diffractometer with PHOTON II detector was employed for single crystal data collection at IIT Madras, India.

2.3. Preparation of N(4) substituted thiosemicarbazones

N(4)-Substituted thiosemicarbazides; Thiomorpholine-4-carbothiohydrazide, 2,6-dimethylmorpholine-4-carbothiohydrazide, Morpholine-4-carbothiohydrazide, *N,N*-dimethylhydrazinecarbothioamide were synthesized by the procedure of Scovill [19]. (*Z*)-*N*'-(5-methoxy-2-oxoindolin-3-ylidene)thiomorpholine-4-carbothiohydrazide *(MeOIstTmor),* (*Z*)-*N*'-(5-methoxy-2-oxoindolin-3-ylidene)−2,6-dimethylmorpholine-4-carbothiohydrazide *(MeOIst-DmMor),* (*Z*)-*N*'-(5-methoxy-2-oxoindolin-3-ylidene)morpholine-4-carbothiohydrazide (*MeOIstMor*) and (*Z*)−2-(5-methoxy-2-oxoindolin-3-ylidene)-*N,N*-dimethylhydrazine-1-carbothioamide (*MeOIstDm*) were synthesized by refluxing the equimolar mixture of respective thiosemicarbazide and 5-methoxyisatin (2.82 mmol) in absolute ethanol (20 mL) and glacial acetic acid (3-drops) at 80 °C for the duration of 6 h (Scheme 1) [20]. The refluxed product was allowed to cool at room temperature, washed with absolute alcohol and dried. The product was re-crystallized with EtOH and again dried.

2.3.1. (Z)-N'-(5-methoxy-2-oxoindolin-3-ylidene)thiomorpholine-4-carbothiohydrazide (MeOIstTmor)

Yield: 56.70%; Color: Orange; MP: 198 °C; Anal. Calc (%) for: $C_{14}H_{16}N_4O_2S_2$ (336.43): C, 49.98; H, 4.79; N, 16.65; Found: C, 49.42; H, 4.60; N, 16.26. FTIR (ν, cm^{-1}): 3172–3037 (br, H–N; indole&azomethine), 1685 (s, C=O), 1539 (s, C=N), 1174, 783 (s, C=S), 1155 (s, N-N), 1282 (s, O-CH_3). ^{1}H NMR (δ, ppm): 13.23 (s, 1H, HN-C=S), 11.10(s, 1H, Indole-NH), 7.01 (d, 1H, C7-H), 6.92 (d, 1H, C4-H), 6.86 (d, 1H,C6-H), 4.24 (s, 3H, -OCH_3), 3.76 (t, 4H, aliphatic-C11, C14-H), 2.81 (t, 4H, aliphatic-C12, C13-H). ^{13}C NMR (δ, ppm): 179.80(C10), 163.25(C2), 155.80(C5), 136.08(C3), 134.96(C9), 121.20(C7), 117.63(C8), 112.43(C6), 105.95(C4), 56.07(OCH_3), 53.36 (C11, C14), 27.04 (C12, C13). ESI-HRMS [*m/z*, Found (Calc.)]: 337.0789 (337.4404) $[M+H]^+$, 359.0611 (359.4221) $[M+Na]^+$. UV–Vis [λ_{max}(nm) ($CHCl_3$)]:283, 356.

2.3.2. (Z)-N'-(5-methoxy-2-oxoindolin-3-ylidene)−2, 6-dimethylmorpholine-4-carbothiohydrazide (MeOIstDmMor)

Yield: 79.92%; Color: Red; MP: 206 °C; Anal. Calc (%) for: $C_{16}H_{20}N_4O_3S$ (348.42): C, 55.16; H, 5.79; N, 16.08; found: C, 55.11; H, 5.54; N, 16.04. FTIR (ν, cm^{-1}): 3176–3064 (br, H–N; indole&azomethine), 1681 (s, C=O), 1568 (s, C=N), 1179, 697(s, C=S), 1151 (s, N-N), 1251 (s, O–CH_3).^{1}H NMR (δ, ppm): 13.19 (s, 1H, HN-C=S), 11.04 (s, 1H, Indole-NH), 6.94 (d, 1H, C7-H), 6.94(d, 1H, C4-H), 6.88 (d, 1H,C6-H), 3.68 (t, 4H, aliphatic-C12, C13-H), 3.74 (s,3H,OCH_3), 2.94 (t, 4H, aliphatic-C11, C14-H), 1.16 (d,6H,methyl-C15,C-16).^{13}C NMR (δ, ppm): 179.58 (C10), 163.18 (C2), 155.75 (C5), 136.02(C3), 134.80 (C9), 121.18 (C7), 117.53 (C8), 112.36 (C6), 105.65 (C4), 71.43 (C12,C13), 55.97 (OCH_3), 55.32(C11,C14), 18.85 (C15,C16). ESI-HRMS [*m/z*, Found (Calc.)]: 349.1332 (349.428) $[M+H]^+$, 371.1150 (371.40) $[M+Na]^+$.UV–Vis [λ_{max}(nm) ($CHCl_3$)]:284, 355.

2.3.3. (Z)-N'-(5-methoxy-2-oxoindolin-3-ylidene)morpholine-4-carbothiohydrazide (MeOIstMor)

The compound (*MeOIstMor*) has been synthesized and characterized by K.N. Aneesrahman [21].

2.3.4. (Z)−2-(5-methoxy-2-oxoindolin-3-ylidene)-N, N-dimethylhydrazine-1-carbothioamide (MeoIstDm)

Yield: 65.95%; Color: Orange; MP: 122–124 °C; Anal. Calc (%) for: $C_{12}H_{14}N_4O_2S$ (278.33): C, 51.78; H, 5.07; N, 20.13; found: C, 51.87; H, 4.97; N, 20.02%. FTIR (ν, cm^{-1}): 3267-3176 (m, H–N; indole&azomethine), 1691 (s, C=O), 1537 (s, C=N), 1182, 775 (s, C = S), 1126 (s, N-N), 1300 (s, O-CH_3). ^{1}H NMR (δ, ppm): 13.48 (s, 1H, HN-C = S), 11.07(s, 1H, Indole-NH), 7.06 (d, 1H, C7-H), 6.89 (d, 1H, C4-H), 6.83 (d, 1H,C6-H), 3.73 (s, 3H, -OCH_3–), 3.50 (t, 3H, aliphatic-C11), 3.36 (t, 3H, aliphatic-C12), ^{13}C NMR (δ, ppm): 180.37(C10), 163.39(C2), 156.64(C5), 133.86(C3,C9), 121.59(C7), 118.28(C8), 112.68(C6), 106.56(C4), 56.26(-OCH_3–),

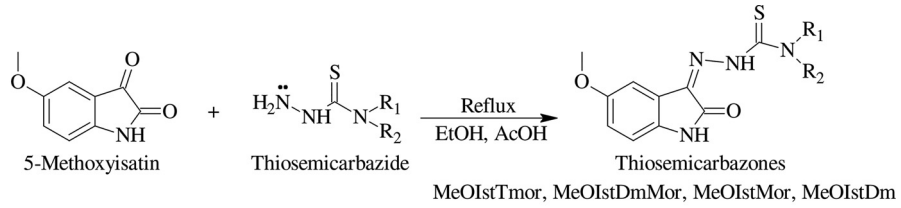

Where,

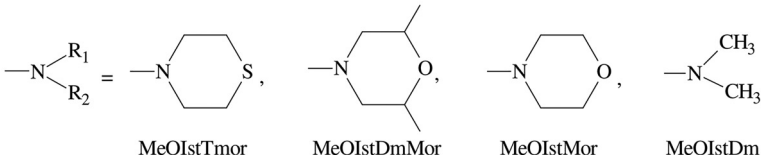

Scheme 1. Synthesis of N(4) Thiomorpholinyl/ (2,6-dimethyl)morpholinyl/ Morpholinyl/ Dimethyl amine 5-methoxyisatin Thiosemicarbazones.

29.92 (C11,C12). ESI-HRMS [*m/z,* Found (Calc.)]: 279.091 (279.338) $[M+H]^+$, 301.0734 (301.31) $[M+Na]^+$. UV–Vis [λ_{max}(nm)($CHCl_3$)]: 284, 350.

2.4. Anticancer screening

2.4.1. Cell lines

A549, MCF-7 and A431 cell lines were cultured in complete DMEM media.

2.4.2. Cell viability assay

Cell viability of A431, MCF-7, and A549 cells were assessed by crystal violet assay. Approximately 5×10^3 cells were seeded in each well of 96 wells plate. Cells were treated with different concentration of compounds and incubated for 72 h. After 72 h, the media was discarded. Cells were stained with 80 mL (0.4%) crystal violet that was prepared in 50% methanol and incubated for 30 min on a bench rocker with 20 oscillations per minute. After that, cells were washed by dipping in a beaker filled with tap water; this prevents the washout of cells. Culture plates were kept overnight for air dry at room temperature. Next day, 150 µL of methanol was added in each well and kept on a rocker for 30 min. Finally, optical density was measured in micro-plate reader at 570 nm.

2.4.3. Colony formation assay

A431 cells were analyzed to form colonies. 1000 cells were seeded in each well of six-well plates and incubated for 24 hrs. The cells were treated with the respective compounds in different concentration (0.1% DMSO as a control, 0.3 µM, 1 µM, 3 µM, and 10 µM). Fresh media was added by replacing the used one in every 72 h, followed by the treatment with respective concentration of compounds. The cell culture was maintained for 10 days with change of media after every two days. After 10 days colonies were washed with DPBS, fixed with methanol and stained with 0.4% crystal violet which was prepared in 50% methanol. The culture plate was air dried and colonies were counted using Image J software.

2.4.4. Propidium iodide staining

Around 1.5×10^5 cells/well were seeded in a six-well plate and after 24 h, treated with different concentration of compound (0.1% DMSO as a control, 0.3 µM, 1 µM, 3 µM, 10 µM). Cells were incubated for 48 h. The cell along with media from the same tube was harvested after 48 h in 1.5 ml micro-centrifuge tubes. Micro-centrifuge tubes were centrifuged at 3000 rpm for 5 min and washed with DPBS twice. Immediately after that, 80% ice-cold ethanol was added while vortexing the tube to minimize the clumping of cells. After that samples were centrifuged and given a DPBS wash twice. After adding PI, cells were incubated at 40 °C for 30 min. The cells were then analyzed with Flow Cytometry.

2.4.5. Cell cycle analysis

For cell cycle analysis, around 1.5×10^5 cells/well were seeded in a six-well plate and were harvested after 48 h of treatment. After three PBS washes, cells were fixed with 80% ice-cold ethanol. After incubation with RNase and PI stain for 30 min, cells were analyzed by FACS machine and cells in different phase were quantified. The percentage of cell with G0/G1 DNA content was used as a measure of apoptosis.

2.4.5. Immunoblotting

2.4.5.1. Cell lysate preparation. After 48 h incubation, cells were washed with DPBS and 50–80 µL of 2X SDS lysis buffer was added (depends upon confluence of cells). The cells were collected with the help of cell scrapper and collected into the MCT. After that cells were sonicated at 30% of amplification for 10 s with 10 s interval for three cycles. Sonication was done by keeping MCT in a 50 mL beaker filled with ice to avoid protein degradation. Samples were centrifuged at 16,000 g for 20 min at 40 °C. Supernatant was collected in fresh MCT and kept at −80 °C.

2.4.5.2. Protein estimation by bca kit. Pierce ™ BCA protein assay kit was used to know the total protein concentration in the samples. BCA reagent A and reagent B were mixed in 50:1 ratio respectively. Then, 200 µL mixtures were added in each well containing 25 µL of protein samples (Protein samples can be diluted by adding PBS). After that, plate was incubated for 30 min at 37 °C. The absorbance was taken at 562 nm. After plotting the absorbance (Y-axis) vs concentration graph (X-axis) we got an equation. From that equation the concentration of protein samples was calculated. To see the expression of particular protein, in each well of SDS gel, we should add equal amount (25 µg) of total protein. Thus, while dividing 25 µg with concentration of protein each MCT gives the volume of protein should be withdrawn for one well. Protein concentration and loading dye should be in 1:0.25.

2.4.5.3. SDS gel running. According to the molecular weight of protein that is of interest, the percentage of gel is determined. For higher molecular weight protein gel with lower percentage of gel is prepared and vice-versa. After transferring the gel into running buffer and then samples were loaded into the separate well.

2.4.5.4. Transferring proteins from gel to PVDF membrane. 1X transfer buffer was prepared and kept in ice to chill down. Foam pads and filter paper was soaked in 1X transfer buffer. PVDF membrane

was taken the same size of the gel and activated by dipping it in Methanol for 2 min. On a transfer cassette, the gel sandwich was prepared in the order: Sponge, filter paper, gel, PVDF membrane, filter paper, and sponge. While putting PVDF membrane above gel, 1X transfer buffer was flooded to avoid the bubbles in between. The transfer cassette was then arranged in a transfer apparatus, which was kept on the gel tank filled with 1X transfer buffer. Ice-pack is kept inside the tank and tank is kept on the ice box. Transfer was done at 90 Vs for 2 h.

2.4.5.5. Blocking the membrane. After the transfer is over, the PVDF membrane is kept in 5% skimmed milk for one hour for the blocking of unspecific proteins. 5% skimmed milk was prepared in TBST. 3% BSA is also used as a blocking agent.

2.4.6. Data and statistical analysis

The results are expressed as the mean ± standard deviation (SD). A Paired *t*-test was used to determine the significant difference between groups. A p-value< 0.05 was considered as significant.

3. Results and discussion

3.1. FTIR spectroscopy

The broad symmetrical stretching band in the range of 3267–3037 cm^{-1} was assigned to *ν*(N-H) of indole and azomethine *ν*(N-H) moieties of thiosemicarbazones [22]. The absence of a stretching band at about 2500–2600 cm^{-1}, specifies to *ν*(S-H) [23] and the presence of two strong bands specific to *ν*(C = S) at 1182–1174 cm^{-1} and 783–697 cm^{-1} indicated the existence of thiosemicarbazone in the thione tautomer [24]. Strong stretching bands appeared in the thiosemicarbazone *MeOIstTmor* at 1685 cm^{-1} and 1539 cm^{-1},respectively, assigned to *ν*(C = O) and (C = N) of thiosemicarbazones [25,26]. Similarly, the synthesized thiosemicarbazones had two significant stretching bands at the range 1691–1681 cm^{-1} and 1568–1537 cm^{-1}, respectively, that assigned to *ν*(C = O) and (C = N) [27]. The strong bands due to *ν*(N-N) of thiosemicarbazones appeared at 1155–1126 cm^{-1} [28]. Strong bands of isatin moieties of thiosmecarbazones appeared at 1300–1251 cm^{-1}, which were assigned to *ν*(-OCH_3–) [29,30] (Supplementary data S5–S7).

3.2. NMR spectroscopy

In the ^{1}H NMR (DMSO-d_6) spectra of N(4) substituted thiosemicarbazones the signals of highly polar H-N-C = S and indol-NH protons were observed downfield as a singlet at 13.48–13.19 ppm [21] and 11.10–11.04 ppm respectively [31]. A singlet peak at 11.10–11.04 ppm related to the NH adjacent to C = S, but absence of peak at 4 ppm attributed to the S–H proton in the thiosemicarbazones indicate the existence of thione tautomer [32]. All the aromatic protons of isatin moiety were seen as singlet or doublet signals at 7.06–6.83 ppm [33]. In the case of N(4) thiomorpholinyl group (*MeOIstTmor*), the signals of ring -CH_2 protons were found as a quartet at 3.76 ppm whereas in N(4) 2,6-dimethyl morpholinyl group (*MeOIstDmMor*), the signals of ring -CH_2 protons were observed as a quartet at 3.68–2.94 ppm [34] and that of methyl protons were observed as a triplet at 3.50 ppm [35] in the compound *MeoIstDm* and triplet at 1.16 ppm in the compound *MeoIstDmMor* [21,27]. The signals of methoxy (-OCH_3–) protons were observed as a singlet at 4.24–3.73 ppm in the thiosemicarbazones [36] (Supplementary data S5–S7).

In the ^{13}C NMR (DMSO-d_6) spectra of the compounds, the HN–C = S (C10) signal of the thioamide carbon was observed at the range of 180.37–179.58 ppm [37]. The characteristic –C = N (C3) and –C = O (C2) peaks were observed at 136.08–133.86 ppm and 163.39–163.18 ppm respectively [38,39]. The aromatic carbons (C4–C9) of the isatin ring were observed at 106.56–105.65(C4), 156.64–155.75 (C5), 112.43–111.68 (C6), 121.59–121.18 (C7), 118.28–117.53 (C8) and 134.96–133.86 ppm (C9) [40,41]. The C(5) (156.64–155.75) carbons atom shifted downfield due to the presence of methoxy group (OCH_3–) and its carbon peaks were observed at 56.26–55.97 ppm [22]. The signals of N(4) thiomorpholinyl group (*MeOIstTmor*) carbon atoms (C11-C14) were seen at 53.36–27.04 ppm [21] whereas the signals in N(4) 2,6-dimethyl morpholinyl group (*MeOIstDmMor*) carbons atoms (C11–C14) of cyclic ring were observed at 71.43–55.32 ppm [14]. The signals of methyl carbon atoms (C15-C16) in the compound (*MeOIstDmMor*) were observed at 18.85 ppm whereas the signal of methyl carbon atoms (C11-C12) in the compound (*MeOIstDm*) were seen at 29.92 ppm [42] (Supplementary data S8–S10).

3.3. ESI-HRMS spectrometry

All the obtained mass spectral data of the synthesized thiosemicarbazones were in agreement with the calculated data of the proposed molecular structures.

The protonated and alkali adduct analyte molecules were seen using the positive mode of the ESI-HRMS investigations for the mass spectral peaks of the compounds. The protonated molecular ion $[M+H]^+$ peaks of thiosemicarbazones were observed at *m/z* = 337.0789 (calc., 337.4404) (*MeOIstTmor*), *m/z* = 349.1332 (calc., 349.4280) (*MeOIstDmMor*) and *m/z* = 279.0910 (279.338) (*MeOIstDm*) [21,43]. Beside the protonated peaks, the thiosemicarbazones showed the molecular ion $[M+Na]^+$ peaks: *m/z* = 371.1150 (calc., 371.4000) (*MeOIstDmMor*), *m/z* = 343.0838 (calc., 343.3565) (*MeOIstMor*) and *m/z* = 301.0734 (calc., 301.31) (*MeOIstDm*). In the compound *MeOIstDmMor*, the fragment N(4)–2,6-dimethylmorpholinyl $[C_{16}H_{20}N_4O_3 + H]^+$ cation caused the prominent peak at *m/z* 317.1606 (calc., 317.3630) [44]. The presence of fragment N(4) dimethylamine $[C_{12}H_{14}N_4O_2 + H]^+$ cation in the compound *MeOIstDm* accounts for the prominent peak at *m/z* 247.1185 (calc., 247.2731). Fragmentation is characterized by loss of one sulfur atom, abbreviated SH (*m/z*; 33 amu) [45]. Mass spectral data of the thiosemicarbazones agree well with those estimated for their putative structures [46] (Supplementary data S11–S13).

3.4. UV–Vis spectroscopy

UV-visible spectral data of the thiosemicarbazones were recorded in $CHCl_3$ in the 600–200 nm range. The compounds exhibited two broad absorption bands with varying intensities and shoulder like appearance in the region 284 nm and 356–350 nm[37] attributed to n→π^* intraligand electronic transition viz. the bands due to the electronic transition of azomethine (-C = N) and that due to thioamide (-HN-C = S) group [44,47,48]. The $\pi \rightarrow \pi^*$ transitions of the imine C = N double bond were seen at 284 nm for all the synthesized thiosemicarbazones, the bands at 356 nm are assigned to the electronic transition n → π^* of the thiosemicarbazone moiety (C = S) [42,49]. Similar observations about the peak position and nature has been observed with isatin thiosemicarbazones [50] (Supplementary data S14–S15).

3.5. X-ray crystallography

Single crystals of *MeOIstDm* and *MeOIstDmMor* suitable for X-ray diffraction studies were grown by slow evaporation in 1:4 mixtures of $CHCl_3$ and EtOH. The single crystal diffraction data were collected at 298 K on Bruker D8 VENTURE diffractometer with

Table 1
Crystal data and structure refinement parameters.

Identification code	MeOIstDm	MeOIstDmMor
Empirical formula	$C_{12}H_{14}N_4O_2S$	$C_{16}H_{22}N_4O_4S$
Formula weight	278.33	366.43
Temperature/K	296.15	296.15
Crystal system	monoclinic	orthorhombic
Space group	$P2_1/c$	$Pna2_1$
a/Å	9.357(2)	16.091(3)
b/Å	9.9370(19)	8.6078(14)
c/Å	14.207(3)	27.098(5)
α/°	90	90
β/°	104.929(9)	90
γ/°	90	90
Volume/Å^3	1276.4(5)	3753.3(11)
Z	4	8
ρ_{calc}g/cm^3	1.448	1.297
μ/mm^{-1}	0.258	0.200
F(000)	584.0	1552.0
Crystal size/mm^3	0.35 × 0.25 × 0.2	0.15 × 0.12 × 0.1
Radiation	Mo/K_α (λ = 0.71073)	Mo/K_α (λ = 0.71073)
2θ range for data collection/°	5.06 to 64	6.932 to 49.998
Index ranges	$-13 \le h \le 13$, $-14 \le k \le 14$, $-21 \le l \le 21$	$-19 \le h \le 19$, $-10 \le k \le 10$, $-32 \le l \le 32$
Reflections collected	47,022	74,084
Independent reflections	4418 [R_{int} = 0.0439, R_{sigma} = 0.0250]	6574 [R_{int} = 0.1318, R_{sigma} = 0.0648]
Data/restraints/parameters	4418/0/175	6574/25/467
Goodness-of-fit on F^2	1.096	1.202
Final R indexes [$I \ge 2\sigma$ (I)]	R_1 = 0.0646, wR_2 = 0.1546	R_1 = 0.0997, wR_2 = 0.1943
Final R indexes [all data]	R_1 = 0.1035, wR_2 = 0.1768	R_1 = 0.1280, wR_2 = 0.2063
Largest diff. peak/hole / e Å^{-3}	0.64/−0.42	0.34/−0.30
Flack parameter	–	0.10(9)

PHOTON II detector with Mo/K_α radiation (λ = 0.71073 Å). The data were corrected for Lorentz and polarization effects. Multi-scan absorption correction was applied. The structure was solved by direct methods using ShelXT [51] and refined by full-matrix least-squares refinement techniques on F^2, using ShelXL-2018/3 [52]. All calculations were done with the help of OLEX^2 version 1.5 crystallographic software [53]. For the molecular graphics, the programme OLEX^2 [53] and Mercury [54] were used. All non-hydrogen atoms were refined anisotropically. All hydrogen atoms were fixed geometrically with Uiso values of 1.2 times the U_{iso}values of their respective carrier atoms. The hydrogen on lattice water were located from difference fourier map and refined using the riding model. For *MeOIstDm,* a total of 47,022 reflections were measured of which 4418 were unique and 3148 were considered observed ($I > 2\sigma$ (I)]. The final residual index are; R_1 = 0.0646, wR_2 = 0.1546 for the observed and R_1 = 0.1035, wR_2 = 0.1768 for all reflections using 175 parameters. For *MeOIstDmMor*, a total of 74,084 reflections were measured of which 6574 were unique and 5048 were considered observed ($I > 2\sigma$ (I)]. The final residual index are; *R* 0.0997, *R*w 0.1943 for the observed and *R* 0.1280, *R*w 0.2063 for all reflections using 467 parameters 25 restraints. Details of the crystallographic data and structure refinement for *MeOIstDm,* and *MeOIstDmMor* are given in Table 1. Selected bond lengths are given in Tables 2 and 3. CCDC reference numbers 2,194,144 *(MeOIstDm)* and 2,194,145 *(MeOIstDmMor)* contains the supplementary crystallographic data for this paper.

3.5.1. Crystal structure description

The structure of compound *MeOIstDm* and *MeOIstDmMor* together with the atom labeling scheme is shown in Fig. 2 and Fig. 3 respectively. The compound *MeOIstDm* crystallizes in monoclinic space group $P2_1/c$ with one molecule in the asymmetric unit (Fig. 2) and the compound *MeOIstDmMor* crystallizes in orthorhombic $Pna2_1$ space group with two molecule of compound and two lattice water molecules in the asymmetric unit (Fig. 3). The quality of data for *MeOIstDmMor* is not very good. The value of R_{int} is 13.2% and the Poor Data/Parameter Ratio of 7.21. The crystal is a weak diffractor and diffract very weakly beyond $2\theta = 42^0$.

Table 2
Bond Lengths for *MeOIstDm*.

Atom	Atom	Length/Å	Atom	Atom	Length/Å
S1	C10	1.6735(19)	N4	C5	1.416(3)
O1	C1	1.430(3)	N4	C9	1.358(3)
O1	C2	1.377(2)	C2	C3	1.390(3)
O2	C9	1.228(3)	C2	C7	1.394(3)
N1	N2	1.354(2)	C3	C4	1.398(3)
N1	C8	1.293(2)	C4	C5	1.371(3)
N2	C10	1.378(2)	C5	C6	1.399(3)
N3	C10	1.335(2)	C6	C7	1.380(3)
N3	C11	1.467(3)	C6	C8	1.455(3)
N3	C12	1.448(3)	C8	C9	1.518(3)

Figs. 1 and 3

In compound *MeOIstDmMor*, a comparison of C-N and N-N bond distances with typical single and double bond lengths [C(9)-N(1) 1.322, C(5)-N(1) 1.405, C(10-N(3) 1.358, C(10)-N(4) 1.334, C(16)-N(4) 1.473, C(11)-N(4) 1.428, C(8)=*N*(2) 1.279, N(2)-N(3)1.354 Å] indicates that charge delocalization is widespread throughout the thiosemicarbazone skeleton. Similarly in compound *(MeOIstDm),* the comparison of C-N and N-N bond distances with typical single and double bond lengths [C(9)-N(4) 1.358, C(10)-N(2) 1.378, C(10)-N(3) 1.335, C(11)-N(3) 1.467, C(12)-N(3) 1.448, C(8)-N(1) 1.293, N(1)-N(2)1.354 Å] also indicates that charge delocalization is widespread throughout the thiosemicarbazone skeleton [55]. All bond distances are normal in the 5-methoxyisatin moiety in the compound *(MeOIstDmMor),* except for the elongated C(9)-C(8) single bond is 1.525 Å whereas in compound *(MeOIstDm)* C(9)-C(8) single bond is 1.518 Å. In 5-methoxyisatin moiety C(9)-O(2) distance for studied *MeOIstDmMor* crystal structure is 1.242 Å whereas in *(MeOIstDm)* C(9)-O(2) bond distance is 1.228 Å [49]. In comparison to the 5-methoxyisatin derivative (*Z*)-*N*-(5-methoxy-2-oxoindolin-3-ylidene)pyrrolidine-1-carbothiohydrazide, the bond lengths C-N, N-N, C(9)-C(8), and

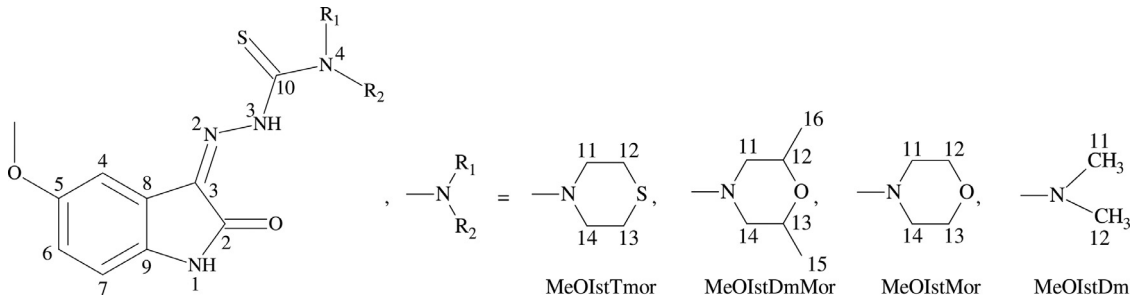

Fig. 1. Structure and numbering of 5-MethoxyisatinThiosemicarbazones.

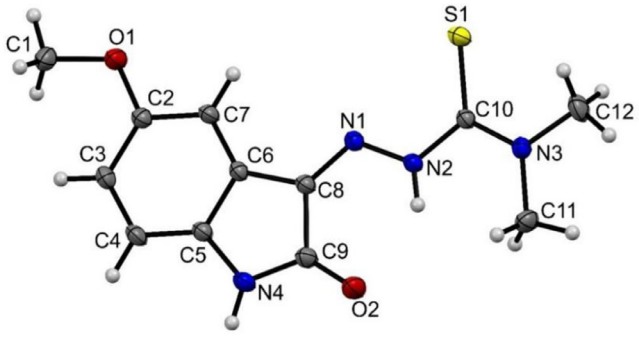

Fig. 2. ORTEP diagram of compound *MeOIstDm* drawn in 30% thermal probability ellipsoids showing atomic numbering scheme.

C(9)-O(2) of the compounds *MeOIstDmMor* and *MeOIstDm* are similar [21]. Indole-3-thiosemicarbazone, {1.696 (3) Å}, and 5-bromo indole-3-thiosemicarbazone, {1.699(2) Å} have identical C = S bond lengths of 1.679(9) Å in *MeOIstDmMor* and 1.6735(19) Å in *MeOIstDm* [56]. The bond angle of N2-N1-C8-C6 is 179.62(19)°, indicating that *MeOIstDm* of the imine N2 atom undergone sp^2 hybridization whereas the torsion angle C5-C4-C8-N2 is 179.11(9)°, indicating that the compound *MeOIstDmMor* has an *E* (trans) configuration, resulting in the double bond character of C = N [47] (Supplementary data S16–S31).

The two molecules in the asymmetric unit of *MeOIstDmMor* are involved in intra as well as intermolecular H-bonding *via* two lattice water molecules (Fig. 4). The sulfur atom S2 shows H-bonding with hydrogen atom H8A of lattice water molecule (O8–H8A.....S2 = 2.535(4) Å), this water molecule further involved in H-bonding with second water molecule (O7–H7C.....O8 = 2.097(10) Å), and oxygen atom (O7) of this water molecule involved in H-bonding with hydrogen atom attached to ring nitrogen (N1) of neighboring molecule (N1–H1.....O7 = 2.080(8) Å). The oxygen atom on this molecule involved in intra as well as intermolecular H-bonding, it shows intramolecular H-bonding with hydrogen (H3A) attached to nitrogen (N3–H3A.....O2 = 1.989(6) Å) and intermolecular H-bonding with hydrogen H5 attached to the ring nitrogen (N5) of neighboring molecule (N5–H5.....O2 = 2.028(6) Å) forming a two dimensional H-bonding network (Fig. 5).

3.6. *Molecular docking studies of compound* MeOIstDmMor

Molecular docking studies were carried out by using Molecular Operating Environment (MOE) software package. Three-dimensional (3D) crystal structure of VEGFR2 was obtained from Protein Data Bank (PDB). The accession code for the downloaded enzyme was 4ASD. Before docking studies, the docking protocol was validated by using re-dock method. Native co-crystallized ligand sorafenib was re-docked into the binding site of prepared enzyme. Comparison of the binding orientation was carried out between the re-docked ligand and experimental ligand. The validated protocol with root-mean square deviation less than 2 Å was used for further docking simulations. The 3-D / 2-D interaction plots of native ligand sorafenib are shown in Fig. 6**: (a-b)**. Native ligand sorafenib forms hydrogen bond interactions with Asp1044, Cys919 and Cys919. While a π-π stacking interaction was also observed

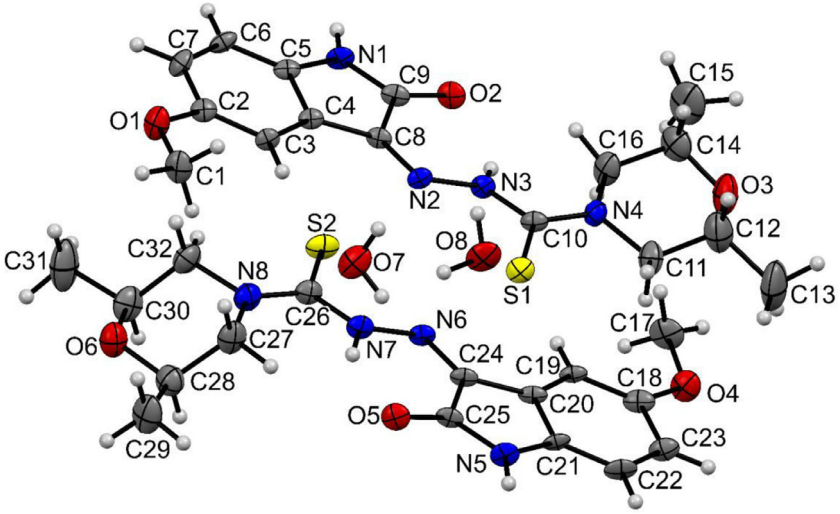

Fig. 3. ORTEP diagram of *MeOIstDmMor* drawn in 20% thermal probability ellipsoids showing atomic numbering scheme. The asymmetric unit contains two crystallographically independents units and two water molecule in the crystal lattice.

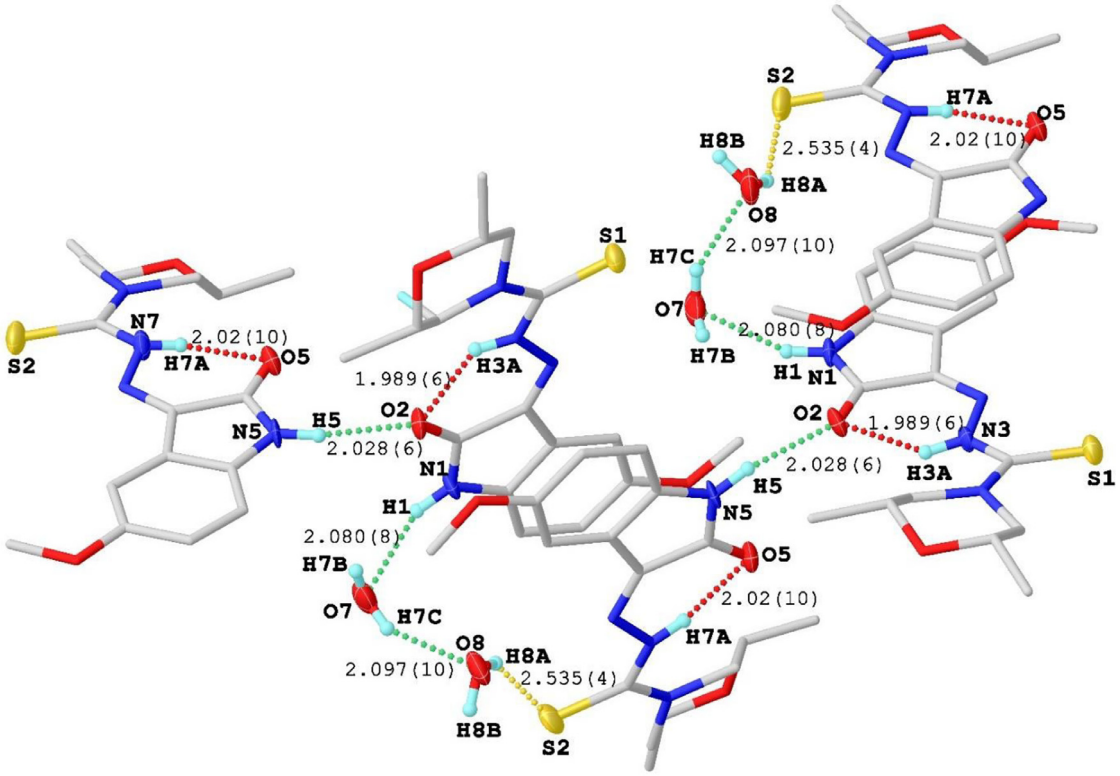

Fig. 4. Hydrogen bonding interactions in the crystal lattice of *MeOIstDmMor* viewed along the crystallographic *c*-axis (Hydrogen bonding interactions with max D–A distance 2.9 Å and minimum angle 120°).

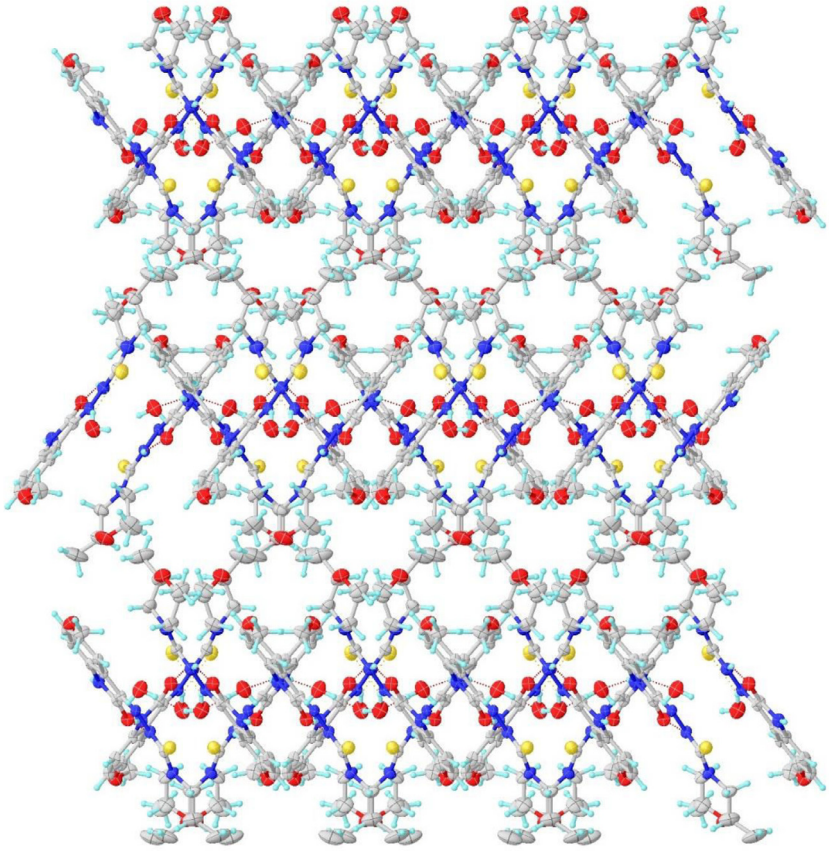

Fig. 5. Two dimensional hydrogen bonding network in the crystal lattice of *MeOIstDmMor* viewed along crystallographic a-axis. (Hydrogen bonding interactions with max D–A distance 2.9 Å and minimum angle 120°).

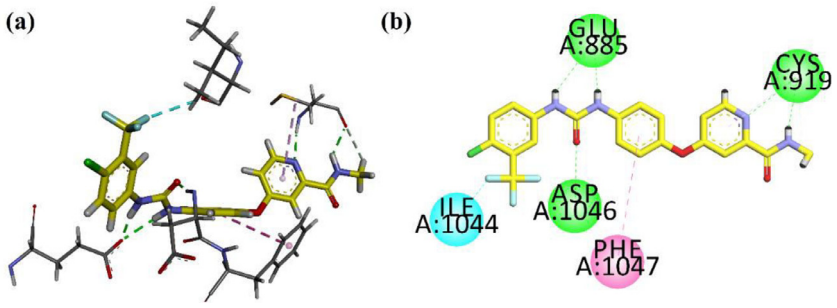

Fig. 6. (a-b) 3D and 2D interaction plots of native ligand sorafenibinto the binding site of VEGFR2 enzyme (PDB ID = 4ASD).

Table 3
Bond Lengths for *MeOIstDmMor*.

Atom	Atom	Length/Å	Atom	Atom	Length/Å
C1	O1	1.411(12)	C18	C19	1.389(14)
C2	C3	1.374(13)	C18	C23	1.415(14)
C2	C7	1.396(14)	C18	O4	1.382(12)
C2	O1	1.378(12)	C19	C20	1.407(12)
C3	C4	1.425(12)	C20	C21	1.391(12)
C4	C5	1.405(12)	C20	C24	1.440(14)
C4	C8	1.424(13)	C21	C22	1.368(14)
C5	C6	1.361(13)	C21	N5	1.396(12)
C5	N1	1.405(12)	C22	C23	1.399(15)
C6	C7	1.389(14)	C24	C25	1.504(11)
C8	C9	1.525(11)	C24	N6	1.319(11)
C8	N2	1.279(11)	C25	N5	1.316(12)
C9	N1	1.322(13)	C25	O5	1.235(12)
C9	O2	1.242(12)	C26	N7	1.356(13)
C10	N3	1.358(12)	C26	N8	1.333(14)
C10	N4	1.334(13)	C26	S2	1.688(10)
C10	S1	1.679(9)	C27	C28	1.487(19)
C11	C12	1.435(19)	C27	N8	1.484(14)
C11	N4	1.428(15)	C28	C29	1.524(17)
C12	C13	1.50(2)	C28	O6	1.437(16)
C12	O3	1.449(18)	C30	C31	1.50(2)
C14	C15	1.59(2)	C30	C32	1.458(18)
C14	C16	1.439(19)	C30	O6	1.414(16)
C14	O3	1.377(18)	C32	N8	1.482(15)
C16	N4	1.473(14)	N2	N3	1.354(10)
C17	O4	1.399(14)	N6	N7	1.351(12)

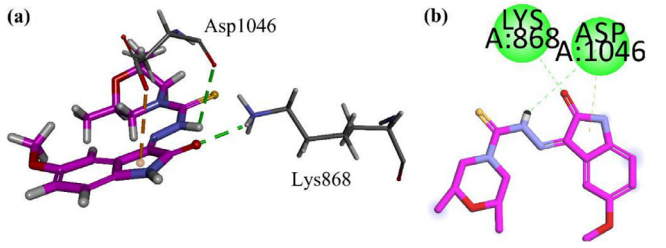

Fig. 7. (a-b) 3D and 2D interaction plots of *MeOIstDmMor* into the binding site of VEGFR2 enzyme (PDB ID = 4ASD).

between Phe1047 and Phenyl ring of sorafenib. Trifluoromethyl (CF_3) group forms halogen interactions with Ile1044. The synthesized 5-methoxyisatin derivative was also docked into the binding site of VEGFR2 enzyme. Its 3-D / 2-D dimensional interaction plots are shown in Fig. 7**: (a-b)**. The synthesized compound interacts with Asp1046 and Lys868 *via* hydrogen bond interactions. The strength of ligand-enzyme complex was computed in terms of binding energy of the docked poses. The computed binding energy value for native sorafenib was −9.0855 Kcal mol^{-1}. While for isatin derivative, it was −6.4015 Kcal mol^{-1}. The interaction plots of 5-methoxyisatin derivative are shown in Fig. 8**: (a-b)**. The compound forms two hydrogen bond interactions with Ile1025 and Arg1027.The computed binding energy value for *MeOIstDmMor*, it was −6.3185 Kcal mol^{-1}.

Table 4
Cell Viability assay (μM) of the compounds in different cell lines with their IC_{50} Values for 72 h.

Compd↓ Cell lines→	MCF-7	A549	A431
MeOIstTmor	2.93	6.81	5.29
MeOIstDmMor	4.41	2.52	4.80
MeOIstMor	5.41	5.64	6.84
MeOIstDm	7.41	3.55	7.25

3.7. Anticancer activity

Breast cancer cells (MCF-7), Lung cancer cells (A549), and Skin cancer cells (A431) were cultured in 96 well plates in DMEM medium for 12 h and treated cells with different concentration (i.e., 1, 3, 10, and 30 μM of *MeOIstTmor, MeOIstDmMor, MeOIstMor* and *MeOIstDm* respectively and incubated for 72 h as shown in Fig. 9: A, B, C and D respectively. All the synthesized compounds showed high inhibitory effects toward cell viability. Table 4, shows the IC_{50} value of different synthetic compounds against different cell lines, the compound *MeOIstDmMor* has exhibited broad spectrum activity towards A549 with IC_{50} value 2.52 μM than rest of compounds whereas the compound *MeOIstTmor* has exhibited high anticancer activity against MCF-7 with IC_{50}; 2.93 μM. All the compounds have shown moderate activity towards A431 with IC_{50} ranging from 4.80 to 7.25 μM.

Cells were seeded at a density of 3000–4000 cells/well in a 96 well plate and incubated at 37 °C for 24 h. Then, the medium was removed, and freshly prepared solutions of the compounds were added (Control, 0.3 μM, 1 μM, 3 μM, and 10 μM). After a 72 h treatment, crystal violet assay was performed. A, B, C, D shows the effect of *MeOIstTmor, MeOIstDmMor, MeOIstMor* and *MeOIstDm* on different cell lines respectively. Data are represented as mean ± SD of three independent experiments. With an IC_{50} of 2.93 μM compared to other compounds, the compound *MeOIstTmor* demonstrated strong anticancer activity against MCF-7.

Out of screened compounds for their effects in cell viability in different cancer cell lines *MeOIstDmMor* showed a better antiproliferative effects against the A431 cell line. It was selected for further studies to determine the ability of the cells to from colonies in presence of *MeOIstDmMor* in a dose dependent manner. A431 cells were seeded in six well plates with low numbers of 3000 cells/well and treated compound in different concentrations (C, 0.3, 1, 3, and 10 μM), every after 72 h fresh media was added with compound. After two weeks of incubation, it was observed that *MeOIstDmMor* inhibited the size and number of colonies in dose dependent manner (Fig. 10**:** A and B). We found colonization of cell was inhibited (100%) above 3 μM as compared to control after two weeks. The number of colonies drastically decreased as compare

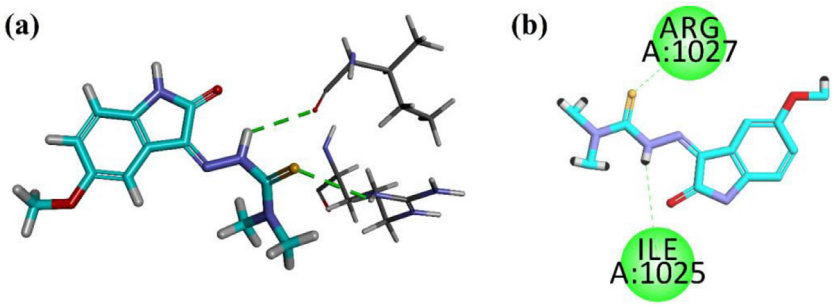

Fig. 8. (a-b) 3D and 2D interaction plots of *MeOIstDmMor* into the binding site of VEGFR2 enzyme (PDB ID = 4ASD).

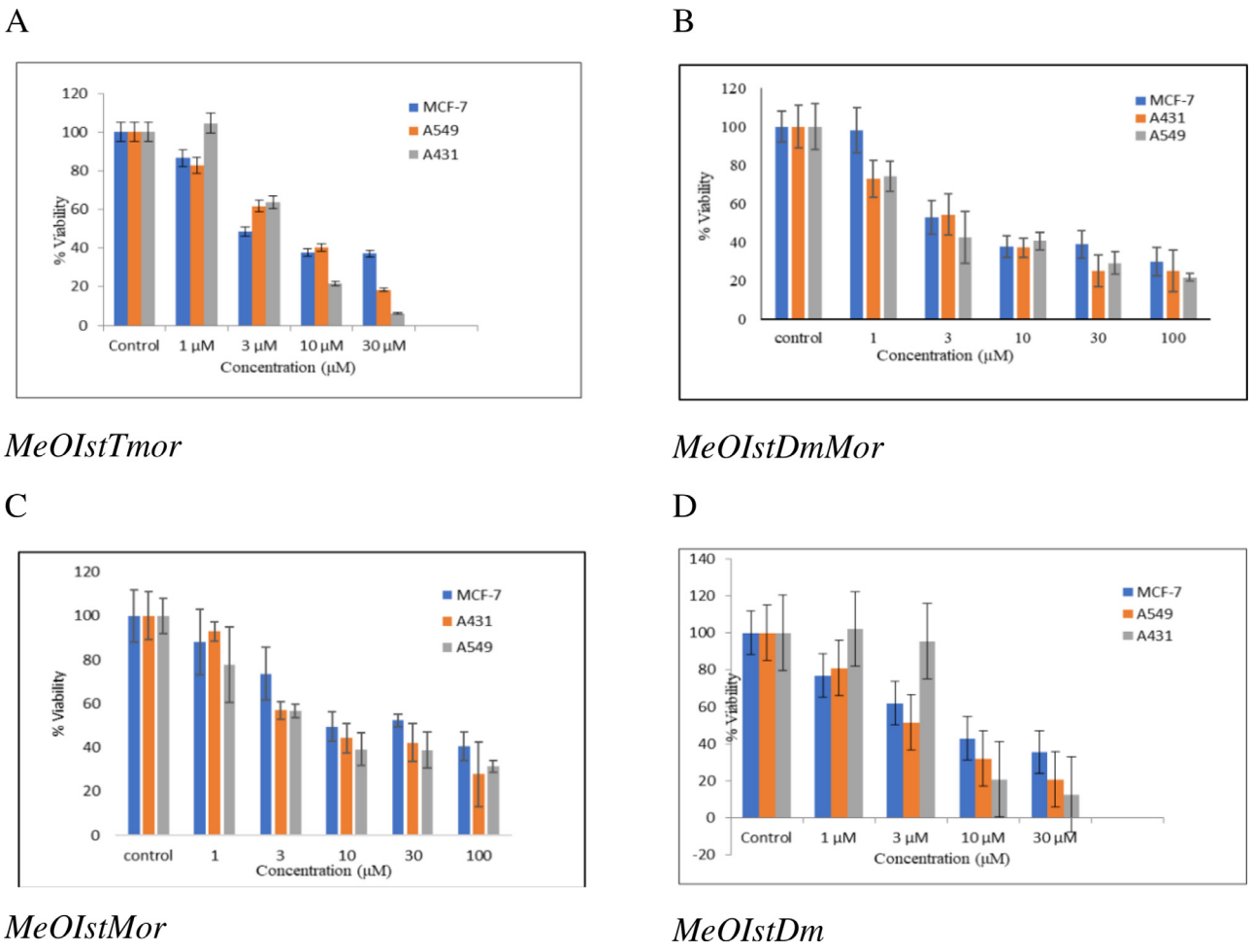

Fig. 9. Cell Viability assay synthetic compounds with different concentration.

to that of control with compound treatment, however the ability to form colony was completely inhibited in 3 µM and 10 µM of concentration.

To analyze the effect on cell death of A431 cells by flow cytometry assay using propidium iodide staining, cells were treated in different concentrations, i.e., control, 0.3 µM, 1 µM, 3 µM, and 10 µM of *MeOIstDmMor*. As shown in Fig. 10**,** in comparison with the control, treatment with *MeOIstDmMor* led to an increase in apoptotic cell population significantly in a concentration dependent manner, which might be due to DNA damage or other survival stresses induced by *MeOIstDmMor* similar to many other thiosemicarbazone derivatives [12]. Furthermore, the effect of *MeOIstDmMor* in cell cycle was evaluated, A431cells were treated with a lower dose of *MeOIstDmMor* i.e., control, 0.3 µM, and 1 µM. Compared to control, significant percentage of cells were arrested in the G0/G1 phase treated with 0.3 µM, and 1 µM (Fig. 11**:** A, B, C, D). It was found that *MeOIstDmMor* changed the profile of the cell cycle with an increase in G0/G1 cell population associated with decline G2/M and S cell population. This increase in percentage of cells in S phase arrest might be attributed to irreparable DNA damage [57].

A431 cells were seeded in six well plates with low numbers of 3000 cells/well and treated compound in different concentrations (C, 0.3, 1, 3, and 10 µM), every after 72 h fresh media was added with compound for 14 days and crystal violet staining was performed. B. A431 cells were seeded at a density of 30,000 cells/well in a 12-well plate and incubated at 37 °C for 24 h and treated compound in different concentrations of *MeOIstDmMor* (C, 0.3, 1, 3, and

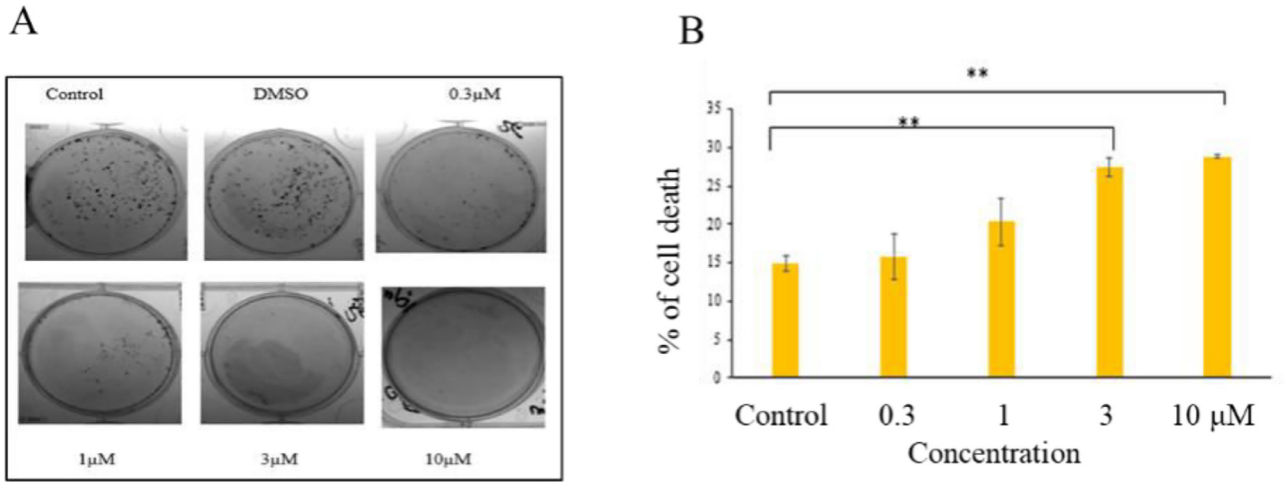

Fig. 10. Colony Formation assay and Flow Cytometric analysis of apoptosis by Propidium Iodide (PI) Staining A.

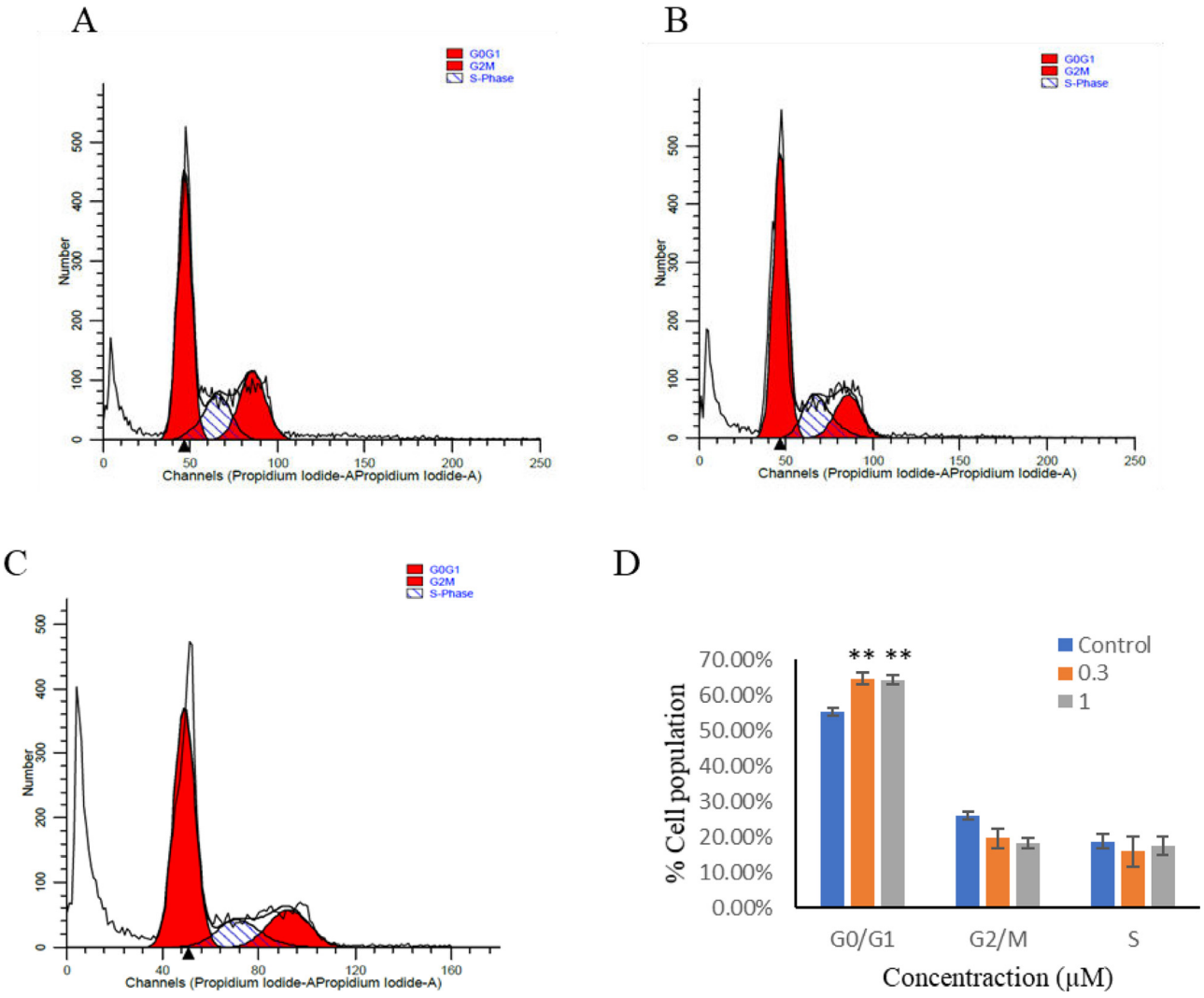

Fig. 11. *MeOlstDmMor* causes G0/G1 cell cycle arrest in A431 cell line (A) Control (DMSO). Hectograph representing PI area vs number of cells when treated with 0.3 (B) and 1 μM (C) of *MeOlstDmMor* were fixed and permeabilized with 80% chilled ethanol and stored for overnight at 4 °C. Then cells were washed and subjected to RNase treatment and PI staining for 30 min at room temperature for flow cytometry to analyze DNA content.

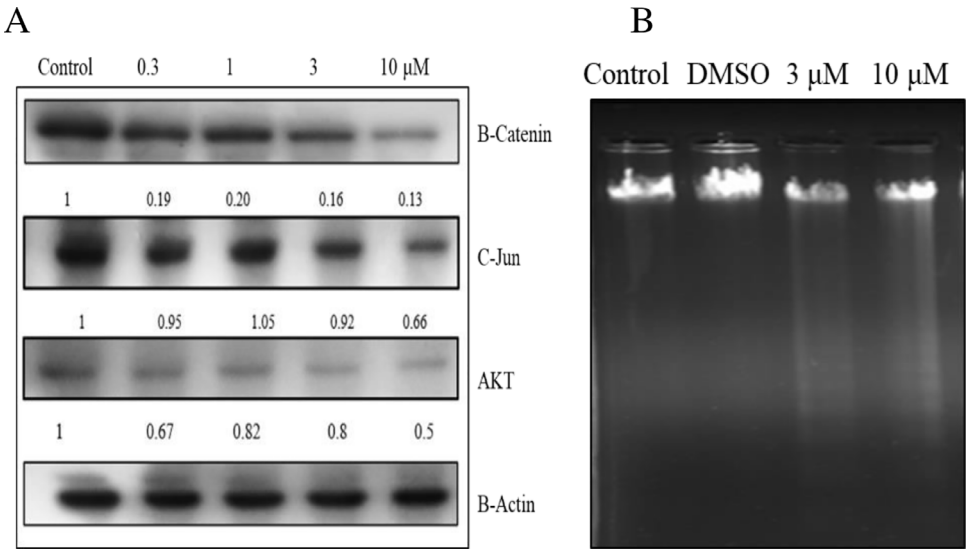

Fig. 12. A; Western blotting analysis of compound *MeOIstDmMor* in A431 cell line.

10 µM). After a 72hPI staining was performed. Data represented as mean ± SD of three independent experiments $p^{**} < 0.01$, $^{*}p<0.05$. Bar graph showing the percentage of cell death compared to vehicle control (DMSO).

To identify the mechanism of action affected by treatment of *MeOIstDmMor* in skin cancer cell line, we examined downstream molecules associated with MAPK signaling path ways that regulate major cellular events including cell proliferation, survival and migration. Improper functioning of MAPK pathways leads to the development and progression of cancer [18]. We found that *MeOIstDmMor* treatment in A431 skin cancer cell line, downregulate the expression of MAPK pathway molecules c-jun. Where in cancer condition, the highly express c-Jun are associated with cell proliferation and angiogenesis [12]. *MeOIstDmMor* induced cell death and apoptosis in A431 cells significantly, to understand its effects in the expression of proteins which are responsible for cancer cell proliferation, we have performed western blot analysis. As shown in Fig. 11:A, the expression level of β-catenin, C-Jun and Akt significantly inhibited after the treatment of cells with *MeOIstDmMor* in concentration dependent manner. It shows that compound *MeOIstDmMor* induce cytotoxic activity with the regulation of β-catenin, C-Jun and Akt which are responsible for cell proliferation, migration and apoptosis in cancer.

Cleavage of chromosomal DNA into oligonucleosomal size fragment is an integral part of apoptosis. So, to evaluate the role of compound *MeOIstDmMor* in A431cell, DNA fragmentation assay was conducted. As shown in Fig. 12**:** B that uncut DNA that is control as well as drug control shows distinct band of DNA. However, typical ladder DNA fragments of 180–200 base pairs and multiples thereof on an agarose gel should be present as the concentration of the drugs increases but, in our experiment, only the formation of DNA smear has been observed as concentration of drugs has increases.

A431 cells were treated with different concentrations of the *MeOIstDmMor* (Control, 0.3 µM, 1 µM, 3 µM and 10 µM) and β-actin was used as loading control. *MeOIstDmMor* inhibit β-Catenin, C-Jun and AKT protein expression in dose dependent manner. **B;** Agarose gel showing fragmentation of DNA, Lane 1 contains control DNA sample while lane 2 contain drug control i.e., DMSO. Lane 3 and 4 contain samples for *MeOIstDmMor* 3 µM and 10 µM respectively.

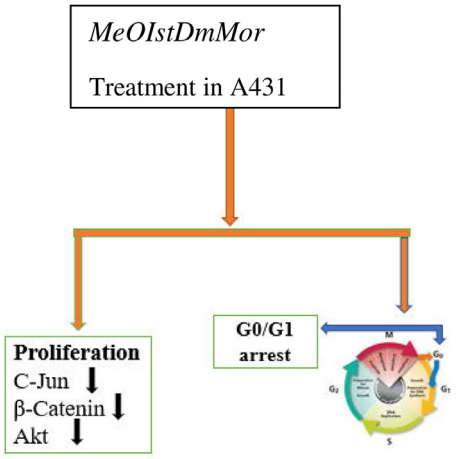

Fig. 13. Graphical abstract of *MeoIstDmMor* mediated anticancer activity in A431 cells lines.

4. Conclusions

The single crystal X-ray diffraction study has proved that the thiosemicarbazones exist as the thione tautomer. Molecular docking studies showed that compound *MeOIstDmMor* interacted strongly with VEGFR2 *via* two hydrogen bonding with Il1025 and Arg1027. Our investigation displayed promising anticancer activity of *MeOIstTmor, MeOIstDmMor, MeOIstMor* and *MeOIstDm* with IC_{50} of 2.52 to 7.41 µM respectively, which may serve as anticancer drugs for skin cancer in the future. *MeOIstDmMor* significantly inhibited cancer cell proliferation in low dose and inhibited A431 cancer cell colony formation, PI staining was conducted and found to undergo apoptosis in a dosage dependent, with G0G1 phase cell cycle arrest. Western blotting analysis of *MeOIstDmMor* treated skin cancer cell lines showed downstream molecules of MAPK (C-Jun), β-catenin and Akt. Experimental data obtained suggest that *MeOIstDmMor* has a significant cytotoxic effect on skin cancer cell viability, and we conclude that this compound can be used as a therapeutic agent for the treatment of cancer in future.

Declaration of Competing Interest

Submission of this manuscript complies with no conflict of interest that exists among the authors to declare.

Data Availability

No data was used for the research described in the article.

Acknowlegements

The authors sincerely acknowledge Nepal Academy of Science and Technology (NAST), Khumaltar, Lalitpur, Nepal for Ph.D. fellowship grant (2018/2019 AD) to UC. The authors gratefully acknowledge IIT Madras, India for CHN analysis and single crystal data collection and Dr. Anupa A Kumbhar, Department of Chemistry at Savitribai Phule Pune University, India for providing NMR and mass spectral data.

Supplementary materials

Supplementary material associated with this article can be found, in the online version, at doi:10.1016/j.molstruc.2022.134549.

References

[1] C. Luo, N. Li, B. Lu, J. Cai, M. Lu, Y. Zhang, H. Chen, M. Dai, Global and regional trends in incidence and mortality of female breast cancer and associated factors at national level in 2000 to 2019, Chin. Med. J. (Engl). 135 (2022) 42–51, doi:10.1097/CM9.0000000000001814.

[2] Sonam Varun, R. Kakkar, Isatin and its derivatives: a survey of recent syntheses, reactions, and applications, Medchemcomm 10 (3) (2019) 351–368, doi:10.1039/c8md00585k.

[3] K.L. Vine, L. Belfiore, L. Jones, J.M. Locke, S. Wade, E. Minaei, M. Ranson, N-alkylated isatins evade P-gp mediated efflux and retain potency in MDR cancer cell lines, Heliyon 2 (2016) 2405-8440, doi:10.1016/j.heliyon.2015.e00060.

[4] Z. Xu, S.J. Zhao, Z.S. Lv, F. Gao, Y. Wang, F. Zhang, L. Bai, J.L. Deng, Fluoroquinolone-isatin hybrids and their biological activities, Eur. J. Med. Chem. 162 (2019) 396–406, doi:10.1016/j.ejmech.2018.11.032.

[5] R. Chen, H. Zhang, T. Ma, H. Xue, Z. Miao, L. Chen, X. Shia, Moxifloxacin/Gatifloxacin-1,2,3-triazole-isatin Hybrids with Hydrogen-Bond Donor and Their In Vitro Anticancer Activity, J. Heterocycl. Chem. 56 (2019) 2691–2694, doi:10.1002/jhet.3670.

[6] M. Rizzo, C. Porta, Sunitinib in the treatment of renal cell carcinoma: an update on recent evidence, Ther, Adv. Urol. 9 (2017) 195–207, doi:10.1177/1756287217713902.

[7] Y.A. Ammar, A.M. Sh El-Sharief, A. Belal, S.Y. Abbas, Y.A. Mohamed, A.B.M. Mehany, A. Ragab, Design, synthesis, antiproliferative activity, molecular docking and cell cycle analysis of some novel (morpholinosulfonyl) isatins with potential EGFR inhibitory activity, Eur. J. Med. Chem. 156 (2018) 918–932, doi:10.1016/j.ejmech.2018.06.061.

[8] K. Khaldoun, A. Safer, N. Boukabcha, N. Dege, S. Ruchaud, M. Souab, S. Bach, A. Chouaih, S. Saidi-Besbes, Synthesis and evaluation of new isatin-aminorhodanine hybrids as PIM1 and CLK1 kinase inhibitors, J. Mol. Struct. 1192 (2019) 82–90, doi:10.1016/j.molstruc.2019.04.122.

[9] B. Shakya, P.N. Yadav, Thiosemicarbazones as potent anticancer agents and their modes of action, Mini-Rev. Med. Chem. 20 (2019) 638–661, doi:10.2174/1389557519666191029130310.

[10] H. Pervez, N. Khan, J. Iqbal, S. Zaib, M. Yaqub, M.M. Naseer, Synthesis and in vitro bio-activity evaluation of N4-benzyl substituted 5-Chloroisatin-3-thiosemicarbazones as Urease and Glycation Inhibitors, Acta Chim. Slov. 65 (2018) 108–118, doi:10.17344/acsi.2017.3649.

[11] B. Shakya, P. Nath, J. Ueda, S. Awale, Discovery of 2-pyridineformamide thiosemicarbazones as potent antiausterity agents, Bioorg. Med. Chem. Lett. 24 (2014) 458–461, doi:10.1016/j.bmcl.2013.12.044.

[12] B. Shakya, N. Shahi, F. Ahmad, P.N. Yadav, Y.R. Pokharel, 2-Pyridineformamide N(4)-ring incorporated thiosemicarbazones inhibit MCF-7 cells by inhibiting JNK pathway, Bioorganic Med. Chem. Lett. 29 (2019) 1677–1681, doi:10.1016/j.bmcl.2019.04.031.

[13] A.I. Matesanz, P. Souza, α-N-heterocyclic thiosemicarbazone derivatives as potential antitumor agents: a structure-activity relationships approach, Mini Rev. Med. Chem. 9 (2009) 1389–1396, doi:10.2174/138955709789957422.

[14] R. Cheng, W. Shi, Q. Yuan, R. Tang, Y. Wang, D. Yang, X. Xiao, J. Zeng, J. Chen, Y. Wang, 5-Substituted isatin thiosemicarbazones as inhibitors of tyrosinase: insights of substituent effects, Spectrochim. Acta - Part A Mol. Biomol. Spectrosc. 255 (2021) 119669, doi:10.1016/j.saa.2021.119669.

[15] N.K. Singh, S. Sharma, A. Krishnakumar, R.K. Choudhary, A.A. Kumbhar, R.J. Butcher, Y.R. Pokharel, P.N. Yadav, Exploration of anticancer potency of N(4) thiomorpholinyl isatin/haloisatin thiosemcarbazones on coordination to Cu^{2+} ion, Inorg. Chem. Commun. (2022) 109767, doi:10.1016/J.INOCHE.2022.109767.

[16] N.K. Singh, S. Shrestha, N. Shahi, R.K. Choudhary, A.A. Kumbhar, Y.R. Pokharel, P.N. Yadav, Study on Enhancement of Anticancer Activity of N(4)1-(2-Pyridyl)piperazinyl 5-Nitroisatin Thiosemicarbazone on Chelation with Copper(II), Asian J. Chem. 33 (2022) 557–564, doi:10.9734/bpi/cacs/v9/1762A.

[17] N.K. Singh, S. Shrestha, N. Shahi, R.K. Choudhary, A.A. Kumbhar, Y.R. Pokharel, P.N. Yadav, Anticancer potential of N(4)substituted 5-nitroisatin thiosemicarbazones and their copper(II) complexes, Rasayan J. Chem. 14 (2021) 1600–1610, doi:10.31788/RJC.2021.1436341.

[18] N. Shahi, V. Pandey, A. Pathak, R.S. Thapa, P. Pokhrel, Y.R. Pokharel, P. N.Yadav, Anticancer potential of 3-hydroxypyridine-2-carboxaldehyde N(4)-methyl and pyrrolidinylthiosemicarbazones and their Zn(II) complexes in different cancers via targeting MAPK superfamily signaling pathway, Results Chem 3 (2021) 1–9, doi:10.1016/j.rechem.2021.100104.

[19] J.P. Scovill, A facile synthesis of thiosemicarbazides and thiosemicarbazones by the transamination of 4-methyl-4-phenyl-3-thiosemicarbazide, Phosphorus. Sulfur. Silicon Relat. Elem. 60 (1991) 15–19, doi:10.1080/10426509108233920.

[20] A. Qasem, S. Guan, A. Salhin, N. Eltaher, Synthesis of isatin thiosemicarbazones derivatives : in vitro anti-cancer, DNA binding and cleavage . activities Spectrochimica Acta Part A : molecular and Biomolecular Spectroscopy Synthesis of isatin thiosemicarbazones derivatives : in vitro anti-cance, Mol. Biomol. Spectrosc. 125 (2014) 440–448, doi:10.1016/j.saa.2014.01.086.

[21] K.N. Aneesrahman, K. Ramaiah, G. Rohini, G.P. Stefy, N.S.P. Bhuvanesh, A. Sreekanth, Synthesis and characterisations of copper(II) complexes of 5-methoxyisatin thiosemicarbazones: effect of N-terminal substitution on DNA/protein binding and biological activities, Inorganica Chim. Acta 492 (2019) 131–141, doi:10.1016/j.ica.2019.04.019.

[22] H. Muğlu, Synthesis, characterization, and antioxidant activity of some new N 4-arylsubstituted-5-methoxyisatin-β-thiosemicarbazone derivatives, Res. Chem. Intermed. 46 (2020) 2083–2098, doi:10.1007/s11164-020-04079-x.

[23] E. Türkkan, U. Sayin, N. Erbilen, S. Pehlivanoglu, E. Gokce, H.U. Tasdemir, A.O. Saf, G. Leyla, E.G. Akgemci, Anticancer, antimicrobial, spectral, voltammetric and DFT studies with Cu(II) complexes of 2-hydroxy-5-methoxyacetophenone thiosemicarbazone and its N(4)- substituted derivatives, J. Organomet. Chem. 831 (2017) 23–35, doi:10.1016/j.jorganchem.2016.12.020.

[24] M.P. Sathisha, V.K. Revankar, K.S.R. Pai, Synthesis, structure, electrochemistry, and spectral characterization of bis-isatin thiocarbohydrazone metal complexes and their antitumor activity against ehrlich ascites carcinoma in Swiss Albino mice, Met. Based. Drugs (2008) 1–11 2008, doi:10.1155/2008/362105.

[25] H. Pervez, M.S. Iqbal, M.Y. Tahir, M.I. Choudhary, K.M. Khan, Synthesis of some N4-substituted isatin-3-thiosemicarbazones, Nat. Prod. Res. 21 (2007) 1178–1186, doi:10.1080/14786410601129770.

[26] P.N. Yadav, M.A. Demertzis, D. Kovala-Demertzi, A. Castineiras, D.X. West, Synthesis, solution and spectral studies of palladium(II) complexes with 2-hydroxyacetophenone N(3)-propylthiosemicarbazone. Crystal structure of a tri-palladium complex, Inorganica Chim. Acta 332 (2002) 204–209, doi:10.1016/S0020-1693(02)00710-7.

[27] J. Haribabu, G.R. Subhashree, S. Saranya, K. Gomathi, R. Karvembu, D. Gayathri, Isatin based thiosemicarbazone derivatives as potential bioactive agents: antioxidant and molecular docking studies, J. Mol. Struct. 1110 (2016) 185–195, doi:10.1016/j.molstruc.2016.01.044.

[28] M. Joseph, M. Kuriakose, M.R.P. Kurup, E. Suresh, A. Kishore, S.G. Bhat, Structural, antimicrobial and spectral studies of copper(II) complexes of 2-benzoylpyridine N(4)-phenyl thiosemicarbazone, Polyhedron 25 (2006) 61–70, doi:10.1016/j.poly.2005.07.006.

[29] A. Esme, S.G. Sagdinc, S.Z. Yildiz, Experimental and theoretical studies on Sudan Red G [1-(2-methoxyphenylazo)-2-naphthol] and its Cu(II) coordination compound, J. Mol. Struct. 1075 (2014) 264–278, doi:10.1016/j.molstruc.2014.07.009.

[30] M.A. Demertzis, P.N. Yadav, D. Kovala-Demertzi, Palladium(II) complexes of the thiosemicarbazone and N-ethylthiosemicarbazone of 3-hydroxypyridine-2-carbaldehyde: synthesis, properties, and X-ray crystal structure, Helv. Chim. Acta 89 (2006) 1959–1970, doi:10.1002/hlca.200690187.

[31] H. Muğlu, M.S. Çavuş, T. Bakır, H. Yakan, Synthesis, characterization, quantum chemical calculations and antioxidant activity of new bis-isatin carbohydrazone and thiocarbohydrazone derivatives, J. Mol. Struct. 1196 (2019) 819–827, doi:10.1016/j.molstruc.2019.07.002.

[32] E.M. Jouad, G. Larcher, M. Allain, A. Riou, G.M. Bouet, M.A. Khan, X.D. Thanh, Synthesis, structure and biological activity of nickel(II) complexes of 5-methyl 2-furfural thiosemicarbazone, J. Inorg. Biochem. 86 (2001) 565–571, doi:10.1016/S0162-0134(01)00220-3.

[33] F. Qi, Q. Qi, J. Song, J. Huang, Synthesis, Crystal Structure, Biological Evaluation and in Silico Studies on Novel (E)-1-(Substituted Benzylidene)-4-(3-isopropylphenyl) thiosemicarbazone Derivatives, Chem. Biodivers 18 (2021) 1–13, doi:10.1002/cbdv.202000804.

[34] H.A. Mahdy, M.K. Ibrahim, A.M. Metwaly, A. Belal, A.B.M. Mehany, M.A.El-Gamal K, A. El-Sharkawy, M.A. Elhendawy, M.M. Radwan, M.A. Elsohly, I.H. Eissa, Design, synthesis, molecular modeling, in vivo studies and anticancer evaluation of quinazolin-4(3H)-one derivatives as potential VEGFR-2 inhibitors and apoptosis inducers, Bioorg. Chem. 94 (2020) 103422, doi:10.1016/j.bioorg.2019.103422.

[35] A. El-Faham, W.N. Hozzein, M.A.M. Wadaan, S.N. Khattab, H.A. Ghabbour, H.K. Fun, M.R. Siddiqui, Microwave synthesis, characterization, and antimicrobial activity of some novel isatin derivatives, J. Chem. (2015) 1–9 2015, doi:10.1155/2015/716987.

[36] B. Ali, K.M. Khana, U. Salar, S.Hussain Kanwal, M. Ashraf, M. Riaz, A. Wadood, M. Tahad, S. Perveen, 1-[(4′-Chlorophenyl) carbonyl-4-(aryl) thiosemicarbazide

derivatives as potent urease inhibitors: synthesis, in vitro and in silico studies, Bioorg. Chem. 79 (2018) 363–371, doi:10.1016/j.bioorg.2018.05.017.
[37] N.T. Akinchan, P.M. Drozdzewski, W. Holzer, Syntheses and spectroscopic studies on zinc(II) and mercury(II) complexes of isatin-3-thiosemicarbazone, J. Mol. Struct. 641 (2002) 17–22, doi:10.1016/S0022-2860(02)00134-5.
[38] G. Munikumari, R. Konakanchi, V.B. Nishtala, G. Ramesh, L.R. Kotha, K.B. Chandrasekhar, C. Ramachandraiah, Palladium(II) complexes of 5-substituted isatin thiosemicarbazones: synthesis, spectroscopic characterization, biological evaluation and in silico docking studies, Synth. Commun. 49 (2019) 146–158, doi:10.1080/00397911.2018.1546400.
[39] G.A. Bain, D.X. West, J. Krejci, J. Valdcs-Martinez, S. Hernbndez-ortega, R.A. Toscanob, Synthetic and spectroscopic investigations of N(4)-substituted isatin thiosemicarbazones and their copper (II) complexes, Polyhedron 16 (1997) 855–862.
[40] S. Saranya, J. Haribabu, V.N.V. Palakkeezhillam, P. Jerome, K. Gomathi, K.K. Rao, V.H.H. Surendra Babu, R. Karvembu, D. Gayathri, Molecular structures, Hirshfeld analysis and biological investigations of isatin based thiosemicarbazones, J. Mol. Struct. 1198 (2019) 126904, doi:10.1016/j.molstruc.2019.126904.
[41] C. Balachandran, J. Haribabub, K. Jeyalakshmi, N.S.P. Bhuvanesh, R. Karvembub, N. Emia, S. Awale, Nickel(II) bis(isatin thiosemicarbazone) complexes induced apoptosis through mitochondrial signaling pathway and G0/G1 cell cycle arrest in IM-9 cells, J. Inorg. Biochem. 182 (2018) 208–221, doi:10.1016/j.jinorgbio.2018.02.014.
[42] M. Muralisankar, S.M. Basheer, J. Haribabu, N.S.P. Bhuvanesh, R. Karvembu, A. Sreekanth, An investigation on the DNA/protein binding, DNA cleavage and in vitro anticancer properties of SNO pincer type palladium(II) complexes with N-substituted isatin thiosemicarbazone ligands, Inorganica Chim. Acta. 466 (2017) 61–70, doi:10.1016/j.ica.2017.05.044.
[43] K.B. Britto, C.S. Francisco, D. Ferreira, B.J.P. Borges, R. Conti, D. Profeti, L.R. Rodrigues, V. Lacerda Jr., P.A.B. Morais, W.S. Borges, Identifying new isatin derivatives with gsk-3β inhibition capacity through molecular docking and bioassays, J. Braz. Chem. Soc. 31 (2020) 476–487, doi:10.21577/0103-5053.20190206.
[44] F. El-Saied, B. El-Aarag, T. Salem, G. Said, S.A.M. Khalifa, H.R. El-Seedi, Synthesis, characterization, and in vivo anti-cancer activity of new metal complexes derived from isatin-N(4)antipyrinethiosemicarbazone ligand against ehrlich ascites carcinoma cells, Molecules 24 (2019) 3313, doi:10.3390/molecules24183313.
[45] M.E. Mahmoud, A.A. Yakout, S.B. Ahmed, M.M. Osman, Speciation, selective extraction and preconcentration of chromium ions via alumina-functionalized-isatin-thiosemicarbazone, J. Hazard. Mater. 158 (2008) 541–548, doi:10.1016/j.jhazmat.2008.01.114.
[46] E. Labisbal, A. Sousa, A. Castiñeiras, J.A. García-Vázquez, J. Romero, D.X. West, Spectral and structural studies of metal complexes of isatin 3-hexamethyleneiminylthiosemicarbazone prepared electrochemically, Polyhedron 19 (2000) 1255–1262, doi:10.1016/S0277-5387(00)00383-1.
[47] M.A. Arafath, F. Adam, F.S.R. Al-Suede, M.R. Razali, M.B. Khadeer Ahamed, A.M.S.A. Majid, M.Z. Hassan, H. Osman, S. Abubakar, Synthesis, characterization, X-ray crystal structures of heterocyclic Schiff base compounds and in vitro cholinesterase inhibition and anticancer activity, J. Mol. Struct. 1149 (2017) 216–228, doi:10.1016/j.molstruc.2017.07.092.
[48] S.S. Konstantinović, B.C. Radovanović, Z.B. Todorović, S.B. Ilić, Spectrophotometric study of Co(II), Ni(II), Cu(II), Zn(II), Pd(II) and Hg(II) complexes with isatin-β-thiosemicarbazone, J. Serbian Chem. Soc 72 (2007) 975–981, doi:10.2298/JSC0710975K.
[49] F. Kandemirli, T. Arslan, N. Karadayi, E.E. Ebenso, B. Köksoy, Synthesis and theoretical study of 5-methoxyisatin-3-(N-cyclohexyl)thiosemicarbazone and its Ni(II) and Zn(II) complexes, J. Mol. Struct. 938 (2009) 89–96, doi:10.1016/j.molstruc.2009.09.009.
[50] M. Muralisankar, S. Sujith, N.S.P. Bhuvanesh, A. Sreekanth, Synthesis and crystal structure of new monometallic and bimetallic copper(II) complexes with N-substituted isatin thiosemicarbazone ligands: effects of the complexes on DNA/protein-binding property, DNA cleavage study and in vitro anticancer activity, Polyhedron 118 (2016) 103–117, doi:10.1016/j.poly.2016.06.017.
[51] G.M. Sheldrick, SHELXT - Integrated space-group and crystal-structure determination, Acta Crystallogr. Sect. A Found. Crystallogr. 71 (2015) 3–8, doi:10.1107/S2053273314026370.
[52] M. Sheldrick, Crystal structure refinement with SHELXL, Acta Crystallogr. Sect. C Struct. Chem. 71 (2015) 3–8, doi:10.1107/S2053229614024218.
[53] O.V. Dolomanov, L.J. Bourhis, R.J. Gildea, J.A.K. Howard, H. Puschmann, OLEX2: a complete structure solution, refinement and analysis program, J. Appl. Crystallogr. 42 (2009) 339–341, doi:10.1107/S0021889808042726.
[54] C.F. Macrae, I. Sovago, S.J. Cottrell, P.T.A. Galek, P. McCabe, E. Pidcock, M. Platings, G.P. Shields, J.S. Stevens, M. Towler, P.A. Wood, Mercury 4 . 0 : from visualization to analysis, design and prediction, J. Appl. Crystallogr. 53 (2020) 226–235, doi:10.1107/S1600576719014092.
[55] A.I. Matesanz, P. Albacete, P. Souza, Synthesis and characterization of a new bioactive mono(thiosemicarbazone) ligand based on 3,5-diacetyl-1,2,4-triazol diketone and its palladium and platinum complexes, Polyhedron 109 (2016) 161–165, doi:10.1016/j.poly.2016.02.008.
[56] A. Khan, J.P. Jasinski, V.A. Smolenski, E.P. Hotchkiss, P.T. Kelley, Z.A. Shalit, M. Kaur, K. Paul, R. Sharma, Enhancement in anti-tubercular activity of indole based thiosemicarbazones on complexation with copper(I) and silver(I) halides: structure elucidation, evaluation and molecular modelling, Bioorg. Chem. 80 (2018) 303–318, doi:10.1016/j.bioorg.2018.06.027.
[57] H. Zhang, R. Thomas, D. Oupicky, F. Peng, Synthesis and characterization of new copper thiosemicarbazone complexes with an ONNS quadridentate system: cell growth inhibition, S-phase cell cycle arrest and proapoptotic activities on cisplatin-resistant neuroblastoma cells, J. Biol. Inorg. Chem. 13 (2008) 47–55, doi:10.1007/s00775-007-0299-6.

Asian Journal of Chemistry; Vol. 35, No. 3 (2023), 605-616

ASIAN JOURNAL OF CHEMISTRY

https://doi.org/10.14233/ajchem.2023.26967

Evaluation of Anticancer Potential of N(4)-Alkyl Substituted 5-Methoxyisatin Thiosemicarbazones: Synthesis, Characterization and Molecular Docking

UPENDRA CHAUDHARY[1], VIJAY GURUNG[2], SAYED TARIQ PACHAKHAN[2], JHASHANATH ADHIKARI SUBIN[3], YUBA RAJ POKHAREL[2,*] and PARAS NATH YADAV[1,*]

[1]Central Department of Chemistry, Tribhuvan University, Kirtipur, Kathmandu 44618, Nepal
[2]Faculty of Life Science and Biotechnology, South Asian University, Akbar Bhawan, Chanakyapuri, New Delhi-110021, India
[3]Department of Chemistry, D.A.V. College, Jawalakhel, Lalitpur 44700, Nepal

*Corresponding authors: E-mail: yrp@sau.ac.in; pnyadav219@gmail.com

Received: 13 November 2022; *Accepted*: 21 January 2023; *Published online*: 27 February 2023; AJC-21152

(*Z*)-*N*-ethyl-2-(5-methoxy-2-oxoindolin-3-ylidene)hydrazine-1-carbothioamide (MeOIstEt) and (*Z*)-2-(5-methoxy-2-oxoindolin-3-ylidene)-*N*-methylhydrazine-1-carbothioamide (MeOIstMe) were synthesized and subjected to elemental analysis and various characterization techniques *viz.* IR, ^{1}H NMR, ^{13}C NMR, UV-Vis and HRMS. The synthesized N(4)-alkyl substituted thiosemicarbazones were evaluated for their anticancer activity against various cancer cell lines like breast cancer (MCF-7), skin cancer (A431) and lung cancer (A549). In micromolar concentrations, the synthesized compounds exhibited moderate anticancer activity (IC_{50}, 6.59-36.49 μM). The compound MeOIstEt was found to be more effective than MeOIstMe against A549 and MCF-7 cell lines, whereas compound MeOIstMe was found to be more potent against A431 cell lines. From flexible receptor molecular docking calculations in a hydrated environment, one of the compounds showed better binding affinity than one FDA approved drug. The insights from computational studies have strengthened the experimental findings and *vice-versa*. This work demonstrates the role of multiple approaches in finding better drug candidate with efficient anti-cancer properties.

Keywords: Anticancer activity, Breast cancer, 5-Methoxyisatin, Molecular docking, Thiosemicarbazones.

INTRODUCTION

Around 13% of all fatalities worldwide every year are attributed to cancer, making it a leading cause of mortality [1]. In affluent countries, cancer is still responsible for even more than 20% of all deaths, making it an extremely high relative mortality rate. Breast cancer is among the most common chronic cancers in women and also the major cause of death [2]. The affinity of 1*H*-indole-2,3-diones for tyrosine kinase, cyclin-dependent kinases (CDKs) and carbonic anhydrase isozymes (CAIs) can be related to anticancer mechanism [3]. Many tyrosine and serine/threonine kinases like CDKs, FLT3 kinase, polo-like kinase 4 (PLK4), glycogen synthase kinase-3β(GSK-3β), aurora B kinase, p90 ribosomal S6 protein kinase 2 (RSK2) and microtubule affinity-regulating kinase 4 (MARK4) were identified as suitable target for inhibition by isatin derivatives [4]. According to Cane *et al.* [5] at a dosage of 0.1 mM, isatin suppressed the growth of a human promyelocytic leukemia (HL60) cancer cell line by 80%, causing DNA fragmentation and chromatin condensation. Cancer cell lines resistant to apoptosis, including such as U373, A549, SKMEL-28 and OE21, as well as apoptosis-sensitive cells, such as HS683, MCF-7, B16F10 and PC-3, were suppressed by isatin-based heterocyclic compounds [6]. In U-937 cells, moderate doses of 5,6,7-tribromoisatin (4 μM) were found to be anti-proliferative, whereas high quantities (130 μM) were found to be cytotoxic [7]. The thiosemicarbazone of 1-morpholino/piperidinomethyl-5-nitroisatin was assessed 60 human tumor cell line *in vitro* on a non-small cell lung cancer cell line (HOP-62, GI_{50} value -8.00) and leukaemia cell lines (HL-60(TB), GI_{50} value -6.30, MOLT-4, GI_{50} value -6.18) [8]. With an IC_{50} of 0.9 μM, 5-fluoro-2-pyridine formamide-4-pyrrolidinyl-3-thiosemicarbazone suppressed anti-apoptotic protein Bcl-2, c-Jun, JNK, MAPK or MAP (mitogen-activated protein) kinase activation and triggering endogenous cell apoptosis in MCF-7 cells [9]. Using the MTT assay, Juranic *et al.* [10] found that isatin-β-thiocarbo-

hydrazone and N-ethylisatin-β-thiocarbohydrazone exhibited cytotoxic effects on B16 (murine melanoma), HeLa (human cervical cancer) and human peripheral blood mononuclear cell lines. N(4) substituted 5-nitroisatin-3-thiosemicarbazones were tested for their ability to inhibit urease *in vitro* and displayed a strong inhibitory effect with an IC_{50} value of 16.4 μM [11]. With an *in vitro* PLA2 inhibition assay and an *in silico* molecular docking analysis, 5-methoxyisatin-3-thiosemicarbazone was explored *in vitro* antioxidant behaviour and cytotoxicity against MCF-7 (breast cancer cell line) [12]. *In vitro* antiproliferative activity of (*Z*)-2-(5-fluoro-2-oxo-indolin-3-ylidene)-*N*-phenylhydrazinecarbothioamide against human colon cancer cell line (HCT-116) with IC_{50} = 31.4 μM was observed [13].

5-Methoxyisatin thiosemicarbazones derivatives were found to be effective against MCF-7, A549 and HeLa cell lines *in vitro*, with an IC_{50} of 14.83 ± 0.45 μM, 17.88 ± 0.16 and 6.89 ± 0.42 μM, respectively [14]. The anticancer activity of 2-acetylpyridine N-ethylthiosemicarbazone moieties on Leukemia P388 cells were examined. Both *in vitro* and *in vivo*, there was a good correlation and effectiveness in cell division delay ($p < 0.01$) [15]. The 5-nitroisatin thiosemicarbazone derivatives displayed *in vitro* antiproliferative activity against HeLa cells with an IC_{50} value of 16.52 ± 1.08 μM and considerable antioxidant activity with an IC_{50} value of 7.24 ± 0.09 μM [16]. Breast cancer cells (MCF-7), epidermoid carcinoma cell (A431) and PNT2 (normal prostate epithelium cell) were tested for their susceptibilities to the *in vitro* antiproliferative effects of N(4)thiomorpholinylisatin/5-haloisatin thiosemicarbazones analogous. The compounds demonstrated cell viability values of 0.94 μM, 0.77 μM, 0.79 μM and 0.61 μM in MCF-7 cell line and 0.56 μM, 0.55 μM, 0.47 μM and 1.19 μM in A431 cell line, respectively [17].

EXPERIMENTAL

5-Methoxyisatin, 4-ethyl-3-thiosemicarbazide and 4-methyl-3-thiosemicarbazide (Alfa-Aesar), carbon disulphide (Qualigens fine chemicals), sodium chloroacetate (Chemical center, India), hydrazine hydrate, 98% (Fisher-Scientific), acetonitrile, 98% (Merck), methyl alcohol, 98% (Fisher-Scientific), ethyl alcohol, 99.9% (Merck), glacial acetic acid, 98% (Fisher-Scientific), concentrated hydrochloric acid (Merck) and sodium hydroxide (Fisher-Scientific) were used as obtained.

Melting points were measured using the Philip Harris Melting Point Apparatus. Elemental analysis was carried out using a LECO Truspec Micro analyzer at IIT Madras, India. FT-IR spectra were recorded using a Shimadzu, Tracer 100 FTIR spectrometer in the 4000-400 cm^{-1} range. SPECORD®200 PLUS UV-visible spectrophotometer was used to collect UV-Visible spectra in MeOH solutions between 600 and 200 nm. NMR spectra were recorded in DMSO-d_6 using TMS as an internal standard on a Bruker Advance III HD NMR, 400 MHz spectrometer and mass spectra were recorded using ESI-HRMS on a Bruker IMPACT HD liquid chromatography mass spectrometer at the Department of Chemistry, Savitribai Phule Pune University, Pune, India.

Synthesis of N(4)-substituted thiosemicarbazones: The compounds (*Z*)-*N*-ethyl-2-(5-methoxy-2-oxoindolin-3-ylidene)-hydrazine-1-carbothioamide (MeOIstEt) and (*Z*)-2-(5-methoxy-2-oxoindolin-3-ylidene)-*N*-methylhydrazine-1-carbothioamide (MeOIstMe) were synthesized by refluxing a stoichiometric ratio of the respective thiosemicarbazide (2.82 mmol) and 5-methoxyisatin (2.82 mmol) in absolute ethanol (20 mL) and glacial acetic acid for 6 h (**Scheme-I**) [18]. The refluxed product was cooled to room temperature, filtered and washed with absolute alcohol. The product was dried and recrystallized in EtOH.

(*Z*)-*N*-Ethyl-2-(5-methoxy-2-oxoindolin-3-ylidene)-hydrazine-1-carbothioamide (MeOIstEt): Yield: 49.39%; colour: brown; m.p.: 250 ºC; Anal. calcd. (found) % for $C_{12}H_{14}N_4O_2S$ (*m.w.* 278.33): C, 51.75 (51.65); H, 5.07 (5.04); N, 20.13 (20.05). FTIR (KBr, ν_{max}, cm^{-1}): 3313 (s, H-N; indole), 3257 (w, H-N; azomethine), 1683 (s, C=O), 1529 (s, C=N), 1288, 783 (s, C=S), 1139 (s, N-N), 1184 (s, -OCH_3). ^{1}H NMR (δ, ppm): 12.69 (s, 1H, HN-C=S & NH), 7.87 (d, 1H, C7-H), 7.75 (d, 1H, C4-H), 7.13 (d, 1H, C6-H), 3.84 (t, 2H, aliphatic-C11), 3.79 (s, 3H, -OCH_3), 1.35 (m, 3H, aliphatic-C12). ^{13}C NMR (δ, ppm): 177.16 (C10), 163.20 (C2), 155.75 (C5), 136.37 (C3), 132.38 (C9), 121.21 (C7), 117.62 (C8), 112.24 (C6), 106.60 (C4), 56.09 (-OCH_3), 39.90 (C11), 14.48 (C12). ESI-HRMS: *m/z* [Found (calcd.)]: 279.0910 (279.0910) $[M+H]^+$, 301.0733 (301.0729) $[M+Na]^+$. UV-Vis [λ_{max} (nm) (MeOH)]: 358 (n-π^*), 283 (π-π^*).

(*Z*)-2-(5-Methoxy-2-oxoindolin-3-ylidene)-*N*-methyl-hydrazine-1-carbothioamide (MeOIstMe): Yield: 86.07%; colour: brown; m.p.: 280-282 ºC; Anal. calcd. (found) % for $C_{11}H_{12}N_4O_2S$ (264.30): C, 49.99 (50.58); H, 4.58 (4.44); N, 21.20 (21.15). FTIR (KBr, ν_{max}, cm^{-1}): 3303 (s, H–N; indole), 3233 (w, H-N; azomethine), 1696 (s, C=O), 1555 (s, C=N),

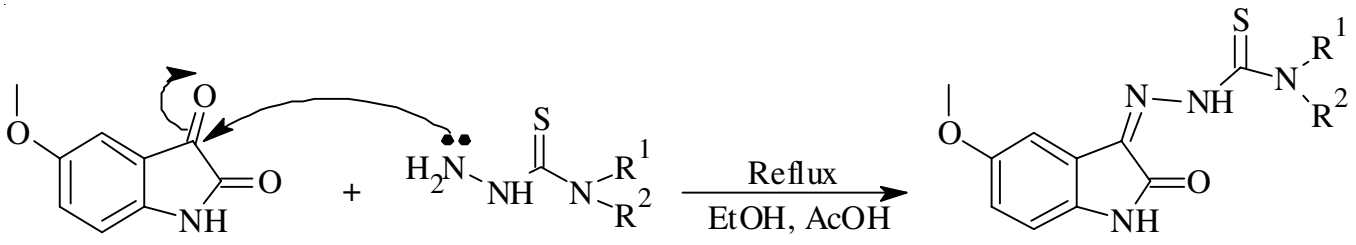

Where, MeOIstEt (R^1 = H, R^2 = -C_2H_5), MeOIstMe (R^1 = H, R^2 = -CH_3)

Scheme-I: Synthesis of N(4)-alkyl substituted thiosemicarbazones

1291, 744 (s, C=S), 1132 (s, N-N), 1196 (s, -OCH_3). ^{1}H NMR (δ, ppm): 12.58 (s, 1H, HN-C=S), 11.01(s, 1H, indole-NH), 7.25 (d, 1H, C7-H), 7.25 (d, 1H, C4-H), 6.94 (m,1H, thiourea), 6.92 (d, 1H, C6-H), 3.76 (s, 3H, -OCH_3), 3.35(m, 3H, aliphatic-C11). ^{13}C NMR (δ, ppm): 178.17 (C10), 163.21 (C2), 155.77 (C5), 136.41 (C3), 132.29 (C9), 121.27 (C7), 117.65 (C8), 112.27 (C6), 106.43 (C4), 56.08 (-OCH_3), 31.78 (C11). ESI-HRMS: *m/z* [Found (calcd.)]: 265.0766 (265.0753) $[M+H]^+$, 287.0569 (287.0573) $[M+Na]^+$. UV-Vis [λ_{max} (nm) (MeOH)]: 356 (n-π^*), 282 (π-π^*).

Anticancer activity

Cell lines: A549, MCF-7 and A431 cell lines were cultured in complete DMEM media.

Cell viability assay: Cell viability of A431, MCF-7 and A549 cells were assessed by crystal violet assay. Approximately 5×10^3 cells were seeded in each well of 96 wells plate. Cells were treated with different concentration of compounds and incubated for 48 h. After 48 h, the media was discarded. Cells were stained with 80 mL (0.4%) crystal violet prepared in 50% methanol and incubated for 30 min on a bench rocker with 20 oscillations per minute. After that cells were washed by dipping in a beaker filled with tap water which prevented the washout of cells. Culture plates were kept overnight for air drying at room temperature. Next day, 150 µL of methanol was added in each well and kept on a rocker for 30 min. Finally, optical density was measured in micro-plate reader at 570 nm.

RESULTS AND DISCUSSION

FTIR studies: In FTIR spectrum of N(4) alkyl substituted thiosemicarbazones, the broad symmetric and asymmetric stretching vibration of indole N-H was observed between 3313-3303 cm^{-1} [19], whereas the N-H stretching vibration of azomethine was observed between 3257-3233 cm^{-1}. The slight shift to higher wavenumbers in indole N-H (3313 cm^{-1}) is probably a consequence of changes in hydrogen bonding. The absence of a stretching band at about 2600-2500 cm^{-1}, which specifies to ν(S-H) and the presence of two strong bands specific to ν(C=S) at 1291-1288 cm^{-1} and 783-744 cm^{-1} indicated the existence of the thione tautomer of thiosemicarbazone [20,.21]. The strong stretching bands appeared in the thiosemicarbazone at the range of 1696-1683 cm^{-1} and 1555-1529 cm^{-1}, respectively, assigned to ν(C=O) and (C=N) [22,23]. The medium stretching bands were assigned to ν(N-N) of thiosemicarbazones and appeared at 1139-1132 cm^{-1} [24]. The strong stretching bands of isatin moieties of thiosemicarbazones appeared at 1196-1184 cm^{-1}, which were assigned to ν(-OCH_3) [25].

NMR studies: In ^{1}H NMR (DMSO-d_6) spectra of N(4) alkyl substituted thiosemicarbazones, the signals of highly acidic H-N-C=S and indol-NH protons were observed downfield as a singlet at δ 12.58 ppm and δ 11.01 ppm in ligand MeOIstMe [12]. The N(4)-ethyl compound in which the signal was attributed to the N(3)-H at δ 12.69 ppm confirmed both by its position at lower field showing an intramolecularly hydrogen-bonded proton and by its stronger dependence on the type of the N(4) substituent [26]. This is supported by the ^{1}H NMR spectra, which shows a singular peak at δ 11.01 ppm relative to the NH adjacent to C=S [11], but no peak at 4 ppm attributed to the S–H proton in the ligand. All the aromatic protons of isatin moiety were seen as doublet signals at δ 7.25 to 6.92 ppm in the ligand, respectively. Similarly, in case of N(4) ethyl group (MeOIstEt), the signals of -CH_2 protons were found as a triplet at δ 3.84 ppm and the signals of -CH_3 protons were found as multiplet at δ 1.35 ppm [27] and N(4) methyl group (MeOIstMe), the signals of -CH_3 protons were found as multiplet at δ 3.35 ppm [28]. The signals of secondary amine of N(4)-H in ligand MeOIstEt was observed as singlet at δ 7.16 ppm whereas the signals of secondary amine of N(4)-H in ligand MeOIstMe was observed as singlet at δ 6.94 ppm [29]. The signals of methoxy (-OCH_3) protons were observed as a singlet at δ 3.79-3.76 ppm in the ligand [30].

The ^{13}C NMR spectra of the synthesized compounds were obtained in DMSO-d_6. In compounds, the –C=S (C10) signals were observed at the range of δ 178.17-177.16 ppm. The characteristic –C=O (C2) and –C=N (C3) peaks were observed at the range of 163.21-163.20 ppm and 136.41-136.37 ppm in thiosemicarbazones, respectively [31]. The aromatic carbons (C4–C9) of the isatin ring were observed at 106.60-106.43 (C4), 155.77-155.75 (C5), 112.27-112.24 (C6), 121.27-121.21(C7), 117.65-117.62 (C8) and 132.38-132.29 ppm (C9) in the thiosemicarbazones, respectively [32]. The C5 carbons atom shifted downfield due to the presence of methoxy group. The signals in N(4)-methyl group (MeOIstEt) carbons atoms (C12) were observed at 14.48 ppm and methylene group (-CH_2) carbon atom (C11) were observed at δ 39.30 ppm [33]. The signals of N(4) methyl group (MeOIstMe) carbon atoms C11) were seen at δ 31.78 ppm. The signals of methoxy (–OCH_3) carbon atoms peak was observed at δ 56.09-56.08 ppm in both the thiosemicarbazones [34].

ESI-HRMS studies: The molecular ion peaks of the proposed molecular structures were in consistent. The protonated and alkali adduct molecules were seen in the positive mode of the ESI-HRMS investigations for the mass spectral peaks of the compounds. The protonated molecular ion $[M+H]^+$ peaks obtained from thiosemicarbazones were observed at *m/z* = 279.0910 (calcd., 279.0910) (MeOIstEt) and *m/z* = 265.0766 (calcd., 265.0753) (MeOIstMe) [14]. Besides protonated peaks, the thiosemicarbazones showed the molecular ion $[M+Na]^+$ peaks: *m/z* = 301.0733 (calcd. 301.0729) (MeOIstEt) and *m/z* = 287.0569 (calcd. 287.0573) (MeOIstMe). The significant peaks at *m/z* 247.1185 (calcd. 247.2961) $[C_{11}H_{11}N_4SO + H]^+$ ion and *m/z* 226.9515 (calcd., 226.2754) $[C_9H_{11}N_3O_2S + H]^+$ ion were observed due to the fragment with the loss of OCH_3 group (*m/z* 31 amu) and C_2N group (*m/z* 38 amu), respectively [35].

UV-Vis studies: In MeOH, UV-visible spectral data of the compounds were recorded in the 600-200 nm region. The compounds showed two broad absorption bands with different intensity and a shoulder-like appearance in the region around 282 nm and 356 nm, which were attributed to n→π* intraligand electronic transitions, namely the bands due to the electronic transition of azomethine (-C=N), carbonyl (-C=O) and the (-HN-C=S) group [21,36]. Due to transitions of π→π* and n→π*, the electronic spectra of these compounds revealed exceptional absorption bands in the aromatic ring (C=C) and

thiosemicarbazone (C=S) and imine (CH=N) region [37]. The bands at around 356 nm were attributed to the electronic transition n→π* of the thiosemicarbazone moiety (C=S) and the bands at around 282 nm were allocated to the electronic transition π→π* of C=O on aldehyde group [18].

Biological activity: The cell viability *in vitro* of the synthesized compounds MeOIstEt and MeOIstMe was investigated at concentrations ranging from 1 to 100 μM and found to be greater than 50%. Therefore, the compounds showed modest anticancer activity against MCF-7 (breast cancer), A549 (lung cancer) and A431 (skin cancer) cells. The compound MeOIstEt was found to be the most potent proliferation inhibitor against the A549 and MCF-7 cells than MeOIstMe whereas compound MeOIstMe was found to be more potent proliferation inhibitor towards A431 cells than MeOIstEt.

Computational method and materials

Density functional theory: The quantum mechanical calculations in the framework of density functional theory (DFT) as implemented in an open-source software suite, CP2K was used [38]. The molecular geometry of the studied compounds was calculated and the models were proposed for molecular docking studies. BFGS optimizer was employed in locating the global minima of the molecules. Localized basis sets (DZVP-MOLOPT-SR-GTH) and exchange-correlation functional (BLYP) were used with 300 Ry cutoff of kinetic energy in minimizing the molecular structure up to the energy convergence of 1.0×10^{-6} Ry and the force convergence (MAX and gradient) of 1.0×10^{-4} Ry/Bohr.

Molecular docking: ADFR suite was used in accessing the best docked pose of the small molecules with the receptor proteins [39]. The active site was located by an option in the molecular docking program and also from the protein database. In some cases, CASTp server results were also considered for unanimous inferences [40]. The number of independent GA searches were set to 50 with each using up to 10,000,000 evaluations of the scoring functions. This high value ensured that the chances of capturing the best possible docked pose was maximized and instead of local minima of the scoring function, a global minima was reached in a solvated environment. The water map setting with the default weight of 0.60 and entropy of -0.20 were chosen for hydrated docking. The amino acids residues (up to 15) of the receptors at the orthosteric site were assigned to be flexible and the small molecule possessed rotational degrees of freedom during the docking process by default. The box sizes for different proteins had large variations depending upon the size of the active site. The largest box of size 22 × 28 × 19 points was chosen for the protein with PDB ID of 7BJ6 as an example. The padding of 2.00, grid spacing of 0.375 Å and smoothing of 0.500 were adopted for all the receptors.

Different clusters of docking results related to different searches were obtained and the pose with best affinity was taken for further analysis. The reference ligand was not provided and consequently the RMSD value of each distinct output was not obtained. As a representative case, one of the receptors with its active site occupied by a small molecule ligand is depicted in Fig. 1.

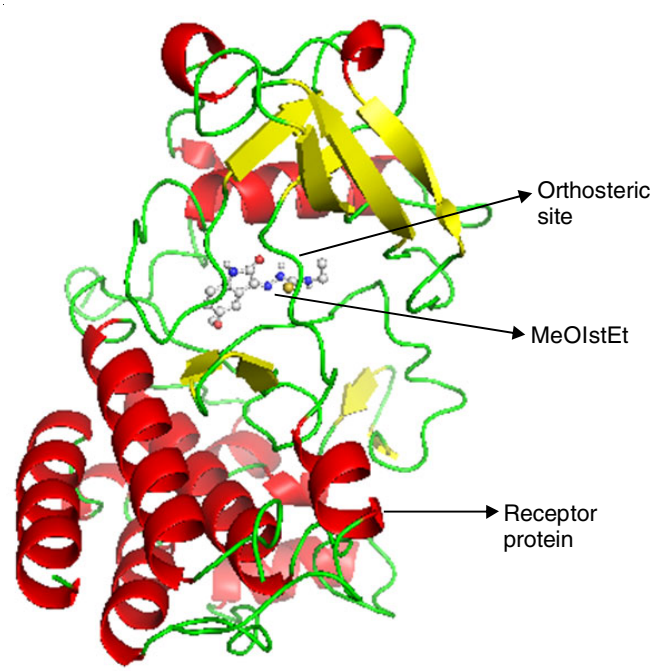

Fig. 1. Cartoon representation of a docked pose of MeOIstEt in the active site of protein with PDB ID: 4ASD (carbon gray, nitrogen blue, oxygen red, sulfur yellow, hydrogen cream spheres)

Target proteins: Various proteins represented as different PDB ID as receptors of the ligands are presented in Table-1. The search for alternate prophylactics of cancerous cell addressing different types of growth factors and other enzymes were considered for spanning a broad range of possible targets. Here, *in silico* approach addresses targeted therapy that deals with the treatment of specific cancer by obstructing the pathways or mutations causing tumor cell proliferation. The receptor with maximum amino acid residue count of 1014 and minimum of 98 were used in this work and the PDB structures were retrieved

TABLE-1
DETAILS OF DIFFERENT KINDS OF RECEPTORS USED IN MOLECULAR DOCKING

PDB ID	Receptor class	Feature	Overall quality factor (Disallowed %)
4ASD	VEGFR2	A monomer with 353 residues	98.64 (0.4%)
3MJG	PDGFR	A hetero-4-mer with 922 residues	82.25 (0%)
3MJK	PDGF precursor	A homo-2-mer with 1014 residues	85.96 (0%)
7BJ6	MDM2 protein	A monomer with 98 residues	100.00 (0%)
2VTA	Cyclin dependent kinase 2	A monomer with 298 residues	88.02 (0%)
3VHE	VEGFR2 kinase domain	A monomer with 359 residues	97.25 (0%)
6LVK	FGFR3	A monomer with 626 residues	98.49 (0%)

from RCSB website (rcsb.org) [41]. The protein structures were cleaned by removing water molecules, ions, metals, ligands and other small molecules. The polar hydrogens were added along with Gasteiger charges.

4ASD is a vascular endothelial growth factor receptor (VEGFR2) with 353 residue count. It is a protein tyrosine kinase receptor that regulate tumor-induced blood vessels formation. 3VHE is a similar target with 359 residue count. 3MJG is a platelet-derived growth factor receptor (PDGFR) and is involved in the development of different types of cancerous cells [42]. Its antagonist could be a good therapeutic candidate. 3MJK is a protein associated with platelet-derived growth factor precursor with 1014 residues. Only A and B chains were considered for molecular docking. 7BJ6 is a murine double minute 2 protein and is considered vital in p53 regulation and cancer cell suppression. 2VTA has been top ranked (fit score of 2.488) by an online program PharmMapper (http://59.78.96.61/pharmmapper) [43] as potential target (cell division protein kinase 2) in cancer treatment. It consists of a single chain with 298 residues and ligands based on its docking have been currently subjected to clinical trials [44]. 6LVK is a fibroblast growth factor receptor 3 used in specially the therapeutics of bladder cancer has been shown to have significant results over VEGFR2 proteins [45]. This protein is a monomer with 626 residues. These target proteins were selected from different domains and class to encompass broad spectrum in the development of therapeutics against different types of cancer by computational methods. The evaluation of protein structure was performed by Protein Structure Analysis and Verification Server [46] using ERRAT [47] and PROCHECK [48] programs. The results showed acceptable quality of the deposited structures that could be used for molecular docking studies without any additional corrections or modifications.

Test compounds and control drugs: Thiosemicarbazones and their derivatives are nitrogen and sulfur containing compounds having diverse biological and therapeutic values [49]. Herein, specifically their anticancer potentials have been explored by using computational methods. The molecular structures (ball and stick models) of these two compounds obtained from DFT calculations are shown in Fig. 2. In order to compare the performances of the test compounds, some FDA drugs (imatinib, ruxolitinib and lenalidomide) have also been considered as references [50]. The structures were optimized by molecular mechanics using conjugate gradient algorithm with Newton's method as line search technique. Universal force field was used for the atoms with energy convergence of 10^{-7} units. The molecular structures were obtained as PDB files and the minimization was performed by Avogadro software [51] without any constraints. Their druglikeness, pharmacodynamics and pharmacokinetics have also been studied by computational methods. Imatinib and ruxolitinib are anticancer drugs of class tyrosine kinase inhibitor (antineoplastic agent). Lenalidomide is an immunomodulatory drug used in the treatment of various types of cancer and is an angiogenesis inhibitor.

Computational resources: All the codes used were open-source software in this computational work. The visualization and interpretation were also performed using free software (Avogadro and PyMol) easily available in the internet [51,52]. A multi core Intel CPU machine with 256 GB of memory and 6 TB of storage was used in the calculations. The operating systems were Ubuntu 20.04 and Windows 8.1.

Druglikeness and pharmacology studies: In order to determine the druglike properties and for ADMET prediction of the test compounds, various parameters were calculated using ADMETlab 2.0 server [53]. The physico-chemical properties are shown as radar plots in Fig. 3 and are self-explanatory. All the parameters lie within the acceptable range (between upper and lower limits) and Lipinski's rule of five is not violated. This verifies the druglikeness and acceptable oral bioavailability.

The different parameters show that the test compounds do not possess extreme toxicity and have moderate ADME profile (Table-2). This suggests that these compounds could be used as potential drug candidates with caution (carcinogenicity and respiratory toxicity) in further clinical trials.

Anticancer properties by graph based signatures: In order to find biologically active compounds having anticancer

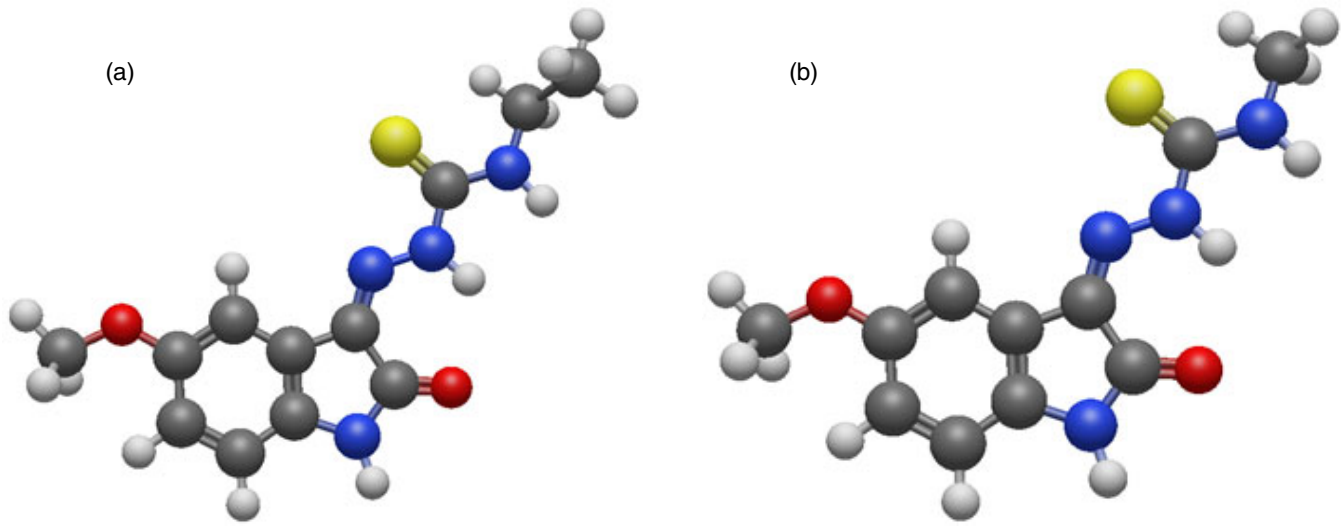

Fig. 2. Geometry optimized molecular structure of (a) MeOIstEt and (b) MeOIstMe (oxygen in red, carbon in gray, sulfur in yellow, nitrogen in blue and hydrogen in shaded white)

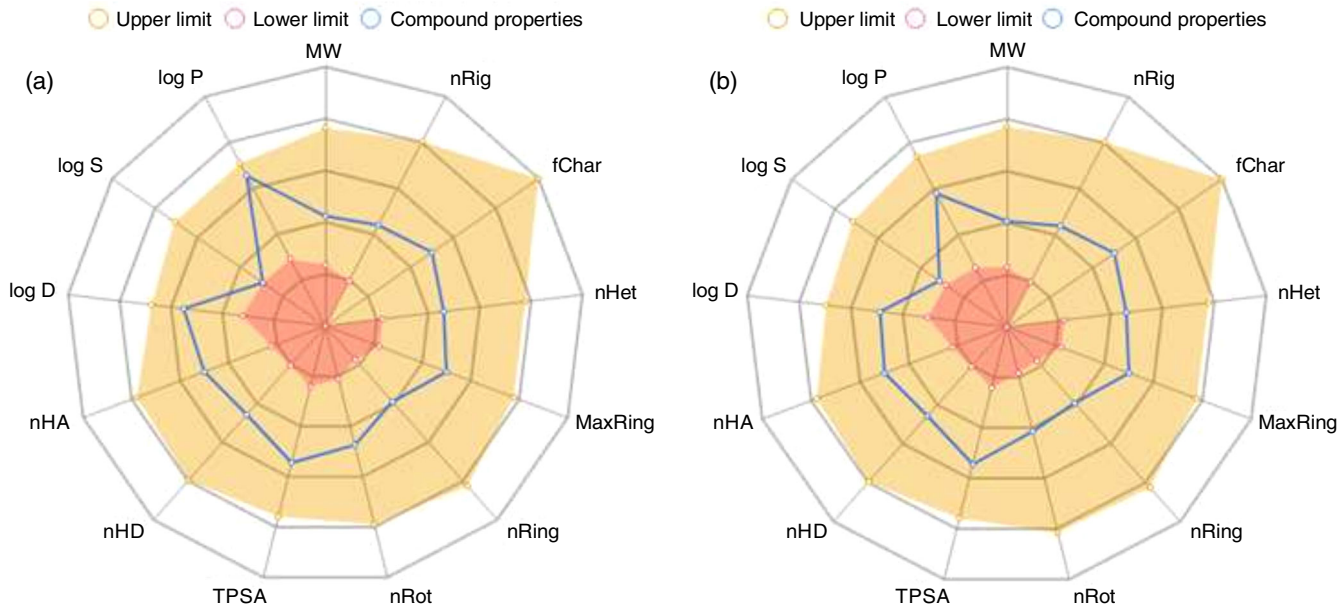

Fig. 3. Radar plots of (a) MeOIstEt and (b) MeOIstMe showing physico-chemical data

TABLE-2
SELECTED PROPERTIES PERTAINING TO ADSORPTION, DISTRIBUTION, METABOLISM, EXCRETION AND TOXICITY OF THE DRUG CANDIDATES

Properties	MeOIstEt	MeOIstMe
Adsorption		
Caco-2 permeability (log cm/s)	-4.78	-4.90
Pgp-inhibitor	Very low probability	Very low probability
Pgp-substrate	Very low probability	Very low probability
Human intestinal absorption	10% probability	10% probability
Distribution		
Plasma protein binding	0.999	0.995
VD (L/Kg)	3.84	1.34
BBB Penetration	Low	Low
Metabolism		
CYP1A2 inhibitor	High	High
CYP1A2 substrate	High	High
CYP2C9 inhibitor	Medium	Medium
CYP2C9 substrate	High	High
Excretion		
Clearance (mL/min/Kg)	5.95	7.26
$T_{1/2}$	Long	Long
Toxicity		
HERG blockers	Low probability	Low probability
Human hepatotoxicity	70% probability of being toxic	70% probability of being toxic
AMES toxicity	Low probability	Low probability
Skin sensitization	Low probability	Low probability
Carcinogenicity	High probability	High probability
Eye irritation	Low probability	Low probability
Respiratory toxicity	High probability	High probability

capability, an online program pdCSM (http://biosig.unimelb.edu.au/pdcsm-cancer) was used [54]. The smiles notations of the test compounds were taken for job submission and no actual three dimensional molecular geometry were required. The graph based signatures as implemented in the algorithm predicts the anticancer activity (GI_{50}) against 74 cancer cell lines.

It was found that the test compound MeOIstEt was active against breast (MCF-7, MDA-MB-468), leukemia (K-562, P388-ADR), ovarian (OVCAR-4), renal (SN12K1) and small cell lung (DMS-273) cancer cell lines. For MeOIstMe, breast (MCF-7, MDA-MB-468, T47D), leukemia (CCRF-CEM, K-562, P388-ADR), ovarian (OVCAR-3, OVCAR-4), renal (SN12K1) and small cell lung (DMS-273) cancer cell lines. Surprisingly, the second compound showed activity in larger number of cases than the first compound despite having lower molecular weight.

It was found that MeOIstEt is a potent CDK2 inhibitor with IC_{50} of less than 10 μM and with pKi of 6.11 (CDK2-ligand binding affinity) from kinCSM predictor (https://biosig.lab.uq. edu.au/kin_csm/). MeOIstMe is also a potent CDK2 inhibitor with IC_{50} of less than 10 μM and with pKi of 6.099. These findings suggest that the test compounds possess notable anticancer properties that is worthy of further investigation. Fragmentation of molecules that affects protein phosphorylation is studied by this online program and it has been found that the potential type of inhibition is type I for both the compounds.

Flexible receptor molecular docking: The data obtained from the flexible receptor molecular docking in hydrated environment of two test molecules and three approved drugs (controls) on to various proteins are tabulated in Table-3. In almost all the cases, the control drugs showed better binding affinities than the two thiosemicarbazones (MeOIstEt and MeOIstMe). Only in case of the receptor with PDB ID: 2VTA, MeOIstEt showed better binding affinity than lenalidomide. In comparing the binding affinities of MeOIstMe with that of MeOIstEt, it can be inferred that the former almost always results in weaker binding and thus may not be distinctly favoured in the inhibition of protein functioning. Apparently, the molecular weight of ligand seems to be a major factor in deter-

TABLE-3
BINDING AFFINITIES (kcal/mol) OF VARIOUS CHEMICAL COMPOUNDS AND DRUGS AGAINST DIFFERENT RECEPTOR PROTEINS (PDB ID) RELATED TO MALIGNANT TUMORS

	m.w.	4ASD	3MJG	3MJK	7BJ6	2VTA	3VHE	6LVK
MeOIstEt	278.33	-8.8	-8.2	-7.4	-6.8	-9.7	-8.7	-8.2
MeOIstMe	264.30	-8.7	-8.1	-7.4	-6.5	-9.1	-8.5	-7.9
Imatinib	493.60	-15.7	-14.9	-9.0	-11.1	-13.1	-13.9	-13.2
Ruxolitinib	306.40	-10.6	-10.1	-8.7	-8.8	-11.4	-10.4	-9.7
Lenalidomide	259.26	-9.7	-9.2	-8.2	-7.8	-9.2	-9.2	-8.4

mining the interaction strength with the amino acid residues with the minor ones being the type, proximity and frequency of non-covalent interactions. A thorough analysis at the atomic level would ultimately provide an exact description of the inherent phenomenon.

Interactions at the atomic-level: The frequency and proximity of different types of non-covalent interactions between the amino acid residues at the orthosteric site of the protein and the docked ligand determines the strength of the protein-ligand complex. Better binding results in a stable complex and the protein would be effectively inhibited resulting in the treatment of the disease. Hence, the pose of the ligand that forms strong bonding with the residues is the ultimate quest in structure-based drug design strategy [55] that is cost effective. Many drugs have been discovered using this technique and have circumvented the expensive experimental high-throughput screenings [56]. The receptor flexibility incorporated into the calculation along with that of the ligand's provides the closest resemblance to the realistic models as in biological systems. Fig. 4 shows the best docked pose of MeOIstEt at the active

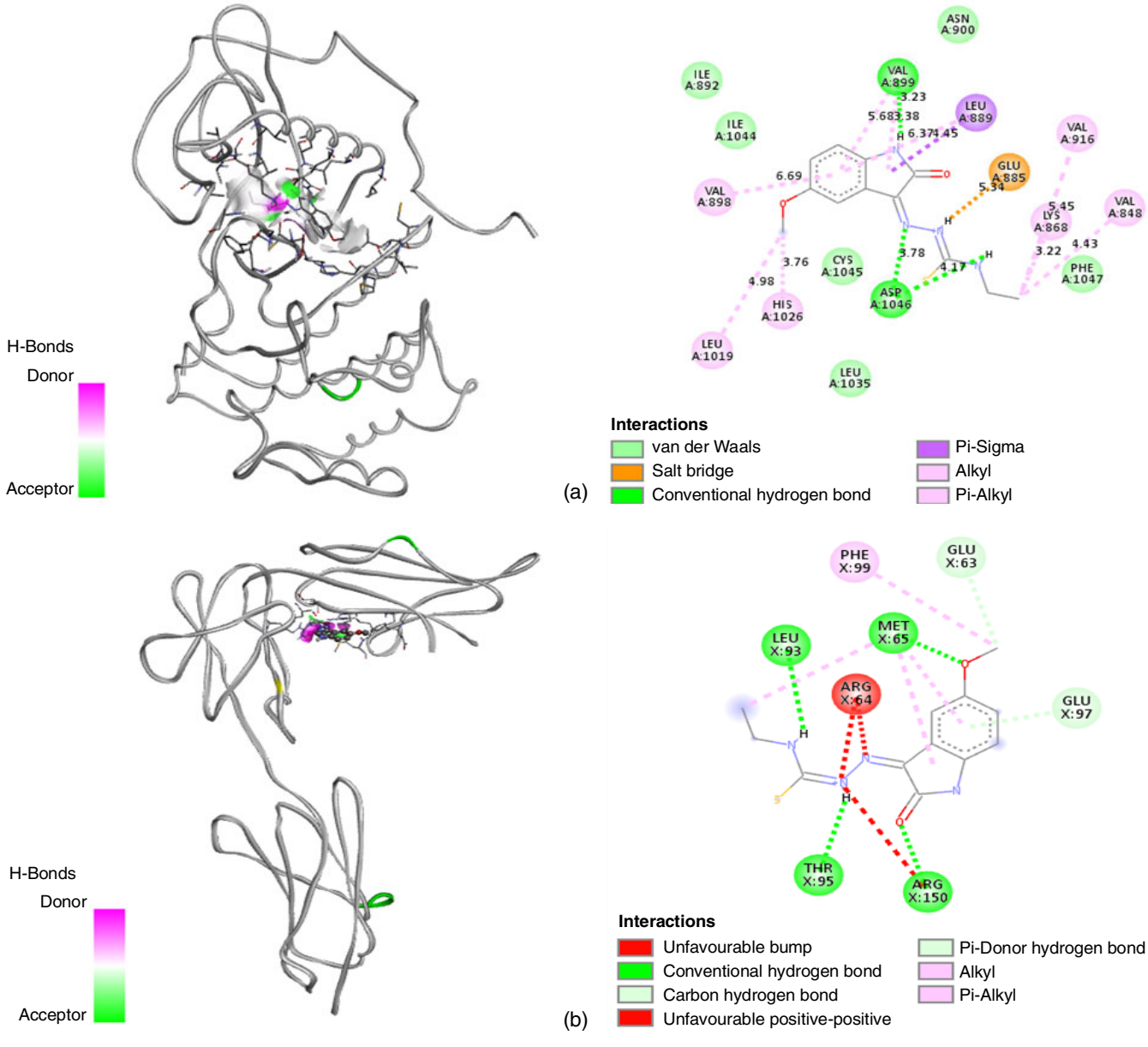

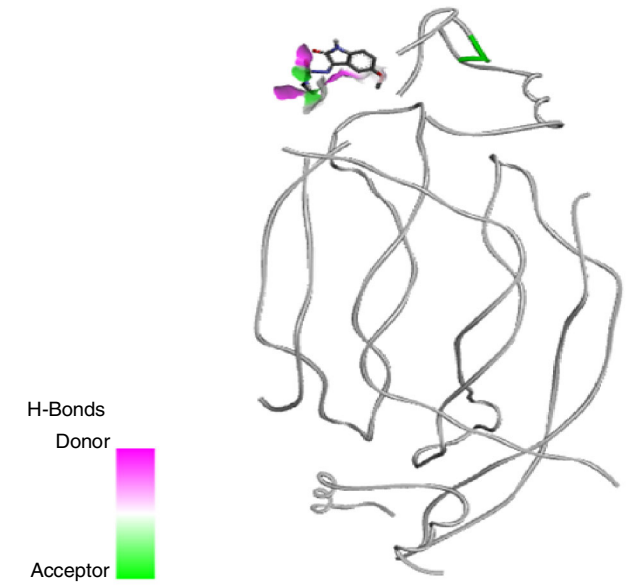
H-Bonds
Donor
Acceptor

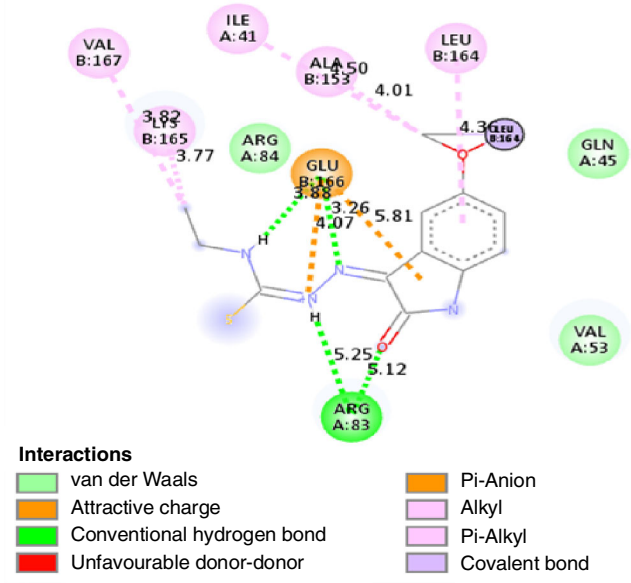
VAL B:167
ILE A:41
ALA B:153
LEU B:164
LYS B:165
ARG A:84
GLU B:166
GLN A:45
VAL A:53
ARG A:83
3.82
3.77
4.50
4.01
4.37
3.88
3.26
4.07
5.81
5.25
5.12
Interactions
van der Waals
Attractive charge
Conventional hydrogen bond
Unfavourable donor-donor
Pi-Anion
Alkyl
Pi-Alkyl
Covalent bond

(c)

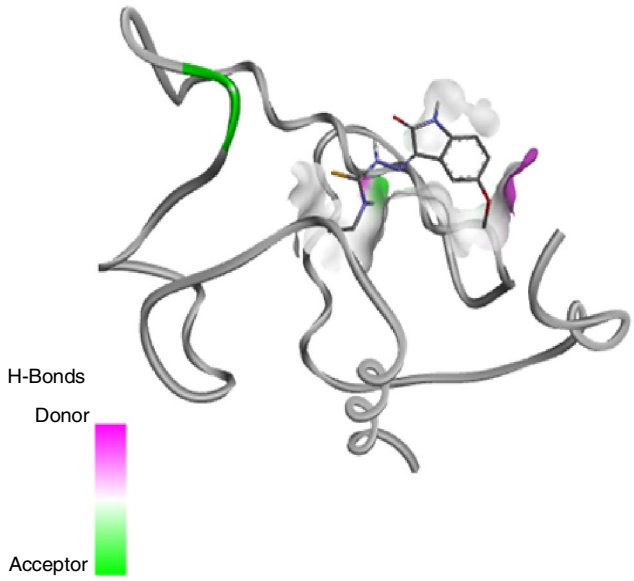
H-Bonds
Donor
Acceptor

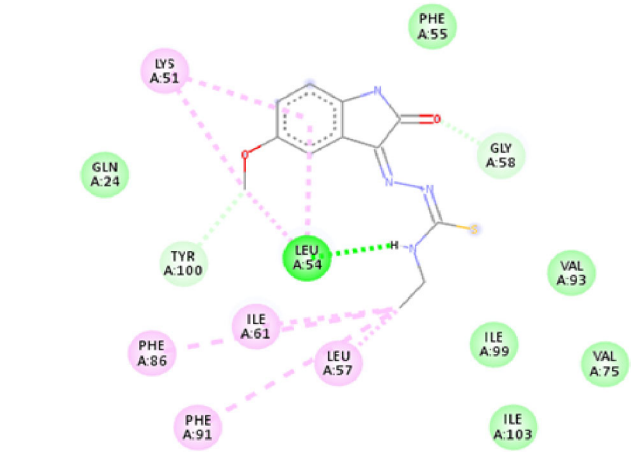
PHE A:55
LYS A:51
GLY A:58
GLN A:24
TYR A:100
LEU A:54
VAL A:93
ILE A:61
PHE A:86
LEU A:57
ILE A:99
VAL A:75
PHE A:91
ILE A:103
Interactions
van der Waals
Conventional hydrogen bond
Carbon hydrogen bond
Alkyl
Pi-Alkyl

(d)

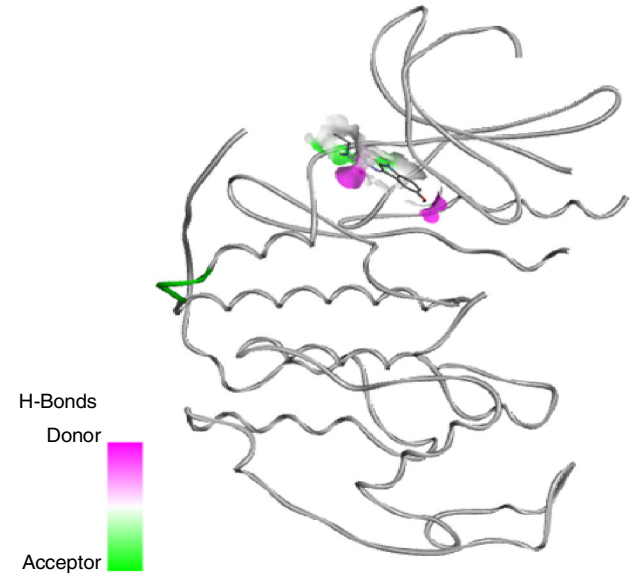
H-Bonds
Donor
Acceptor

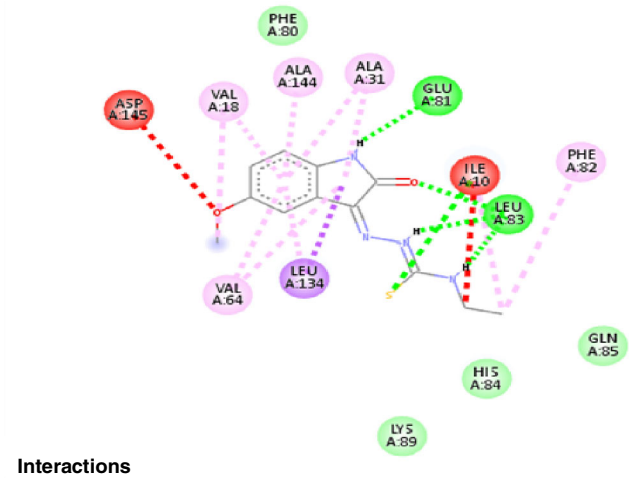
PHE A:80
ALA A:144
ALA A:31
VAL A:18
ASP A:145
GLU A:81
ILE A:10
PHE A:82
LEU A:83
LEU A:134
VAL A:64
GLN A:85
HIS A:84
LYS A:89
Interactions
van der Waals
Unfavourable bump
Conventional hydrogen bond
Unfavourable acceptor-acceptor
Pi-Sigma
Alkyl
Pi-Alkyl

(e)

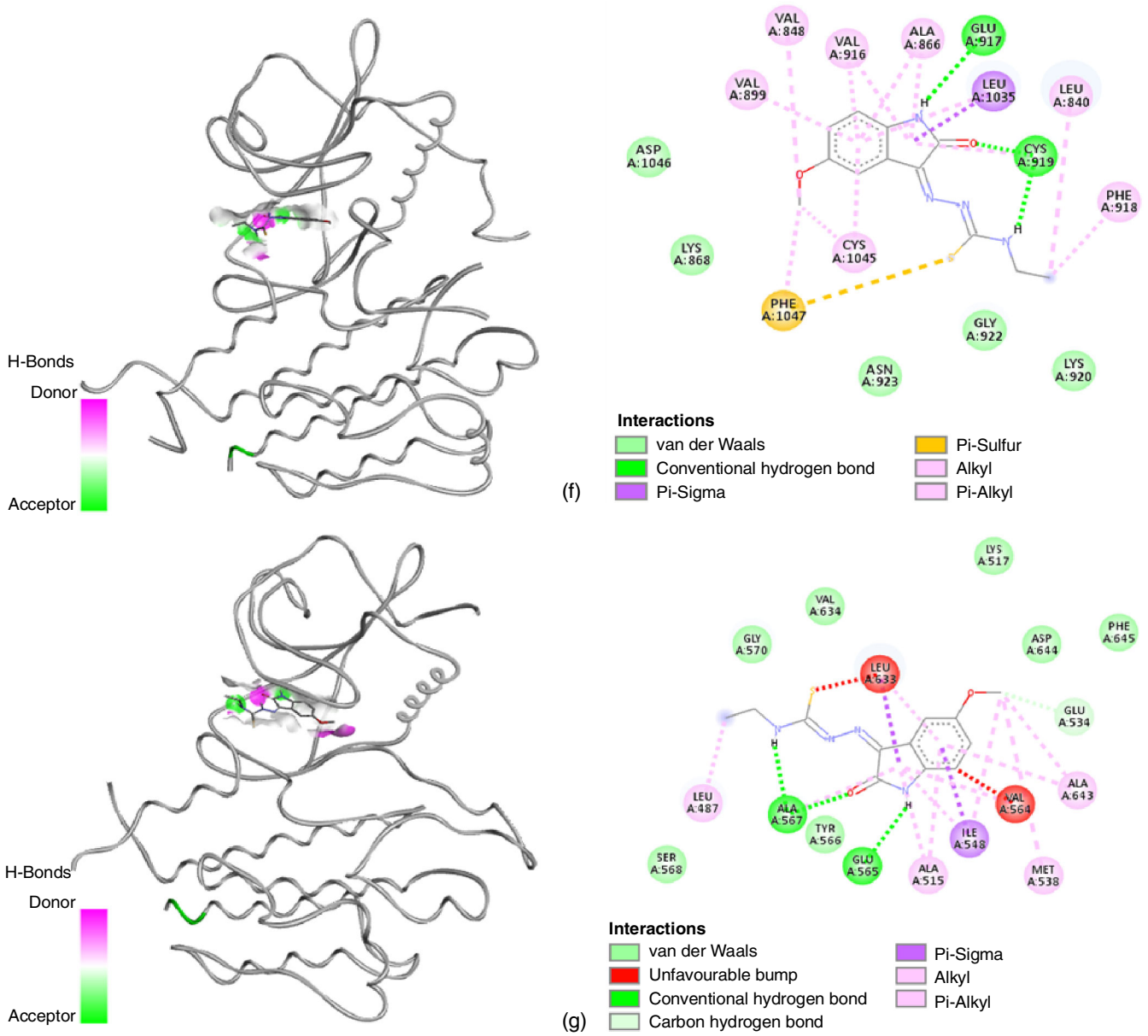

Fig. 4. 3D Plots with H-bond surface and 2D plots of Best docked pose of MeOIstEt with 4ASD (a); with 3MJG (b); with 3MJK (c); with 7BJ6 (d); with 2VTA (e); with 3VHE (f) and with 6LVK (g)

site of the receptor molecules [57]. The plots on the left are 3D representations while those at the right are the 2D projections. The pocket areas with hydrogen bonding donors are purple while the acceptors are green. Since, MeOIstMe did not yield distinctly better binding affinities than MeOIstEt, its atomic level interactions are not presented in the figures.

The occurrences of hydrogen bonding, ionic, unfavourable, pi-related and alkyl related interactions with different amino acid residues of various proteins are presented in Table-4. In case of hydrogen bonding, the distances are also shown. Even though some interactions are unfavourable, the presence of other strong non-covalent interactions makes the complex

TABLE-4
AMINO ACID RESIDUES INVOLVED IN MAJOR INTERACTIONS WITH MeOIstEt AND DISTANCES (Å)

PDB ID	Hydrogen-bonds	Salt-bridge/others	Pi related	Alkyl related
4ASD	ASP1046 (4.17, 3.78), VAL899 (3.23)	GLU885	LEU889	LYS868, HIS1026
3MJG	MET65 (1.77), LEU93 (1.95), THR95 (1.88), ARG150 (1.83)	ARG64	GLU63, GLU97	MET65, PHE99
3MJK	ARG83 (5.12, 5.25)	LEU164	GLU166	LYS165, VAL167
7BJ6	LEU54 (2.14)	–	PHE86, PHE91	LEU57
2VTA	GLU81 (4.80), LEU83 (4.23, 5.33), ILE10 (4.32)	ILE10, ASP145	LEU134	ALA31, VAL18
3VHE	CYS919 (3.66), GLU917 (4.03)	PHE1047	LEU1035	ALA866
6LVK	GLU565 (1.88), ALA567 (1.84, 2.08)	VAL564, LEU633	ILE548, LEU633	ALA643, LEU487

stable in nature. In case of 4ASD, the key amino acid residues ASP1046, VAL899, LYS868 and GLU885 are involved and have also been reported in case of docking with compounds derived from well-known drugs [58] for cancer. In case of 3MJG protein the major interaction is with the residues MET65, LEU93, THR95 and ARG150 with short hydrogen bonding distances. Other key residues THR86 and THR88 have been reported to be involved in interaction with a different compound, indigocarpan [59]. 3MJK protein involves a residue ARG83 with weak hydrogen bonding and other interactions with GLU166, LYS165 and VAL167. However, CYS96, LYS97, SER143, HIS146, ARG148, GLU176 and CYS177 are the key residues reported with Litreol. With titerpenes the key residues are ILE38, HIS39, VAL95, LYS97, THR98, TRP120, PRO121, VAL124, ARG148, VAL152 and VAL160 [60]. None of the residues match thus pointing towards different site for docking of the small molecule. The key residue in case of 7BJ6 are LEU54, PHE86, PHE91 and LEU57 as shown in Fig. 4d. But other set of key residues GLN72, MET62, GLY58, GLN59 and VAL93 have been reported [61] for its native ligand, an isoindolinone. This is due to slight shifting of docking position by the compound. The protein 2VTA has been found to interact with the test compound with the residues VAL18, GLU81, LEU83, ILE10, ASP145, LEU134 and ALA31. All the residues are same as in its native ligand except PHE80, PHE82 and ALA144. 3VHE protein has residues CYS919 and GLU917 involved in weaker hydrogen bonding. CYS919 and LYS920 have been reported as key residues while interacting with indigocarpan in other studies [59]. In case of 6LVK, there are two amino acid residues GLU565 and ALA567 with strong hydrogen bonding (short distances) with MeOIstEt and similar residues have been reported with the native ligand. In most of the cases, the involvement of same amino acid residues suggests that the test compound is bound at the vicinity of the active site of the protein and thus may lead to its effective inhibition.

Based on the observation of interactions at the methoxy end of the compound, it can be inferred that its replacement with other larger functional groups like butoxy or phenyl rings with diverse substituents (electron withdrawing or even electron donating) may lead to stronger binding at the active pocket. Thus, the synthesis of different compounds with the same scaffold but with slight variation in substituent that favour non-covalent interactions (hydrogen bond, ionic and pi-related) with the key amino acid residues would be appropriate. The presence of donors for hydrogen bond formation from the residues of the protein in most of the cases suggests the inclusion of functional group with electronegative elements. This proposition is in accordance to the composition of the FDA approved drug imatinib, which contains multiple nitrogen atoms and has long molecular structure. A trial and error method or virtual screening (pharmacophore modeling) of a library of compounds with multiple types of substituent that may fulfill this criteria may usher to a better lead candidate than some of the control drugs.

Conclusion

Two thiosemicarbazones, MeOIstEt and MeOIstMe were synthesized and characterized by various spectral techniques. They were tested for anticancer activity *in vitro* in different cancer cell lines like A549, MCF-7 and A431. Moderate anticancer activity with IC_{50} values in the range of 6.59-36.49 μM were obtained. Also, the anticancer properties of two test compounds were investigated *in silico* by various computational methods using either free software or online servers. One of these compounds, MeOIstEt hint of being biologically active and showed better binding affinity than one FDA approved drug from flexible receptor molecular docking calculations in a hydrated environment. Atomic level non-covalent interactions were determined in the receptor-ligand complexes and drug likeness along with ADMET predictions made using different programs showed acceptable properties. The compounds require further *in vitro* experiments (different cell lines) and could be subjected to further *in vivo* trials. Further functionalization of the test compounds with suitable groups leading to even better binding with the target receptor may help in improving the efficacy and effectiveness of the proposed compound as a good cancer drug. In order to determine the stability of complex, the trajectory of the ligand inside the active site, its RMSD and free energy needs to be analyzed. It requires molecular dynamics simulation of the complex with production run of 200 nanoseconds or longer and is currently being pursued. This work shows that computational technique could be synergistically used with experiments for better insights and proper justification in the search of therapeutics against different diseases.

ACKNOWLEDGEMENTS

Upendra Chaudhary express his gratitude to the Nepal Academy of Science and Technology (NAST) for supporting financially through the Ph. D. scholarship program (2018/2019 AD). The authors also express their sincere thanks to Dr. Anupa A. Kumbhar, Department of Chemistry, Savitribai Phule Pune University, Pune, India for providing NMR and mass spectral data.

CONFLICT OF INTEREST

The authors declare that there is no conflict of interests regarding the publication of this article.

REFERENCES

1. H.A. Mahdy, M.K. Ibrahim, A.M. Metwaly, A. Belal, A.B.M. Mehany, K.M.A. El-Gamal, A. El-Sharkawy, M.A. Elhendawy, M.M. Radwan, M.A. Elsohly and I.H. Eissa, *Bioorg. Chem.*, **94**, 103422 (2020); https://doi.org/10.1016/j.bioorg.2019.103422
2. V.R. Solomon, C. Hu and H. Lee, *Bioorg. Med. Chem.*, **17**, 7585 (2009); https://doi.org/10.1016/j.bmc.2009.08.068
3. R.L.D. Havrylyuk, B. Zimenkovsky, O. Vasylenko, A. Gzella and R. Lesyk, *J. Med. Chem.*, **55**, 8630 (2012); https://doi.org/10.1021/jm300789g
4. R. Sribalan, G. Banuppriya, M. Kirubavathi and V. Padmini, *J. Mol. Struct.*, **1175**, 577 (2019); https://doi.org/10.1016/j.molstruc.2018.07.114
5. A. Cane, M.C. Tournaire, D. Barritault and M. Crumeyrolle-Arias, *Biochem. Biophys. Res. Commun.*, **276**, 379 (2000); https://doi.org/10.1006/bbrc.2000.3477
6. N.M. Evdokimov, I.V. Magedov, D. McBrayer and A. Kornienko, *Bioorg. Med. Chem. Lett.*, **26**, 1558 (2016); https://doi.org/10.1016/j.bmcl.2016.02.015

7. K.L. Vine, J.M. Locke, M. Ranson, S.G. Pyne and J.B. Bremner, *Bioorg. Med. Chem.*, **15**, 931 (2007); https://doi.org/10.1016/j.bmc.2006.10.035
8. N. Karali, *Eur. J. Med. Chem.*, **37**, 909 (2002); https://doi.org/10.1016/S0223-5234(02)01416-2
9. B. Shakya, N. Shahi, F. Ahmad, P.N. Yadav and Y.R. Pokharel, *Bioorg. Med. Chem. Lett.*, **29**, 1677 (2019); https://doi.org/10.1016/j.bmcl.2019.04.031
10. N.V.Z. Juranic, F. Anastasova, I. Juranic, T. Stanojkovic and S. Radulovic, *J. Exp. Clin. Cancer Res.*, **3**, 317 (1999).
11. H. Pervez, N. Manzoor, M. Yaqub, A. Khan, K.M. Khan, F.H. Nasim and M.I. Choudhary, *Lett. Drug Des. Discov.*, **7**, 102 (2010); https://doi.org/10.2174/157018010790225840
12. S. Saranya, J. Haribabu, V.N. Vadakkedathu Palakkeezhillam, P. Jerome, K. Gomathi, K.K. Rao, V.H.H. Surendra Babu, R. Karvembu and D. Gayathri, *J. Mol. Struct.*, **1198**, 126904 (2019); https://doi.org/10.1016/j.molstruc.2019.126904
13. A.Q. Ali, S.G. Teoh, A. Salhin, N.E. Eltayeb, M.B. Khadeer Ahamed and A.M.S.A. Majid, *Spectrochim. Acta A Mol. Biomol. Spectrosc.*, **125**, 440 (2014); https://doi.org/10.1016/j.saa.2014.01.086
14. K.N. Aneesrahman, K. Ramaiah, G. Rohini, G.P. Stefy, N.S.P. Bhuvanesh and A. Sreekanth, *Inorg. Chim. Acta*, **492**, 131 (2019); https://doi.org/10.1016/j.ica.2019.04.019
15. M.A. Demertzis, P.N. Yadav and D. Kovala-Demertzi, *Helv. Chim. Acta*, **89**, 1959 (2006); https://doi.org/10.1002/hlca.200690187
16. G. Munikumari, R. Konakanchi, V.B. Nishtala, G. Ramesh, L.R. Kotha, K.B. Chandrasekhar and C. Ramachandraiah, *Synth. Commun.*, **49**, 146 (2019); https://doi.org/10.1080/00397911.2018.1546400
17. P.N. Yadav, N.K. Singh, S. Sharma, A. Krishnakumar, R.K. Choudhary, A.A. Kumbhar, R.J. Butcher and Y.R. Pokharel, *J. Inorg. Biochem.*, (2022); https://doi.org/10.2139/ssrn.4042515
18. M. Muralisankar, S. Sujith, N.S.P. Bhuvanesh and A. Sreekanth, *Polyhedron*, **118**, 103 (2016); https://doi.org/10.1016/j.poly.2016.06.017
19. J. Haribabu, G.R. Subhashree, S. Saranya, K. Gomathi, R. Karvembu and D. Gayathri, *J. Mol. Struct.*, **1110**, 185 (2016); https://doi.org/10.1016/j.molstruc.2016.01.044
20. L.M. Finkielsztein, E.F. Castro, L.E. Fabian, G.Y. Moltrasio, R.H. Campos, L.V. Cavallaro and A.G. Moglioni, *Eur. J. Med. Chem.*, **43**, 1767 (2008); https://doi.org/10.1016/j.ejmech.2007.10.023
21. N.K. Singh, S. Shrestha, N. Shahi, R.K. Choudhary, A.A. Kumbhar, Y.R. Pokharel and P.N. Yadav, *Rasayan J. Chem.*, **14**, 1600 (2021); https://doi.org/10.31788/RJC.2021.1436341
22. A.Q. Ali, S.G. Teoh, A. Salhin, N.E. Eltayeb, M.B.K. Ahamed and A.M.S.A. Majid, *Inorg. Chim. Acta*, **416**, 235 (2014); https://doi.org/10.1016/j.ica.2014.03.029
23. P.N. Yadav, M.A. Demertzis, D. Kovala-Demertzi, A. Castineiras and D.X. West, *Inorg. Chim. Acta*, **332**, 204 (2002); https://doi.org/10.1016/S0020-1693(02)00710-7
24. M. Joseph, V. Suni, M.R. Prathapachandra Kurup, M. Nethaji, A. Kishore and S.G. Bhat, *Polyhedron*, **23**, 3069 (2004); https://doi.org/10.1016/j.poly.2004.09.026
25. M.S. Çavus, H. Yakan, H. Muglu and T. Bakir, *J. Phys. Chem. Solids*, **140**, 109362 (2020); https://doi.org/10.1016/j.jpcs.2020.109362
26. G.A. Bain, D.X. West, J. Krejci, J. Valdés-s-Martinez, S. Hernández-Ortega and R.A. Toscano, *Polyhedron*, **16**, 855 (1997); https://doi.org/10.1016/S0277-5387(96)00323-3
27. C. Balachandran, J. Haribabu, K. Jeyalakshmi, N.S.P. Bhuvanesh, R. Karvembu, N. Emi and S. Awale, *J. Inorg. Biochem.*, **182**, 208 (2018); https://doi.org/10.1016/j.jinorgbio.2018.02.014
28. D. Kovala-Demertzi, M. Demertzis, P.N. Yadav, A. Castiñeiras and D.X. West, *Transition Met. Chem.*, **24**, 642 (1999); https://doi.org/10.1023/A:1006989117072
29. A.J. Abdulghani and N.M. Abbas, *Bioinorg. Chem. Appl.*, **2011**, 706262 (2011); https://doi.org/10.1155/2011/706262
30. H. Muglu, *Res. Chem. Intermed.*, **46**, 2083 (2020); https://doi.org/10.1007/s11164-020-04079-x
31. N.K. Singh, S. Shrestha, N. Shahi, R.K. Choudhary, A.A. Kumbhar, Y.R. Pokharel and P.N. Yadav, *Asian J. Chem.*, **33**, 557 (2021); https://doi.org/10.14233/ajchem.2021.23004
32. A.M.S. El-Sharief, Y.A. Ammar, A. Belal, M.A.M.S. El-Sharief, Y.A. Mohamed, A.B.M. Mehany, G.A.M. Elhag Ali and A. Ragab, *Bioorg. Chem.*, **85**, 399 (2019); https://doi.org/10.1016/j.bioorg.2019.01.016
33. R. Bhuvaneswari, M. Divya Bharathi, G. Anbalagan, G. Chakkaravarthi and K.S. Murugesan, *J. Mol. Struct.*, **1173**, 188 (2018); https://doi.org/10.1016/j.molstruc.2018.06.109
34. U. Chaudhary, D. Dawa, I. Banerjee, S. Sharma, K. Mahiya, A. Rauf, Y.R. Pokharel and P.N. Yadav, *J. Mol. Struct.*, **1274**, 134549 (2023); https://doi.org/10.1016/j.molstruc.2022.134549
35. E. Labisbal, A. Sousa, A. Castiñeiras, J.A. García-Vázquez, J. Romero and D.X. West, *Polyhedron*, **19**, 1255 (2000); https://doi.org/10.1016/S0277-5387(00)00383-1
36. N.T. Akinchan, P.M. Drozdzewski and W. Holzer, *J. Mol. Struct.*, **641**, 17 (2002); https://doi.org/10.1016/S0022-2860(02)00134-5
37. Y.H. Lu, Y.W. Lu, C.L. Wu, Q. Shao, X.L. Chen and R.N.B. Bimbong, *Spectrochim. Acta A Mol. Biomol. Spectrosc.*, **65**, 695 (2006); https://doi.org/10.1016/j.saa.2005.12.032
38. T.D. Kühne, M. Iannuzzi, M. Del Ben, V.V. Rybkin, P. Seewald, F. Stein, T. Laino, R.Z. Khaliullin, O. Schütt, F. Schiffmann, D. Golze, J. Wilhelm, S. Chulkov, M.H. Bani-Hashemian, V. Weber, U. Borštnik, M. Taillefumier, A.S. Jakobovits, A. Lazzaro, H. Pabst, T. Müller, R. Schade, M. Guidon, S. Andermatt, N. Holmberg, G.K. Schenter, A. Hehn, A. Bussy, F. Belleflamme, G. Tabacchi, A. Glöß, M. Lass, I. Bethune, C.J. Mundy, C. Plessl, M. Watkins, J. VandeVondele, M. Krack and J. Hutter, *J. Chem. Phys.*, **152**, 194103 (2020); https://doi.org/10.1063/5.0007045
39. P.A. Ravindranath, S. Forli, D.S. Goodsell, A.J. Olson and M.F. Sanner, *PLOS Comput. Biol.*, **11**, e1004586 (2015); https://doi.org/10.1371/journal.pcbi.1004586
40. W. Tian, C. Chen, X. Lei, J. Zhao and J. Liang, *Nucleic Acids Res.*, **46(no. W1)**, W363 (2018); https://doi.org/10.1093/nar/gky473
41. H.M. Berman, *Nucleic Acids Res.*, **28**, 235 (2000); https://doi.org/10.1093/nar/28.1.235
42. R. Board and G.C. Jayson, *Drug Resist. Updat.*, **8**, 75 (2005); https://doi.org/10.1016/j.drup.2005.03.004
43. X. Wang, Y. Shen, S. Wang, S. Li, W. Zhang, X. Liu, L. Lai, J. Pei and H. Li, *Nucleic Acids Res.*, **45(no. W1)**, W356 (2017); https://doi.org/10.1093/nar/gkx374
44. P.G. Wyatt, A.J. Woodhead, V. Berdini, J.A. Boulstridge, M.G. Carr, D.M. Cross, D.J. Davis, L.A. Devine, T.R. Early, R.E. Feltell, E.J. Lewis, R.L. McMenamin, E.F. Navarro, M.A. O'Brien, M. O'Reilly, M. Reule, G. Saxty, L.C.A. Seavers, D.M. Smith, M.S. Squires, G. Trewartha, M.T. Walker and A.J.-A. Woolford, *J. Med. Chem.*, **51**, 4986 (2008); https://doi.org/10.1021/jm800382h
45. I. Kuriwaki, M. Kameda, H. Hisamichi, S. Kikuchi, K. Iikubo, Y. Kawamoto, H. Moritomo, Y. Kondoh, Y. Amano, Y. Tateishi, Y. Echizen, Y. Iwai, A. Noda, H. Tomiyama, T. Suzuki and M. Hirano, *Bioorg. Med. Chem.*, **28**, 115453 (2020); https://doi.org/10.1016/j.bmc.2020.115453
46. L. Mazumder, M.R. Hasan, K. Fatema, M.Z. Islam and S.K. Tamanna, *BioMed Res. Int.*, **2022**, 4302625 (2022); https://doi.org/10.1155/2022/4302625
47. C. Colovos and T. Yeates, *Protein Sci.*, **2**, 1511 (1993); https://doi.org/10.1002/pro.5560020916
48. D.K.A. Mohan and P. Gangwar, *World J. Pharm. Res.*, **2**, 1114 (2013).
49. B.Z. Sibuh, P.K. Gupta, P. Taneja, S. Khanna, P. Sarkar, S. Pachisia, A.A. Khan, N.K. Jha, K. Dua, S.K. Singh, S. Pandey, P. Slama, K.K. Kesari and S. Roychoudhury, *Biomedicines*, **9**, 1375 (2021); https://doi.org/10.3390/biomedicines9101375
50. S. Kim, J. Chen, T. Cheng, A. Gindulyte, J. He, S. He, B.A. Shoemaker, Q. Li, P.A. Thiessen, B. Yu, L. Zaslavsky, J. Zhang and E.E. Bolton, *Nucleic Acids Res.*, **49(no. D1)**, D1388 (2021); https://doi.org/10.1093/nar/gkaa971

51. K. Tallapragada, J. Chewning, D. Kombo and B. Ludwick, *J. Cheminform.*, **4**, 1 (2012); https://doi.org/10.1186/1758-2946-4-1
52. B. Schiffrin, S.E. Radford, D.J. Brockwell and A.N. Calabrese, *Protein Sci.*, **29**, 1851 (2020); https://doi.org/10.1002/pro.3902
53. G. Xiong, Z. Wu, J. Yi, L. Fu, Z. Yang, C. Hsieh, M. Yin, X. Zeng, C. Wu, A. Lu, X. Chen, T. Hou and D. Cao, *Nucleic Acids Res.*, **49(no. W1)**, W5 (2021); https://doi.org/10.1093/nar/gkab255
54. R. Al-Jarf, A.G.C. de Sá, D.E.V. Pires and D.B. Ascher, *J. Chem. Inf. Model.*, **61**, 3314 (2021); https://doi.org/10.1021/acs.jcim.1c00168
55. J. Blaney, *J. Comput. Aided Mol. Des.*, **26**, 13 (2012); https://doi.org/10.1007/s10822-011-9518-x
56. M. Batool, B. Ahmad and S. Choi, *Int. J. Mol. Sci.*, **20**, 2783 (2019); https://doi.org/10.3390/ijms20112783
57. D. Systèmes, BIOVIA Discovery Studio Visualizer, San Diego: Dassault Systèmes (2020); https://3ds.com/products-services/biovia/products
58. N.A.A.M. Aziz, R.F. George, K. El-Adl and W.R. Mahmoud, *RSC Adv.*, **12**, 12913 (2022); https://doi.org/10.1039/D2RA01119K
59. S.K. Paramashivam, K. Elayaperumal, B. Natarajan, M. Ramamoorthy, S. Balasubramanian and K.N. Dhiraviam, *Bioinformation*, **11**, 73 (2015); https://doi.org/10.6026/97320630011073
60. A.B. Mahajanakatti, G. Murthy, N. Sharma and S. Skariyachan, *Interdiscip. Sci.*, **6**, 13 (2014); https://doi.org/10.1007/s12539-014-0170-8
61. G. Chessari, I.R. Hardcastle, J.S. Ahn, B. Anil, E. Anscombe, R.H. Bawn, L.D. Bevan, T.J. Blackburn, I. Buck, C. Cano, B. Carbain, J. Castro, B. Cons, S.J. Cully, J.A. Endicott, L. Fazal, B.T. Golding, R.J. Griffin, K. Haggerty, S.J. Harnor, K. Hearn, S. Hobson, R.S. Holvey, S. Howard, C.E. Jennings, C.N. Johnson, J. Lunec, D.C. Miller, D.R. Newell, M.E.M. Noble, J. Reeks, C.H. Revill, C. Riedinger, J.D. St. Denis, E. Tamanini, H. Thomas, N.T. Thompson, M. Vinkovic, S.R. Wedge, P.A. Williams, N.E. Wilsher, B. Zhang and Y. Zhao, *J. Med. Chem.*, **64**, 4071 (2021); https://doi.org/10.1021/acs.jmedchem.0c02188

Nepal Academy of Science and Technology (NAST)

CERTIFICATE OF PARTICIPATION

Awarded to

UPENDRA CHAUDHARY

for Presentation in Oral / Poster / Participation in the

9th National Conference on Science and Technology

June 26-28,2022 (Asar 12-14, 2079)

Khumaltar, Lalitpur, Nepal

Ms. Luna Vajra
Chief, Promotion Division

Prof. Dr. Mahesh K. Adhikari
Secretary

Dr. Sunil Babu Shrestha
Vice Chancellor